Errata Sheet for

Performance Assessment for the Tank Farm Facility at the Idaho National Engineering and Environmental Laboratory

DOE/ID-10966

Section 2.1.6.2, "Grout K_d Values," page 2-55

This section states that "Concrete K_d values for reducing conditions have been chosen." This is true for the tank contents; however, the concrete vault was assigned K_d values for oxidizing conditions. The section further states that "The concrete K_d values were chosen from Region II of Bradbury and Sarott (1995)." This is also true; however, in Region II, the reducing and oxidizing K_d values are the same for all elements except technicium and uranium. The technicium K_d values for reducing and oxidizing conditions are 1 and 0.001 m^3/kg, respectively. The uranium K_d values for reducing and oxidizing conditions are 5 and 2 m^3/kg, respectively.

TFF PA Results for ^{14}C

The projected doses for ^{14}C are extremely low in the final performance assessment (PA). ^{14}C was originally modeled in error with a low K_d value for grout in the draft PA report. Therefore, ^{14}C was maintained in the final PA analyses to show continuity with the draft reports; however, the K_d value was corrected for grout and the ^{14}C doses were significantly reduced in the draft final PA report.

Revised Table 3-6, page 3-34

Table 3-6 now includes data for ^{129}I and the K_d concrete vault values.

Table 3-6. Non-decay chain DUST-MS input parameters.

Nuclide	Half-life (yr)	K_d Sand Pad (m^3/kg)	K_d Grout (m^3/kg)	K_d Concrete Vault (m^3/kg)
^{14}C	5.73E+03	5.00E–03	5.00E+00	5.00E+00
^{129}I	1.57E+07	1.00E–03	8.00E–03	8.00E–03
^{90}Sr	2.86E+01	1.50E–02	3.00E–03	3.00E–03
^{99}Tc	2.13E+05	1.00E–04	2.50E+00	1.00E–03

Revised Table 7-3, page 7-5

Table 7-3 now includes data for the sand pad sorption and concrete vault sorption coefficients.

Table 7-3. Overview of the parameter values for sensitivity and uncertainty analysis.

	Measured Item	Best Scenario	Realistic Scenario	Conservative Scenario	Worst-Case Scenario
Solid Radionuclide Inventory		50% reduction from worst case	25% reduction from worst case	10% reduction from worst case	Depicts sodium-bearing waste (undiluted tank-heel residual)
Liquid Radionuclide Inventory		95% reduction from worst case	80% reduction from worst case	50% reduction from worst case	Depicts sodium-bearing waste (undiluted tank-heel residual)
Infiltration		1.1 cm/yr	1.1 cm/yr	4.1 cm/yr	12.4 cm/yr
Grout Sorption Coefficients (m^3/kg)	C	10	10	5.0	1.0
	I	0.03	0.03	0.008	0.002
	Sr	0.006	0.006	0.003	0.001
	Tc	5	5	2.5	1
Sand Pad Sorption Coefficients (m^3/kg)	C	0.005	0.005	0.005	0.005
	I	0.001	0.001	0.001	0.001
	Sr	0.015	0.015	0.015	0.015
	Tc	0.0001	0.0001	0.0001	0.0001
Concrete Vault Sorption Coefficients (m^3/kg)	C	10	10	5	1
	I	0.03	0.03	0.008	0.002
	Sr	0.006	0.006	0.003	0.001
	Tc	0.001	0.001	0.001	0.001
Unsaturated Zone Longitudinal Dispersivities (m)	Sediment	0.52	0.52	0.29	0.052
	Basalt	3.36	3.36	1.85	0.34
Unsaturated Zone Transverse Dispersivities (m)	Sediment	0.26	0.26	0.14	0.026
	Basalt	1.7	1.7	0.94	0.17
Interbed Sediment Sorption Coefficients (mL/g)	C	20	20	10	2
	I	5	5	0.1	0.01
	Sr	24	24	18	12
	Tc	0.1	0.1	0.01	0
Basalt Sorption Coefficients (mL/g)	C	7.1	7.1	5.0	1.7
	I	1	1	0.1	0
	Sr	13	13	6	1
	Tc	0.24	0.24	0.01	0

Inventory Error and Effect on Results

An error in the inventory for liquids was found for ^{129}I and ^{99}Tc. This error consisted of a 34% reduction in the ^{99}Tc liquid inventory of the realistic and best cases, and a 46% reduction in the ^{129}I liquid inventory of the best case. Because the error reduces the total inventory, the projected doses for this inventory would also be proportionally reduced. The corresponding inventories for ^{129}I and ^{99}Tc have been corrected in Table A-2 (beginning on page A-12). The correct concentrations are shown in the table below.

Table A-2. Liquid radionuclide inventory.

Tank Source Inventory in 2016										
		Liquids - Based on WM-188 Analytical Data of 4,989 L			Conservative Scenario 50% Reduction of Liquid Concentration (Through Flushing)		Realistic Scenario 80% Reduction of Liquid Concentration (Through Flushing)		Best Scenario 95% Reduction of Liquid Concentration (Through Flushing)	
Nuclide	ORIGEN2 or Analytical Ratio	Ratio Factor	Activity (Ci/L)	Total Ci	(Ci/L)	Total Ci	Ci/L	Total Ci	Ci/L	Total Ci
Tc-99							1.19E–05	5.96E–02	2.99E–06	1.49E–02
I-129									7.44E–09	3.71E–05

DOE/ID-10966
Revision 1
April 2003

Performance Assessment for the Tank Farm Facility at the Idaho National Engineering and Environmental Laboratory

Volume 1
Sections 1 through 9

DOE/ID-10966
Revision 1

Performance Assessment for the Tank Farm Facility at the Idaho National Engineering and Environmental Laboratory

Volume 1
Sections 1 through 9

April 2003

Prepared for the
U.S. Department of Energy
Idaho Operations Office

ABSTRACT

This report documents the projected radiological dose impacts associated with the closure of the Tank Farm Facility at the Idaho Nuclear Technology and Engineering Center at the Idaho National Engineering and Environmental Laboratory. The performance assessment analysis is based on conservative assumptions and parameters. The calculations involved modeling (a) the release of radionuclides from the tanks, sand pads, and piping, and subsequent transport through the environment and (b) exposures to members of the public via air, groundwater, and food chain pathways. This performance assessment analysis includes responses to comments received during reviews by the Nuclear Regulatory Commission and the Department of Energy. Additional analyses have been performed on the Tank Farm Facility to further evaluate the expected performance. In addition, a complete sensitivity/uncertainty analysis has been conducted to ensure that the reported doses for compliance purposes are conservative. The results of the analyses indicate compliance with the established performance objectives and provide reasonable assurance that public health and safety will be protected.

EXECUTIVE SUMMARY

Performance assessments (PAs) involve estimating radiological exposure to future members of the public. These analyses include comparing exposure estimates to specific performance measures to determine whether there is a reasonable expectation that the performance measures will be met in the future. This report documents the projected radiological dose impacts associated with the closure of the Tank Farm Facility (TFF) at the Idaho Nuclear Technology and Engineering Center (INTEC). INTEC is one of the facilities at the Idaho National Engineering and Environmental Laboratory (INEEL). The performance objectives and other performance-related factors required to be considered in this performance assessment are for deactivated high-level waste facility closure actions that contain residual low-level waste. This PA includes responses to comments received during reviews by the Nuclear Regulatory Commission and the Department of Energy.

The potential risks posed by closure of the TFF were assessed by conservatively estimating the release and transport of radionuclides from (a) the release of radionuclides from the tanks, sand pads, and piping and subsequent transport through the environment and (b) exposures to members of the public via air, groundwater, and food chain pathways. Contaminated soils associated with the TFF are not addressed in the TFF closure or this PA. Instead, past releases of contaminants are being addressed under the Comprehensive Environmental Response, Compensation, and Liability Act (CERCLA). Contaminated soils are also addressed in the TFF Composite Analysis.

Two receptor types were assessed. The first was a member of the public. During the operational and institutional control periods, it is assumed that this individual resides at the INEEL Site boundary. During the post-institutional control period, the member of the public resides at the INTEC facility. This receptor was used to evaluate the drinking water pathway, all pathways (including food chains), and air pathway doses for comparison to the performance objectives.

The second type of receptor evaluated was an intruder. This hypothetical receptor was assumed to inadvertently intrude onto the TFF during the post-institutional control period. Four intruder scenarios were evaluated in this PA. The first was an acute scenario, which consisted of exposure while developing a water well. In the well-drilling scenario, the receptor was exposed to contaminated drill cuttings spread over the ground. The second scenario involved an acute scenario where the intruder was assumed to excavate a basement. The third scenario was chronic exposure in an agricultural scenario based on drill cuttings from the development of the water well. The well cuttings were assumed to be spread over the ground, and the intruder then began farming activities. The fourth scenario was also a chronic exposure, which consisted of an agricultural scenario based on the excavation of contaminated soil for the development of a basement.

The performance assessment process consists of conceptual models that link radionuclide inventory, release (or source term), environmental transfer, and

impact assessment. The waste inventory used in the TFF PA was based upon bounding calculations, process knowledge, and sample analysis. The final step is determining radiological doses to receptors.

The exposure pathways evaluated included the ingestion of contaminated water, ingestion of contaminated food, inhalation of contaminated airborne particulates, and external exposure to radionuclides in the air and on the ground (or soil) surface. Contaminated agricultural products consumed by members of the public also were considered. The analysis of the potential transport pathways from the TFF indicates that the groundwater pathway was the most significant in terms of radionuclide transport to the receptors.

Several computer models were used in the TFF PA including DUST-MS, PORFLOW, GWSCREEN, and RadDecay. Each model was used for a specific analysis. DUST-MS was used to evaluate the release of radionuclides from the tanks, sand pads, and piping. PORFLOW was used to evaluate the transport of radionuclides through the groundwater pathway for the 1,000-yr compliance period. GWSCREEN was used to evaluate the groundwater transport of radionuclides over very long periods of time. RadDecay was used to evaluate the ingrowth of radionuclide progeny in the waste.

In addition to computer codes, several analytical models were developed to evaluate the degradation of concrete vaults, stainless steel tanks, and piping. Multiplicative models also were developed to evaluate the doses to intruders and public receptors.

As shown in the table below, the conservative analysis results indicate compliance with all performance objectives.

Performance Objective	PA Result
All-pathways 25 mrem/yr	1.35 mrem/yr (groundwater pathway) 0.51 mrem/yr (atmospheric pathway)
Airborne emissions excluding radon 10 mrem/yr	0.51 mrem/yr
Average annual radon flux 20 pCi/m^2/s	0.39 pCi/m^2/s
Protection of groundwater 4 mrem/yr	0.77 mrem/yr
Acute drilling scenario 500 mrem	232 mrem
Acute construction scenario 500 mrem	0.80 mrem
Chronic post-drilling scenario 100 mrem/yr	91.1 mrem/yr
Chronic post-construction scenario 100 mrem/yr	26.1 mrem/yr

To ensure that the sensitivities and uncertainties of the groundwater pathway modeling were thoroughly understood, a sensitivity/uncertainty analysis was conducted. A total of four scenarios were considered for the groundwater pathway analyses. These scenarios were termed (1) worst case, (2) conservative case, (3) realistic case, and (4) best case. The conservative case was used in the PA analyses to demonstrate compliance with the performance objectives. The worst-case scenario was used to evaluate the potential worst-case doses from the use of worst-case parameter values including the inventories and transport characteristics. The realistic scenario presents the analyses in relation to the expected behavior of the groundwater transport and the contaminant inventories expected to remain after cleaning of the tanks and piping. The best scenario uses the same transport parameter values as the realistic case; however, the inventory was further reduced to the level expected from the best available analysis of the cleaning technology. Such an evaluation was intended to demonstrate that the conservative case was, in fact, conservative and appropriate to use as the compliance case.

The following table provides the results of the sensitivity/uncertainty analysis for the four groundwater pathway scenarios.

Groundwater Scenario	Drinking Water Dose (mrem/yr)	All-Pathway Dose (mrem/yr)
Worst Case	23.1	85.8
Conservative Case	0.77	1.35
Realistic Case	0.04	0.07
Best Case	0.03	0.04

This sensitivity/uncertainty analysis indicates that the performance objectives for the groundwater pathway are met for three cases (i.e., conservative, realistic, and best). However, the worst-case scenario doses are above the performance objectives. To assess the degree of uncertainty in the groundwater doses, the four groundwater scenarios were run for the matrix of possibilities: (1) inventory, (2) infiltration rate, and (3) transport parameters (i.e., distribution coefficients). This matrix resulted in 36 groundwater scenario combinations.

The matrix analysis of parameter combinations resulted in a worst-case scenario considered to be a realistic “upper-bound” of the dose analysis. This combination was the worst-case transport parameters, conservative inventory, and a conservative infiltration rate. The conservative inventory is considered to be the upper bound of the final closure inventory based on preliminary data obtained from cleaning Tank WM-182. The cleaning process has been effective and the final inventories are expected to be less than those predicted in the conservative inventory calculations. The infiltration rate of 4.1 cm/yr is also considered to be the upper bound of the infiltration rate at the TFF. The TFF currently has a soil cover; the 4.1 cm/yr infiltration rate is based on measurements at the INEEL Central Facilities Area soil-covered landfill. Again, the infiltration rate will likely be reduced since an engineered cover is proposed

for the TFF. However, the PA analyses do not take credit for this reduction for the compliance case. The realistic and best cases do include a reduction in the infiltration rate. The largest uncertainty in the analyses was considered to be the distribution coefficients for the TFF grout and the unsaturated zone.

The combination of the worst-case distribution coefficients, conservative inventory, and conservative infiltration rate resulted in a realistic, "upper-bound," worst-case dose of 3.4 mrem/yr for the drinking water pathway (i.e., groundwater protection) and a dose of 15 mrem/yr for the all-pathways dose. These doses are less than the performance objectives. In summary, the worst-case groundwater doses were found to exceed the performance objectives; however, a combination of parameters in the matrix analysis presents a realistic, "upper-bound" dose estimate for the worst-case that shows compliance with the performance objectives.

Uncertainty in the atmospheric pathway, radon flux, and intruder analyses doses were also investigated based on the four inventories for the TFF (i.e., worst-case, conservative, realistic, and best). The following table summarizes the results of the uncertainty analysis.

Scenario and Performance Objective	Worst-Case Inventory	Conservative Inventory	Realistic Inventory	Best Inventory
Acute Drilling Intruder (500 mrem)	276	232	193	144
Chronic Drilling Intruder (100 mrem/yr)	106	91.1	75.1	52.8
Acute Construction Intruder (500 mrem)	0.89	0.80	0.67	0.45
Chronic Construction Intruder (100 mrem/yr)	29.1	26.1	21.8	14.5
Rn Flux (20 $pCi/m^2/s$)	0.48	0.39	0.29	0.19
Atmospheric (10 mrem/yr)	1.1	0.51	0.22	0.05

The uncertainty analysis for the intruder, atmospheric releases, and radon fluxes indicate that the performance objectives are attained for all inventory scenarios except for the chronic intruder post-drilling scenario. The worst-case inventory is based on the assumption that the tank internals have been washed and the remaining heel is unaltered at a depth of 1 in. However, cleaning of Tank WM-182 has proven the effectiveness of the cleaning process, and the heel is much less is than 1 in. The residual radionuclide inventory in Tank WM-182 is less than any of the inventories presented in the analysis. Also, the intruder doses are the result of short-lived radionuclides remaining after the end of institutional control. The analysis assumed that the intruder would drill through the reinforced concrete vault at 100 years. Credit for the reinforced concrete vault deterring the

intruder from drilling through the vault was not taken in the analysis. The doses are reduced dramatically as the time of intrusion is extended a few years.

The sensitivity/uncertainty analysis indicates that the conservative case analyses provide a "bounding analysis" of the potential doses to the public from the closure of the TFF. The sensitivity/uncertainty analysis indicates that the potential for the doses exceeding the performance objectives are low, and that a combination of worst-case assumptions would be required to result in the doses exceeding the performance objectives.

CONTENTS

FIGURES

TABLES

ACRONYMS

ALARA	as low as reasonably achievable
amsl	above mean sea level
bgs	below ground surface
BLM	Bureau of Land Management
BRA	baseline risk assessment
CEDE	committed effective dose equivalent
CERCLA	Comprehensive Environmental Response, Compensation, and Liability Act
CFA	Central Facilities Area
CFR	Code of Federal Regulations
CPP	Chemical Processing Plant (now INTEC)
DCF	dose conversion factor
DEQ	(Idaho) Department of Environmental Quality
DOE	Department of Energy
DOE-ID	Department of Energy Idaho Operations Office
DUST-MS	Disposal Unit Source Term–Multiple Species
EBR-I	Experimental Breeder Reactor-I
EDE	effective dose equivalent
EIS	environmental impact statement
EPA	Environmental Protection Agency
ESRP	Eastern Snake River Plain
FDF	Flood-Diversion Facility (INEEL)
FFA/CO	Federal Facility Agreement and Consent Order
FORTRAN	Formula Translation
HLLW	high-level radioactive liquid waste
HLW	high-level waste
HWMA	Idaho Hazardous Waste Management Act

ICRP	International Commission on Radiological Protection
IDAPA	Idaho Administrative Procedures Act
IDHW	Idaho Department of Health and Welfare
INEEL	Idaho National Engineering and Environmental Laboratory
INTEC	Idaho Nuclear Technology and Engineering Center
Ka	kilo annum
LLW	low-level waste
M	magnitude
Ma	million annum
MCL	maximum contaminant level
mpy	mils per year
MTR	Materials Test Reactor
MW	monitoring well
NEA	Nuclear Energy Agencies
NOAA	National Oceanic and Atmospheric Administration
NRC	Nuclear Regulatory Commission
OU	operable unit
PA	performance assessment
PMF	probable maximum flood
PMP	probable maximum precipitation
PW	perched water
RCRA	Resource Conservation and Recovery Act
RESL	Radiological and Environmental Sciences Laboratory
RI/FS	remedial investigation/feasibility study
RI/BRA	remedial investigation/baseline risk assessment
ROD	record of decision
RWMC	Radioactive Waste Management Complex

SDA	Subsurface Disposal Area
TAN	Test Area North
TEDE	total effective dose equivalent
TFF	Tank Farm Facility
TRA	Test Reactor Area
TRU	transuranic waste
USC	United States Code
USGS	United States Geological Survey
WAG	Waste Area Group
WCC	Woodward-Clyde Consultants
WCFS	Woodward-Clyde Federal Services
WIR	Waste-Incidental-to-Reprocessing

NOMENCLATURE

Ac	actinium
Ag	silver
Am	americium
At	astatine
Ba	barium
Be	beryllium
Bi	bismuth
C	carbon
Cd	cadmium
Ce	cerium
Cf	californium
Cl	chlorine
Cm	curium
Co	cobalt
Cr	chromium
Cs	cesium
Eu	europium
Fe	iron
Fr	francium
Gd	gadolinium
H	hydrogen
Hg	mercury
Ho	holmium
HTO	tritiated water, occurs when a water molecule exchanges a hydrogen atom for a tritium atom
I	iodine
In	indium

Kr	krypton
La	lanthanum
Nb	niobium
Nd	neodymium
Ni	nickel
Np	neptunium
Pa	protactinium
Pb	lead
Pd	palladium
Pm	promethium
Po	polonium
Pr	praseodymium
Pu	plutonium
Ra	radium
Rb	rubidium
Rh	rhodium
Rn	radon
Ru	ruthenium
Sb	antimony
Se	selenium
Sm	samarium
Sn	tin
Sr	strontium
Tc	technetium
Te	tellurium
Th	thorium
Tl	thallium

Tm	thulium
U	uranium
Y	yttrium
Zr	zirconium

Performance Assessment for the Tank Farm Facility at the Idaho National Engineering and Environmental Laboratory

1. INTRODUCTION

In 1949, the Atomic Energy Commission, predecessor to the Department of Energy (DOE), established the National Reactor Testing Station, now known as the Idaho National Engineering and Environmental Laboratory (INEEL). Here, the Atomic Energy Commission built, tested, and operated various types of nuclear reactors, support facilities, and equipment. The INEEL became the setting for the world's largest concentration of nuclear reactors. Fifty-two test reactors were built and tested. Of these reactors, only three are still operating.

In the 1970s, laboratory work expanded into the fields of systems engineering, environmental remediation, waste management, technology development, and energy research. In 1974, the laboratory's name was changed to the Idaho National Engineering Laboratory to reflect this new mission. The following year, the INEEL became the nation's second largest national environmental research park.

In 1997, DOE changed the laboratory's name to the Idaho National Engineering and Environmental Laboratory to underscore projects in developing waste cleanup and other environment-related technologies. Today, the INEEL is a federally-funded research and development center emphasizing applied engineering. It is also DOE's lead laboratory for environmental management.

The INEEL occupies approximately 890 mi^2 (2300 km^2)[a] of desert in a rural, sparsely populated area of southeastern Idaho on the Eastern Snake River Plain. The eastern boundary of the INEEL Site is 22 mi (35 km) west of Idaho Falls, Idaho.

The Idaho Nuclear Technology and Engineering Center (INTEC) is one of the facilities at the INEEL. Prior to May 1998, INTEC was named the Idaho Chemical Processing Plant (CPP). INTEC covers approximately 200 acres (80 ha) and encompasses more than 150 buildings, including storage, treatment, and laboratory facilities for spent nuclear fuel, mixed high-level waste (HLW), and mixed transuranic waste. The employees at INTEC are focused primarily on four areas:

- Safely storing spent nuclear fuel
- Preparing spent nuclear fuel for shipment to an offsite repository
- Developing technologies to safely treat high-level and liquid radioactive waste
- Remediating past environmental releases.

With the exception of that at Argonne National Laboratory-West, all HLW at the INEEL exists at INTEC (Palmer et al. 1999). The HLW was created from 1953 until 1988, from reprocessing spent nuclear fuel at INTEC. The resulting radioactive waste exists in both liquid and solid forms. All of the liquid waste is stored in the INTEC Tank Farm Facility (TFF). The TFF is a collection of 15 belowground stainless-steel tanks. The eleven 300,000-gal tanks are enclosed in belowground concrete vaults, while the four 30,000-gal tanks are directly buried in the soil. Figure 1-1 shows the relative locations of the INEEL, INTEC, and the TFF. The INEEL HLW Program manages all of the liquid waste stored at the TFF.

a. The measurements for this report were originally made in U.S. customary units. Where conventional, we have converted these to SI units and preserved the correct number of significant digits. In some cases, numbers end with a period; this is to preserve the correct number of significant digits. Flow rates and specifications have not been converted.

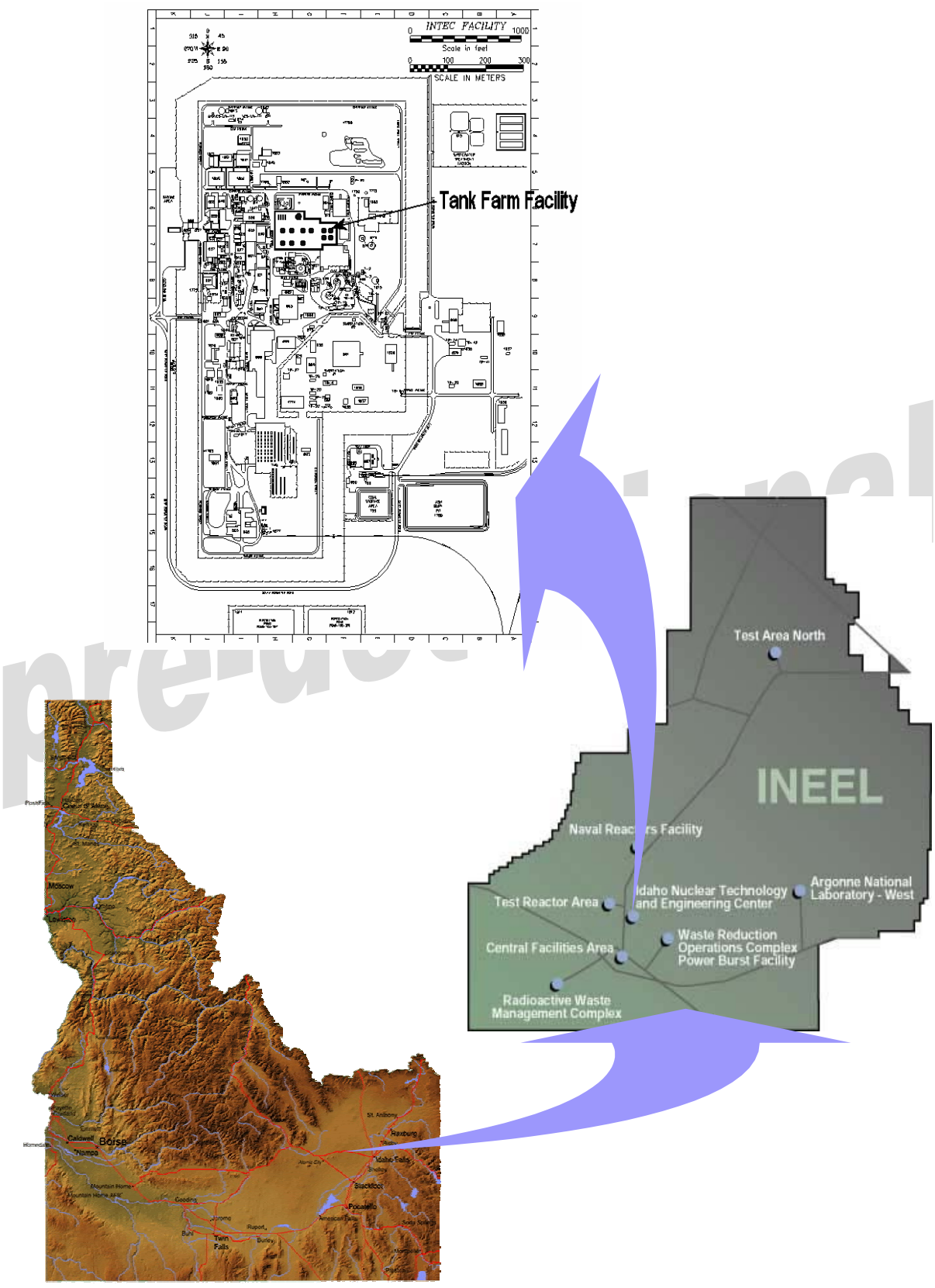

Figure 1-1. Location of the INEEL, INTEC, and the TFF in relation to the surrounding region.

Two types of liquid waste have been stored at the TFF: high-level liquid waste (HLLW), sometimes referred to as non-sodium-bearing waste, and sodium-bearing waste. The HLLW was generated as a direct result of reprocessing spent nuclear fuel; the sodium-bearing waste was generated from incidental activities, such as decontamination, associated with INTEC operations.

In April 1992, then Secretary of Energy James Watkins announced that spent nuclear fuel reprocessing would halt and he called for the shutdown of reprocessing facilities at INTEC. In 1988, the dissolution of nuclear fuel and creation of HLW ceased at INTEC. Since that time, no HLLW has been generated. The production of sodium-bearing waste is dependent on the type of work done at INTEC in the future. Sodium-bearing waste is generated primarily from decontamination and from operations associated with laboratories, fuel basins, and closure activities.

Under the terms of a 1992 Consent Order (and subsequent modifications) between the Idaho Department of Health and Welfare (IDHW)[b] and DOE (IDHW 1992), DOE must permanently cease use of tanks in the TFF at the INEEL or bring the tanks into compliance with secondary containment requirements as set forth by the Idaho Administrative Procedures Act (IDAPA) 58.01.05.009 (2002) (40 *Code of Federal Regulations* [CFR] 265.193, 2002). The Consent Order further specifies that this compliance cannot be achieved through an equivalency demonstration or by obtaining a variance as provided by IDAPA 58.01.05.009 [40 CFR 265.193(d)(4) and (h)]. DOE plans to close the TFF tanks because high radiation fields would make compliance with secondary containment requirements difficult, and a need for such storage is not evident after 2012.

The TFF includes 11 belowground 300,000-gal and 318,000-gal tanks (hereinafter referred to as 300,000-gal tanks) and four belowground 30,000-gal tanks. The 300,000-gal tanks are numbered WM-180 through WM-190, and the 30,000-gal tanks are designated as WM-103 through WM-106. The second modification to the Consent Order specifies that DOE must cease use of Tanks WM-182, WM-183, WM-184, WM-185,[c] and WM-186 by June 30, 2003, and the remaining tanks by December 31, 2012. Ceasing use of the tanks, as defined in the Consent Order, means that "DOE must empty the tanks down to their heels, i.e., the liquid level remaining in each tank will be lowered to the greatest extent possible by the use of existing transfer equipment" (IDHW 1998). According to the Idaho Hazardous Waste Management Act of 1983 (HWMA) and the Resource Conservation and Recovery Act (RCRA), the TFF is an interim status hazardous waste management unit (State of Idaho 1983; 42 *United States Code* [USC] 6901, 1976). Because of this status, the requirements of 40 CFR 265 (2002) apply to the TFF closure (rather than 40 CFR 264 [2002]).

The TFF will continue to operate until 2012 while various parts of the facility are being closed. The final closure of any component of the TFF will not be complete until all the tanks have been closed and the remedial investigation/feasibility study (RI/FS) for operable unit (OU) 3-14 (Tank Farm Soils) is completed. The final closure plan will address closure and any required post-closure care of the TFF. A decision to close the unit as a landfill or as clean closure will be determined during final closure. Clean closure is anticipated, as discussed in the HWMA/RCRA Closure Plan (DOE-ID 2001a).

Two significant releases from TFF ancillary equipment to surrounding soils occurred in 1955 and 1972. No releases have occurred from the tanks to environmental media. These releases are subject to investigation and remediation as necessary under the INEEL Comprehensive

b. On July 1, 2000, the Idaho legislature elevated the Division of Environmental Quality, a part of the Idaho Department of Health and Welfare, to the Idaho Department of Environmental Quality (DEQ). DEQ now oversees the implementation of the Consent Order. As such, citations and references to IDAPA 16 Title 01 (under IDHW), are now IDAPA 58 Title 01 (under DEQ).

c. The Consent Order allows Tank WM-185 to be used as an emergency spare tank.

Environmental Response, Compensation, and Liability Act (CERCLA) (42 USC 9601–9675, 1980) program as described in the Federal Facility Agreement and Consent Order (FFA/CO) (IDHW, Environmental Protection Agency [EPA], and DOE Idaho Operations Office [DOE-ID] 1991).

Performance assessments (PAs) are used by DOE to ensure a reasonable expectation that low-level waste (LLW) disposal will meet the radiological performance objectives in DOE Manual 435.1-1 (DOE 2001a). This PA addresses closure of the TFF, including the 11 belowground 300,000-gal stainless-steel tanks and corresponding vaults, four belowground 30,000-gal stainless-steel tanks, and associated ancillary equipment (e.g., piping and jets). This PA evaluates only the radiological waste constituents of the TFF; the hazardous constituents are addressed in the *HWMA/RCRA Closure Plan for Tanks WM-182 and WM-183* (DOE-ID 2001a).

1.1 General Approach

As required by Sections I.2.F, "Field Element Managers," and II.U(3), "Closure," of DOE Manual 435.1-1 (2001a), the responsible Field Element Manager is required to prepare two facility/site closure plans (Tier 1 and Tier 2) for each deactivated HLW facility or site or a combination of facilities (named a site) that are to be analyzed and closed together due to similarities or proximity. The closure plans will

> *Define the approach that will be taken for ensuring the long-term protection of the public and the environment from the closure of deactivated HLW facilities containing residual LLW or* [transuranic] *TRU wastes. This two-phase closure plan process is considered appropriate and necessary because much of the site-specific and detailed facility and waste characterization data needed to conduct projected performance analysis of the closure action may not be available at the time the closure action is being defined and resources are being solicited* (DOE 2000).

The Tier 1 Closure Plan defines and bounds the parameters of the TFF closure action and must be approved by the Deputy Assistant Secretaries for Waste Management and Environmental Restoration before physical closure activities begin. This review and approval is intended to reduce the risk of committing a significant amount of resources to the closure before the appropriate levels of management have approved the closure plan. The Tier 2 Closure Plan, which will be approved by the Field Element Manager, will provide the detailed information related to the TFF closure using the bounding conditions contained in the Tier 1 Closure Plan. The Tier 2 Plan is considered an extension of the Tier 1 Plan and will give facility/site-specific analyses of each facility defined and bounded by the Tier 1 Closure Plan. Thus, the Tier 2 Plan documentation should demonstrate that the performance objectives and other commitments identified in the Tier 1 Plan can be met and maintained.

This PA has been developed to support the DOE-ID *Tier 1 Closure Plan for the TFF* (DOE-ID 2003a). The methodology employed for the preparation of the TFF PA has been based on a logical sequence of steps as described by

- *Guidelines for Radiological Performance Assessment of DOE Low-Level Radioactive Waste Disposal Sites* (Case and Otis 1988)
- Guidance from DOE Order 435.1 (2001b), Manual 435.1-1 (2001a), and Guidance 435.1-1 (1999a)
- Tier 1 Closure Plan Content Guide (DOE 2000)
- *Format and Content Guide for U.S. Department of Energy Low-Level Waste Disposal Facility Performance Assessments and Composite Analyses* (DOE 1999b).

In addition, an approved LLW PA for the Radioactive Waste Management Complex (RWMC) at the INEEL was used to support the development of the TFF PA (Maheras et al. 1994 and 1997).

1.1.1 Steps in Developing the Performance Assessment

The initial step in a PA is to set the scope of the analysis and identify the applicable performance objectives. The result of this process is documented in the remainder of Section 1.

The next step is to document relevant site characterization data, relevant features of the environment and facility design features that are important to the development of conceptual models, and the definition of analysis parameters. The relevant site characterization data and facility design features for the TFF PA are provided in Section 2.

Since the TFF PA supports the Tier 1 Closure Plan, the analysis must be bounding and is based on limited waste characterization data. An important parameter used in a PA is the estimated residual radionuclide inventory. Limited characterization data are available for determining the radionuclide inventory for the TFF. In addition, the projected final result of decontamination for the tanks and associated piping is currently unknown. Closure of the TFF tanks will be performed in phases; Tanks WM-182 and WM-183 will be closed in the first phase. The closure of these two tanks will serve as a proof-of-process demonstration of the waste removal, decontamination, and sampling techniques for the closure of the remaining TFF tanks. However, until the closure of the first two tanks is complete, professional judgment and bounding calculations are required to determine a radionuclide inventory for the TFF.

The radionuclide inventory for the TFF is based on computer modeling, professional judgment, process knowledge, and limited sampling data. This inventory was then assumed to be contained in each of the eleven 300,000-gal tanks. Similar calculations were performed for contaminated sand pads located beneath two tanks. The piping inventory was based on analytical data collected during closure of tank WM-182. The radionuclide inventories for the tanks, sand pads, and piping are given in Section 2.3. A full description of the development of the radionuclide inventory is given in Appendix A.

The analysis of performance begins with developing and selecting scenarios for evaluation. Several deterministic site-specific scenarios have been developed. (In a deterministic model, relationships are fixed and no probabilities are entered, so a given input produces one predictable output.) A scenario is defined here as a description of all the features, events, and processes influencing the waste disposal system performance. Each scenario consists of several scenario modules that have a corresponding conceptual model and mathematical representation.

Scenarios are developed by preparing a comprehensive list of features, events, and processes. This list is then screened to remove processes or events that will not influence performance, are deemed physically improbable, or are extremely rare. This approach may lead to the creation of more than one scenario. In this PA, the scenarios consist of the groundwater transport model, radon release model, and volatile radionuclide release model. Associated with each of these scenarios is a dose model. The scenario "features" lists were used to develop conceptual models by making assumptions about the magnitude, timing, consequences, and detailed mechanisms of the events and processes. The conceptual models were used to formulate the mathematical models ultimately used to simulate site performance.

The approach used throughout the model development and parameter selection process was to make reasonable assumptions and select best estimate parameter values. Where parameter values were not well-defined or it was necessary to limit model-complexity, conservative assumptions have been made. The conceptual models, scenario models, dose models, and associated dose models are described in Section 3. The results of the models for each scenario are presented in Section 4.

The intruder scenario also was evaluated for the TFF PA. This scenario was developed based upon the physical environment at the TFF. The development of the intruder scenario, mathematical representations, results, and

sensitivity/uncertainty analysis are described in Section 5.

The remainder of the TFF PA presents an interpretation and evaluation of (a) the performance analysis results compared to the performance objectives and of (b) the sensitivity and uncertainty of the analyses to ensure a reasonable expectation of facility performance.

1.1.2 Conservative Parameters Used in Performance Assessment

Every effort has been made in this PA to use very conservative inventory and modeling parameters and demonstrate that performance criteria are met, especially in the radionuclide inventory development, sand pad inventory, degradation analysis, and performance models. In determining the radionuclide inventory, recent analytical results from sampling Tanks WM-182, WM-183, and WM-188 were considered. Generally, the highest radionuclide concentrations were found in the WM-188 analytical data. These concentrations were used in the radionuclide inventory calculations rather than an average of the analytical data from the three tanks. In addition, the same radionuclide inventory is attributed to each of the 300,000-gal tanks.

For the sand pad inventory, which is necessary because of accidental releases in 1962 that contaminated the sand pads in Tanks WM-185 and WM-187, several conservative assumptions were used. For example, the surface available for diffusive transport is assumed to instantaneously remove all radionuclides that reach the surface (the liquid/sand pad interface). This assumption results in greater mass transfer than if a concentration gradient is assumed to exist in the sand pad. Also, the sand pad is assumed to be saturated from the release and air does not occupy the pore space, providing an increased mass of diffusing radionuclides into the sand pad. Complete flushing of the sand pad is assumed to occur annually, completely draining the liquid and removing radionuclides from the sand pad. Finally, a conservatively high effective diffusion coefficient value for each radionuclide from the liquid to the sand pad was used.

The degradation analysis also incorporates several conservative assumptions. For instance, the degradation rate parameters for the vault, grout between the vault and tank, piping, and the tank and grout inside the tank are 100, 100, 500, and 500 yr, respectively. These degradation step changes are within the ranges predicted by the degradation analysis, even for the minimum degradation case, which indicates 100, 500, 1,750, and 1,750 yr, respectively. (A summary of the degradation analysis is provided in Table 7-9.)

Other conservative assumptions used in the degradation analysis include determining the rates of modeled chemical attacks from experiments involving degrading instead of intact concrete and not taking credit for the chemical barrier provided by the chemically-reducing grout, vault, and tank. Only the physical barrier to flow and transport is modeled, while the chemical barrier is probably more significant in affecting radionuclide release rates.

In addition, the vault failure, modeled as occurring from the expansion reaction in reinforcement corrosion, is assumed to be 100 yr, but no credit is taken for the non-aggressive corrosion environment surrounding the vault. Finally, the corrosion rates that were determined for coupons placed in the tank liquid and used in corrosion rate calculations are expected to be greater than corrosion rates in the grouted tank and piping and in the water contacting the vault wall.

The performance models used in this PA were designed to reflect the physical setting of the INEEL site to the extent possible, which contributes to the integrity of the PA. The site comprises a very complex geography, including the influence of the Big Lost River. Comparison of the modeled results to actual conditions was favorable.

The numerical model developed to simulate water and radionuclide transport was structured to use reliable and verified information where available and incorporated conservative ranges for less-certain data. Where appropriate, existing hydrologic data were used extensively to describe subsurface hydraulic conditions. For example, the distribution of basalt units and interbeds closely

followed the geologic cross sections presented in several USGS reports (Anderson 1991; Anderson and Bartholomay 1995; Anderson, Ackerman, and Liszewski 1996; Anderson, Liszewski, and Cecil 1997; Anderson, Kuntz, and Davis 1999). In cases where data from several references conflicted, attempts were made to confirm the data used in the model from different sources. For example, if the drilling logs indicate that a selected interbed consists of both fine and coarse grain sediments, separate hydraulic information such as the hydraulic conductivity or unsaturated hydraulic characteristic was evaluated to confirm the lithologic information. If no information was available to confirm lithologic or hydraulic data, then a conservative approach was adopted that resulted in using the value that yielded the highest transport rates.

The calibration of the PORFLOW water transport model was conducted under existing site conditions. These conditions included water from the percolation ponds and the Big Lost River. The model was calibrated against existing water level data that defined the location and depth of perched water. Once the calibration was completed and a reasonable match obtained, the base flow model from radionuclide transport simulations contained only the Big Lost River input. The percolation ponds will be removed from service prior to the1000-yr simulation period. The existing model simulates the cascading of water from discontinuities in the perched zone. This approach provides a dynamic model of the flow in the unsaturated zone. This modeling scenario is considered to be conservative since the percolations would increase the perched zone's ability to restrict downward contaminant transport.

The modeling assumed that the system would begin failing at 100 yr; at 500 yr the entire vault would fail. At 500 yr, the entire vault structure was assumed to be a porous media with the permeability the same as the surrounding alluvium. This assumption is very conservative because the grout and concrete would most likely fracture. Transport would occur as unsaturated flow in the fractures with diffusion limited transport from the surrounding porous blocks to the fracture. Transport under these conditions is significantly less that the model scenario.

At every stage of model development, a conservative approach was used to select hydraulic and transport properties. This approach resulted in a dynamic model capable of a wide range of simulations for testing a wide range of hydraulic and transport parameters in a realistic manner. Further, implementing conservative values for less-certain data yielded transport rates that are at the upper range for a realistic numerical simulation.

The PA was conducted in accordance with the quality assurance requirements given in Appendix B.

1.2 General Facility Description

1.2.1 Tank Farm Facility

The TFF is part of INTEC and includes 11 belowground 300,000-gal and four belowground 30,000-gal stainless-steel tanks. Aboveground structures in the TFF include the TFF Control House (CPP-628) as the most significant building, several other ancillary buildings, condenser pits, valve boxes, and tank and vault sump riser covers. A perimeter fence encloses the TFF (see Figure 1-2). Gates are located on the west and north sides of the fence.

A detailed description of the INTEC TFF is provided in Appendix C. The Computer Interface Building is not associated with the TFF. Portions of the piping associated with WM-182 and WM-183 will be decontaminated and capped or otherwise sealed during this closure. Condenser pits, valve boxes, and tank and vault sump riser covers will be closed during closure of WM-182 and WM-183.

From 1953 to 1988, DOE processed spent nuclear fuel at INTEC. The process was designed to recover the highly enriched uranium in the fuel using a three-step solvent extraction process. The first solvent extraction cycle resulted in a highly radioactive liquid that was considered HLW and was stored at the TFF. Subsequent extraction cycles and decontamination activities generated a liquid waste that was concentrated by evaporation and also stored at the TFF.

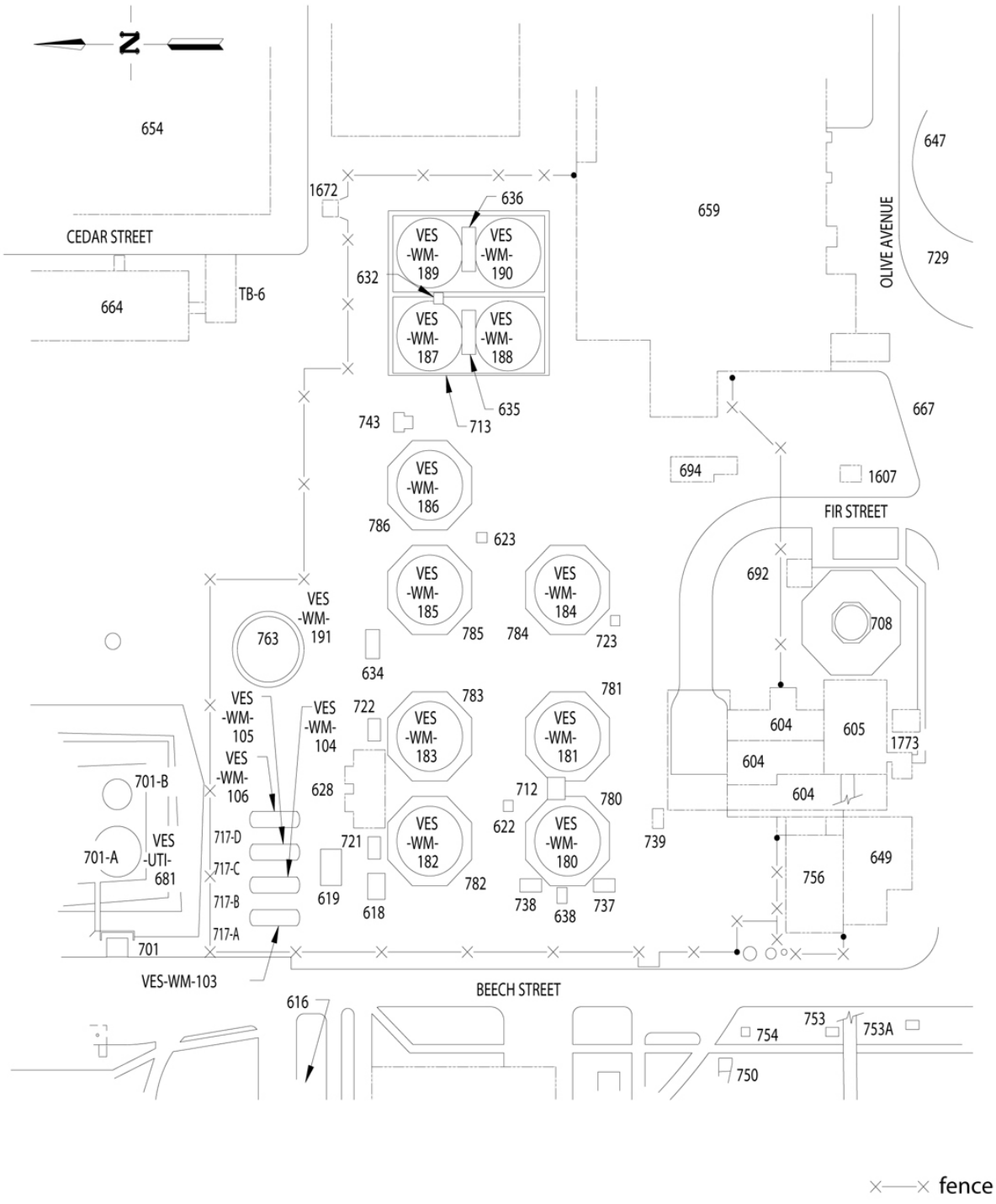

Figure 1-2. A map of the INTEC Tank Farm Facility. The numbers shown are building or structure numbers.

Construction of the TFF began in 1951 with Tanks WM-180 and WM-181. Tanks WM-182 through WM-184 were completed in 1955, Tanks WM-185 and WM-186 were completed in 1957, and Tanks WM-187 and WM-188 were completed in 1959. The last tanks, WM-189 and WM-190, were constructed in 1964. Construction of the four 30,000-gal tanks was completed in 1955. The HLW was removed from the 30,000-gal tanks and the tanks were flushed in 1974 and 1975. The 30,000-gal tanks were reused in 1982 and 1983 but the waste was Process Equipment Waste Evaporator condensate (DOE-ID 2000).

Eight of the tanks (WM-180, WM-182, WM-183, WM-185, and WM-187 through WM-190) contain stainless-steel cooling coils to cool the waste contents in the tanks. Risers provide access to each tank. Each tank has four or five 12-in.-diameter risers. Tanks WM-184 through WM-190 also has two 18-in.-diameter risers (see Figure 1-3). Most risers also house equipment, such as radio frequency probes for level measurement, corrosion coupons, or waste transfer equipment (steam jets and airlifts). Two steam jets are located inside each tank, except for Tanks WM-189 and WM-190. These two tanks each have one steam jet and one airlift pump. A single steam jet can transfer waste out of a tank at approximately 50 gpm, and an airlift can transfer waste out of a tank also at approximately 50 gpm (INEEL 2000a).

Each vault contains at least one sump and steam jet pump to remove any liquid waste or surface water that may leak into the vault. The sumps have liquid-level detectors and high-level alarms.

Each 300,000-gal tank is contained in a concrete vault. The vaults are located approximately 45 ft (14 m) belowground and are configured in one of three basic designs: monolithic octagonal, pillar and panel octagonal, or monolithic square (see Figures 1-4 through 1-6). The 6-in. thick concrete vault roofs are covered with approximately 10 ft (3 m) of soil to provide radiation shielding. Tanks WM-182 and WM-183 are contained in pillar and panel octagonal vaults. Because vaults of this design were constructed with prefabricated components, these vaults are not considered as robust as vaults of monolithic design (Palmer et al. 1999).

Liquid wastes transferred to, from, and among the tanks are managed through a system of piping, valves, and monitoring boxes. The liquid waste is routed through waste transfer valves located in underground, stainless steel-lined concrete boxes, referred to as valve boxes. Liquid releases resulting from decontamination efforts or leakage of liquids from the valve boxes and piping or valve and liquid in piping encasements (secondary containment for piping) is drained to tanks (INEEL 1998).

1.2.2 Closure Concept

In general, the closure strategy for the TFF involves the removal of waste from the tanks. The piping (except the abandoned piping that was previously flushed and decontaminated) and tank vaults will be decontaminated. Confirmatory sampling and analysis will then be performed, followed by grouting of the tanks and vaults. Grout also will be pushed through decontaminated waste lines. Grouting activities will use chemically-reducing grout to further minimize any potential leaching of radionuclides. An overview of the TFF closure concept is shown in Figure 1-7.

Each TFF tank will be closed using the following general sequence:

1. Remove liquid waste in tanks
2. Empty tank to heel with existing jets
3. Flush tank and piping
4. Empty to heel with existing jets
5. Wash tank and remove waste
6. Video and sample heel residuals
7. Evaluate tank residuals against closure performance objectives
8. Displace heel with grout

Figure 1-3. Vault and dome of Tank WM-185 showing the concrete beams and concrete risers on top.

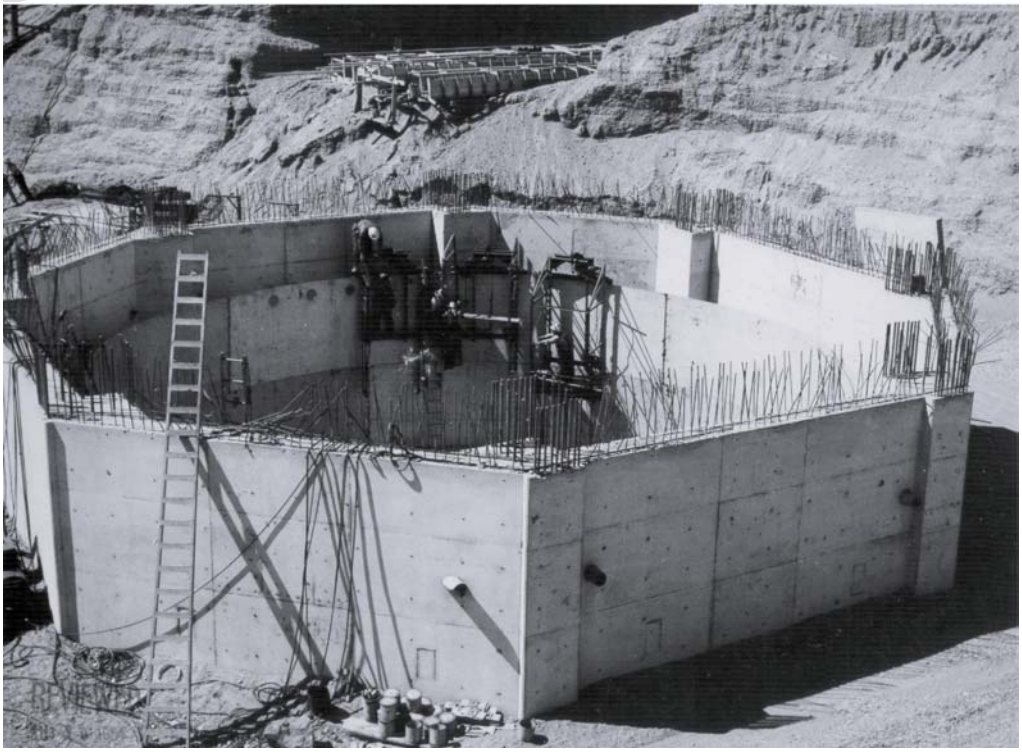

Figure 1-4. Monolithic octagonal vault for Tank WM-180.

Figure 1-5. Pillar and panel octagonal vault for Tank WM-183.

Figure 1-6. Monolithic square vault for Tank WM-190.

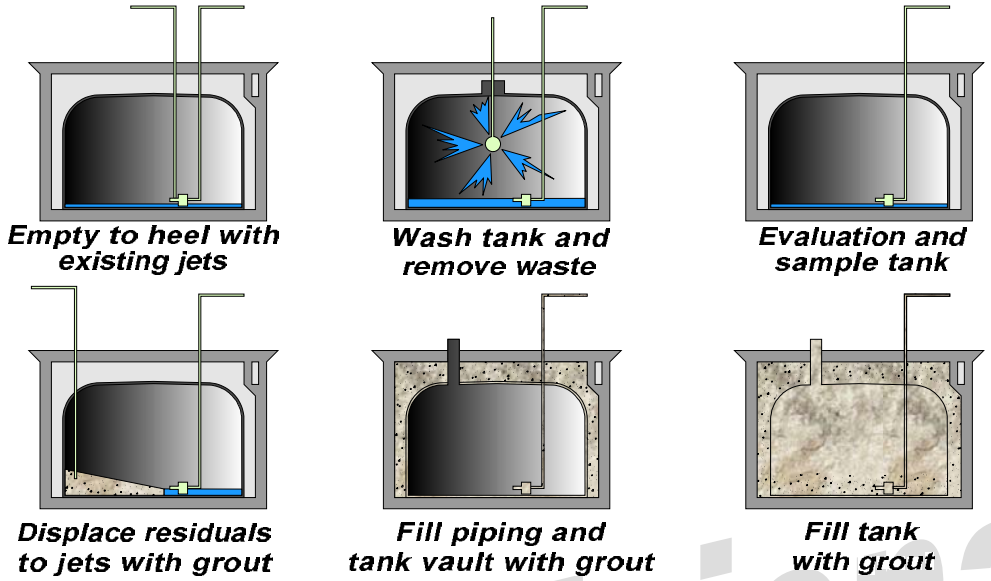

Figure 1-7. Simplified tank closure sequence.

9. Fill piping with grout

10. Fill tank vault with grout

11. Fill tank with grout.

Steps 1 through 3 are considered part of the tank deactivation. Steps 4 through 7 are required to remove waste and decontaminate a given tank. These steps may be repeated, as necessary, until the decontamination sequence is no longer effective (i.e., additional decontamination is no longer economically practical). The last four steps will remove remaining tank residuals to the extent readily feasible, stabilize the residuals, and leave the wastes in a solid physical form.

Contaminated soils associated with the TFF are not addressed in the TFF closure or this PA. Instead, past releases of contaminants from the TFF are being addressed under CERCLA as described in the FFA/CO signed in 1991 (IDHW, EPA, and DOE-ID 1991). However, the potential interaction of contaminants in the surrounding TFF soils with potential future releases from the TFF tanks and associated systems are addressed in the TFF Composite Analysis Report (DOE-ID 2003b).

Closure of the TFF tanks will be performed in phases; Tanks WM-182 and WM-183 will be closed in the first phase. The closure of these two tanks will serve as a proof-of-process demonstration of the waste removal, decontamination, and sampling techniques for the closure of the remaining TFF tanks. This demonstration is necessary because of the uniqueness and complexity of the TFF closure. The closure is unique because similar tanks have not been closed previously at the INEEL. It is complex because of the nature of the waste and the configuration of the tanks. High radiation fields in the tanks and associated equipment preclude manual decontamination of most areas so remote-handling techniques must be used. Furthermore, access to the tanks and vaults is available only through risers, which prevents the use of routine decontamination and sampling procedures. Therefore, the closure strategy may be refined for subsequent closure phases based on information obtained during the closure of Tanks WM-182 and WM-183.

The closure of Tanks WM-182 and WM-183 will be executed in three phases: the planning phase, the pre-closure phase, and the closure demonstration phase. The planning phase encompasses activities such as document

preparation, reviews, and notifications. Pre-closure phase activities include site preparation and decontamination studies. The closure demonstration phase includes evaluation of results from pre-closure phase decontamination studies, and tank decontamination and grouting. The pre-closure and closure activities are described in detail in the conceptual closure approach report for closure of Tanks WM-182 and WM-183 (INEEL 1999a).

The final closure of the TFF will not occur until all tanks have been closed and the RI/FS for OU 3-14 completed. However, the requirements for and the general features of the cover design for the TFF can be described. The TFF cover will, at a minimum, meet the standards described in 10 CFR 61, "Licensing Requirements for Land Disposal of Radioactive Waste," (2003).

The general features of a cover for the closed TFF are similar to a conceptual cover design for the Idaho CERCLA Disposal Facility and are based on the functions and sequence of engineered layers that are commonly called the "Hanford Barrier" (Ward and Gee 2000). The Hanford Barrier was developed to provide long-term protection (1,000 yr) of certain types of waste in semiarid environments and exceeds RCRA cover design requirements, including life expectancy and hydraulic conductivity. The main function of a surface barrier is to ensure that buried wastes are contained and protected from environmental and biotic forces. Surface barriers have been identified as a critical component in management of buried wastes and other sources of subsurface contamination. Barrier technology, particularly for long-term deployment, remains largely unproven at the field scale (Myers and Duranceau 1994).

The overriding technical purpose of the cover is to minimize movement of precipitation into the volume of contaminated materials. Other important roles are to discourage human intruders and to minimize the long-term maintenance that might be needed to ensure that the overriding purpose is not compromised by subsidence, intrusion from plants and animals, or by other natural forces.

The evapotranspiration part of the cover removes as much of the precipitation falling on the cover as possible through evaporation and transpiration. To the extent that this layer is successful in carrying out this purpose, the likelihood of water reaching the residual contamination and mobilizing contaminants will be greatly reduced.

Because the evapotranspiration layer cannot ensure that no water will pass through the upper part of the cover, additional protection to prevent water from reaching the residual contamination is needed. A layer of low-permeability clay is frequently used to provide that protection; however, the clay must remain moist to prevent cracking and a consequent significant increase in permeability. The capillary break portion of the cover keeps the clay from drying out due to a loss of moisture and provides, at the bottom of the capillary break section, a drain for any excess moisture that would come through from above. Part of the capillary break also serves as a barrier to intrusion and to erosion if natural forces remove the upper layers of the cap. The nominal design for the Hanford Barrier uses low-permeability asphalt, not clay, as the water barrier, but the other purposes of the layers in the capillary barrier dictate that the clay not be eliminated.

Any water that is not removed by evapotranspiration or drained off by through the sand layer at the bottom of the capillary break portion of the cover is prevented from entering the zone of residual contamination by the infiltration barrier. Figure 1-8 shows this part of the cover as - consisting of a low-permeability asphalt layer and a base layer. Typical thicknesses for these layers are 4 to 6 in. each.

In most disposal facilities, a major purpose of the fill layer is to help provide a physical buffer between the waste and the infiltration barrier, thereby protecting the barrier from any possible damage from objects in the waste and from minor waste settling. This function is not needed, however, because the tank vaults being covered are already overlain with considerable soil, the vaults do not present any protruding physical features at their tops, and the vaults are unlikely to

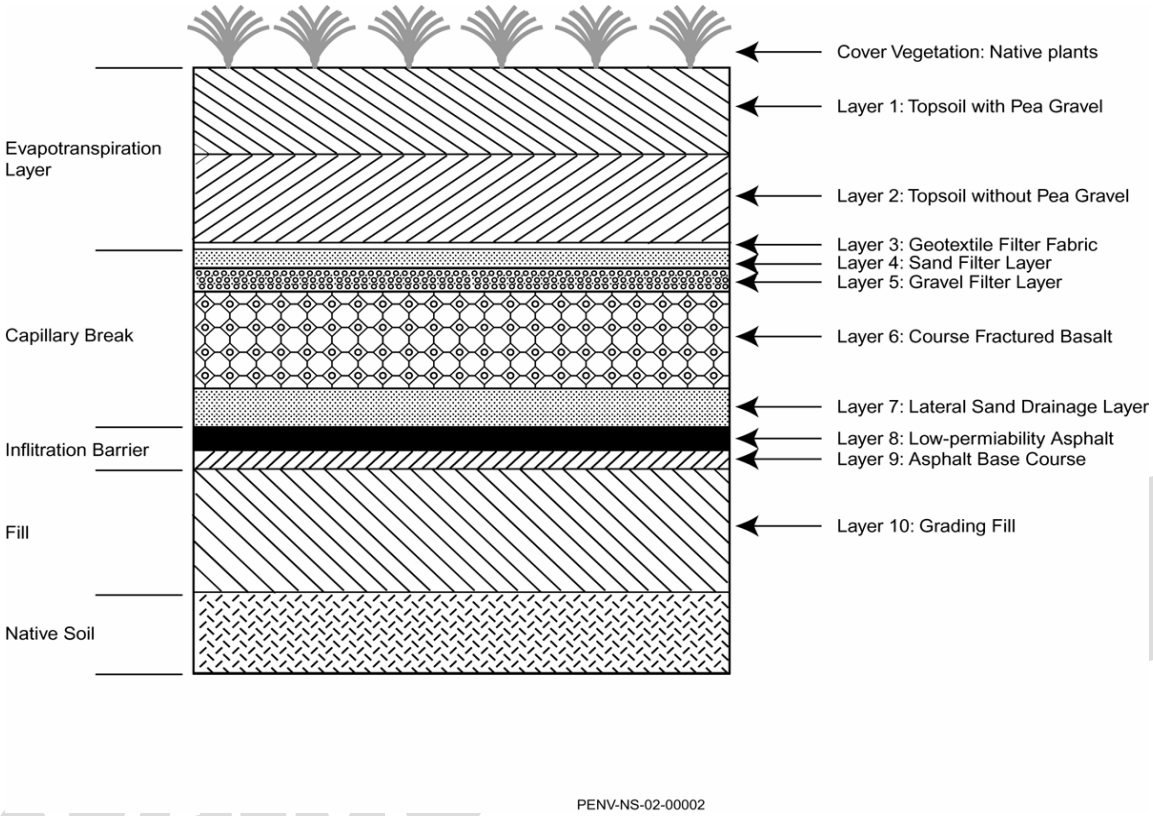

Figure 1-8. Typical cover layering.

experience any settling. A second purpose for the fill is to define the vertical contours of the cover.

The ability of any cover over residual waste to fulfill its design goals effectively is influenced by many factors. Subsidence of some kinds of waste can cause local low spots in the cover and trap infiltrating water instead of letting it run off harmlessly. This is very unlikely to happen with the fully grouted high-level waste tanks because there will be no voids under the cover that can cause subsidence.

The effects of wind and water erosion and plant and animal intrusion are difficult to predict. Any cover placed over the tanks, however, will be designed to minimize these effects over the long term based on site-specific parameters.

In projecting the performance of waste management systems, the presence of completely man-made materials such as geotextile filter fabric or a flexible membrane liner is sometimes conservatively ignored. At other times those components are assumed to perform for hundreds of years. No information is available about the durability of the man-made asphalt layer in the Hanford Barrier but as long as it is covered to prevent exposure to ultraviolet rays it should be expected to perform as designed for at least hundreds of years.

1.2.3 Waste Characterization and Certification Program

During and at the conclusion of the pre-closure activities for Tanks WM-182 and WM-183, samples of tank residuals will be collected to determine the concentrations of hazardous constituents (to support HWMA/RCRA closure) and radionuclides (to support DOE Tier 1 and Tier 2 closure) remaining in the tanks. A phased approach will be used for sampling the tanks. Existing equipment will be used to measure concentrations of gamma-emitting radionuclides that are being removed from the tank. This real-time monitoring of the waste stream will be trended as it is moved from Tanks WM-182 and

WM-183. As the concentrations are reduced and begin to stabilize, personnel will collect the data set to determine the decontamination factor attained. The sampling and analysis approach is described in detail in the *Sampling and Analysis Plan for the Post-Decontamination Characterization of the WM-182 and WM-183 Tank Residuals* (Portage Environmental 2002). Tank sample results will be used to evaluate the final status of the tank contamination and to compare to the PA inventory to ensure that a bounding analysis was performed for the Tier 1 Closure Plan (DOE-ID 2003a).

1.2.4 General Land Use Patterns

The INEEL *Comprehensive Facility and Land Use Plan* (DOE-ID 1997a) and the *INTEC Final Record of Decision* (ROD) (DOE-ID 1999) describe the land use for the INEEL and INTEC. Land use at the INEEL is currently government-controlled industrial use. The term controlled means that unrestricted public access to INTEC and the INEEL is not available. Presently, access to INEEL facilities requires proper clearance, training, or escort and controls to limit the potential for unacceptable exposures. A security force is used to limit access to approved personnel and visitors. These controls are estimated to be in place for a minimum of 100 yr.

Future land use scenarios are identified in the *Long-Term Land Use Future Scenarios for the Idaho National Engineering Laboratory* (DOE-ID 1995a). This document was developed using a stakeholder process that involved a public participation forum, a public comment period, and the INEEL Citizens Advisory Board. Following review and comment by the public participation forum, the document underwent a 30-day public comment period, and was subsequently submitted to the Citizens Advisory Board for review and recommendations.

To date, no recommendations have been received for residential use of any portion of the INEEL until at least year 2095. Until 2095, the reasonably anticipated future use for the TFF is as a government-controlled industrial facility (DOE-ID 1999).

Planning assumptions in the INEEL *Comprehensive Facility and Land Use Plan* (DOE-ID 1997a) are that the INEEL will remain under government control for a minimum of 100 yr. This PA assumes that the institutional control period begins at the end of closure for the TFF. The anticipated date of completion for the TFF closure project is 2016. Therefore, the end of institutional control is assumed to be 2116 for the purposes of dose calculations in this PA.

1.3 Related Documents

As an interim status hazardous waste management unit, the TFF closure must comply with applicable HWMA/RCRA requirements (State of Idaho 1983; 42 USC 6901, 1976). However, the TFF also is a HLW facility regulated by DOE, and must meet the requirements of DOE Order 435.1 (DOE 2001b) and its associated manual (DOE 2001a) and guidance (DOE 1999a). Three closure paths are allowed by DOE 435.1-1: decommissioning, the CERCLA process, and closure by an approved closure plan. The TFF will be closed under an approved DOE closure plan.

DOE requires a two-tiered approach to closure plan development, review, and approval. The Tier 1 Closure Plan (DOE-ID 2003a) defines and bounds the parameters of the TFF closure actions. It must be approved by the Deputy Assistant Secretaries of Waste Management and Environmental Restoration before physical closure activities may begin. This PA supports the Tier 1 Closure Plan. The Tier 2 Closure Plan will give specific analyses of the TFF closure. It should show that the performance objectives and other commitments made in the Tier 1 Plan can be met and maintained. The Tier 2 Closure Plan will be approved by DOE-ID.

The *Composite Analysis for Tank Farm Closure* (DOE-ID 2003b) is a planning tool used to ensure that the combined effect of all sources of residual radioactive material that could contribute to the radioactive dose calculated will not compromise the requirements to protect the public.

In addition, IDAPA 58.01.05.009 [40 CFR 265.197(c)(l), 2002] specifies that if a tank system does not have adequate secondary containment,

then the owner or operator of a tank system must prepare both a closure plan for clean closure and a contingent closure plan for closure as a landfill. The decision to close the TFF to clean closure standards under HWMA/RCRA or as a landfill will be made when all the tanks have been closed and the RI/FS for OU 3-14 is complete. Because this decision has not been made, both a closure plan and a contingent plan have been written. The *Idaho Hazardous Waste Management Act/Resource Conservation and Recovery Act Closure Plan for Idaho Nuclear Technology and Engineering Center Tanks WM-182 and WM-183* describes the strategy for clean closure of the tanks (DOE-ID 2001a). The *Contingent Landfill Closure and Post-Closure Plan for Idaho Nuclear Technology and Engineering Center Tanks WM-182 and WM-183* discusses the landfill closure strategy (DOE-ID 2001b).

Because the TFF was used to store HLW, a Waste-Incidental-to-Reprocessing (WIR) determination report[d] is being prepared in accordance with DOE Order 435.1. In the WIR report, the TFF residuals are evaluated to determine whether the residuals can meet the incidental waste criteria of LLW, rather than HLW (DOE 2001a). It is anticipated that the WIR determination will allow the residuals to be managed as LLW.

Several other important related documents define the scope of the TFF PA and provide resources and background information relevant to the analyses.

Under the terms of a 1992 Consent Order (and subsequent modifications) between IDHW and DOE, DOE must permanently cease use of tanks in the TFF or bring the tanks into compliance with secondary containment requirements as set forth by IDAPA 58.01.05.009 (40 CFR 265.193, 2002). The Consent Order further specifies that this compliance cannot be achieved through an equivalency demonstration or by obtaining a variance as provided by IDAPA 58.01.05.009 [40 CFR 265.193(d)(4) and (h)]. DOE plans to close the TFF tanks because high radiation fields would make compliance with secondary containment requirements difficult, and a need for such storage is not evident after 2012.

The TFF is located within the boundaries of the INTEC facility at the INEEL. Past releases of hazardous and radiological contaminants from INTEC, including the TFF, are being addressed under CERCLA (42 USC 9601–9675, 1980), as described in the FFA/CO signed by DOE, EPA, and IDHW in 1991 (IDHW, EPA, and DOE-ID 1991). Also, an RI/FS (Rodriguez et al. 1997) and a ROD (DOE-ID 1999) have been completed for Waste Area Group 3 (WAG 3), which encompasses INTEC. Past releases from leaking pipes and associated soil contamination are being addressed by this CERCLA action and therefore are not considered in this PA. The *Composite Analysis for Tank Farm Closure* (DOE 2002b) considers the contribution to the groundwater all pathways dose from all radionuclide sources at the INEEL.

The *Idaho High-Level Waste & Facilities Disposition Final Environmental Impact Statement* (EIS) analyzes the potential environmental consequences of managing two waste types at the INEEL: high-level waste in calcine form and liquid mixed waste (historically known as sodium-bearing waste and newly generated waste). This EIS evaluates several alternatives to the disposition of the TFF.

The *INTEC TFF Tanks WM-182 and WM-183 Closure Study* provides the closure methodology for the TFF.[e] This document provides information on the proposed process for closure of the tanks, vaults, and associated ancillary equipment including piping.

Two additional reports that support this PA are the *Idaho Chemical Processing Plant Safety Document* (INEEL 1998) and the *Idaho Nuclear*

d. DOE-ID, 2002, *Idaho Nuclear Technology and Engineering Center Tank Farm Facility Residual-Waste-Incidental-to-Reprocessing Report,* DOE/ID-10777, Draft B, December.

e. LMITCO, 1998, *INTEC TFF Tanks WM-182 and WM-183 Closure Study (Draft)*, August 31.

Technology and Engineering Center Safety Analysis Report (INEEL 2001a).

1.4 Performance Criteria

In July 1999, DOE issued Order 435.1, "Radioactive Waste Management." This Order and its associated manual and guidance set forth the authorities, responsibilities, and requirements for the management of DOE's inventory of HLW, transuranic waste, and low-level waste. DOE Manual 435.1-1 requires that

> *A site-specific radiological performance assessment shall be prepared and maintained for DOE low-level waste disposed of after September 26, 1988. The performance assessment shall include calculations for a 1,000 year period after closure of potential doses to representative future members of the public and potential releases from the facility to provide a reasonable expectation that the performance objectives identified in this Chapter are not exceeded as a result of operation and closure of the facility.* (DOE 2001a)

This requirement is applicable to the TFF closure plan.

Performance assessments involve estimating radiological exposure to future members of the public. These exposure estimates are then compared to specific performance measures to determine whether there is a reasonable expectation that the performance measures will be met in the future. Performance measures consist of specific performance objectives identified in DOE Manual 435.1-1 and other performance-related factors required by DOE Manual 435.1-1 for deactivated HLW facility/site closure actions that contain residual LLW.

This section describes each performance criterion used to assess the performance of the TFF closure facility/site and the points of assessment. These criteria include the performance objectives in DOE Manual 435.1-1, Section IV.P.(1), other performance criteria derived from the requirements in DOE Manual 435.1-1, Section IV.P.(2), and the points of assessment. Performance criteria not explicitly called out in the manual (e.g., site-specific regulatory agency agreements) also are discussed.

1.4.1 Public Protection Performance Objectives

The first applicable performance objective, from DOE Manual 435.1-1, IV P.(1)(a), states

> *Dose to representative members of the public shall not exceed 25 mrem (0.25 mSv) in a year total effective dose equivalent from all exposure pathways, excluding the dose from radon and progeny in air.*

This performance objective is interpreted as requiring the performance analysis to provide a reasonable expectation that the "all-pathways" dose to a hypothetical future member of the public will not exceed 25 mrem (effective dose equivalent [EDE]) in a year, excluding doses from inhalation of radon and its short-lived progeny. "All pathways" include any and all modes by which a receptor at the point of public access could be exposed, including the air pathway. The analysis is to cover 1,000 yr following closure of the disposal facility. Analysis beyond 1,000 yr to calculate the maximum dose and the time of that dose shall be included in the sensitivity and uncertainty analyses as a means of increasing confidence in the outcome of the modeling. Normally, the point of compliance for this performance objective should be at the point of highest calculated dose beyond a 100-m buffer zone surrounding the waste. A larger or smaller buffer zone may be used with justification (DOE 2000).

The second performance objective, from DOE Manual 435.1-1, IV.P. (1)(b), states

> *Dose to representative members of the public via the air pathway shall not exceed 10 mrem (0.10 mSv) in a year total effective dose equivalent, excluding the dose from radon and its progeny.*

Consistent with the National Emission Standards for Hazardous Air Pollutants (40 CFR 61, Subpart H, 2002), ^{220}Rn, ^{222}Rn, and their progeny need not be included in the air pathway analysis for comparison with the 10 mrem/yr EDE performance objective; separate controls for the emission of radon are discussed below. For the air pathway dose analysis, the point of compliance should be the point of highest calculated dose beyond a 100-m buffer zone surrounding the waste. With justification, a larger or smaller buffer zone may be used. The 10 mrem/yr limit should be recognized to refer to all sources, not just the disposal facility. Therefore, if the performance assessment assumes a point of compliance that corresponds to the future land use boundary, a limit that is a fraction of the 10 mrem/yr dose limit should be used in recognition of the potential presence of other sources (DOE 2000).

The third performance objective, from DOE Manual 435.1-1, IV.P.(1)(c), states

> *Release of radon shall be less than an average flux of 20 pCi/m^2/s (0.74 Bq/m^2/s) at the surface of the disposal facility. Alternately, a limit of 0.5 pCi/l (0.0185 Bq/l) of air may be applied.*

For radon, a separate limit is applied. In most cases, the limit to be applied should be an average ground surface emanation rate of 20 pCi/m^2/s directly over the disposal unit. There may be special cases involving the disposal of material that radiologically resembles uranium or thorium mill tailings in isolated locations that warrant using an alternative limit. The alternative limit is an incremental increase of 0.5 pCi/L of radon in the air concentration at the point of assessment (DOE 2000).

Table 1-1 gives a summary of the DOE performance objectives and the corresponding points of compliance.

1.4.2 Water Resource Impact Assessment

DOE Order 5820.2A (1998), superseded by DOE Order 435.1, contained a performance objective for protection of groundwater resources. DOE Manual 435.1-1 does not contain a specific performance objective (e.g., dose or concentration standard) for water resource impacts. The approach in DOE Manual 435.1-1 was chosen by DOE for consistency with Nuclear Regulatory Commission (NRC) methods for LLW disposal and radiation protection principles articulated by the National Council on Radiation Protection and Measurements and the International Commission on Radiological Protection (ICRP). In accordance with these principles, it is appropriate to assign a

Table 1-1. Preliminary performance assessment components, objectives, and points of compliance.[a]

Component	Performance Objective	Point of Compliance
All pathways	25 mrem in a year, not including doses from radon and progeny	The point of highest projected dose or concentration beyond a 100-m buffer zone surrounding the disposed waste
Air pathway	10 mrem in a year, not including doses from radon and progeny	The point of highest projected dose or concentration beyond a 100-m buffer zone surrounding the disposed waste
Radon	For ^{220}Rn, ^{222}Rn, and their progeny either (1) an average flux of ≤ 20 pCi/m^2/s or	Disposal facility surface
	(2) an air concentration of ≤ 0.5 pCi/L unless constrained by applicable laws, regulations, or agreements	The point of highest projected dose or concentration beyond a 100-m buffer zone surrounding the disposed waste

a. Source: DOE 2000.

fraction (e.g., 25 mrem) of the 100 mrem/yr public dose performance measure to a particular practice (e.g., radioactive waste disposal) but it is not recommended to further fraction performance objectives to specific pathways (e.g., groundwater). Thus, exposure by water pathways is included in the all-pathways analysis but there is no specific performance objective for exposure by water pathways. In the case of the air pathway, the 10 mrem/yr performance objective is based on a specific federal regulatory requirement. There is no comparable requirement for water resources (DOE 2000).

DOE Manual 435.1-1, IV.P.(2)(g), states

For the purposes of establishing limits on radionuclides that may be disposed of near-surface, the performance assessment shall include an assessment of impacts to water resources.

For water resources protection, impacts were assessed on a site-specific basis in accordance with a hierarchical set of criteria. This approach recognizes that there are no federal requirements for protection of water resources for a radioactive waste disposal facility or closure action. The site-specific hierarchical approach, rather than mandating specific performance measures for all sites, is consistent with the EPA strategy for groundwater protection. EPA recognizes that groundwater protection is a regional and local matter (EPA 2001). Accordingly, the hierarchy for establishing water resources protection is as follows (from the *DOE Deactivated High-Level Waste Facility Closure Manual*, DOE 2000):

- First, the closure action must comply with any applicable state or local law, regulation, or other legally applicable requirement for water resource protection.
- Second, the closure action must comply with any formal agreement applicable to water resource protection that is made with appropriate state or local officials.
- Third, if neither of the above conditions applies, the site should select assumptions for use in the performance assessment based on criteria established in the site groundwater protection management program and any formal land-use plans.
- If none of the above conditions apply, the site may select assumptions for use in the performance assessment for the protection of water resources that are consistent with the use of water as a drinking water source.

For assessments addressing the use of groundwater as a drinking water source, the point of assessment normally should be the location of the highest groundwater concentration outside a 100-m buffer zone. A larger or smaller buffer zone may be used with justification (DOE 2000).

In terms of protecting the groundwater as a resource, assuming some volume averaging based on projected use may be appropriate. Applying the performance measure at an assumed wellhead mixed with a reasonable volume of groundwater, based on site-specific assumptions regarding groundwater use, is appropriate. This assumes mixing is consistent with state or local laws, regulations, or agreements (DOE 2000).

1.4.2.1 Sole Source Aquifer Designation.

The Eastern Snake River Plain Aquifer has been designated by EPA as a sole source aquifer (58 FR 138, 1991). After sole source designation, any federal financial assistance projects are subject to EPA approval to ensure that these projects do not contaminate the aquifer and create a significant hazard to public health. However, the INEEL is operated by direct federal funding and is not funded through federal financial assistance projects (Maheras et al. 1997). Therefore, the designation of the Eastern Snake River Plain Aquifer as a sole source aquifer has no regulatory impact on the performance objectives used in performance assessments at the INEEL.

1.4.2.2 Groundwater Protection.

DOE Order 435.1 and the supporting manual and guidance do not specify radiation dose or concentration limits that would constitute performance objectives for protection of groundwater (DOE 2001a, 2001b, 1999a). DOE Manual 435.1 uses a hierarchy approach that

requires an analysis of potential applicable state and local requirements or agreements for groundwater protection.

Maheras et al. (1997) assessed the federal, state, and local requirements for groundwater protection at the INEEL for the RWMC PA. Five different options for the groundwater protection performance objective were evaluated.

Option 1. Groundwater protection would be defined by the performance objective specified in IDHW Rules, IDAPA 58.01.11, "Groundwater Quality Rule" (2002). IDAPA 58.01.11.200, "Ground Water Quality Standards" (1997), states that the concentration of radioactive materials or radioactivity in potable water supplies shall not exceed the values listed in 10 CFR Part 20, Appendix B, Table 2, Column 2, "Effluent Concentrations" (2003). These concentrations are equivalent to a radiation dose of 50 mrem/yr EDE based on a water consumption rate of 2 L/d (0.5 gal/d).

Option 2. Groundwater protection would be defined as compliance with the 25 mrem/yr total effective dose equivalent (TEDE) all-pathways standard contained in DOE Guide 435.1. Instead of being based solely on the consumption of drinking water, the evaluation of compliance would be based on all applicable exposure pathways (i.e., an "all-pathways" analysis).

Option 3. Groundwater protection would be defined as compliance with the maximum contaminant levels (MCLs) for radionuclides specified in 40 CFR 141 (2002), promulgated in 65 FR 236 (2000). EPA groundwater standards for radionuclides are compared, from 1976 to the present, in Table 1-2. The current radionuclide standards include (a) a limit on the concentration of 5 pCi/L for ^{226}Ra and ^{228}Ra combined, (b) a limit on the concentration of 15 pCi/L for gross alpha particle activity, not including radon or uranium, (c) a limit on the dose equivalent to the total body or any given internal organ of 4 mrem/yr from man-made beta particle and photon radioactivity, and (d) a limit of 30 μg/L for uranium. The definition of man-made radionuclides excludes the beta-emitting progeny of ^{232}Th, ^{235}U, and ^{238}U. In addition, the definition of gross alpha activity in 40 CFR 141 (2002) specifies that the gross alpha activity is to be inferred from measurements made from a dry sample. Therefore, any gaseous ^{222}Rn originally present in the sample would not be present when the sample was counted. Consequently, the short-lived alpha-emitting ^{222}Rn progeny and ^{218}Po and ^{214}Po also would not be present and would be excluded from the gross alpha activity. 40 CFR 141 also specifies that the concentrations that yield 4 mrem/yr for ^{3}H and ^{90}Sr should be calculated based on a water intake of 2 L/d (0.5 gal/d) and the 168-hr data listed in *Maximum*

Table 1-2. Comparison of MCLs for radionuclides.

Radionuclide	1976 Interim Standards	1991 Proposed Standards	2000 Standards
Combined ^{226}Ra, ^{228}Ra (pCi/L)	5	20	5
Total Gross α (pCi/L)	15 with ^{226}Ra (excluding U and Rn)	15 without ^{226}Ra	15 without ^{226}Ra
βγ emitters (mrem)	4	4 (EDE)	4
Uranium	No standard	20 μg/L (kidney toxicity)[a] 170 pCi/L (radiotoxicity)	30 μg/L

a. Drinking water equivalent level of 100 μg/L and relative source contribution factor of 20%.

Permissible Body Burdens and Maximum Permissible Concentration of Radionuclides in Air or Water for Occupational Exposure (Department of Commerce 1963). For ^{3}H and ^{90}Sr, the concentrations that yield 4 mrem/yr total body dose are specified to be 20,000 pCi/L and 8 pCi/L, respectively.

Option 4. The current MCLs specified in 40 CFR 141 (2002) of 5 pCi/L for ^{226}Ra and ^{228}Ra (combined) and 15 pCi/L for gross alpha activity, including ^{226}Ra but excluding radon and uranium, would be retained. The 4 mrem/yr dose limit for beta particle and photon radioactivity from man-made radionuclides also would be retained but the 4 mrem/yr would now be an EDE, not a total body dose. The EDE would be calculated using a water intake of 2 L/d and ICRP-30 dosimetry, as implemented in EPA (1988), not using the ICRP-2 dosimetry that served as the basis for the data listed in the Department of Commerce report (1963). The concentrations that yield 4 mrem/yr total body dose specified in 40 CFR 141 of 20,000 pCi/L for ^{3}H and 8 pCi/L for ^{90}Sr would be retained.

Option 5. A dose limit of 4 mrem/yr (EDE) for all radionuclides would be used as the performance objective for the protection of groundwater resources, without the use of the MCLs. A water intake of 2 L/d and ICRP-30 dosimetry, as implemented in EPA (1988), would be used to calculate the EDE.

The reasoning for this option is based on an analysis of the 1976 EPA interim water quality standards (41 FR 298) and the proposed standards that have been published. In regard to standards for beta/gamma-emitting radionuclides, EPA clearly intended to replace the 1976 interim limits based on the dose limit for whole body or any organ by a limit based on EDE. This intention was shown in the proposed standards for 1991. Thus, for these radionuclides, the assumed groundwater protection requirement for the TFF disposal facility is the same as the proposed 1991 revision of the EPA drinking water. The only exception is that dose (not risk) is evaluated in the PA. Replacement of dose limits for whole body or any organ by a limit based on EDE is in agreement with the current radiation protection policies of DOE, NRC, and EPA.

EPA has used concentration limits, rather than dose limits, for alpha-emitting radionuclides so the standard is expressed in terms of quantities that could be measured directly by operators of public drinking water systems. This approach has not been used for man-made, beta/gamma-emitting radionuclides because EPA has presumed that only naturally-occurring, alpha-emitting radionuclides would be of concern for public drinking water supplies. EPA states in 65 FR 236 (2000) that "a newly proposed MCL expressed mrem EDE could result in a more consistent risk level within the Agency's target risk range." However, in the final rule, they ratified the current standard since it was protective of public health. Commenters that supported EPA's final rule stated that there was no appreciable occurrence of man-made beta emitters in drinking water, so it was not a pressing public health concern to revise the MCL.

The final rule states that

> *EPA agrees that review of the MCL for beta particle and photon radioactivity is a priority and, as previously stated..., the Agency intends to review this standard within the general time frame established for the DOE submission of the licensing application for the Yucca Mountain site.*

EPA's discussion in the final rule regarding the standards indicates that they realize the difficulty of applying the current MCLs to waste management and cleanup decisions. However, since the main focus of the MCLs was for water treatment plants, EPA chose to maintain the standards and review them at a later date.

In a prospective analysis such as a performance assessment, there is clearly no intent to demonstrate compliance with a groundwater protection requirement by actual measurement at a water treatment plant. Therefore, there is no need to express the performance objective for alpha-emitting radionuclides in terms of concentration limits. Indeed, using a single dose limit for all radionuclides provides a consistent and transparent approach.

1.4.2.3 Selection of Groundwater Performance Objectives.

The various groundwater protection performance objectives available for use in the TFF PA are summarized in Table 1-3. The selection of a site-specific groundwater protection performance objective was based on guidance in DOE Guide 435.1.

The performance objective Option 5 discussed in Section 1.4.2.2 for groundwater protection (i.e., 4 mrem/yr EDE for all radionuclides) is more restrictive than the EPA's 2000 revisions of the drinking water standards for radionuclides. In the EPA revised standards, the dose limit of 4 mrem/yr applies only to beta/gamma-emitting radionuclides; the concentration limits for alpha-emitting radionuclides are in addition to this dose limit. However, a 4 mrem/yr EDE in the Option 5 performance objective applies to all radionuclides. To illustrate this point, the current EPA standard for radium of 5 pCi/L corresponds to an EDE of about 5 mrem/yr. The inclusion of alpha-emitting radionuclides in the dose limit provides a performance objective that is more restrictive than EPA's revisions of drinking water standards and provides a common basis for determining concentration limits in groundwater for all radionuclides.

The INEEL FFA/CO does not specifically address the issue of groundwater protection for LLW. Risk assessments done as part of the FFA/CO have used MCLs as applicable or relevant and appropriate requirements. The use of Option 5 does not preclude the use of MCLs. The MCLs for those radionuclides specified in 40 CFR 141 also can be calculated in addition to the 4 mrem/yr EDE specified in Option 5. The use of MCLs is not considered necessary for a performance assessment. Option 5 provides a performance objective that is more protective of the public health than that offered by Option 4 and the use of MCLs.

The use of Option 5 as the performance objective for groundwater protection simplifies the assessment of the groundwater pathway. The need to separate radionuclides in terms of dose or concentration is not deemed necessary. The use of Option 5 allows for a single dose limit to be applied to all radionuclides and provides a consistent approach with other potential pathways (i.e., air). Radionuclide concentrations will be available from the groundwater analysis to compare to the MCLs, which can then be compared to other groundwater programs.

Table 1-3. Summary of groundwater protection performance objective options.

Option	Total Dose (mrem/yr)	Man-made Beta-Gamma Dose (mrem/yr)	Gross Alpha Concentration (pCi/L)	^{226}Ra and ^{228}Ra Concentration (pCi/L)	Uranium Concentration (μg/L)
1	50[a]	—[b]	—[b]	—[b]	—[b]
2	25[a]	—[b]	—[b]	—[b]	—[b]
3	—	4[c,d]	15[e,f]	5[g]	—
4	—	4[a,d]	15[e,f]	5[g]	—
5	4[a]	—[b]	—[b]	—[b]	—[b]

a. Based on ICRP-30 dosimetry.

b. Incorporated into total dose (EDE).

c. Based on ICRP-2 dosimetry.

d. For ^{3}H and ^{90}Sr, the concentrations that yield 4 mrem/yr total body dose are specified to be 20,000 pCi/L and 8 pCi/L, respectively.

e. Excluding uranium and radon isotopes.

f. Excludes beta-gamma progeny of ^{238}U, ^{235}U, and ^{232}Th.

g. ^{226}Ra and ^{228}Ra, combined.

1.4.3 Intruder Analysis

DOE Order 5820.2A, which has been superseded by DOE Order 435.1, contained a performance objective for the dose to individuals who inadvertently intrude into the LLW disposal facility after loss of active institutional control. DOE Manual 435.1-1 does not contain a specific performance objective for inadvertent intruders. As with the water resource impact assessment (Section 1.4.2), the approach in DOE Manual 435.1-1 was chosen by DOE for consistency with NRC methods for LLW disposal and radiation protection principles articulated by the National Commission on Radiological Protection and the ICRP. In accordance with these principles, it is appropriate to assign a fraction (e.g., 25 mrem) of the 100-mrem/yr public dose performance measure to a particular practice (e.g., radioactive waste disposal) but it is not recommended to further fraction performance objectives to derivative activities (e.g., inadvertent intrusion). Thus, inadvertent intrusion is considered in the performance assessment but there is no specific performance objective for inadvertent intrusion (DOE 2000).

DOE Manual 435.1-1, IV.P.(2)(h), states

> *For purposes of establishing limits on the concentration of radionuclides that may be disposed of near-surface, the performance assessment shall include an assessment of impacts calculated for a hypothetical person assumed to inadvertently intrude for a temporary period into the low-level waste disposal facility. For intruder analyses, institutional controls shall be assumed to be effective in deterring intrusion for at least 100 years following closure. The intruder analyses shall use performance measures for chronic and acute exposure scenarios, respectively, of 100 mrem (1 mSv) in a year and 500 mrem (5 mSv) total effective dose equivalent excluding radon in air.*

Intruder analyses are to be performed as one of the mechanisms for establishing concentration limits for waste considered acceptable for near-surface disposal. DOE intends to exercise control of the closure sites until it can be safely released pursuant to DOE Order 5400.5 (1993) (or 10 CFR 834 when promulgated). Hence, intrusion is an accidental, temporary event. However, for purposes of conducting intruder analyses, the intrusion event should be considered to occur because of a lapse in institutional controls that would be remedied within a few years. The focus of the intruder analysis should be on the selection of reasonable scenarios and reasonably conservative parameters (DOE 2000).

Intrusion is assumed to occur no sooner than 100 yr following facility closure and should not be analyzed beyond 1,000 yr post-closure. The onset of intrusion can be extended beyond 100 yr if adequate justification is provided (e.g., continued DOE presence for facility decommissioning). Passive controls, such as marker systems and engineered features of the disposal system, may be effective in deterring accidental intrusion into the closure site and may be used as justification for extending the onset of intrusion (DOE 2000).

Considering regional social customs and regional construction practices (e.g., well-drilling and excavation), the 500-mrem EDE should be used in assessing acute exposure from individual events that reasonably could occur at the site. Different individual events may be considered as appropriate for the site-specific conditions (DOE 2000).

The 100-mrem/yr EDE should be used in assessing chronic exposure from residing at or frequently visiting the disposal site. In the analysis of chronic exposure of a hypothetical intruder, doses should be assumed to come from external exposure to and inhalation and ingestion of materials exhumed from the site. Exposure may occur through a variety of pathways but need not include the consumption of contaminated groundwater or the irrigation of crops with contaminated groundwater. Groundwater consumption and crop irrigation are excluded because the impacts of groundwater contamination are evaluated separately in the all-pathways analysis, the water resource protection analysis, or both. Similarly, intruder doses need not include consideration of doses from airborne radon and its

short-lived progeny because these are dealt with in the air pathway analysis. Doses from the progeny of radon that are deposited in the disposed waste should be included in the intruder analyses (DOE 2000).

1.4.4 ALARA Analysis

DOE's approach to radiation protection for closure sites is based on two key components. One component is the performance objectives described in Section 1.4.1, which specify maximum doses for various pathways. The other component is the ALARA principle, which requires doses to be maintained "as low as reasonably achievable."

DOE Manual 435.1-1, IV.P.(2)(f), states

Performance assessments shall include a determination that projected releases of radionuclides to the environment shall be maintained as low as reasonably achievable (ALARA).

The goal of the ALARA process is to attain the lowest practical dose level after taking into account social, technical, economic, and public policy considerations (DOE 2000). Thus, expected doses can never exceed the performance objectives but also must be as far below the performance objective as can reasonably be achieved. Therefore, in addition to providing a reasonable expectation that the performance objectives described in Section 1.4.1 will not be exceeded, the performance assessment also needs to show that the closure action is being conducted in a manner that maintains releases of radionuclides to the environment ALARA. The TFF ALARA analysis is given in Appendix D.

1.4.5 Summary of Performance Criteria

The previous sections have identified all the applicable performance objectives for the TFF PA in support of the DOE *Tier 1 Closure Plan*. Tables 1-4 thru 1-6 are summaries of the adopted performance objectives for the TFF PA for each time interval of interest.

Table 1-4. Summary of adopted performance objectives for the period of active institutional control.

Compliance Interval	Pathway	Compliance Point	Performance Objective
Period of active institutional control	All pathways (excluding radon)	Maximum point of impact at INEEL boundary	25 mrem/yr
2016 to 2116	Air emissions (excluding radon)	Maximum point of impact at INEEL boundary	10 mrem/yr
	Radon emissions	TFF surface	20 pCi/m^2/s
	Groundwater	Maximum point of impact at INEEL boundary	4 mrem/yr

Table 1-5. Summary of adopted performance objectives for the post-institutional control period.

Compliance Interval	Pathway	Compliance Point	Performance Objective
Post-institutional control	All pathways (excluding radon)	Maximum dose beyond 100 m	25 mrem/yr
2116 to 3016	Air emissions (excluding radon)	Maximum dose beyond 100 m	10 mrem/yr
	Radon emissions	TFF surface	20 pCi/m^2/s
	Groundwater	Maximum dose beyond 100 m	4 mrem/yr

Table 1-6. Summary of adopted performance objectives for inadvertent intruders.

Compliance Interval	Pathway	Compliance Point	Performance Objective
Post-institutional control 2116 to 3016	All pathways (excluding radon in air and groundwater)	Point of maximum dose	500 mrem (acute) 100 mrem/yr (chronic)

1.5 Summary of Key Assumptions

It is inherent in modeling exercises to make simplifying assumptions in the models to represent the real system of components. These simplifying assumptions have been made in several areas of this PA. The key assumptions are presented in the following sections and are discussed in further detail under the applicable sections of this PA.

This PA assumes 2016 as the closure date for the TFF. DOE is now moving to have the TFF closed by 2012 because of the INEEL accelerated cleanup program. The 4-yr difference will have little impact on the PA conclusions for compliance to the performance objectives. Long-lived radionuclides contribute significantly to the groundwater dose. The groundwater predicted peak doses will not increase but will occur 4 yr earlier than predicted. The intruder scenario doses will increase slightly in all cases. The dominant contributors to dose in these scenarios are the relatively short-lived radionuclides $^{137}Cs/^{137m}Ba$ and $^{90}Sr/^{90}Y$. Reducing the decay will slightly increase the final inventory in 3012. Based simply on the difference in time of decay, the dose estimates in the intruder scenario would increase by approximately 1%.

1.5.1 Radionuclide Inventory

The tank radionuclide source inventory estimate is based on the most recent analytical results from sampling of Tanks WM-182, WM-183, and WM-188 and historical data regarding the contents of the eleven 300,000-gal tanks. The concentrations for radionuclides lacking current analytical data have been estimated using the ORIGEN2 model (Croff 1980). The model used sodium-bearing waste as the nuclear fuel waste stream and radionuclide concentrations based on closure in 2016. The inventory is designed to be conservative based on data of liquid and solid tank contents and recent sampling data. The conservative approach was maintained by using the highest radionuclide concentrations (Tank WM-188) in the radionuclide inventory calculations, rather than averaging the recently sampled tanks. The least conservative scenario appears to overestimate the amount of residual radioactivity remaining in the tanks after closure. The cleaning of the first of 10 tanks shows removal effectiveness greater than anticipated and similar to the tank cleaning mockup results. Assumptions for the development of the radionuclide inventory and supporting documentation are given in Appendix A.

Contaminated sand pads are located beneath Tanks WM-185 and WM-187 because of previous operational upsets. The contamination of these sand pads has been evaluated for mechanisms of contaminant removal associated with the filling and draining of the vaults during rainfall or snowmelt. Radionuclides with low distribution coefficients were assumed to be removed from the sand pad, while those with high distribution coefficients were assumed to remain in the sand pads. This analysis also is presented in Appendix A.

Contamination contained in piping associated with the transfer of material throughout the facility also was evaluated to determine the potential impact of this source on future doses. Appendix A gives an estimate of the final composition of contamination in the process lines after a series of washing and decontamination steps.

1.5.2 Degradation Analysis

An analysis of the degradation of the vaults, grout, tanks, and piping was completed for the

TFF PA. This analysis, presented in Appendix E, contains several key assumptions necessary for the simplification of the analysis. The analysis indicated that the concrete vaults turn to rubble approximately 500 yr after closure. The grout and tanks were predicted to turn to rubble after 5,000 yr. Using the degradation analysis, key assumptions were made in the conceptual model such that the concrete vault was assumed to be completely degraded at 100 yr and the tanks and grout at 500 yr. These assumptions show that a very conservative analysis is being conducted in relation to the results of the degradation analysis.

The piping associated with the tank systems at the TFF was modeled based on the assumption that the stainless-steel piping and associated grout inside and enveloping the pipe in the secondary containment degrade similar to the tank environment and release contaminants beginning 500 yr after closure. The degradation analysis for the piping is presented in Appendix E.

1.5.3 Groundwater Model

Based on the availability of geotechnical information and the inherent uncertainty regarding this information, several assumptions were necessary for the model simulations. Listed below are the key hydrologic assumptions inherent in the groundwater and contaminant transport modeling.

- The hydrostratigraphy presented by numerous United States Geological Survey (USGS) reports is accurate and reliable, and thus forms the basis for numerical simulations of groundwater flow and contaminant transport.
- Literature-based values for recharge indicate that the Big Lost River and the INTEC percolation ponds are the major sources of recharge to the unsaturated zone and aquifer at INTEC.
- Infiltration from the Big Lost River and the INTEC percolation ponds is constant over time. The amount of seepage from the Big Lost River was based on stream gaging studies. INTEC plant discharge records were used for the percolation pond estimates.
- The percolation ponds were only used in the calibration of perched water bodies at INTEC. The ponds will be closed in the future; therefore, the ponds are not used the flow model for transport of radionuclides at INTEC from the TFF. The water infiltration from the ponds was shut off in the model after the assumed TFF closure date of 2016.
- Water usage from the Big Lost River and flood diversion of the river were assumed to be constant over the time of the simulations. However, separate analysis for flooding of the Big Lost River was evaluated.
- The fundamental assumption for simulating water transport and developing the initial hydrologic conditions for contaminant transport simulations is that there are no perched water zones due solely to infiltrating water from precipitation.
- The interbeds are the controlling geological units responsible for the formation of perched water zones whether the hydraulic conductivity of a sedimentary interbed might be smaller than that of an overlying basalt flow or alterations in the baked zone exist between two flows that contribute to reduced vertical hydraulic conductivity.
- Because of the lack of direct information on the hydraulic conductivity of the interbed units, values were assigned in modeling simulations based on lithologic properties, residual moisture contents, and the existence of perched water in nearby monitoring wells.
- Hydraulic conductivity values for the basalt units were based on the thickness. Thin basalt units were assigned higher hydraulic conductivity values.
- Fractured basalts were treated as a porous medium with low residual moisture contents and unsaturated hydraulic characteristic curves that yield high water releases at low capillary pressures.
- For calibration involving seepage losses from the Big Lost River and the INTEC percolation ponds, the location and extent of perched

water zones is controlled by variations in hydraulic conductivity.

- Based on the volume of water available from the Big Lost River seepage losses, compared with estimates from other potential sources of recharge, the source of the perched water in the northern portion of the INTEC facility was due primarily to the Big Lost River seepage.
- Similarly, the INTEC percolation ponds were the principle source of water for the perched zones in the southern portion of INTEC.
- Since there was a lack of site-specific information, such as K_d values for specific radionuclides or dispersion coefficients for geologic materials underlying the site, information from similar sites or previously conducted PA investigations was incorporated into the model.

1.6 Summary

This document has been prepared to describe the methods and results of the PA for the TFF. The results of the analyses indicate compliance with the established performance objectives and provide reasonable assurance that public health and safety will be protected.

The basic concept of a performance assessment is to develop a simplified representation of the physical setting at the INEEL using research data, assumptions, documented information, and modeling techniques in an attempt to understand contaminant transport within the physical system and along potential pathways of human exposure. This PA begins with site-specific physical data that are used to formulate a conceptual model and provide a listing of the performance objectives. Information in Section 2 includes description of geography, demography, meteorology, climatology, ecology, geology, and hydrology. Also included are the design features of the TFF and the waste characteristics. The specific processes in the conceptual model are then described mathematically.

The PA includes scenarios in which an inadvertent intruder receives both an acute dose and a chronic dose. Section 5 defines the intruder scenarios and gives the results of intruder scenario analysis.

The results of the PA are described in Section 6. The results show reasonable assurance that the potential dose will be below the regulatory standards.

Section 7 provides an evaluation of the PA results with respect to the performance objectives. A PA does not produce an absolute answer but rather a bounding approximation. This approximation is dependent on the accuracy of the input data, the conceptual and mathematical models, and the computer codes. A sensitivity/uncertainty analysis was prepared as part of this PA.

Section 7 contains a sensitivity/uncertainty analysis based on several scenarios involving the sensitive parameters for the transport of radionuclides. Different inventories, sorption coefficients, hydraulic diffusivity values, and infiltration rates are varied in numerical simulations for four different scenarios and the results are also discussed. Selection criteria are discussed for the radionuclide inventory, radionuclide screening analysis, TFF degradation analysis, modeled releases, and the groundwater analysis. Four scenarios were established for this PA: best, realistic, conservative, and worst-case. The conservative scenario is shown in Section 3 as the compliance scenario and is compared to the performance objectives. The criteria for the selection and quantification of four radionuclide inventories and transport scenarios are also presented in this section.

2. CLOSURE FACILITY AND SITE CHARACTERISTICS

This section provides descriptive information and data for the INEEL site, environment, and TFF site, and the characteristics of the residual waste. This description gives the basis for the TFF conceptual model and an understanding of the method of analysis. The emphasis of this section is on the characteristics that are important to the performance of the closure action.

2.1 Site Characteristics

2.1.1 Geography and Demography

2.1.1.1 Closure Action Location. The INEEL is located in southeastern Idaho, on the west-central portion of the Eastern Snake River Plain (ESRP) (Figure 2-1). Included in its 890 mi^2 (2,300 km^2) of area are portions of five Idaho counties (Bingham, Bonneville, Butte, Clark, and Jefferson) (see Figure 2-2). The nearest INEEL boundaries are 22 mi (35 km) west of Idaho Falls, 23 mi (37 km) northwest of Blackfoot, 44 mi (71 km) northwest of Pocatello, and 7 mi (10 km) east of Arco, Idaho. There are no permanent residents within an 11-mi (18-km) radius of INTEC and there is a relatively low population base in the surrounding areas. The significant communities in close proximity to the INEEL are Atomic City (1 mi [2 km]), population 25; Arco (7 mi [10 km]), population 1,026; Idaho Falls (22 mi [35km]), population 50,730; Blackfoot (23 mi [37 km]), population 10,419; and Pocatello (44 mi [71 km]), population 51,466. The INEEL also lies approximately equidistant from three larger metropolitan areas: Salt Lake City, Utah (211 mi [340 km]), population 181,743; Boise, Idaho (257 mi [414 km]), population 185,787; and Butte, Montana (214 mi [344 km]) population 33,892 (Sehlke and Bickford 1993, Department of Commerce 2001).

The INEEL HLW Program is conducted at INTEC, located in the south-central portion of the INEEL. INTEC occupies approximately 200 acres (80 ha) and consists of more than 150 buildings. Primary facilities include storage, treatment, and laboratory facilities for spent nuclear fuel, mixed HLW, and mixed transuranic waste/sodium-bearing waste (Figure 2-3). Located outside the INTEC perimeter fence are parking areas, a helicopter landing pad, the wastewater treatment lagoon, various pits, and percolation ponds. These areas occupy approximately 55 acres (22 ha).

INTEC began operations in 1953 and was, historically, a fuel reprocessing facility for defense projects, research, and storage of spent nuclear fuel. In 1992, DOE decided to end the fuel-reprocessing mission at INTEC. This decision led to the phase-out of fuel dissolution, solvent extraction, product denitration, and other processes. The current mission of INTEC is to safely receive and store spent nuclear fuel and radioactive wastes, prepare spent nuclear fuel for shipment to an off-site repository, develop new technologies for waste and waste management for DOE, and remediate past environmental releases.

2.1.1.2 Closure Site Description. The TFF lies within the boundaries of the INTEC facility in the northern portion of the facility. The HLLW generated from fuel reprocessing operations were stored in stainless-steel storage tanks at the TFF. The TFF comprises nine 300,000-gal tanks, two 318,000-gallon tanks, and four 30,000-gal tanks (Figure 2-4). All of the tanks, except for the 30,000-gal tanks, are contained within concrete vaults under the ground surface. The 30,000-gal tanks were directly buried in the ground without concrete vaults.

The principal surface materials at the INEEL are basalt, alluvium, lakebed or lacustrine sediments, slope wash sediments and talus, silicic volcanic rocks, and sedimentary rocks. The natural plant life consists mainly of sagebrush and various grasses. The vegetation of the INEEL is limited by soil type, meager rainfall, and extended drought periods. Only a few deciduous trees, located principally along the Big Lost River, exist on the INEEL. The most prominent ground cover is a mixture of sagebrush (*Artemisia tridentata*) and a variety of grasses. Lanceleaf rabbitbrush (*Crysothamnus viscidiflorus*) covers about 80% of the INEEL and can be found in any given area. The soil at the INEEL TFF site is previously disturbed sandy gravel; the flat terrain precludes erosion (INEEL 2001a.

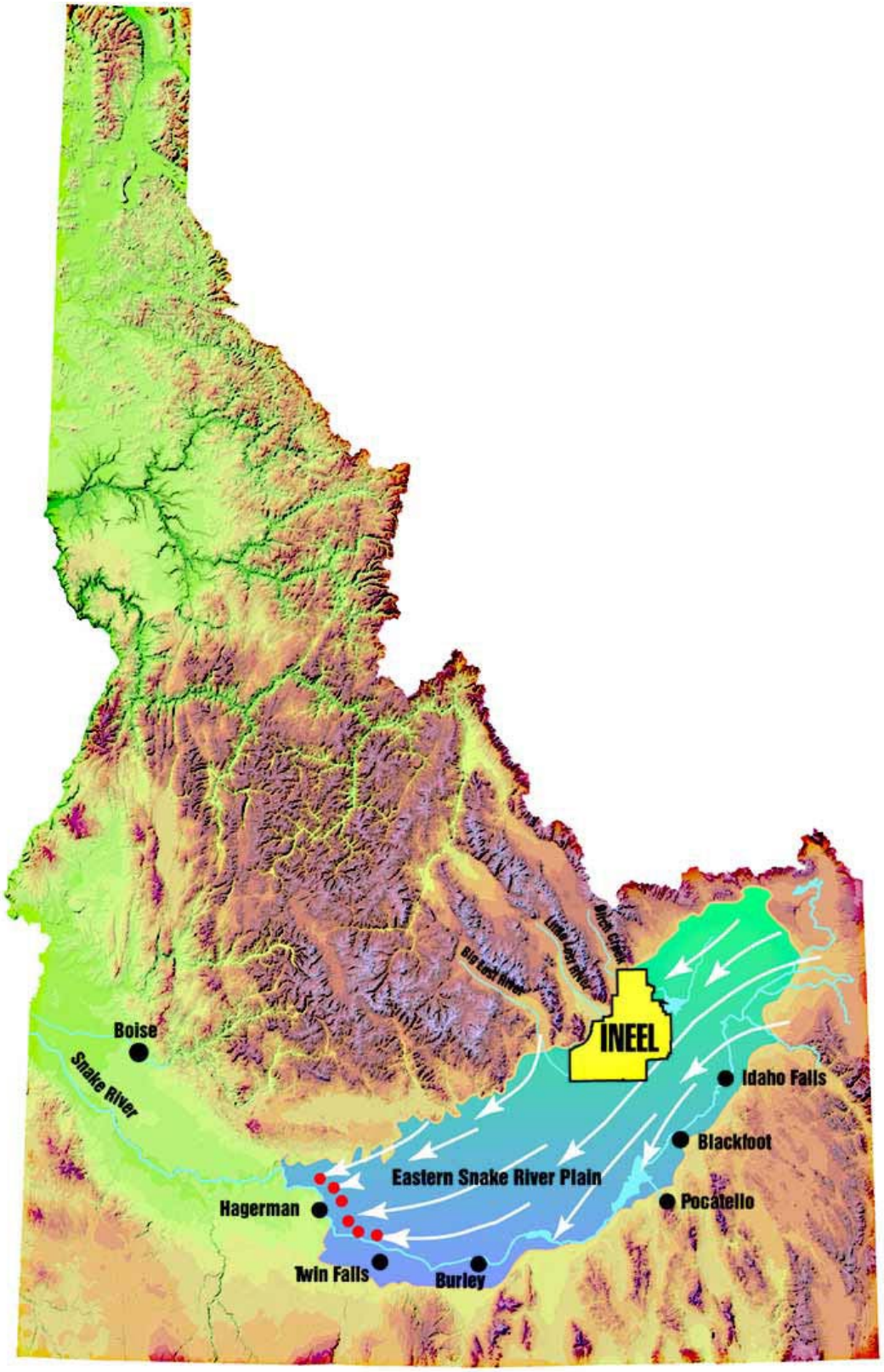

Figure 2-1. Idaho map showing the location of the INEEL on the Eastern Snake River Plain.

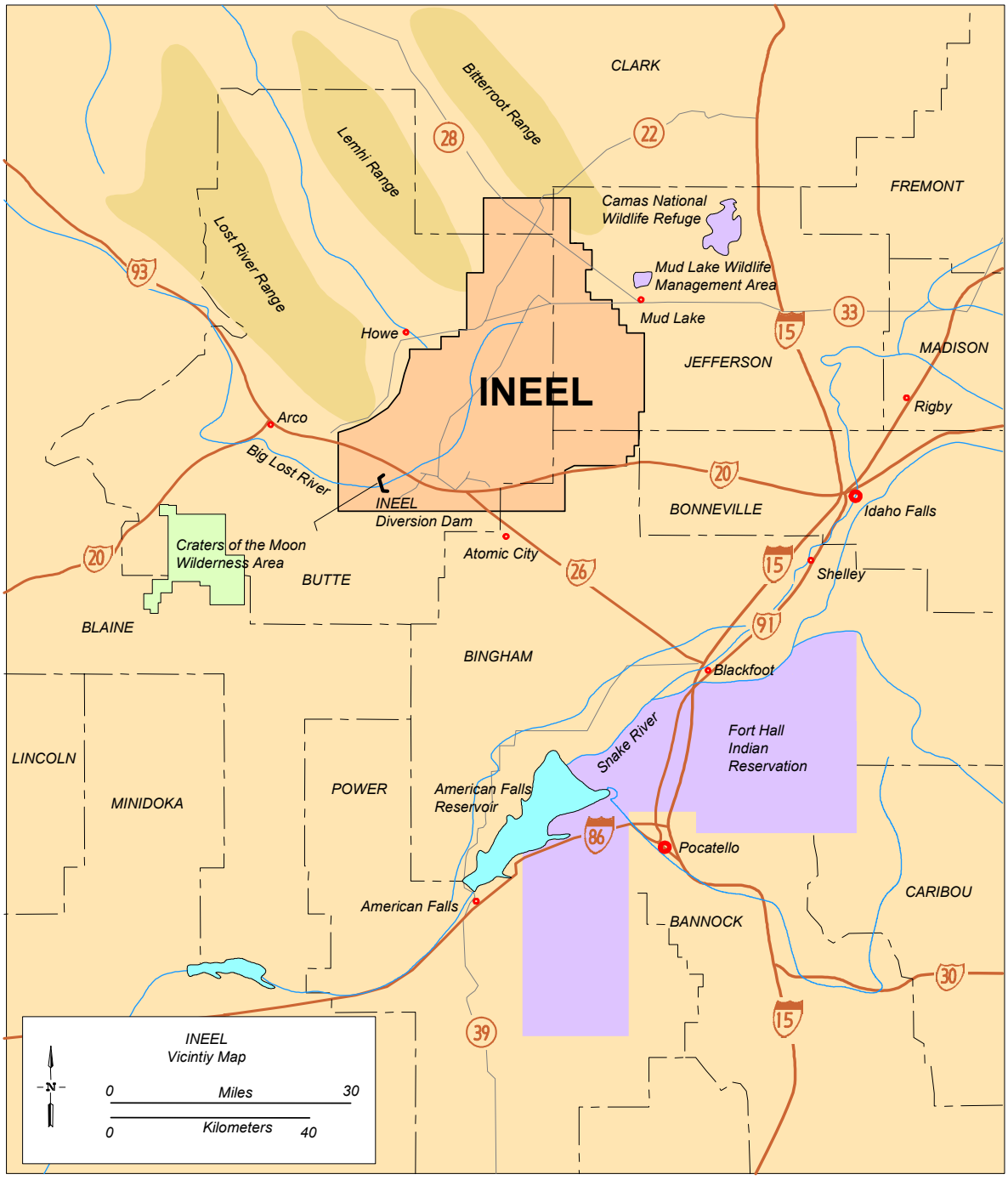

Figure 2-2. INEEL vicinity map.

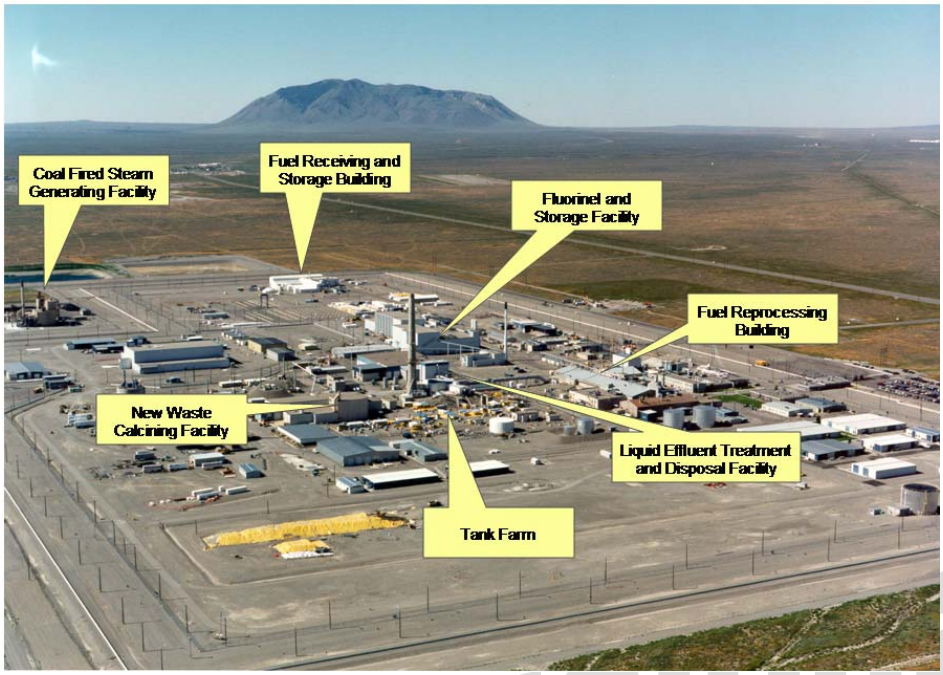

Figure 2-3. Major facilities at INTEC.

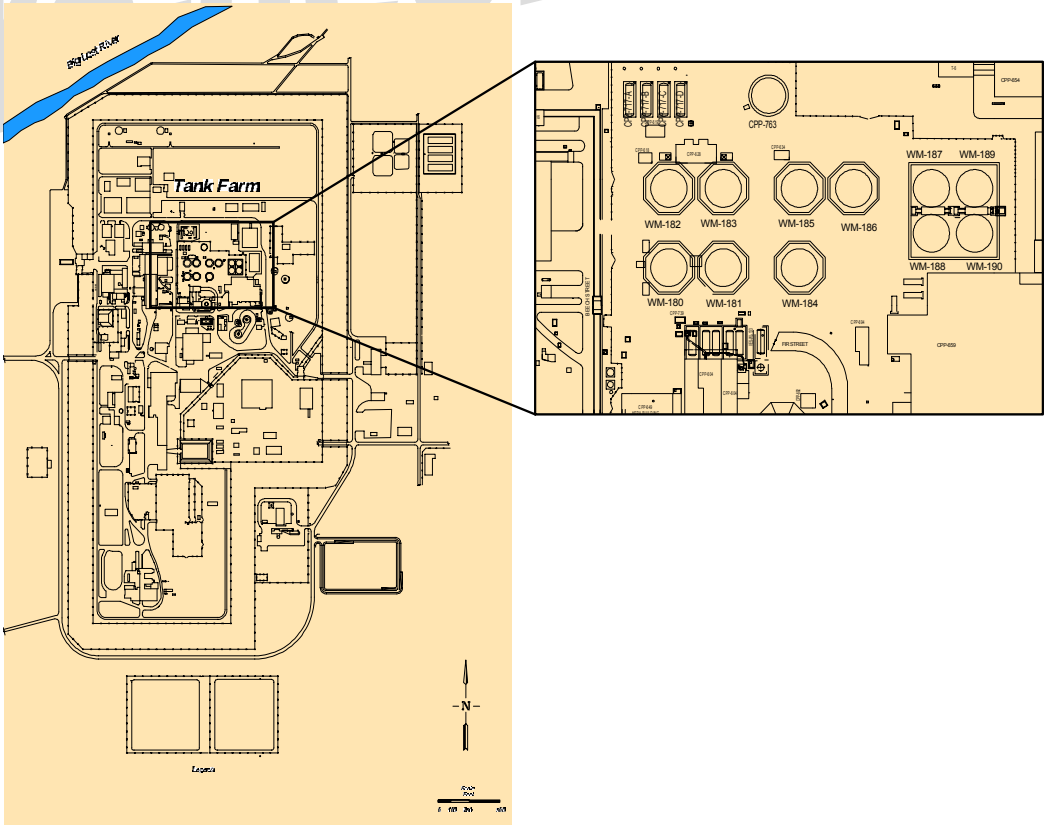

Figure 2-4. Location of the TFF tanks and vaults at INTEC.

INTEC is located on an alluvial plain approximately 200 ft (60 m) from the Big Lost River channel, near the channel intersection with the INEEL's Lincoln Boulevard. INTEC is surrounded by a stormwater drainage ditch system (DOE-ID 1998). Stormwater runoff from most areas of INTEC flows through ditches to an abandoned gravel pit on the northeast side of INTEC. From the gravel pit, the runoff infiltrates the ground. The system is designed to handle a 1-in-25-yr, 24-hr storm event. Because the land is relatively flat (slopes of generally less than 1%) and annual precipitation is low, stormwater runoff volumes are small and are generally spread over large areas where they may evaporate or infiltrate the ground surface.

The INEEL is located in the Pioneer Basin. This closed drainage basin includes three main streams: Big Lost River, Little Lost River, and Birch Creek. These three streams drain the mountain areas to the north and west of the INEEL, although most flow is diverted for irrigation in the summer months before it reaches the site boundaries. Flow that reaches the INEEL infiltrates the ground surface along the length of the streambeds in the spreading areas at the southern end of the INEEL and, if the stream flow is sufficient, in the ponding areas (playas or sinks) in the northern portion of the INEEL. During dry years, there is little or no surface water flow on the INEEL. Because the Pioneer Basin is a closed drainage basin, water does not flow off the INEEL. Rather, the water either infiltrates the ground surface to recharge the aquifer or is consumed by evapotranspiration.

The Big Lost River flows southeast from Mackay Dam, past Arco, and onto the Snake River Plain (see Figure 2-2). Near the INEEL's southwestern boundary, a diversion dam prevents flooding of downstream areas during periods of heavy runoff by diverting water to a series of natural depressions or spreading areas (DOE-ID 1995b). During periods of high flow or low irrigation demand, the Big Lost River continues northeastward past the diversion dam, passes within 200 ft (60 m) of INTEC, and ends in a series of playas 15 to 20 mi (24 to 30 km) northeast of INTEC, where water infiltrates the ground surface.

Flow from Birch Creek and the Little Lost River infrequently reaches the INEEL. In the summer months, the water in Birch Creek and the Little Lost River is diverted for irrigation prior to reaching the INEEL. During periods of unusually high precipitation or rapid snowmelt, water from Birch Creek and the Little Lost River may enter the INEEL from the northwest and infiltrate the ground.

Flood studies at the INEEL have examined the flooding potential at INEEL facilities due to failure of the Mackay Dam, 45 mi (72 km) upstream from the INEEL (Koslow and Van Haaften 1986). The USGS made preliminary estimates of the 100-yr flood plain along the Big Lost River (Berenbrock and Kjelstrom 1998). DOE commissioned additional studies to refine the 100-yr flood plain and delineate the 500-yr flood plain, including a two-dimensional model analysis and a paleohydrologic and geomorphic assessment of the flood risk along the Big Lost River (Ostenaa et al. 1999). There is no record of any historical flooding at INTEC since 1952. Section 2.1.5.3 discusses in detail the potential for flooding at INTEC.

The Snake River Plain has a relatively low rate of seismicity, whereas the surrounding basin and range has a fairly high rate of seismicity [Woodward-Clyde Federal Services (WCFS) 1996]. The primary seismic hazards from earthquakes to INEEL facilities consist of the effects from ground shaking and surface deformation (surface faulting and tilting). Other potential seismic hazards such as avalanches, landslides, mudslides, and soil liquefaction are not likely to occur at the INEEL because the local geological conditions and terrain are not conducive to these types of hazards. Based on the seismic history and geologic conditions, earthquakes greater than moment magnitude of 5.5 and associated strong ground shaking and surface fault ruptures are not likely to occur within the Snake River Plain [Woodward-Clyde Consultants (WCC) 1990; WCFS 1996]. However, moderate to strong ground shaking could affect the INEEL from earthquakes in the surrounding basin and range. Section 2.1.4.2 provides detailed discussions on seismology.

Volcanic hazards include the effects of lava flows, fissures, uplift, subsidence, volcanic earthquakes, and ash flows or airborne ash deposits. Most of the basalt volcanic activity occurred from 4 million to 2,100 yr ago in the INEEL area. The most recent and closest volcanic eruption occurred at the Craters of the Moon National Monument, 26.8 mi (43.1 km) southwest of INTEC (Kuntz, Covington, and Schorr 1992). Based on a probability analysis of the volcanic history in and near the south-central INEEL area, the Volcanism Working Group estimated that the conditional probability that basaltic volcanism would affect a south-central INEEL location is less than once per 100,000 yr or longer (Volcanism Working Group 1990). The probability is associated primarily with the Axial Volcanic Zone and the Arco Volcanic Rift Zones. INTEC is located in a lesser lava flow hazard area of the INEEL, more than 5 mi (8 km) from the Axial Volcanic Zone and any volcanic vent younger than 400,000 yr. Section 2.1.4.3 provides additional discussions on the volcanic hazards.

2.1.1.3 Population Distribution.

Population growth surrounding the INEEL (i.e., within a seven-county region comprising Bannock, Bingham, Bonneville, Butte, Clark, Jefferson, and Madison counties) has paralleled statewide growth from 1960 to 1990. During this time, the regional population increased an average of approximately 1.40% annually, while the annual growth rate for the state was 1.53% (Department of Commerce 1995). From 1990 to 1999, state population growth accelerated to nearly 2.45% per year, but the regional population growth dropped to 1.32% (Department of Commerce 2000). Population growth for the state is projected to slow after the year 2000 (Department of Commerce 1997). Table 2-1 lists 1990 and 2000 census data for the counties surrounding the INEEL and growth projections for 2010 and 2025. The projections are based on an annual growth rate of 1.05%, derived from the average of the projected state growth rates from 2000 to 2025 (Department of Commerce 1997).

In the year 2000, Bannock and Bonneville counties had the largest populations in the region, and together accounted for 46.9% of the total regional population (Department of Commerce 2001). Butte and Clark are the most sparsely populated counties and together contained 1.57% of the regional population in 2000. The largest cities in the region are Pocatello (Bannock County) and Idaho Falls (Bonneville County), with year 2000 populations of approximately 51,466 and 50,730, respectively.

Figures 2-5 through 2-7 show population densities, based on the 1990 census, for the years 2000 through 2020 at 10-yr intervals for the 50-mi (80-km) radius around INTEC (INEEL 1999b). The nearest populated area to the INEEL is Atomic City, population about 25 (Department of Commerce 2001), located approximately 1 mi (2 km) from the southern INEEL boundary and about 11 mi (18 km) from INTEC.

No permanent residents live within a 10-mi (20-km) circle centered at INTEC on the INEEL (DOE 2002). No cities or towns are within 10 mi (20 km) of the INTEC TFF. However, several INEEL facilities, such as the Central Facilities Area (CFA), the Test Reactor Area (TRA), and RWMC are within 10 mi (20 km) of the INTEC TFF. Also, the Experimental Breeder Reactor I (EBR-I), a National Historic Landmark, is located southwest and within 10 mi (20 km) of the INTEC TFF.

The INEEL has become a major part of the eastern Idaho community and economy. During fiscal year 2001, the INEEL employed an average of over 8,000 people and had a budget of nearly $1 billion (INEEL 2001b). The INEEL contractors are the largest employers in the area and one of the five largest in the state. The 2001 impact analysis indicates that INEEL activities and its workforce support an additional 10,250 jobs statewide (INEEL 2001b). Therefore, over 18,000 Idaho jobs can be attributed to the facility. The INEEL workforce is projected to decrease by approximately 450 people by fiscal year 2005 (INEEL 2000b).

2.1.1.4 Uses of Adjacent Lands.

The INEEL occupies approximately 890 mi^2 (570,000 acres or 230,000 ha) of land in Bingham, Bonneville, Butte, Clark, and Jefferson counties in southeastern Idaho. Approximately 2% of this land (11,400 acres [4,610 ha]) has been developed to

Table 2-1. Regional population of the INEEL; selected years 1990–2025.

County	1990 [a]	2000 [b]	2010	2025
Bannock	66,026	75,565	83,886	98,116
Bingham	37,583	41,735	46,329	54,187
Bonneville	72,207	82,522	91,608	107,147
Butte	2,918	2,899	3,217	3,762
Clark	762	1,022	1,135	1,328
Jefferson	16,543	19,155	21,264	24,870
Madison	23,674	27,467	30,491	35,663
Total	219,713	250,365	277,930	325,073

a. Source: Department of Commerce 1990.

b. Source: Department of Commerce 2001.

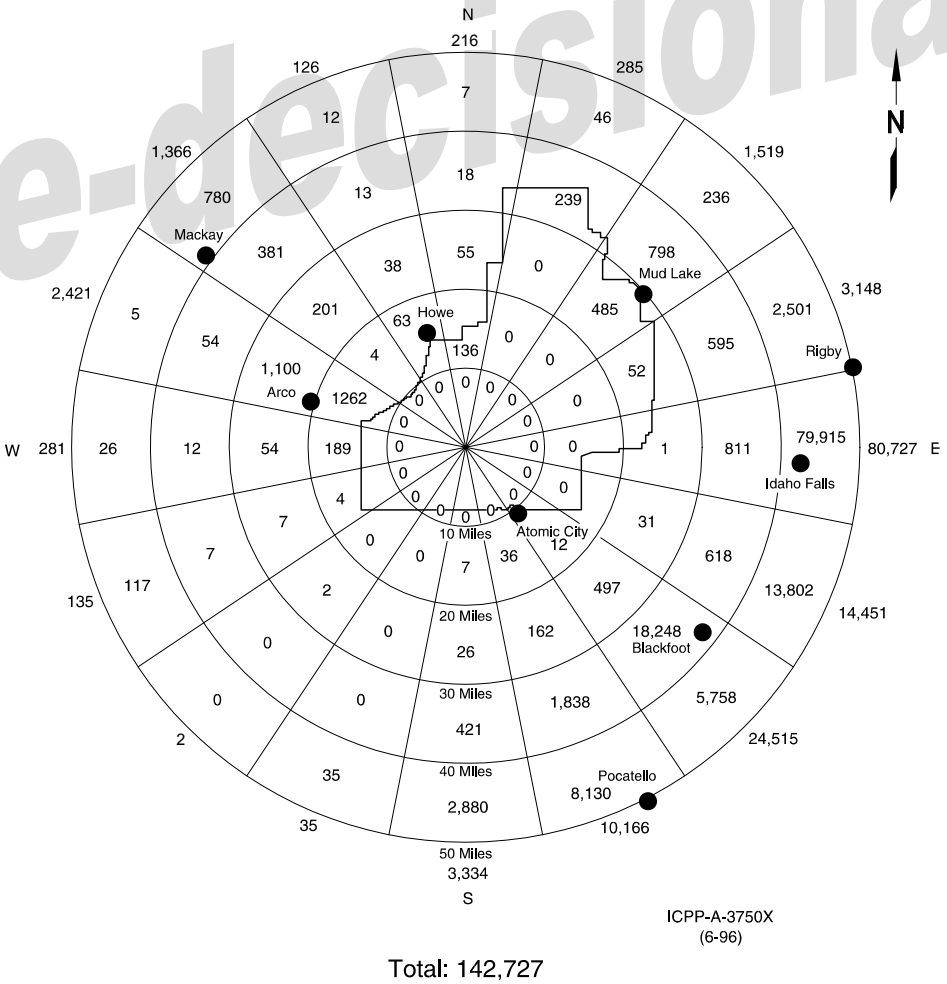

Figure 2-5. 2000 population distribution for the area surrounding INTEC (INEEL 1999b).

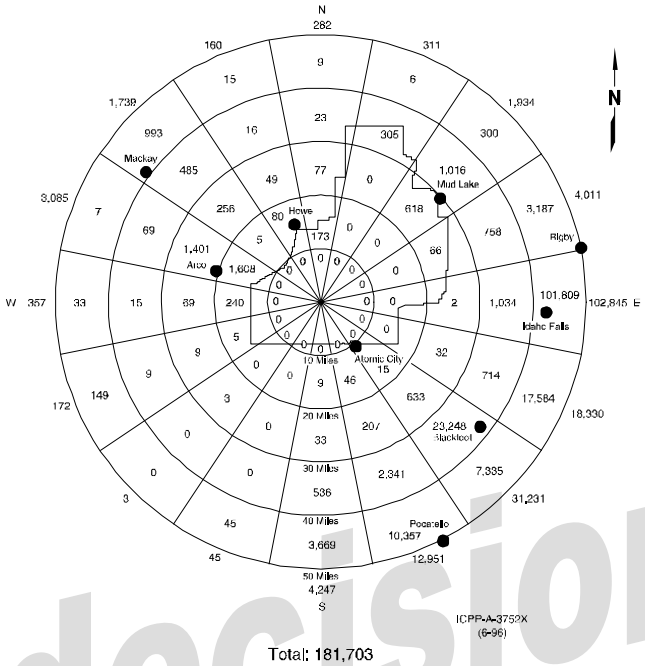

Figure 2-6. 2010 projected population distribution for the area surrounding INTEC (INEEL 1999b).

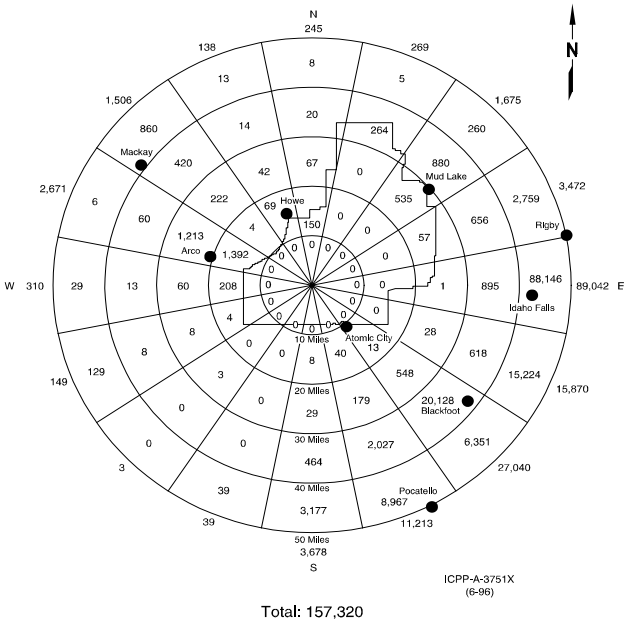

Figure 2-7. 2020 projected population distribution for the area surrounding INTEC (INEEL 1999b).

support INEEL facility and program operations associated with energy research and waste management activities (DOE 1995). INEEL operations are performed within the Site's primary facility area (CFA, TRA, INTEC, etc.), which occupies 2,032 acres (822.3 ha). A 345,000-acre (140,000 ha) security and safety buffer zone is located around the core development area, which also accommodates environmental research and ecological and socio-cultural preservation.

Approximately 6% of the INEEL (34,000 acres [14,000 ha]) is devoted to utility rights-of-way and public roads, including Highway 20 (which runs east and west and crosses the southern portion of the INEEL), Highway 26 (which runs southeast and northwest intersecting Highway 20), and Idaho State Highways 22, 28, and 33 (which cross the northeastern part of the INEEL) (DOE 1995).

Up to 340,000 acres (140,000 ha) of the INEEL is leased for cattle and sheep grazing (DOE 1995); the Bureau of Land Management (BLM) administers grazing permits. However, grazing of livestock is prohibited within 0.5 mi of any primary facility boundary and within 2 mi (3 km) of any nuclear facility. In addition, 900 acres (400 ha) located at the junction of Idaho State Highways 28 and 33 are used by the U.S. Sheep Experiment Station as a winter feedlot (DOE-ID 1997a). Figure 2-8 shows land use in the vicinity of the INEEL.

On July 17, 1999, the Secretary of Energy and representatives of the U.S. Fish and Wildlife Service, BLM, and Idaho State Fish and Game Department designated 73,263 acres (29,648 ha) of the INEEL as the Sagebrush Steppe Ecosystem Reserve (DOE 1999c). In 1995, the National Biological Service listed the ungrazed sagebrush steppe ecosystem in the Intermountain West and big sagebrush (*Artemisia tridentata*) in Idaho's Snake River Plain as critically endangered (Noss, LaRoe, and Scott 1995). The INEEL Sagebrush Steppe Ecosystem Reserve was designated to ensure this portion of the ecosystem receives special, scientifically-controlled consideration. Conservation management in this area is intended to maintain the current vegetation and provide the opportunity for study of an undisturbed sagebrush steppe ecosystem. Traditional rangeland uses, such as livestock grazing, which exist in a portion of the area, are continuing under this management designation. The designated INEEL Sagebrush Ecosystem Reserve is located in the northwest portion of the area. The southern boundary of the Reserve, which runs east and west along section lines, is about 11 mi (18 km) north of INTEC at the closest point (DOE 2002).

Recreational uses of the INEEL include public tours of general facility areas and EBR-I, a National Historic Landmark. Controlled hunting also is permitted on the INEEL, but is restricted to 0.5 mi inside the Site boundary. These restricted hunts are intended to assist the Idaho Department of Fish and Game in reducing crop damage caused by wild game on adjacent private agricultural lands. The INEEL also is designated as a National Environmental Research Park, functioning as a field laboratory set aside for ecological research and evaluation of the environmental impacts from nuclear energy development (DOE 2002).

The INEEL does not lie within any of the land boundaries established by the Fort Bridger Treaty of 1868. The entire INEEL is land occupied by DOE; therefore, the provision in the Fort Bridger Treaty that allows the Shoshone-Bannock Tribes to hunt on unoccupied lands of the United States does not presently apply to any INEEL land (DOE 2002).

Land use at the INEEL is in a state of transition. Emphasis is moving toward radioactive and hazardous waste management, environmental restoration and remedial technologies, and technology transfer, resulting in more development of the INEEL within some facility areas and less development in others. DOE has projected land use scenarios at the INEEL for the next 25, 50, 75, and 100 yr. Future development is projected to take place in the central portion of the INEEL within existing facility areas.

For further review, see the *Long-Term Land Use Future Scenarios for the Idaho National Engineering Laboratory* (DOE-ID 1995a) and the *Idaho National Engineering and Environmental Laboratory Comprehensive Facility and Land Use Plan* (DOE-ID 1997a).

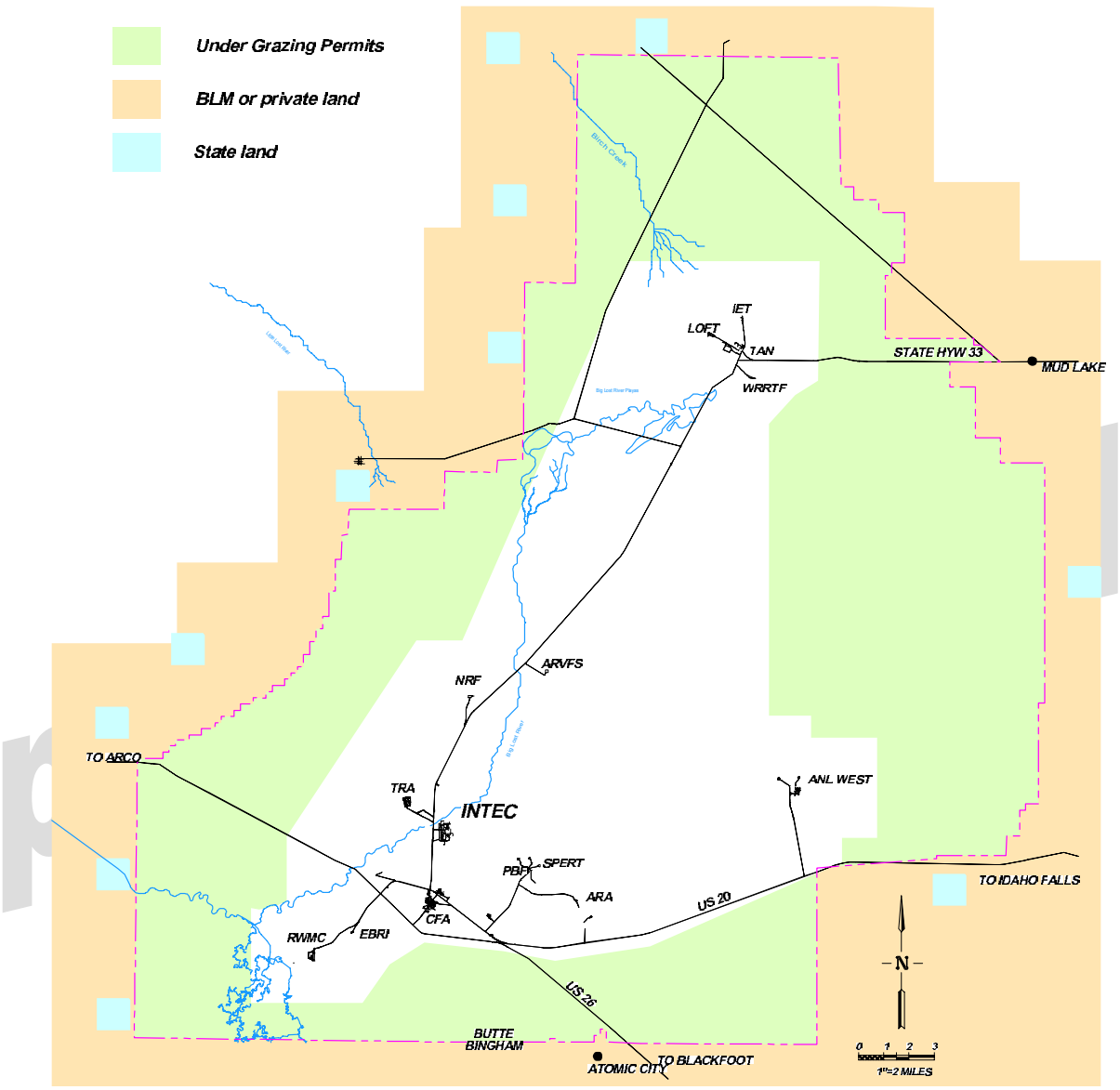

Figure 2-8. Selected land use of the INEEL and surrounding vicinity.

Approximately 75% of the land adjacent to the INEEL is owned by the federal government and administered by BLM. Land uses on this federally-held land consist of wildlife management, mineral and energy production, grazing, and recreation. The State of Idaho owns approximately 1% of the adjacent land. This land also is used for wildlife management, grazing, and recreation. The remaining 24% of the land adjacent to the INEEL is privately owned and is primarily used for grazing and crop production (INEEL 1999b).

Small communities and towns located near the INEEL boundaries include Mud Lake to the east; Arco, Butte City, and Howe to the west; and Atomic City to the south. The larger communities of Idaho Falls/Ammon, Rexburg, Blackfoot, and Pocatello/Chubbuck are located to the east and southeast of the INEEL Site. The Fort Hall Indian Reservation is located southeast of the INEEL Site.

All county plans and policies encourage development adjacent to previously developed

areas to minimize the need to extend infrastructure improvements and to avoid urban sprawl. Because the INEEL is remotely located from most developed areas, its lands and adjacent areas are not likely to experience residential and commercial development and no new development is planned near the INEEL Site. However, recreational and agricultural uses are expected to increase in the surrounding area in response to greater demand for recreational areas and the conversion of rangeland to cropland (Sehlke and Bickford 1993).

The four most prominent tourist/recreation areas or attractions in the INEEL area include:

- Yellowstone National Park, which is approximately 72.5 mi (117 km) northeast of the INEEL and 99.5 mi (160 km) from INTEC
- EBR-I, which is situated on the INEEL
- Craters of the Moon National Monument, which is located approximately 19 mi (31 km) southeast of the INEEL
- The resort areas of Ketchum and Sun Valley, which are approximately 59.5 mi (95.8 km) west of the INEEL and 72 mi (120 km) from INTEC (INEEL 1999b).

Other recreation and tourist attractions in the region surrounding the INEEL Site include Hell's Half Acre Wilderness Study Area, Black Canyon Wilderness Study Area, Camas National Wildlife Refuge, Market Lake State Wildlife Management Area, North Lake State Wildlife Management Area, Targhee and Challis National Forests, Sawtooth National Recreation Area, Sawtooth Wilderness Area, Sawtooth National Forest, Grand Teton National Park, Jackson Hole recreation complex, and the Snake River.

The *Idaho National Engineering and Environmental Laboratory Comprehensive Facility and Land Use Plan* (DOE-ID 1997a) and the *Final Record of Decision, Idaho Nuclear Technology and Engineering Center* (DOE-ID 1999) describe the land use for the INEEL and INTEC. Land use at the INEEL is currently government-controlled industrial use. The term controlled means that unrestricted public access to INTEC and the INEEL is not available. Presently, access to INEEL facilities requires proper clearance, training, or escort and controls to limit the potential for unacceptable exposures. A security force limits access to approved personnel and visitors. These controls are estimated to be in place for the next 100 yr.

Future land use scenarios are identified in the *Long-Term Land Use Future Scenarios for the Idaho National Engineering Laboratory* (DOE-ID 1995a). This document was developed using a stakeholder process that involved a public participation forum, a public comment period, and the INEEL Citizens Advisory Board. Following review and comment by the public participation forum, the document underwent a 30-day public comment period and was subsequently submitted to the Citizens Advisory Board for review and recommendations. To date, no recommendations have been received for residential use of any portion of the INEEL until at least the year 2095. Until 2095, the reasonably anticipated future use for the TFF is as a government-controlled industrial facility (DOE-ID 1999).

Planning assumptions in the INEEL *Comprehensive Facility and Land Use Plan* (DOE-ID 1997a) are that the INEEL will remain under government control for at least the next 100 yr. Future government management and control becomes increasingly uncertain with time. No residential development will be allowed to occur within INEEL boundaries during the next 100 yr.

INTEC was one of the facilities that had a future use scenario projected in the *Long-Term Land Use Future Scenarios for the Idaho National Engineering Laboratory* (DOE-ID 1995a). The scenarios are broken down into 25-yr increments.

- Present: Interim storage of spent nuclear fuels, disposition of fuels, managing and improving waste, and water management techniques.
- 25-yr: Continued use as industrial area, planned new waste treatment facility.
- 50-yr: Approaching end of useful life if no new mission identified, decontamination and

decommissioning with all or selected areas for restricted industrial use.

- 75-yr: Standby mode for restricted industrial use, reuse permitted but no new development outside existing fence line.
- 100-yr: Continuation as a restricted industrial area.

2.1.2 Meteorology and Climatology

Meteorological data have been collected periodically at over 45 locations on and near the INEEL since 1949. The longest and most complete record of air temperature and precipitation observations (over 35 yr) at the INEEL was collected from the weather station at CFA. The CFA station is located approximately 3 mi (5 km) south of INTEC. Differences in climate between the CFA monitoring station and INTEC are minimal. INTEC and CFA are at approximately the same terrain elevation and have the same exposure to wind, snow, and cloud cover.

The National Oceanic and Atmospheric Administration (NOAA) Air Resources Laboratories conducts most of the meteorological monitoring within 50 mi (80 km) of the INEEL. An overview of climatological data is available from data summaries collected from the CFA monitoring station. A summary of the climatology of the INEEL is available in *Climatography of the Idaho National Engineering Laboratory* (Clawson, Start, and Ricks 1989).

2.1.2.1 Temperature. Temperatures at the INEEL vary widely over the course of the year. Records for CFA indicate that the highest and lowest daily maximum temperatures range from 101°F (38.3°C) to –47°F (–44°C), respectively. The average annual temperature at the INEEL exhibits a gradual seven-month increase, beginning with the first week in January and continuing through the third week in July. During the summer months of April through October, the average monthly temperature varies from 41 to 68°F (5 to 20°C). The temperature then decreases over the course of five months until the minimum average temperature is reached again.

2.1.2.2 Wind. The prevailing wind direction at INTEC and at most locations on the INEEL is southwesterly (DOE-ID 1995a). In summer, a sharp reversal in wind direction occurs daily; winds from the southwest predominate during daylight hours, and northeasterly winds predominate at night. The reversals normally occur shortly after sunrise and sunset. The wind rose diagrams in Figure 2-9 show the annual wind flow at the INEEL at three of the meteorological monitoring sites from 1988 to 1992. Multi-year wind roses exhibit little variability and are representative of typical patterns.

The average monthly wind speed varies from approximately 3.1 mph (4.9 km/h) in December to 9.3 mph (15 km/h) in April and May (DOE-ID 1995a). The highest hourly average speed was recorded at 51 mph (82 km/h), from the west-southwest. Strong wind gusts can occur during thunderstorm activity. On average, strong wind gusts occur 2 or 3 days per month during June, July, and August.

The highest instantaneous speed, recorded 18 ft (5.5 m) aboveground at CFA, was 78 mph (130 km/h), with the wind from the west-southwest. Calm conditions prevail 11% of the time.

Atmospheric particulate matter is routinely monitored using low-volume air sampling stations at various locations across the INEEL and a total suspended particulate monitor at CFA. In 1989 and 1990, the INEEL mean value from the low-volume air samplers ranged from 17 to 20 $\mu g/m^3$, and the CFA annual average ranged from 28 to 40 $\mu g/m^3$ (Hoff et al. 1990, 1991).

2.1.2.3 Precipitation. The average annual precipitation at CFA is 8.7 in. (22 cm). The highest recorded annual amount of precipitation recorded was 14.4 in. (36.6 cm) in 1963, and the lowest amount was 4.5 in. (11 cm) in 1966. A precipitation peak of approximately 1.2 in./mo (3.0 cm/mo) is associated with thunderstorms in May and June each year (DOE-ID 1995a). Other months generally receive one-half or less of this amount.

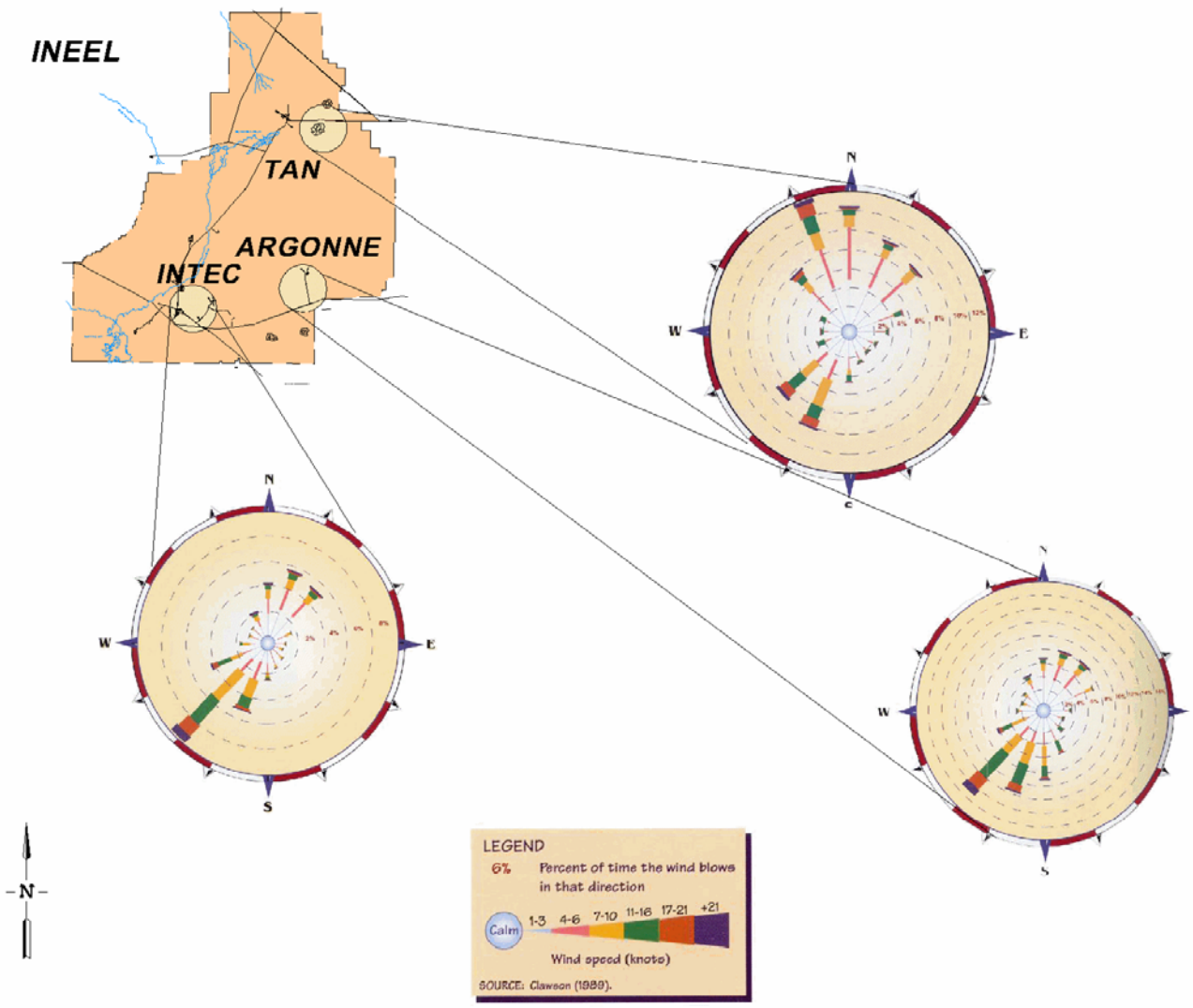

Figure 2-9. Annual average wind direction and speed at INEEL meteorological monitoring stations.

Snowfall is a substantial contributor to total annual precipitation. Snowfall and snow depth records are available from the CFA monitoring station. Snowfall ranges from 6.7 to 60 in./yr (17 to 200 cm/yr) with an annual average of 28 in. (71 cm). Although snow falls mostly during November through April, it does occasionally fall during May, September, and October (Clawson, Start, and Ricks 1989). The maximum average monthly snowfall is 6.4 in. (16 cm), occurring in December. The water content of melted snow probably contributes between one-quarter and one-third of the average annual precipitation (Sehlke and Bickford 1993).

2.1.2.4 Evaporation. The potential annual evaporation from a saturated ground surface at the INEEL is approximately 36 in. (91 cm), with 80% of the evaporation occurring between May and October. During July, the warmest month of the year, the daily potential evaporation rate is approximately 0.2 in. (0.5 cm) (Hull 1989). Evaporation occurring during the remainder of the year is small. Actual evaporation rates are much lower than potential rates because the ground surface is rarely saturated. Transpiration by the native vegetation of the Snake River Plain is estimated at 5.9 to 9.1 in./yr (15 to 23 cm/yr). From late winter to spring, precipitation is most likely to infiltrate into the ground because of the

low evapotranspiration rates (Mundorff, Crosthwaite, and Kilburn 1964). For evaporation from surface water bodies (ponds), a pan evaporation rate of approximately 42.9 in./yr (109 cm/yr) has been estimated (Clawson, Start, and Ricks 1989).

2.1.2.5 Relative Humidity. Average relative humidity at CFA ranges from a monthly average minimum of 15% in August to a monthly average maximum of 89% in December and February. On a daily basis, humidity reaches a maximum just before sunrise, at the time of the lowest temperature, and a minimum late in the afternoon, near the time of the highest temperature.

2.1.2.6 Tornadoes. Most of the tornado activity in the U.S. occurs east of the Rocky Mountains. In Idaho, tornadoes have been reported only in the spring and summer seasons (April through August). In the 42-year period of 1916 through 1957, 19 tornadoes were reported in Idaho. With expanding population and better surveillance methods, the average number of tornadoes per year will probably continue to increase slowly in Idaho. Compared to areas in the Midwest, however, the frequency will remain very small. With very few tornadoes occurring in the state per year, the chances of any one location being struck are remote.

When taken in context with maximum atmospheric moisture content, surrounding geography, and other statistics, the national tornado statistics allow a realistic assessment of tornado risk and establish a value for the maximum credible tornado expected at the INEEL. For the years 1950 to the present, the NOAA record indicates there have been a total of five funnel clouds sighted within the boundaries of the INEEL. The calculated return period for a tornado on the INEEL with wind speeds exceeding 120 mph (190 km/hr) is 1E+06 years (Coats and Murray 1985).

2.1.2.7 Dust Devils. Although tornadoes are rare at the INEEL, the whirling winds of the less violent dust devils are common. These dust devils pick up dust and pebbles and can overturn, blow down, or carry off insecure objects. They usually occur on warm, sunny days with little or no wind. The dust cloud may be several hundred yards in diameter and extend several hundred feet into the air.

2.1.2.8 Hurricanes and Tropical Storms. Because of the moderating influence of the Pacific Ocean and the isolating influence of surrounding mountains, neither hurricanes nor tropical storms occur at the INEEL.

2.1.2.9 Precipitation Extremes. The highest precipitation extremes at the INEEL (regardless of location) are cited in Table 2-2 (NOAA 1984). The greatest amounts recorded during 1-hr and 24-hr periods are listed monthly and annually. The high hourly amounts during May and June were the result of heavy thunderstorms passing over the rain gauge. The maximum for one hour was 1.15 in. (2.92 cm) at Test Area North (TAN). Precipitation amounts greater than 1 in./d (3 cm/d) have occurred during 10 of the calendar months within the period of record. Some months have had multiple occurrences.

2.1.3 Ecology

2.1.3.1 Flora. In 1975, the INEEL Site was dedicated as one of five DOE National Environmental Research Parks. It is an outdoor laboratory used to study ecological relationships and the effects of human activities on natural systems. In addition, it provides a unique setting for scientific investigation because the public has been excluded from much of the area for the past 25 yr. Ecological data collected from the Idaho National Environmental Research Park provide a basis for analyzing environmental changes over time and assessing the effect of human influence on the environment.

Research on the flora and fauna of the INEEL Site has largely been conducted by or in conjunction with the DOE Radiological and Environmental Sciences Laboratory (RESL). The physical aspects of the INEEL Site and its flora and fauna are typical of cold, high altitude, sagebrush ecosystems found in many parts of the western United States. The following discussion of the flora and fauna at the INEEL is from the

Table 2-2. Greatest precipitation measured at the INEEL (regardless of location).[a]

Month	1-hr[b] (in.)	24-hr[c] (in.)
January	0.18	1.08
February	0.18	0.96
March	0.17	0.61
April	0.24	1.51
May	1.00	1.78
June	1.15	1.73
July	0.24	1.33
August	0.45	1.44
September	0.55	1.55
October	0.34	1.12
November	0.25	1.02
December	0.23	1.18
Maximum	1.15	1.78

a. Source: NOAA 1984.

b. From January 1950 through December 1964; hourly amounts were not available from 1965 through 1982.

c. From January 1950 through December 1982.

Environmental Resource Document for the Idaho National Engineering Laboratory (Irving 1993). This report contains additional detailed information and references to specific ecological studies. The common and scientific names for the flora discussed here are presented in Table 2-3. For ease of reading, only the common names are used in this discussion.

Extensive surveys of INEEL vegetation were carried out in 1952, 1958, and 1967 using 150 permanent transects established and maintained for this purpose (Harniss and West 1973). Reports by McBride et al. (1978) and Jeppson and Holte (1978) also have described vegetation.

The common vegetation type, found on approximately 80% of the INEEL Site, is a mixture of big sagebrush, green rabbitbrush, and perennial grasses. Most of the trees on the INEEL Site are scattered along the Big Lost River and the Twin Buttes area. Figure 2-10 depicts the distribution of vegetation at the INEEL.

Vegetation in low-lying areas and along playa borders consists primarily of alkaline-tolerant species including shadscale saltbush, nuttal saltbush, and winterfat. Important associated grasses are bottlebrush squirreltail, giant wildrye, and Indian ricegrass.

Prickly pear, painted milkvetch, and skeletonweed are common in sandy areas in the north. Willows, baltic rush, and povertyweed grow along the Big Lost River channel.

Several studies have been conducted at the INEEL on the plant rooting depths, especially for the RWMC Subsurface Disposal Area (SDA). Vegetation studies of plant uptake of radionuclides at the INEEL have focused primarily on (a) determining if deep-rooted plants are a mechanism for waste pit intrusion and subsequent

Table 2-3. Flora at the INEEL Site.

Common Name	Latin Name
Cactus Family—*Cactaceae*	
Coryphantha	*Coryphantha* sp.
Prickly pear cactus	*Opuntia polyacantha*
Goosefoot Family—*Chenopodiaceae*	
Shadscale saltbush	*Atriplex confertifolia*
Nuttall saltbush	*Atriplex nuttallii*
Winterfat	*Ceratoides lanata*
Summer cypress	*Kochia scoparia*
Povertyweed	*Monolepsis nuttalliana*
Russian thistle	*Salsola kali*
Composite or Aster Family—*Compositae*	
Big sagebrush	*Artemisia tridentata*
Threetip sagebrush	*Artemisia tripartite*
Hoary false-yarrow	*Chaenactis douglasii*
Green rabbitbrush	*Chrysothamnus viscidiflorus*
Skeleton weed	*Lygodesmia grandiflora*
Common dandelion	*Taraxacum officinale*
Gray horsebrush	*Tetradymia canescens*
Goatsbeard or yellow salsify	*Tragopogon dubius*
Mustard Family—*Cruciferae*	
Flixweed tansy mustard	*Descurainia Sophia*
Grass Family—*Gramineae*	
Crested wheatgrass	*Agropyron cristatum*
Bluebunch wheatgrass	*Agropyron spicatum*
Cheatgrass	*Bromus tectorum*
Giant wildrye	*Elymus cinereus*
Indian ricegrass	*Oryzopsis hymenoides*
Bottlebrush squirreltail	*Sitanion hystrix*
Rush Family—*Juncaceae*	
Baltic rush	Juncus balticus
Pea Family—*Leguminosae*	
Painted milkvetch	*Astragalus ceramicus* Sheld. var. *apus* Barneby
Thistle milkvetch	*Astragalus kentrophyta* Gray var. *kentrophyta*
Woolly-pod milkvetch	*Astragalus purshii* Dougl. var. *ophiogenes* Barneby
Phlox Family—*Polemoniaceae*	
Large-flowered gymnosteris	*Gymnosteris nudicaulis* Greene
Longleaf phlox	*Phlox longifolia*
Buckwheat Family—*Polemoniaceae*	
Buckwheat	*Oxytheca dendroides*,[a] Nutt.
Willow Family—*Salicaceae*	
Willows	*Salix* sp.
Parsley Family—*Umbelliferae*	
Desert parsley	*Lomatium* sp.

a. Source: Hitchcock and Cronquist 1974.

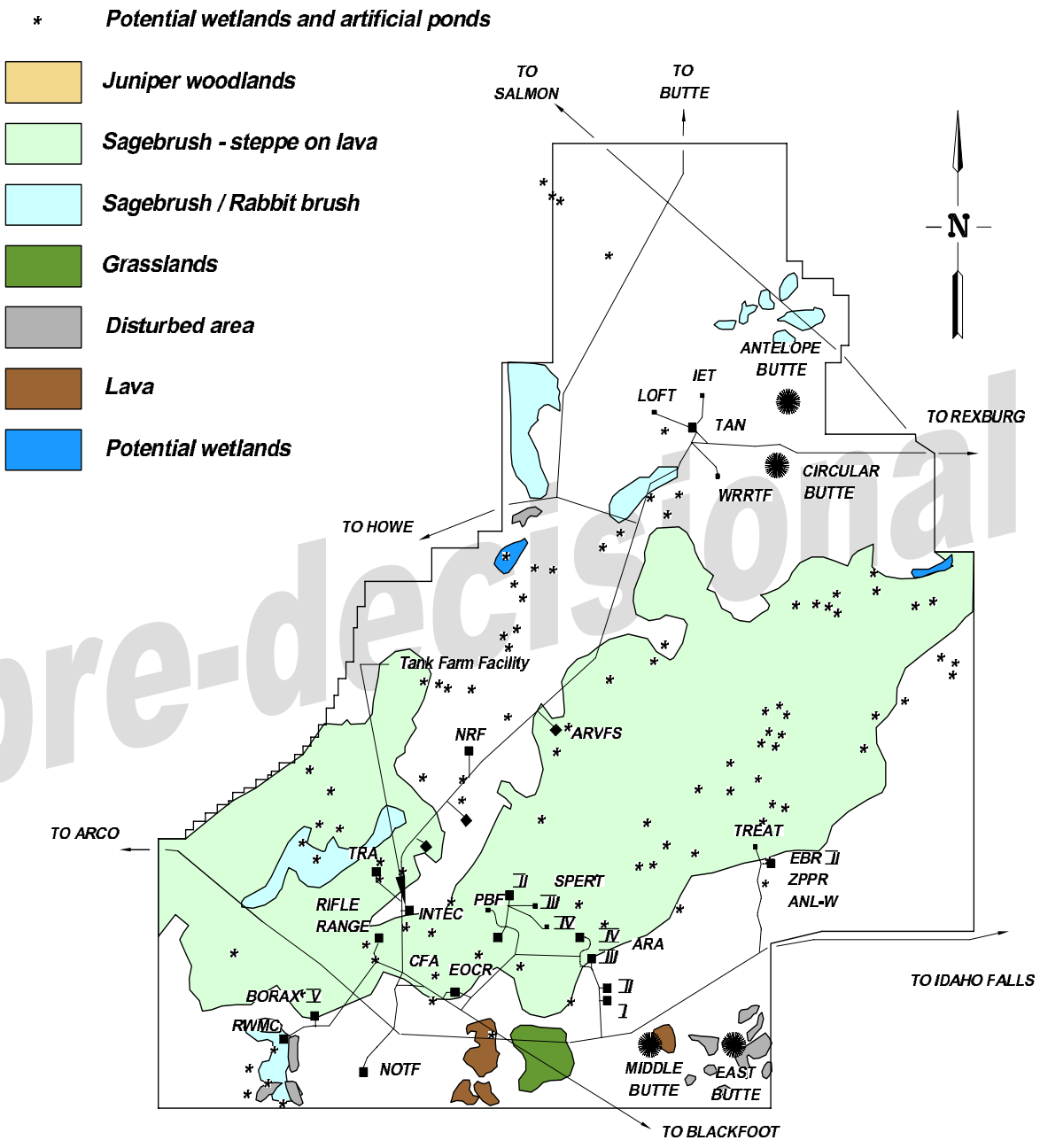

Figure 2-10. Approximate distribution of vegetation at the INEEL (INEEL 1999b).

uptake of radionuclides, and (b) analyzing inventories of radionuclides in aerial portions of plants. Aerial portions of plants are important because they can potentially transport subsurface contaminants through dispersal of leaves, consumption by herbivores, and use by birds as nesting materials.

One RWMC SDA study compared radionuclide uptake by crested wheatgrass (rooting depth 3 to 4.9 ft [0.9 to 1.5 m]) to that of Russian thistle (rooting depth 3 to 16 ft [0.9 to 4.9 m]). The study showed higher radionuclide concentrations in the deeper-rooted species (Arthur 1982). Examples of other deep-rooting species are rabbitbrush and sagebrush. General examples of shallow-rooting plant types are grasses and annual forbs.

Reynolds and Fraley (1989) found that the roots of big sagebrush extended to a depth of 88.7 in. (225 cm), green rabbitbrush to a depth of 74.9 in. (190. cm), and Great Basin wildrye had roots up to 78.8 in. (200. cm) deep at the SDA. Maximum lateral spread of the roots of both big sagebrush and Great Basin wildrye was 35.5 in. (90.2 cm) and occurred at a depth of 15.8 in. (40.1 cm). In addition, studies indicate root penetration of up to 5.2 ft (1.6 m) for sodar and crested wheatgrass at the INEEL (Markham 1987).

A survey of rare plants on the INEEL Site was initiated in 1980 (Cholewa and Henderson 1984). The survey identified the following plants: painted milkvetch and woolly-pod milkvetch, which were under federal review for endangered or threatened status; coryphantha, large-flowered gymnosteris, and oxytheca, on the Idaho State Watch List; and thistle milkvetch, which was previously unknown to occur in Idaho. Since then, painted and woolly-pod milkvetch have been removed from endangered or threatened candidate status (Mosely and Groves 1990).

2.1.3.2 Fauna. The INEEL supports a variety of wildlife including small mammals, birds, reptiles, and a few large mammals. The common and scientific names for the fauna discussed here are presented in Table 2-4. For ease of reading, only the common names are used in this discussion.

The mammals include chipmunks, ground squirrels, several species of mice, kangaroo rats, cottontail rabbits, bats, jackrabbits, and coyotes. Commonly occurring game animals are sage grouse, mourning dove, elk, pronghorn, and mule deer.

Limited data are available on the number of game animals seasonally inhabiting the INEEL and the harvest of these animals by hunters. Pronghorn inhabit the INEEL during the entire year; however, many are migratory and summer to the north of the INEEL. Pronghorn often bear young within the INEEL.

Aquatic life on the INEEL is limited and depends mainly upon the flow of the Big Lost River. During several months of the year, and even during some entire years, the river does not flow. However, during spring runoff and periods of high rainfall, the diversion system (at the southern boundary of the INEEL) and the Big Lost River sinks (at the northern boundary of the INEEL) support water flow when water accumulates. This normally occur less than 2 or 3 months in the spring. Fish species observed in the Big Lost River on the INEEL include rainbow trout, mountain whitefish, eastern brook trout, Dolly Varden char, Kokanee salmon, and shorthead sculpin (Overton et al. 1976).

An investigation of amphibians and reptiles within the INEEL was conducted from May through September 1975 (Reynolds et al. 1986). The Great Basin spadefoot toad was the only amphibian recorded, typically associated with the Big Lost River, the Big Lost River sinks, and the spreading areas near the RWMC. The sagebrush lizard and the short-horned lizard are common; the sagebrush lizard is the most abundant reptile. The western skink and the leopard lizard also have been observed. Four species of snakes, including the Great Basin rattlesnake and Great Basin gopher snake, were recorded. The western terrestrial garter snake and the desert-striped whipsnake are present in lesser numbers and have more restricted distributions.

Table 2-4. Fauna at the INEEL.

Common Name	Latin Name
Fish[a]	
Rainbow trout	*Salmo gairdneri*
Eastern brook trout	*Salvelinus fontinalis*
Dolly varden char	*Salvelinus malma*
Kokanee salmon	*Oncorhynchus nerka*
Mountain whitefish	*Prosooium williamsoni*
Shorthead sculpin	*Cottus confuses*
Reptiles and Amphibians[b]	
Leopard frog	*Rana pipiens*
Great Basin spadefoot toad	*Spea intermontanus*
Leopard lizard	*Gambelia wislizenii*
Sagebrush lizard	*Scel6porus graciosus*
Short-horned lizard	*Phrynosoma douglassi*
Western skink	*Eumeces skiltonianus*
Desert-striped whipsnake	*Masticophis taeniatus*
Great Basin gopher snake	*Pituophi-s melanoleucus*
Western Terrestrial garter snake	*Thamnophis elegans*
Great Basin rattlesnake	*Crotalus viridis*
Mammals[c]	
Family—*Canidae*	
Coyote	*Canis latrans*
Family—*Felidae*	
Bobcat	*Lynx rufus*
Family—*Antilocapridae'*	
Pronghorn	*Antilocapra americans*
Family—*Cervidae*	
Mule deer	*Odocoileus hemionus*
Elk	*Cervus canadensis*
Family—*Vespertilionidae*	
Big-brown bat	*Eptesicus fuscus*
Townsend's big-eared bat	*Plecotus townsendii*
Family—*Leporidae*	
White-tailed jackrabbit	*Lepus townsendii*
Black-tailed jackrabbit	*L. californicus*
Nuttall's cottontail	*Sylvilagus nuttallii*
Family—*Sciuridae*	
Least chipmunk	Tamias minimus
Townsend's ground squirrel	*Spermophilus townsendii*
Family—*Geomyidae*	
Northern pocket gopher	Thomomys talpoides
Family—*Heteromyidae*	
Ord's kangaroo rat	*Dipodomys ordii*
Family—*Cricetidae*	
Western harvest mouse	*Reithrodontomys megalotis*
Deer mouse	*Peromyscus maniculatus*

Table 2-4. (continued).

Common Name	Latin Name
Birds[d]	
Family—*Accipitridae*	
Golden eagle	*Aquila chrysaetos*
Ferruginous hawk	*Buteo regalis*
Bald eagle	*Haliaeetus leucocephalus*
Family—*Falconidae*	
Merlin	*Falco columbarius*
Prairie falcon	*Falco mexicanus*
Peregrine falcon	*Falco peregrinus*
Family—*Phasianidae*	
Sage grouse	*Centrocercus urophasianus*
Family—*Scolopacidae*	
Long-billed curlew	*Numenius americanus*
Family—*Strigidae*	
Burrowing owl	*Athene cunicularia*
Family—*Columbidae*	
Mourning dove	*Zenaida macroura*
Family—*Corvidae*	
Blackbilled magpie	*Pica pica*
Family—*Mimidae*	
Sage thrasher	*Oreoscoptes montanus*
Family—*Turdidae*	
American robin	*Turdus migraturius*
Family—*Tyrannidae*	
Say's phoebe	*Sayornis saya*
Family—*Alaudidae*	
Horned lark	*Eremophila alpestris*
Family—*Emberizidae*	
Western meadowlark	*Sturnella neglecta*
Sage sparrow	*Amphispiza belli*
Brewer's sparrow	*Spizella breweri*

a. Source: Simpson and Wallace 1978.
b. Source: Nussbaum, Brodie, and Storm 1983.
c. Source: Jones, Carter, and Genoways 1979.
d. Source: American Ornithologist's Union 1983.

A total of 740 insect species have been recorded at the INEEL; 226 of these species have not yet been identified beyond the family level. The majority of the abundant species belong to the orders Hymenoptera (wasps and ants) and Diptera (flies). About half of the abundant species are parasitic or predatory.

Over 185 species of birds have been recorded on the INEEL, and about 60 of these species probably breed on the INEEL. Many of the bird species are relatively uncommon, and only a few species are very abundant. The most common species are the Brewer's sparrow, sage thrasher, sage sparrow, horned lark, sage grouse, mourning dove, western meadowlark, blackbilled magpie, and robin (Reynolds et al. 1986).

Species on the INEEL that merit special consideration because of their sensitivity to disturbance or their threatened status include the ferruginous hawk, merlin, long-billed curlew,

Townsend's big-eared bat, common loon, white pelican, great egret, and trumpeter swan (Reynolds et al. 1986; Mosely and Groves 1990). The bald eagle and peregrine falcon are on the Federal Endangered Species List and occasionally visit the INEEL.

Studies have been performed on burrowing characteristics of small mammals such as ground squirrels, deer mice, and voles (Arthur, Grant, and Markham 1983; Markham 1987; Reynolds and Laundre 1988). Results of the studies indicate burrows no deeper than 140 cm (55 in.) at the INEEL.

2.1.4 Geology, Seismology, and Volcanology

2.1.4.1 Regional and Site-Specific Geology. The bulk of the geology sections in this report are taken primarily from previous work conducted by Maheras et al. (1994) and Anderson, Kuntz, and Davis (1999). The INEEL is located on the west-central part of the ESRP, a northeast-trending structural basin about 200 mi (300 km) long and 50 to 70 mi (80 to 100 km) wide (Figure 2-11). The INEEL is underlain by a sequence of Tertiary and Quaternary volcanic rocks and sedimentary interbeds that are more than 10,000 ft (3,000 m) thick (Whitehead 1992). The volcanic rocks consist mainly of basalt flows in the upper part of the sequence and rhyolitic ash-flow tuffs in the lower part. Basalt and sediment generally range in age from about 200 thousand to 4 million years before present (Anderson, Liszewski, and Cecil 1997), and underlie the plain at depths ranging from about 2,200 to 3,800 ft (670 to 1,200 m) below ground surface (bgs).

Hundreds of basalt flows, basalt-flow groups, and sedimentary interbeds underlie the INEEL. Basalt makes up about 85% of the volume of deposits in most areas. A basalt flow is a solidified body of rock formed by the surficial outpouring of molten lava from a vent or fissure (Bates and Jackson 1980). A basalt-flow group consists of one or more distinct basalt flows deposited during a single, brief eruptive event. All basalt flows of a group erupted from the same vent or several nearby vents represent the accumulation of one or more lava fields from the same magma and have similar geologic ages, paleomagnetic properties, potassium contents, and natural-gamma emissions (Anderson and Bartholomay 1995). The basalt flows consist mainly of medium- to dark-gray vesicular to dense olivine basalt. Individual flows generally range from 10 to 50 ft (3 to 20 m) thick, and are locally interbedded with scoria and thin layers of sediment. Sedimentary interbeds are as thick as 50 ft (20 m) and consist of well-sorted to poorly-sorted deposits of clay, silt, sand, and gravel. In places, the interbeds contain or consist mainly of scoria and basalt rubble. Sedimentary interbeds accumulated on the ancestral land surface for hundreds to hundreds of thousands of years during periods of volcanic quiescence and are thickest between basalt-flow groups.

At least 178 basalt-flow groups and 103 sedimentary interbeds underlie the INEEL above the effective base of the aquifer (Anderson, Ackerman, and Liszewski 1996; Anderson, Liszewski, and Cecil 1997). Basalt-flow groups and sedimentary interbeds are informally referred to as A through S5. Basalt-flow groups LM through L, and related sediment, range in age from about 200 to 800 thousand years old and make up the unsaturated zone and the uppermost areas of the INEEL. Most wells in the southern and eastern parts of the INEEL are completed in basalt-flow groups AB through I and the related sediments. Flow groups AB through I and related sediments range in age from about 200 to 640 thousand years old and make up a stratigraphic section characterized by horizontal to slightly inclined layers. Anderson, Liszewski, and Cecil (1997) estimated the geologic ages of basalts and sediments in the unsaturated zone and the Snake River Plain Aquifer to be from about 200 thousand to 1.8 million years; average accumulation rates are reflective of a subsidence rate of 164 ft (50.0 m)/100,000 yr.

The nomenclature for the stratigraphy underlying the INTEC facility and the surrounding area is based on work presented by Anderson (1991). A north-south geologic cross section, illustrated in Figure 2-12, forms the framework for the conceptual model and numerical simulations discussed in Sections 3 and 4.

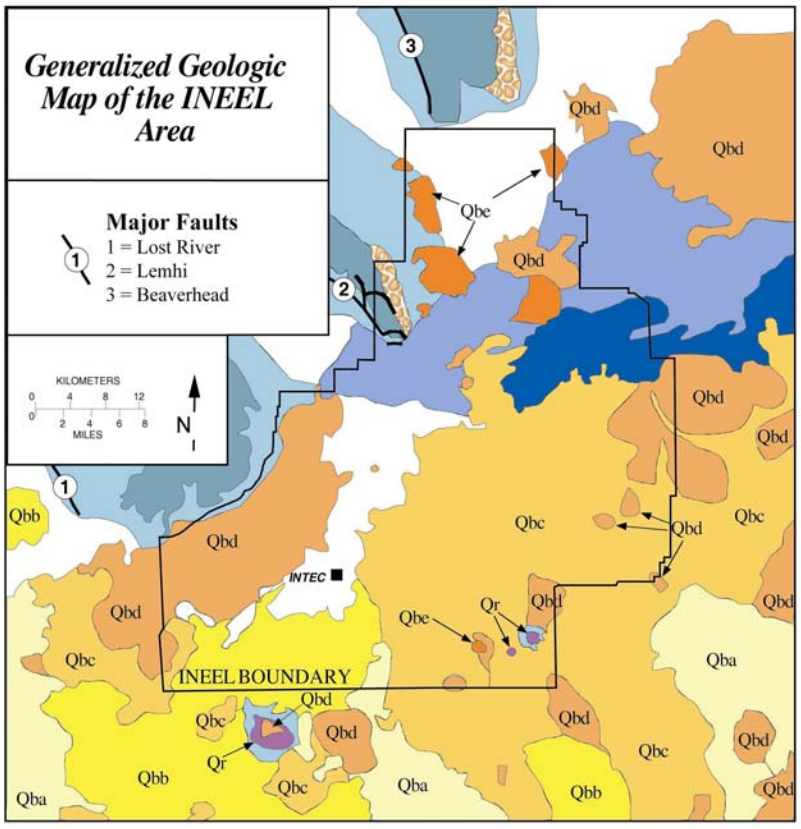

Deposits

Mainstream Alluvium. Includes deposits of modern floodplains (Holocene) and older deposits in terraces above modern floodplains (upper to middle Pleistocene). Composed mostly of gravel and sand with minor silt and clay. Older deposits host well-developed soils and partial to complete loess cover. Up to 20 m thick in southern INEEL, and much thicker in mainstreams to the north.

Alluvial Fans Deposits. Debris flow and stream deposits of clast-supported pebble and boulder gravels with matrix of silty sand to clayey silt (Holocene to upper Pliocene). Middle to lower Pleistocene units commonly locally faulted along the west flanks of the Lost River, Lemhi, and Beaverhead ranges. Includes colluvial debris fans on steep slopes of East, Middle, and Big Southern Buttes.

Eolian Deposits. Very fine to coarse sand in mostly stabilized dunes, 1 to 5 m thick. Some areas of active deflation and migrating sand (Holocene to upper Pleistocene).

Lacustrine Deposits. Mostly lake-floor deposits of Pleistocene Lake Terreton. Silty clay to sandy silt, 1 to >100 m thick. Locally includes sandy lake margin deposits and Holocene playa deposits.

Bedrock Units

Basaltic Lava Flows. Black to gray pahoehoe and 'a'a lava flows, with bedded, oxidized, scoria, cinders, and ash near vents. Locally weathered and oxidized. Olivine basalts composed of crystals of olivine, pyroxene, plagioclase, titanomagnetite, and ilmenite in a matrix of brown glass.

Qba Holocene to uppermost Pleistocene (<15K yr). No cover of eolian or alluvial deposits.

Qbb Upper to Middle Pleistocene (15–200K yr). Locally covered by up to 1 m of eolian sand and loess.

Qbc Middle Pleistocene (200–400K yr). Covered by as much as several meters of eolian sand and loess.

Qbd Middle to Lower Pleistocene (400–730K yr). Mostly covered by several meters of eolian sand and loess.

Qbe Lower Pleistocene (>730K yr). Mostly covered by several meters of eolian sand and loess. Reversed magnetic polarity.

Quaternary Rhyolite

Qr **Rhyolite Domes.** Pleistocene (0.3–1.2M yr) tan to pink, flow laminated rhyolite, with minor vent breccia and banded obsidian composed of microcrystalline intergrowths of quartz, and alkali feldspar with rare phenocrysts of quartz clinopyroxene and magnetite.

Tertiary Volcanics

Volcanic Rocks. Basaltic lava flows, rhyolitic ash flow tuffs, and rhyolitic lava flows. Mostly Miocene and Pliocene (about 4–12M yr).

Pre-Tertiary Rocks

Pre-Tertiary Rocks. Late Precambrian to Triassic. Mostly Mississippian shelf carbonates of the Overthrust Belt. Also includes Permian to Triassic fine clastic deposits and phosphatic silts; Cambrian to Ordovician quartzites, sandstone, conglomerates, and siltstones; Devonian dolostones and argillites; and Precambrian sandstones and quartzites.

Figure 2-11. General geologic map of the INEEL (Kuntz et al. 1994).

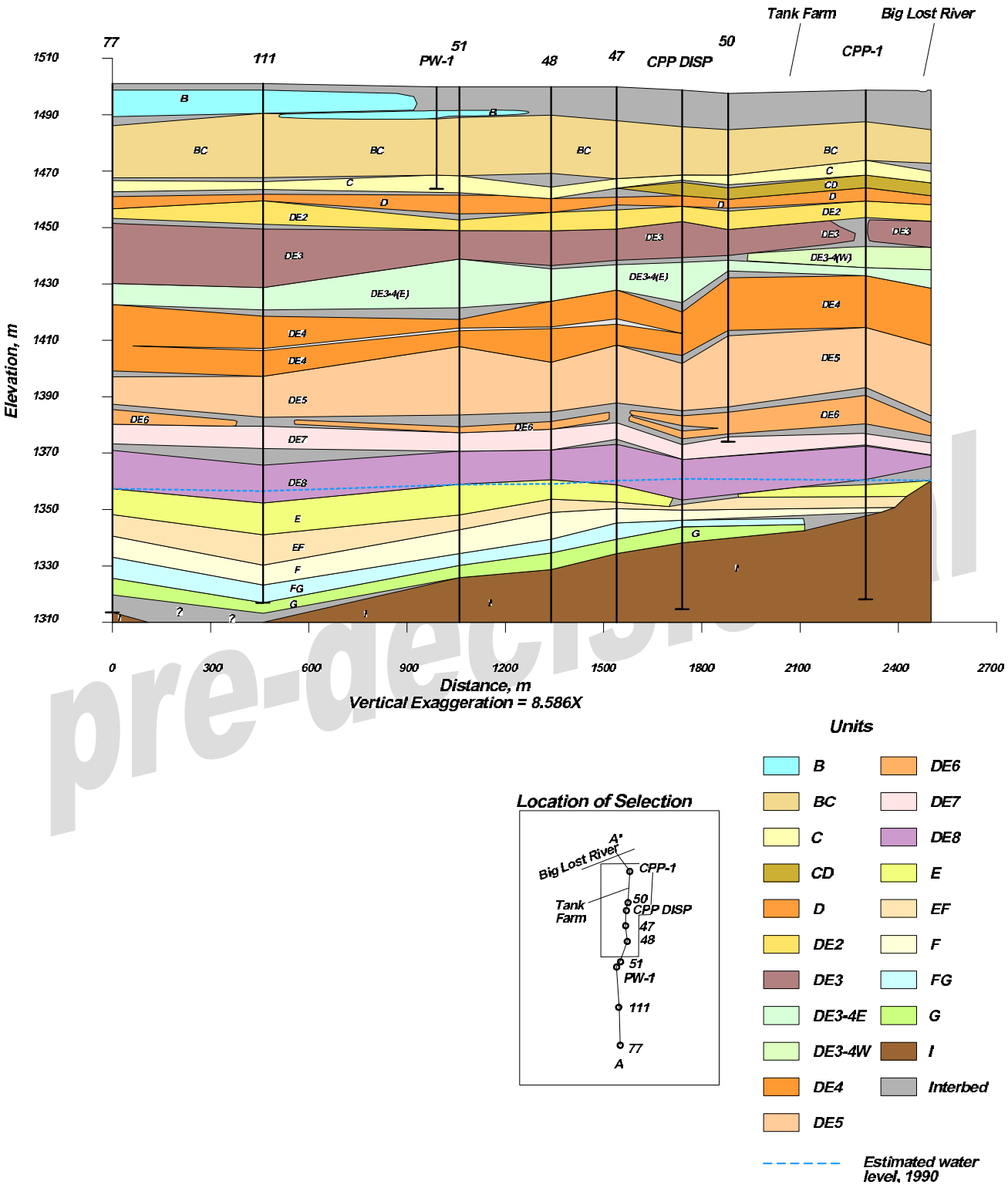

Figure 2-12. North-south geological cross section.

The stratigraphy of the aquifer at and near INTEC is dominated by thick, massive basalt flows of flow group I and thin, overlying flows of flow groups B through H. The basalt flows, as interpreted, appear to be relatively uniform in thickness beneath INTEC. Significant changes in the flow thickness are often related to changes in the lithology of the flow or are caused by the flow margins in which the flow appears as a lobe of basalt. The lithologic changes that may cause a change in the flow thickness are the existence of pyroclastic deposits on or within a flow, or a flow being very vesicular, and thus, more susceptible to the effects of erosion.

Based on the Anderson (1991) geologic cross section, the unsaturated zone and upper regional aquifer underlying INTEC are comprised of 19 basalt-flow groups, 11 sedimentary interbeds, and surficial alluvium. The characteristics of these individual flow groups and their impact on the site hydrology are discussed in detail in Section 3. The sediments, as interpreted, appear to be primarily made up of sands and silts with some small clay lenses. The majority of the sediments are thin 1- to 5-ft (0.3- to 2-m) layers of silt between the major basalt flows. Sediments were most likely deposited in eolian or fluvial type environments. Two major sediment sequences are shown on the cross sections: the upper sequence associated with the CD, thick D, and DE2 sands and silts and the lower sediments associated with the DE6, DE7, and DE8 stratigraphic units.

The cross sections show a very thick sequence of sediments, particularly in the northern end of the north-south section, which are stratigraphically shown as the CD, D, and DE2 units. These sediments appear to be a thick sequence of sands over and underlain by silts and clays. The sediments associated with the DE6, DE7, and DE8stratigraphic units appear to be made up of gravels, silts, and clays. These sediments were most likely deposited in a fluvial environment and may indicate a braided stream deposit. This is the last major sediment deposit above the Snake River Plain Aquifer.

Holocene surficial geology and archaeology suggest that fluvial and eolian deposition and tectonic subsidence in the INEEL area have been in approximate net balance for at least the past 10,000 yr. A reversal of the long-term, regional pattern of ESRP subsidence, sedimentation, and volcanism into an erosional rather than a depositional regime would require major changes from the Holocene tectonic or climatic configuration of the ESRP. Worldwide geologic evidence indicates that the Quaternary epoch (approximately the past 2 million years) has been a time of major climatic fluctuations. During colder and wetter periods, glaciers occupied high-elevation areas. Lowland areas such as the ESRP received thick, widespread loess blankets. Lowland areas also were periodically impacted by local catastrophes (such as the large, late-Pleistocene, glacial outburst flood(s) that traveled down the Big Lost River Valley), eroded upland surfaces on the ESRP and deposited sediment in the INTEC area. If the future ESRP climate were to become warmer and more arid, the probable consequences would be decreased vegetation and increased eolian transport of fine-grained sediment, mainly as longitudinal dunes of fine sand.

Future climate fluctuations on the ESRP (to either colder/wetter or warmer/drier conditions) are not expected to erode the INTEC land surface. Quaternary geologic and Holocene archaeological data suggest the INEEL area will probably continue its long-term history of regional subsidence and net accumulation of sedimentary and volcanic materials, although sedimentation patterns on the ESRP will change in response to future climate fluctuations.

INTEC soil cover erosion could occur as a consequence of faulting and uplift but this erosion would involve a major change in the Quaternary tectonic configuration of the ESRP. Therefore, this scenario is improbable within the next 10,000 yr, considering

- The regional seismicity and tectonic history of the INEEL area
- The absence of Quaternary tectonic faults on the ESRP in the vicinity of the INEEL

- The long response time for significant erosion to occur as a result of protracted faulting and uplift.

In summary, the following impacts from volcanic and tectonic activity are relevant to INTEC radiological performance assessment:

- During the past 4 million years, the ESRP and the INTEC area have undergone regional subsidence, basaltic volcanism, and fluvial and eolian sedimentation. Erosion has not been a significant process on the ESRP.

- Surficial- and subsurface-geologic data indicate that the INTEC area has both subsided and accumulated basalt lava flows and sediments at an average rate of 0.01 in./yr (0.25 mm/yr). Significant uplift or erosion has not interrupted this long-term trend.

- Lava inundation or magma intrusion associated with volcanism from the nearby Arco Volcanic Rift Zone is improbable considering the volcanic history of the area. Lava inundation or magma intrusion would not likely result in the release of radionuclides to the environment.

Detailed discussions of the site geology and stratigraphy are presented in Anderson (1991) and Anderson, Liszewski, and Cecil (1997).

2.1.4.2 Seismology. The seismically active Intermountain seismic belt surrounds the ESRP and Centennial Tectonic seismic belts. The Intermountain seismic belt is a zone of concentrated seismicity that extends from northwestern Montana through eastern Idaho and Utah into southern Nevada. The Centennial seismic belt, also a seismically active zone, extends from the Hebgen Lake, Montana, area westward into central Idaho.

The INEEL, USGS, Montana Bureau of Mines and Geology, United States Bureau of Reclamation, and the University of Utah Seismograph Stations have compiled earthquake data for 1884 to 1989 (shown in Figure 2-13). The distribution of epicenters indicates that the ESRP is devoid of earthquakes relative to the active areas surrounding it, with the possible exception of the 1905 earthquake located at Shoshone, Idaho. Historical records suggest that the epicenter for the 1905 earthquake is not located within the ESRP, but rather near the Idaho-Utah border.

A large earthquake, in the vicinity of the INEEL but outside the ESRP, occurred in the Centennial seismic belt on October 28, 1983, with a surface-wave magnitude (M) of 7.3. The earthquake resulted from slippage along the Lost River fault—a northwest rupture along a normal fault with relative vertical movement downward to the west. The epicenter for this event was located in the Thousand Springs Valley near the western flank of Borah Peak, approximately 55 to 60 mi (89 to 100 km) from INEEL facilities. There was substantial damage to masonry structures in the local communities of Mackay and Challis near the epicentral area. Although the earthquake ground motions were felt at the INEEL Site, only minor nonnuclear building damage occurred in the form of hairline cracks and settlement (Gorman and Guenzler 1983). INTEC did not experience structural failures or waste spills as a result of the earthquake and waste storage facilities did not show evidence of permanent movement or resulting damage. Peak ground accelerations ranging from 0.022 to 0.078 g were recorded at several INEEL facility areas. The INEEL was located in Modified Mercalli Intensity Zone VI during the earthquake (Jackson 1985).

The largest earthquake in the region occurred on August 17, 1959, at Hebgen Lake, Montana, located approximately 120 mi (190 km) northeast of the INEEL Site. The event had a surface-wave magnitude of 7.5; it was felt at the INEEL, but caused no damage there.

The INEEL has maintained a seismic network for monitoring earthquake activity on and around the ESRP since December 1971. Currently, the seismic network consists of 24 seismic stations and 21 strong-motion accelerographs. The seismic stations continually record seismic data and their data are used to calculate the locations and magnitudes of microearthquakes ($M < 3.5$) that occur locally. When triggered, the strong-motion accelerographs record earthquake ground motions from local, moderate to large, earthquakes.

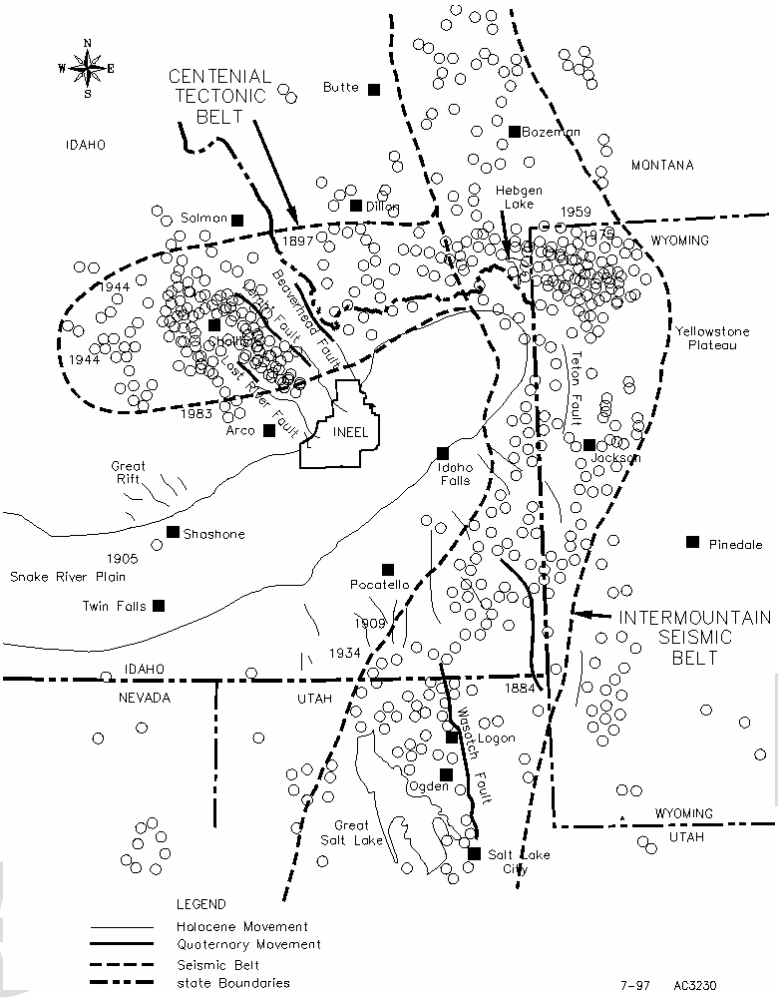

Figure 2-13. Seismicity map showing the ESRP in relation to the Intermountain seismic belt and the Centennial Tectonic belt (WCFS 1996).

From 1972 to 1990, approximately 15 microearthquakes occurred within the ESRP, indicating that infrequently-occurring, small magnitude earthquakes (M < 1.3) are characteristic of ESRP seismicity (Jackson et al. 1993; Pelton, Vincent, and Anderson 1990). These data are in agreement with the historical earthquake data compiled for the surrounding region (Figure 2-14). Recent modifications to the seismic network, such as placing sensors in 18- to 21-m (59- to 69-ft) boreholes, will lower the magnitude threshold of detecting microearthquakes within the ESRP.

Because the seismically-active Intermountain and Centennial seismic belts surround the ESRP, and several Quaternary faults are located near the western boundary of the INEEL, seismic hazard assessments are being updated for all facility areas at the INEEL. These assessments are being performed to quantitatively estimate peak ground motions that INEEL facilities may experience from nearby large magnitude earthquakes. Most of the INEEL is located in Seismic Zone 2B and a small portion is located in Zone 3. The seismic design levels for INEEL facilities exceed those required for these classifications.

Uplift and erosion of the INTEC area could result from faulting and uplift of the southern Lost River Fault if the fault encroached southward onto the ESRP to a position several kilometers west of INTEC. Assuming immediate initiation of this faulting and maximum-uplift rates from the most recently active fault segments of the nearby Basin and Range Province (1 to 2 m [3 to 7 ft]/1,000 yr),

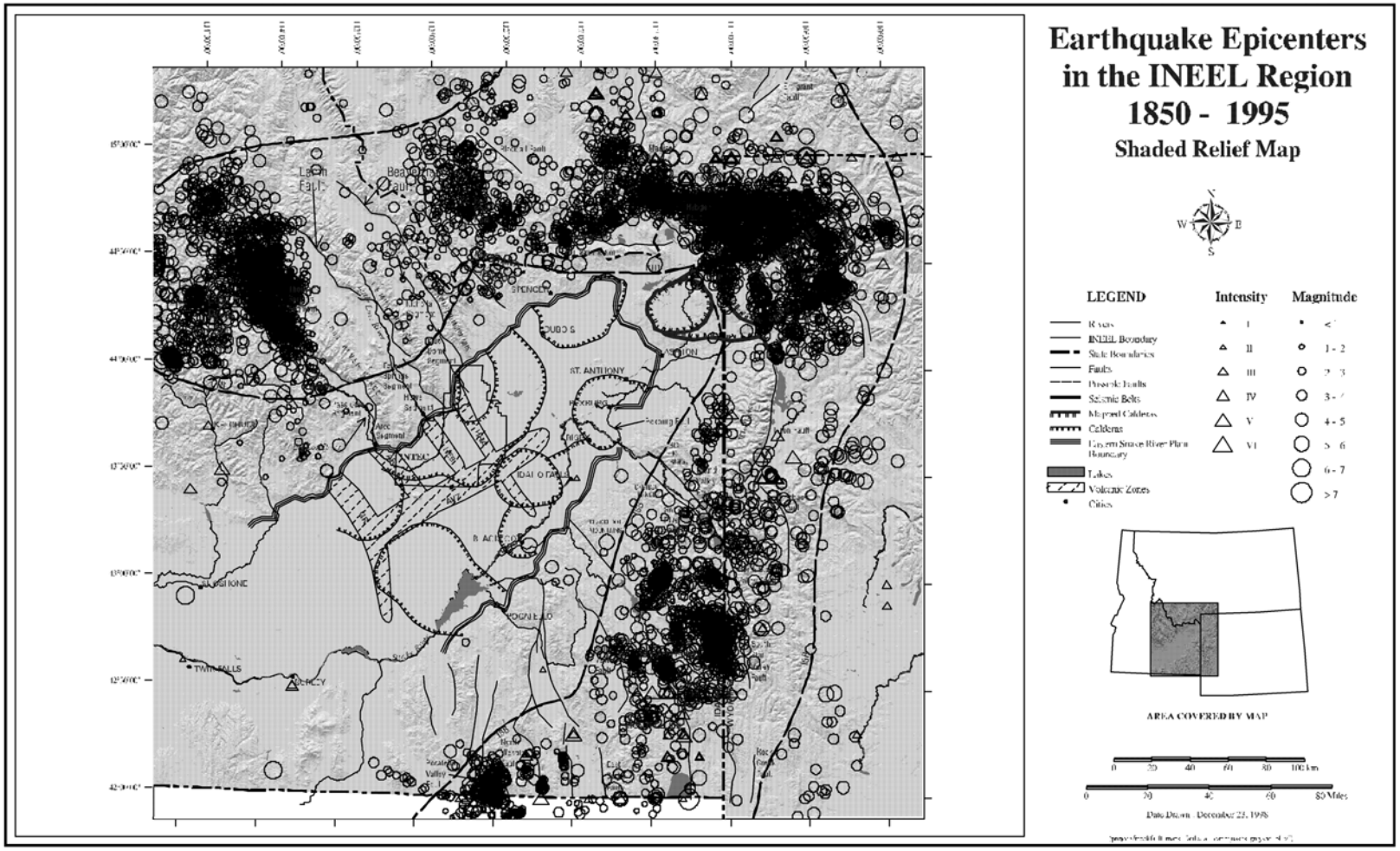

Figure 2-14. Earthquake epicenters in the INEEL region, 1850–1995 (INEEL 1999b).

significant uplift and erosion of the INTEC area would require 10,000 to 100,000 yr.

Additional information on seismic hazards for the region is presented in *Environmental Resource Document for the Idaho National Engineering Laboratory* (Irving 1993).

2.1.4.3 Volcanology. Most of the INEEL is underlain by a 0- to 0.6-mi (0- to 1-km) thick sequence of late Tertiary and Quaternary basalt lava flows and interbedded sediments. Based on drill-hole information, regional mapping along the margins of the ESRP, and geophysical information, the basalt/sediment sequence is underlain by an older section (up to several kilometers thick) of late Tertiary rhyolitic volcanic rock. These two volcanic sequences are a consequence of the passage of the Yellowstone mantle plume (hotspot) through the INEEL area of the ESRP in late Tertiary time (Malde 1991). The Tertiary rhyolitic volcanic rocks were erupted at 6.5 to 4.3 million annum (Ma) when the hotspot resided beneath the INEEL area. They consist mostly of ash-flow tuffs erupted during large, violent explosive episodes and large rhyolitic lava flows. They are analogous to the ash-flow tuffs and lava flows that erupted from calderas in the Yellowstone Plateau at 2.0 to 0.6 Ma.

These types of large-scale explosive eruptions can occur only directly over the mantle hotspot because large inputs of heat into the lower and middle crust are required to generate such large volumes of rhyolitic magma. Because the hotspot is now situated beneath Yellowstone National Park, recurrence of this type of volcanic activity in the INEEL area is nearly impossible. Residual heat in the upper mantle after passage of the hotspot has continued to produce basaltic magmas that have risen to the surface and erupted onto the subsiding ESRP. Basaltic eruptions in the INEEL area began at about 4 Ma, soon after passage of the hotspot, and have continued. The most recent activity occurred along the Great Rift about 2,100 yr ago.

Basalt vents on the ESRP include broad, nearly circular, low-relief shield volcanoes, small spatter cones, and spatter ramparts along eruptive fissures. Lava fields related to single vents range in surface area from 2 to 400 km^2 (0.7 to 154 mi^2) and in volume from 0.05 to 7 km^3 (0.01 to 1.7 mi^3) (Kuntz, Covington, and Schorr 1992). Volcanic vents are not randomly distributed on the ESRP; they are concentrated in northwest-trending linear zones known as volcanic rift zones (Figure 2-15). In addition, vents are concentrated in a northeast-trending zone, known as the Axial Volcanic Zone, along the central axis of the ESRP. The Axial Volcanic Zone is a constructional highland caused by more voluminous magma output along the axis of the ESRP.

Based on radiometric age determinations of basalt lava flows, the Arco Volcanic Rift Zone north of the Big Southern Butte was active between 600 and 100 kilo annum (Ka) (Kuntz, Covington, and Schorr 1992). The Cerro Grande and North and South Robbers flows (10,500 to 12,000 Ka) near the Big Southern Butte occur at the intersection of the Arco Volcanic Rift Zone and the Axial Volcanic Zone. Except for volcanism along the Great Rift, all of the Holocene volcanic fields of the ESRP occur along the Axial Volcanic Zone (Figure 2-15). Recurrence of volcanism in the ESRP has a greater likelihood of occurring along the Great Rift or the Axial Volcanic Zone.

Additional information on the site volcanism is presented in "Quarternary Volcanism, Tectonics, and Sedimentation in the Idaho National Engineering Laboratory Area" (Hackett and Smith 1992).

2.1.5 Hydrology

2.1.5.1 Surface Water. The following sections discuss the surface water hydrology of the region. References for further information on the surface water features and resources of the INEEL site include Lamke (1969), Carrigan (1972), Tullis and Koslow (1983), and Bennett (1990).

Most of the INEEL and all of INTEC are in the Pioneer Basin. The Pioneer Basin is a closed topographic depression on the ESRP that receives intermittent runoff from the Big Lost River, Little Lost River, and Birch Creek drainage (see Figure 2-16). The Pioneer Basin is not crossed by any perennial streams because of the permeability

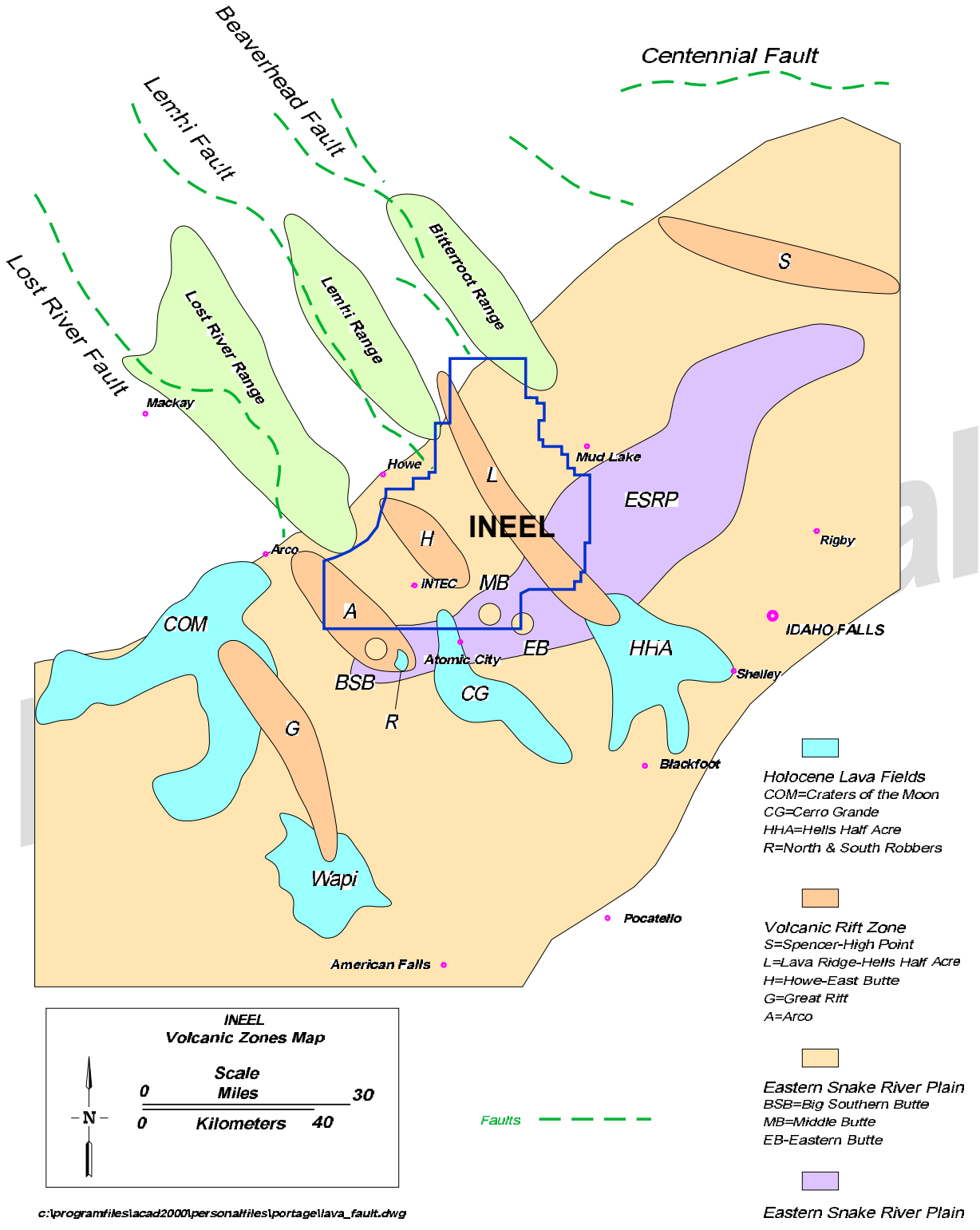

Figure 2-15. Volcanic rift zones at the INEEL.

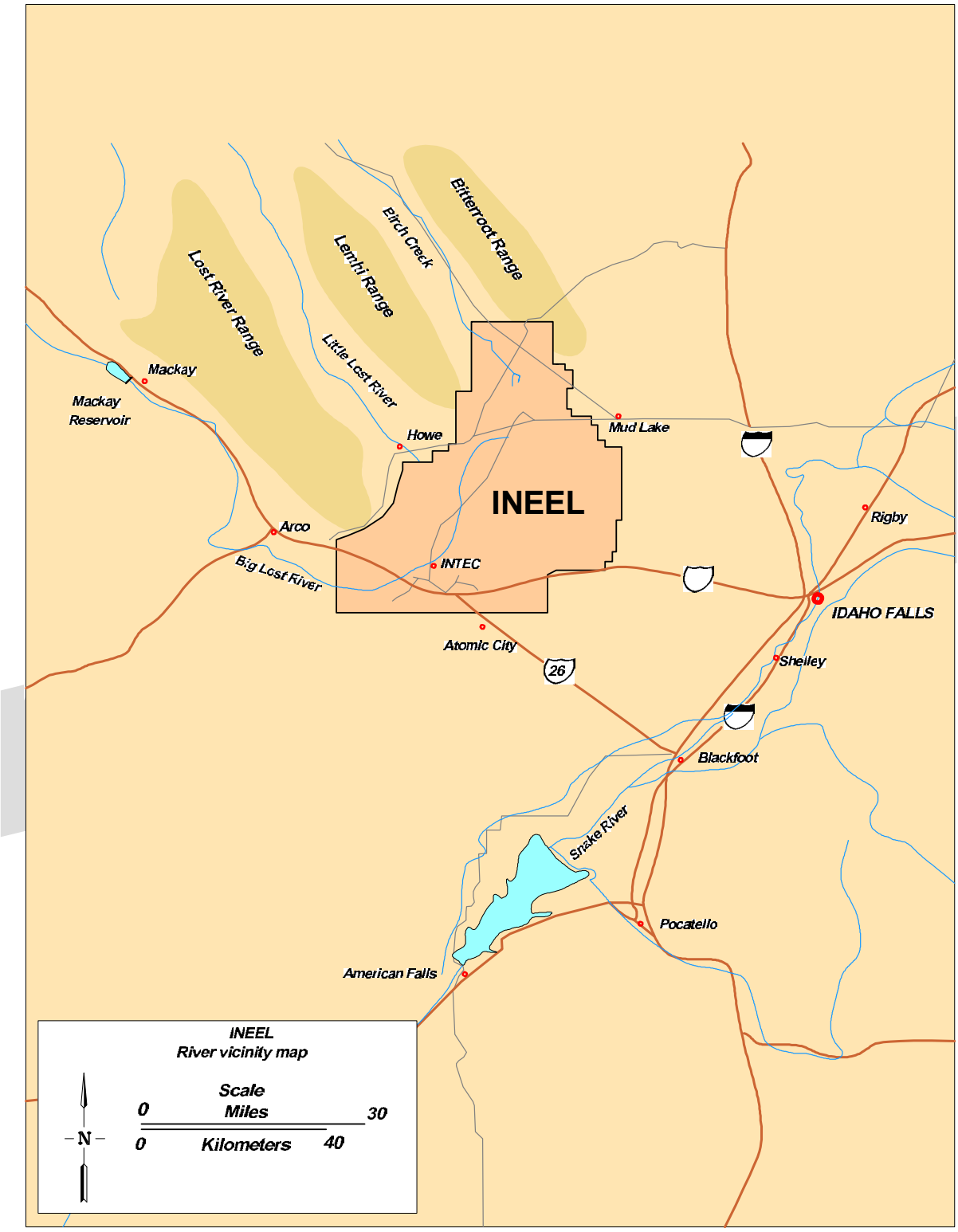

Figure 2-16. Surface water features of the INEEL and surrounding vicinity.

of alluvium and underlying rock of the basin, which causes the water to infiltrate into the ground. In addition, much of the water from the tributary drainage basins is diverted for irrigation upstream of the INEEL. The largest stream, the Big Lost River, enters the INEEL near the southern end from the west. During exceptionally wet years, the Big Lost River flows in a large arc north to the foot of the Lemhi Mountain Range, where it ends in a series of playas (sinks). The only other naturally occurring stream on-Site is Birch Creek, which enters from the north. This stream is usually dry, except during heavy spring runoff when water may flow onto the INEEL. The Little Lost River approaches the INEEL from the northwest through Howe and ends in a playa just off the INEEL Site.

The Big Lost River discharges an average of 211,000 acre-ft/yr (260E+08 m^3/yr) below Mackay Dam, 30 mi (50 km) northwest of Arco. The largest recorded annual flow of the Big Lost River for the entire period of record occurred in 1984 and amounted to 476,000 acre-ft/yr (5.87E+08 m^3/yr), which was measured below Mackay Dam. The second largest annual flow occurred in 1965 and amounted to roughly three-quarters of the 1984 record.

Other than these intermittent streams, playas, and man-made percolation, infiltration, and evaporation ponds, there is little surface water at the INEEL Site. Surface water that reaches the INEEL is not used for consumptive purposes (e.g., irrigation, manufacturing, or drinking). In addition, there are no identified future uses of surface water that reach the INEEL.

The northwest boundary of INTEC is closest to the Big Lost River channel, approximately 200 ft (60 m) away. This is near the point where the channel intersects with Lincoln Boulevard on the INEEL. The Big Lost River is the principle natural surface water feature on the INEEL and the only stream with potential impacts to the TFF. The Big Lost River flows southeast from Mackay Dam, through the Big Lost River Basin past Arco, Idaho, and onto the ESRP. Stream flows are often depleted before reaching the INEEL by irrigation diversions and infiltration losses along the river. When flow in the Big Lost River does reach the INEEL, it is either diverted to the flood diversion facilities or flows northward across the INEEL in a shallow, gravel-filled channel to its terminus in the Big Lost River playas. In the playas, its flow is lost to evaporation and infiltration recharging the Snake River Plain Aquifer. See Table 2-5 for monthly discharge values of the Big Lost River at Lincoln Boulevard near INTEC.

Major control on the Big Lost River upstream of the INTEC site includes the Mackay Dam and the INEEL flood diversion facility, each of which is discussed in greater detail below.

2.1.5.1.1 Mackay Dam—Mackay Dam, located about 45 mi (72 km) upstream from the INEEL, impounds water from the Big Lost River for irrigation purposes downstream. Mackay Dam is a 1,430-ft (436-m) long, 79-ft (24-m) high earth-filled dam built for the Big Lost River Irrigation District. The dam was completed in 1917 and has a storage capacity of 44,500 acre-ft (5.49E+07 m^3) and a surface area of 1,241 acres (502.2 ha) at a water-surface elevation of 6,066.5 ft (1,849.1 m) (Table 2-6). An ungated overflow spillway with a weir length of 75 ft (23 m) at an elevation of 6,066.5 ft (1,849.1 m) above mean sea level (amsl) is located near the west abutment of the dam. The spillway is designed for a discharge of 3,250 ft^3/s (92.0 m^3/s) with 4 ft (1 m) of freeboard on the dam. The outlet works also are located near the west abutment and extend through the embankment and under the spillway to form an outlet channel. The outlet works consist of five motor-operated slide gates measuring 4 × 8 ft, mounted in an upstream control tower. The arched-roof outlet tunnel measures 10 × 10 ft, and reaches 500 ft downstream into a 10-ft diameter steel pipe, which extends to the outlet. At the outlet, the pipe branches into six 4-ft diameter pipes, emptying into a stilling basin at the toe of the dam. The total discharge capacity of Mackay Dam is less than 10,000 ft^3/s (300 m^3/s). Water from the Big Lost River is impounded for the irrigation of about 57,500 acres (23,300 ha) of land downstream from the reservoir and for recreational opportunities. Another 10,200 acres (4,130 ha) of land upstream from the reservoir also is irrigated with Big Lost River water (INEEL 1999b).

Table 2-5. Monthly discharge of the Big Lost River at Lincoln Boulevard near INTEC (ft^3).[a]

Year	Jan	Feb	Mar	Apr	May	Jun	Jul	Aug	Sep	Oct	Nov	Dec	Annual
1965	0	0	2,380	10,300	15,400	29,600	31,100	16,900	10,900	0	0	0	116,580
1966	0	0	0	3,660	981	0	0	0	0	0	0	0	4,641
1967	0	0	0	0	2,030	20,180	18,376	4,400	9,050	8,740	0	0	62,776
1968	0	0	2,280	3,390	16	524	0	1,053	1,130	3,290	4,500	0	16,183
1969	0	0	0	3,960	33,000	33,500	21,800	4,780	9,840	6,710	3,290	0	116,880
1970	0	0	501	1,650	793	13,800	17,700	1,510	6,080	5,280	4,750	8	52,072
1971	0	0	0	10,600	12,300	17,200	20,800	7,760	13,400	14,400	13,100	0	109,560
1972	0	0	1,540	4,920	504	1,710	861	84	2,990	3,520	3,099	0	19,228
1973	0	0	0	2,830	405	0	0	0	0	0	0	0	3,235
1974	0	0	3,240	5,520	6,940	16,200	9,390	1,170	1,160	3,760	4,200	0	51,580
1975	0	0	0	3,180	12,000	12,100	18,700	3,560	6,520	8,210	7,990	0	72,260
1976	0	0	333	1,450	1,660	1,120	0	0	300	620	1,100	76	6,659
1977	0	0	0	0	0	0	0	0	0	0	0	0	0
1978	0	0	0	0	0	0	0	0	0	0	0	0	0
1979	0	0	0	0	0	0	0	0	0	0	0	0	0
1980	0	0	0	0	0	0	1,140	0	0	0	0	0	1,140
1981	0	0	0	1,300	5,092	7,560	0	0	0	0	0	0	13,952
1982	0	0	0	5,930	17,200	13,400	15,100	4,820	8,190	10,500	5,740	600	81,480
1983	600	600	900	12,800	15,800	18,900	18,200	9,780	7,320	6,200	5,660	1,200	97,960
1984	1,200	1,200	1,200	2,200	2,230	4,550	3,950	5,790	5,140	5,980	8,710	2,120	44,270
1985	3	0	0	7,170	6,430	0	0	0	9,950	10,707	1,275	0	35,535
1986	0	96	537	8,370	14,825	20,315	2,900	1,016	14,753	8,220	1,190	2	72,224
1987	0	0	531	491	0	0	0	0	0	0	0	0	1,022
1988	0	0	0	0	0	0	0	0	0	0	0	0	0
1989	0	6	0	0	0	0	0	0	0	0	0	0	6
1990	0	0	0	0	0	0	0	0	0	0	0	0	0
1991	0	0	0	0	0	0	0	0	0	0	0	0	0
1992	0	0	0	0	0	0	0	0	0	0	0	0	0
1993	0	0	0	0	0	5,116	0	0	0	0	0	0	5,116
1994	0	0	0	0	0	0	0	0	0	0	0	0	0

a. Sources: INEEL 1999b.

Table 2-6. Characteristics of Mackay Dam and the INEEL Diversion Dam and reservoir.[a]

Characteristic	Mackay Dam	INEEL Diversion Dam
Dam crest elevation (ft amsl)	6,076.0	5,064.7
Dam crest length (ft)	1,430	500
Dam height (ft)	79	22
Spillway	Ungated overflow crest, 75 ft long	None
Spillway crest elevation (ft amsl)	6,066.5	NA
Gate centerline elevation (ft amsl)	6,036.6 (upper)	5,045.6
	6,007.8 (lower)	
Dam base elevation (ft amsl)	5,997.0	5,042.6
Spillway maximum capacity (ft^3/s)	6,588	NA
Gate maximum capacity (ft^3/s)	2,960	1,121
Reservoir capacity[b] (acre-ft)	55,091 at 6,076.0 ft	58,000 at 5,050.0 ft
	44,500 at 6,066.5 ft	18,200 at 5,040.0 ft
	8,750 at 6,030.0 ft	
	500 at 6,010.0 ft	

a. Sources: Koslow and Van Haaften 1986; INEEL 1999b.

b. It has been estimated that Mackay Reservoir has lost 22% of its mid- and late-season irrigation capacity because of sedimentation of the reservoir. Reservoir capacity given for the INEEL Diversion Dam is for the spreading areas; no water is held immediately behind the Diversion Dam.

2.1.5.1.2 INEEL Flood Diversion Facility—

The INEEL Flood-Diversion Facility (FDF) includes a diversion dam, dikes, and spreading areas located about 10 mi (20 km) upstream from INTEC. The FDF was constructed in 1958 and enlarged in 1984 to reduce the threat of flood on the INEEL from the Big Lost River. The FDF controls or divides the flow in the Big Lost River between the spreading areas to the south and the playas to the north where the water can be temporarily stored until it infiltrates into the ground. This prevents floodwaters from impacting INTEC and other INEEL facilities. The FDF has an elevation between 5,030 and 5,064.7 ft (1,530 and 1,543.7 m) amsl. INTEC lies at about 4,917 ft amsl (1,499 m) amsl, and the playas, located about 18 mi amsl (29 km) downstream from INTEC, lie between about 4,780 and 4,790 ft amsl (1,457 and 1,460 m amsl).

The FDF's diversion dam consists of a small earthen diversion dam and headgate that diverts water from the main channel, through a connecting channel, and into a series of four natural depressions, called spreading areas. Flow in the diversion channel is uncontrolled at discharges that exceed the capacity of the culverts. The diversion channel is capable of carrying 7,200 ft^3/s (2.0E+02 m^3/s) from the Big Lost River channel into the spreading areas. Two low swales located southwest of the main channel will carry an additional 2,100 ft^3/s (59 m^3/s) for a combined diversion capacity of 9,300 ft^3/s (260 m^3/s). The capacity of the spreading areas is about 58,000 acre-ft (7.2E+07 m^3) at an elevation of 5,050 ft (1,540 m) amsl. Runoff from the Big Lost River has never been sufficient to exceed the capacity of the spreading areas and overflow the weir. Gates placed on two 6-ft diameter corrugated steel culverts control flow downstream onto the INEEL. At full capacity, the culverts are capable

of handling up to 900 ft^3/s (30 m^3/s) of flow through the diversion dam. As stated previously, there are no users of the surface water that reaches the INEEL (INEEL 1999b).

2.1.5.2 Floods. A study of recorded discharge data suggests a history of low-magnitude floods. The data are from several USGS stream-flow stations along the Big Lost River upstream of the INEEL. Flooding in the basin is associated with peak flows during the snowmelt season and occasional flooding caused by ice jams in the stream channel. Big Lost River flows seem to be attenuated because of the gravel, deep alluvium, and permeable basalt found in the channel bed. These streamflow losses, combined with controlled streamflow, diversion canals, and irrigation use, significantly impact the natural flood peaks. Downstream on the INEEL, the local semi-arid climate, relief, and geology combine to regulate local runoff. Local flooding in the past has been associated with unseasonably warm temperatures and rain on frozen ground as the following local flood history describes (INEEL 1999b).

2.1.5.2.1 Flooding in 1965—A record snowpack occurred in the Big Lost River Basin in the winter of 1964–65. The maximum runoff occurred in late June. The Mackay Reservoir was full and most of the runoff was passed down to the basin and through the FDF on the INEEL. During the flood peak, June 29, 1965, approximately 1,800 ft^3/s (51 m^3/s) was diverted to the spreading areas from a peak flow of 2,215 ft^3/s (62.72 m^3/s). The Big Lost River overflowed its banks above Arco through most of June. On the INEEL, the flood was controlled by the FDF and by the storage and infiltration in the river channels, playas, and sinks. The water did not reach the end of the Big Lost River channel at the Birch Creek playa during this flood. This flood is significant because it exhibited the largest crest and largest water volume to be discharged onto the INEEL in 65 years of record, yet caused no damage to INEEL facilities.

2.1.5.2.2 Flooding in 1984—High stream flows in the Big Lost River and a severe cold spell during the winter of 1983–84 caused ice jams that imposed a danger of localized flooding. Ice buildup in the spreading areas resulted in waters backing up in the diversion channel and ultimately threatening to overtop a dike. The high stream flows in the Big Lost River in 1983 and 1984 were largely the result of the Borah Peak earthquake of October 28, 1983. The earthquake created new springs upstream of Mackay Reservoir, which significantly increased the inflows to the reservoir. Outflows from the reservoir also were increased to reduce the storage behind the dam. In response to this flood threat, the diversion area was upgraded to provide additional flood control, increasing the diversion channel flow capacity of 2,500 ft^3/s (71 m^3/s) to over 9,000 ft^3/s (300 m^3/s). Downstream, INEEL facilities were not threatened or damaged by the accumulation of ice in the diversion channel.

Generally during the winter months there is no flow in the Big Lost River downstream on the INEEL; however, if there is flow, nearly all the flow is diverted to the FDF to avoid the accumulation of ice in the main channel, reducing the possibility of flooding downstream. In a review of the historical information, no flooding or inundation from storms or runoff has caused flooding of the INTEC site.

2.1.5.3 Potential Flooding Considerations. As discussed in the following sections, the bounding flood scenario for the INEEL TFF is the overtopping failure of the Mackay Dam from a general storm probable maximum precipitation (PMP) (INEEL 1999b). A detailed discussion of this general storm PMP may be found in the following sections. The INTEC TFF site elevation is near or at the extent of floodwaters 4,917 ft (1,498 m) amsl predicted for this hypothetical dam failure scenario.

2.1.5.3.1 Probable Maximum Flood on Streams and Rivers—The probable maximum flood (PMF) represents the hypothetical flood that is considered to be the most severe flood event reasonably possible, based on the hydro-meteorological application of maximum precipitation and other hydrologic factors. Either an unusually severe storm or some catastrophic event, such as a dam failure, may cause the PMF. For conservatism in safety and design, the bounding scenario used for INEEL facilities is a

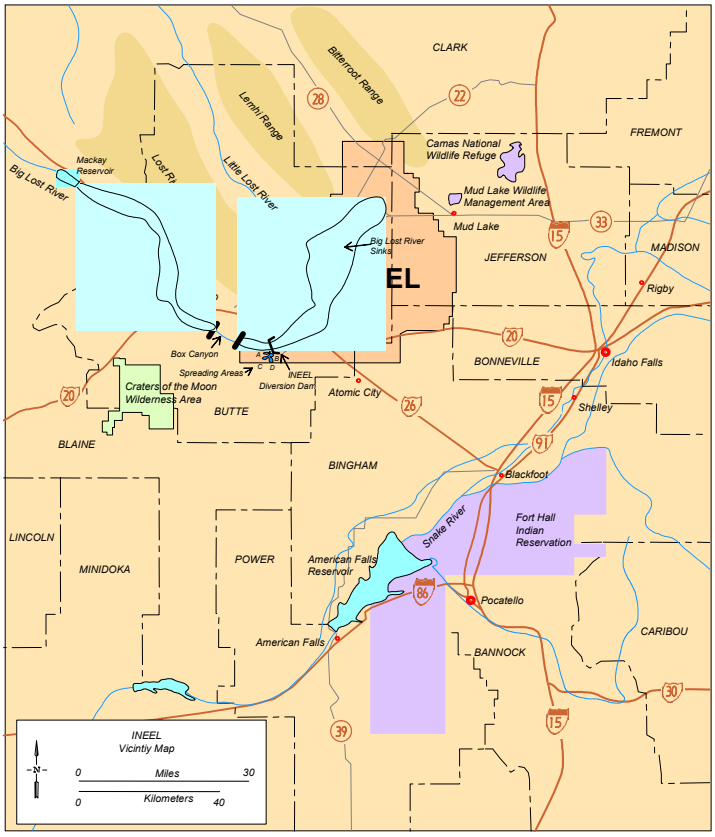

ground may be frozen or fully saturated. The peak flow for the PMF is 82,100 ft^3/s, occurring 154 hr after the beginning of the storm. The PMF estimate falls within the 50,000–200,000 ft^3/s Myers envelope curve used by the U.S. Army Corps of Engineers (INEEL 1999b). The PMF peak flow is almost 20 times higher than the highest flow of 4,420 ft^3/s recorded at Howell

12,600 ft (3,840 m) amsl. Thus, this area has over 7,546 ft (2,300. m) of relief, resulting in large differences in temperature and climate at any given time. The low land in the Pioneer Basin is subjected to periods of warm wind, rain, and snowmelt during the winter months. These cor
lower basins during regional storms and

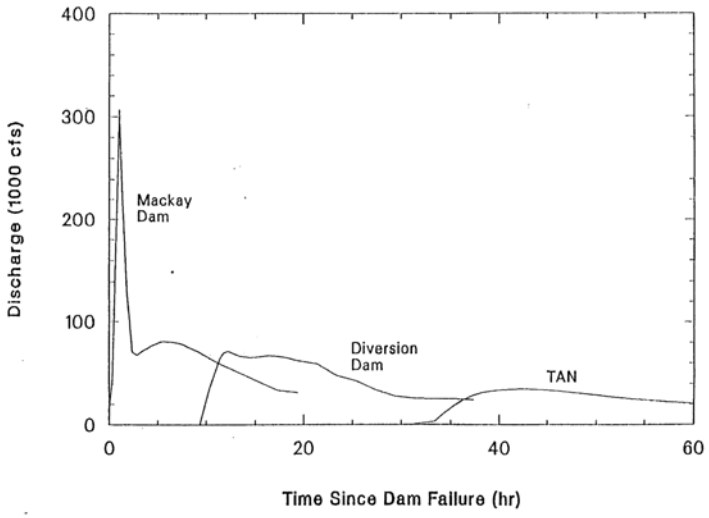

Figure 2-17. Probable maximum flood hydrograph (INEEL 1999b).

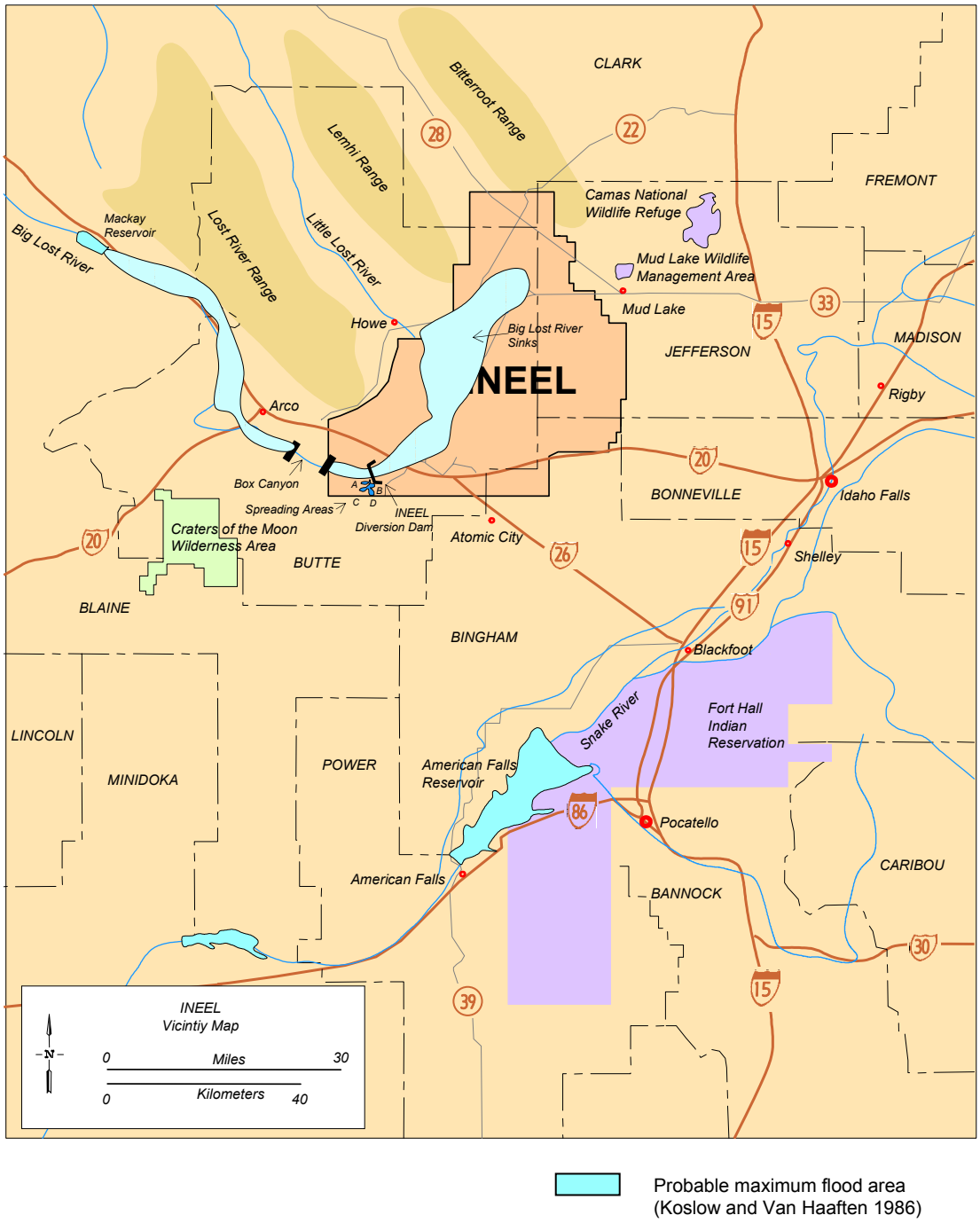

Figure 2-18. Probable maximum flood INEEL inundation map (INEEL 1999b).

Table 2-7. Results of probable maximum flood induced overtopping failure of Mackay Dam. [a,b,c]

Location (approximate elevation, ft amsl)	Streambed elevation (ft amsl)	Peak water surface elevation (ft amsl)	Peak flood flow (ft^3/s)	Peak water velocity (ft/s)	Time of wave arrival (hr)
Mackay Dam (6,076)	5,997	6,078	306,700	8.5	0.0
Arco (5,310–5,410)	5,309	5,319	147,720	5.6	6.7
INEEL Diversion (5,065)	5,043	5,073	71,850	1.0	10.0
CFA (4,928–4,940)	4,935	4,942	67,830	3.4	12.8
TRA (4,920–4,925)	4,919	4,924	67,170	2.8	13.2
INTEC (4,914–4,930)	4,911	4,917	66,830	2.7	13.5
NRF (4,845–4,850)	4,846	4,851	61,620	1.9	16.4
TAN (4,780–4,795)	4,778	4,786	34,810	1.1	34.5

a. Sources: Koslow and VanHaaften 1986; INEEL 1999b.

b. Total flow to INEEL diversion spreading areas = 27,460 acre-ft.

c. Total Mackay Reservoir release = 142,330 acre-ft.

substantially increase the snowpack in the uplands. The largest documented runoff periods in the lower parts of the basins have occurred in January, February, or March; the maximum runoff from the highlands is usually in May or June. Generally, frost leaves the ground in the Pioneer Basin and the valley floors of the mountain basins in March or April; the permeable soils and gravels can then accept surface water by infiltration before the bulk of the snow pack starts to melt. Most surface water reaching the Pioneer Basin from the tributary drainage basins eventually infiltrates beneath the soil and rock to the groundwater reservoir. The remainder is lost through evaporation.

2.1.5.3.5 Probable Maximum Flood Flow—

The spillway of Mackay Dam is not adequate to pass the PMP safely, therefore overtopping and subsequent breaching of the dam because of this PMP storm were analyzed. During this overtopping failure, the inflow is sufficient to raise the water surface above 6,077 ft (1,852 m) amsl, 1 ft (0.3 m) above the crest of the dam. A trapezoidal breach was assumed to develop over a 1-hr period and extend to the base of the dam. The computer code DAMBRK (National Weather Service 1991), was used in the flood-routing analysis.

The peak flow resulting from the PMP-induced overtopping failure is 306,700 ft^3/s in the reach immediately downstream of the Mackay Dam. This peak flow attenuates to 71,850 ft^3/s at the INEEL Diversion Dam and 66,830 ft^3/s at INTEC. The flood wave reaches the INEEL Diversion Dam in 10 hours. Water velocities are approximately 1 to 3 ft/s downstream on the INEEL. The computer program DAMBRK identified the water levels at specified locations for the PMF-induced overtopping failure. The wind activity at the INEEL, coincident with the largest projected flood crest, could not produce waves that would exceed 0.5 ft (0.2 m) primarily because of the shallow depth of water surrounding most INTEC buildings (LITCO 1994). Thus, the static and dynamic effects of wave activity would be negligible.

2.1.5.3.6 Potential Dam Failures—

Mackay Dam is classified as a "high hazard" dam by the State of Idaho with reference to the U.S. Army Corps of Engineers guidelines for safety inspection of dams (Army Corps of Engineers 1995). This high hazard classification is based on the concentration of people and property downstream, the size of the dam, and its storage capacity, not on any aspect of the dam's current condition or operation.

Mackay Dam is located in a region of historical seismicity as evidenced by the 1983 Borah Peak earthquake. The performance of the dam during this earthquake demonstrated the stability of the embankment during moderate ground motion. However, Mackay Dam was built without any seismic design criteria; therefore, a seismically-induced dam failure has been analyzed to determine potential impacts at the INEEL. This analysis assumed a postulated seismic failure of Mackay Dam during an inflow to the reservoir equal to the 25-yr recurrence interval flood (peak flow 4,030 ft^3/s). Because a seismic event may potentially disrupt a significant part of the dam's structure, the breech was assumed trapezoidal, extending to the bottom of the structure at 5,997 ft (1,828 m) amsl, and developing over a 1-hr period. The peak flow from the seismic dam failure in the reach immediately downstream of the dam is 107,480 ft^3/s. This peak flow attenuates to 45,410 ft^3/s at the INEEL Diversion Dam and to 39,080 ft^3/s at INTEC. The leading edge of the wave reaches the INEEL Diversion Dam in about 12 hours. Average water velocities on the INEEL are 1 to 3 ft/s.

Other dam failure permutations examined include two hydraulic (piping) failures concurrent with 100-yr and 500-yr inflow floods to the reservoir. The INEEL Diversion Dam would be overtopped by the floodwaters released from the failure of Mackay Dam. This overtopping of the INEEL Diversion Dam would contribute to the flooding downstream on the INEEL. The DAMBRK analysis assumes that the INEEL Diversion Dam begins to fail when floodwaters reach 5,065 ft (1,544 m) amsl, an overtopping depth of 0.3 ft (9 cm). Because of the small size of this dam, the breach is assumed to be fully developed after 0.1 hr, an essentially instantaneous failure.

The flood from dam failure would initially travel down a valley between basalt flows. The initial velocity would be high near the failure, but the average velocity would decrease to approximately 1 ft/s near the FDF. Water entering the FDF from this flood is much less than the actual capacity of the spreading area (Koslow and Van Haaften 1986). Water that bypasses the FDF would continue to spread out across the floodplain and have a peak water velocity of 2.7 ft/s at INTEC. This would result in flood water within the INTEC controlled area up to 4,917 ft (1,499 m). The existing ground elevation of the INTEC TFF site varies between 4,914 to 4,917 ft (1,498 to 1,499 m) amsl, with the majority of the tanks located in an area with an elevation of 4,916 ft (1,498 m).[a]

An additional study of the MacKay Dam failure was conducted by Van Haaften, Koslow, and Naretto (1984) for the flooding analysis of the New Production Reactor site. A PMF event above Mackay Dam was assumed to result in a 1.1 m (3.7 ft) overtopping of the dam, with a 0.5 hr dam failure, 42.6 m (140 ft) breach in the dam, and no flow losses downstream. This flooding analysis scenario resulted in flooding of the INTEC facility with 1 to 2 m (3 to 7 ft) of water covering the site and a peak flow of 3292.5 m^3/s (116,272 ft^3/s). The flood hydrograph for the base-case discharge shows a peak flow that lasts only 7.5 hrs (Figure 2-19). Since the INTEC facility is located at the boundaries of the flood, the area would be inundated for a lesser period of time.

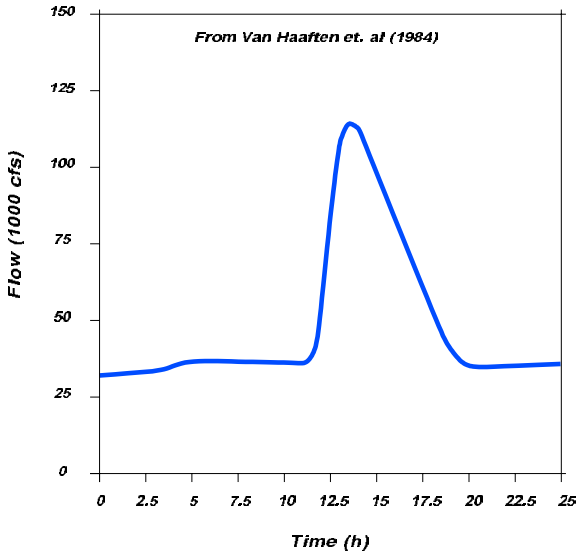

Figure 2-19. Flood hydrograph at INTEC.

a. Based on E.K. Roemer, Portage Environmental, personal communication with Randy Lee, a senior Geographical Information System analyst at the INEEL, 2000, and GPS mapping of INTEC.

The impact of the worst possible flooding condition on the INTEC facility is expected to be minimal. The elevation of the INTEC facility is near the highest elevation that floodwaters could potentially reach. Since the facility is near the edge of the floodwaters, surface water flow velocities would have minor erosional effects. One to two meters of water could cover the facility, but this would occur only for a short duration. A small wetting front infiltrating into the unsaturated zone would occur. However, based on infiltration rates measured by Dunnivant et al. (1998) and the short duration that ponded water could occur at the facility, the wetting front would only advance 16 to 33 ft (4.9 to 10. m) into the underlying alluvial soils.

2.1.5.3.7 Perched Water. There are several perched water zones underlying the INTEC facility, which can be divided into an upper and lower perched water zone. The upper basalt perched water zone was initially discovered in the late 1950s. Perched water was encountered in Wells USGS-50 and USGS-52 at 126 and 174 ft (38.4 and 53.0 m) bgs, respectively. The occurrence of this perched water was attributed to operational practices based on the presence of radioactive and chemical contaminants. Since then, numerous monitoring wells have been installed in the upper perched water zone to identify the source of recharge, delineate the perched water bodies, and determine the nature and extent of contamination.

A lower perched water zone also was identified in the basalt at depths between 340 and 400 ft (1.0E + 02 and 100 m) bgs (Robertson, Schoen, and Barraclough 1974). This water was first discovered in 1956 while drilling Well USGS-40; perched water was encountered at a depth of 348 ft (106 m). An analysis of this perched water detected abnormally high total dissolved solids (303 mg/L), sodium (25 mg/L), and chloride (81 mg/L), indicating the water is of waste origin (Olmsted 1962). According to Robertson, Schoen, and Barraclough (1974), this was a reasonable level for the perched groundwater because of the presence of a clay bed "aquitard" at 370 ft (110 m) bgs. In the late 1950s, only wells drilled in the northern INTEC area encountered the lower perched groundwater zone. Since 1984, a lower perched groundwater zone also has formed in the southern INTEC area because of the disposal of process waste through the percolation ponds. The location of this lower perched water zone is indicated by Well MW-17 and borehole neutron logs from Well USGS-51.

Stratigraphy controls the hydrogeologic characteristics of the subsurface at INTEC, particularly in the formation and movement of perched groundwater. The formation of perched groundwater can be attributed to lithologic features contributing to contrasts in the vertical hydraulic conductivity of basalt layers and sedimentary interbeds in the unsaturated zone. Cecil et al. (1991) attributed four lithologic features to the formation of perched groundwater at INTEC. Perched groundwater can form where (a) a sedimentary interbed with a reduced vertical hydraulic conductivity underlies a more conductive basalt layer, (b) altered baked zones between two basalt flows reduce the hydraulic conductivity, (c) dense unfractured basalt having low vertical hydraulic conductivity is present, or (d) sedimentary and chemical filling of fractures near the upper contact of a basalt flow reduces the vertical hydraulic conductivity.

Water movement in the basalt units located in the unsaturated zone is poorly understood. The presence of perched water at the surficial sediment-basalt contact indicates how water moves into the underlying fractured basalts. Water in a partially saturated medium is held under negative pressure or tension. This capillary tension prevents water from moving from a region with small pore spaces (such as the sediment interbeds) into a region of larger pore spaces (such as the fractured basalts) until the tension is nearly reduced to zero pressure. In other words, the overlying sediment interbeds reach saturation. As a result, water movement into the fractured basalts is likely dominated by fracture density (Maheras et al. 1994). Fracture spacing measurements documented by Knutson et al. (1992) indicate that near perimeter zones of basalt flows, the spacing between fractures decreases to 0.25 m (0.82 ft).

A large-scale field infiltration test conducted by Dunnivant et al. (1998) showed that infiltrating water moved downward through isolated fractures

and did not spread horizontally until reaching an interbed located at a depth of 180 ft (55 m). As water reached the interbed, a perched water body developed that was characterized by direct current resistivity measurements and confirmed by the recovery of water from monitoring wells. Water moved outward from the area coinciding with geological abnormalities and with topographic lows on the interbed surfaces. Depending on the amount of water and the horizontal extent of the interbed, water would continue to move laterally until a discontinuity in the interbed was reached, at which point the downward migration of water would continue.

In modeling studies conducted by Maheras et al. (1994) for the RWMC area, water movement through the fractured basalts is assumed to be rapid, on the order of 98 ft/mo (30 m/mo). Conceptually, the model for the RWMC area excluded the fractured basalts and only included the sediment interbeds stacked together so that they were in direct contact with each other. The fractured basalts were assumed to have negligible water travel times and were not included in the simulations.

Modeling conducted for the *WAG 3 RI/FS* assumed that the basalts could be treated as an anisotropic "single porosity" media, where the matrix is neglected and only the fractures are considered for the transport of water (Rodriguez et al. 1997). For this modeling approach, a horizontal and vertical fracture permeability of 90,000 mDarcy and 300 mDarcy, respectively, and an effective porosity of 5% were applied. Figure 2-20 illustrates the unsaturated moisture characteristic curve and unsaturated hydraulic conductivity as a function of moisture content based on data presented in Rodriguez et al. (1997).

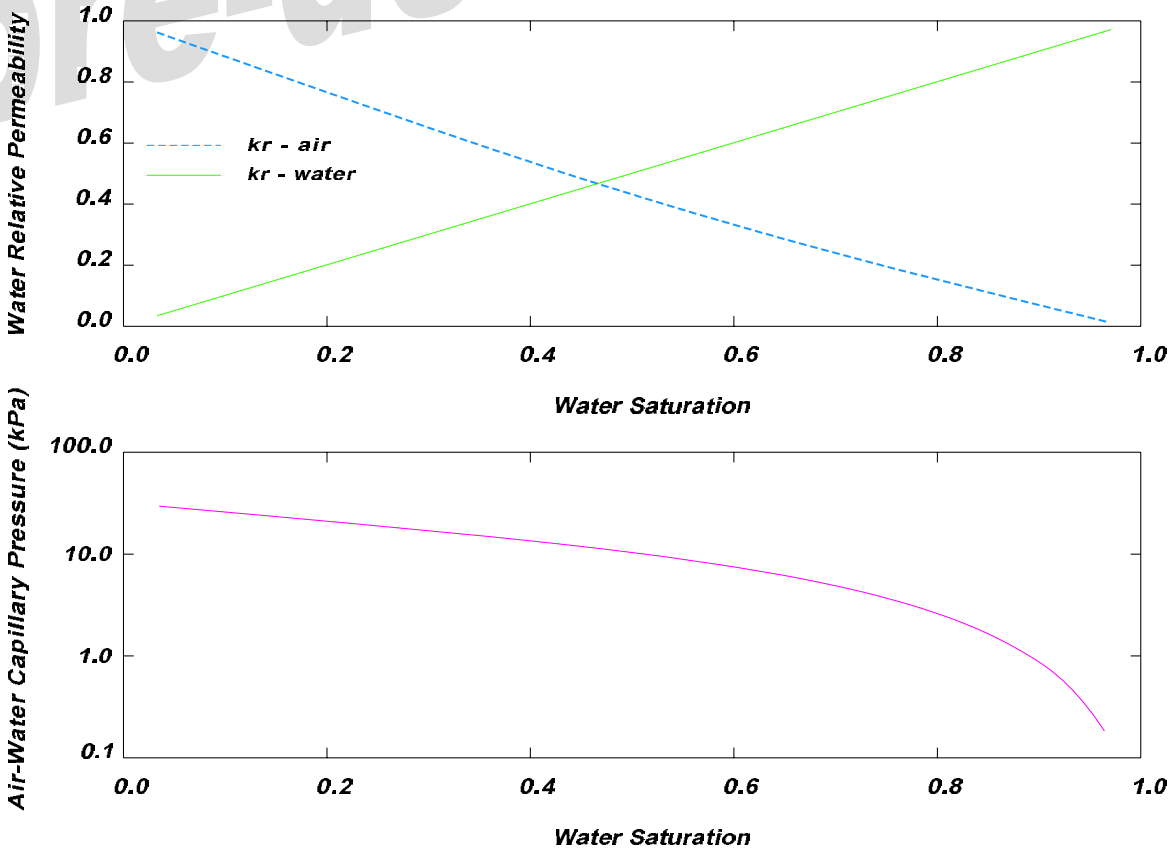

Figure 2-20. Basalt moisture curve.

The unsaturated moisture curve assumes the rapid dewatering of the fractures in response to pressure decreases. The relative permeability decreases linearly in response to decreases in moisture content. This linear permeability response is consistent with a similar approach presented in the *Handbook of Vadose Zone Characterization and Monitoring* (Wilson, Everett, and Cullen 1995), where the effective conductivity for fractured media is a function of the fracture density. Because of the fractured and the porous media interaction, this type of formulation assumes instantaneous equilibrium of total head between the two media and essential features of the flow dynamics are overlooked. Such phenomena as capillary barriers (in which an unsaturated fracture impedes fluid flow) and rapid transient responses are not inherent in this approach (Wilson, Everett, and Cullen 1995). Consequently, the use of porous media unsaturated curves to represent flow in the fractured basalt is a rough approximation of unsaturated fluid flow characteristics.

It is difficult to quantify this approach as conservative or non-conservative since both capillary barriers and rapid transient responses are not incorporated into the analysis. The net result is uncertainty in predicting unsaturated flow and contaminant transport in the fractured basalts that is difficult to quantify.

Additional information on perched water zones at the INEEL is presented by Rightmire and Lewis (1987), Cecil et al. (1991, 1992), Magnuson and McElroy (1993), and McElroy (1993).

2.1.5.3.8 Upper Perched Zone—

Based on the perched water data, it appears the upper perched groundwater bodies are formed by the relatively low vertical hydraulic conductivity in the sedimentary interbeds. Of particular importance to the formation of perched groundwater are the CD, D, and DE3 interbeds. Figure 2-21 shows the location of the upper basalt perched water zone that occurs between depths of 100 to 190 ft (30 to 58 m).

The location and extent of the upper perched water zones are dependent not only on the stratigraphy but also on the location of the recharge source. It appears that water sources vary from the northern to the southern portions of the INTEC facility. Consequently, each area will be discussed in detail in the following sections.

Northern INTEC. Twenty-three monitoring wells (including multiple completion wells) have been installed in the northern INTEC area to monitor the upper perched groundwater (i.e., groundwater that occurs less than 190 ft [58 m] bgs). Only a few of these wells still exist. Two perched groundwater bodies have been identified in the northern INTEC area. The upper perched groundwater body is present above the CD and D interbeds, and the lower perched groundwater body has been identified on the DE3 interbed. According to the lithology, the CD interbed occurs at depths between 113 and 119 ft (34.4 and 36.3 m) bgs, the D interbed occurs at depths between 128 and 135 ft (39.0 and 41.1 m) bgs, and the DE3 interbed occurs at depths between 163 and 170 ft (49.7 and 52 m) bgs. Based on available information, it appears that the perched groundwater between the CD and D interbeds is continuous over much of the northern INTEC area since these interbeds are only separated by 9 ft (3 m).

In addition to these wells, Well MW-4 (1-in.-diameter) is completed at the bottom of the D interbed and Well MW-10 (1-in. diameter) is completed in a fracture zone associated with the BC interbed. Historically, both of these wells have been dry.

The extent of the upper basalt perched groundwater body is shown in Figure 2-21. Water-level elevations range from 4,797.3 to 4,845.3 ft (1,462.2 to 1,476.8 m) amsl and represent the average water table level throughout the monitoring period. The extent of the perched water above the CD and D interbeds is also illustrated in this figure. Perched groundwater is not known to occur above these interbeds outside the areas illustrated on the map. Where the perched water bodies overlap (i.e., in the vicinity of Wells CPP-33-4, CPP-33-1, and MW-5), the entire region between the CD and D interbeds is likely to be saturated. Otherwise, perched groundwater is only present above the associated interbed.

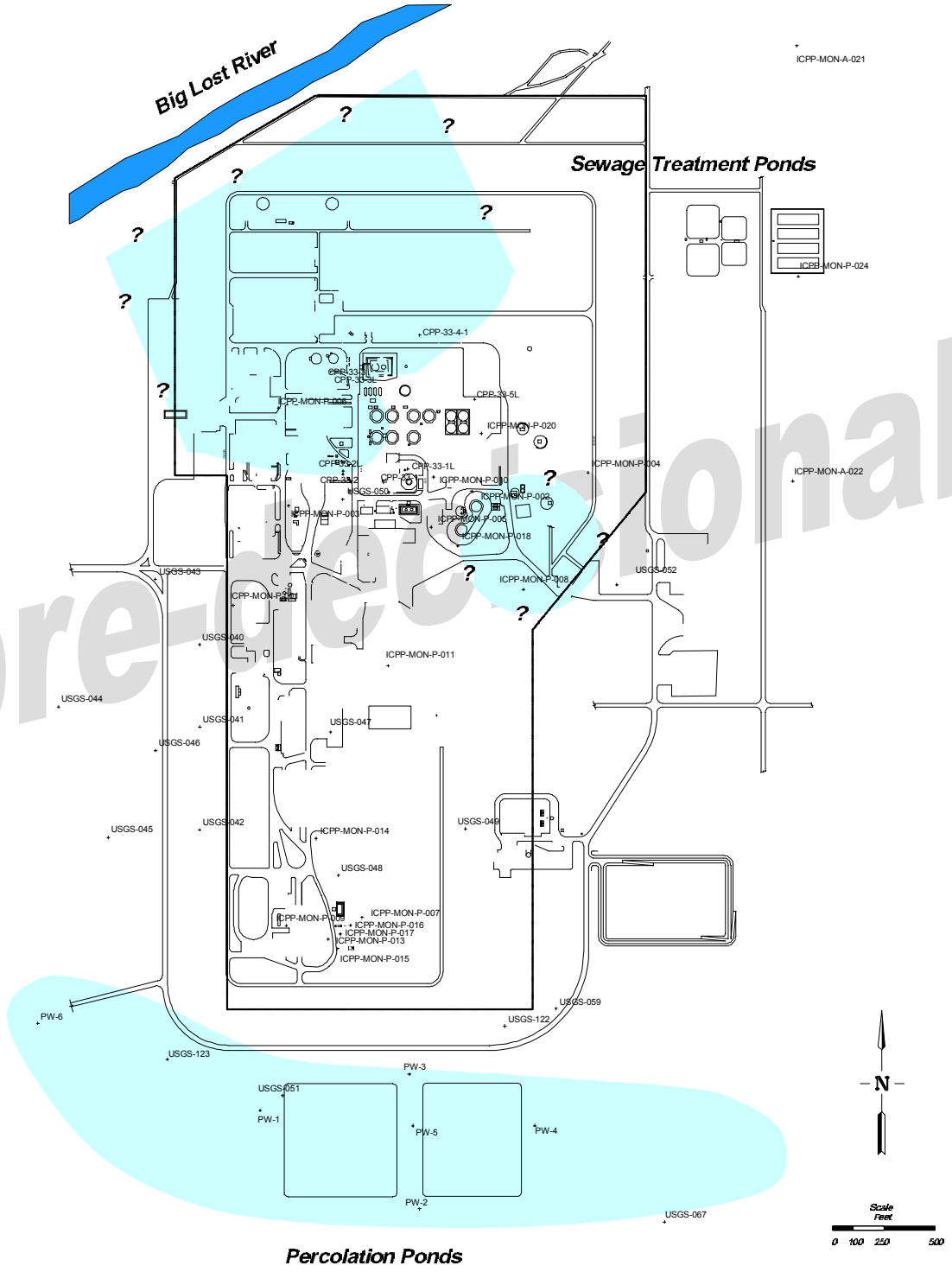

Figure 2-21. Upper perched water at INTEC.

Based on the water-table configuration, it appears that multiple water sources are providing recharge to the upper basalt perched water body in the northern INTEC area. Seepage from the Big Lost River is a potential source of water in this area. The sewage treatment ponds, located east of the facility, provide approximately 1.25E+06 gal (4.73E+06 L) per month of recharge to the perched water body. This recharge has resulted in a water table elevation of 4,845 ft (1,477 m) amsl in the well completed near the sewage treatment ponds (Well CPP-MON-P-024). In the western portion of the perched water body and beneath the main portion of the facility, the recharge has produced a maximum water-table elevation of 4,817.5 ft (1,468.4 m) in Well CPP-33-2. Between the eastern and western portions of the upper perched water body, the average groundwater elevation is 4,809.2 ft (1,465.8 m) in Well CPP-37-4. This water-table configuration indicates separate sources of water providing recharge to the eastern and western portions of the uppermost perched water body. The sewage treatment ponds have minimal, if any, impact upon the western portion of this perched water body.

Occurring beneath the upper perched groundwater body, a deeper perched groundwater body has been identified at a depth of approximately 140 ft (43 m) bgs. This groundwater appears to be the result of the DE3 interbed, which occurs between 163 and 169 ft bgs (49.7 and 51.5 m) in the northern INTEC area. Only three wells (MW-10 [2 in.], MW-12 [1 in.], and MW-20 [2 in.]) are completed in this perched groundwater body. Based upon monitoring data, the water-table elevation within this perched water zone varies from 4,769 to 4,779 ft (1,454 to 1,457 m) amsl.

Southern INTEC. The upper perched water bodies identified in the southern INTEC area are shown in Figure 2-21. The largest perched water body is the result of discharge to the percolation ponds and is monitored by Wells PW-1 through PW-6. In the vicinity of CPP-603, six wells (MW-7, MW-9, and MW-13 through MW-16) were installed to monitor perched water on the upper interbed that is present between 110 and 130 ft (34 and 40 m) bgs. One triple completion well (MW-17) was installed to monitor for perched water on a deeper interbed occurring at approximately 190 ft (58 m) bgs.

Wells PW-1 through PW-6 were installed adjacent to the percolation ponds to monitor the perched groundwater beneath the ponds. The hydrographs for these wells show similar fluctuation in the water level observed for Wells PW-1, PW-3, and PW-6, indicating these wells are effective in monitoring infiltration from the western percolation pond. The water-level fluctuation in Well PW-4 is opposite to the response observed in Wells PW-1, PW-3, and PW-6, indicating this well monitors infiltration from the eastern percolation pond. The water-level fluctuations in Wells PW-2 and PW-5 are fairly consistent, indicating these wells are influenced by discharge to either pond.

Field aquifer tests were performed to determine the hydraulic conductivities for both basalts and sedimentary interbeds. Hydraulic conductivities determined in the field were fairly consistent, varying over only two orders of magnitude. Field hydraulic conductivities ranged from 0.11 to 8.3 ft/d (3.4 cm/d to 2.5 m/d), with an average of 3.3 ft/d (1.0 m/d). Significant differences in hydraulic conductivities were not observed between tests performed on basalts versus tests performed on sedimentary interbeds (i.e., interbeds CD, D, and DE2). The depths are approximately 110, 140, and 230 ft (34, 43, and 70. m) bgs. A complete discussion of the sample collection and laboratory data package is described in *Interim Data Results from the FY 93/94 Perched Ground Water Investigation* (INEL 1994).

The range of hydraulic conductivities determined from the field aquifer tests is within the range of hydraulic conductivities measured in the laboratory. The average hydraulic conductivity determined from the field tests is 3.3 ft/d (1.0 m/d), compared to an average of 1.96 ft/d (0.597 m/d) determined from the laboratory tests. Some of the difference between the two hydraulic conductivities may be attributed to the fact that the field tests measured horizontal hydraulic conductivity, whereas the laboratory tests measured vertical hydraulic conductivity. Typically, horizontal hydraulic conductivities are

higher than the corresponding vertical hydraulic conductivities.

Good correlation in the hydraulic conductivity values occurred from the boreholes where both field and laboratory measurements were performed. From the same zone in Well MW-4, the average hydraulic conductivity determined in the laboratory was 0.1 ft/d (3 cm/d), compared to the field-determined value of 0.11 ft/d (3.4 cm/d). Similarly in Well MW-6, the hydraulic conductivity determined in the laboratory was 6.2 ft/d (1.9 m/d), compared to the field-determined value of 3.7 ft/d (1.1 m/d). These two wells are the only locations where both field and laboratory measurements were performed.

2.1.5.3.9 Lower Basalt Perched Water Zone—A lower perched groundwater zone has been identified in the basalt between 320 and 420 ft (98 and 130 m) bgs (see Figure 2-22). This water was first discovered in 1956 while drilling Well USGS-40; perched groundwater was encountered at a depth of 348 ft (106 m) (Robertson, Schoen, and Barraclough 1974). Since then, groundwater has been encountered in this zone during the drilling of Wells USGS-41, -43, -44, -50, -52, and MW-1, -17, and -18. Borehole neutron logs run in 1993 indicate perched water may still be present in this zone from Wells USGS-40, -43, -46, -51, and -52.

Only four wells are completed in the lower perched water zone that presently monitor water-level changes. Wells MW-1, MW-18, and USGS-50 are completed in the northern portion of the facility. Water in these wells is encountered at approximately 322, 407, and 383 ft (98.1, 124, and 117 m) bgs, respectively. In the southern portion of the facility, only Well MW-17 is completed in this zone; water in this well is encountered at a depth of approximately 315 ft (96.0 m) bgs. Based on water quality information, the deep perched groundwater encountered by Well MW-17 is the result of discharge to the percolation ponds.

Similar to the upper basalt perched water zone, the lower zone is thought to be formed by decreased permeability associated with sedimentary interbed layers. It appears that the lower perched groundwater has formed primarily on the DE8 interbed. The top of this interbed occurs beneath INTEC at depths ranging from 383 to 426 ft (117 to 130 m) bgs. In the western portion of the facility, however, the DE6 interbed is responsible for creating perched groundwater associated with Wells USGS-40 and USGS-43. However, these data contain a high degree of uncertainty, since they consist of a combination of original driller's logs (some dating back 40 yr), geophysical borehole logs, and monitoring wells that are completed in this zone.

As shown in Figure 2-22, the lower perched water zone is probably not continuous beneath the entire facility and may actually consist of several individual perched water bodies. The north-south separation of the lower perched water bodies is based on the lack of perched groundwater (either through drilling or subsequent neutron logging) identified in Wells USGS-42, -45, -47, -48, and -49. Recharge to the southern perched water body is from wastewater discharged to the percolation ponds. Seepage from the Big Lost River is believed to be the source of recharge to the western portion of the northern perched water body.

Water levels in this lower perched water zone have been monitored since the early 1960s in Well USGS-50. Other than during the late 1960s and early 1970s, the water level in this well has been fairly consistent. The water level during the stable period generally ranged between 4,530. and 4,540. ft (1,381 and 1,384 m) amsl. In the late 1960s/early 1970s, however, the water level increased by approximately 90 ft (30 m) in response to failure of the INTEC injection well. During this period, wastewater was discharged directly to the vadose zone from the INTEC injection well at a reported depth of 226 ft (68.9 m) bgs.

The presence of a deep perched groundwater zone beneath the percolation ponds is indicated by the borehole neutron response from Wells USGS-51 and MW-17. Figure 2-23 shows the natural gamma log, stratigraphy, and epithermal

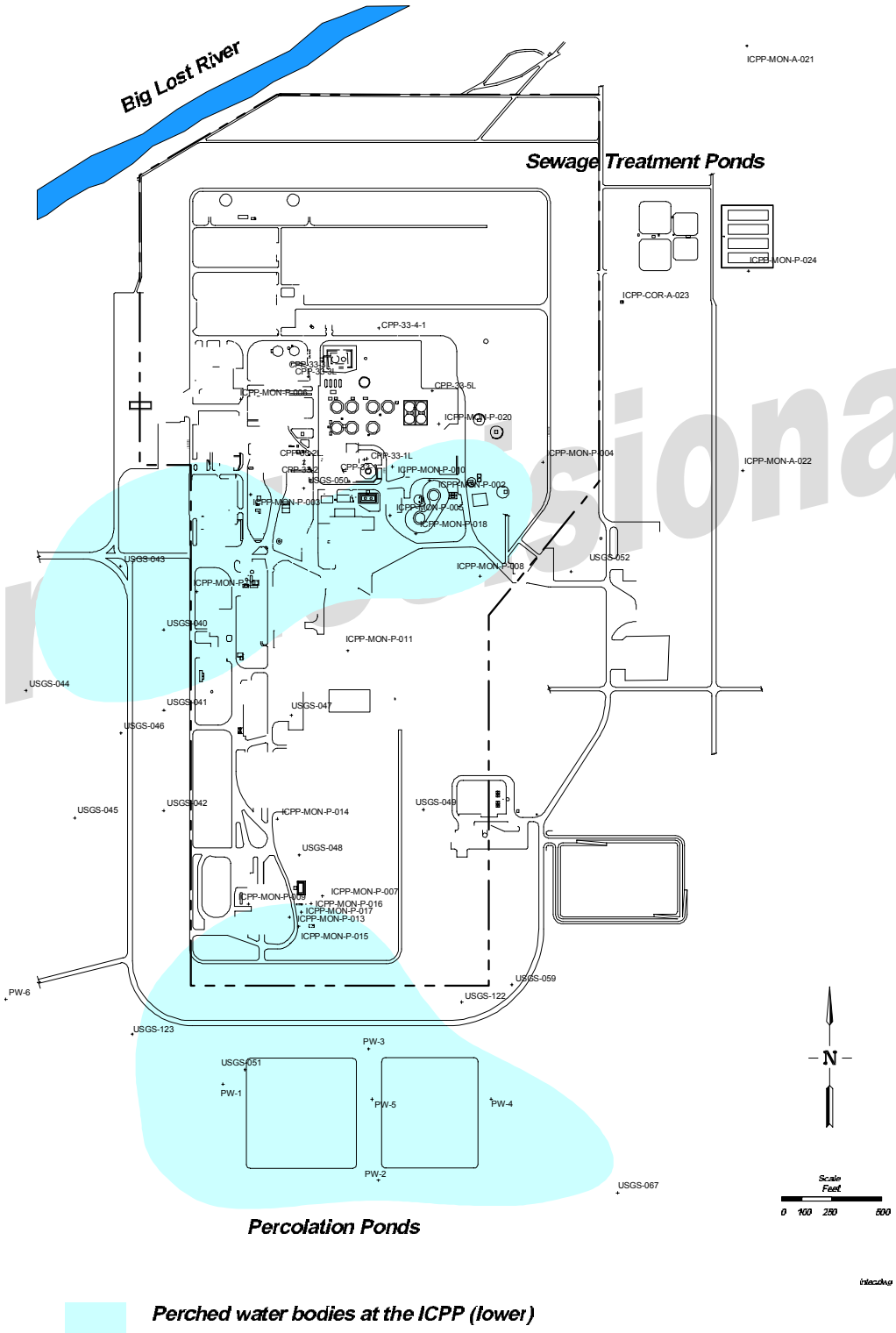

Figure 2-22. Lower perched water zone at INTEC.

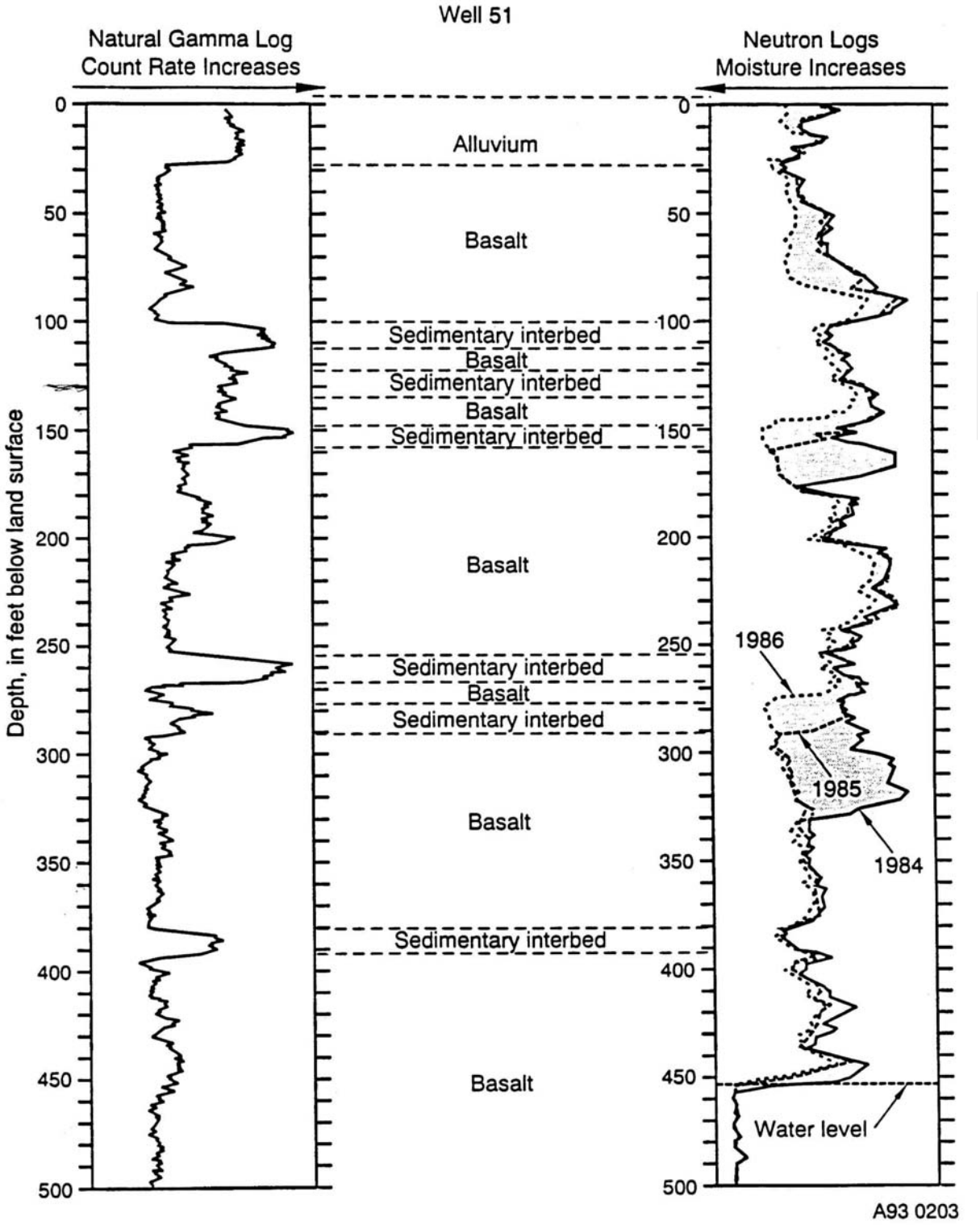

Figure 2-23. Natural gamma and neutron log for Well USGS-51.

neutron logs run in 1984, 1985, and 1986 for Well USGS-51. Deflections of the neutron log to the left indicate increases in moisture content. As shown in this figure, two zones illustrate significantly increasing moisture content since the percolation ponds were placed into service in February 1984. These two zones occur from 145 to 178 ft (44.2 to 54.3 m) and 274 to 332 ft (83.5 to 101 m) bgs.

2.1.5.4 Regional Aquifer. The general direction of regional groundwater movement underlying the INEEL is to the south and southwest. The average slope of the water table is about 4 ft/mi. In the northern part of the INEEL, near Birch Creek Valley, the water-table gradient is relatively low, sloping southward about 1 ft/mi (0.2 m/km) (Barraclough et al. 1967).

Groundwater in the Snake River Plain Aquifer generally occurs under unconfined conditions, but locally may be quasi-artesian or artesian (Nace et al. 1959). Layers of dense, massive basalt or sediments cause the quasi-artesian or artesian conditions as a result of their relatively low permeability. Nace et al. described quasi-artesian as the situation in which the groundwater level is first recognized in a borehole during drilling at a depth below the regional water table, and then the level rises significantly (5 to 50 ft) [2 to 20 m] to the level of the water table. This rise of the water level simulates artesian pressure but the conditions are not truly artesian. Nace et al. also noted that water levels in some wells in the Snake River Plain Aquifer respond to fluctuations in barometric pressure similar to wells in confined aquifers, indicating tight zones in the basalt may impede pressure equalization. True artesian or flowing artesian conditions in the Snake River Plain Aquifer were identified at Rupert, in parts of the Mud Lake Basin, and north of the American Falls Reservoir (Nace et al. 1959). Recharge to the aquifer is primarily by valley underflow from the mountains to the north and northeast of the plain and from infiltration of irrigation water. A small amount of recharge occurs directly from precipitation. Recharge to the aquifer within INEEL boundaries is primarily by underflow from the northeastern part of the plain and the Big Lost River (Bennett 1990). Significant amounts of recharge from the Big Lost River have caused water levels in some wells at the INEEL to rise as much as 6 ft (2 m) in a few months after high flows in the river (Barraclough, Lewis, and Jensen 1982). Locally, the direction of groundwater flow is temporarily changed by recharge from the Big Lost River (Bennett 1990).

The effective hydraulic conductivity of the basalt and interbedded sediments that compose the Snake River Plain Aquifer at and near the INEEL ranges from 1.0E–02 to 3.2E+04 ft/d (3.0E–03 to 9.8E+03 m/d). This six-order-of-magnitude range was estimated from single-well aquifer tests in 114 wells, and is mainly attributed to the physical characteristics and distribution of basalt flows and dikes (Anderson, Kuntz, and Davis 1999). According to Anderson, Kuntz, and Davis, the relative hydraulic conductivity distribution through a typical buried shield volcano in the ESRP suggests that the conductivity of a single lava field is greatest in near-vent volcanic deposits consisting of shelly pahoehoe and slab pahoehoe flows and bedded scoria, spatter, and ash. These near-vent deposits typically cover about 10 to 20% of the lava field. Hydraulic conductivity of basalt flows is least for thick, tube-fed pahoehoe flow and ponded flow inside the vent craters and topographic depressions.

Anderson, Kuntz, and Davis (1999) compared the relationship between the thickness of the basalt and sediment layers in relation to the hydraulic conductivity. They concluded that stratigraphic intervals comprising thin basalt layers have more contacts, rubble zones, and cooling fractures. Hence, stratigraphic intervals have greater hydraulic conductivity than intervals of equal thickness comprising thick layers of basalt.

Detailed analyses of the geologic control related to hydraulic conductivity, along with hydraulic testing results for the regional aquifer, are presented in reports by Walker (1960), Ackerman (1991), and Anderson, Kuntz, and Davis (1999).

2.1.5.5 Infiltration.

2.1.5.5.1 Rainfall—Natural recharge from precipitation also is available to support perched water bodies. Long-term average annual

precipitation at the INEEL is 8.7 in. (22 cm), and pan evaporation is on the order of 43 in./yr (110 cm/yr). Nevertheless, water from snowmelt or heavy rains may infiltrate to a depth where it cannot be evaporated. Furthermore, many areas within INTEC are impervious and precipitation runs off to drainage ditches. The ditches are unlined and a significant fraction of infiltration is likely to occur along the ditches.

A wide range in the rate of infiltration rates at the site is reported in the literature and site-specific studies. These values range from a low of 0.16 in./yr (0.41 cm/yr) to a high of 4.9 in./yr (12 cm/yr). Most of the reported values in the literature are estimates based on the amount of precipitation and best guess estimates of the evapotranspiration rates for the area.

One of the few actual field measurements conducted at the site is reported by Cecil et al. (1992). By measuring tritium and ^{36}Cl profiles in the soil, test results yielded a range of 0.16 to 4.3 in./yr (0.4 to 1.1 cm/yr) infiltration.

A detailed investigation of water infiltration rates was conducted at the Central Facilities Area Landfill by Miller, Hammel, and Hall (1990). The CFA Landfill is covered by an earthen-based material from the surrounding area. Based on soil analysis, precipitation, and evapotranspiration estimates, a range of infiltration rates from 1.0 in./yr (2.5 cm/yr) to 1.6 in./yr (4.1 cm/yr) was reported. This measured value is the same infiltration rate used in the WAG 3 modeling analysis (Rodriquez et al. 1997) for the Tank Farm area.

The analysis of contaminant migration from the TFF was modeled using the measured value of 1.6 in./yr (4.1 cm/yr) for the CFA Landfill. This is considered an appropriate value since the TFF area will be covered with an engineered barrier under the CERCLA program. Therefore, this infiltration rate was considered for the base-case modeling estimates.

The infiltration rates at the INEEL are uncertain, especially for a given area such as the TFF. Therefore, the infiltration rates were treated as an uncertain parameter in the sensitivity/uncertainty analysis presented in Section 7. Three infiltration rates were considered in the uncertainty analysis: 12.4 cm/yr as the highest rate, 4.1 cm/yr as the base-case infiltration, and 1.1 cm/yr as the best-case infiltration. The low infiltration rate of 1.1 cm/yr is considered applicable to a well-engineered landfill cover.

2.1.5.5.2 Man-Made Sources—

INTEC uses approximately 2.1 million gal (7.9 million L) of water per day. Two raw water wells and one potable water well supply water to INTEC. The water is used for process cooling, equipment cooling, steam production, process solutions, decontamination, fuel storage basin makeup, chemical laboratory use, regeneration of ion exchange units, fire protection, and human uses. Piping systems external to facility buildings are either buried or enclosed in utility tunnels. The INTEC water systems that were considered relevant to the water inventory study included the raw water, fire water, treated (softened) water, demineralized water, steam condensate, landscape water, potable water, service waste (industrial wastewater), and sanitary waste systems. The steam distribution system, HLLW process lines, and pipes used to distribute cooling water to the HLLW storage tanks in the Tank Farm were eliminated from leak testing during the water inventory study. The criteria used to eliminate these areas were low volume, secondary containment, distinct radiological or chemical signature, and close monitoring or visibility.

The primary water systems at INTEC include the raw water system, fire water system, water softeners (treated water system), and demineralizer (demineralized water system). The raw water system piping has an approximate length of 6,250 ft (1,910 m) and an average flow of 389 gal/min (1,470 L/m). Raw water is pumped from the aquifer from two production wells to the fire water storage tanks. The raw water feed tanks supply water to three distribution pumps. The firewater piping system has a length of 5 mi (8 km) with an average flow of 45 gal/min (170 L/min). This flow in the system is water used for watering lawns, safety showers, cooling of waste tanks and sump pump bearings, and flushing radiation monitor bowls. The treated (softened) water system has a length of 4,000 ft (1,000 m)

and an average flow of 900 gal/min (3,000 L/min). Treated water is used for chemical process makeup and heat exchangers. The demineralized water system has a length of 4,200 ft (1,300 m) and an average flow of 1.5 gal/min (5.7 L/min). Demineralized water is used for process cooling, steam, and fuel storage basins.

The steam condensate piping system has a length of 4,200 ft (1,300 m) and an average flow of 74 gal/min (280 L/min) between September and April. Primary steam use occurs between the months of September and March because of seasonal demands such as heating and freeze protection. Most of the steam is condensed and recycled or routed to the service waste system. Approximately 10% of the steam is either released to the atmosphere or discharged to the ground.

The potable water system has a length of 2 mi (3 km) with an average flow of 61 gal/min (230 L/min). Potable water is supplied from two wells completed in the Snake River Plain Aquifer. Water is pumped to a storage tank. From there, three distribution pumps in building CPP-606 are used to supply potable water to INTEC facilities. The potable water system includes a chlorination system.

The service waste piping system has a length of 2.4 mi (3.9 km) and an average flow of 1,320 gal/min (5.00E+03 L/min). Raw water, treated water, demineralized water, and steam condensates are discharged to the service waste system. Waste streams that might be contaminated with radioactive materials are monitored before being discharged to the service waste system. If contamination is detected, the water is diverted to a holding tank for processing in the Process Equipment Waste Evaporator. Water in the service waste system is discharged to two percolation ponds located on the south end of the facility.

The sanitary sewer piping system is 1.5 mi (2.4 km) long, and has an average flow rate of 29 gal/min (110 L/min). Potable water and sanitary waste from INTEC facilities are discharged to the sanitary sewer system and gravity-drained to lift stations, where the waste is pumped to the INTEC Sewage Treatment Plant. The waste is then transferred to a series of treatment lagoons located at the northeast corner of INTEC.

The seven landscape watering systems at INTEC are all located in the northern area and have historically covered a total area of 1.5 acres (0.61 ha). Approximately 20,000 gal/d (80,000 L/d) from the raw water, fire water, and potable water systems has been used to maintain lawns and landscaping at INTEC during the summer months. A total volume of 2.35 million gal (8.90 million L) is used to water INTEC lawns each year. Consumptive use is calculated to require 784,000 gal (2,970,000 L) per growing season. Subtracting the consumption and evapotranspiration from the supplied water yields a net volume of 1.57 million gal (5.94 million L) available for infiltration and recharge of the perched water bodies.

A summary of the estimated amount of water available to recharge the perched water bodies at INTEC is given in Table 2-8. Historically, approximately 720 million gal/yr (2.7 billion L/yr) are known to be recharging the perched water bodies at INTEC. This does not include an additional 38.4 million gal (145 million L) that could be leaking through the facility piping and going undetected by the current metering system.

2.1.6 Geochemistry

Site-specific geochemical modeling was not performed for this PA. However, assumptions based on basic geochemistry were used in the PA development.

2.1.6.1 Sediment and Basalt K_d Values.

Knowledge of the sorptive properties of contaminants is key to understanding contaminant movement at the TFF. The subsurface comprises surficial sediments, sedimentary interbeds, and basalt. There is limited site-specific adsorption information for contaminants in the subsurface environment at the INEEL (Del Debbio and Thomas 1989; Schmalz 1972). Distribution coefficients are available for cobalt, chromium, strontium, cesium, cadmium, mercury, and selenium for alluvium. For interbed sediments and basalt, distribution coefficients are available for cadmium, mercury, selenium, and strontium.

Table 2-8. Estimated volume of water recharging the perched water bodies at INTEC.

	Northern INTEC		Facility-Wide	
Source	Volume (gal/yr)	Percent	Volume (gal/yr)	Percent
Service wastewater	None	0	690,000,000	95.8
Sewage treatment ponds	15,000,000	58	15,000,000	2.1
Water system leaks[a]	3,980,000	16	3,980,000	0.6
Landscape irrigation[a]	1,568,000	6	1,568,000	0.2
Precipitation infiltration	3,800,000	15	8,000,000	1.1
Steam condensate	1,300,000	5	1,700,000	0.2
CPP-603 Basins	None	0	49,275	0.1
Total	25,648,000	100	720,297,275	100

a. Estimate based on past leaks and irrigation practices. Actual loss from piping leaks is unknown.

Limited availability of site-specific adsorption information for other radionuclides for sediments and basalts at the INEEL has resulted in the use of adsorption parameters measured for sediments and basalts from other sites. Table 2-9 summarizes the measured K_d values for the INEEL.

Several investigators have published compendia of soil and sediment distribution coefficient data (Baes and Sharp 1983; Coughtrey, Jackson, and Thorne 1985; Sheppard and Thibault 1990). The most thorough of these compendia is Sheppard and Thibault (1990), which contains a breakout of the distribution coefficients by major soil types (i.e., sand, loam, clay, and organic). Past compendia grouped all soil types together.

Distribution coefficient data for basalts are not as readily available as data for soils and sediments. The main source of K_d values is basalts from the Nuclear Energy Agencies (NEA) sorption database (Ticknor and Ruegger 1989). These basalt sorption values are provided in Table 2-10.

In addition, a survey of the literature for the WAG 3 modeling study (Rodriquez et al. 1997) is provided in Table 2-11.

Sorption coefficient (K_d) values are considered sensitive parameters in predictive modeling of radionuclide transport in the subsurface. There are a limited number of actual measurements available for the radionuclides that are specific to the INEEL soils and basalt, as indicated by Table 2-9. Consequently, it was necessary to survey the literature for similar sites where actual radionuclide sorption studies have been conducted. Table 2-12 provides a list of K_d values for key radionuclides used in the predictive transport modeling. The rationale for the selection criteria is presented in Table 2-13. In the sensitivity/uncertainty analysis presented in Section 7, three separate combinations of the sorption coefficients were modeled to evaluate the sensitivity of this important transport parameter, 1) worst-case transport, 2) conservative transport, and 3) realistic/best transport sorption coefficients. This method provided a means of comparing the bounding-case analysis (i.e., conservative transport sorption coefficients), presented in Sections 3 and 4, with the range of values presented in the literature.

Column studies conducted on basalts at various moisture contents from saturation to 20% consistently resulted in essentially the same K_d values (Porro, Newman, and Dunnivant 2000). This evidence indicates that K_d values for the saturated zone are applicable to the unsaturated zone. While the reliability of K_d values obtained from batch tests is still being debated, using

Table 2-9. Summary of sorption coefficients measured at the INEEL.

	K_d Values (mL/g)[a]			
Element	Alluvium	Interbed Sediment	Basalt	Reference
Cd	4891-2864	10,115-8622	2319-785	Del Debbio and Thomas (1989)
Co	56	Not measured	Not measured	Schmalz (1972)
Cr	1.2	Not measured	Not measured	Schmalz (1972)
Cs	950	Not measured	Not measured	Schmalz (1972)
Hg	1921-236	673-72	87-9.2	Del Debbio and Thomas (1989)
Se	63-5.8	17-4.9	3.4-0.29	Del Debbio and Thomas (1989)
Sr	35-52	110-186	1.1-2.7	Del Debbio and Thomas (1989)
	24	Not measured	Not measured	Schmalz (1972)

a. K_d values reported by Del Debbio and Thomas (1989) were measured using batch equilibrium sorption methods on crushed materials, which were passed through a 2-mm sieve.

Table 2-10. Basalt K_d values from the NEA database.

Element	NEA Basalt K_d Ranges (mL/g)
I	5.0E−02
Sr	2.0 to 1000
Tc	1.5E−01 to 5.5

Table 2-11. Sorption coefficient ranges identified in WAG 3.[a]

Element	Sediment K_d (Range) mL/g	Basalt K_d (Range) mL/g
C	5 (2-20)[b]	—
I	0.1 (0.02-5)	—
Sr	60 (35-186)[c,d]	6 (1-13)[c,d]
Tc	0[d]	0[d]

a. Source: Rodriquez et al. 1997.

b. Range from NEA (Ticknor and Ruegger 1989) and Sheppard and Thibault (1990).

c. Source: Newman et al., in preparation, *Evaluation of the Mobility of Am, Cs, Co, Pu, Sr, and U through INEEL Basalt and Interbed Materials: Summary Report of the INEL/Clemson University Laboratory Studies*, ER-WAG7-82, INEEL internal report.

d. Source: Del Debbio and Thomas 1989.

Table 2-12. Overview of the radionuclide sorption coefficients (mL/g) used in transport modeling.

		Best Scenario	Realistic Scenario	Conservative Scenario	Worst-Case Scenario
Interbed Sediment Sorption Coefficients (mL/g)	C	20	20	5	2
	I	5	5	0.1	0.01
	Sr	24	24	18	12
	Tc	0.1	0.1	0.01	0
Basalt Sorption Coefficients (mL/g)	C	7.1	7.1	5	1.7
	I	1	1	0.1	0
	Sr	13	13	6	1
	Tc	0.24	0.24	0.01	0

Table 2-13. Selection rationale for the range of K_d values (mL/g) used in the sensitivity analysis.

Radionuclide	Range for K_d values (mL/g) used in transport model	Selection Rationale[a]
C (sediment)	2–20	Default: Ref. #1 loam soil K_d = 20 Site Values: WAG 3 Ref. #2 and #3 K_d = 2–20 Literature Confirmation: Sand Ref. #1 K_d = 5
C (basalt)	1.7–7.1	Site Values: WAG 3 K_d = not reported Literature Confirmation: The lowest reported Ref. #4 K_d = 1.7
I (sediment)	0.01–5	Default: Ref .#1 loam soil K_d = 5 Site Values: WAG 3 Ref. #2 K_d = 5 Literature Confirmation: No referenced value as low as K_d = 0.01
I (basalt)	0–1	Site Values: WAG 3 Ref. #2 K_d = 0 Literature Confirmation: Ref. #3 K_d = 0.05, Ref. #1 for sand K_d = 1
Sr (sediment)	12–24	Ref. #1 loam soil K_d = 20 Site Values: WAG 3 Ref.#2 K_d = 12–24 Literature Confirmation: Ref. #5 reports a range of 35–52 alluvium and 110–186 for interbed sediments
Sr (basalt)	1–13	Site Values: WAG 3 Ref. #2 K_d = 1–13 Literature Confirmation: Ref. #5 reports a range of 1.1–2.7 for crushed basalt column tests, Ref. #4 K_d = 2–1000
Tc (sediment)	0–0.1	Default: Ref. #1 loam soil K_d = 0.1 Site Values: WAG 3 Ref. #2 K_d = 0 Literature Confirmation: Ref. #3 lowest measured sand K_d = 0.02
Tc (basalt)	0–0.24	Site Values: WAG 3 Ref. #2 K_d = 0 Literature Confirmation: Ref. #5 measured K_d = 0.016 for crushed basalt column tests; Ref. #3 K_d = 0.15–5.5

a. References:

1. Sheppard and Thibault 1990.
2. Rodriquez et al. 1997.
3. NEA database (Ticknor and Ruegger 1989).
4. Thibault, Sheppard, and Smith 1990.
5. Del Debbio and Thomas 1989.

saturated K_d values for unsaturated transport simulation is not a specific concern.

The modeling study conducted for the *Remedial Investigation/Baseline Risk Assessment* (RI/BRA) *for INTEC* (Rodriguez et al. 1997) used the sediment distribution coefficient for the alluvium and the interbed sediments, a zero distribution coefficient for the vadose zone basalts, and 1/25 of the sediment distribution coefficient for the aquifer basalts. The vadose zone basalts were assumed to have a zero distribution coefficient in the RI/BRA, based on the assumption that the water moves more quickly through vertical fractures in the vadose zone. This allows very little time for the contaminant to sorb to the basalt. In the aquifer, the RI/BRA modeling assumed that the water moves more slowly through the basalt fractures and matrix and there is sufficient time for the contaminants to sorb in the basalts.

The RI/BRA modeling also based the aquifer basalt distribution coefficients on an evaluation of the ratio of the distribution coefficient for sediments to that for basalts from the Del Debbio and Thomas (1989) report. Here they found the ratio to the 1/25. The Del Debbio and Thomas (1989) report, however, provides conflicting information on the differences in sediment and basalt distribution coefficients. This report provides for higher distribution coefficients in the basalts (based on breakthrough curve studies) in comparison to the batch distribution coefficient study. Because of this, the distribution coefficients for basalts were treated as uncertain as well as the sediment distribution coefficients.

Three separate combinations of sorption coefficients were evaluated in the uncertainty of the K_d values (see Section 7). The sorption coefficients listed for the conservative case were used in the bounding analysis presented in Sections 3 and 4. The remaining cases (i.e., worst-case and realistic/best) were used in the uncertainty analysis presented in Section 7. Listed below are guidelines and criteria used in the distribution coefficient selection process.

2.1.6.1.1 Strontium—The basalt values were based on the range presented in Table 2-13, with the worst-case scenario being assigned the lowest reported values in the range and the best/realistic case being assigned the highest value in the reported range. The conservative values (i.e., bounding case) were assigned the mid-point of the reported basalt K_d range.

The sediments (i.e., interbed sediments in the unsaturated zone) were assigned K_d values based upon the modeling conducted for WAG 3 CERCLA groundwater modeling at INTEC (Rodriquez et al. 1997). This modeling showed that a K_d value of 12 for the sediment resulted in ^{90}Sr groundwater concentrations higher than measured. A sediment value of 24 also was investigated and showed a closer match of the modeled concentrations with the measured concentrations. Therefore, the best/realistic scenario was assigned a K_d value of 24 for the interbed sediments, while the worst-case scenario was assigned a value of 12. The conservative case was assigned the mid-point value of the range.

2.1.6.1.2 Carbon—The basalt values were based on the Atomic Energy Commission range presented in Table 2-13. The worst-case scenario was assigned the lowest reported value, while the best/realistic scenario was assigned the high value for the range.

The sediment K_d values were taken from the range reported in Table 2-13, with the worst-case scenario being assigned the low value of the range and the best/realistic scenario being assigned the high value of the range. The conservative case was assigned a value of 5 mL/g, which was closer to the low end of the reported range.

As noted above, sand K_d values were selected for ^{14}C for transport simulations in the basalts where site-specific basalt K_d values were not available (Table 2-9). The published sand K_d values were obtained from Sheppard and Thibault (1990). It was assumed that the lower sand K_d values are more representative of the sorptive behavior of ^{14}C in basalt. This assumption is based on the coating of weathered mineral or chemical precipitates on sand grains and the irregular fracture surfaces that can react with the radionucludies. While the surface area to the void-

space ratio for fractured media is less than a porous media (thereby reducing the sorptive capability for a fractured media), the presence of abundant iron oxides in basalt fractures capable of sorbing radionuclides offset the surface area effects. The degree of this offset is uncertain and difficult to apply to natural systems.

This approach allows a degree of retardation of ^{14}C in the basalts. The lower sand K_d values, compared with the higher K_d values for finer-grain sediment, are conservative on a relative basis. However, there is an acknowledged degree of uncertainty because of the lack of direct K_d measurements available for ^{14}C in basalt.

2.1.6.1.3 Technetium—The basalt value for the worst-case scenario was based on the value in Table 2-13 of zero. The best/realistic case was assigned a low K_d value of 0.24, which is in the low end of the range. This was done due to the fact that technetium has been found to be mobile at the INEEL Site. The conservative value was set to a very low value of 0.01, again due to reports that technetium is mobile at the INEEL.

The sediment K_d value for the worst-case was taken as zero, while the realistic case was assigned a value of 0.1 based on values in Table 2-13 for loam soil. The conservative value was assigned a value one order of magnitude less than the loam soil value.

2.1.6.1.4 Iodine—The basalt value for the worst-case was assigned a value of zero, while the best/realistic case was assigned a value of 1.0 based on a reasonable upper end for the values reported in Table 2-13. The sediment K_d value for the worst-case was assigned a value of 0.01, while the best/realistic case was assigned a value of 5.0. The conservative case was assigned a value of 0.1.

2.1.6.2 Grout K_d Values. The grout sorption coefficients K_d values were evaluated for the three groundwater pathway scenarios. A review of the Bradbury and Sarott (1995) study on "Sorption Databases for the Cementitious Near-Field of a LLW Repository for Performance Assessment" indicates that the K_d values presented in their study were based on the conservative end of the possible choices (i.e., lower K_d values). Therefore, a combination of grout K_d values were chosen based on Bradbury and Sarott (1995), Allard (1985), and other studies specific to the elements of interest.

Concrete K_d values for reducing conditions have been chosen. The concrete is expected to exhibit strong reducing conditions (Eh from –300 to –500 mV) as do most concrete systems. In addition, the closure system will also consist of a mixture of concrete and fly ash, slag, or other substances to ensure reducing conditions in the grout.

The concrete K_d values were chosen from Region II of Bradbury and Sarott (1995). In Region II, the pore water composition is dominated by portlandite ($Ca(OH)_2$), which fixes the pH at 12.5. The portlandite will be removed slowly by groundwater flow but the quantities contained in the cement are so large that this phase buffers the system over very long periods of time.

Bradbury and Sarott (1995) also discuss a Region III for concrete systems, where the removal of $Ca(OH)_2$ has become significant and the pH falls continuously. The calcium-silicate-hydrate (CSH) gel is no longer stable and begins to dissolve incongruently. However, investigation into the original paper on these concrete regions by Atkinson, Everitt, and Gappy (1989) reveals that concrete is not expected to reach this state until 100,000 yr. Since the PA compliance period is only 1000 yr, the concrete K_d values are not expected to change over this period of time and therefore are held constant. This assumption is supported by the concrete degradation analysis presented in Appendix E. Graphs of the hydraulic conductivity for the tank/grout show no increase over the 1000-yr time period. The concrete degradation sensitivity analysis also shows that the tank/grout hydraulic conductivity does not increase until 800 yr, for the least conservative case, with only a one order of magnitude change in the hydraulic conductivity. Thus, the amount of water available for loss of $Ca(OH)_2$ is still minimal. For conservatism, the PA assumes that the tank fails at 500 yr; however, the degradation analysis indicates the tank/grout life is much longer. In addition, graphs of carbonation degradation and calcium hydroxide leaching do

not show any significant changes during the 1000-yr compliance period for loss of $Ca(OH)_2$.

The selection of concrete K_d values for the three groundwater pathway scenarios are presented in Table 2-14. The following discussion provides justification for each set of sorption coefficients for each element shown in Table 2-14.

2.1.6.2.1 Strontium—Ewart, Terry, and Williams (1985) report strontium distribution ratios for hardened cement paste and concrete between 0.001 and 0.004 m^3/kg with very little dependency on concentration. Atkinson and Nickerson (1988) summarized the results from different types of tests and gave a best-estimate range for strontium of 0.003 to 0.006 m^3/kg. Due to the small difference in K_d values reported for strontium, the worst-case scenario was assigned the low value of 0.001 m^3/kg, and the value was scaled for the other scenarios to a high value of 0.006 m^3/kg for the best/realistic scenario.

2.1.6.2.2 Technetium—Sorption data for technetium on cementitious materials are sparse. Under reducing conditions, technetium is present as hydrolyzed technetium (IV) species. In some recent work, using technetium (IV) at trace levels, distribution ratios of 5 m^3/kg have been reported (Bayliss et al. 1991). Technetium may be expected to sorb strongly under reducing conditions at high pH and Bradbury and Sarott (1995) chose a conservative value (i.e., low value) of 1 m^3/kg for reducing conditions. Therefore, for the TFF PA the conservative value of 1 m^3/kg was chosen for the worst-case scenario, with the K_d values being scaled up to the measured value of 5 m^3/kg for the best/realistic K_d value.

2.1.6.2.3 Iodine—Iodine is assumed to be present as I^- under oxidizing and reducing conditions (Bradbury and Sarott 1995). Many studies on the sorption of I^- on cement paste at high pH indicate that its sorption is low but finite. Bradbury and Sarott (1995) selected a conservative value (i.e., lower value) of 0.002 m^3/kg for I^- in reducing concrete systems. Allard et al. (1985) recommended a K_d value of 0.03 m^3/kg for I^- in concrete systems. Therefore, for the TFF PA the conservative value of 0.002 m^3/kg was chosen for the worst-case scenario, with the K_d value being scaled up to the recommend value of 0.03 m^3/kg by Allard et al. (1985) for the best/realistic case.

Table 2-14. Solubility limits for the TFF grout.

Nuclide	Half-life (yr)	Specific Activity (Ci/g)	Solubility Limit		
			Moles/L	Atoms/L	Ci/L
^{241}Am	4.32E+02	3.44E+00	3.70E–06	2.23E+18	3.06E–03
^{243}Am	7.38E+03	2.00E–01	3.70E–06	2.23E+18	1.79E–04
^{237}Np	2.14E+06	7.05E–04	1.00E–10	6.02E+13	1.67E–11
^{238}Pu	8.78E+01	1.71E+01	3.20E–11	1.93E+13	1.30E–07
^{239}Pu	2.41E+04	6.22E–02	3.20E–11	1.93E+13	4.74E–10
^{240}Pu	6.54E+03	2.28E–01	3.20E–11	1.93E+13	1.75E–09
^{241}Pu	1.44E+01	1.03E+02	3.20E–11	1.93E+13	7.93E–07
^{242}Pu	3.76E+05	3.93E–03	3.20E–11	1.93E+13	3.04E–11
^{230}Th	7.70E+04	2.02E–02	2.50E–10	1.51E+14	1.16E–09
^{234}U	2.45E+05	6.24E–03	2.50E–11	1.51E+13	3.64E–11
^{235}U	7.04E+08	2.16E–06	2.50E–11	1.51E+13	1.27E–14
^{236}U	3.42E+06	4.43E–04	2.50E–11	1.51E+13	2.61E–12
^{238}U	4.47E+09	3.36E–07	2.50E–11	1.51E+13	2.00E–15

2.1.6.2.4 Carbon—Allard, Persson, and Torstenflt (1985) recommend a K_d value for carbon of 5 m^3/kg. Studies by Allard, Torstenflt, and Andersson (1981) and Bayliss et al. (1988) have investigated the sorption of ^{14}C as $^{14}CO_3^{2-}$ in cement/concrete systems. Generally, very high sorption values (approximately 10 m^3/kg) have been reported. Therefore, for the TFF PA the value of 10 m^3/kg has been chosen for the best/realistic case and the value scaled down to 1 m^3/kg for the worst-case scenario.

2.1.6.3 Solubility Limits. Solubility limits for selected nuclides important to the groundwater pathway are shown in Table 2-14 and were taken from Allard, Persson, and Torstenflt (1985). (Solubility limits were not applied to the contaminants in the grout for this PA). Evaluation of the maximum solubility limits from Allard, Persson, and Torstenflt (1985) and a comparison to the pore-water concentrations in the tank grout system indicated little difference between the solubility limits and pore-water concentrations (i.e., a factor of 10 or less). Therefore, solubility limits were not applied in this PA.

2.1.7 Natural Resources

2.1.7.1 Geologic Resources. Geologic resources at the INEEL are very limited in nature. INEEL mineral resources include sand, gravel, pumice, silt, clay, and aggregate. These resources are extracted at several quarries or pits at the INEEL and are used for road construction and maintenance, waste burial activities, and ornamental landscaping. INTEC uses mineral materials extracted from the TRA Gravel Pit, 1 mi (2 km) west of INTEC, and the Lincoln Boulevard Gravel Pit, approximately 7 mi (10 km) north of INTEC. The geologic history of the ESRP makes the potential for petroleum products at the INEEL very low. The potential for geothermal energy exists at the INEEL; however, a study conducted in 1979 identified no economic geothermal resources (Mitchell, Johnson, and Anderson 1980).

2.1.7.2 Water Resources. The Snake River Plain Aquifer, one of the largest and most productive groundwater resources in the United States, underlies the INEEL and adjacent properties. The aquifer is listed as a Class I aquifer and was designated by EPA as a sole-source aquifer in 1991 (EPA 1990). Groundwater from this aquifer supplies most of the water for the area surrounding the INEEL and essentially all drinking water consumed within the ESRP (INEEL 1999b). The water from the aquifer is used for agriculture, food processing, aquaculture, and domestic, rural, public, and livestock water supplies. In total, nearly 4.7 trillion gal (18 trillion L) of water are drawn from the aquifer annually, with the majority going to agriculture (DOE-ID 1998).

Irrigated agriculture provides a significant portion of the economic base for the people of southern Idaho and the Snake River Plain Aquifer plays a major role in meeting irrigation requirements. The aquifer provides ground water for irrigation of over one third of the three million irrigated acres of the ESRP. It is estimated that over 127,000 people depend on the aquifer for domestic and municipal water needs. Total domestic water consumption is approximately 46,000 acre-ft/yr (5.7 million m^3/yr); ground water discharge from well pumpage equals approximately 1.92 million acre-ft (2.37 billion m^3/yr) (EPA 1990).

In addition to providing water for INEEL Site operations and agriculture, the aquifer supplies water for other industries. Water discharged from springs in the Twin Falls-Hagerman area is used to commercially raise fish. The spring water flow of 1,660 ft^3/s (47.0 m^3/s) constitutes 76% of the water used for the commercial production of fish in Idaho. Most of the fish farms discharge water directly into the Snake River. The discharges from Hagerman Springs also significantly contribute to the flow of the Snake River downstream of Twin Falls, Idaho.

Groundwater in the aquifer generally flows from the northeastern recharge areas to the southwestern discharge areas. Nearly 6.5E+06 acre-ft (8.0E+09 m^3) of water is discharged by the aquifer annually. Most of the discharge occurs as spring flow between Hagerman and Twin Falls. About 2.1E+06 acre-ft (2.6E+09 m^3/yr) of irrigation water is pumped from the Snake River Plain Aquifer in a typical

year. About half of this water reenters the ground as return flow to the aquifer (INEEL 1999b).

The altitude of the regional groundwater surface underlying the INEEL ranges from about 4,600 ft (1,400 m) in the north to about 4,400 ft (1,300 m) near the southwest boundary of the INEEL. The average hydraulic gradient slopes to the south and southwest on the INEEL at about 4 ft/mi (0.8 m/km). Within the INEEL boundaries, the depth below the land surface to the regional groundwater table ranges from 200 ft (60 m) in the northeast to 900 ft (300 m) in the west-southwest (INEEL 1999b).

The Snake River Plain Aquifer is the only source of water used at the INEEL. The combined groundwater withdrawal averages approximately 7E+06 gal/d (3E+07 L/d) or 8,000 acre-ft/yr (1E+07 m^3/yr). Table 2-15 lists the INEEL production wells, the depth of the wells, the depth to water at the wells, and the annual volume of water withdrawn from the wells. All wells withdraw water from the main body of the Snake River Plain Aquifer. The water withdrawn from each well is used for potable water on the Site, for ground maintenance, and for necessary facility operations (INEEL 1999b).

The underflow of the INEEL (i.e., the amount of water passing directly under the INEEL boundaries) is approximately 4.7E+11 gal/yr (1.8E+12 L/yr). The INEEL consumption is less than 1% of the INEEL underflow and less than 0.1% of the total annual aquifer discharge (INEEL 1999b).

2.1.8 Natural Background Radiation

Monitoring and assessment activities are conducted to characterize existing radiological conditions at the INEEL and the surrounding environment. Results of these activities show that exposures resulting from airborne radionuclide emissions are well within applicable standards and are a small fraction of the dose from background sources.

DOE has compared radiation levels monitored on and near the INEEL with those monitored at distant locations to determine radiological conditions. Results from onsite and boundary community locations include contributions from background conditions and INEEL emissions. These data show that over the most recent 5-yr period for which results are available (1992 through 1996), average radiation exposure levels for boundary locations were no different than those at distant stations. The average annual dose measured by the Environmental Science and Research Foundation Inc. during 1996 was 123 mrem for distant locations and 124 mrem for boundary community locations (DOE-ID 1997b). The corresponding 5-yr averages were 127 mrem for the distant group and 125 mrem for the boundary group. These differences are well within the range of normal variation.

The offsite population could receive a radiation dose as a result of radiological conditions directly attributable to INEEL operations. The dose associated with radiological emissions is assessed annually to demonstrate compliance with the National Emissions Standards for Hazardous Air Pollutants (40 CFR 61, Subpart H, 2002). The effective annual dose equivalent to the maximally exposed individual resulting from radionuclide emissions from INEEL facilities during 1995 and 1996 has been estimated at 0.018 mrem and 0.031 mrem, respectively (DOE-ID 1996, 1997c). These doses are well below both the EPA dose limit (10 mrem/yr) and the dose received from background sources (about 360 mrem/yr).

The annual collective dose to the population surrounding the INEEL, based on 1990 U.S. Census Bureau data, was estimated at 0.3 person rem. This estimate is based on the air emissions from all facilities that were expected to become operational before June 1, 1995 (DOE 1995). The dose applies to a total population of about 120,000 people, resulting in an average individual dose of less than 0.003 mrem. For comparison, this population receives an annual collective dose from background sources of about 43,000 person rem. In 1999, the population doses were revised in the *High-Level Waste Environmental Impact Statement* (DOE 2002); as a result, the dose was estimated at about 0.09 person rem per year.

Table 2-15. INEEL production wells and annual volume pumped.[a,b]

Well Name	Depth of Well (ft bgs)	Depth to Water (ft bgs)	Annual Volume Pumped (gal)
ANP-01	360	208	2.561E+06
ANP-02	340	211	1.433E+06
ANP-08	309	218	3.908E+05
Badging Facility Well	644	489	5.760E+04
CFA-1	639	468	1.473E+07
CFA-2	681	471	1.448E+05
CPP-01	586	460	1.834E+08[c]
CPP-02	605	460	1.834E+08[c]
CPP-04	700	462	1.834E+08[c]
CPP-05	695	447	1.834E+08[c]
EBR-I	1075	596	4.491E+04
EBR II-1	745	632	2.767E+06[d]
EBR II-2	753	630	2.767E+06[d]
FET-1	330	199	1.427E+06
FET-2	455	200	5.067E+05
Fire Station Well	516	420	1.057E+04
NRF-1	535	363	2.594E+06
NRF-2	529	362	9.368E+06
NRF-3	546	363	9.802E+04
NRF-4	597	363	1.649E+07
Rifle Range Well	620	508	9.115E+04
RWMC Production	685	568	4.824E+05
SPERT-1	653	456	3.871E+05
SPERT-2	1,217	463	3.450E+05
TRA-01	600	453	3.595E+07
TRA-03	602	456	2.074E+06
TRA-04	965	463	9.006E+07

a. Note: All wells are withdrawing water from the main body of the Snake River Plain Aquifer and are used as drinking water wells with the exception of Wells ANP-08, Fire Station Well, and NRF-4, which are production wells for facility operations.

b. Source: INEEL 1999b.

c. Total for Wells CPP-01, CPP-02, CPP-04, and CPP-05.

d. Total for Wells EBR II-1 and EBR II-2.

2.2 Principal Facility Design Features

This PA has been developed to support the DOE-ID *Tier 1 Closure Plan for the TFF*. Thus, the PA analysis is intended to define and bound the parameters of a closure action. Much of the site-specific and detailed facility and waste characterization data needed to conduct a projected performance analysis of the TFF closure action are not available at this time. Therefore, several simplifying and bounding assumptions have been made for the TFF PA. This section presents an overview of the TFF design features and factors considered in the TFF PA.

2.2.1 Water Infiltration

Currently, the tanks and vaults at the TFF are covered with 10 ft (3 m) of soil to provide shielding from the liquid waste. The contaminated soils contained in the TFF from historical liquid releases (mainly from piping) are being evaluated under CERCLA. Therefore, at the present time, consideration of a cover and designs to limit water infiltration are not available. The CERCLA ROD for INTEC describes the proposed remedy for the TFF soils (DOE-ID 1999).

The ROD for INTEC and the TFF soils states that a final remedial action selection decision concerning the Tank Farm soils release sites has been postponed and will be developed following additional site characterization, risk analysis, and remedial alternative evaluation. An interim action is selected at the Tank Farm until a final decision is made by the Agencies. The remedy selected for the Tank Farm Soils Interim Action is Alternative 3—Institutional Controls with Surface Water Control. The interim remedy for controlling surface water infiltration includes (a) surface water run-on diversion channels sized to accommodate a 1-in-25-yr, 24-hr storm event and (b) grading and surface sealing the Tank Farm soils or sufficiently covering the Tank Farm so as to divert 80% of the precipitation falling atop the Tank Farm soils area. The interim action is projected to last 8 yr or until a final risk management decision is made and implemented by the Agencies.

Because of the uncertainty of the CERCLA action, the timing, and final remedial action, the infiltration rate was treated as uncertain. Three infiltration rates are analyzed in the uncertainty analysis presented in Section 7. The interim action was not considered in the PA calculations. The 8-yr life of the covering would not have a significant controlling influence on infiltration or radiation dose.

Therefore, the use of an engineered cover at the TFF was not assessed for the conservative case (i.e., coompliance case) groundwater analyses. The higher 4.1 cm/yr infiltration rate for earthen cover material was used for the compliance analyses.

2.2.2 Disposal Unit Cover Integrity

As stated in Section 2.2.1, future actions in the TFF to remediate contaminated soils will be conducted under CERCLA. As such, the future cover design is not known at this time. Therefore, a bounding analysis was conducted for the TFF PA. The overlying 10 ft (3 m) of cover soil was assumed to be the only cover available for the bounding TFF analyses. An infiltration rate of 4.1 cm/yr for an earthen cover was used in the analysis presented in Sections 3 and 4. Since a conservative analysis is being conducted by assuming that no cover is in place, the erosion of the overlying 10 ft (3 m) of soil also was assumed to not take place. In this way, the conservative analysis does not become a “worst-case” analysis. Additional uncertainty analyses are presented in Section 7, where three infiltration rates are investigated.

2.2.3 Structural Stability

The structural stability of the vaults and tanks is provided by the closure concept of grouting all voids. The *High-Level Waste Environmental Impact Statement* (DOE 2002) considered several alternatives for the TFF tanks, including filling them with low-level contaminated grout or leaving a remaining void above the first grout lift. In this PA, the entire tank is assumed to be filled with grout. Therefore, no voids will be available in the TFF system and structural failure (i.e., collapse) is not considered.

An analysis was conducted for the TFF PA to evaluate degradation of the concrete vaults, tanks, and grouted systems (see Section 3 and Appendix E). The degradation analysis was conducted to ensure that assumptions were bounding, including degradation of the vault and outer grout systems at 100 yr, piping releases at closure, and tank degradation at 500 yr. However, the degradation analysis was conducted on the assumption that the entire void space in the vaults and tanks was filled with grout. Therefore, no structural collapse was predicted. Instead, the degradation analysis was conducted to facilitate an evaluation of the changes in hydraulic properties with time.

2.2.4 Inadvertent Intruder Barrier

The concrete vault structures and the closure concept of grouting the void spaces in the tanks provide some protection from intruders. However, the main component of intruder prevention for the TFF PA involves the depth of waste in relation to the ground surface. In most intruder scenarios, the intruder is assumed to excavate a basement for housing construction. The depth of the waste in the TFF tanks precludes the intruder from contacting the waste. The concrete system may preclude an intruder from drilling through the vault/tank structure. Opinions on this protective quality vary, however, depending on the type of drilling equipment employed. An evaluation of the intruder scenarios and the potential barrier to intrusion provided by the TFF closure concept are discussed in detail in Section 5.

2.3 Waste Characteristics

Physical characteristics, hazardous constituents, and radionuclide concentrations have been measured in Tanks WM-182, WM-183, and WM-188. The hazardous constituent concentrations are documented in the *Idaho Hazardous Waste Management Act/Resource Conservation and Recovery Act Closure Plan for Idaho Nuclear Technology and Engineering Center Tanks WM-182 and WM-183* (DOE-ID 2001a). The analytical results and the radionuclide inventory are presented below. The tanks, sand pads, and piping all contribute to the radionuclide inventory. An inventory for each is described in the following sections.

2.3.1 Tank Inventory

The single tank radionuclide inventory is based on the most recent analytical results from sampling of Tanks WM-182, WM-183, and WM-188 and historical data regarding the contents of the eleven 300,000-gal tanks. The TFF radionuclide inventory includes ten 300,000-gal tanks (WM-190 was never used), two sand pads, piping, and the four 30,000-gal tanks. The concentrations for radionuclides lacking current analytical data have been estimated using the ORIGEN2 model (Croff 1980). The model used sodium-bearing waste as the nuclear fuel waste stream and radionuclide concentrations based on closure in 2016. The inventory is designed to be conservative based on data of liquid and solid tank contents and recent sampling data. The conservative approach was maintained by using the highest radionuclide concentrations in the radionuclide inventory calculations, rather than averaging the recently sampled tanks.

To provide for a thorough sensitivity/ uncertainty analysis, four radionuclide inventories were prepared. The conservative inventory has been prepared as the compliance inventory for comparison to the radiation dose criteria established in DOE Order 435.1, "Radioactive Waste Management." The other radionuclide inventories have been prepared to be included in the PA uncertainty analysis described in Section 7 of this report. The scenarios include the worst-case, realistic, and best inventories.

The conservative radionuclide inventory adjusted the radionuclide quantity and concentration to produce a very conservative yet more realistic scenario than used in the worst-case scenario. The worst-case scenario assumes the tank cleaning will not be effective (sodium-bearing waste remains unaltered at a depth of 1 in.). The conservative scenario assumes the tank cleaning is marginally successful. The solid residual is reduced by 10% to 2,085 kg, and the liquid concentration reduced by half. The conservative scenario and the remaining scenarios use predicted values for ^{129}I and ^{99}Tc.

The concentrations of ^{129}I and ^{99}Tc were recognized as being higher than expected based on process knowledge and the fission yield of ^{235}U. Historically, it has been difficult to measure ^{129}I and ^{99}Tc in TFF liquids and solids. Excellent radiochemical separations are difficult to achieve in a sample matrix with relatively high concentrations of ^{137}Cs and ^{90}Sr. Detection of ^{129}I and ^{99}Tc are biased high by interference of these radionuclides.[b]

The conservative (compliance) inventory is significantly greater than the expected results of the planned tank cleaning. Recent cleaning of Tank WM-182 has shown a dramatic decrease in solid mass and liquid concentrations. Additionally, using WM-188 solid sample data is conservative because this tank contained the highest radionuclide content of any of the three recently sampled tanks. Based on past tank operating history and solids sample data, Tank WM-188 solids should represent the highest radionuclide concentrations remaining in tank solids (Tyson 2002).

The assumption that 2,085 kg of solids in the compliance inventory is conservative because tank mockup testing and recent cleaning in Tank WM-182 have shown that tank solids can be flushed and pumped to much lower quantities. Only partial credit is taken for the liquid-waste concentration reduction that will occur during cleaning. The radionuclide concentration is assumed to be 50 % of the sodium-bearing waste sampled in Tank WM-188.

The two additional inventories, the realistic and best scenarios included more efficient waste removal. The realistic scenario assumes a 25% reduction in solid waste and an 80% reduction in liquid concentration. The best scenario assumes a a 50% reduction in solid waste and an 95% reduction in liquid concentration.

b. Letter from M. C. Swenson, INEEL, to V. L. Jacobson, INEEL, 2002, "Response to NRC Questions on the Radiological Source Term for I-129 and TC-99 in Tank Farm Waste," MCS-05-02, October 22.

TFF Tanks WM-182, WM-183, and WM-188 were sampled recently to determine the presence and quantity of radioactive and hazardous constituents (Portage Environmental 2002, Patterson 1999). These three tanks are the only Tank Farm tanks that have been sampled recently and directly. The samples were collected using a remote sampling device. Previously, samples were collected by jetting (steam jets) primarily liquid waste to holding tanks in the New Waste Calcining Facility (NWCF) and the Waste Calcining Facility. The samples were collected for operational data and not intended for characterizing the solid and liquid in the tanks. The recent sampling events were designed to collect solid and liquid data directly from the tank heels. The heels in this case refer to the condition when the tanks are emptied to 10,000 to 15,000 gal of liquid and solid. The data from these tanks serve as an initial characterization of the waste stream and provide the most recent and defensible data of tank solids and liquids.

The most recent data from the tanks were examined to determine which tank contained the greatest radionuclide concentrations.

The analytical data obtained from Tanks WM-182, WM-183, and WM-188 reflect the quantities of radionuclides present when the tank samples were analyzed. Tank WM-188 radionuclide concentrations were the highest of the three tanks and were used to calculate the bounding tank. ^{137}Cs was used as an indicator for residual radionuclide concentrations in the tanks during preparation of this source term. Historically, ^{137}Cs has been used in conjunction with ORIGEN2 to characterize waste for treatment in the NWCF. ^{137}Cs was used as the indicator radionuclide because it is detected accurately and easily using gamma spectroscopy. Solid and liquid data are accurately produced by this method. ^{137}Cs has been consistently monitored during fuel reprocessing operations, and its gamma energy (0.662 Mev) is high enough to provide good detection. ^{137}Ba is the daughter of ^{137}Cs. ^{137}Ba produces the gamma photon measured at (0.662Mev). By convention, the result is reported as ^{137}Cs. ^{137}Ba and ^{137}Cs are in secular equilibrium.

Historically, ^{137}Cs has been used during the operations period of the NWCF to predict concentrations of other nuclides that could not be detected as easily or efficiently. The ^{137}Cs data and the ORIGEN2 numerical code for predicting nuclide concentration in nuclear fuel (or in this case, nuclear fuel waste streams during and after reprocessing) has successfully been used in the past by INTEC Operations to predict concentrations of various nuclides in waste streams to be calcined (Staiger and Millet 2000).

The radionuclide inventory for the tanks is based on the same premise that was used by INTEC Operations. The source term was established initially based on ORIGEN2 data, then adjusted to the ^{137}Cs concentration in Tank WM-188. The mean concentration of ^{137}Cs in Tank WM-188 was used in the calculations to adjust the source term generated by ORIGEN2. Radionuclides detected in WM-188 were input directly into the source term and the ORIGEN2 values were removed. Many nuclides are not detected in the TFF waste stream because of the relatively high concentrations of radioactivity in the waste. The sample matrix makes it difficult to detect radionuclides with low energy emissions or those in relatively low concentrations. The utility of using ORIGEN2 data is increased because it provides a starting point to calculate a concentration. Total strontium is used for ^{90}Sr because of the short half-lives of other strontium isotopes. The analytical data are presented in Appendix A.

The mean concentration for each nuclide in the respective media (solid, liquid) was calculated and then decayed to 2016 using the following formula:

$$A = A_0 e^{-0.693\, t / T_{1/2}} \qquad (2\text{-}1)$$

where

A = activity after time t

A_0 = initial activity

e = natural log

t = decay time

$T_{1/2}$ = radioactive half-life of the nuclide.

Activity levels for radionuclides that weren't analyzed came from ORIGEN2 modeling results (Staiger and Millet 2000). The following description of ORIGEN2 was taken from the Radiation Safety Information Computational Center home page of the Oak Ridge National Laboratory, Oak Ridge, Tennessee (Radiation Safety Information Computational Center 2002):

> *ORIGEN is a computer code system for calculating the buildup, decay, and processing of radioactive materials. ORIGEN2 is a revised version of ORIGEN and incorporates updates of the reactor models, cross sections, fission product yields, decay data, and decay photon data, as well as the source code.*
>
> *ORIGEN2 uses a matrix exponential method to solve a large system of coupled, linear, first-order ordinary differential equations with constant coefficients.*
>
> *ORIGEN2 has been variably dimensioned to allow the user to tailor the size of the executable module to the problem size and/or the available computer space.*

The radionuclide quantities in the ORIGEN2 output were based on the burnup rates and relative percentages of fuel types present in the sodium-bearing waste. These numbers had been normalized to a ^{137}Cs quantity of 1 Ci. The ratio of the ^{137}Cs level in ORIGEN2 to the ^{137}Cs level in the WM-188 samples provided a factor by which the ORIGEN2 radionuclide quantities could be multiplied to provide equivalent WM-188 radionuclide quantities. The ratio between ^{137}Cs in the ORIGEN2 numbers and the sample data for ^{137}Cs in Tank WM-188 is the ratio factor listed in Tables A-7 and A-8.

Closure of the individual TFF tanks is currently planned to occur using the following general sequence (see Section 1.2.2):

1. Remove liquid waste in tanks
2. Empty tank to heel with existing jets
3. Flush tank and piping
4. Empty to heel with existing jets
5. Wash tank and remove waste
6. Video and sample heel residuals
7. Evaluate tank residuals against closure performance objectives
8. Displace heel with grout
9. Fill piping with grout
10. Fill tank vault with grout
11. Fill tank with grout.

Steps 1 through 3 are considered part of the tank deactivation. Steps 4 through 7 are required to remove waste and decontaminate a given tank. These steps may be repeated, as necessary, until the decontamination sequence is no longer effective (i.e., additional decontamination is no longer economically practical). The last four steps will remove remaining tank residuals to the extent readily feasible, stabilize the residuals, and leave the wastes in a solid physical form.

The assumptions given below are based on the closure concept presented above. The bounding tank inventory does not assume that dilution of the liquid or solid waste occurs during washing of the tanks. Credit is only taken for emptying the tanks to a 1-in. (3-cm) solid heel and a 1,318-gal (5,992-L) liquid heel. However, as presented later in the groundwater pathway and intruder analyses, credit for washing and removal of a portion of the liquid fraction of the waste is necessary to meet the performance objectives.

The radionuclide inventory for closure of the 300,000-gal tanks is based on the slurry heel volumes for solids and liquid stated in EDF-1920 (Tyson 2002). The following assumptions were used in the development of the bounding source inventory (Staiger and Millet 2000):

1. A waste consisting of the highest measured concentration of the radionuclides found in any of the solutions or solids currently stored in Tanks WM-182, WM-183, and WM-188 represents the concentration of residual species in the worst-case inventory.

2. Estimates of non-measured residuals are based on the highest calculated amounts conforming to those estimated by D. R. Wenzel,[c] normalized to the highest ^{137}Cs concentration.

3. The tank internals are flushed with water to clean material from all internal surfaces.

4. The acid concentration in the liquid heel after flushing is > pH 2.

5. Residuals associated with the solids heel are neither dissolved nor diluted.

6. Closure operations are successful in removing the liquid heel to a final volume of 1,318 gal (4,989 L of waste).

7. The solids heel is thoroughly mixed, leaving the interstitial liquid with a chemistry equivalent to the liquid heel.

8. The makeup of the solids heel is 27% solid-interstitial liquid and 73% free liquid.

9. The solids heel is removed from the tank down to a level of 1 in.

Based on ORIGEN2 and analytical sampling results, the bounding tank source inventory in 2016 will be 24,102 Ci. Activity in the solids portion accounts for 92% (22,133 Ci) of the total curies. Only a small number of the total nuclides contribute significantly to the radionuclide inventory. ^{238}Pu, ^{241}Pu, ^{90}Sr, ^{90}Y, ^{137}Cs, ^{137}Ba, and ^{151}Sm are major contributors to the transuranic activity and fission product activity, respectively. The conservative tank inventory at the assumed time of facility closure (2016) is provided in Table 2-16.

c. Letter from D. R. Wenzel, INEEL, to N. E. Russel, INEEL, 1997, "Calculation of Radionuclide Inventories for Sodium-Bearing Wastes," WEN-23-97, November 26.

Table 2-16. Conservative single tank inventory.

Nuclide	Liquid Activity (Ci)	Solid Activity (Ci)	Total Activity (Ci)	Nuclide	Liquid Activity (Ci)	Solid Activity (Ci)	Total Activity (Ci)
Ac-225	5.7E–09	3.4E–08	4.0E–08	Pb-212	3.0E–05	1.8E–04	2.1E–04
Ac-227	8.6E–07	5.2E–06	6.0E–06	Pb-214	2.0E–07	1.2E–06	1.4E–06
Ac-228	1.0E–11	6.2E–11	7.2E–11	Pd-107	2.5E–04	1.5E–03	1.7E–03
Ag-108m	6.3E–09	3.8E–08	4.4E–08	Pm-146	1.5E–04	8.9E–04	1.0E–03
Am-241	1.8E–01	4.4E–01	6.2E–01	Pm-147	8.6E–02	5.2E–01	6.0E–01
Am-242	2.2E–04	1.3E–03	1.6E–03	Po-210	8.6E–08	5.2E–07	6.0E–07
Am-242m	2.2E–04	1.3E–03	1.6E–03	Po-211	0.0E+00	0.0E+00	0.0E+00
Am-243	3.2E–04	1.9E–03	2.2E–03	Po-212	1.8E–05	1.1E–04	1.3E–04
At-217	5.7E–09	3.4E–08	4.0E–08	Po-213	5.7E–09	3.4E–08	4.0E–08
Ba-137m	5.7E+02	3.4E+03	4.0E+03	Po-214	2.0E–07	1.2E–06	1.4E–06
Be-10	4.6E–08	2.8E–07	3.2E–07	Po-215	8.6E–07	5.2E–06	6.0E–06
Bi-210	8.6E–08	5.2E–07	6.0E–07	Po-216	3.0E–05	1.8E–04	2.1E–04
Bi-210m	3.3E–21	2.0E–20	2.3E–20	Po-218	2.0E–07	1.2E–06	1.4E–06
Bi-211	8.6E–07	5.2E–06	6.0E–06	Pr-144	9.1E–08	5.5E–07	6.4E–07
Bi-212	2.9E–05	1.7E–04	2.0E–04	Pr-144m	1.1E–09	6.5E–09	7.6E–09
Bi-213	5.7E–09	3.4E–08	4.0E–08	Pu-236	1.7E–06	1.0E–05	1.2E–05
Bi-214	2.0E–07	1.2E–06	1.4E–06	Pu-238	2.8E+00	1.4E+01	1.7E+01
C-14	4.9E–01	1.1E–05	4.9E–01	Pu-239	3.5E–01	9.0E–01	1.2E+00
Cd-113m	2.7E–02	1.7E–01	1.9E–01	Pu-240	1.6E–01	9.6E–01	1.1E+00
Ce-142	4.6E–07	2.8E–06	3.2E–06	Pu-241	2.1E+00	1.3E+01	1.5E+01
Ce-144	9.1E–08	5.5E–07	6.4E–07	Pu-242	1.2E–04	7.2E–04	8.4E–04
Cf-249	2.6E–13	1.5E–12	1.8E–12	Pu-244	1.0E–11	6.2E–11	7.2E–11
Cf-250	1.1E–13	6.5E–13	7.6E–13	Ra-223	8.6E–07	5.2E–06	6.0E–06
Cf-251	4.1E–15	2.4E–14	2.8E–14	Ra-224	3.0E–05	1.8E–04	2.1E–04
Cm-242	1.8E–04	1.1E–03	1.3E–03	Ra-225	5.7E–09	3.4E–08	4.0E–08
Cm-243	3.2E–04	1.9E–03	2.2E–03	Ra-226	2.0E–07	1.2E–06	1.4E–06
Cm-244	1.6E–02	9.6E–02	1.1E–01	Ra-228	1.0E–11	6.2E–11	7.2E–11
Cm-245	4.6E–06	2.8E–05	3.2E–05	Rb-87	4.5E–07	2.7E–06	3.1E–06
Cm-246	3.0E–07	1.8E–06	2.1E–06	Rh-102	5.7E–07	3.4E–06	4.0E–06
Cm-247	3.3E–13	2.0E–12	2.3E–12	Rh-106	1.8E–06	1.1E–05	1.3E–05
Cm-248	3.6E–13	2.2E-12	2.5E–12	Rn-219	8.6E–07	5.2E–06	6.0E–06
Co-60	7.0E–02	1.4E–01	2.1E–01	Rn-220	3.0E–05	1.8E–04	2.1E–04
Cs-134	6.0E–03	4.7E–02	5.3E–02	Rn-222	2.0E–07	1.2E–06	1.4E–06
Cs-135	1.4E–02	8.3E–02	9.6E–02	Se-79	6.9E–03	4.1E–02	4.8E–02
Cs-137	5.7E+02	3.4E+03	4.0E+03	Sm-146	4.2E–09	2.5E–08	3.0E–08
Eu-150	1.7E–07	1.0E–06	1.2E–06	Sm-147	1.1E–07	6.9E–07	8.0E–07

Table 2-16. (continued).

Nuclide	Liquid Activity (Ci)	Solid Activity (Ci)	Total Activity (Ci)	Nuclide	Liquid Activity (Ci)	Solid Activity (Ci)	Total Activity (Ci)
Eu-152	2.0E–02	1.2E–01	1.4E–01	Sm-148	5.7E–13	3.4E–12	4.0E–12
Eu-154	9.1E–01	3.0E–01	1.2E+00	Sm-149	5.2E–14	3.1E–13	3.6E–13
Eu-155	1.1E–01	2.4E+00	2.6E+00	Sm-151	4.7E+00	2.8E+01	3.3E+01
Fr-221	5.7E–09	3.4E–08	4.0E–08	Sn-121m	7.3E-4	4.5E–03	5.2E–03
Fr-223	1.2E–08	7.2E–08	8.4E–08	Sn-126	6.3E–03	3.8E–02	4.4E–02
Gd-152	2.2E–14	1.3E–13	1.6E–13	Sr-90	4.1E+02	7.6E+03	8.0E+03
H-3	8.0E–02	4.8E–01	5.6E–01	Tc-98	3.9E–08	2.4E–07	2.8E–07
Ho-166m	6.9E–07	4.1E–06	4.8E–06	Tc-99	1.5E–01	9.0E–01	1.0E+00
I-129	3.7E–04	2.2E–03	2.6E–03	Te-123	5.7E–15	3.4E–14	4.0E–14
In-115	1.5E–12	8.9E–12	1.0E–11	Te-125m	1.9E–03	1.1E–02	1.3E–02
La-138	3.0E–12	1.8E–11	2.1E–11	Th-227	8.6E–07	5.2E–06	6.0E–06
Nb-93m	2.9E–02	1.7E–01	2.0E–01	Th-228	3.0E–05	1.8E–04	2.1E–04
Nb-94	1.7E–02	7.7E+00	7.7E+00	Th-229	5.7E–09	3.4E–08	4.0E–08
Nd-144	2.5E–11	1.5E–10	1.7E–10	Th-230	1.4E–05	8.3E–05	9.6E–05
Ni-59	1.3E–02	1.6E–01	1.7E–01	Th-231	3.2E–04	1.9E–03	2.2E–03
Ni-63	4.3E–01	2.6E+00	3.0E+00	Th-232	1.1E–11	6.5E–11	7.6E–11
Np-237	1.7E–03	5.9E–03	7.6E–03	Th-234	3.2E–04	1.9E–03	2.2E–03
Np-238	1.1E–06	6.5E–06	7.6E–06	Tl-207	8.6E–07	5.2E–06	6.0E–06
Np-239	3.2E–04	1.9E–03	2.2E–03	Tl-208	1.0E–05	6.2E–05	7.2E–05
Np-240m	1.0E–11	6.2E–11	7.2E–11	Tl-209	1.3E–10	7.6E–10	8.8E–10
Pa-233	4.5E–02	2.7E–01	3.1E–01	Tm-171	6.9E–14	4.1E–13	4.8E–13
Pa-231	1.5E–06	8.9E–06	1.0E–05	U-232	2.9E–05	1.7E–04	2.0E–04
Pa-234	4.1E–07	2.4E–06	2.8E–06	U-233	3.7E–06	2.2E–05	2.6E–05
Pa-234m	3.2E–04	1.9E–03	2.2E–03	U-234	1.3E–02	7.6E–02	8.8E–02
Pb-209	5.7E–09	3.4E–08	4.0E–08	U-235	6.0E–05	4.1E–04	4.7E–04
Pb-210	8.6E–08	5.2E–07	6.0E–07	U-236	3.2E–05	3.1E–03	3.1E–03
Pb-211	8.6E–07	5.2E–06	6.0E–06	U-237	5.3E–05	3.2E–04	3.7E–04
Ru-106	1.8E–06	1.1E–05	1.3E–05	U-238	8.2E–05	2.4E–04	3.3E–04
Sb-125	7.4E–03	4.5E–02	5.2E–02	U-240	1.0E–11	6.2E–11	7.2E–11
Sb-126	8.6E–04	5.2E–03	6.0E–03	Y-90	4.1E+02	7.6E+03	8.0E+03
Sb-126m	6.3E–03	3.8E–02	4.4E–02	Zr-93	3.3E–02	2.0E–01	2.3E–01
Ru-106	1.8E–06	1.1E–05	1.3E–05				

The TFF also has four belowground 30,000-gal stainless-steel tanks designated as Tanks WM-103, -104, -105, and -106. These tanks last stored HLW in 1974 and stored evaporator condensate until 1983. The tanks were taken out of service in 1983 and the tank inlets have been cut and capped (INEEL 1999a). The contents of these tanks were sampled for RCRA constituents in 1990 and then emptied. The sampling analysis provided limited radionuclide information, as follows[d]:

- The sample for Tank WM-103 was 35 mR/hr and had a ^{137}Cs content of 398 ± 17 disintegration per second per milliliter (d/s/mL) (11 ± 0.46 nCi/mL).

- The sample for Tank WM-104 was 35 mR/hr and had a ^{137}Cs content of 2,780 ± 150 d/s/mL (75 ± 4.0 nCi/mL) and a ^{154}Eu content of 4.5 ± 1 d/s/mL (0.12 ± 0.03 nCi/mL).

- The sample for Tank WM-105 was 35 mR/hr and had a ^{137}Cs content of 192 ± 9 d/s/mL (5.2 ± 0.24 nCi/mL).

- The sample for Tank WM-106 was 35 mR/hr, had a ^{137}Cs content of 1,280 ± 59 d/s/mL (35 ± 1.6 nCi/mL), and a ^{134}Cs concentration of 10.8 ± 1.3 d/s/mL (0.29 ± 0.035 nCi/mL).

Using the same analogy used in the development of the conservative tank inventory for the 300,000-gal tanks, an estimate of the total ^{137}Cs activity in a 30,000-gal tank was made using the data from Staiger and Millet (2000):

- The 30,000-gal tanks have the same composition in terms of the contributions to activity for liquid and solids as the 300,000-gal tanks.

- The 30,000-gal tanks contain 10% of the residuals contained in the 300,000-gal tanks.

- The 300,000-gal tanks have 4.9E+06 mL of liquids and 1.25E+06 mL of solids. Therefore, the 30,000-gal tanks contain 4.9E+05 mL of liquids and 1.25E+05 mL of solids, for a total volume of 6.2E+05 mL of residual contamination.

- The maximum ^{137}Cs content of a given 30,000-gal tank was calculated based on the sample for WM-104, with a ^{137}Cs concentration of 75 nCi/mL.

These assumptions result in a maximum ^{137}Cs tank content of 0.046 Ci for the 30,000-gal tanks.

A comparison of the ^{137}Cs activity calculated for the 30,000-gal tanks (i.e., 0.046 Ci) with the ^{137}Cs content of the 300,000-gal tanks from the inventory indicates that the contamination levels in the 30,000-gal tanks are insignificant by comparison. Therefore, the inventory for the 300,000-gal tanks is considered to bound any additional contamination that may be released from the 30,000-gal tanks.

2.3.2 Sand Pad Inventory

The sand pads in Tanks WM-185 and WM-187 are contaminated from accidental releases into the vaults in 1962. A description of the leakage into the tanks is available in Latchum et al. (1962). Subsequent to these releases, liquid from sources such as precipitation and irrigation was periodically pumped out of the vaults.

This section presents the background information and the approach, assumptions, and data used to estimate the activity of radionuclides contained in the sand pad beneath the tanks at the TFF. The results from the analysis are provided for each radionuclide in the year 2016, which is the expected closure date. These activities have been estimated by modeling diffusion of radionuclides from the liquid into the sand pad for the contaminating event in 1962. The analysis then models radioactive decay and periodic flushing of the sand pad to estimate activities in 2016.

2.3.2.1 Background Information. Surface water leaking into the tank vault has been a

c. E-mail communication between K. Poor, Portage Environmental, Idaho Falls, Idaho, and Duke Engineering, Idaho Falls, Idaho, April 11, 2000.

common occurrence since the beginning of Tank Farm operations. The top of the vault and tank structure allow surface water to partially fill the vault. Before and subsequent to the 1962 releases, water from precipitation, spring runoff and irrigation has been pumped out of the tank vaults at least semiannually.

The amount of water collected in the vaults is documented in the INEEL internal memorandum, "HLLW Tank Sump Transfer History."[e] The report documents over 100 transfers from Tanks WM-185 and WM-187. Reports are not available before 1962 but water transfers from the vaults are known to have occurred. Water transfers continue from vault sumps. The residual inventory predicted for 2016 is based on 38 "flushing" events when water infiltrated to the vault from leaks in the tank/vault roof and was then jetted out of tank vaults. The 38 events correspond to the number of years from 1962 to 2000. The actual number of water transfers from the tank vaults and associated leaching of radionuclides from the sand pad likely exceeds 130 for each vault to date. Water was jetted from the tank vault sumps at least twice yearly and will continue until each tank is closed.

Details of the sand pad analysis are shown in Appendix A. The results from the analysis are provided for each radionuclide at activities in 2016, which is the expected closure date. These activities have been estimated by modeling diffusion of radionuclides from the liquid into the sand pad for the contaminating event in 1962. The analysis then models radioactive decay and periodic flushing of the sand pad to estimate activities in 2016.

The curb and sand pad at the bottom of the concrete vault were designed to cushion the tank bottom. Additionally, the curb, which has drain holes, allows liquid to drain from the sand pad beneath the tanks to the sumps outside the curb. The sumps were periodically used to remove water that had accumulated in the vaults. Liquid may have been present in the vault from sources such as precipitation, irrigation activities, and accidental spills. The curb is an octagonal shape, creating and area 51 ft between the sides of the octagon (or 52 ft including the 6-in. curb). Because the vault floor is conical and the tank bottom is flat, the thickness of the sand pad ranges from about 2 in. (5 cm) at the tank center to about 6 in. (15 cm) at the curb. The 6-in. × 6-in. curb was installed 6 ft (2 m) from the outside edge of the vault floor. This curb encircles the sand pad and creates an area that is 51 ft (16 m) wide. Because the vault floor is conical and the tank bottom is flat, the thickness of the sand pad ranges from about 3 or 4 in. (8 or 10 cm) at the tank center to about 5 or 6 in. (13 or 15 cm) at the curb.

2.3.2.2 Estimating Approach. The approach to estimate the activities of the radionuclides contained in the TFF sand pad in 2016 is described in this section. The analysis represents a different approach to determine the mass of radionuclides in the sand pad than previous analyses (Poloski 2000). Previous analyses assumed radionuclides entered the entire sand pad and reached an equilibrium partitioning in the sand and the sand pad was subsequently flushed.

The approach presented in this report assumes radionuclides enter the sand pad through diffusion at the curb/sand pad interface. This assumption is reasonable since the contaminated liquid, which entered the vault in 1962, appears to have filled the concrete vault from the bottom toward the vault top (i.e., there was no horizontal pressure gradient driving the liquid through the sand pad). Once contained in the sand pad, radioactive decay and periodic (annual) flushing were modeled to determine the present-day activities. Flushing is assumed to occur 38 times and then the inventory is decayed over 16 years to estimate 2016 activities of all radionuclides.

There are numerous published reference materials that present solutions to diffusion modeling equations (e.g., Crank 1975; Choy and Reible 2000). The following equation describes one-dimensional diffusion from a semi-infinite media with uniform initial concentration and zero

e. Letter from K.J. Rebish, INEEL, to J.M. Roberts and B.H. O'Brien, INEEL, 1993, "HLLW Tank Sump History," KJR-10-93, October 15.

concentration at the surface. Equation (2-2) is shown in Choy and Reible (2000).

$$\frac{\partial C_A}{\partial t} = \left(\frac{D_{A(eff)}}{R_{fA}} \right) \frac{\partial^2 C_A}{\partial z^2} \qquad z \in [0, \infty) \quad (2\text{-}2)$$

where

C_A = concentration of radionuclide A (M/L^3)

t = time (T)

$D_{A(eff)}$ = diffusion coefficient of radionuclide A, assumed to be 10^{-5} cm^2/s, which is conservative for sand (L^2/T)

R_{fA} = retardation factor of radionuclide A in sand (unitless)

z = distance (L).

The boundary conditions associated with Equation (2-2) and its solution include the following:

$$C_A(z,t)\big|_{z=0} = 0 \qquad t > 0 \qquad (2\text{-}3)$$

$$C_A(z,t)\big|_{z \to \infty} = C_{A0} \qquad t > 0 \qquad (2\text{-}4)$$

$$C_A(z,t)\big|_{t=0} = C_{A0} \qquad z \in [0, \infty) \quad (2\text{-}5)$$

where

C_{A0} = initial concentration of radionuclide A (M/L^3).

The boundary and initial conditions [Equations (2-3) through (2-5)] for Equation (2-2) describe a semi-infinite system with a constant initial concentration of radionuclide A (C_{A0}) and represent transport (diffusion) toward the surface, where the concentration is maintained at zero. The zero concentration boundary condition implies that as soon as the contaminant diffuses to the surface, it is immediately removed. For mass transport in the sand pad, this assumption is conservative (i.e., it does not underestimate mass transfer at the liquid/sand pad interface).

The analytical solution to Equation (2-2), using boundary and initial conditions in Equations (2-3) through (2-5) for the surface flux, $j_A(t)$, in units of M/L^2T is offered in Choy and Reible (2000):

$$j_A(t)\big|_{z=0} = C_{A0} \sqrt{\frac{D_{A(eff)} R_{fA}}{\pi t}} \qquad t > 0 \qquad (2\text{-}6)$$

Equation (2-6) determines the amount of a contaminant that diffuses through the liquid/sand pad interface. Records from the accident in 1962 (Latchum et al. 1962) indicate that the time from the introduction of the liquid into the vault to the time when the liquid was pumped out of the vault was approximately 24 hr. Thus, for this analysis the diffusion of radionuclides from the liquid into the sand pad is modeled for 24 hr. Equation (2-6) is used to compute the flux through the liquid/sand pad interface, and the flux time history is integrated over 24 hr to determine the total mass of each radionuclide that enters the sand pad.

After the accident, the mass of each radionuclide in the sand pad is assumed to be impacted by radioactive decay and flushing. These processes are modeled by assuming the mass of radionuclides in the sand pad undergoes radioactive decay for a period of time representing the length of time between flushing events. Then the system is flushed. During flushing, the sand pad is assumed to be saturated and the radionuclides are partitioned at equilibrium between the liquid and solid phase according to their K_d values. The flushing is assumed to remove all liquid and radionuclides that have partitioned into the liquid phase from the sand pad except for the residual liquid. Thus, the radionuclides remaining in the sand pad are contained in the residual liquid and sorbed onto the sand. Then the mass of radionuclides in the sand pad is again calculated, assuming radioactive decay occurs over a period of time that represents the time between flushing events. The cycle of modeling radioactive decay and flushing is repeated until present-day activities are computed.

In the absence of data, it was assumed that the flushing events occurred once a year for 38 yr (i.e., each year the seasonal effects of precipitation and irrigation are purged from the vaults). After present-day activities are computed, these results are decayed over 16 years to 2016, which corresponds to the time of TFF closure.

To determine the mass of radionuclides in the sand pad following the initial event in 1962, the radioactive decay and flushing of the sand pad is modeled. A number of existing programs were examined, including the DUST-MS computer code (Sullivan 1993 and 1996). However, the repeated radioactive decay and flushing cycles made using these models, especially data entry, a burden. Consequently, a FORTRAN computer code was developed to model radioactive decay and then flushing of the sand pad based on partition coefficients and the volume of sand, void space, and residual saturation. The mathematical formulation of this approach is provided below; the FORTRAN source code is presented in Appendix A.

Radioactive decay is modeled using a first-order differential equation with a rate constant that represents the radionuclide's half-life. For chain decay, the same first-order differential equation is applicable; however, an additional term accounts for the increase in the mass of a daughter product. The following illustrates the appropriate equations for a three-member decay chain (Thorne et al. 2000).

The differential equations that define the rate change of atoms in each compartment (i.e., for each radionuclide in the decay chain) are as follows:

$$\frac{dq_1}{dt} = -k_1\, q_1 \qquad (2\text{-}7)$$

$$\frac{dq_2}{dt} = k_1\, q_1 - k_2\, q_2 \qquad (2\text{-}8)$$

$$\frac{dq_3}{dt} = k_2\, q_2 - k_3\, q_3 \qquad (2\text{-}9)$$

where

q_i = atoms of radionuclide i (unitless)

t = time (yr)

k_i = decay constant for radionuclide i (yr^{-1}).

Solutions to the above differential equations obtained by Laplace transforms are as follows:

$$q_1(t) = q_1(0)\, e^{-k_1 t} \qquad (2\text{-}10)$$

$$q_2(t) = \frac{k_1\, q_1(0)}{k_1 - k_2}\left(e^{-k_2 t} - e^{-k_1 t}\right) + q_2(0)\, e^{-k_2 t} \qquad (2\text{-}11)$$

$$q_3(t) = \frac{k_1 k_2\, q_1(0)}{(k_2 - k_1)(k_3 - k_1)} e^{-k_1 t} + \frac{k_1 k_2\, q_1(0)}{(k_1 - k_2)(k_3 - k_2)} e^{-k_2 t} + \frac{k_1 k_2\, q_1(0)}{(k_1 - k_3)(k_2 - k_3)} e^{-k_3 t} + \frac{k_2\, q_2(0)}{(k_3 - k_2)} e^{-k_2 t} - e^{-k_3 t} + q_3(0)\, e^{-k_3 t} \qquad (2\text{-}12)$$

The activity (Ci) of each compartment may be determined from these equations by multiplying by the appropriate decay constant. The activity for individual radionuclides that were not part of a decay chain was determined according to Equation (2-10).

After accounting for radioactive decay, this analysis models flushing of the liquid in the sand pad using the following equations. For any radionuclide A, the total mass of radionuclide A in the sand pad is either sorbed onto the solid phase (i.e., sand) or in the liquid phase. That is,

$$M_{TA} = M_{SA} + M_{LA} \qquad (2\text{-}13)$$

where

M_{TA} = total mass of radionuclide A in the sand pad

M_{SA} = mass sorbed onto solid phase

M_{LA} = mass sorbed into liquid phase.

The partitioning between the solid and liquid phases is described according to the following equation.

$$K_{dA} = \frac{C_{SA}}{C_{LA}} \quad (2\text{-}14)$$

where

K_{dA} = partition coefficient of radionuclide A (mL/g)

C_{SA} = solid concentration (g A/g sand)

C_{LA} = liquid concentration (g A/mL liquid).

The solid concentration and liquid concentration of radionuclide A are defined as

$$C_{SA} = \frac{M_{SA}}{M_S} \quad (2\text{-}15)$$

where

M_{SA} = mass of radionuclide A in sand

M_S = mass of sand

and

$$C_{LA} = \frac{M_{LA}}{V_L} \quad (2\text{-}16)$$

where

M_{LA} = mass of radionuclide A in liquid

V_L = volume of liquid in sand void space.

Substituting Equations (2-15) and (2-16) into Equation (2-14) and simultaneously solving for the two unknown variables (i.e., M_{SA} and M_{LA}) in the resulting equation and in Equation (2-13), yields (2-17).

$$M_{LA} = \frac{M_{TA}}{\left(1+\frac{K_{dA}M_S}{V_L}\right)} \quad (2\text{-}17)$$

Substituting this equation into Equation (2-13) and solving for M_{SA} yields

$$M_{SA} = \left(1 - \frac{1}{\left(1+\frac{K_{dA}M_S}{V_L}\right)}\right) M_{TA} \quad (2\text{-}18)$$

After flushing the sand pad, the amount of radionuclide A removed is $(1-\Theta_{res})M_{LA}$, where Θ_{res} is the residual saturation of the sand pad. The amount of radionuclide A remaining in the sand pad is $M_{SA}+(\Theta_{res})M_{LA}$. This remaining amount is then decayed. The radioactive decay and flushing is repeated annually 38 times to determine the present-day activity of radionuclide A. This activity is decayed 16 yr to calculate activities in 2016. The cycle is repeated for each radionuclide.

2.3.2.3 Data and Assumptions. The accidental spill in 1962 is modeled assuming the liquid is present in the vault 24 hr. The 24-hr time is consistent with the estimated time from the beginning of the spill to the time when the spilled liquid was removed by pumping the vault (Latchum et al. 1962). The area of the flux surface (i.e., the liquid/sand pad interface) is assumed to be an annular region having a radius equal to the tank radius and a thickness equal to the maximum sand pad height. That is, this area is approximately equal to the area of a rectangle with a length of $2\pi r$, where r is the radius of the tank (25 ft), and a width of 6 in. (i.e., the maximum estimated height of the sand pad).

The initial amount of each radionuclide in the tanks at the time of the accidental spills was evaluated with limited sampling of Tanks WM-185 and WM-187 on February 14, 1962. A sample also was obtained from each vault during the siphoning; however, limited analyses were conducted. Due to the limited number of radionuclides provided by the analysis, an alternative method was used to determine the radionuclide inventory. An ORIGEN2 simulation of a pseudo aluminum-clad fuel with an initial ^{235}U enrichment of 93% and a burnup of the processed fuel of 18%, Wenzel (1997) evaluated the expected radionuclide content of the tank. The fuel from Materials Test Reactor (MTR) Cycle No. 198 (Dykes 1963) was taken as typical for the fuel processed. Tanks WM-185 and WM-187 only contained aluminum waste prior to the incident in

1962 (Palmer et al. 1999). The reactor contained 4,842 g ^{235}U and had 684 MWd of operation over a 417-day period. For calculation purposes, inventories were normalized to the activity in a typical 200-g element. The 1972 analysis using the ORIGEN2 code is appropriate because the waste source was the same type of MTR fuel that was present in Tanks WM-185 and WM-187 in 1962 when the siphoning event occurred. The ORIGEN2 analysis is the best estimate of the 1962 inventory. The analysis did not account for the decay of radionuclides. The ORIGEN2 data were corrected to the concentration of ^{137}Cs in Tank WM-185 one month before the incident. Data for Tanks WM-185 and WM-187 were shown in the record of the incident (Latchum et al. 1962). Tank WM-185 data were used because of the slightly higher ^{137}Cs concentration. The ^{137}Cs concentration used was 1.71 Ci/L. Appendix A presents the initial (i.e., 1962) inventories of the liquid in Ci/mL for all radionuclides and associated half-lives. Appendix A also gives the data used for decay chain calculations and the partitioning coefficients used in the analysis.

The effective diffusion coefficient for each radionuclide from the liquid to the sand pad is set conservatively high for a liquid diffusion coefficient (1.0E–05 cm^2/s). The sand pad void fraction and residual saturation are 0.34 and 0.30, respectively (typical values for sand) (Thorne et al. 2000). Using the dimensions of the tank and sand pad and a typical density of sand (1.75 g/cm^3), the total mass of sand (M_s) is about 4.14E+07 g. Additionally, the volume of water in the sand pad (V_L) can be computed (i.e., the product of the volume of sand and the void fraction).

Using the input parameters described in this section, Equation (2-6) is used to compute the mass of each radionuclide entering the sand pad in the 24-hr period the liquid was in the vault. With this inventory, radioactive decay is modeled for one year and the sand pad is flushed. Flushing represents the periodic pumping of liquid that collected inside the vault, and is assumed to occur once every year for the 38 yr from 1962 to 2000.

In flushing, the sand is assumed to be saturated and the amount of each radionuclide in the liquid and solid phases is assumed to be partitioned and in equilibrium according to Equation (2-14). Liquid is assumed to be removed from the void space in the sand until the degree of saturation changes from saturated conditions to the residual saturation. The amount of each radionuclide remaining in the sand and residual liquid is then calculated. This mass is decayed for another year, at which time the sand pad is assumed to be flushed again. The decay and flushing cycle is repeated 38 times to determine the activities of each radionuclide in 2000 and the inventory is decayed 16 yr to estimate the activities at the time of closure in 2016.

These assumptions and the data used in the analysis are considered reasonably conservative. That is, available data that represent the modeled system are used; however, when data are not available, conservative assumptions are made. For example, the surface available for diffusive transport in this analysis is assumed to instantaneously remove all radionuclides that reach the surface (i.e., the liquid/sand pad interface). Thus, mass transfer is greater under these conditions than if a concentration gradient is assumed to exist in the sand pad.

Using conservative assumptions and the available data, the analysis is expected to provide a reasonable and conservative estimate of the mass of each radionuclide contained in the sand pad. That is, the actual sand pad inventories are not expected to be larger than these estimates. Table 2-17 lists a summary of results from the diffusion, radioactive decay, and flushing modeling.

2.3.3 Piping Inventory

Analysis of residual metal contamination in process waste piping has recently been performed. The radionuclide inventory for piping has been based on the metal contamination data collected in 2002. The calculations determined a total ancillary piping residual mass of 15.5 kg. The estimate of residual radionuclide inventory in piping is described in Appendix A. The estimate used for the compliance scenario is based on analytical data.

Table 2-17. Inventory for the sand pads at the time of closure (2016).

Nuclide	Ci	Nuclide	Ci	Nuclide	Ci	Nuclide	Ci
^{225}Ac	2.23E–08	^{154}Eu	1.29E+00	^{214}Po	1.13E–05	^{228}Th	1.93E–05
^{227}Ac	1.40E–05	^{221}Fr	2.23E–08	^{215}Po	1.40E–05	^{229}Th	2.23E–08
^{228}Ac	2.33E–01	^{223}Fr	1.93E–07	^{216}Po	2.03E–05	^{230}Th	5.49E–04
^{108}Ag	2.86E–09	^{152}Gd	3.23E–14	^{218}Po	1.13E–05	^{231}Th	8.41E–03
^{108m}Ag	2.86E–09	^{3}H	2.47E–22	^{236}Pu	4.23E–11	^{232}Th	4.44E–12
^{241}Am	1.89E+00	^{166m}Ho	4.15E–07	^{238}Pu	2.00E+00	^{234}Th	8.99E–05
^{242}Am	1.64E–05	^{129}I	1.08E–06	^{239}Pu	1.57E+00	^{207}Tl	1.40E–05
^{242m}Am	1.64E–05	^{115}In	3.71E–12	^{240}Pu	3.54E–01	^{208}Tl	7.33E–06
^{243}Am	1.47E–04	^{138}La	5.33E–11	^{241}Pu	1.88E+00	^{209}Tl	4.82E–10
^{217}At	2.23E–08	^{93m}Nb	1.98E–01	^{242}Pu	5.69E–05	^{210}Tl	1.13E–05
^{137m}Ba	1.50E+03	^{94}Nb	2.29E–02	^{243}Pu	4.11E–16	^{232}U	1.88E–05
^{10}Be	1.80E–07	^{63}Ni	1.64E–10	^{244}Pu	5.99E–12	^{233}U	1.35E–06
^{210}Bi	5.74E–06	^{235}Np	1.79E–24	^{223}Ra	1.40E–05	^{234}U	3.13E–01
^{211}Bi	1.40E–05	^{237}Np	3.72E–04	^{224}Ra	2.03E–05	^{235}U	8.41E–03
^{212}Bi	2.03E–05	^{238}Np	7.77E–08	^{225}Ra	2.23E–08	^{236}U	1.06E–02
^{213}Bi	2.23E–08	^{239}Np	1.47E–04	^{226}Ra	1.13E–05	^{237}U	3.75E–05
^{214}Bi	1.13E–05	^{240}Np	6.59E–15	^{228}Ra	2.33E–01	^{238}U	8.99E–05
^{14}C	3.90E–07	^{240m}Np	5.99E–12	^{87}Rb	7.69E–07	^{240}U	5.99E–12
^{113m}Cd	1.60E–02	^{231}Pa	2.02E–05	^{219}Rn	1.40E–05	^{90}Y	2.26E+02
^{249}Cf	2.42E–16	^{233}Pa	3.72E–04	^{220}Rn	2.03E–05	^{93}Zr	2.11E–01
^{250}Cf	1.37E–17	^{234}Pa	1.44E–07	^{222}Rn	1.13E–05		
^{251}Cf	5.95E–19	^{234m}Pa	8.99E–05	^{126}Sb	1.65E–02		
^{252}Cf	2.79E–25	^{209}Pb	2.23E–08	^{126m}Sb	1.65E–02		
^{242}Cm	1.35E–05	^{210}Pb	5.74E–06	^{79}Se	2.00E–02		
^{243}Cm	7.91E–07	^{211}Pb	1.40E–05	^{146}Sm	3.77E–10		
^{244}Cm	2.21E–04	^{212}Pb	2.03E–05	^{147}Sm	2.53E–06		
^{245}Cm	5.11E–08	^{214}Pb	1.13E–05	^{151}Sm	3.76E+01		
^{246}Cm	1.14E–09	^{107}Pd	4.21E–04	^{121m}Sn	2.06E–03		
^{247}Cm	4.11E–16	^{146}Pm	1.71E–05	^{126}Sn	1.65E–02		
^{248}Cm	1.26E–16	^{147}Pm	3.23E–03	^{90}Sr	2.26E+02		
^{60}Co	1.60E–03	^{210}Po	5.74E–06	^{98}Tc	6.18E–20		
^{135}Cs	5.99E–03	^{211}Po	3.83E–08	^{99}Tc	2.02E–12		
^{137}Cs	1.50E+03	^{212}Po	1.30E–05	^{123}Te	4.93E–16		
^{152}Eu	9.28E–03	^{213}Po	2.19E–08	^{227Th}	1.40E–05		

2.3.4 Residual Radionuclide Inventory in Piping

The *Sampling and Analysis Plan for the Post-Decontamination Characterization of the Process Waste Lines from INTEC Tank Farm Facility Tanks WM-182 and WM-183* (Portage Environmental 2001) was prepared to define the data collection steps for residual contamination in piping. The process waste lines in the TFF have carried acidic waste in solution and have routinely been flushed after waste transfer with either acid or acid plus a water flush. During closure of the tank systems, the piping was triple rinsed with water to remove loose residual waste.

Sections of horizontal and vertical process waste line have been removed from Tank WM-182. Samples from the decontaminated process waste lines were collected; these data are used to represent the effectiveness of triple rinsing all of the lines remaining in the WM-182 and WM-183 tank systems. The piping was removed from the system and 2- to 6-in.-long sections of the pipe were removed from each end using a wheel pipe cutter. Rinsate samples from the pipes were collected and analyzed for metals. The piping was filled with water (sealed at one end with an inert cap), allowed to equilibrate for a minimum of 30 min, decanted, and analyzed for total metals.

The analytical results for the metals are shown in Appendix A. The concentration of metals in liquid (mg/L) sodium-bearing waste is greater than the concentration of radionuclides (mg/L). Therefore, the residual metal concentration in piping is a conservative estimate of residual radionuclide concentration. The maximum concentration of each metal in the piping rinsate samples was summed with the remaining 23 data points. This yielded a concentration of 2,922 µg/L. The rinsate was collected from 18-in. lengths of the 2.5-in. outside diameter pipe. Several assumptions were made to ensure the estimate of the piping residuals is conservative:

- The mass of metals was assumed to be equal to 1 ft of piping. Therefore, the starting value was 1/3 greater than indicated by the analysis.
- The sample volumes were less than 1 L (less than 300 mL). The data were not adjusted downward to correspond with the actual sample volumes.
- A safety factor of 500 was applied to the data. This safety factor was used to provide a conservative estimate and to provide for the possibility of greater concentrations being found in other piping.

Below are the equations and results that form a basis for this approach. The comparability of metals data to radionuclide data on a mass per unit volume was established by using the specific activity for a few radionuclides that are significant contributors to the inventory. Equation (2-19) shows the calculation for determining grams of ^{137}Cs.

$$Cs_g = Ci / SpA \qquad (2\text{-}19)$$

where

Cs_g = ^{137}Cs grams

Ci = curies of ^{137}Cs in the liquid inventory (1142.5 Ci)

SpA = ^{137}Cs specific activity (87 Ci/g).

Equation (2-20) shows the calculation to determine the mass per unit volume. There is 4,989 L of liquid in each tank.

$$g / L = 13.13g / 4989L \qquad (2\text{-}20)$$

This equation yields a concentration of 3 mg/L. The same equation can be used to determine the concentration in mg/L of the remaining radionuclides. The mass of metals in the tank is found to be greater than the mass of radionuclides. The total concentration of radionuclides is approximately 73 mg/L, while the mass of metals is near 15 g/L.

It is not assumed that the chemical properties of radionuclides and metals are the same; therefore, the conservative assumptions shown above were used to ensure the decontamination

factor for metals was not overstated and the fixed contamination would be included in the estimate. The following equations show the estimated mass of radionuclides in the piping residual based on the conservative inventory.

$$\sum C\max_i = 2922 \mu g / L \qquad (2\text{-}21)$$

where

$Cmax_i$ = maximum concentration of each metal in the rinsate samples.

2,922 µg is assumed to correspond with the mass of metals in 18 in. of process waste pipe. Some waste piping is up to 3 in. outside diameter. To arrive at a conservative estimate, the mass is assumed to correspond to 1 ft of piping. 10,600 linear ft of process waste piping is located in the TFF.

$$m_p = m \times ft_l \times k \qquad (2\text{-}22)$$

where

m_p = total mass in piping

m = mass per linear ft (2,922 µg)

ft_l = total linear ft of pipe (10,600)

k = safety factor of 500.

This equation yields 15.5 kg of sodium-bearing waste solid in the residual piping. The sodium-bearing waste in the conservative inventory is then apportioned to mass. Table 2-18 shows the total Ci by radionuclide for the piping.

Previous estimates were based on work contained in *INTEC Tank Farm Facility Process Waste Line Source Term Estimate* (Wilcox 2000). Wilcox estimated the residual contamination contained in the pipes based on a 0.002-in. film thickness coating the internal surface of process waste piping, not including vessel off-gas lines. Wilcox conducted conversations with INTEC Operations personnel in which they estimated the piping residue thickness within the C2 valve box piping to be about 2 mil (0.002 in.) on the bottom portion of the piping. For conservative reasons, the entire internal piping surface was given a 2-mil thickness. The inventory that is predicted for the piping is approximately one-fourth of the estimate in Wilcox. The inventories of both estimates are similar except for the added conservative assumption to include a 2-mil thickness of the internal pipe surface.

Table 2-18. Radionuclide inventory for piping at 2016.

Nuclide	Ci	Nuclide	Ci	Nuclide	Ci	Nuclide	Ci
^{225}Ac	2.6E−10	^{137}Cs	2.6E+01	^{210}Po	3.8E−09	^{148}Sm	2.6E−14
^{227}Ac	3.8E−08	^{150}Eu	7.7E−09	^{212}Po	8.2E−07	^{149}Sm	2.3E−15
^{228}Ac	4.6E−13	^{152}Eu	9.0E−04	^{213}Po	2.6E−10	^{151}Sm	2.1E−01
^{108m}Ag	2.8E−10	^{154}Eu	2.2E−03	^{214}Po	9.0E−09	^{121m}Sn	3.3E−05
^{241}Am	3.3E−03	^{155}Eu	1.8E−02	^{215}Po	3.8E−08	^{126}Sn	2.8E−04
^{242}Am	1.0E−05	^{221}Fr	2.6E−10	^{216}Po	1.3E−06	^{90}Sr	5.6E+01
^{242m}Am	1.0E−05	^{223}Fr	5.4E−10	^{218}Po	9.0E−09	^{98}Tc	1.8E−09
^{243}Am	1.4E−05	^{152}Gd	1.0E−15	^{144}Pr	4.1E−09	^{99}Tc	7.0E−02
^{217}At	2.6E−10	^{3}H	3.6E−03	^{144m}Pr	4.9E−11	^{123}Te	2.6E−16
^{137m}Ba	2.6E+01	^{166m}Ho	3.1E−08	^{236}Pu	7.7E−08	^{125m}Te	8.4E−05
^{10}Be	2.0E−09	^{129}I	3.6E−05	^{238}Pu	1.0E−01	^{227}Th	3.8E−08
^{210}Bi	3.8E−09	^{115}In	6.6E−14	^{239}Pu	6.7E−03	^{228}Th	1.3E−06
^{210m}B	1.5E−22	^{138}La	1.3E−13	^{240}Pu	7.2E−03	^{229}Th	2.6E−10
^{211}Bi	3.8E−08	^{93m}Nb	1.3E−03	^{241}Pu	9.5E−02	^{230}Th	6.1E−07
^{212}Bi	1.3E−06	^{94}Nb	5.7E−02	^{242}Pu	5.4E−06	^{231}Th	1.4E−05
^{213}Bi	2.6E−10	^{144}Nd	1.1E−12	^{244}Pu	4.6E−13	^{232}Th	4.9E−13
^{214}Bi	9.0E−09	^{59}Ni	1.2E−03	^{223}Ra	3.8E−08	^{234}Th	1.4E−05
^{14}C	8.2E−08	^{63}Ni	1.9E−02	^{224}Ra	1.3E−06	^{207}Tl	3.8E−08
^{113m}Cd	1.2E−03	^{237}Np	4.4E−05	^{225}Ra	2.6E−10	^{208}Tl	4.6E−07
^{142}Ce	2.0E−08	^{238}Np	4.9E−08	^{226}Ra	9.0E−09	^{209}Tl	5.6E−12
^{144}Ce	4.1E−09	^{239}Np	1.4E−05	^{228}Ra	4.6E−13	^{171}Tm	3.1E−15
^{249}Cf	1.2E−14	^{240m}Np	4.6E−13	^{87}Rb	2.0E−08	^{232}U	1.3E−06
^{250}Cf	4.9E−15	^{233}Pa	2.0E−03	^{102}Rh	2.6E−08	^{233}U	1.7E−07
^{251}Cf	1.8E−16	^{231}Pa	6.6E−08	^{106}Rh	8.2E−08	^{234}U	5.6E−04
^{242}Cm	8.2E−06	^{234}Pa	1.8E−08	^{219}Rn	3.8E−08	^{235}U	3.1E−06
^{243}Cm	1.4E−05	^{234m}Pa	1.4E−05	^{220}Rn	1.3E−06	^{236}U	2.3E−05
^{244}Cm	7.2E−04	^{209}Pb	2.6E−10	^{222}Rn	9.0E−09	^{237}U	2.4E−06
^{245}Cm	2.0E−07	^{210}Pb	3.8E−09	^{106}Ru	8.2E−08	^{238}U	1.8E−06
^{246}Cm	1.3E−08	^{211}Pb	3.8E−08	^{125}Sb	3.3E−04	^{240}U	4.6E−13
^{247}Cm	1.5E−14	^{212}Pb	1.3E−06	^{126}Sb	3.8E−05	^{90}Y	5.6E+01
^{248}Cm	1.6E−14	^{214}Pb	9.0E−09	^{126m}Sb	2.8E−04	^{93}Zr	1.5E−03
^{60}Co	1.0E−03	^{107}Pd	1.1E−05	^{79}Se	3.1E−04		
^{134}Cs	3.5E−04	^{146}Pm	6.6E−06	^{146}Sm	1.9E−10		
^{135}Cs	6.1E−04	^{147}Pm	3.8E−03	^{147}Sm	5.1E−09		

3. ANALYSIS OF PERFORMANCE

The methods used to analyze the long-term performance of the TFF are described in this section. Figure 3-1 illustrates the steps taken in the analysis of performance with the final point comparing the dose to the performance objectives.

Five main models were selected and used in the analysis of performance. These models are

1. Groundwater flow/transport models (see Section 3.3.2)

2. Groundwater release model (see Section 3.3.3)

3. Radon flux model (see Section 3.3.4)

4. Atmospheric transport (see Section 3.3.5)

5. Intruder (see Section 5).

Source term development is discussed in Section 3.1. This section includes a description of the inventories assumed, potential mechanisms of contaminant release from the facility, and potential mechanisms responsible for loss of integrity of the engineered TFF barriers.

Following the source term discussion, potential receptors are identified in Section 3.2 by recognizing the time periods of concern in this PA, the potentially significant pathways to human exposure, and exposure scenarios. In this section, the TFF radionuclide inventory for the groundwater pathway is screened to eliminate radionuclides that, under conservative conditions, are insignificant with respect to potential human exposures.

The conceptual models developed and the computational approach used to assess the performance of the TFF also are described in Section 3.2. The conceptual models are derived from technical information presented in Section 2. These models embody a number of simplifying assumptions to facilitate the computational analysis required to assess the long-term performance of the TFF. The dose calculations are presented in Section 3.3.5.

3.1 Source Term

This section discusses factors affecting the rate at which radionuclides are released from the disposal facility. Source term considerations are typically a large source of uncertainty. The uncertainty includes prediction of future conditions of the tanks, vaults, and piping contamination after the closure sequence is completed. The uncertainty is compounded by issues related to the release mechanisms from the waste form. Once releases from the waste form occur, the effectiveness and longevity of the concrete/grout system must be considered. Each of these topics is discussed in the following sections.

3.1.1 Radionuclide Inventory

The inventory used for the analysis of compliance (i.e., conservative case inventory) for a given 300,000-gal tank presented in Section 2.3 was applied to each individual tank. The development of the conservative case is documented in Appendix A and is provided in Section 2.3. The inventory is provided for the year 2016, which is the assumed year of completion of closure activities at the TFF. Two of the tanks contain contaminated sand pads located beneath the tanks (Tanks WM-185 and WM-187). The sand pad activities also are discussed in Section 2.3. In addition, the sand pad contamination was evaluated for the effect of rinsing from water infiltration into the vaults and drainage that occurred from 1962 to 2000. This analysis is provided in Appendix A. Contamination in the piping also was considered. The piping inventory calculations also are provided in Appendix A.

The estimated residual inventory for the INTEC TFF tanks contains several decay chains. Decay chains are important because radionuclides with low inventories at the time of closure may increase over the time of interest because of the decay of their parent radionuclide. The inventory can be divided between radionuclides that are not part of a decay chain, short decay chains (two to three radionuclides), and large decay chains. The

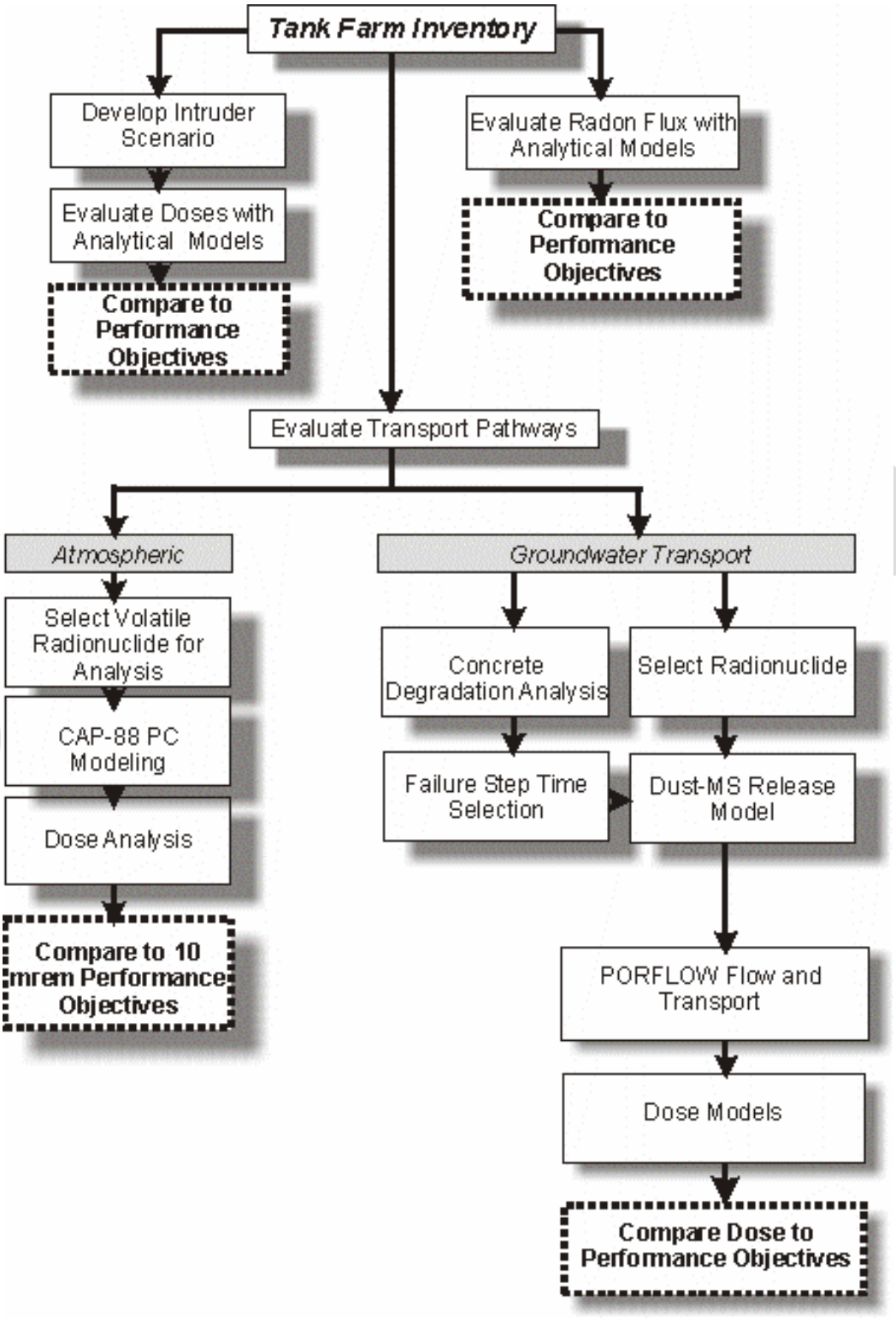

Figure 3-1. Flow chart for the PA analyses.

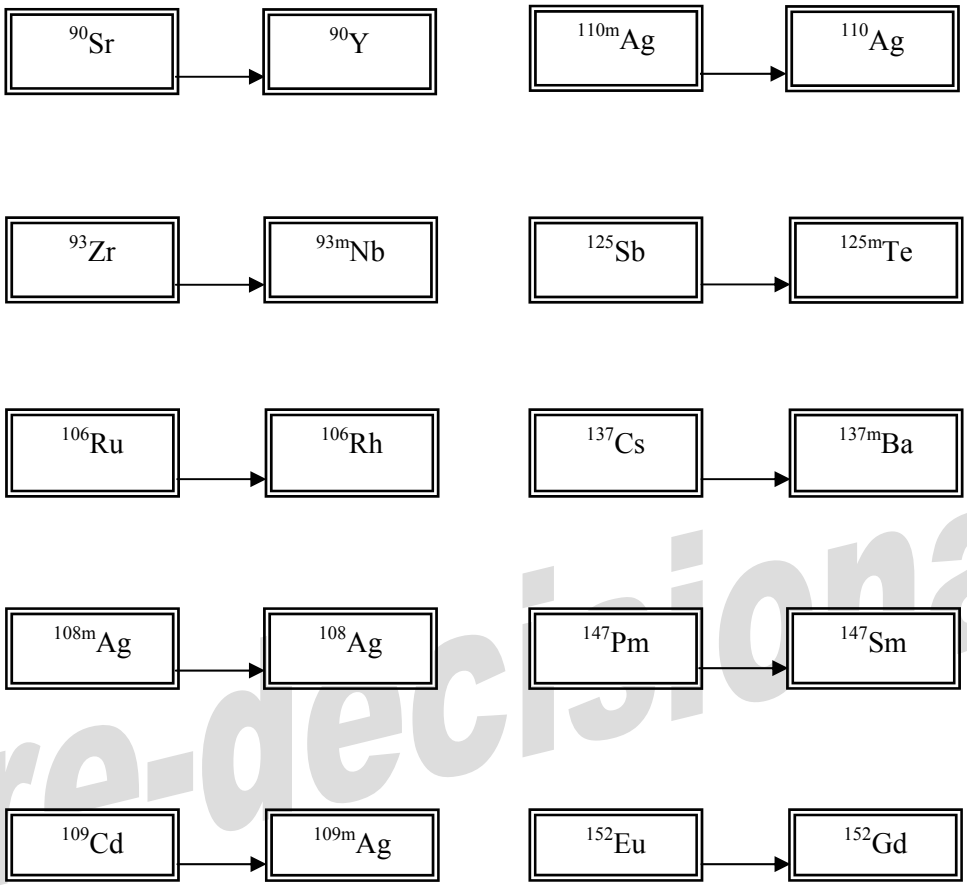

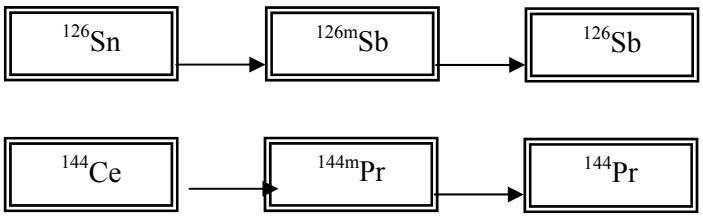

The decay and ingrowth of short decay chain radionuclides are controlled by the following equations. These equations are based on a three-box model defined as

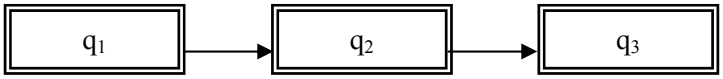

following decay chains were identified in the TFF tank inventories:

The differential equations that define the rate change of atoms in each compartment (i.e., for each radionuclide in the decay chain) are as follows

$$\frac{dq_1}{dt} = -k_1 q_1 \quad (3\text{-}1)$$

$$\frac{dq_2}{dt} = k_1 q_1 - k_2 q_2 \quad (3\text{-}2)$$

$$\frac{dq_3}{dt} = k_2 q_2 - k_3 q_3 \quad (3\text{-}3)$$

where

q = atoms of radionuclide of interest

t = time (yr)

k = decay constant for radionuclide of interest (yr^{-1}).

Solutions to the above differential equations were obtained by Laplace transforms as follows:

$$q_1(t) = q_1(0)\, e^{-k_1 t} \quad (3\text{-}4)$$

$$q_2(t) = \frac{k_1\, q_1(0)}{k_1 - k_2}\left(e^{-k_2 t} - e^{-k_1 t}\right) + q_2(0)\, e^{-k_2 t} \quad (3\text{-}5)$$

$$q_3(t) = \frac{k_1 k_2 q_1(0)}{(k_2 - k_1)(k_3 - k_1)} e^{-k_1 t} + \frac{k_1 k_2 q_1(0)}{(k_1 - k_2)(k_3 - k_2)} e^{-k_2 t} + \frac{k_1 k_2 q_1(0)}{(k_1 - k_3)(k_2 - k_3)} e^{-k_3 t} + \frac{k_2 q_2(0)}{(k_3 - k_2)}\left(e^{-k_2 t} - e^{-k_3 t}\right) + q_3(0) e^{-k_3 t} \quad (3\text{-}6)$$

The activity of each compartment may be determined from these equations by simply multiplying by the appropriate decay constant. The activity for individual radionuclides that were not part of a decay chain was determined according to Equation (3-4).

Four major decay chains were identified in the TFF tank residual inventories: ^{252}Cf, ^{249}Cf, ^{251}Cf, and ^{250}Cf. These decay chains are shown in Figures 3-2 through 3-5. Radionuclides in italics are short-lived progeny that are considered to be in equilibrium with their parent radionuclide. The radionuclide activities as a function of time for the analyses were determined using the RadDecay computer code (Grove Engineering 1990).

3.1.2 Engineered Barriers Degradation and Failure

The following sections address degradation of the cover and the TFF closure system (i.e., vault, tank, grout, and piping). The degradation analyses were conducted to provide support for the PA analyses that assume degradation step changes of 100 yr for the vault and 500 yr for the tanks and piping.

3.1.2.1 Cover Degradation. As stated in Section 2.2.1, future actions in the TFF to remediate contaminated soils will be conducted under CERCLA. As such, the future cover design is not known at this time. Therefore, a bounding analysis was conducted for the TFF PA (i.e., compliance analysis based on the conservative case parameters) and no additional cover was assumed to be available. The overlying 10 ft (3 m) of cover soil was assumed to be the only cover available for the TFF analyses. The erosion of the overlying 10 ft (3 m) of soil also was assumed to not take place. In this way, the analysis conservative case does not become a "worst-case" analysis. Since the TFF lies within an area of relatively flat terrain and a future cover will be placed over the facility, the assumption of no erosion of the existing 10 ft (3 m) of soil cover is considered appropriate.

3.1.2.2 Degradation of the Vault, Grout, Tank, and Piping. The degradation analysis of the TFF closure system (i.e., vaults, tanks, grout, and piping) is described in detail in Appendix E. The following discussion provides an overview of the degradation analysis and the assumptions incorporated into the TFF PA analyses.

Potential degradation mechanisms for the concrete, grout, piping and tanks, and the preferential water pathways were assessed for the TFF PA. The potential degradation mechanisms

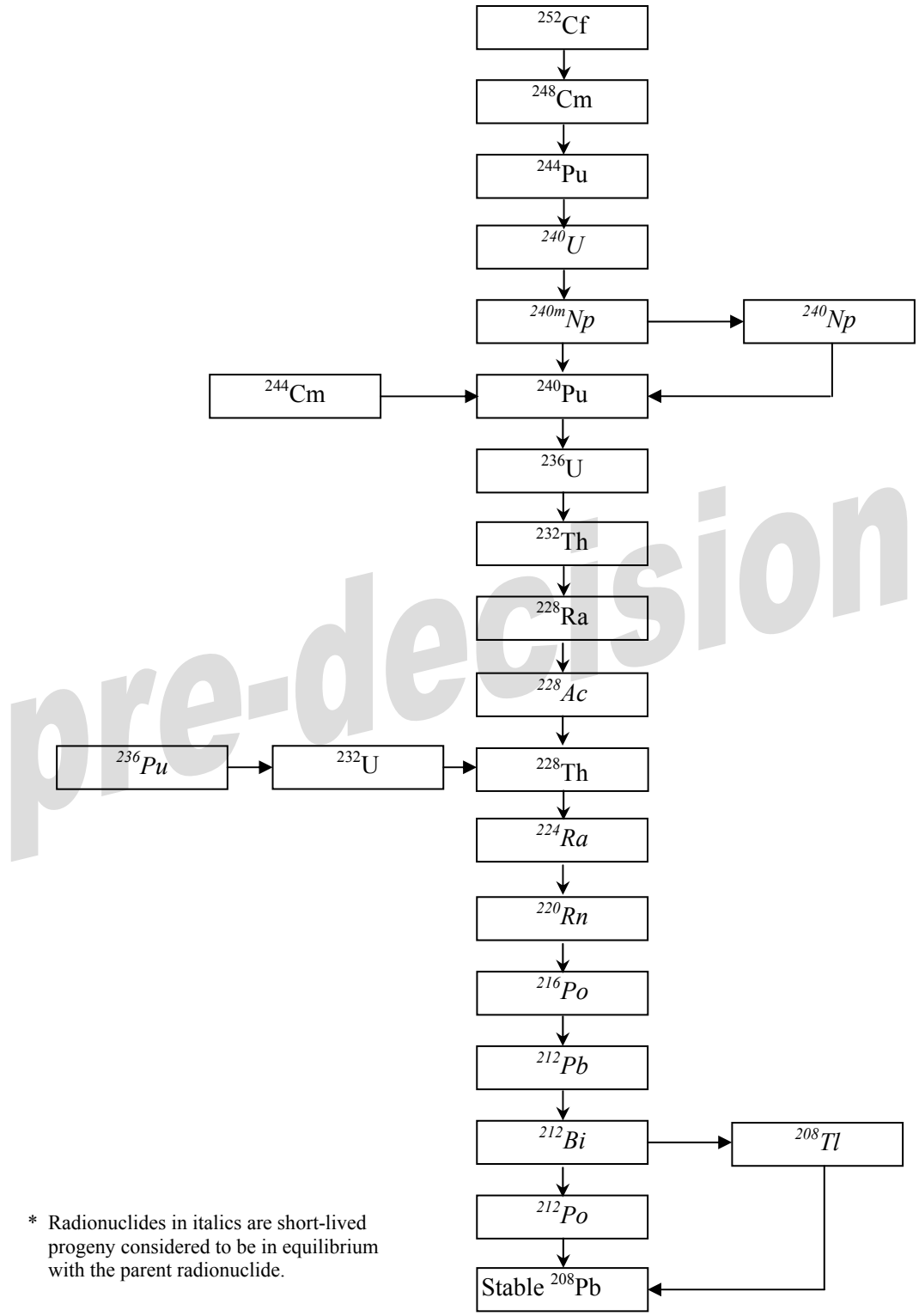

Figure 3-2. ^{252}Cf radionuclide decay chain.

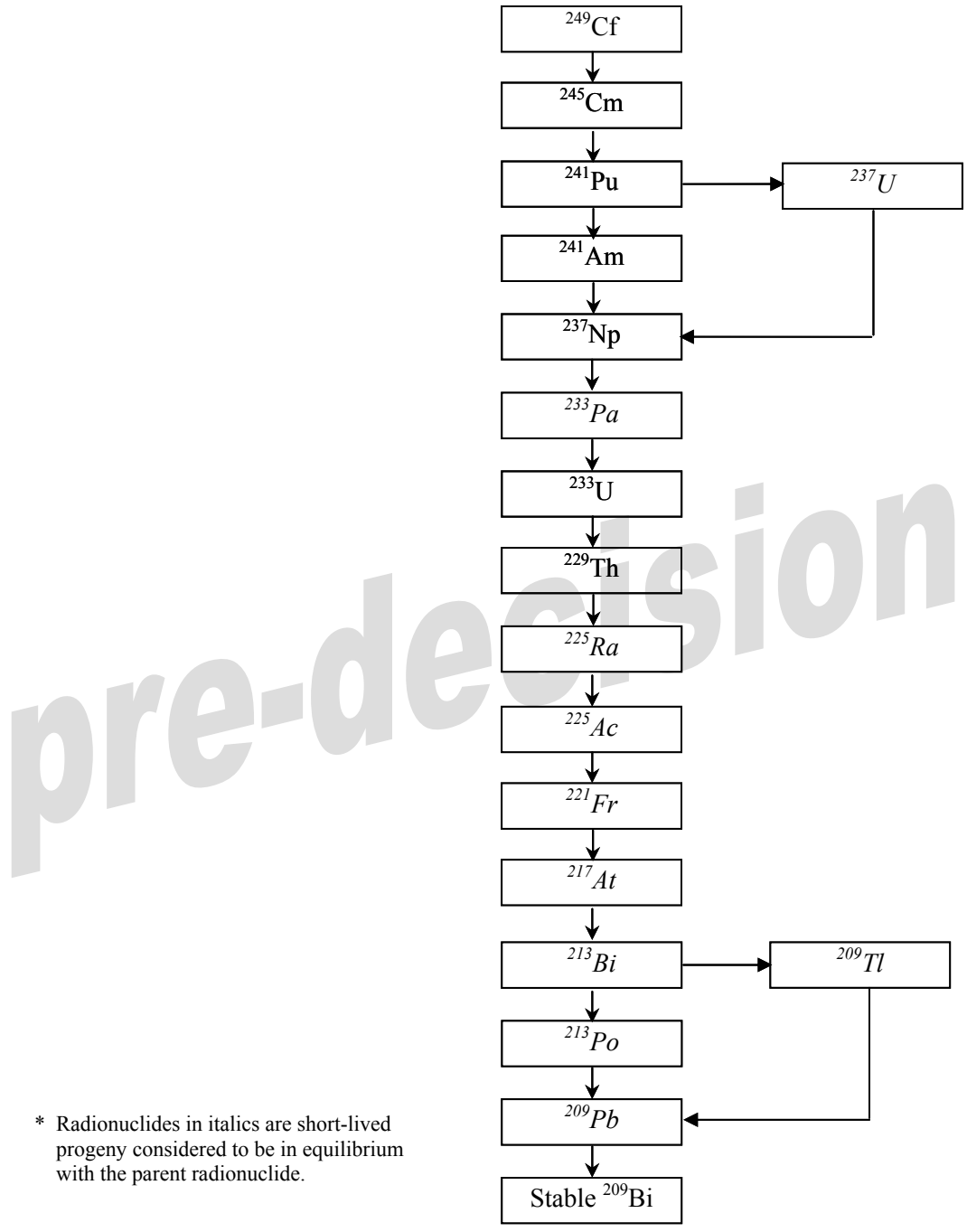

Figure 3-3. ^{249}Cf radionuclide decay chain.

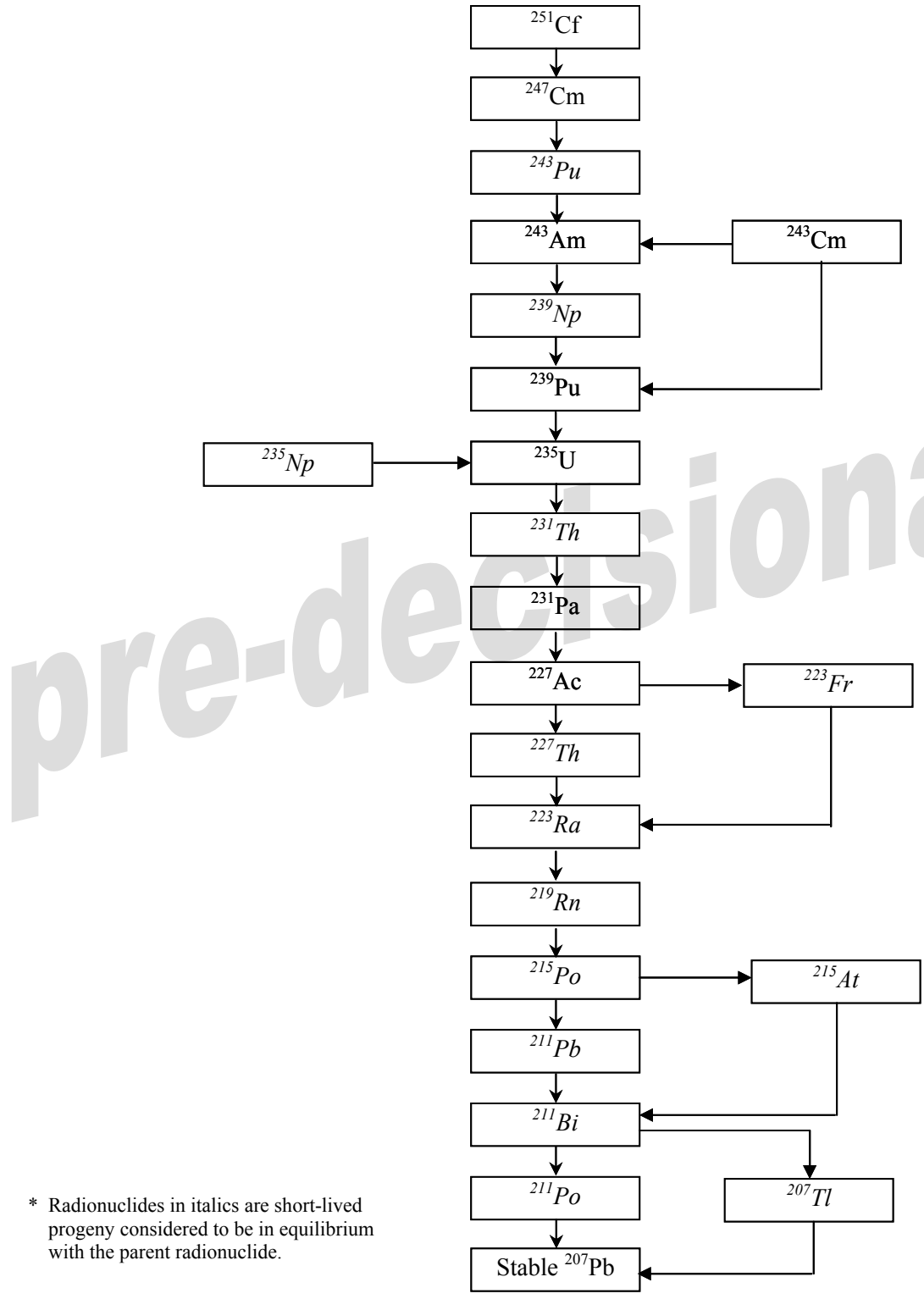

Figure 3-4. ^{251}Cf radionuclide decay chain.

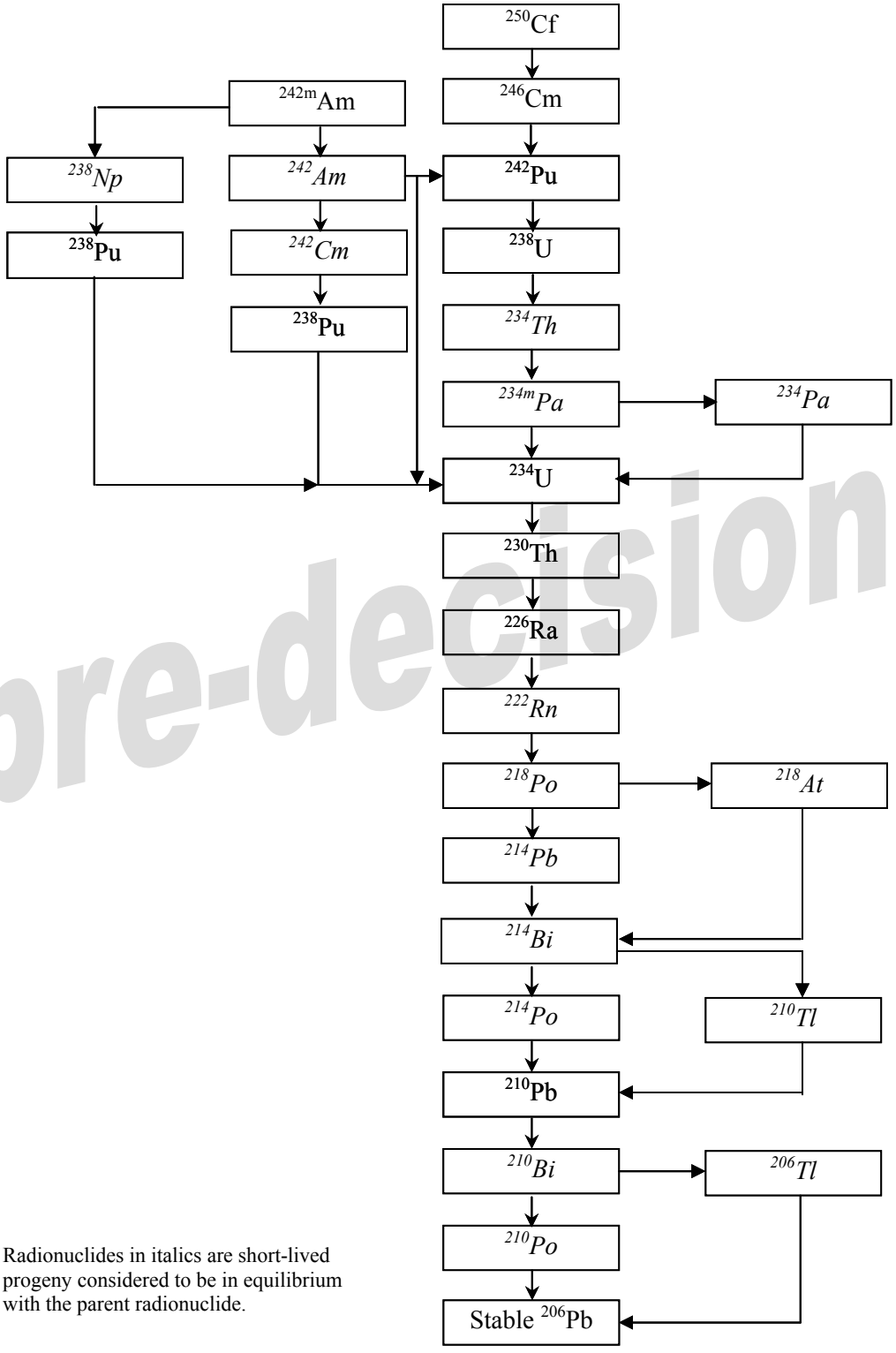

Figure 3-5. ^{250}Cf radionuclide decay chain.

and factors that can affect the permeability include cracks and voids, sulfate and magnesium attack, calcium hydroxide leaching, alkali-aggregate reaction, carbonation, acid attack, and corrosion of the tank, pipes, and reinforcement. This section provides a summary of these degradation mechanisms. A complete discussion of the approach used to model these mechanisms is presented in Appendix E.

Because of the limited availability of site-specific data (e.g., properties of the concrete and grout, chemistry of the soil moisture and water entering the vault), a number of assumptions were made and simple models used. The assumptions rely on using values for the conservative case model input parameters that are viewed as reasonably conservative (i.e., expected values). To compare the sensitivity of the model results to the expected values, a sensitivity analysis was performed and is presented in Appendix E. The sensitivity analysis evaluates the models using input parameters with the maximum protection and minimum protection parameter values.

The analysis modeled sulfate and magnesium attack, carbonation, and calcium hydroxide leaching. Reinforcement corrosion of the outer vault and localized corrosion that results in complete corrosion of the tank also were modeled. Based on the expected conditions at the TFF following closure, effects of acid attack, alkali-aggregate reaction, and corrosion of the pipes on the concrete and grout degradation are assumed to be insignificant compared to the three modeled chemical attacks. This approach is discussed in Appendix E.

In the closure of the TFF tanks, the tanks, vaults, and piping leading to the tanks will be filled with grout (INEEL 1999a). For modeling purposes, each of the 11 tanks and vaults and the piping external to the vaults is conceptualized as a representative tank, vault, or piping having average dimensions. Thus, because only a representative system is modeled, the same permeabilities are computed for each of the 11 tanks, vaults, and piping systems. Considering the limited data and the lack of information regarding variabilities between the tanks, it is reasonable to model a single tank, vault, and piping that represents each of the 11 tanks, vaults, and piping systems.

Figure 3-6 shows the system conceptualization and the grout degradation sequence of the representative vault, tank, grout, and piping. This sequence was used as the basis to develop the approach and mathematical models for the degradation analysis.

Figure 3-6a shows the conceptualized individual tank/vault unit. The concrete and grout are not cracked, all voids are filled, and the tank has no penetrations.

Figure 3-6b displays a tank/vault unit following the grout pour. A few shrinkage cracks are present in the outer vault and grout (Odler and Jawed 1991). A small number of localized penetrations have occurred in the tank wall. These penetrations could occur from pitting corrosion, galvanic corrosion related to pipe entrances, or stress corrosion cracking. In order to take a conservative approach to degradation, this figure is used as the initial condition assumed in the failure calculations. Multiple studies indicate that none of these initial failures are likely to be present in any of the vault/tank units now.

In Figure 3-6c, the steel reinforcement in the outer concrete vault is assumed to corrode. As the steel corrodes, it expands, leading to disruption of the concrete. The gravel texture in the figures is intended to represent a rubble condition where the concrete has lost its structural properties. Even after structural failure, the concrete still acts as a chemical barrier that conditions water and air reaching the outer grout layer. This condition occurs at about 500 yr.

Figure 3-6d depicts the vault/tank unit after the grout outside the tank has failed from chemical attack. Chemical attack must penetrate the outer vault rubble before initiating attack on the grout. No steel reinforcement is present in the outer grout. Thus, steel corrosion is eliminated as a failure mechanism. This condition occurs at about 5,000 yr.

Figure 3-6e illustrates the final stage where the tank has corroded substantially and all concrete

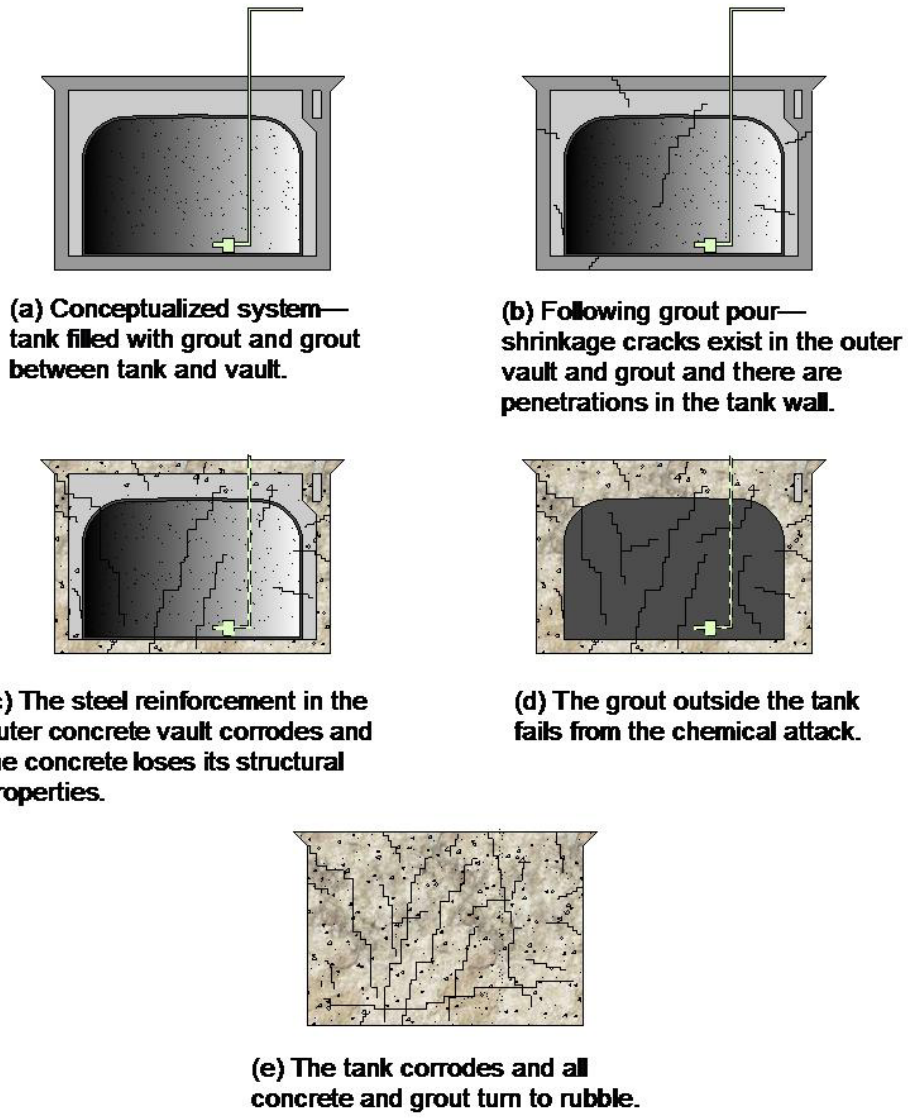

Figure 3-6. Conceptualization of the degradation sequence for the representative tank, grout, vault, and piping system at the TFF.

and grout have turned to rubble. At this point, the vault/tank unit has lost all hydraulic control of contaminant leaching. The chemically-reducing grout formulation may slow the migration of many radionuclides, but no credit is taken for this effect in the degradation modeling. This condition occurs at about 40,000 yr.

A representative vertical cross section of the tank, vault, and grout system and its dimensions are shown in Figure 3-7. The system conceptualization consists of four zones:

- The tank and the grout inside the tank (Zone a)
- The grout inside the vault but outside the tank (Zone b)
- The outer concrete vault walls, roof, and floor (Zone c)
- The piping (Zone d).

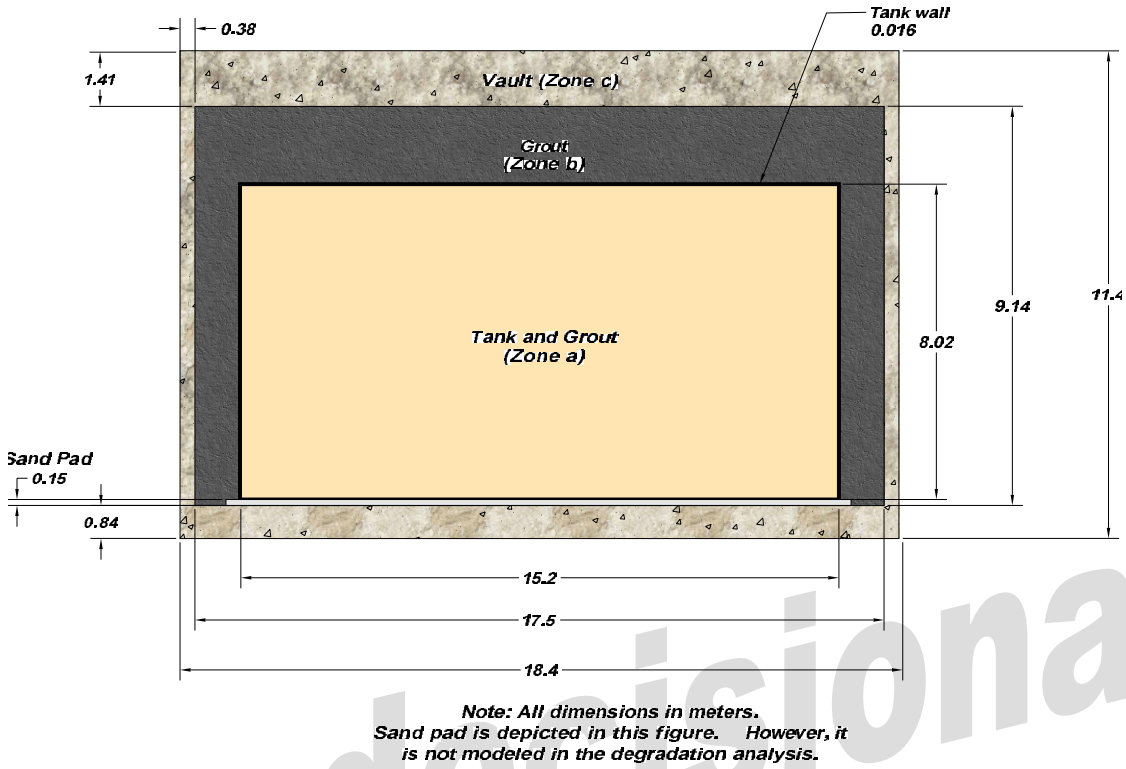

Figure 3-7. Representative tank, vault, and grout showing the dimensions for the degradation analysis.

Conceptually, because these zones contain potential water pathways arising from initial voids and cracks, each zone has a nonzero initial permeability (Seitz and Walton 1993). Over time, various mechanisms that increase the permeability cause the tank to corrode and the concrete and grout to degrade. The degradation mechanisms and processes considered in this analysis that can affect the system permeability include cracks and voids, sulfate and magnesium attack, calcium hydroxide leaching, alkali-aggregate reaction, carbonation, acid attack, and corrosion of the tank, pipes, and reinforcement.

The likely degradation processes of the representative system are conceptualized as occurring at the outside of the vaults and moving inward to the center of the system (i.e., from Zone c to Zone b to Zone a). For Zones a, b, and c, this approach is analogous to peeling an onion. Once the outer concrete vault (Zone c) completely turns to rubble, the next layer (Zone b) begins to degrade. After the grout in Zone b turns to rubble, the grout in Zone a begins to degrade. Additionally, the permeability of Zone a is not only affected by the degradation of the grout inside the tank but also by general and localized corrosion of the tank. Because the piping is separate from Zones a, b, and c, Zone d is modeled independent of the other three zones. However, the grout in Zone d is subject to the same chemical attack as Zones a, b, and c.

During the degradation period for each zone, the permeability increases from its initial permeability. Conceptually, the increasing permeability reflects an increase in the pathways available for water flow. Following complete degradation of the concrete vault and grout in Zones a through d, including complete corrosion of the tank and piping, all zones are assumed to have the same permeability (i.e., the permeability of rubble).

All zones of the modeled system were assigned reasonable values for an initial permeability (Breysse and Gerard 1997; Walton and Seitz 1991). Water can flow through cement and grout matrix, shrinkage cracks, and voids. For example, although the autogenous healing in

cracks is a well-known physical phenomenon (Edvardsen 1999; Hearn, Detwiler, and Sframeli 1994), the concrete permeability is significantly affected by the number of cracks and the crack width (Wang, Jansen, and Shah 1997) and shrinkage cracks (Hearn 1999). The presence of cracks and voids is conservatively assumed in this analysis, even though the grouting operation is designed to ensure (a) good pours without voids around and within pipes, and (b) a minimum of shrinkage or thermal stress cracking.

The reinforced concrete vaults either were poured in place or constructed using pillars and panels. Because of the difficulty of verifying initial conditions and predicting future conditions, very little performance credit is taken for the vaults. The initial permeability of the vaults (Zone c) is taken as 10^{-9} m/s. The fresh grout inside and outside of the tank is assumed to have an initial permeability of 10^{-13} m/s (Iriya et al. 1992).

In order to flow through the inside of the tank, water must pass through a flaw in the tank roof or side, flow through the grout inside the tank, then exit through a second hole in the tank. Permeability of the grouted tank (Zone a) is computed in this analysis as a lumped permeability that takes into account the status of the tank and the inner grout. Thus, the initial permeability for the grouted tank in Zone a is assumed to be 10^{-16} m/s.

The models used in the degradation analysis of Zones a, b, and c for sulfate and magnesium attack, calcium hydroxide leaching, and carbonation are presented in detail in Appendix E.

The results are shown in Figure 3-8. The figure indicates that the percent of concrete or grout lost from sulfate and magnesium attack occurs much faster than carbonation and calcium hydroxide leaching, with Zone c completely degrading after about 2,000 yr. Figure 3-9 shows the percent of grout lost for Zone d (piping) and reveals that the piping (assuming no credit for the pipe) completely degrades after 500 yr from sulfate and magnesium attack. The overall degradation for each zone is shown in Figure 3-10. This figure shows corrosion of the reinforcement steel fails the vault (Zone c) at about 500 yr. Note that the degradation of Zone c is faster by reinforcement corrosion than by sulfate attack in Figure 3-8. However, the time for failure of Zones a and b is the same in Figures 3-8 and 3-10. The reason for this consistency is the model assumes that although reinforcement corrosion can fail Zone c, chemical attack must still penetrate the cracked concrete vault before the grout in Zone b is affected.

The hydraulic conductivities for Zones a, b, c, and d are displayed in Figures 3-11 and 3-12. These figures show the effects of chemical attack on all four zones, reinforcement corrosion on Zone c, and corrosion of the tank on Zone a. The results also are consistent with the percent of loss provided in Figures 3-8 through 3-10.

As discussed in Appendix E, the permeability of Zone a is modeled assuming localized corrosion produces holes in the tank walls. The number of holes and the permeability of the material surrounding the holes (i.e., the grout in Zones a and b) determines the permeability of Zone a. The model used to predict the permeability of Zone a is based on the approach from Walton et al. (1997).

Using this model, the permeability in Zone a for each chemical attack is computed. For the maximum degradation shown in Figure 3-8, the permeability in Zone a begins to increase because of the increased number of holes in the tank at about 2,000 yr. After Zone b turns to rubble at 5,000 yr, the grout inside the tank degrades and the Zone a permeability begins to increase at a faster rate until about 10,000 yr. At about 10,000 yr, the grout inside the tank has turned to rubble. The remaining tank walls continue to corrode at a decreased rate until the entire tank has corroded at about 40,000 yr, when the permeability of Zone a equals the permeability of rubble. This time corresponds to the time when localized corrosion causes enough holes in the tank walls to completely fail the tank. This time also is consistent with the time the tanks are expected to fail from general corrosion (as estimated using data for corrosion rates measured from the coupons retrieved from the TFF tanks) (Palmer et al. 1999).

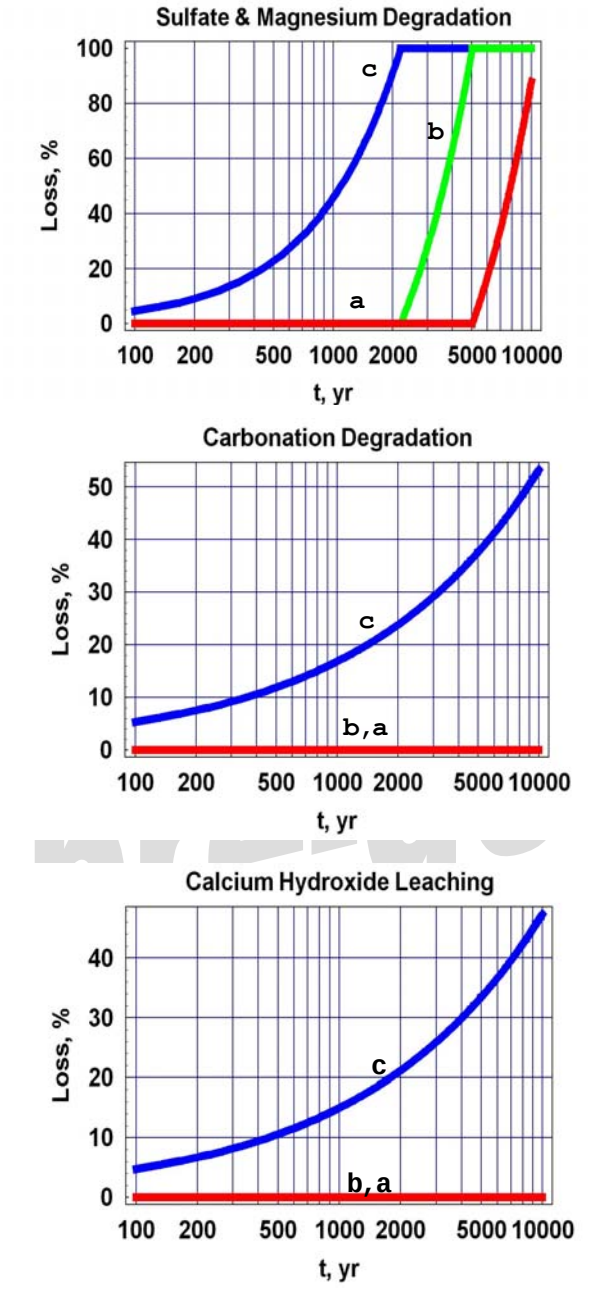

Figure 3-8. Base-case results for the percentage of concrete and grout degraded from sulfate and magnesium attack, carbonation, and calcium hydroxide leaching for Zones a (tank and grout), b (grout), and c (vault).

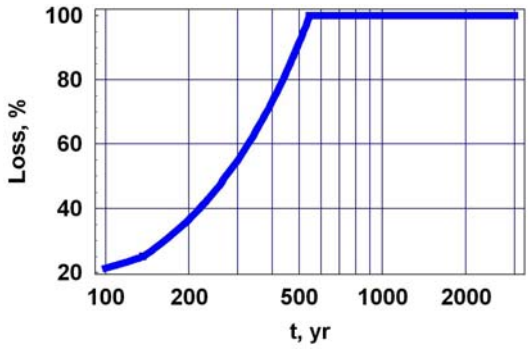

Figure 3-9. Base-case results for percent grout loss for the maximum degradation from sulfate and magnesium attack, carbonation, and calcium hydroxide leaching for Zone d (piping).

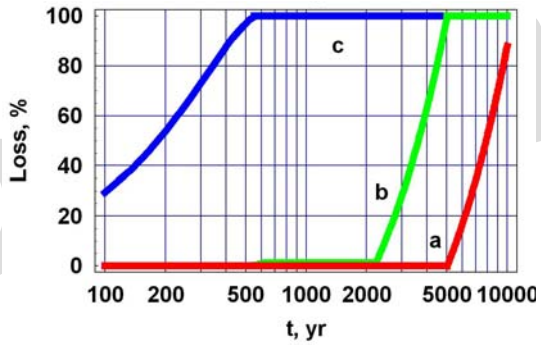

Figure 3-10. Base-case results for the maximum percent of concrete and grout degraded from reinforcement corrosion, sulfate and magnesium attack, carbonation, and calcium hydroxide leaching for Zones a (tank and grout), b (grout), and c (vault).

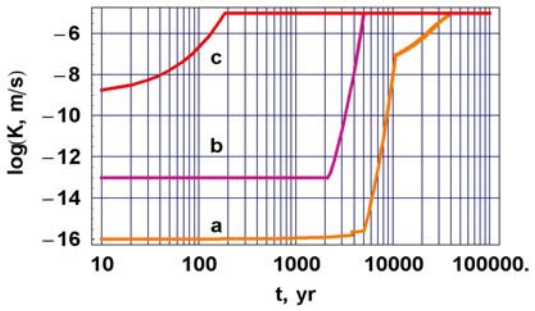

Figure 3-11. Base-case results of the hydraulic conductivity of Zone a (tank and grout), Zone b (grout inside vault and outside tank), and Zone c (vault).

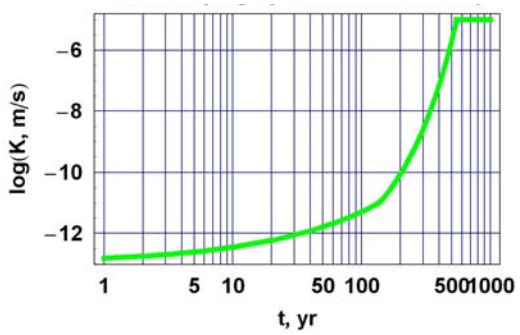

Figure 3-12. Base-case results of the hydraulic conductivity of Zone d (piping).

The model results show reinforcement corrosion, which cracks the concrete, causes the outer vault to turn to rubble in an estimated 500 yr. Once the outer vault completely degrades, the grout between the vault and the tank turns to rubble at approximately 5,000 yr. The tank and grout contained in the tank completely degrade and turn to rubble at approximately 40,000 yr. The grout associated with the piping turns to rubble after approximately 500 yr. The predominant chemical attack on the grout is from sulfate and magnesium. Sensitivity analysis indicates the times for the four zones to turn to rubble can vary greatly from tens of years to tens of thousands of years or beyond (see Appendix E).

In the above discussion, the grouted pipe and encasement system was assumed to degrade by sulfate and magnesium attack, carbonation, and calcium hydroxide leaching. The pipe was assumed to corrode instantaneously and have no affect on (a) the permeability of the grouted pipe and encasement system and (b) contaminant releases. To provide a more realistic representation of contaminant transport from the grouted pipe and encasement system into the vadose zone, a more detailed alternative analysis was conducted to include the effects of the pipe on contaminant releases. The analysis assumed that the pipe is 3-in. schedule 40 stainless steel, which (according to ANSI B36.10 [1970]) has a wall thickness of 0.216 in. Corrosion rates reported by Palmer et al. (1999) for coupons placed into the TFF stainless-steel tanks were applied to the pipe degradation. This is reasonable since the assumption implies the water contacting the pipe has the same characteristics as the water contacting the tank. For consistency in calculations, the rate at which localized corrosion in the tanks results in the tank wall holes also occurs at the same rate in the pipes (i.e., holes in the tank and pipe walls are assumed to appear with the same frequency).

Using the corrosion rates in Palmer et al. (1999), the pipe will completely corrode from general corrosion in about 40,000 yr. Additionally, the model for localized corrosion used in the degradation analysis predicts the first hole in the tank (which is assumed to occur at the same rate as in the pipes) appears at approximately 10,000 yr.

The current PA analysis used the following step degradation times (i.e., complete failure) for the TFF closure system: (1) outer vault/grout fail at 100 yr post-closure, (2) tank and grout in the tank fails at 500 yr post-closure, and (3) piping fails at 500 yr post-closure. These assumptions are conservative based on the best estimates provided from the degradation analysis and, due to the uncertainty in the degradation results, are considered appropriate for the PA analyses.

3.2 Pathways and Scenarios

The following sections describe the time periods of concern and pathways of human exposure to TFF constituents potentially released after closure. The information provided in this section was subsequently used to develop models for evaluating potential doses.

3.2.1 Time Periods of Concern

For the purposes of assessing the performance of the TFF closure facility, two time periods were addressed. The time periods include the institutional control period and the post-institutional control period. Each period of interest is described in the following sections.

3.2.1.1 Institutional Control Period. The institutional control period is the 100-yr time interval specified in DOE Manual 435.1-1 (2001) following closure of the TFF. The assumed closure date of the TFF is currently 2016. Periodic maintenance and monitoring activities are conducted during the institutional control period. The TFF site is assumed to be stabilized and no

longer operational during this period but will remain part of the INEEL and, therefore, fenced and patrolled to eliminate the possibility of inadvertent intruders. Institutional control is assumed to last 100 yr (i.e., until 2116) for the purposes of this PA.

3.2.1.2 Post-Institutional Control Period.

The final time period of concern is when the facility is no longer maintained by the INEEL and could be accessed by the public. For the purpose of this PA, the total duration of this period is 1,000 yr from the time of closure (i.e., 3016). Projections of conditions and activities during this period are uncertain and difficult to assess. In addition, peak doses may not occur from TFF releases until several thousand years after closure because of the presence of long-lived radionuclides. The potential peak doses from these long-lived radionuclides are in the sensitivity analysis. However, for compliance purposes, the performance period is 1,000 yr after facility closure. Reasonable human activities are assumed to occur over this period of time based on the existing population patterns for the INEEL region.

3.2.2 Transport Pathways

This section identifies potential pathways of human exposure to radionuclides released from the TFF and justifies eliminating some of these pathways from further consideration. The results of this section were used to develop exposure scenarios for off-site members of the public.

3.2.2.1 Pathway Identification.

Radionuclides released from the TFF to the geosphere have the potential of reaching humans through numerous pathways. Most conceivable pathways for a buried LLW source are indicated in Figure 3-13, and each pathway is briefly defined. The pathways identified in this figure are for facilities undisturbed from the standpoint of human intrusion. Pathways pertinent to intruder exposures are addressed separately in Section 5.

3.2.2.2 Pathway Screening. The pathways listed in Figure 3-13 are generic in nature, and the significance of each pathway must be evaluated on a site-specific basis to develop an exposure model. Many pathways may be removed from consideration for particular sites because of a negligible contribution to human exposure.

For the TFF, leaching and transport of radionuclides to the saturated zone [pathway (1)] is the predominant means that radionuclides may be subsequently transported in the environment. Thus, this pathway must be addressed in developing an exposure model and is addressed in the groundwater model of this PA. Other pathways that may contribute to human exposure are those tied to groundwater concentrations of contaminants. Irrigation with contaminated groundwater may lead to contamination of agricultural crops and animals [pathways (3), (21), (23), (25) and (26)]. Ingestion of contaminated groundwater by terrestrial animals [pathway (19)] may lead to human exposure, and can be tied to groundwater contamination. Human exposure may occur as a result of direct human ingestion of contaminated groundwater [pathway (41)] as a result of consumption of contaminated food supplies [pathways (44) and (45)]. These were all considered for the TFF PA exposure scenarios.

Discharge of contaminated groundwater to surface water [pathway (6)] may result in contamination of the aquatic ecosystem including the water body itself, sediment, and aquatic plants and animals [pathways (13), (14), (15), (34), (35), (36), (37), (38), and (39)]. The groundwater at the INEEL does not intersect the Big Lost River in the vicinity of the INEEL. The groundwater at the INEEL does interact with surface water as springs that flow into the Snake River. Major areas of springs and seepages from the aquifer occur in the vicinity of the American Falls Reservoir (southwest of Pocatello), approximately 44 mi (71 km) from the TFF, and the Thousand Springs area (near Twin Falls) between Milner Dam and King Hill, approximately 100 mi (200 km) from the TFF (Garabedian 1986). These spring locations are at such great distances from the TFF that contributions to the human dose from surface water at these locations would be insignificant because of groundwater dilution. Therefore, these pathways are not considered further in the TFF PA. In addition, exposure pathways associated with the ingestion of surface water, swimming, aquatic animals, or associated plant/animal uptake of radionuclides from surface water [pathways

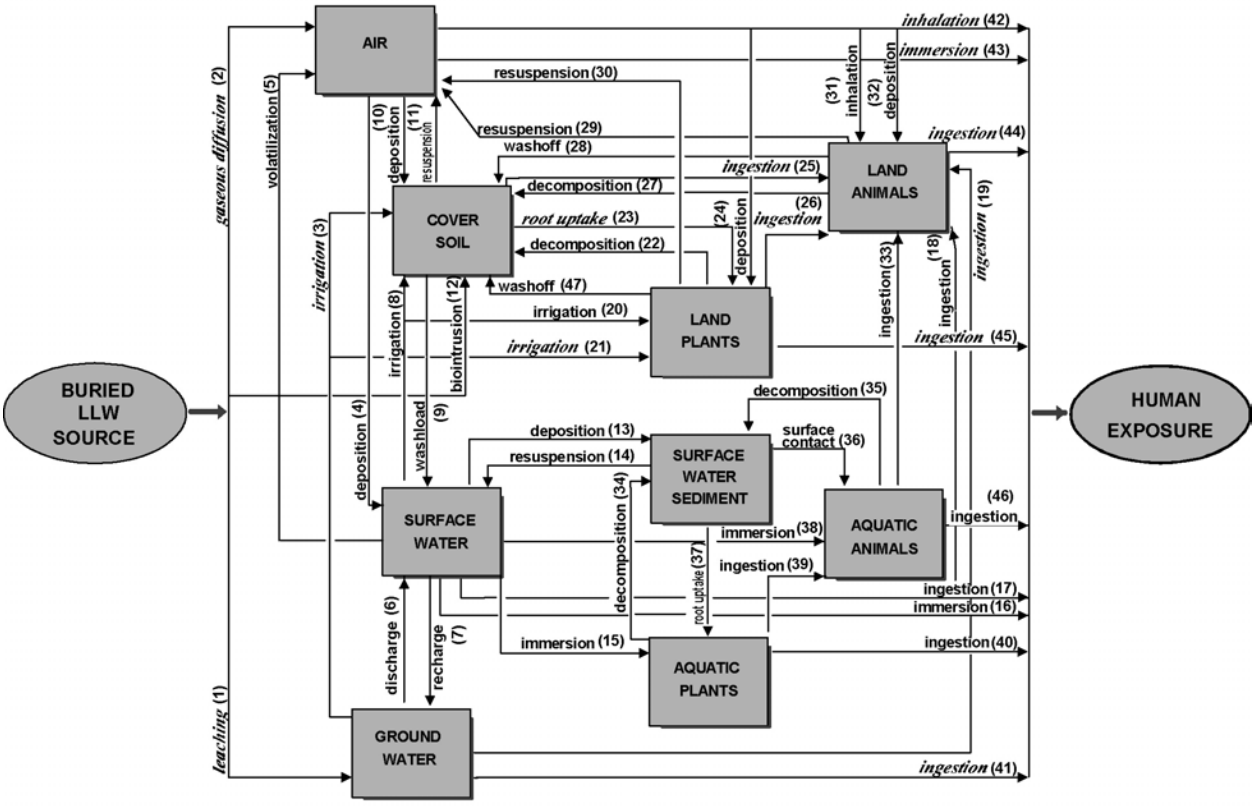

Figure 3-13. Potential transport and exposure pathways from a near-surface facility (pathways selected for analysis are identified by italics).

(1) *Leaching*—migration of radionuclides from the waste form by a combination of dissolution, diffusion, and advection.

(2) *Gaseous Diffusion*—upward migration of gaseous radionuclides from the waste form by diffusion through the caps and cover soils to the atmosphere.

(3) *Irrigation*—contamination of cover soil by radionuclides that have reached groundwater, which is subsequently used for irrigation.

(4) Deposition—contamination of surface water by radionuclides that have reached the atmosphere; represents deposition of particulate-associated radionuclides or gaseous species partitioning at the air-water interface.

(5) Volatilization—partitioning of volatile radionuclides species present in surface water into air above the water body.

(6) Discharge—discharge of radionuclides present in groundwater into surface water.

(7) Recharge—movement of radionuclides into the groundwater from contaminated surface water.

(8) Irrigation—contamination of cover soil by radionuclides that have reached surface water, which is subsequently being used for irrigation.

(9) Washload—contamination of surface water by soil containing radionuclides as a result of erosion by rain or irrigation water.

(10) Deposition—contamination of cover soil by radionuclides that have reached the atmosphere and have become associated with airborne particulate matter.

(11) Resuspension—Resuspension of soil-associated radionuclides as a result of wind erosion.

(12) Biointrusion—contamination of cover soil by soil-associated radionuclides that are brought to the surface from the vicinity of the waste form by burrowing animals, such as rodents or ants, or by intruding plant roots.

(13) Deposition—deposition of radionuclides in surface water that have partitioned onto suspended sediment.

(14) Resuspension—resuspension of particulate-borne radionuclides in the sediment of surface water as a result of hydrodynamic forces at the sediment-water interface.

(15) Immersion—contamination of aquatic plants by radionuclides in surface water attributable to the immersion of the plants in the contaminated water.

(16) Immersion—human exposure to radionuclides as a result of immersion in contaminated surface water.

(17) Ingestion—human exposure to radionuclides as a result of ingestion and inhalation of radionuclides present in surface water.

(18) Ingestion—contamination of terrestrial animals from their ingestion of radionuclides in surface water.

(19) *Ingestion*—contamination of terrestrial animals from their ingestion of radionuclides in groundwater.

(20) Irrigation—contamination of terrestrial plants as a result of irrigation with surface water containing radionuclides.

(21) *Irrigation*—contamination of terrestrial plants as a result of irrigation with groundwater.

(22) Decomposition—contamination of cover soil as a result of decomposition of terrestrial plants in the soil.

(23) *Root uptake*—contamination of terrestrial plants by uptake through roots of soil water containing radionuclides.

(24) Deposition—deposition of airborne radionuclides onto terrestrial plant surfaces.

(25) *Ingestion*—ingestion of radionuclides by grazing animals as a result of contaminated soil ingestion.

(26) *Ingestion*—ingestion of radionuclide-containing vegetation by terrestrial animals.

(27) Decomposition—contamination of cover soil as a result of decomposition of terrestrial animals in the soil.

(28) Washoff—contamination of surface soil as a result of washoff of externally-contaminated terrestrial animals.

(29) Resuspension—resuspension of surficial radionuclides on terrestrial animals to the atmosphere.

(30) Resuspension—resuspension of surficial radionuclides on terrestrial plants to the atmosphere.

(31) Inhalation—contamination of terrestrial animals as a result of inhalation of radionuclides in the atmosphere.

(32) Deposition—surface contamination of terrestrial animals via deposition of particulate-borne radionuclides in the atmosphere.

(33) Ingestion—contamination of terrestrial animals as a result of their ingestion of aquatic animals.

(34) Decomposition—contamination of surface water sediment as a result of decomposition of aquatic plants in the sediment.

(35) Decomposition—contamination of surface water sediment as a result of decomposition of aquatic animals in the sediment.

(36) Surface contact—surface contamination of aquatic animals as a result of contact with contaminated sediment.

(37) Root uptake—contamination of aquatic plants via radionuclide uptake through roots.

(38) Immersion—contamination of aquatic animals as a result of immersion in surface water containing radionuclides.

(39) Ingestion—contamination of aquatic animals as a result of their ingestion of aquatic plants containing radionuclides.

(40) Ingestion—human exposure to radionuclides as a result of ingestion of contaminated aquatic flora.

(41) *Ingestion*—human exposure to radionuclides as a result of ingestion of contaminated groundwater.

(42) *Inhalation*—human exposure to radionuclides as a result of inhalation of airborne radionuclides.

(43) *Immersion*—human exposure to radionuclides as a result of immersion in contaminated air.

(44) *Ingestion*—human exposure to radionuclides as a result of ingestion of contaminated terrestrial animals and animal products (such as milk).

(45) *Ingestion*—human exposure to radionuclides as a result of ingestion of contaminated terrestrial plants.

(46) Ingestion—human exposure to radionuclides as a result of ingestion of contaminated aquatic animals.

(47) Washoff—contamination of surface soil below vegetation due to rain-induced surface washoff.

(16), (17), (18), (33), (40), and (46)] also were not considered for further analysis.

Pathway (7) considers contamination of groundwater due to recharge by surface water. This pathway is not considered significant for the TFF since migration of radionuclides to the nearby surface water body (i.e., Big Lost River) is not considered possible. The waste will be in a grouted form buried beneath the ground surface such that the interaction of the waste with surface water is not physically possible. Pathways (8) and (20), representing contamination of cover soil and terrestrial plants as a result of irrigation with contaminated surface water, also not considered. They were withdrawn because of a lack of a physical mechanism to move the radionuclides from the source to the surface water. Contamination of surface water from erosion of contaminated soil [pathway (9)] was not considered significant because movement of the contaminants from their present location below the ground surface to the surface is not considered feasible [i.e., no erosion of 10-ft (3-m) cover soil]. In addition, pathways (22) and (27), representing the pathways to surface soil via decomposition of terrestrial plants and animals, were not considered significant relative to the exposure resulting from direct consumption of these potentially contaminated products.

Pathways that result in human exposure directly or indirectly as a result of atmospheric dispersion and deposition [pathways (4), (5), (10), (11), (24), (28), (29), (30), (31), (32), and (47)] are not included in exposure scenarios for the TFF PA for the following reasons:

- The only potentially volatile radioactive components of the TFF are ^{3}H and ^{14}C. Calculations providing an upper bound on doses received from volatilization of these radionuclides from the TFF facility after disposal are described in Section 3.3.5.

- Pathways leading to exposure from resuspended contaminated soil [pathway (11)] are not considered since there is no mechanism for releasing particulates from the TFF (i.e., grouted waste form).

- Other atmospheric pathways are indirect in nature (e.g., the contaminants must first be suspended or volatilized from one medium, then redeposited in another). These indirect pathways are not believed to be more significant than the direct pathways (2, 42, and 43), and thus, are not addressed in this PA.

Therefore, pathways (2), (42), and (43) are included in the dose analysis for atmospheric releases of ^{3}H and ^{14}C. Please note that the requirements for radon are specified as a flux term in the performance objectives and are dealt with separately in this PA.

Finally, contamination of cover soil over the TFF as a result of biointrusion of burrowing animals or plant roots [pathway (12)] also is not considered a major transport pathway. It is acknowledged that biointrusion is a potentially significant pathway of contamination of cover soil over a LLW facility (McKenzie et al. 1983). However, studies at the INEEL have indicated that burrowing animals and plant roots for species of the area do not exceed 7ft (2 m) in depth (Arthur 1982, Reynolds and Fraley 1989; Markham 1987; Arthur, Grant, and Markham 1983; Reynolds and Laundre 1988). Therefore, given the 10 ft (3 m) of cover over the vaults, this pathway is not considered in this PA. Data on burrowing animals and plant roots are provided in Section 2.1.3.

In summary, of the original 47 pathways identified in Figure 3-13, the following are considered to be of possible consequence to off-site members of the public and are considered further in this PA:

- Pathways related to contaminated groundwater believed to be of potential consequence. This includes leaching of the waste form, resulting in contamination of groundwater and contamination of agricultural crops and animals as a result of irrigation with contaminated groundwater [pathways (1), (3), (19), (21), (23), (25), (26), (41), (44), and (45)].

- The release of the volatile radionuclides ^{3}H and ^{14}C [pathways (2), (42), and (43)].

Radon releases are considered separately from these volatile radionuclides because the performance objective is defined in terms of flux rate for radon.

3.2.3 Exposure Scenarios

Three exposure scenarios were considered in the TFF PA: 1) drinking water dose from groundwater, 2) all-pathways dose from groundwater, and 3) air dispersion pathways. In addition, the intruder pathway and radon flux analyses also were considered and are described in Sections 3.3.4 and 5.

3.2.3.1 Protection of Groundwater. As discussed in Section 1.4.2, the groundwater protection standard chosen for evaluation in this PA is a drinking water dose of 4 mrem/yr. The nearest location from the disposal site for off-site members of the public depends on the time period after disposal. During the period of active institutional control for the first 100 yr after facility closure, off-site members of the public are assumed to be located no closer to the disposal site than the present boundary of the INEEL. However, after active institutional control ceases, off-site members of the public could be located as close as 100 m (300 ft)[a] from the TFF. However, for the groundwater pathway, the member of the public is assumed to have a well located in the groundwater at the point of maximum concentration, which for the analyses presented in this PA is located 600 m (2,000 ft) from the facility.

As discussed in Section 3.2.2, the primary mechanism for transport of radionuclides from the TFF is expected to be leaching of radionuclides to the groundwater and subsequent human consumption. Thus, in the dose analysis for groundwater protection, an off-site member of the public is assumed to use water from a well for domestic purposes. The well is assumed to be located where the maximum concentrations of radionuclides in groundwater are predicted to occur.

3.2.3.2 All-Pathways Exposure Scenario. As stated previously, the primary mechanism for transport of radionuclides from the TFF is expected to be leaching to the groundwater and subsequent human consumption. Thus, in the all-pathways dose analysis, an off-site member of the public is assumed to use water from a well for domestic purposes. The well is assumed to be located where the maximum concentrations of radionuclides in groundwater are predicted to occur.

The following exposure pathways involving the use of contaminated well water are assumed to occur:

- Direct ingestion of contaminated water
- Ingestion of milk and meat from dairy and beef cattle that drink contaminated water
- Ingestion of vegetables grown in garden soil irrigated with contaminated water
- Ingestion of milk and meat from dairy and beef cattle that eat fodder from pasture irrigated with contaminated water.

Additional exposure pathways for off-site members of the public could involve releases of radionuclides into the air (i.e., volatile radionuclides). Exposures from the air pathway also are considered in this PA.

***3.2.3.3* Air Dispersion Scenario.** Volatile radionuclides ^{3}H and ^{14}C were evaluated in the air dispersion scenario. The depth to the waste and the waste physical characteristics (i.e., grouted waste) limits the analysis to volatile radionuclides in the waste form. Additional details on the air dispersion scenario are provided in Section 3.3.5.

3.2.4 Groundwater Transport Radionuclide Screening

The TFF inventory includes several radionuclides that will not be significant in terms of projected receptor doses from the groundwater

a. Inputs to the modeling software must be in metric units. Therefore, in these sections, measurements are given in metric units, followed by U.S. customary units.

pathway. Therefore, screening analysis methods were investigated for use in the TFF PA to reduce the number of radionuclides considered in the groundwater analysis. A more detailed analysis of releases from the disposal facility and transport in groundwater is required for the radionuclides selected by the screening procedure.

The groundwater screening analysis considered that active institutional control will be maintained over the disposal site for 100 yr after facility closure and, furthermore, that the performance of the facility will be monitored to detect and/or prevent significant releases of radionuclides to the environment throughout the period of active institutional control. This consideration eliminates from concern any radionuclide with a half-life less than about 5 yr because the inventory in the waste at 100 yr after facility closure will be reduced to innocuous levels by radioactive decay. However, radionuclides with half-lives less than 5 yr cannot be neglected if the radionuclide appears in a decay chain. This is because its activity may increase with time due to decay of a parent radionuclide, unless the parent is also short-lived.

The use of the 5-yr half-life screening criteria results in the elimination of the following radionuclides from further consideration: ^{102}Rh, ^{119m}Sn, ^{134}Cs, ^{150}Eu, ^{153}Gd, ^{155}Eu, ^{55}Fe, and ^{171}Tm. In addition, the following radionuclides in short decay chains were eliminated from further analysis since the parent and progeny each have half-lives less than 5 yr: ^{106}Ru/^{106}Rh, ^{109}Cd/^{109m}Ag, ^{110m}Ag/^{110}Ag, ^{125}Sb/^{125m}Te, and ^{144}Ce/^{144m}Pr/^{144}Pr. Additional radionuclides were screened from further consideration since their half-lives indicate that they are either stable or have such long half-lives that their specific activity, and thus contribution, to dose would be insignificant. These radionuclides include ^{142}Ce (5E+16 yr), ^{149}Sm (1E+15 yr), ^{144}Nd (2.4E+15 yr), and ^{148}Sm (2E+14 yr).

The screening procedure used for the TFF source inventory was based first on the concentrations of radionuclides in the waste pore-water that would give an annual effective dose EDE of 4 mrem/yr from consumption of 70 oz/d (2 L/d) [i.e., 190 gal/yr (730 L/yr)] of contaminated water. The 4 mrem/yr standard was used for screening each nuclide because this portion of the screening process does not consider transport from the waste form to the groundwater. Prior groundwater transport analyses provided in Appendix F show that the screening analysis based on an individual drinking the pore water in the waste is very conservative because it does not consider transport through the unsaturated zone and subsequent dilution. Therefore, the entire limit was applied to each radionuclide because of the conservative nature of the screening analysis based on waste pore-water concentrations to limit the number of radionuclides considered in the analysis. Thus, for radionuclide i, the limiting concentration in the waste pore-water in units of μCi/L is given by

$$C_{iw,limit} = \frac{4\ mrem}{730\ L/yr \cdot DCF^{i}\ (mrem/\mu Ci)} \qquad (3\text{-}9)$$

where

$C_{iw,limit}$ = limiting concentration in drinking water for radionuclide i (μCi/L)

730 L/yr = drinking water ingestion rate

DCF_i = ingestion dose conversion factor for radionuclide I (mrem/μCi).

Given the assumption of a 100-yr active institutional control period, the screening procedure can be based on the concentrations of radionuclides in the waste at 100 yr after disposal. In addition, radionuclide concentrations in the waste at 500 and 1,000 yr after closure were calculated to evaluate progeny ingrowth from decay chains.

The next step in the screening procedure is to convert the assumed radionuclide concentration in the waste-form to concentrations in the waste pore-water. These concentrations are clearly maximum (conservative) values, as they represent the pore-solution concentration in the waste form and do not consider the transport time out of the waste-form or the dilution due to transport in the unsaturated zone. Given the concentrations in the

disposal facility at 100, 500, and 1,000 yr after disposal, the maximum concentrations in groundwater obtained from the screening model are given by

$$C_{iw,max(t)} = \frac{C_{iv}(t)}{\theta + K_d \rho_s} \quad (3\text{-}10)$$

where

$C_{iw,max(t)}$ = maximum radionuclide concentration in groundwater for radionuclide i at time t μCi

$C_{iv}(t)$ = concentration in the disposal facility for radionuclide i at time t μCi

0.001 = conversion factor to convert the waste concentration from μCi/m^3 to μCi/L of the solid waste

θ = porosity of the waste form (unitless)

K_d = equilibrium solid/solution distribution coefficient (L/kg)

ρ_s = bulk density of the waste form (kg/L).

The concentration in the waste forms, C_{iv}, were based on the worst-case inventories for the tanks and sand pad presented in Appendix A. The conservative case presented in Section 2.3 was not used for the screening analysis. This was done to ensure that all radionuclides of importance would remain after screening. The volume of the waste in a tank was based on 55.5 m^3, while the sand pad volume was 23.4 m^3.

The denominator of Equation (3-10) accounts for the waste concentration being a total value. The denominator of the equation partitions the total activity of each radionuclide from the solid portion of the waste-form to the pore-water of the waste-form. A simple division by the K_d is no applicable in this case, since the inventories are the totals in the waste (i.e., both liquid fraction and solid fractions) before the waste has been grouted. Therefore, after grouting the total inventory must be partitioned into the grout pore-water.

The worst-case inventory (see Appendix A) and worst-case equilibrium solid/solution distribution coefficients were used in the screening analysis to ensure a complete list of radionuclides.

The porosity of the grout was assumed to be 0.2; the sand pad had an assumed porosity of 0.34. The grout porosity will change over time because of degradation to approximately 0.4. However, this change does not result in different radionuclides being chosen from the screening analysis. The bulk density of grout was assumed to be 2.1E+06 g/m^3, while the sand pad was assumed to be at a density of 1.76E+06 g/m^3.

Given $C_{iw,limit}$ and $C_{iw,max}$, at 100, 500, and 1000 yr, a radionuclide is selected for further analysis only if the following inequality is satisfied:

$$C_{iw,max(t)} > C_{iw,limit} \quad (3\text{-}11)$$

The screening procedure is sufficiently conservative so that any radionuclides eliminated from further consideration would not contribute more than a small fraction of the dose limit of 4 mrem/yr (EDE) from contamination of groundwater, considering that the waste pore-water concentration were used.

The development of pore-water concentrations in the tank grout required the evaluation of distribution coefficients (i.e., K_d values) specific to grout. These grout distribution coefficients were taken from studies conducted by Allard, Persson, and Torstenflt (1985) and Bradbury and Sarott (1995) (see Section 2.1.6). The development of pore-water concentrations in the sand pad required the evaluation of K_d values specific to sand. These coefficients were taken from Sheppard and Thibault (1990) (see Section 2.1.6). The selected distribution coefficients for grout and sand are provided in Table 3-1.

The worst-case TFF inventories, presented in Appendix A, were screened according to the above calculations. The screened inventory for the tank is provided in Table 3-2. The same process was used

Table 3-1. Distribution coefficients for grout and sand.

Nuclide	Grout[a] (m^3/kg)	Sand[a] (m^3/kg)	Nuclide	Grout[a] (m^3/kg)	Sand[a] (m^3/kg)
^{10}Be	1.00E–03	2.50E–01	^{94}Nb	5.00E–01	1.60E–01
^{14}C	1.00E–02	5.00E–03	^{63}Ni	1.00E–01	4.00E–01
^{113m}Cd	1.00E–01	8.00E–02	^{107}Pd	1.00E–01	5.50E–02
^{60}Co	1.00E–01	6.00E–02	^{146}Pm	0.00E+00	0.00E+00
^{135}Cs	2.00E–03	2.80E–01	^{87}Rb	0.00E+00	5.50E–02
^{150}Eu	5.00E+00	0.00E+00	^{79}Se	1.00E–04	1.50E–01
^{154}Eu	5.00E+00	1.90E+00	^{146}Sm	5.00E+00	2.45E–01
^{3}H	0.00E+00	0.00E+00	^{151}Sm	5.00E+00	2.45E–01
^{166m}Ho	5.00E+00	2.50E–01	^{121m}Sn	1.00E+00	1.30E–01
^{129}I	2.00E–03	1.00E–03	^{98}Tc	1.00E+00	1.00E–04
^{115}In	1.00E–01	0.00E+00	^{99}Tc	1.00E+00	1.00E–04
^{138}La	5.00E+00	0.00E+00	^{123}Te	0.00E+00	1.25E–01
Short Decay Chains					
^{108}Ag	1.00E–03	9.00E–02	^{126}Sb	0.00E+00	4.50E–02
^{108m}Ag	1.00E–03	9.00E–02	^{126m}Sb	0.00E+00	4.50E–02
^{137m}Ba	1.00E–03	4.00E–04	^{147}Sm	5.00E+00	2.45E–01
^{137}Cs	2.00E–03	2.80E–01	^{126}Sn	1.00E+00	1.30E–01
^{152}Eu	5.00E+00	1.90E+00	^{90}Sr	1.00E–03	1.50E–02
^{152}Gd	0.00E+00	0.00E+00	^{90}Y	1.00E–03	1.70E–01
^{93m}Nb	5.00E–01	1.60E–01	^{93}Zr	5.00E+00	6.00E–01
^{147}Pm	0.00E+00	0.00E+00			
^{252}Cf Decay Chain					
^{228}Ac	5.00E+00	4.50E–01	^{240}Pu	5.00E+00	5.50E–01
^{212}Bi	5.00E–01	1.00E–01	^{244}Pu	5.00E+00	5.50E–01
^{252}Cf	0.00E+00	0.00E+00	^{224}Ra	5.00E–02	5.00E–01
^{244}Cm	5.00E+00	4.00E+00	^{228}Ra	5.00E–02	5.00E–01
^{248}Cm	5.00E+00	4.00E+00	^{220}Rn	0.00E+00	0.00E+00
^{240}Np	5.00E+00	5.00E–03	^{228}Th	5.00E+00	3.20E+00
^{240m}Np	5.00E+00	5.00E–03	^{232}Th	5.00E+00	3.20E+00
^{212}Pb	5.00E–01	2.70E–01	^{208}Tl	0.00E+00	0.00E+00
^{212}Po	5.00E–01	1.50E–01	^{232}U	2.00E+00	3.50E–02
^{216}Po	5.00E–01	1.50E–01	^{236}U	2.00E+00	3.50E–02
^{236}Pu	5.00E+00	5.50E–01	^{240}U	2.00E+00	3.50E–02
^{249}Cf Decay Chain					
^{225}Ac	5.00E+00	4.50E–01	^{209}Pb	5.00E–01	2.70E–01
^{241}Am	5.00E+00	1.90E+00	^{213}Po	5.00E–01	1.50E–01
^{217}At	0.00E+00	0.00E+00	^{241}Pu	5.00E+00	5.50E–01

Table 3-1. (continued).

Nuclide	Grout[a] (m^3/kg)	Sand[a] (m^3/kg)	Nuclide	Grout[a] (m^3/kg)	Sand[a] (m^3/kg)
^{213}Bi	5.00E–01	1.00E–01	^{225}Ra	5.00E–02	5.00E–01
^{249}Cf	0.00E+00	0.00E+00	^{229}Th	5.00E+00	3.20E+00
^{245}Cm	5.00E+00	4.00E+00	^{209}Tl	0.00E+00	0.00E+00
^{221}Fr	0.00E+00	0.00E+00	^{233}U	2.00E+00	3.50E–02
^{237}Np	5.00E+00	5.00E–03	^{237}U	2.00E+00	3.50E–02
^{233}Pa	5.00E+00	5.50E–01			
^{251}Cf Decay Chain					
^{227}Ac	5.00E+00	4.50E–01	^{211}Po	5.00E–01	1.50E–01
^{243}Am	5.00E+00	1.90E+00	^{215}Po	5.00E–01	1.50E–01
^{211}Bi	5.00E–01	1.00E–01	^{239}Pu	5.00E+00	5.50E–01
^{251}Cf	0.00E+00	0.00E+00	^{243}Pu	5.00E+00	5.50E–01
^{243}Cm	5.00E+00	4.00E+00	^{223}Ra	5.00E–02	5.00E–01
^{247}Cm	5.00E+00	4.00E+00	^{219}Rn	0.00E+00	0.00E+00
^{223}Fr	0.00E+00	0.00E+00	^{227}Th	5.00E+00	3.20E+00
^{235}Np	5.00E+00	5.00E–03	^{231}Th	5.00E+00	3.20E+00
^{239}Np	5.00E+00	5.00E–03	^{207}Tl	0.00E+00	0.00E+00
^{231}Pa	5.00E+00	5.50E–01	^{235}U	2.00E+00	3.50E–02
^{211}Pb	5.00E–01	2.70E–01			
^{250}Cf Decay Chain					
^{242}Am	5.00E+00	1.90E+00	^{210}Po	5.00E–01	1.50E–01
^{242m}Am	5.00E+00	1.90E+00	^{214}Po	5.00E–01	1.50E–01
^{210}Bi	5.00E–01	1.00E–01	^{218}Po	5.00E–01	1.50E–01
^{214}Bi	5.00E–01	1.00E–01	^{238}Pu	5.00E+00	5.50E–01
^{250}Cf	0.00E+00	0.00E+00	^{242}Pu	5.00E+00	5.50E–01
^{242}Cm	5.00E+00	4.00E+00	^{226}Ra	5.00E–02	5.00E–01
^{246}Cm	5.00E+00	4.00E+00	^{222}Rn	0.00E+00	0.00E+00
^{238}Np	5.00E+00	5.00E–03	^{230}Th	5.00E+00	3.20E+00
^{234}Pa	5.00E+00	5.50E–01	^{234}Th	5.00E+00	3.20E+00
^{234m}Pa	5.00E+00	5.50E–01	^{210}Tl	0.00E+00	0.00E+00
^{210}Pb	5.00E–01	2.70E–01	^{234}U	2.00E+00	3.50E–02
^{214}Pb	5.00E–01	2.70E–01	^{238}U	2.00E+00	3.50E–02

a. Distribution coefficients assumed to be zero for all radionuclides not listed in the references.

Table 3-2. Tank activity groundwater screening for the drinking water pathway.

Nuclide	Half-life (yr)	K_d (m^3/kg)	Ingestion DCF (mrem/μCi)	$C_{iw,\ limit}$ Allowable Concentration (μCi/L)	100 yr $C_{iw,max}$ (μCi/L)	500 yr $C_{iw,max}$ (μCi/L)	1000 yr $C_{iw,max}$ (μCi/L)
^{225}Ac	2.74E–02	5.00E+00	1.11E+02	4.94E–05	6.24E–10	3.42E–09	8.29E–09
^{227}Ac	2.18E+01	5.00E+00	1.41E+04	3.89E–07	2.25E–08	3.07E–08	4.05E–08
^{228}Ac	6.99E–04	5.00E+00	2.16E+00	2.54E–03	1.83E–13	2.98E–13	4.41E–13
^{108}Ag	4.51E–06	1.00E–03	0.00E+00	NA[a]	2.24E–08	2.53E–09	1.65E–10
^{108m}Ag	1.27E+02	1.00E–03	7.62E+00	7.19E–04	2.41E–07	2.72E–08	1.77E–09
^{241}Am	4.32E+02	5.00E+00	3.64E+03	1.51E–06	2.09E–03	1.11E–03	4.96E–04
^{242}Am	1.83E–03	5.00E+00	1.41E+00	3.89E–03	2.04E–06	3.29E–07	3.36E–08
^{242m}Am	1.52E+02	5.00E+00	3.52E+03	1.56E–06	2.05E–06	3.30E–07	3.38E–08
^{243}Am	7.38E+03	5.00E+00	3.62E+03	1.51E–06	4.59E–06	4.42E–06	4.22E–06
^{217}At	1.02E–09	0.00E+00	0.00E+00	NA	3.37E–05	1.85E–04	4.48E–04
^{137m}Ba	4.86E–06	1.00E–03	0.00E+00	NA	3.60E+03	3.68E–01	3.77E–06
^{10}Be	1.60E+06	1.00E–03	4.66E+00	1.18E–03	3.03E–06	3.03E–06	3.03E–06
^{210}Bi	1.37E–02	5.00E–01	6.40E+00	8.56E–04	1.05E–07	1.14E–06	3.74E–06
^{211}Bi	4.05E–06	5.00E–01	0.00E+00	NA	2.25E–07	3.07E–07	4.05E–07
^{212}Bi	1.15E–04	5.00E–01	1.06E+00	5.17E–03	1.62E–06	3.45E–08	2.85E–10
^{213}Bi	8.68E–05	5.00E–01	7.22E–01	7.59E–03	6.24E–09	3.42E–08	8.29E–08
^{214}Bi	3.78E–05	5.00E–01	2.83E–01	1.94E–02	1.47E–07	1.27E–06	3.95E–06
^{14}C	5.73E+03	1.00E–02	2.09E+00	2.62E–03	8.05E–01	7.67E–01	7.22E–01
^{113m}Cd	1.37E+01	1.00E–01	1.61E+02	3.40E–05	1.26E–04	2.06E–13	2.13E–24
^{249}Cf	3.51E+02	0.00E+00	4.74E+03	1.16E–06	1.65E–10	7.46E–11	2.78E–11
^{250}Cf	1.31E+01	0.00E+00	2.13E+03	2.57E–06	4.24E–13	2.64E–22	8.20E–34
^{251}Cf	9.00E+02	0.00E+00	4.85E+03	1.13E–06	2.94E–12	2.16E–12	1.47E–12
^{252}Cf	2.64E+00	0.00E+00	1.08E+03	5.07E–06	3.52E–40	8.30E–86	7.66E–143
^{242}Cm	4.47E–01	5.00E+00	1.15E+02	4.76E–05	1.69E–06	2.73E–07	2.79E–08
^{243}Cm	2.85E+01	5.00E+00	2.51E+03	2.18E–06	4.07E–07	2.42E–11	1.27E–16
^{244}Cm	1.81E+01	5.00E+00	2.02E+03	2.71E–06	5.04E–06	1.13E–12	5.52E–21
^{245}Cm	8.50E+03	5.00E+00	3.74E+03	1.47E–06	6.56E–08	6.35E–08	6.10E–08
^{246}Cm	4.75E+03	5.00E+00	3.70E+03	1.48E–06	4.24E–09	4.00E–09	3.71E–09
^{247}Cm	1.56E+07	5.00E+00	3.42E+03	1.60E–06	4.80E–15	4.80E–15	4.80E–15
^{248}Cm	3.39E+05	5.00E+00	1.36E+04	4.03E–07	5.21E–15	5.21E–15	5.20E–15
^{60}Co	5.27E+00	1.00E–01	2.69E+01	2.04E–04	4.79E–08	6.94E–31	1.96E–59
^{135}Cs	2.30E+06	2.00E–03	7.07E+00	7.75E–04	4.74E–01	4.74E–01	4.74E–01
^{137}Cs	3.02E+01	2.00E–03	5.00E+01	1.10E–04	1.99E+03	2.03E–01	2.08E–06

Table 3-2. (continued).

Nuclide	Half-life (yr)	K_d (m^3/kg)	Ingestion DCF (mrem/μCi)	$C_{iw,\ limit}$ Allowable Concentration (μCi/L)	100 yr $C_{iw,max}$ (μCi/L)	500 yr $C_{iw,max}$ (μCi/L)	1000 yr $C_{iw,max}$ (μCi/L)
^{152}Eu	1.36E+01	5.00E+00	6.48E+00	8.46E–04	1.77E–06	2.48E–15	2.13E–26
^{154}Eu	8.80E+00	5.00E+00	9.55E+00	5.74E–04	1.36E–06	2.85E–20	2.26E–37
^{221}Fr	9.13E–06	0.00E+00	0.00E+00	NA	3.37E–05	1.85E–04	4.48E–04
^{223}Fr	4.14E–05	0.00E+00	8.62E+00	6.36E–04	1.68E–05	2.29E–05	3.02E–05
^{152}Gd	1.10E+14	0.00E+00	1.61E+02	3.40E–05	1.80E–11	1.80E–11	1.80E–11
^{3}H	1.23E+01	0.00E+00	6.40E–02	8.56E–02	2.21E–01	3.48E–11	1.94E–23
^{166m}Ho	1.20E+03	5.00E+00	8.07E+00	6.79E–04	9.37E–09	7.44E–09	5.57E–09
^{129}I	1.57E+07	2.00E–03	2.76E+02	1.99E–05	2.77E–02	2.77E–02	2.77E–02
^{115}In	4.60E+15	1.00E–01	1.58E+02	3.47E–05	1.07E–12	1.07E–12	1.07E–12
^{138}La	1.12E+11	5.00E+00	5.88E+00	9.32E–04	4.30E–14	4.30E–14	4.30E–14
^{93m}Nb	1.46E+01	5.00E–01	5.22E–01	1.05E–02	4.79E–03	4.80E–03	4.79E–03
^{94}Nb	2.03E+04	5.00E–01	7.14E+00	7.67E–04	1.42E–01	1.40E–01	1.38E–01
^{59}Ni	7.50E+04	1.00E–01	2.10E–01	2.61E–02	1.60E–04	1.60E–04	1.60E–04
^{63}Ni	1.00E+02	1.00E–01	5.77E–01	9.50E–03	1.57E–01	9.85E–03	3.09E–04
^{235}Np	1.08E+00	5.00E+00	2.43E–01	2.26E–02	2.91E–61	2.69E–172	0.00E+00
^{237}Np	2.14E+06	5.00E+00	4.44E+03	1.23E–06	1.67E–05	1.69E–05	1.70E–05
^{238}Np	5.80E–03	5.00E+00	4.00E+00	1.37E–03	9.75E–09	1.57E–09	1.61E–10
^{239}Np	6.45E–03	5.00E+00	3.26E+00	1.68E–03	4.59E–06	4.42E–06	4.22E–06
^{240}Np	1.24E–04	5.00E+00	2.37E–01	2.31E–02	1.64E–16	1.64E–16	1.64E–16
^{240m}Np	1.41E–05	5.00E+00	0.00E+00	NA	1.49E–13	1.49E–13	1.49E–13
^{231}Pa	3.28E+04	5.00E+00	1.06E+04	5.17E–07	2.35E–08	3.14E–08	4.12E–08
^{233}Pa	7.39E–02	5.00E+00	3.63E+00	1.51E–03	1.67E–05	1.69E–05	1.70E–05
^{234}Pa	7.64E–04	5.00E+00	2.16E+00	2.54E–03	1.16E–09	1.16E–09	1.16E–09
^{234m}Pa	2.22E–06	5.00E+00	0.00E+00	NA	7.25E–07	7.25E–07	7.25E–07
^{209}Pb	3.71E–04	5.00E–01	2.13E–01	2.57E–02	6.24E–09	3.42E–08	8.29E–08
^{210}Pb	2.23E+01	5.00E–01	5.37E+03	1.02E–06	1.05E–07	1.14E–06	3.74E–06
^{211}Pb	6.86E–05	5.00E–01	5.25E–01	1.04E–02	2.25E–07	3.07E–07	4.05E–07
^{212}Pb	1.21E–03	5.00E–01	4.55E+01	1.20E–04	1.62E–06	3.45E–08	2.85E–10
^{214}Pb	5.10E–05	5.00E–01	6.25E–01	8.77E–03	1.47E–07	1.27E–06	3.95E–06
^{107}Pd	6.50E+06	1.00E–01	1.49E–01	3.68E–02	1.78E–04	1.78E–04	1.78E–04
^{146}Pm	5.53E+00	0.00E+00	3.67E+00	1.49E–03	4.23E–07	7.46E–29	4.79E–56
^{147}Pm	2.62E+00	0.00E+00	1.05E+00	5.22E–03	2.25E–10	2.83E–56	1.20E–113
^{210}Po	3.79E–01	5.00E–01	1.90E+03	2.88E–06	1.05E–07	1.14E–06	3.74E–06
^{211}Po	1.64E–08	5.00E–01	0.00E+00	NA	6.14E–10	8.39E–10	1.11E–09

Table 3-2. (continued).

Nuclide	Half-life (yr)	K_d (m^3/kg)	Ingestion DCF (mrem/μCi)	$C_{iw,\ limit}$ Allowable Concentration (μCi/L)	100 yr $C_{iw,max}$ (μCi/L)	500 yr $C_{iw,max}$ (μCi/L)	1000 yr $C_{iw,max}$ (μCi/L)
^{212}Po	9.44E–15	5.00E–01	0.00E+00	NA	1.04E–06	2.21E–08	1.82E–10
^{213}Po	1.33E–13	5.00E–01	0.00E+00	NA	6.10E–09	3.34E–08	8.11E–08
^{214}Po	2.02E–12	5.00E–01	0.00E+00	NA	1.47E–07	1.27E–06	3.95E–06
^{215}Po	2.47E–11	5.00E–01	0.00E+00	NA	2.25E–07	3.07E–07	4.05E–07
^{216}Po	4.63E–09	5.00E–01	0.00E+00	NA	1.62E–06	3.45E–08	2.85E–10
^{218}Po	5.80E–06	5.00E–01	0.00E+00	NA	1.47E–07	1.27E–06	3.95E–06
^{236}Pu	2.85E+00	5.00E+00	1.17E+03	4.68E–06	6.86E–19	3.99E–61	6.42E–114
^{238}Pu	8.78E+01	5.00E+00	3.20E+03	1.71E–06	1.62E–02	6.87E–04	1.33E–05
^{239}Pu	2.41E+04	5.00E+00	3.54E+03	1.55E–06	2.82E–03	2.79E–03	2.75E–03
^{240}Pu	6.54E+03	5.00E+00	3.54E+03	1.55E–06	2.29E–03	2.20E–03	2.08E–03
^{241}Pu	1.44E+01	5.00E+00	6.85E+01	8.00E–05	2.49E–04	6.36E–08	6.11E–08
^{242}Pu	3.76E+05	5.00E+00	3.36E+03	1.63E–06	1.73E–06	1.73E–06	1.73E–06
^{243}Pu	5.65E–04	5.00E+00	3.34E–01	1.64E–02	4.80E–15	4.80E–15	4.80E–15
^{244}Pu	8.26E+07	5.00E+00	3.32E+03	1.65E–06	1.49E–13	1.49E–13	1.49E–13
^{223}Ra	3.13E–02	5.00E–02	6.59E+02	8.31E–06	2.25E–06	3.07E–06	4.05E–06
^{224}Ra	1.00E–02	5.00E–02	3.66E+02	1.50E–05	1.62E–05	3.45E–07	2.84E–09
^{225}Ra	4.05E–02	5.00E–02	3.85E+02	1.42E–05	6.23E–08	3.41E–07	8.27E–07
^{226}Ra	1.60E+03	5.00E–02	1.32E+03	4.15E–06	1.47E–06	1.27E–05	3.94E–05
^{228}Ra	5.75E+00	5.00E–02	1.44E+03	3.81E–06	1.83E–11	2.97E–11	4.41E–11
^{87}Rb	4.73E+10	0.00E+00	4.92E+00	1.11E–03	3.48E–04	3.48E–04	3.48E–04
^{219}Rn	1.25E–07	0.00E+00	0.00E+00	NA	1.21E–03	1.66E–03	2.19E–03
^{220}Rn	1.76E–06	0.00E+00	0.00E+00	NA	8.77E–03	1.87E–04	1.54E–06
^{222}Rn	1.05E–02	0.00E+00	0.00E+00	NA	7.95E–04	6.84E–03	2.13E–02
^{126}Sb	3.40E–02	0.00E+00	1.07E+01	5.12E–04	6.87E–01	6.85E–01	6.83E–01
^{126m}Sb	3.62E–05	0.00E+00	9.36E–02	5.85E–02	4.91E+00	4.89E+00	4.88E+00
^{79}Se	6.50E+04	1.00E–04	8.70E+00	6.30E–04	2.57E+00	2.56E+00	2.55E+00
^{146}Sm	7.00E+07	5.00E+00	2.04E+02	2.69E–05	6.12E–11	6.12E–11	6.12E–11
^{147}Sm	6.90E+09	5.00E+00	1.85E+02	2.96E–05	1.65E–09	1.65E–09	1.65E–09
^{151}Sm	9.00E+01	5.00E+00	3.89E–01	1.41E–02	3.14E–02	1.44E–03	3.07E–05
^{121m}Sn	7.60E+01	1.00E+00	1.55E+00	3.54E–03	2.49E–04	6.49E–06	6.80E–08
^{126}Sn	1.00E+05	1.00E+00	1.95E+01	2.81E–04	4.54E–04	4.53E–04	4.52E–04
^{90}Sr	2.86E+01	1.00E–03	1.42E+02	3.86E–05	6.25E+03	3.85E–01	2.10E–06
^{98}Tc	4.20E+06	1.00E–03	4.88E+00	1.12E–03	2.61E–06	2.61E–06	2.61E–06
^{99}Tc	2.13E+05	1.00E–03	1.46E+00	3.75E–03	8.60E+01	8.59E+01	8.58E+01

Table 3-2. (continued).

Nuclide	Half-life (yr)	K_d (m^3/kg)	Ingestion DCF (mrem/μCi)	$C_{iw,\ limit}$ Allowable Concentration (μCi/L)	100 yr $C_{iw,max}$ (μCi/L)	500 yr $C_{iw,max}$ (μCi/L)	1000 yr $C_{iw,max}$ (μCi/L)
^{123}Te	1.00E+13	0.00E+00	4.18E+00	1.31E–03	4.47E–12	4.47E–12	4.47E–12
^{227}Th	5.12E–02	5.00E+00	3.81E+01	1.44E–04	2.22E–08	3.03E–08	4.00E–08
^{228}Th	1.91E+00	5.00E+00	3.96E+02	1.38E–05	1.62E–07	3.45E–09	2.85E–11
^{229}Th	7.34E+03	5.00E+00	3.53E+03	1.55E–06	6.24E–10	3.42E–09	8.29E–09
^{230}Th	7.70E+04	5.00E+00	5.48E+02	1.00E–05	3.65E–07	1.06E–06	1.92E–06
^{231}Th	2.91E–03	5.00E+00	1.35E+00	4.06E–03	9.60E–07	9.61E–07	9.62E–07
^{232}Th	1.41E+10	5.00E+00	2.73E+03	2.01E–06	1.86E–13	3.00E–13	4.44E–13
^{234}Th	6.60E–02	5.00E+00	1.37E+01	4.00E–04	7.25E–07	7.25E–07	7.25E–07
^{207}Tl	9.07E–06	0.00E+00	0.00E+00	NA	1.21E–03	1.66E–03	2.18E–03
^{208}Tl	5.81E–06	0.00E+00	0.00E+00	NA	3.15E–03	6.70E–05	5.53E–07
^{209}Tl	4.18E–06	0.00E+00	0.00E+00	NA	7.28E–07	3.99E–06	9.67E–06
^{210}Tl	2.47E–06	0.00E+00	0	NA	0.00E+00	0.00E+00	0.00E+00
^{232}U	7.20E+01	2.00E+00	1.31E+03	4.18E–06	3.95E–07	8.41E–09	6.82E–11
^{233}U	1.59E+05	2.00E+00	2.89E+02	1.90E–05	1.53E–07	2.26E–07	3.18E–07
^{234}U	2.45E+05	2.00E+00	2.83E+02	1.94E–05	4.71E–04	4.85E–04	4.85E–04
^{235}U	7.04E+08	2.00E+00	2.66E+02	2.06E–05	2.40E–06	2.40E–06	2.41E–06
^{236}U	3.42E+06	2.00E+00	2.69E+02	2.04E–05	1.45E–05	1.45E–05	1.46E–05
^{237}U	1.85E–02	2.00E+00	3.17E+00	1.73E–03	1.53E–08	3.90E–12	3.74E–12
^{238}U	4.47E+09	2.00E+00	2.55E+02	2.15E–05	1.81E–06	1.81E–06	1.81E–06
^{240}U	1.61E–03	2.00E+00	4.44E+00	1.23E–03	3.72E–13	3.72E–13	3.72E–13
^{90}Y	7.32E–03	1.00E–03	1.08E+01	5.07E–04	6.25E+03	3.85E–01	2.10E–06
^{93}Zr	1.53E+06	5.00E+00	1.66E+00	3.30E–03	4.80E–04	4.80E–04	4.80E–04

for the sand pads; these results are provided in Table 3-3. The radionuclides selected for analysis are given in Table 3-4.

The next step in the screening process involved evaluation of the release of the radionuclides from the waste-form and the resulting groundwater concentrations. Releases and groundwater concentrations were previously analyzed. The results are presented in Appendix F. Based on these analyses, only ^{129}I, ^{99}Tc, ^{90}Sr, and ^{14}C were found to result in appreciable groundwater concentrations and significant doses.

The *Idaho High-Level Waste & Facilities Disposition Final Environmental Impact Statement* (DOE 2002) also conducted screening and groundwater transport analyses for the TFF. Their screening and analyses found that only ^{99}Tc and ^{129}I resulted in significant doses from the groundwater pathway.

Therefore, base on previous modeling of the TFF presented in Appendix F, four radionuclides (i.e., ^{129}I, ^{99}Tc, ^{90}Sr, and ^{14}C) were determined to result in appreciable groundwater concentrations and doses. Therefore, the groundwater analysis was focused on the four radionuclides.

The releases calculated with DUST-MS (Sullivan 1993, 1998) discussed in Section 3.3, show that several radionuclides are never released from the waste form during the 1,000-yr compliance period. This is because distribution coefficients (K_d values) are used in the DUST-MS release model, whereas the screening method does not take into account the transport from the tank and sand pad. Therefore, radionuclides not released in significant quantities during the 1,000-yr compliance period were not modeled in the PORFLOW (Runchal 1997; ACRi 2000) groundwater model. However, all radionuclides selected in the groundwater screening were run using the long-term groundwater model GWSCREEN (Rood 1998) in previous modeling analyses for the TFF. Results from the previous analyses conducted for all radionuclides are presented in Appendix F: input parameters used in those analyses are provided in tables in this section. The modeling conducted in this report focused on the four radionuclides found to be the major contributors to the groundwater pathway doses in the previous modeling exercise (i.e., ^{90}Sr, ^{99}Tc, ^{129}I, and ^{14}C).

3.3 Models and Assumptions

3.3.1 Source Term Model

For the TFF concrete vaults, release rates of radionuclides were estimated using the Disposal Unit Source Term-Multiple Species (DUST-MS) computer code (Sullivan 1993, 1996). One-dimensional DUST-MS transport simulations were conducted for radionuclide sources in the grouted tank, piping, and the sand pad beneath the tank.

Infiltration was assumed to contact and transport radionuclides after concrete degradation and tank corrosion. The concrete vault and grout between the vault wall and the tank were assumed to completely degrade after 100 yr, at which time infiltrating water contacted radionuclides in the sand pad and transported the radionuclides through the sand pad and the degraded vault floor to the basalt. At 500 yr, the stainless-steel tanks were assumed to have totally corroded and the grout inside the tank was assumed to have completely degraded. At this time, infiltrating water contacting radionuclides contained in the grout inside the tank was assumed to transport radionuclides through the degraded grout in the tank, sand pad, and degraded vault floor to the basalt. Piping releases were assumed to occur in the same manner as the tanks. The DUST-MS computer code modeled these two releases as separate and independent events.

The two waste forms for these DUST-MS simulations were the radionuclides in the grouted tank and piping and the radionuclides in the sand pad. The DUST-MS waste form release rate model selected for these simulations was a surface rinse model. The surface rinse model accounts for partitioning between the infiltrating water and the radionuclides in the waste form. Additionally, partitioning and retardation were modeled in DUST-MS for radionuclide transport occurring in the grouted tank, sand pad, and vault floor. Radionuclide source locations specified in the DUST-MS computer code for the two waste forms

Table 3-3. Sand pad activity groundwater screening for the drinking water pathway.

Nuclide	Half-life (yr)	K_d (m^3/kg)	Ingestion DCF (mrem/μCi)	$C_{iw,\ limit}$ Allowable Concentration (μCi/L)	100 yr $C_{iw,max}$ (μCi/L)	500 yr $C_{iw,max}$ (μCi/L)	1000 yr $C_{iw,max}$ (μCi/L)
^{225}Ac	2.74E–02	4.50E–01	1.11E+02	4.94E–05	2.67E–10	8.00E–10	1.84E–09
^{227}Ac	2.18E+01	4.50E–01	1.41E+04	3.89E–07	2.42E–07	7.72E–07	1.43E–06
^{228}Ac	6.99E–04	4.50E–01	2.16E+00	2.54E–03	1.02E–08	1.96E–12	3.91E–12
^{108}Ag	4.51E–06	9.00E–02	0.00E+00	NA	5.77E–12	6.50Ev13	4.24E–14
^{108m}Ag	1.27E+02	9.00E–02	7.62E+00	7.19E–04	6.20E–11	6.99E–12	4.56E–13
^{241}Am	4.32E+02	1.90E+00	3.64E+03	1.51E–06	2.96E–03	1.56E–03	6.99E–04
^{242}Am	1.83E–03	1.90E+00	1.41E+00	3.89E–03	1.84E–08	2.96Ev09	3.03E–10
^{242m}Am	1.52E+02	1.90E+00	3.52E+03	1.56E–06	1.85E–08	2.98E–09	3.05E–10
^{243}Am	7.38E+03	1.90E+00	3.62E+03	1.51E–06	2.58E–07	2.49E–07	2.37E–07
^{217}At	1.02E–09	0	0.00E+00	NA	6.22E–07	1.87E–06	4.29E–06
^{137m}Ba	4.86E–06	4.00E–04	0.00E+00	NA	8.13E+02	8.30E–02	8.51E–07
^{10}Be	1.60E+06	2.50E–01	4.66E+00	1.18E–03	2.43E–09	2.43Ev09	2.43E–09
^{210}Bi	1.37E–02	1.00E–01	6.40E+00	8.56E–04	1.02E–06	7.91E–06	2.33E–05
^{211}Bi	4.05E–06	1.00E–01	0.00E+00	NA	1.09E–06	3.47E–06	6.41E–06
^{212}Bi	1.15E–04	1.00E–01	1.06E+00	5.17E–03	3.17E–07	5.28E–09	6.03E–11
^{213}Bi	8.68E–05	1.00E–01	7.22E–01	7.59E–03	1.20E–09	3.59E–09	8.26E–09
^{214}Bi	3.78E–05	1.00E–01	2.83E–01	1.94E–02	1.35E–06	8.67E–06	2.45E–05
^{14}C	5.73E+03	5.00E–03	2.09E+00	2.62E–03	2.51E–07	2.39E–07	2.25E–07
^{113m}Cd	1.37E+01	8.00E–02	1.61E+02	3.40E–05	4.29E–06	7.00E–15	7.26E–26
^{249}Cf	3.51E+02	0.00E+00	4.74E+03	1.16E–06	3.48E–15	1.58E–15	5.87E–16
^{250}Cf	1.31E+01	0.00E+00	2.13E+03	2.57E–06	1.19E–18	7.43E–28	2.31E–39
^{251}Cf	9.00E+02	0.00E+00	4.85E+03	1.13E–06	9.64E–18	7.08E–18	4.82E–18
^{252}Cf	2.64E+00	0.00E+00	1.08E+03	5.07E–06	1.91E–35	4.50E–81	4.15E–138
^{242}Cm	4.47E–01	4.00E+00	1.15E+02	4.76E–05	7.24E–09	1.17E–09	1.19E–10
^{243}Cm	2.85E+01	4.00E+00	2.51E+03	2.18E–06	5.86E–11	3.49E–15	1.83E–20
^{244}Cm	1.81E+01	4.00E+00	2.02E+03	2.71E–06	4.05E–09	9.10E–16	4.44E–24
^{245}Cm	8.50E+03	4.00E+00	3.74E+03	1.47E–06	4.28E–11	4.14E–11	3.97E–11
^{246}Cm	4.75E+03	4.00E+00	3.70E+03	1.48E–06	9.50E–13	8.96E–13	8.33E–13
^{247}Cm	1.56E+07	4.00E+00	3.42E+03	1.60E–06	3.47E–19	3.47E–19	3.47E–19
^{248}Cm	3.39E+05	4.00E+00	1.36E+04	4.03E–07	1.06E–19	1.06E–19	1.06E–19
^{60}Co	5.27E+00	6.00E–02	2.69E+01	2.04E–04	1.75E–10	2.53E–33	7.13E–62
^{135}Cs	2.30E+06	2.80E–01	7.07E+00	7.75E–04	7.21E–05	7.21E–05	7.21E–05
^{137}Cs	3.02E+01	2.80E–01	5.00E+01	1.10E–04	1.82E+00	1.86E–04	1.90E–09
^{152}Eu	1.36E+01	1.90E+00	6.48E+00	8.46E–04	1.01E–07	1.41E–16	1.21E–27
^{154}Eu	8.80E+00	1.90E+00	9.55E+00	5.74E–04	8.69E–07	1.81E–20	1.44E–37
^{221}Fr	9.13E–06	0	0.00E+00	NA	6.22E–07	1.87E–06	4.29E–06
^{223}Fr	4.14E–05	0	8.62E+00	6.36E–04	7.81E–06	2.49E–05	4.60E–05
^{152}Gd	1.10E+14	0.00E+00	1.61E+02	3.40E–05	5.70E–13	5.70E–13	5.70E–13
^{3}H	1.23E+01	0.00E+00	6.40E–02	8.56E–02	1.53E–23	2.41E–33	1.34E–45
^{166m}Ho	1.20E+03	2.50E–01	8.07E+00	6.79E–04	5.28E–09	4.19E–09	3.14E–09
^{129}I	1.57E+07	1.00E–03	2.76E+02	1.99E–05	3.05E–06	3.05E–06	3.05E–06

Table 3-3. (continued).

Nuclide	Half-life (yr)	K_d (m^3/kg)	Ingestion DCF (mrem/μCi)	$C_{iw,\ limit}$ Allowable Concentration (μCi/L)	100 yr $C_{iw,max}$ (μCi/L)	500 yr $C_{iw,max}$ (μCi/L)	1000 yr $C_{iw,max}$ (μCi/L)
^{115}In	4.60E+15	0.00E+00	1.58E+02	3.47E–05	6.49E–11	6.49E–11	6.49E–11
^{138}La	1.12E+11	0.00E+00	5.88E+00	9.32E–04	9.33E–10	9.33E–10	9.33E–10
^{93m}Nb	1.46E+01	1.60E–01	5.22E–01	1.05E–02	4.45E–03	4.45E–03	4.45E–03
^{94}Nb	2.03E+04	1.60E–01	7.14E+00	7.67E–04	4.81E–04	4.75E–04	4.67E–04
^{63}Ni	1.00E+02	4.00E–01	5.77E–01	9.50E–03	6.92E–13	4.34E–14	1.36E–15
^{235}Np	1.08E+00	5.00E–03	2.43E–01	2.26E–02	2.03E–52	1.88E–163	3.03E–302
^{237}Np	2.14E+06	5.00E–03	4.44E+03	1.23E–06	2.79E–04	3.83E–04	4.46E–04
^{238}Np	5.80E–03	5.00E–03	4.00E+00	1.37E–03	3.21E–08	5.19E–09	5.30E–10
^{239}Np	6.45E–03	5.00E–03	3.26E+00	1.68E–03	9.44E–05	9.09E–05	8.68E–05
^{240}Np	1.24E–04	5.00E–03	2.37E–01	2.31E–02	4.28E–15	4.28E–15	4.28E–15
^{240m}Np	1.41E–05	5.00E–03	0.00E+00	NA	3.89E–12	3.89E–12	3.89E–12
^{231}Pa	3.28E+04	5.50E–01	1.06E+04	5.17E–07	2.33E–07	6.66E–07	1.20E–06
^{233}Pa	7.39E–02	5.50E–01	3.63E+00	1.51E–03	2.64E–06	3.61E–06	4.21E–06
^{234}Pa	7.64E–04	5.50E–01	2.16E+00	2.54E–03	8.82E–10	8.82E–10	8.82E–10
^{234m}Pa	2.22E–06	5.50E–01	0.00E+00	NA	5.51E–07	5.51E–07	5.51E–07
^{209}Pb	3.71E–04	2.70E–01	2.13E–01	2.57E–02	4.44E–10	1.33E–09	3.06E–09
^{210}Pb	2.23E+01	2.70E–01	5.37E+03	1.02E–06	3.77E–07	2.93E–06	8.65E–06
^{211}Pb	6.86E–05	2.70E–01	5.25E–01	1.04E–02	4.04E–07	1.29E–06	2.38E–06
^{212}Pb	1.21E–03	2.70E–01	4.55E+01	1.20E–04	1.17E–07	1.96E–09	2.24E–11
^{214}Pb	5.10E–05	2.70E–01	6.25E–01	8.77E–03	5.00E–07	3.22E–06	9.10E–06
^{107}Pd	6.50E+06	5.50E–02	1.49E–01	3.68E–02	2.57E–05	2.57E–05	2.57E–05
^{146}Pm	5.53E+00	0.00E+00	3.67E+00	1.49E–03	1.09E–09	1.92E–31	1.23E–58
^{147}Pm	2.62E+00	0.00E+00	1.05E+00	5.22E–03	1.89E–13	2.39E–59	1.01E–116
^{210}Po	3.79E–01	1.50E–01	1.90E+03	2.88E–06	6.75E–07	5.27E–06	1.55E–05
^{211}Po	1.64E–08	1.50E–01	0.00E+00	NA	1.98E–09	6.32E–09	1.17E–08
^{212}Po	9.44E–15	1.50E–01	0.00E+00	NA	1.35E–07	2.26E–09	2.58E–11
^{213}Po	1.33E–13	1.50E–01	0.00E+00	NA	7.82E–10	2.35E–09	5.39E–09
^{214}Po	2.02E–12	1.50E–01	0.00E+00	NA	9.00E–07	5.79E–06	1.64E–05
^{215}Po	2.47E–11	1.50E–01	0.00E+00	NA	7.26E–07	2.31E–06	4.28E–06
^{216}Po	4.63E–09	1.50E–01	0.00E+00	NA	2.11E–07	3.52E–09	4.02E–11
^{218}Po	5.80E–06	1.50E–01	0.00E+00	NA	9.00E–07	5.79E–06	1.64E–05
^{236}Pu	2.85E+00	5.50E–01	1.17E+03	4.68E–06	7.17E–24	4.18E–66	6.71E–119
^{238}Pu	8.78E+01	5.50E–01	3.20E+03	1.71E–06	5.56E–03	2.36E–04	4.55E–06
^{239}Pu	2.41E+04	5.50E–01	3.54E+03	1.55E–06	9.63E–03	9.52E–03	9.38E–03
^{240}Pu	6.54E+03	5.50E–01	3.54E+03	1.55E–06	2.15E–03	2.06E–03	1.95E–03
^{241}Pu	1.44E+01	5.50E–01	6.85E+01	8.00E–05	9.34E–05	3.02E–10	2.89E–10
^{242}Pu	3.76E+05	5.50E–01	3.36E+03	1.63E–06	3.49E–07	3.48E–07	3.48E–07
^{243}Pu	5.65E–04	5.50E–01	3.34E–01	1.64E–02	2.52E–18	2.52E–18	2.52E–18
^{244}Pu	8.26E+07	5.50E–01	3.32E+03	1.65E–06	3.67E–14	3.67E–14	3.67E–14
^{223}Ra	3.13E–02	5.00E–01	6.59E+02	8.31E–06	2.18E–07	6.95E–07	1.28E–06
^{224}Ra	3.62E+00	5.00E–01	3.66E+02	1.50E–05	6.34E–08	1.06E–09	1.21E–11

Table 3-3. (continued).

Nuclide	Half-life (yr)	K_d (m^3/kg)	Ingestion DCF (mrem/μCi)	$C_{iw,\ limit}$ Allowable Concentration (μCi/L)	100 yr $C_{iw,max}$ (μCi/L)	500 yr $C_{iw,max}$ (μCi/L)	1000 yr $C_{iw,max}$ (μCi/L)
^{225}Ra	4.05E–02	5.00E–01	3.85E+02	1.42E–05	2.40E–10	7.20E–10	1.65E–09
^{226}Ra	1.60E+03	5.00E–01	1.32E+03	4.15E–06	2.70E–07	1.74E–06	4.92E–06
^{228}Ra	5.75E+00	5.00E–01	1.44E+03	3.81E–06	9.14E–09	1.76E–12	3.52E–12
^{87}Rb	4.73E+10	5.50E–02	4.92E+00	1.11E–03	4.70E–08	4.70E–08	4.70E–08
^{219}Rn	1.25E–07	0	0.00E+00	NA	5.65E–04	1.80E–03	3.33E–03
^{220}Rn	1.76E–06	0	0.00E+00	NA	1.64E–04	2.74E–06	3.13E–08
^{222}Rn	1.05E–02	0	0.00E+00	NA	7.01E–04	4.51E–03	1.27E–02
^{126}Sb	3.40E–02	4.50E–02	1.07E+01	5.12E–04	1.72E–04	1.72E–04	1.71E–04
^{126m}Sb	3.62E–05	4.50E–02	9.36E–02	5.85E–02	1.23E–03	1.23E–03	1.22E–03
^{79}Se	6.50E+04	1.50E–01	8.70E+00	6.30E–04	4.49E–04	4.47E–04	4.44E–04
^{146}Sm	7.00E+07	2.45E–01	2.04E+02	2.69E–05	5.19E–12	5.18E–12	5.18E–12
^{147}Sm	6.90E+09	2.45E–01	1.85E+02	2.96E–05	3.48E–08	3.48E–08	3.48E–08
^{151}Sm	9.00E+01	2.45E–01	3.89E–01	1.41E–02	2.40E–01	1.10E–02	2.34E–04
^{121m}Sn	7.60E+01	1.30E–01	1.55E+00	3.54E–03	2.14E–05	5.58E–07	5.84E–09
^{126}Sn	1.00E+05	1.30E–01	1.95E+01	2.81E–04	4.26E–04	4.25E–04	4.24E–04
^{90}Sr	2.86E+01	1.50E–02	1.42E+02	3.86E–05	4.44E+00	2.74E–04	1.50E–09
^{98}Tc	4.20E+06	1.00E–04	4.88E+00	1.12E–03	7.12E–19	7.12E–19	7.12E–19
^{99}Tc	2.13E+05	1.00E–04	1.46E+00	3.75E–03	2.33E–11	2.32E–11	2.32E–11
^{123}Te	1.00E+13	1.25E–01	4.18E+00	1.31E–03	1.33E–17	1.33E–17	1.33E–17
^{227}Th	5.12E–02	3.20E+00	3.81E+01	1.44E–04	3.36E–08	1.07E–07	1.98E–07
^{228}Th	1.91E+00	3.20E+00	3.96E+02	1.38E–05	9.90E–09	1.65E–10	1.89E–12
^{229}Th	7.34E+03	3.20E+00	3.53E+03	1.55E–06	3.75E–11	1.13E–10	2.59E–10
^{230}Th	7.70E+04	3.20E+00	5.48E+02	1.00E–05	8.75E–07	2.06E–06	3.53E–06
^{231}Th	2.91E–03	3.20E+00	1.35E+00	4.06E–03	8.87E–06	8.87E–06	8.87E–06
^{232}Th	1.41E+10	3.20E+00	2.73E+03	2.01E–06	5.97E–14	2.80E–13	5.55E–13
^{234}Th	6.60E–02	3.20E+00	1.37E+01	4.00E–04	9.48E–08	9.48E–08	9.48E–08
^{207}Tl	9.07E–06	0	0.00E+00	NA	5.64E–04	1.80E–03	3.32E–03
^{208}Tl	5.81E–06	0	0.00E+00	NA	5.90E–05	9.85E–07	1.13E–08
^{209}Tl	4.18E–06	0	0.00E+00	NA	1.34E–08	4.03E–08	9.26E–08
^{210}Tl	2.47E–06	0	0	NA	0.00E+00	0.00E+00	0.00E+00
^{232}U	7.20E+01	3.50E–02	1.31E+03	4.18E–06	6.87E–07	1.46E–08	1.19E–10
^{233}U	1.59E+05	3.50E–02	2.89E+02	1.90E–05	1.46E–07	2.32E–07	3.66E–07
^{234}U	2.45E+05	3.50E–02	2.83E+02	1.94E–05	3.00E–02	3.00E–02	3.00E–02
^{235}U	7.04E+08	3.50E–02	2.66E+02	2.06E–05	8.07E–04	8.07E–04	8.07E–04
^{236}U	3.42E+06	3.50E–02	2.69E+02	2.04E–05	1.01E–03	1.01E–03	1.01E–03
^{237}U	1.85E–02	3.50E–02	3.17E+00	1.73E–03	3.58E–08	1.16E–13	1.11E–13
^{238}U	4.47E+09	3.50E–02	2.55E+02	2.15E–05	8.62E–06	8.62E–06	8.62E–06
^{240}U	1.61E–03	3.50E–02	4.44E+00	1.23E–03	5.74E–13	5.74E–13	5.74E–13
^{90}Y	7.32E–03	1.70E–01	1.08E+01	5.07E–04	3.97E–01	2.44E–05	1.34E–10
^{93}Zr	1.53E+06	6.00E–01	1.66E+00	3.30E–03	1.19E–03	1.19E–03	1.19E–03

a. Allowable concentration not calculated since ingestion DCF not reported for these nuclides in EPA 1988.

Table 3-4. Radionuclides remaining from the initial screening based on waste pore-water concentrations.

Nuclide	Half-life (yr)	Nuclide	Half-life (yr)	Nuclide	Half-life (yr)
^{241}Am	4.32E+02	^{94}Nb	2.03E+04	^{224}Ra	1.00E–02
^{242m}Am	1.52E+02	^{63}Ni	1.00E+02	^{226}Ra[b]	1.60E+03
^{243}Am	7.38E+03	^{237}Np	2.14E+06	^{79}Se	6.50E+04
^{14}C	5.73E+03	^{210}Pb	2.23E+01	^{151}Sm	9.00E+01
^{113m}Cd	1.37E+01	^{210}Po	3.79E–01	^{126}Sn+D[a]	1.00E+05
^{244}Cm	1.81E+01	^{238}Pu	8.78E+01	^{90}Sr+D[a]	2.86E+01
^{135}Cs	2.30E+06	^{239}Pu	2.41E+04	^{99}Tc	2.13E+05
^{137}Cs+D[a]	3.02E+01	^{240}Pu	6.54E+03	^{234}U	2.45E+05
^{3}H	1.23E+01	^{241}Pu	1.41E+01	^{236}U	3.42E+06
^{129}I	1.57E+07	^{242}Pu	3.76E+05		

a. +D indicate there is a daughter to consider in the groundwater and dose analysis.

b. ^{226}Ra is included for the groundwater analysis because it will provide activity to ^{210}Pb during transport and decay.

were at the center of the 1-ft layer of grout in the tank (i.e., the bottom 1 ft of the grouted tank was conservatively assumed to contain all of the tank contamination) and at the center of the sand pad.

Radionuclide inventories used to determine the DUST-MS release rates for the tank and sand pad are provided in Section 2.3. Justification for the times required for vault degradation and tank corrosion (i.e., 100 and 500 yr, respectively) is summarized in Section 3.1.2.2 and presented completely in Appendix E. Additional DUST-MS input parameters are discussed subsequently in this section.

The release rates computed in the DUST-MS simulations were estimated at the location of the vault floor/basalt interface. These release rates were used in the PORFLOW unsaturated/saturated zone transport simulations discussed in Section 3.2. The following sections present a more detailed discussion of the DUST-MS model, the modeling approach, the input parameters, and verification of DUST-MS model results.

3.3.1.1 DUST-MS Model Description.

DUST-MS considers four major processes: fluid flow, container degradation, waste form leaching, and contaminant transport. The DUST-MS model permits selection of a unique failure time and waste form type for each container. To simulate different waste forms, DUST-MS has four different models to estimate release rates: rinse with partitioning, diffusion, uniform degradation, and solubility-limited release. For these four processes, DUST-MS computes release rates with an analytical model or a finite difference model. After calculating waste form releases, the movement of the contaminants through subsurface system materials is determined using a one-dimensional finite difference procedure with material- and contaminant-specific distribution coefficients, diffusion coefficients, dispersion coefficients, and bulk densities. The governing transport equation simulates the distribution and movement of contaminants from advection, dispersion, diffusion, radioactive production and decay, sorption, and sources and sinks external to the containers. The DUST-MS code has received extensive testing and verification. DUST-MS code predictions compare favorably to known analytical solutions as well as other code predictions.

3.3.1.2 Conceptual Model.

The conceptual model for computing release rates of radionuclides out of the TFF vault is illustrated in Figure 3-14. Infiltrating water from the ground surface contacts the waste inside the vaults. As shown in

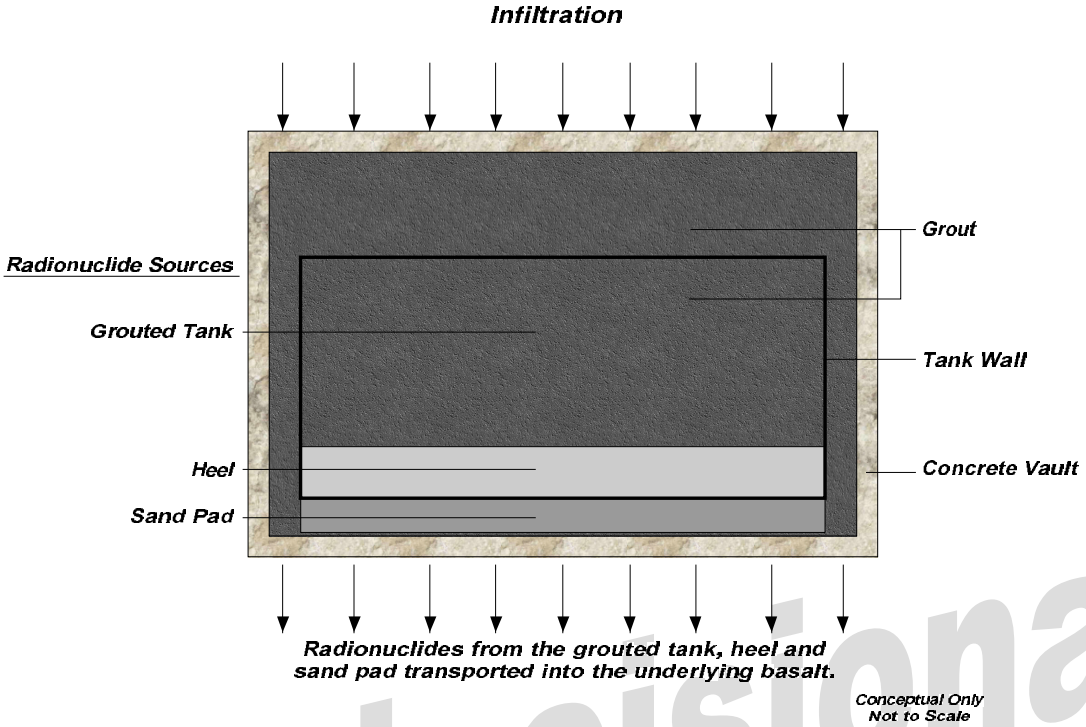

Figure 3-14. DUST-MS conceptual model for release from the TFF vaults and tanks.

Figure 3-14, radionuclides are assumed to be located in the grouted tank heel and in the sand pad beneath the tank. The release of radionuclides from the grouted tank heel and from the sand pad is modeled in DUST-MS assuming surface rinsing. The vault is assumed to remain intact for 100 yr. The tanks are assumed to remain intact for 500 yr. Upon vault and tank failure, radionuclides are released from the two sources.

The DUST-MS code calculates release rates out of the vault and tanks into the unsaturated zone. Release rates are computed for transport through the grout inside the tank (0.15 m [5.9 in.]), the sand pad (0.15 m [5.9 in.]), and the degraded concrete (0.76 m [30. in.]). Retardation is assumed to occur in the waste release model (surface rinsing), in the grout inside the tank, in the sand pad, and in the degraded concrete.

3.3.1.3 Model Input Parameters. Input parameter values that describe source geometry, infiltration rates, failure times, dispersion coefficients, and computational options used in all DUST-MS simulations are included in Table 3-5. Vadose zone transport properties (infiltration and moisture content) also are listed in Table 3-5.

Table 3-6 lists the modeled radionuclides; half-lives; partition coefficients (K_d values) for the sand pad, liquid tank waste, solid tank waste, and concrete vault; and sand pad liquid tank waste and solid tank waste initial inventories. The distribution coefficients for grout were taken from studies conducted by Allard, Persson, and Torstenflt (1985) and Bradbury and Sarott (1995). The distribution coefficients for sand were taken from Sheppard and Thibault (1990) (see Appendix A).

3.3.1.4 Verification of DUST-MS Model Results. The PORFLOW computer code was initially used to estimate tank and sand pad release rates. However, because of the numerically-intensive calculations associated with grid discretization and modeling the entire source term and unsaturated/saturated model domain, the DUST-MS computer code was used. The DUST-MS computer code minimized the computational time required in PORFLOW simulations to

Table 3-5. Parameter values for source term analysis using the DUST-MS model.

Parameter	Value	Comments
Number of finite difference nodes	200	Reasonable number
Spatial discretization (cm)	1.3	Reasonable number
Geometry of grouted tank heel	Cylindrical	Based on tank geometry
Radius of tank heel (cm)	762	Based on tank geometry
Failure time of vault (yr)	100	Based on degradation analysis
Failure time of tank (yr)	500	Based on degradation analysis
Geometry of underlying sand	Cylindrical	Based on tank geometry
Radius of underlying sand (cm)	762	Based on tank geometry
Dispersion coefficient (cm)	1.2	Reasonable value
Thickness of grouted heel (m)	0.30	Reasonable value
Transport distance in tank (m)	0.15	One-half total thickness
Thickness of sand pad (m)	0.15	Reasonable value
Transport distance in sand pad (m)	0.075	One-half total thickness
Thickness of vault floor (m)	0.76	Average value
Boundary condition top	No flux	Reasonable condition
Boundary condition bottom	Zero concentration	Reasonable condition
Initial time interval (yr)	1.0	Reasonable step
Fractional change in time interval (yr)	0.001	Reasonable step
Time step maximum (yr)	1000.0	Reasonable step
Number of time steps	10,000	Reasonable value
Maximum simulation time (yr)	1.0E+06	Value computing peaks
Darcy velocity (cm/s)	4.0E–07	Based on vadose zone flow modeling
Grouted tank moisture content (by volume)	0.242	Average based on vadose zone modeling
Sand pad moisture content (by volume)	0.05	Average based on vadose zone modeling
Vault concrete moisture content (by volume)	0.282	Average based on vadose zone modeling
Grout density (g/cm^3)	2.12	Reasonable value
Sand pad density (g/cm^3)	1.75	Reasonable value
Concrete vault density (g/cm^3)	2.12	Reasonable value
Location of release rate output	Bottom of vault	Source location for vadose and saturated zone modeling

Table 3-6. Non-decay chain DUST-MS input parameters.

Nuclide	Half-life (yr)	K_d Sand Pad (m^3/kg)	K_d Grout/Concrete (m^3/kg)
^{14}C	5.73E+03	5.00E–03	5.00E+00
^{90}Sr	2.86E+01	1.50E–02	3.00E–03
^{99}Tc	2.13E+05	1.00E–04	2.50E+00

calculate release rates from the tank and the sand pad.

To verify DUST-MS release rates, results from PORFLOW simulations for selected radionuclides were compared to DUST-MS results. Release rates, computed with DUST-MS using Table 3-5 input parameters and with PORFLOW yielded similar predictions and justified the use of the DUST-MS computer code with these input parameters to estimate release rates from the grout tank and the sand pad. These results are discussed in Appendix F. In addition, Section 7 presents the sensitivity/uncertainty analysis for the analyses.

3.3.2 Groundwater Flow and Transport Modeling

A two-dimensional unsaturated/saturated PORFLOW model was used to simulate water and contaminant transport in the subsurface at the INTEC facility (see Figure 3-15). By using a two-dimensional model, it was possible to digitize the problem domain using a detailed 250 × 103 node grid. This approach allowed a detailed approximation of the complex geology underlying the facility as discussed in Section 3.3.2.2.1 at reasonable computational speeds. The two-dimension problem domain represented a vertical slice in a north-south direction beginning at the Big Lost River, through the center of two tank vaults, and southward in the downgradient direction for a total distance of 2500 m (8,200 ft). The top of the model is located at land surface and extends to a depth of 200 m (700 ft)—well below the top of the water table located at 134 to 139 m (440. to 456 ft) bgs. A variable grid was used with a high density of nodes in the tank vault area where complex construction and highly variable hydraulic conductivities for the various materials exist. By default, the unit thickness of the two-dimensional model in an east-west direction is 1 m (3 ft).

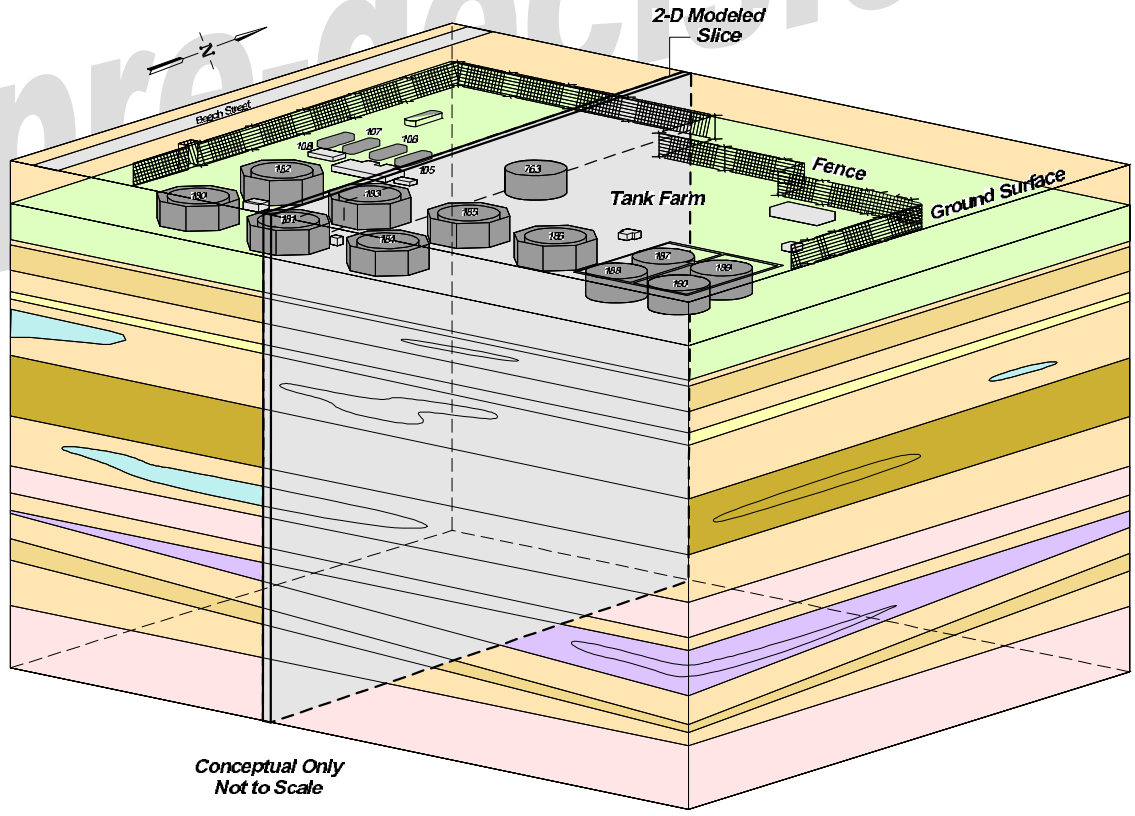

Figure 3-15. Illustration of the two-dimensional modeling slice used in PORFLOW.

For the top of the model, a constant flux boundary was set at the infiltration rate based on precipitation in the area. For simulations where seepage from the Big Lost River is incorporated, two nodes located in the uppermost northern edge of the model at the location of the Big Lost River were injected with water. The injection rate is equal to the average seepage lost per meter of river, based on historical gaging data presented in Bennett (1990). The seepage loss rate is consistent with the unit thickness (1 m [3 ft]) of the model.

The base of the model is set as a no flow boundary. This is based on the assumption of horizontal flow in the regional aquifer and nonexistent future pumping of the aquifer for water supply.

The sides of the model are set as mixed boundaries. In the unsaturated zone, the boundaries are set as no flow. The boundaries in the unsaturated zone are located at sufficient distances so as to not impact movement of water from the tank vault area. Constant head boundary conditions are used in the saturated portion of the model based on the regional potentiometric map at the location of the boundary.

Initial conditions are discussed in detail in Section 3.3.2.4 since different modeling simulations used different initial conditions. For the first simulation, initial conditions for steady-state runs of the base-case model assumed unsaturated conditions except in the regional aquifer, recharge rate equal to precipitation, no Big Lost seepage, and no perched water zones.

For contaminant transport simulations, the initial contaminant concentrations in the model domain and the boundaries are set equal to zero. Consequently, all predicted contaminant concentrations in the model domain are the result of releases from the Tank Farm vaults and associated piping. This is a reasonable assumption for the unsaturated zone considering that the presence of existing contamination, particularly for future estimates, is minimal in the region based on existing sampling data.

For the source area releases, the conceptual model of the tank vault included initial hydraulic conductivity values that represented the materials of the vaults including grout, concrete, and steel. At selected time periods, based on degradation studies presented in Section 3.1.2, the hydraulic conductivities were changed to the degraded values. Contaminants were released as a result of the higher hydraulic conductivity values for the tank vault materials.

Because of the large contrast in hydraulic conductivity values for the tank vaults compared with the surrounding geologic material, it was necessary to use small time steps during the simulations to minimize computational errors. This resulted in extensive run times for the model simulations. To reduce run times because of the numerous simulations for both the transport predictions and the subsequent uncertainty analysis, the model DUST-MS, as detailed in Section 3.3.1, was used to compute release rates of radionuclides out of the TFF vault. As discussed in Section 3.3.1.4, a comparative analysis between DUST-MS and PORFLOW was conducted. The DUST-MS and PORFLOW transport simulation results compared favorably.

For contaminant transport simulations, the calibrated unsaturated and saturated flow model was used to set the transport velocity vector field. All transport simulations were conducted under steady-state conditions. It was assumed that the percolation ponds had been taken out of service and the resulting percolation was no longer a factor in the transport of water in the subsurface. Only steady infiltration from precipitation and seepage from the Big Lost River, at rates discussed in the following sections, were incorporated into the water transport model.

As noted earlier, DUST-MS was used to predict the release rates from the various waste forms. Radionuclide releases coincided with degradation rates of the waste forms discussed in Section 3.1.2.2. Release rates calculated by DUST-MS were incorporated as input in PORFLOW, with the initial radionuclide releases beginning at the time of degradation. For example, the outer vault began to release radionuclides after 100 yr and the tanks/piping after 500 yr. These assumptions are conservative, based on the best estimates provided from the degradation analysis.

Because of the small region of the two tanks simulated in the 2-D model compared with the large model domain, releases from only one tank were simulated. Radionuclide concentrations downgradient were subsequently doubled to incorporate releases from both tanks. Earlier simulations conducted using releases from both tanks yielded similar results.

For initial conditions, the radionuclide concentrations were set equal to zero. All model boundaries also were set with initial radionuclide concentrations of zero. Contaminants were released from nodes that coincided with the location of the piping, sand pad, vaults, and tanks. Transport simulations were conducted for a time period of 1,000 yr.

An important component of the conceptual model for the transport of contaminants is the relationship of dispersion in the two-dimensional model. Since the model uses a unit thickness of 1 m, there is no lateral dispersion of contaminants beyond this thickness. It is assumed that contaminants disperse or diffuse out of the lateral boundary at the same rate as contaminants move into the unit thickness of the model domain. Essentially, all dispersion of contaminants occurs in the longitudinal direction, with zero transverse dispersion. This is a conservative approach to predicting downgradient contaminant concentrations.

Since the model domain is located in the center of the tanks, the highest contaminant concentrations are located in the source area of the model. Although it is assumed that the same amount of contaminants disperse in a transverse direction out of, as into the model domain, in reality there would be the same loss of contaminants, albeit small, in the transverse direction. Consequently, downgradient contaminant concentrations will be slightly higher for the two-dimensional simulation compared to a fully three-dimensional simulation.

Radionuclide concentrations were observed downgradient in the regional aquifer at the location where the highest concentrations occur. During unsaturated flow simulations, it was observed that the perched water zones deflected the contamination. Consequently, the usual 100-m downgradient location was inappropriate to quantify the maximum impacts of radionuclide releases from the tanks and vaults. Based on the radionuclide concentrations distribution, the maximum observed concentrations occur approximately 600 m downgradient from the tanks.

3.3.2.1 Numerical Model Selection. The PORFLOW code (Runchal 1997; ACRi 2000) was selected to perform the proposed fluid and contaminant transport simulations for the TFF PA. PORFLOW was selected based on the following criteria:

- Application to the multiphase contaminant transport problem at INTEC
- Model validation
- A history of applications similar to the model simulations to be performed at INTEC facilities.

PORFLOW is a comprehensive mathematical model used for the simulation of multi-phase fluid flow, heat transfer, and mass transport processes in variably saturated porous and fractured media. The code can simulate transient or steady-state problems in one, two, or three dimensions using either Cartesian or cylindrical geometry**.** The geologic medium may be anisotropic and heterogeneous and may contain distinct embedded elements such as discrete fractures or boreholes within a porous matrix. In partially saturated zones, liquids and gases are assumed to co-exist. The degree of saturation of each phase is determined at each grid node as part of the solution. The dependent variable, or its change from the current state, approximates the flux terms. Finally, several options are provided for the incorporation of sources or sinks of fluid, heat, or mass. Fluid injection or withdrawal, sources or sinks of heat, or chemical species may occur anywhere in the interior of the domain of interests. For chemical species, the sources can be limited by their inventory, solubility, or both.

PORFLOW numerically solves a variable set of equations for general transport, multi-phase

pressure, temperature, and one or more chemical species. The method of nodal point integration is used to integrate the governing differential equations by temporal and spatial discretization over each control volume (element) of the physical domain. It leads to solutions that automatically conserve fluid, heat, and mass locally within every grid element, as well as for the entire flow domain. The storage terms are approximated by a modified Newton-Raphson method (Runchal 1997).

The PORFLOW code is particularly well suited for simulating the transport of fluid and contaminants from the Tank Farm waste forms, through the underlying unsaturated zone, and into the regional aquifer. PORFLOW can be used to simulate the release of contaminants from the waste form and the subsequent transport through the underlying geological media. Because of the number of simulations conducted for the numerous radionuclides discussed in Section 4, time restraints required the use of DUST-MS for computing the release of radionuclides from the waste forms. PORFLOW was designed especially for problems of fluid and mass transport in geologic media.

Several features of PORFLOW are especially important regarding the proposed modeling simulations for the INTEC area. First, data exist for the waste inventory and solubility of the contaminants that will be used as part of the PA. This information can be input to PORFLOW to estimate the contaminant source emanating from the Tank Farm waste forms. These sources terms are automatically input into the underlying unsaturated zone, transported to the regional aquifer based on hydraulic and retardation characteristics of the unsaturated zone, and then transported by the regional aquifer. PORFLOW can simulate transport under partially or completely saturated conditions. Second, the geologic media underlying the facility consists of fractured basalts and unconsolidated porous media. PORFLOW incorporates the planar geologic features, such as fractures or faults, with different length scales and properties to distinguish these features from the parent geologic media. This feature will be useful for simulating flow in the fractured basalt instead of assuming a representative hydraulic conductivity for the entire basalt matrix. Finally, PORFLOW can calculate contaminant flux values at any location in the problem domain. This feature allows the user to assess the flux of contaminants from the waste forms, the amount of contaminants that are being held in the unsaturated zones, and the flux of contaminants entering the regional aquifer.

PORFLOW can simulate the decay of a radionuclide and up to three daughters in a conservative manner. Using the law of radioactive disintegration and the half-life input by the user, PORFLOW computes the remaining concentrations of the parent radionuclides and the subsequent increase and/or decrease in the daughters' concentrations. The code maintains a mass balance of the initial radionuclide and the subsequent concentrations of the parent and daughters at selected time intervals.

PORFLOW has been extensively peer-reviewed (Runchal 1997). INEEL, Battelle Pacific Northwest, and Professor R. Allan Freeze of the University of British Columbia have formally reviewed PORFLOW and its derivatives. Additionally, it has been reviewed by ANDRA (France), Bae-SEMA (United Kingdom), British Petroleum (United Kingdom), Exxon Production Research, Failure Analysis Associates Inc., Fluor Daniels Inc., Gaz de France (France), SAIC, Shell Oil, SOHIO, and Westinghouse Hanford Company. Over 100 publications and project reports on the benchmarking, verification, and applications of PORFLOW are currently available.

PORFLOW has a history of use specific to the PA presented in this report. The code was successfully used for the Radiological *Performance Assessment for the Z-Area Saltstone Facility* and E-Area at the Savannah River Site (Westinghouse Savannah River Company 1992). This use of PORFLOW is very similar to the proposed application at the INEEL Site. PORFLOW also was used at RWMC at the INEEL, near the INTEC area (Maheras et al. 1994).

In summary, PORFLOW is a robust simulation code that has a direct application to the multi-phase contaminant transport problem at INTEC. The code has been extensively validated

by independent researchers and has been used to model similar hydrogeologic systems at other DOE facilities.

3.3.2.2 General Modeling Assumptions.

Based on a review of the available technical information for INTEC and the surrounding sites at the INEEL, three general conclusions can be drawn regarding the ability to accurately simulate hydrologic conditions underlying INTEC and subsequent predictive estimates relative to the necessary assumptions. The first conclusion is that there is a large amount of data available from previous investigations. These data provide important information about the stratigraphy and hydrologic parameters that control the subsurface movement of water and contaminants. Conversely, the second conclusion, based on a thorough review of the available technical data, is that there is a large degree of uncertainty regarding this information. The uncertainty is due to conflicting information from the available technical references, such as large ranges in the values of certain hydraulic parameters, conflicting lithologies, and the selection of appropriate technical data that results in a bias relative to the hydrologic properties representing certain subsurface conditions. The final conclusion is that there is a significant lack of important technical data necessary to reduce the uncertainty of model simulations for existing hydrologic conditions and future predictions. The uncertainties associated with the available technical data and the lack of important data will be discussed in detail in the following sections.

These three conclusions required certain assumptions to provide a reasonable model of present and future hydrologic conditions at INTEC. Once again, these assumptions will be discussed in detail in the following sections. In general terms, however, the following rules were used as guidelines for selecting the assumptions inherent in the model simulation performed as part of this PA. First, where appropriate, existing hydrologic data were used extensively to describe subsurface hydraulic conditions. For example, the distribution of basalt units and interbeds closely followed the geologic cross sections presented in several USGS reports (Anderson 1991; Anderson and Bartholomay 1995; Anderson, Ackerman, and Liszewski 1996; Anderson, Liszewski, and Cecil 1997; Anderson, Kuntz, and Davis 1999). Second, because of the conflicting nature of the data from several references, attempts were made to confirm the data used in the model from different sources. For example, if the drilling logs indicate that a selected interbed consists of both fine and coarse grain sediments, separate hydraulic information such as the hydraulic conductivity or unsaturated hydraulic characteristic was evaluated to confirm the lithologic information. Finally, if there is no available information to confirm lithologic or hydraulic data, then a conservative approach was adapted that resulted in using the value that yielded the highest transport rates. For example, if the only available information for a particular geologic unit is a range in hydraulic conductivity values, then the upper portion of the range is used in the model.

3.3.2.2.1 Subsurface Geology Assumptions—

As noted in the geology section, the geology underlying INTEC consists of a series of basalt flows and sedimentary interbeds with an alluvial veneer. There are over 30 individual geologic units that compose the unsaturated zone and upper regional aquifer at the site. Previous modeling programs at the INEEL (Thomas 1988; Maheras et al. 1997; Rodriguez et al. 1997) simplified the subsurface geology to perform three-dimensional modeling. It was assumed for this PA that a two-dimensional model can be used to simulate the movement of water and contaminants in the subsurface. The advantage of the two-dimensional model is that greater detail is possible for defining the subsurface features.

The PA model is based on a USGS cross section of the subsurface geology at INTEC presented by Anderson (1991) and shown in Figure 2-12. This detailed geologic cross section shows the alluvium, 18 basalt flows, and nine continuous and discontinuous sedimentary interbeds. With the exception of basalt flows E through I, which form the upper regional aquifer and were combined into a single hydrologic unit, all of the remaining geologic units are represented as individual units within the problem domain.

The USGS cross section runs north-south across INTEC and is aligned to parallel the

regional groundwater flow direction. Hydraulic properties are based on the lithologic descriptions and published values and are assigned to the individual units in accordance with their locations.

3.3.2.2.2 Infiltration Assumptions—

A fundamental assumption for simulating the perched groundwater zones discussed in the subsequent section is that the amount of infiltrating water, either from precipitation, the Big Lost River, or human activities, is based on reasonable values from the site literature. Surface sources are set at a maximum reasonable value regardless of the resultant formation of perched zones. The controlling factor for the development of perched groundwater zones will be the vertical permeability contrasts in subsurface units that result in perched water.

3.3.2.2.3 Perched Groundwater Assumptions—

The mechanisms surrounding the hydrologic and hydraulic factors that control the perched water zones underlying INTEC are not well understood and remain controversial. The source of water causing the perched zones and the subsurface units responsible for restricting the downward movement of infiltrating water are not fully understood. Further, it is not known if perched water zones existed before site activities began. Finally, there is disagreement on the subsurface units responsible for restricting the downward movement of infiltrating water. Most scientific studies state that fine-grain interbeds form the base of the perched water zones. Conversely, the interbeds and highly fractured basalts adjacent to the interbed zones commonly are the highest permeable regions in basalt flows. Cecil et al. (1991) state that lithologic features contributing to the contrasts in the vertical hydraulic conductivity of basalt layers and sedimentary interbeds in the unsaturated zone provide the mechanisms for the development of perched groundwater zones.

Perched water at TRA, INTEC, and RWMC can be attributed to at least four lithologic features. First, the vertical hydraulic conductivity of a sedimentary interbed might be smaller than that of an overlying basalt flow. Second, alterations in the baked zone between two flows can contribute to reduced vertical hydraulic conductivity. Third, dense, unfractured basalt may inhibit unsaturated groundwater movement, contributing to the formation of perched groundwater zones. Fourth, sedimentary and chemical filling of fractures near the upper contact of a basalt flow reduces the vertical hydraulic conductivity. Selecting which of these mechanisms is responsible for the observed perched zones is an important assumption in the model simulation.

The assumptions involving the perched zones are perhaps the most important in developing and interpreting the numerical model. They control the amount of water input into the system as well as the hydraulic characteristics of the underlying formation. All model results should be viewed in light of these initial assumptions.

For the initial phase of the model, it is assumed that there are no perched water zones due solely to infiltrating water from precipitation. This assumption is supported by age-dating studies using ^{36}Cl ratios conducted by Cecil et al. (1992). The pore water from soil cores was extracted and analyzed for ^{36}Cl. ^{36}Cl was produced during nuclear weapons tests conducted over the oceans from 1952 to 1958. In the subsequent 40 yr, infiltrating water from precipitation containing the higher concentrations of ^{36}Cl has only penetrated to a depth of 1.3 m (4.3 ft). Based on this evidence, it appears unlikely that precipitation is a significant source of recharge for the perched groundwater underlying the site.

The best estimate of the subsurface stratigraphy, hydraulic parameters, and volume of infiltrating water from the various sources initially was coded into the model. Subsurface stratigraphy and the volume of infiltrating water remained constant during the model simulations. For subsequent simulations involving seepage losses from the Big Lost River and the percolation ponds, it was assumed that the development of perched water zones was due to variations in the vertical hydraulic conductivity of selected subsurface units. Consequently, the development of perched zones and the thickness and aerial extent of perched water are determined by (a) comparing the model results with the existing hydrologic information and (b) adjusting the vertical permeability of the appropriate subsurface unit

with measured perched water to match model predictions with actual conditions.

Based on the lithologic features presented by Cecil et al. (1991) and discussed in detail in Section 2.1.5.4, sedimentary interbeds in the unsaturated zone exhibit lower permeability and restrict the movement of infiltrating water. Selection of the appropriate interbeds for reduced permeability and subsequent formation of perched water zones was based on the known location of perched water at the site in relation to the individual interbeds and the limited amount of lithologic and hydraulic information available. For example, 12 soil borings in the C-D interbed reported fine-grain material as the dominant lithology for this unit. Hydraulic data indicated high residual moisture content indicative of fine-grain material. And, finally, wells completed at a similar depth as the C-D interbed reported perched water. Consequently, this unit was assigned a lower permeability consistent with the lithology that was sufficient to form perched water zones.

A similar approach was taken with assigning permeability values for the other sedimentary interbeds. For the lower perched zones, there was a limited amount of lithologic and hydraulic information available. Therefore, the location of perched water zones, as defined by the available monitoring wells, was the primary factor for determining the vertical permeability.

3.3.2.2.4 Hydraulic Transport Parameter Estimations—Transport parameter estimations involve the hydrodynamic dispersion and molecular diffusion terms in the transport equation. Both terms can have a significant effect, particularly in the unsaturated zone where flux rates may be low but pore water velocities may be significant. Relatively high dispersion and diffusion terms can result in significant transport and spreading of contaminants that may or may not be representative of actual contaminant transport conditions.

The one-dimensional form of the advective-dispersive equation for nonreactive dissolved containment under steady-state conditions is

$$D_l \frac{\partial^2 C}{\partial l^2} - v_l \frac{\partial C}{\partial l} = \frac{\partial C}{\partial t} \qquad (3\text{-}12)$$

where

D_l = coefficient of hydrodynamic dispersion in the longitudinal direction

C = solute concentration

l = curvilinear coordinate direction

v_l = average linear velocity.

The coefficient of hydrodynamic dispersion can be expressed in terms of two components:

$$D_l = \alpha_l v + D^* \qquad (3\text{-}13)$$

where

α_l = dynamic dispersion or dispersivity

v = velocity

D^* = coefficient of molecular diffusion for the solute in a porous medium (Freeze and Cherry 1979).

The hydrodynamic dispersion is dependent on the pore water velocity as illustrated in Equation (3-13). In the unsaturated zone, low moisture contents can result in a low effective porosity, resulting in a relatively high pore-water velocity. When these high pore-water velocities are multiplied by the dispersivity, the net result can yield unrealistically high transport rates in the unsaturated zone.

Previous modeling studies at the site set the dispersivity values to zero to yield a conservative estimate of the maximum concentrations of contaminants (Maheras et al. 1994). This approach was based on the limited availability of data on unsaturated water movement and virtually no data on dispersivity values in the unsaturated zone.

In evaluating the best estimate of dispersivity values for the unsaturated zone modeling, several factors were incorporated into the analysis. The

transport scale is on the order of 130 m for transport through the unsaturated zone to the underlying water table. There are 20 separate zones that are assigned a specific hydraulic conductivity value that differs from the adjacent zones. The variations in hydraulic conductivity inherently impart dispersion on the transport of solutes. The scale of transport in the individual geologic units or zones is on the order of a few to tens of meters. As shown by Mills et al. (1985), the scale of the transport distances for the individual stratigraphic units results in a range of longitudinal dispersivity of 0.01 to 1.0 m. The results of an extensive review of the literature for measured dispersivity values in porous and fractured material are presented in Section 7. The range in measured dispersivity values is significantly less than the calculated site values for the Snake River Plain Aquifer. In addition, the measurement scale for the literature values is closer to the scale of transport for the individual geologic units in the unsaturated zone underlying the site.

Longitudinal dispersivity values of 0.29 m for sediments and 1.85 m for basalts were assigned for transport simulations. Transverse dispersivities were set at one half the value of the longitudinal dispersivity. This approach minimizes the amount of dispersion in the unsaturated zone resulting in conservative estimates of radionuclide concentrations but allows the contaminant plumes to spread during transport.

3.3.2.3 Numerical Model Description and Parameterization

3.3.2.3.1 Alluvium—The upper alluvial unit is consistently identified as a coarse-grain unit consisting of predominantly sand and gravel. Lithologic logs from CPP-2 and CPP-3, along with the PW series wells (PW-1 through PW-6; Figure 3-19) and numerous USGS wells, all show the coarse-grain nature of the alluvium. Consequently, the hydraulic parameters in the model are set to reflect the nature of the coarse-grain deposits. Unfortunately, there is little technical data available for the hydraulic properties because of the unsaturated nature of the alluvium. The average hydraulic conductivity for the alluvial sediments, as reported by Thomas (1988), indicates a relatively low value of 0.16 m/d (0.52 ft/d). Based on the lithologic logs, this value appears to be low. Therefore, adapting a conservative approach, the hydraulic conductivity value for the alluvium was increased to 80 m/d (300 ft/d), a value consistent with the lithologic descriptions as described by Freeze and Cherry (1979).

Total and effective porosities for the alluvium are based on values presented by Magnuson (1995). The moisture characteristic curve, adapted from a publication by Blumb, Murphy, and Everett (1992), represents coarse-grain sediment similar to the alluvium. Low residual moisture contents reported in the RI/FS also were used to select the representative curve (Rodriguez et al. 1997). The curve for the unsaturated hydraulic conductivity as a function of moisture content was developed using the methodology presented by Van Genuchten (1978).

3.3.2.3.2 Basalts—Hydraulic data for the basalts in the unsaturated zone are very limited at the site. This is due in part to the lack of field testing of hydraulic properties in the unsaturated basalt. Conventional test methods such as pumping or slug tests are not applicable for unsaturated basalts. This lack of data is further exacerbated by the difficulty in predicting the unsaturated hydraulic parameters, such as moisture characteristic curves and unsaturated hydraulic conductivity, as a function of moisture contents in a fractured medium.

Because of these problems, it is necessary to estimate the hydraulic properties indirectly based on a number of limiting assumptions. Hydraulic conductivities in the basalts are directly related to the size and distribution of fractures with the individual flow units. Characterizing these basalt fractures using conventional drilling techniques is difficult at best. Consequently, recent research has focused on the characteristics of the basalt flows as a general guide to predicting the magnitude of the hydraulic conductivity. Comparing the range and frequency distribution of hydraulic conductivity, Anderson, Kuntz, and Davis (1999) found that three main rock types at the INEEL affect the magnitude of the hydraulic conductivity. These rock types are (1) thin, tube-fed pahoehoe

flows, (2) thick, tube-fed pahoehoe flows, and (3) near-vent volcanic deposits consisting of shelly pahoehoe and slab pahoehoe flows and bedded scoria, splatter, and ash. The hydraulic conductivity of thin, tube-fed pahoehoe flows ranges from 2.4E–02 to 7E+03 m/d (7.9E–02 to 2.3E+04 ft/d) compared with 3E–03 to 1.5E+03 m/d (1E–02 to 4.9E+03 ft/d) for the thick, tube-fed pahoehoe flows. The higher hydraulic conductivity range for the thin flows is due to voids associated with the contacts, rubble zones, and cooling fractures of thin, tube-fed flow that are more predominant in the thinner flows. The thick, greater-than-10 m (30 ft), tube-fed flows are characterized by fewer contacts, fewer rubble zones, and less extensive cooling fractures. Where they have ponded in topographic depressions, these units are so massive that their hydraulic conductivity values may be extremely low. Near-vent volcanic deposits represent only about 10 to 20% of most lava fields, and thick, ponded, tube-fed flows are rare. Hydraulic conductivity values associated with near-vent deposits are similar to those of the more permeable thin, tube-fed pahoehoe flows.

Anderson (1991) provides a detailed discussion of the characteristics of the individual basalt units underlying INTEC. These characteristics include the number of flows that compose a basalt unit, the thickness of the basalt units, and the probable source vent for the individual flows. Using this lithological information as a guide, the basalt units were divided into broad categories: basalt units comprising thin flows and units comprising thick flows. Basalt units comprising thick flows are initially assigned a hydraulic conductivity value of 10 m/d (30 ft/d). These values were modified for the perched groundwater simulations, as discussed in subsequent sections. This thicker-flow basalt includes the flow groups BC, DE3, DE3-4, DE4, DE5, and I. The remaining basalt units comprising thin flows are assigned a hydraulic conductivity value of 1,000 m/d (3,000 ft/d). Both hydraulic conductivity values assigned to the basalt units are not the highest values but represent the upper range of values reported.

Although there is a large range of hydraulic conductivity values reported for the individual units, the *RI/FS for INTEC* (Rodriguez et al. 1997) reports a range in hydraulic conductivity for the BC group (a thick basalt flow) of 0.4 to 2.1 m/d (1 to 6.9 ft/d). Conversely, the CPP-02 and CPP-DISP well tests indicate hydraulic conductivity values for 1,000 to 823 m/d (3,000 to 2,700 ft/d) for DE3, believed to consist of thin-flow units. The noted exception to this generalized approach was for thick-flow Basalt Group I that had several hydraulic tests conducted and yielded a higher hydraulic conductivity value of 170 m/d (560 ft/d).

3.3.2.3.3 Sedimentary Interbeds—

Sedimentary interbeds exhibit a wide range of lithologic and hydraulic characteristics, both within the same interbed unit and between individual units. Hydraulic conductivity values for individual units can range as high as four or five orders of magnitude. Further, there are often inconsistencies between reported lithologies and hydraulic conductivities for the respective units. In addition, there is a lack of detailed information for several of the interbed units—especially the deeper units. Consequently, several basic assumptions were implemented in selecting the hydraulic properties based on drilling logs, hydraulic tests, and moisture contents.

The first step in determining the appropriate hydraulic parameters for an individual unit is a review of the lithologic descriptions from the drilling logs. These descriptions can range from clay to gravel for the same interbed unit. Therefore, several logs were evaluated and the dominant lithology type was identified. Lithologies were then compared with available hydraulic testing data from laboratory core testing and field hydraulic testing. Commonly, the field tests incorporated both the sedimentary interbed and the surrounding basalt, resulting in an average value for the two geologic units. Next, available moisture content data were compared with the lithologic and hydraulic data to select the most representative unsaturated hydraulic parameters. It was assumed that the limited number of available in-situ moisture measurements were representative of the residual moisture content. (Higher moisture contents are often associated with finer-grained sediments as a result of higher capillary forces.) Finally, based on the best determination of the

lithologic properties and residual moisture contents, moisture characteristic curves were selected from the available literature that represented the type of material comprising the individual interbed.

Based on this approach, the C-CD and D-DE2 interbeds were assigned relatively low vertical permeability values of 0.005 and 0.0025 m/d (0.02 and 0.0082 ft/d), respectively. Assigning low permeable values to these units is important because the permeability will control the movement of infiltrating water in the subsurface, restricting the downward movement of water, and forming a perched water zone. The lower permeability values for these upper sedimentary interbeds are supported by existing perched water at these depths in both the northern and southern portion of the INTEC area.

The other sedimentary units assigned a low permeability value were interbeds DE4 and DE4-DE5. These units are discontinuous across the site but together can restrict the downward movement of infiltrating water across the entire site. Both units are thin and located within massive basalt flows. By lowering their permeabilities, the effects of restricting infiltration and forming perched water bodies is consistent with the factors resulting in perched water as outlined by Cecil et al. (1991). As discussed earlier, whether the low vertical permeability is a result of a sedimentary interbed or alterations in the baked zone between two flows that can contribute to reduced vertical hydraulic conductivity, the net result is the same.

The remaining interbeds were assigned hydraulic characteristics for coarser-grained sediments such as sands and gravels. Based on the modeling simulations and the resulting formation of perched water, these hydraulic values may be modified to reflect actual conditions.

3.3.2.4 Model Development. An incremental modeling process was used to assess the impacts of key input parameters on the resulting numerical simulations. This process involved a base-case simulation in which the only source input is the infiltration from precipitation. Once a mass balance was achieved, a second simulation was conducted, inputting the losses caused by infiltration from the Big Lost Creek. Results were evaluated to check the mass balance and the validity of the initial assumptions outlined in the previous sections. Upon completion of the second simulation, the base model was assumed to be complete and represented hydrologic conditions before human impact at the site. Subsequent modeling used this flow base case as a starting point for the simulation of human impacts, such as seepage from percolation ponds and the simulation of contaminant migration in the subsurface. Based on the modeling results and assumptions, hydraulic parameters, such as hydraulic conductivity, were modified in the subsequent modeling simulations. These changes are noted in the following discussions.

3.3.2.4.1 Flow Base-Case Model Infiltration Simulations—The first modeling simulation involved the implementation of a two-dimensional model as shown in Figure 3-16. A detailed cross section based on the work of Anderson (1991) was discretized to include the major basalt flow units, sedimentary interbeds, and surface alluvium. Using the existing technical literature and the assumptions outlined in the previous section, the best available hydraulic parameters were incorporated in the model. This approach allowed an evaluation of the existing technical data to test the relevance of the assumption that no perched water was present in the subsurface due solely to precipitation.

Results the base-case model simulation show that surface infiltration dominates flow in the unsaturated zones. Downward movement of water at a flux rate comparable to the infiltration rate was observed in the unsaturated zone. Movement was dominantly vertical in the unsaturated zone at a rate and direction consistent with infiltration conditions. Saturated zone simulations will be modified in later simulations.

Moisture contents in the unsaturated portion of the problem domain yielded values that were consistent with the moisture characteristic curves for the individual units. All of the moisture content values input to the PORFLOW code represented the residual moisture contents (Θ_r) for the moisture characteristic curves of the individual hydrologic units. These results are consistent with

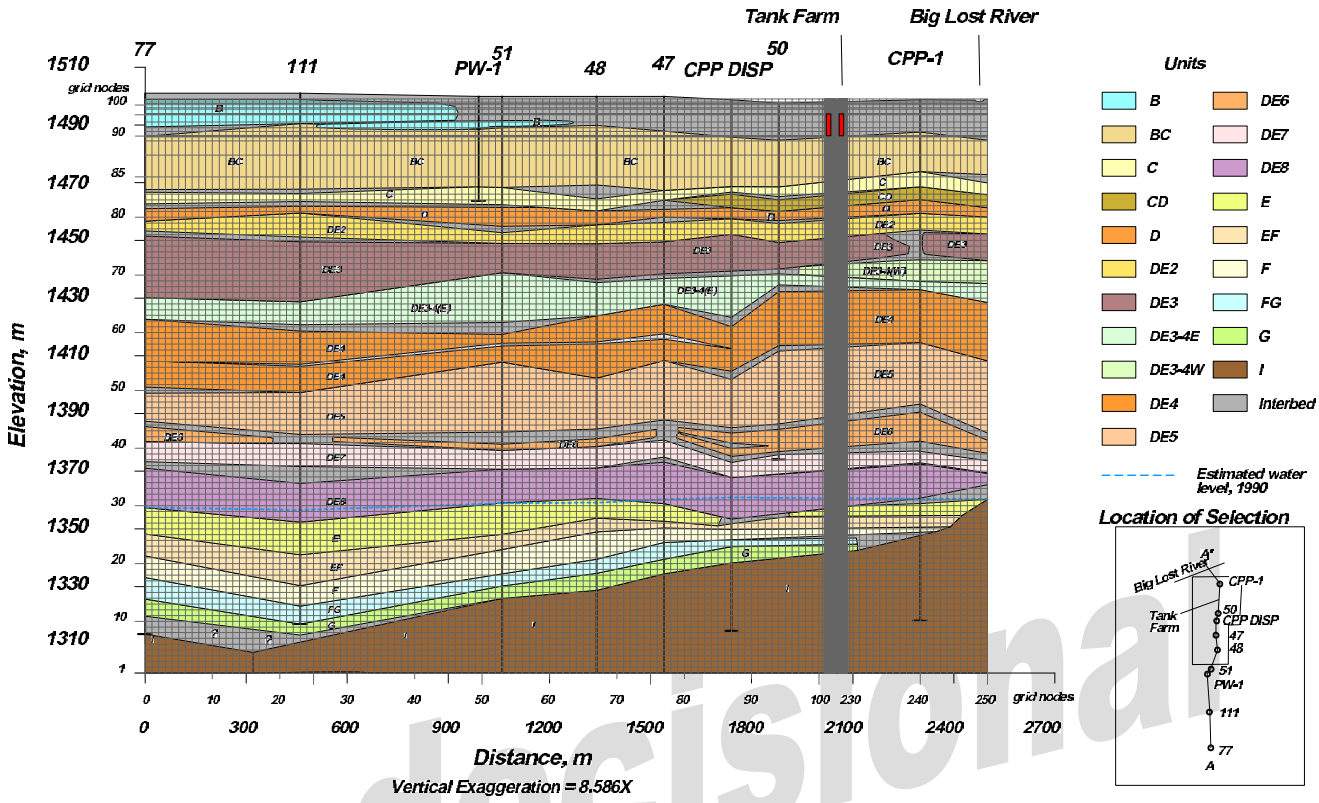

Figure 3-16. Model grid superimposed on geologic cross section for groundwater model.

the initial unsaturated hydraulic parameters input into the model indicating that the unsaturated hydraulic conductivity at Θ_r is sufficient to transport precipitation through the unsaturated zone without developing a significant increase in moisture conditions. More importantly, no perched water zones developed, which is consistent with the initial assumptions.

Water balances for the initial simulation were consistent with the amount of precipitation entering the upper boundary of the model, plus the upgradient groundwater inflow equaling the downgradient groundwater discharge.

3.3.2.4.2 Base-Case Model Simulations of Big Lost River Losses—

The next modeling simulation involved inputting water into the model to simulate seepage losses from the Big Lost River. Seepage losses from the Big Lost River occur sporadically over time as a result of periodic flows in the river channel. These flows are dependent on precipitation, releases from upstream dams, and irrigation diversions. For modeling purposes, it was assumed to be a constant source, based on seepage records for the site. This approach is consistent with earlier modeling simulations presented in the RI/FS report (Rodriguez et al. 1997).

The amount of water that seeps into the ground from the Big Lost River near INTEC was based on estimates provided by Bennett (1990). Using stream flow data from gaging stations located at Lincoln Blvd. (Site 9) and the playas site (Site 14) for the period of 1965 through 1987, Bennett reports average seepage losses of 82,000 to 210,000 m^3/d (2,000 to 5,100 acre-ft/mo). Dividing the seepage losses by the distance between the two gaging stations, 30.1 km (18.7 mi) yields an effective seepage rate of 2.72 and 6.98 m^3/d. For conservative purposes, the higher seepage value was used in the simulation.

Results of the simulation, using the additional water input from the Big Lost River seepage, show the development of several perched zones directly below the river and extending southward into the

INTEC area, as illustrated in Figure 3-17. The upper perched zone is formed by the combination of C-D, D-DE2, and DE2-DE3 interbeds acting as the restricting layer. This upper perched zone is consistent with the shallow perched water found at several locations across the INTEC site. The extent of the alluvial perched zone is controlled by the permeability of the restricting layer. It is reasonable to decrease the vertical permeability of these interbeds within hydraulic conductivity values consistent with the lithology to increase the southern extent of the alluvial perched zone. This issue will be addressed during subsequent simulations when water from man-made sources is introduced into the system. However, the model predictions suggest that the source of water in the northern INTEC facility could be solely from seepage losses along the Big Lost River.

There are three lower perched layers that form as the result of interbeds DE3-DE4, DE4-DE5, and DE6. Unfortunately, due to the lack of monitoring wells, there is little available information to confirm these perched zones. One exception is Well USGS-50, which is an open borehole from 109 to 123 m (358 to 404 ft) bgs. Based on the well completion interval, it is possible that the lower perched zones emanating from the Big Lost River seepage could be responsible for the groundwater observed at Well USGS-50. Once again, it is reasonable to decrease the vertical permeability of the restricting interbeds and increase the southern extent of these lower perched zones to intersect Well USGS-50.

This modeling supports the case that the Big Lost River is at least a partial source of groundwater for the northern INTEC area. Furthermore, results suggest that perched water existed, at least on a limited aerial extent, in the INTEC area before human influences. The issue of modifying subsurface permeability units to extend the perched zones will be determined in subsequent modeling simulations after evaluating the results of inputting man-made sources of water.

3.3.2.4.3 Percolation Ponds—The next step in the modeling process is to evaluate the impact of the percolation ponds on the underlying perched zones. These ponds have been in service since 1984, receiving service water from INTEC operations. According to the RI/FS, approximately 96% of all water recharging the perched water bodies from man-made sources is a result of seepage from the percolation ponds (Rodriguez et al. 1997). The percolation ponds are unlined ponds that were excavated into the surface alluvium. The two ponds have been used alternatively, receiving an approximate average volume of 5.85E+03 m3/d (1.54E+06 gal/d).

There appears to be a discrepancy in the amount of water recharged to the perched zones

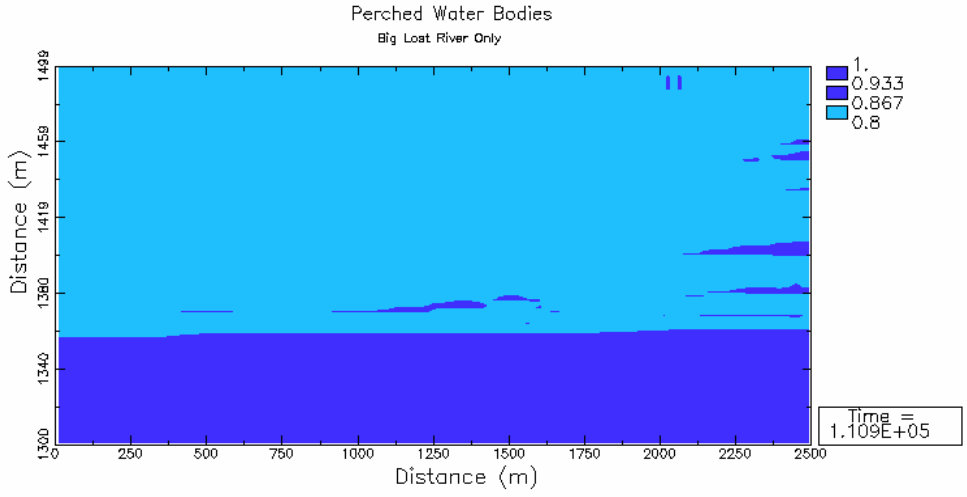

Figure 3-17. Model prediction of the hydrologic conditions illustrating the perched water zones resulting from the Big Lost River seepage.

from the percolation ponds according to the RI/FS. This document reports a recharge value because of seepage from the percolation ponds of 7.16E+03 m^3/d (1.89E+06 gal/d), compared with the estimated average volume discharged to the ponds of 5.85E+03 m^3/d (1.55E+06 gal/d). The higher seepage number cannot be confirmed; however, the amount of water discharged to the percolation ponds reported in the RI/FS is confirmed in a separate report by Cecil et al. (1991).

The seepage volume from the percolation ponds does not account for any evaporative losses from the ponds. The RI/FS reports an annual pan evaporation rate of 109 cm/yr (42.9 in./yr) for the area. This pan evaporation rate is supported by regional data presented by Dunne and Leopold (1978). Using this pan evaporation value and assuming that only one pond is used at a time, the resulting losses due to evaporation are 5.75 m^3/d (1,520 gal/d). This evaporation loss amounts to less than 1% of the seepage volume and, therefore, is not considered significant.

The model consists of a 1-m wide vertical cross section in a north-south direction through the west pond. For input into the model, the total amount of discharge to the ponds was divided by two to incorporate the discharge to the individual ponds and then multiplied by the ratio of the area of the pond area intersected by the model by the total area of the west pond. As a result, only water lying directly above the model in the region of the pond was input into the model. Water was injected into the boundary nodes along the top of the model in the area of the pond at a total rate equal to the percolation rate calculated above.

To determine the size and location of the perched zones, the subsurface lithology is compared to the existing well information used to select where the permeability should decrease in selected subsurface units to form a restricting layer. One well that provides a detailed picture of subsurface perched zones is Well USGS-51. Detailed neutron logging of this well, as presented by Cecil et al. (1991), shows three perched zones located beneath the percolation ponds. The base of the upper perched zone is located at a depth of 32 m (10E+02 ft). This zone coincides with the C-D and C-CD interbeds. The base of the middle perched zone is located at a depth of 54 m (180 ft) and coincides with the DE2-DE3 interbed. The base of the lower perched zone is located at a depth of 102 m (335 ft) and roughly approximates the DE6 and DE7-DE8 interbeds. Consequently, the vertical permeability of these interbeds was decreased to the lower end of the reported range for the simulations conducted in this model simulation.

Modeling results presented in Figure 3-18 show the development of several additional perched zones, plus the enhancement of existing perched zones predicted by the previous Big Lost River simulation. A large upper perched zone directly below the percolation ponds is evident because of the C-D and D-DE2 interbeds. Other perched zones have developed on the DE2-DE3 and DE4 interbeds. In addition, the existing perched zones developed by seepage from the Big Lost River show an increase in thickness and extent because of the additional water provided by the percolation ponds. The lower perched zones exhibit a larger degree of variability because of the lithology. These perched zones are formed by interbeds DE6 and DE7-DE8 that are stratigraphically located at different depths. This difference in depths results in a confining layer that ranges from 106.8 to 126.7 m (350.4 to 415.7 ft) bgs, yielding a lower perched zone that changes with depth across the site. The lower perched zone is discontinuous but extends across the majority of the site.

3.3.2.5 Model Calibration. There are only a limited number of wells completed in the unsaturated zone at the site. Compounding the lack of wells is the numerous perched zones possible at the site. Consequently, a combined approach was used for calibrating the model. This approach initially relied on an accurate and detailed definition of the hydrostratigraphy, incorporation of the best available hydraulic information, and the input of accurate sources of water to the model as previously discussed. Finally, two simulations, the first with the Big Lost River seepage and then a combined simulation with both the Big Lost River and the southern percolation ponds, were compared with the existing well information for calibration purposes.

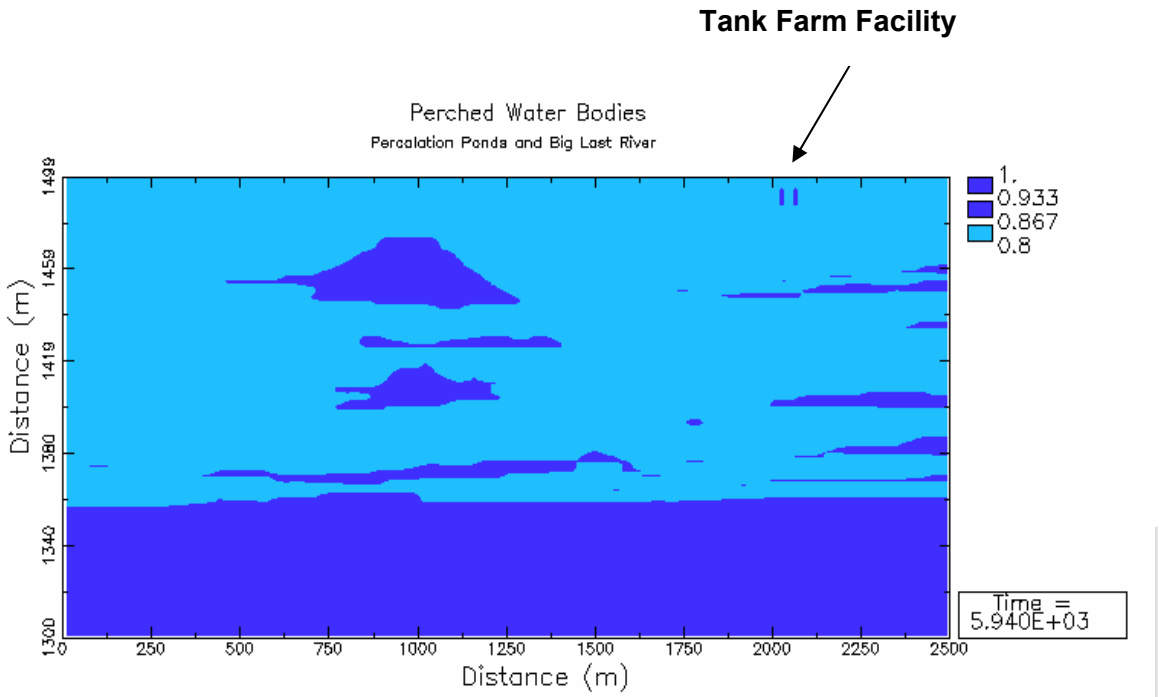

Figure 3-18. Model prediction of the hydrologic conditions illustrating the perched water zones resulting from the Big Lost River and percolation ponds seepage.

The remaining portion of this section discusses the assumption, available data, and calibration of the unsaturated portion of the model.

Figure 3-17 shows the moisture distribution resulting from Big Lost River seepage. There are several perched zones that develop as a result of water from the Big Lost River. An upper perched zone that forms as a result of the lower permeability values assigned to C-D, D-DE2, and the DE2-DE3 interbeds extends approximately 250 m (820 ft) southward across the INTEC facility. The extent of perched water in the upper unsaturated zone is in general agreement with the *Hydrologic and Geochemical Assessment* (INEL 1983), which states that seepage from the Big Lost River may extend laterally outward from 30 to 500 m (100 to 2,000 ft) from the river. In addition to the upper perched zone, there is a discontinuous lower perched zone that forms as a result of the lower permeability values assigned to the DE3(4)-DE4, DE4, DE4-DE5, and DE6 interbeds. Although these interbeds were assigned similar permeability values, their distribution, extent, and thickness (as defined by the geologic cross section) results in varied distributions and thicknesses of the perched water zones. For several of these lower perched zones, there are no monitoring wells to confirm or deny their existence.

Figure 3-18 illustrates the distribution of perched zones resulting from both seepage from the Big Lost River and the percolation ponds at the south end of the INTEC facility. The number, extent, and thickness of perched zones increase significantly because of additional water seepage from the percolation ponds. This is expected because of the large volume of water associated with the percolation ponds compared with the Big Lost River. A large perched zone is located directly beneath the percolation pond because of the low permeability of the interbed units C-D and D-DE2. In addition, a smaller perched zone developed below this large perched zone because of the lower permeability associated with the DE2-DE3 interbed. The increased extent of the upper perched zones resulting from Big Lost River

seepage reflects the increase in soil moisture because of the percolation pond seepage. Finally, the lower perched zones initially established by Big Lost River seepage also increase in thickness and extent because of the additional percolation pond seepage.

To calibrate the development of perched groundwater zones caused by seepage from the Big Lost River and the percolation ponds, Table 3-7 lists the available monitoring wells, including surface elevations, well depths, screen intervals, and water level elevations.

The bulk of the monitoring wells are located in the upper portion of the unsaturated zone, with only four wells available to define the lower perched zones. In addition to the well data, the lithologic and neutron log of Well USGS-51 from Cecil et al. (1991) is presented in Figure 2-23. This well log shows the presence of several perched zones that can be used to calibrate the perched zone below the percolation ponds.

The following subsections compare the available well information and geophysical data to calibrate the upper and lower perched zones predicted by the numerical simulations. All well locations discussed in the following sections are shown in Figure 3-19. Monitoring wells presented in Table 3-7 are designated in general as ICPP-MON-P--#. These wells also are referenced to as MW wells at the INEEL. The nomenclature in the following discussions are designated as MW, which can be directly referenced to the ICPP-MON-P well number designations in Table 3-7 and Figure 3-19.

3.3.2.5.1 Upper Perched Zones—For the purpose of this report, the upper perched zones are defined as saturated water zones above, and including, the DE2-DE3 interbed. Figure 3-18 illustrates a vertical cross section of the site showing relative moisture contents resulting from the Big Lost River and percolation ponds seepage. The model predicts two upper perched zones. The northern perched zone is a thin, perched water body that results from the Big Lost River seepage. This perched water body extends approximately 700 m (2,000 ft) from the edge of the Big Lost River. Compared with the modeling result for seepage solely from the Big Lost River as shown in Figure 3-17, this perched zone extends another 450 m (1,500 ft) because of the additional water in the unsaturated zone provided by seepage from the percolation ponds. The other upper perched zone is a thick saturated body that results from percolation pond seepage. As noted in previous sections, there is a substantial quantity of water available for seepage from the percolation ponds based on estimates presented in the RI/FS report (Rodriguez et al. 1997).

Figure 3-19 compares the extent of the upper perched zones with the existing monitoring well network. Note that this map differs from the previous definition of the upper perched water presented in Figure 2-21. For purposes of model calibration, it was determined that the vertical hydraulic conductivity of the D-DE2 interbed provided the controlling influence on the extent and thickness of the upper perched zone. Available lithologic and hydraulic data indicate that this interbed exhibits the lowest vertical hydraulic conductivity values for the upper perched zone. Interbeds C-D and DE2-DE3 also are important for restricting infiltration and forming perched water zones. However, based on the water level information presented in Table 3-7, the base of the upper perched zone coincides with the depth and location of the D-DE2 interbed.

Changes of 0.001 m/d (0.04 in./d) in the vertical hydraulic conductivity of the D-DE2 interbed results in changes of hundreds of meters in the lateral extent of the northern upper perched zone. Consequently, for calibration purposes, the vertical hydraulic conductivity of this interbed was adjusted until the lateral extent of the northern perched zone matched the extent predicted by the monitoring wells. In addition, water levels for both the upper perched zones also were compared with the predicted head values. For the extent of the northern perched zone, it was assumed that the southern edge is located between Wells MW-02, -04, -05, and -18 (wells showing perched water) and Wells MW-08 and-11 (wells reported to be dry).

Table 3-7. Perched water wells at INTEC.

Well No.	Other Well Designation	Surface Elevation (m)	Well Depth (m bgs)	Screen Interval (m amsl)	Average Water Level Elevation (m)	Range in Water Level Elevation (m)
CPP-33-1 (5 cm)		1498.15	30.2	1468.0–1471.0		Dry–1468.4
CPP-33-2 (5 cm)		1497.85	32.3	1465.6–1471.7	1468.2	1467.3–1468.0
CPP-33-3 (5 cm)		1498.00	37.2	1460.8–1463.9	1462.7	
CPP-33-4 (5 cm)	CPP-33-4E	1497.14	36.0	1461.1–1467.2	1466.7	
CPP-37-4					1465.8	
CPP-55-06 (5 cm)		1497.33	34.4	1462.8–1468.9	1465.0	1465.2
MW-1 (2.5 cm)	ICPP-MON-P-001	1498.55	120.4	1386.1–1389.1		Dry
MW-1 (10 cm)		1498.55	120.4	1396.1–1399.2	1402.1	1400.6–1402.42
MW-2	ICPP-MON-P-002	1497.5	38.7	1463.4–1466.4	1464.9	1465.9
MW-3 (2.5 cm)	ICPP-MON-P-003	1498.4	46.1	1462.4–1462.9		Dry
MW-3 (5 cm)		1498.4	46.1	1456.3–1459.4		Dry–1456.5
MW-4 (2.5 cm)	ICPP-MON-P-004	1497.0	39.9	1457.5–1458.0		1457.9
MW-4 (5 cm)		1497.0	39.9	1463.3–1466.3	1464.9	1465.2
MW-5	ICPP-MON-P-005	1498.5	43.0	1460.0–1466.1	1464.9	1463.6
MW-6	ICPP-MON-P-006	1498.5	49.1	1456.8–1462.9	1461.8	1461.9
MW-7 (2.5 cm)	ICPP-MON-P-007	1498.8	53.9	1467.1–1467.6		Dry
MW-7 (5 cm)		1498.8	53.9	1455.5–1458.6	1456.6	1442.4(?)–1456.9
MW-8	ICPP-MON-P-008	1497.1	43.0	1459.0–1462.0		Dry–1459.4
MW-9 (2.5 cm)	ICPP-MON-P-009	1499.5	48.2	1467.3–1467.7		Dry
MW-9 (5 cm)		1499.5	48.2	1459.9–1462.9	1460.3	Dry
MW-10 (2.5 cm)	ICPP-MON-P-010	1498.0	55.2	1474.2–1474.7		Dry–1474.6
MW-10 (5 cm)		1498.0	55.2	1452.0–1455.0	1453.9	1453.9
MW-11 (2.5 cm)	ICPP-MON-P-011	1498.1	45.9	1463.5–1463.9		Dry
MW-11 (5 cm)		1498.1	45.9	1456.6–1458.1	1457.9	Dry
MW-12 (2.5 cm)	ICPP-MON-P-012	1497.5	46.6	1451.7–1452.2		Blocked
MW-12 (5 cm)		1497.5	46.6	1461.2–1464.3		Dry
MW-13	ICPP-MON-P-013	1499.6	39.0	1467.6–1469.1		Dry
MW-14	ICPP-MON-P-014	1499.3	42.1	1467.6–1470.7		Dry–1467.3(?)
MW-15	ICPP-MON-P-015	1499.2	43.6	1459.3–1465.4	1461.9	1462.9
MW-16	ICPP-MON-P-016	1499.3	38.4	1466.7–1469.8		Dry
MW-17 (2.5 cm)	ICPP-MON-P-017	1499.1	116.1	1415.6–1418.7		Dry
MW-17 (5 cm)		1499.1	116.1	1440.7–1443.7	1441.0	1441.89
MW-17 (10 cm)		1499.1	116.1	1383.0–1389.4	1388.1	1388.91
MW-18 (2.5 cm)	ICPP-MON-P-018	1497.8	150.6	1371.6–1377.7	1373.7	Dry
MW-18 (5 cm)		1497.8	150.6	1460.1–1463.2		Dry
MW-18 (10 cm)		1497.8	150.6	1351.2–1358.0	1356.7	1357.3–1357.7
MW-19	ICPP-MON-P-019					
MW-20 (2.5 cm)	ICPP-MON-P-020	1498.0	46.2	1465.8–1468.8		Dry–1465.9
MW-20 (5 cm)		1498.0	46.2	1452.8–1457.5	1457.3	1457.3
PW-1		1498.85	36.3	1462.6–1468.4	1474.9	1476.4–1478.3
PW-2		1498.70	39.9	1458.8–1464.9	1461.8	1461.5–1461.2
PW-3		1498.55	37.5	1461.1–1467.1	1462.4	1462.6
PW-4		1498.03	45.7	1452.3–1464.5	1475.2	1472.1–1472.8
PW-5		1500.80	39.3	1461.5–1467.6	1477.7	1476.4–1478.0
PW-6		1499.74	38.1	1461.6–1467.7	1462.4	1462.8–1463.6
USGS-50		1498.7	123.4	1375.3–1389.9	1378.0	Dry–1378.0

Sources: INEL 1993; Rodriguez et al. 1997; DOE-ID 1994.

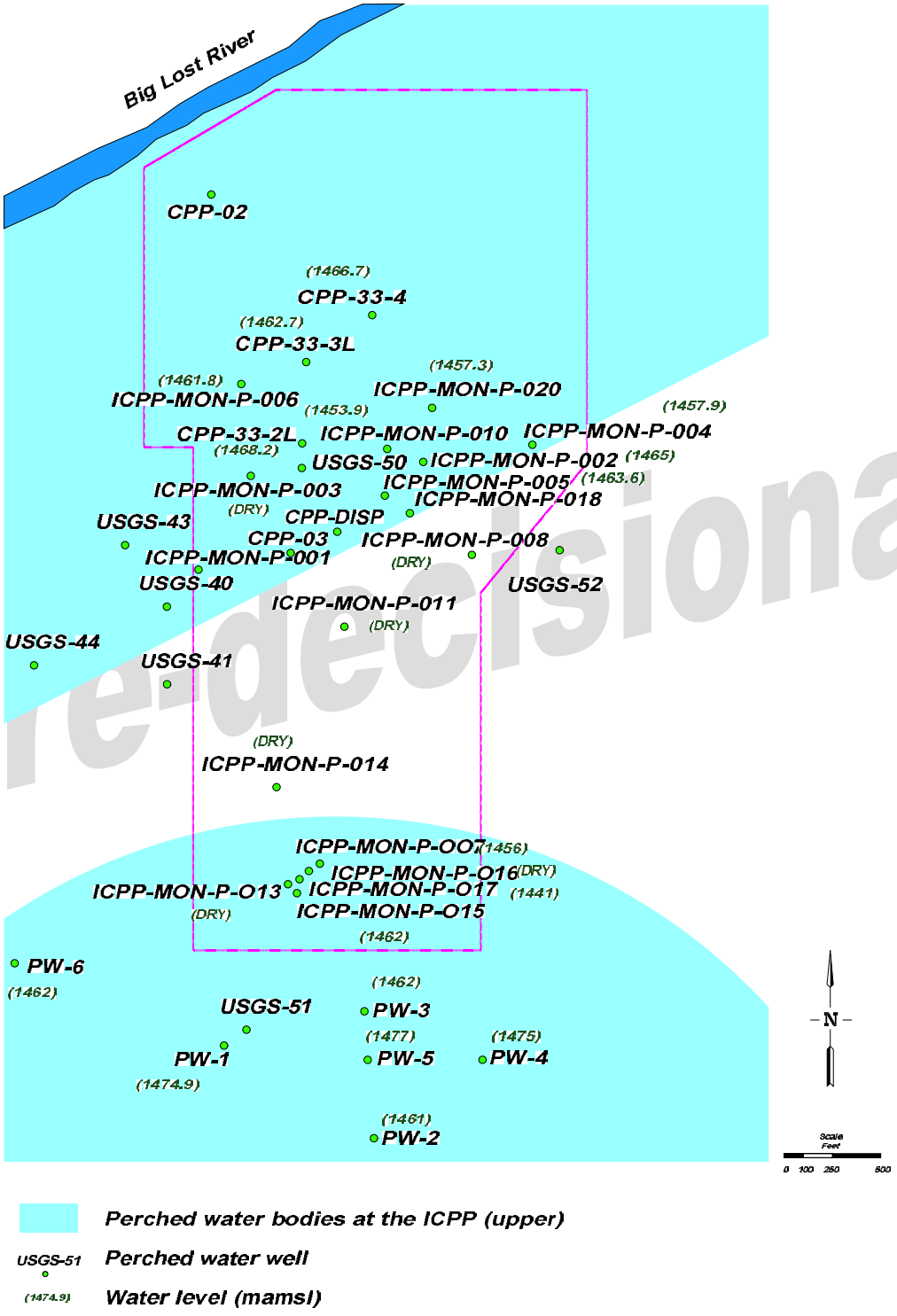

Figure 3-19. The extent of upper perched water at the INTEC facility based on perched water well data in Table 3-7.

As shown in Figure 3-19, the extent of the perched zone resulting from the Big Lost River seepage is approximately 670 m (2,200 ft). The southern extent of the Big Lost River perched unit is located between Wells MW-02, -04, -05, and -18 and Wells MW-08 and -11—consistent with the calibration requirements discussed in the previous paragraph. Since the volume of water required to form a perched water zone from other possible sources has not been clearly defined in previous investigations, it appears more likely that the assumption of the Big Lost River as the source of the upper northern perched zones is valid. For example, the RI/FS for the site reports that the seepage from the sewage lagoon is only 2.1% of the estimated volume of water recharging the perched water bodies at the INTEC site. This compares with 95.8% for the percolation ponds. Water system leaks that could possibly provide water to the previously defined perched zone in Well MW-18 are only 0.6%. In comparison, reported infiltration from precipitation accounted for only 1.1% of the estimated volume of water recharging the perched zones and previous model simulations showed that no perched water zones developed at the site due solely to precipitation.

The elevation of the upper perched water emanating from the Big Lost River is predicted by the numerical simulation ranges from approximately 1,460 m (4,790 ft) amsl to approximately 1,450 m (4,760 ft) amsl in the southern portion of this perched unit. Table 3-7 shows water-level elevations in the northern portion of this perched unit are as high as 1,468 m (4,817 ft) amsl and as low 1,453 m (4,767 ft) amsl in the southern portion of the perched unit. Because the monitoring wells used for calibration purposes are screened at various depths and the model predicts generally lower water-level elevations as the perched unit moves southward, there is a reasonable agreement between the model prediction and the actual site data for the upper perched zone emanating from the Big Lost River.

The upper perched zone resulting from the percolation ponds' seepage also is shown in Figure 3-19. The model predicts that this upper perched water body is the largest perched zone at the site—consistent with the fact that the percolation ponds are the largest source of water seepage in the area. The model further predicts that water-level elevations range from 1,475 m (4,839 ft) amsl directly below the ponds, to 1,444 m (4,738 ft) at the base of the perched zone. The southern extent of this perched unit is not shown in the figure but is located 420 m (1,400 ft) south of the southern edge of the pond. For calibration purposes, the first set of wells, compared with the model prediction, is the perched water (PW)-series wells, PW-1 through PW-6, (Figure 3-19). These wells show water-level elevations that range from 1,462 to 1,478 m (4,797 to 4,849 ft) amsl. Most of the PW-series wells are located adjacent to the ponds, where the steep decline in water levels is evident in the model simulation. The observed water levels in these adjacent PW-series wells are comparable to the water levels based on the model prediction. The variation of the water-level data from the PW-series wells is due in part to different screen intervals measuring different hydrologic units.

The second set of wells used to evaluate the depth and extent of the upper perched zone associated with the percolation ponds includes MW-07, -13, -15, -16, and -17. The model predicts that all five wells are located within the extent of the upper perched zone. However, Wells MW-13 and MW-16 are dry, while the other three wells contain water. The explanation appears to be the location of the screen interval for these wells. The dry wells, MW-13 and MW-16, are screened above the perched water with the base of the well screens located at 1,468 and 1,467 m (4,817 and 4,813 ft) amsl, respectively. The saturated wells are screened 8 to 28 m (30 to 92 ft) lower and intersect the perched water zone, predicted by the model. This evidence is strong confirmation on the northern extent of the upper perched zone associated with the percolation ponds.

3.3.2.5.2 Lower Perched Zones—For the purpose of this report, the lower perched zones are defined as those located below the DE2-DE3 interbed. Figure 3-18 illustrates the location of perched groundwater zones based on the results of the unsaturated flow model. The lower perched zones are discontinuous and controlled by the discontinuous low-permeable interbed units. Water sources for these lower perched zones

include seepage losses from the Big Lost River and the percolation ponds.

There are only a few wells completed in the deeper perched zones at the site that can be used to evaluate the accuracy of the model predictions. Monitoring Wells MW-1 (10-cm inside diameter), MW-17 (10-cm inside diameter), MW-18 (2.5-cm inside diameter), and USGS-50 are completed in the lower perched aquifer and showed water-level elevations that ranged from 1,356.7 to 1,441.0 m (4,451.3 to 4,727.9 ft) in 1995. This compares with the model that predicts a range of water-level elevation for the lower perched zone of approximately 1,367 to 1,436 m (4,485 to 4,712 ft). This is a favorable comparison between actual and predicted water levels considering the large degree of variability in both the location of the deep perched zone and the reported water-level data. However, there are several lower perched zones that have no wells screened at their location or depth. Consequently, it is not possible to calibrate the existence of these lower perched zones. The existence of several lower perched zones relies on the accuracy of the geologic cross section used as a basis of the model and the relative permeability values based on limited lithologic data.

Comparing individual water-level data for the limited number of monitoring wells with the predicted water-level elevations based on model predictions yields a reasonable agreement. Monitoring Well MW-01 (10 cm) has a water-level elevation of approximately 1,402 m (4,600. ft) amsl. The model results show a perched zone resulting from the low-permeable DE4-DE5 interbed extending southward from the Big Lost River. The water-level elevation predicted by the model is approximately 1,400 m (4,600 ft)—only a 2-m (7-ft) difference than the water level in MW-01. Well MW-17 (10 cm) has a water-level elevation of 1,388 m (4,554 ft) amsl, compared with the model that shows a water-level elevation of 1,381 m (4,531 ft) for the perched zone resting upon the DE6 interbed. Well MW-18 (2.5 and 10 cm) has water-level elevations of 1,374 and 1,357 m (4,508 and 4,452 ft) amsl, respectively. The model predicts several small scattered perched zones at the location that approximate the reported data. Since the MW-18 wells have previously reported dry conditions, the scattered thin perched zones are consistent with the limited amount of perched water in this area.

Well USGS-50 has a water-level elevation of 1,378 m (4,521 ft) amsl, compared with 1,380 m (4,530 ft) for the perched zone controlled by the DE-6 interbed—a difference of only 2 m (7 ft). Well USGS-50 is located at the southern edge of this DE-6 perched zone, perhaps explaining why this well has occasionally been observed to be dry.

A second source of important data for the calibration of the lower perched zones is the detailed geophysics conducted on Well USGS-51 (Figure 2-23). This well was repeatedly logged in 1984, 1985, and 1986, showing the development of several perched zones with depth. The lowest perched zone associated with the DE6 interbed as predicted by the model is not evident in the geophysical logs from Well USGS-51. The next lowest perched zone, from 83 to 102 m (270 to 335 ft) bgs, coincides with the DE4 perched zone predicted by the model that shows saturated conditions from approximately 83 to 101 m (270 to 331 ft) bgs. Well USGS-51 intersects the DE2-DE3 interbed perched zone at the thinnest saturated portion, and therefore is not evident in the geophysical log for the well. The other two perched zones identified in the geophysical log correspond to the upper perched zone associated with the percolation ponds.

The final source of data for the calibration of the lower perched zones is information presented in the RI/FS report (Rodriguez et al. 1997), which lists perched zones for several USGS wells. This information is reproduced in Table 3-8. There is concern regarding this information because the majority of the USGS wells listed in the table are completed in the underlying regional aquifer. It is hard to conceive water levels above the regional aquifer, considering the substantially higher transmissivities exhibited by the regional aquifer. There is information provided, however, that the reported water levels occurred during the drilling of the wells.

USGS Wells-40, -41, -43, and -44 have water levels from 1,382 to 1,395 m (4,534 to 4,577 ft) amsl. Comparing the perched zones

Table 3-8. Perched layer, depth to water, and water table elevations for the wells encountering the lower perched zone (Rodriguez et al. 1997).

Well[a]	Water level (m bgs)	Year	Interbed	Interbed Depth (m)	Water Table Elevation (m amsl)
MW-1	98	1995	Unknown	Unknown	1401
MW-17	111	1995	DE8	>116	1389
MW-18	124	1995	DE8	125–129	1388
USGS-40	104	1956	DE6	112–116	1395
USGS-41	117	1956	DE8	123–131	1382
USGS-43	110	1957	DE6	112–131	1388
USGS-44	117	1957	DE8	125	1382
USGS-50	117	1995	DE8	120–123	1382
USGS-51	82	1986	DE6	117–122	1428
USGS-52	117	1960	DE8	126–130	1379

a. MW wells also are designated as ICCP-MON-P at the INEEL.

developed solely by seepage from the Big Lost River, the DE6 interbed, resulting in a perched layer, yields the highest water level of 1,381 m (4,531 ft) amsl. This comparison indicates that the DE6 perched zones associated with the Big Lost River as predicted by the model are real and supported by the available data.

In summary, there is general agreement in the location, depth, and water-level elevations between the numerically predicted perched zones and the perched zones defined by the available monitoring well network. There is uncertainty regarding the exact locations of all of the perched zones because of the limited number of wells available for calibration. The biggest difference in modeling results presented in this report and previous modeling exercises is the number and locations of sources providing water for the formation of perched zones. The approach presented in this report relies on estimates of precipitation and seepage from the Big Lost River and the percolation ponds with the adjustment of interbed hydraulic conductivity to calibrate the location and extent of the perched zones. Based on this approach, the existing distribution of perched zones can be reasonably matched.

Previous investigations relied on several sources of water for the formation of perched zones. The INTEC RI/FS used a similar approach of including water from several sources at the site. However, these additional sources provide only a few percent of the total source of water available for the formation of perched water and are not significant when compared to the total amount of water provided by precipitation, the Big Lost River, and the percolation ponds.

To reiterate, the fundamental approach used in the numerical simulation of the unsaturated zone was to rely on the USGS definition of the site hydrostratigraphy, estimates of precipitation, and Big Lost River and percolation pond seepage values confirmed by several sources from the available literature. The hydraulic conductivity of the low-permeable interbed was varied within reasonable ranges based on lithologic descriptions to predict the location and extent of the numerous perched water bodies underlying INTEC.

3.3.2.5.3 Transport Verification—

The disposal of tritium in the percolation ponds and the monitoring data from surrounding PW-series wells provide a tracer test to compare the transport of tritium predicted by the model with actual conditions. According to Cecil et al. (1991), the first percolation pond was placed into service in February 1984. It is further reported that 960 Ci of tritium was discharged to the percolation ponds

from 1984 through 1988. Orr and Cecil (1991) report a tritium disposal rate of 185 Ci/yr from 1986 to 1988. In November 1988, the PW-series wells surrounding the percolation ponds reported tritium values in the perched groundwater ranging from 5.5 to 36.7 pCi/mL (Cecil et al. 1991).

Using the Big Lost River seepage model as the flow base case, the percolation ponds simulation was run for approximately 5 yr to simulate wastewater from the percolation ponds entering the unsaturated zone. Reported tritium disposal volumes were averaged over the 5-yr run period. Results, shown in Figure 3-20, illustrate the contaminant plume in the unsaturated zone. Based on the model predictions, tritium concentrations range from 10 to 80 pCi/mL. This is higher than that reported by Cecil et al. (1991) (5.5 to 36.7 pCi/mL), yet comparable to observed results.

3.3.2.5.4 Final Flow and Transport Model—During the radionuclide transport simulations, the percolation ponds will no longer be in service. Consequently, the water transport portion of the model is based on the hydraulic values selected during the calibration of the model but without the input of the percolation ponds. The extent of the perched water is due solely to the Big Lost River seepage and precipitation. The extent of future perched water is similar to the extent shown in Figure 3-17.

It was necessary to calibrate the water transport model using the percolation ponds because the well data used in the calibration were collected during the operation of the ponds. By using the calibrated model without the percolation ponds, a realistic simulation of future subsurface conditions was obtained. The PORFLOW flow and transport input files are provided in Appendix G.

3.3.3 Radon Transport Model

This report considers the flux of radon from a grouted slab of residual waste, which has finite thickness in one spatial direction and is of infinite thickness in the other two spatial directions (i.e., a 1-dimensional model). The slab is submersed in air containing no radon. This model is conservative for the TFF LLW site for several reasons:

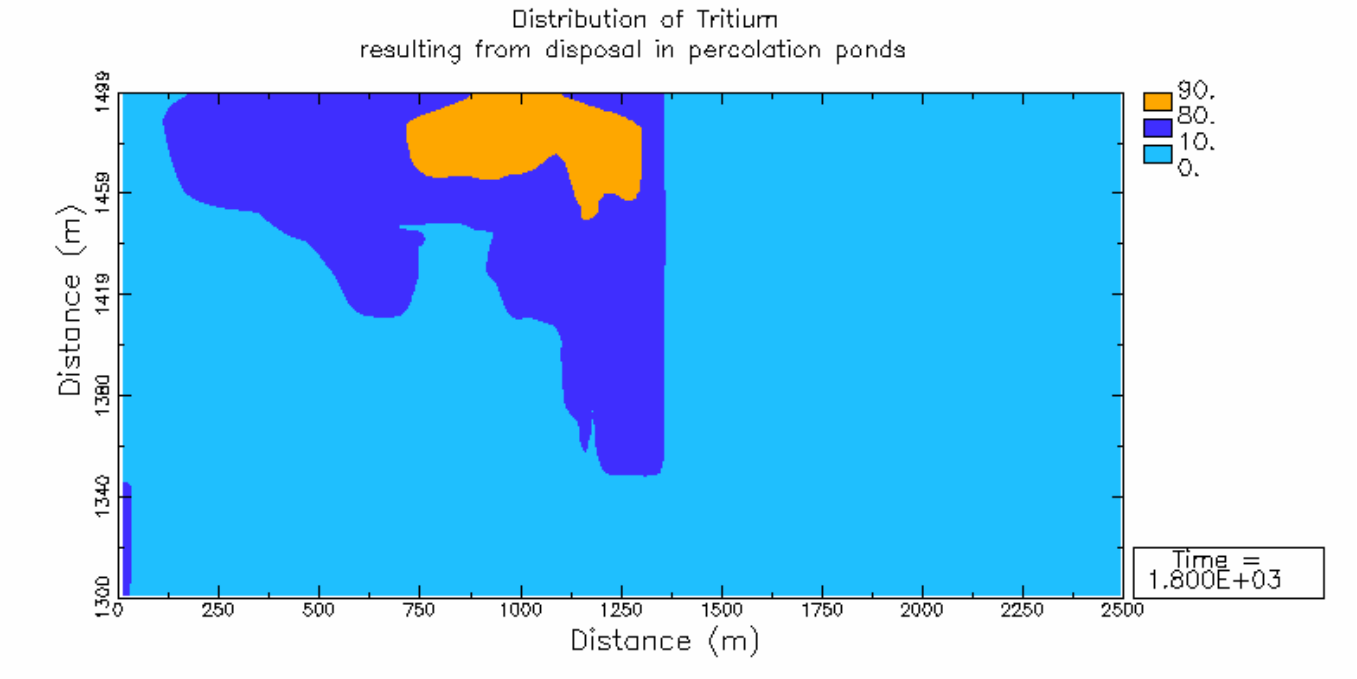

Figure 3-20. Distribution of tritium resulting from discharge into percolation ponds (units in pCi/mL).

- No credit for the tank or vault is assumed.[b] These materials provide a significant barrier for radon transport to the surface of the facility.

- Submersion of the slab in radon-free air allows for the greatest possible diffusive flux out of the slab.

This conservative model is chosen to simplify the calculations, making them more transparent and easier to understand.

3.3.3.1 The Transport Model. The model presented herein is a one-dimensional diffusion-only model for radon transport out of a grouted heel slab. Advective flow is not considered in this model because cementitious materials are too impermeable for pressure-driven flow to be a significant means of radon transport in the slab (Renken and Rosenberg 1995; Tanner 1990; Rogers and Nielson 1992). Also, since the waste is being buried at depth, it is difficult to envision a scenario where a pressure gradient across the slab could be established. Figure 3-21 shows a schematic diagram of this model.

The equation describing the diffusive transport of radon in this slab is

$$\frac{\partial C_{Rn}(x,t)}{\partial t} = D_G \nabla^2 C_{Rn}(x,t) - \lambda_{Rn} C_{Rn}(x,t) + S_{Rn} \qquad (3\text{-}14)$$

where

$C_{Rn}(x,t)$ = time and space-dependent radon concentration in the air-filled pore space in the slab (atoms/m^3)

D_G = bulk diffusion coefficient for radon in the grouted slab (m^2/s)

λ_{Rn} = radioactive decay constant for radon (s^{-1})

S_{Rn} = source of radon (atoms/m^3·s) (footnote c)

^{222}Radon (half-life of 3.82 d) is much longer-lived than either ^{220}Rn (half-life of 55.6 s) or ^{219}Rn (half-life of 3.96 s). Hence, the diffusive transport in the slab will be dominated by ^{222}Rn because of its relative abundance on an atomic fraction basis. This fact means that ^{220}Rn and ^{219}Rn can be treated as trace gases flowing in the presence of a more dominant gas. The shorter-lived isotopes would need to be present in *activity* concentrations at least three or four orders of magnitude larger than ^{222}Rn to invalidate this assumption. Inventories given in Section 2.3 do not show these trace isotopes to be present in such high quantities. Therefore, the rest of this section will consider ^{222}Rn. A later section of this chapter will demonstrate that the shorter-lived isotopes cannot penetrate even a modest barrier.

For the TFF, the steady-state solution is of interest. Hence, the time derivative is neglected and Equation (3-14) becomes

$$0 = D_G \nabla^2 C_{Rn}(x) - \lambda_{Rn} C_{Rn}(x) + S_{Rn} \qquad (3\text{-}15)$$

which has the general solution of the form

$$C_{Rn}(x) = \frac{S_{Rn}}{\lambda_{Rn}} + A_1 \exp\left(\sqrt{\lambda_{Rn}/D_G}\cdot x\right) + A_2 \exp\left(-\sqrt{\lambda_{Rn}/D_G}\cdot x\right) \qquad (3\text{-}16)$$

where A_1 and A_2 are constants that are determined by boundary conditions.

The boundary conditions for this problem are

b. This assumption is somewhat modified for the short-lived nuclides (^{220}Rn and ^{219}Rn) to show compliance. It is shown that a very moderate overburden (i.e., much less than the 10 ft of overburden currently projected) is sufficient to prevent release of these two short-lived isotopes flowing in the presence of the more dominant isotope, ^{222}Rn.

c. This term can be treated as a constant in this analysis because the radium concentration in the slab is varying much more slowly (from ingrowth and decay) than the radon concentration.

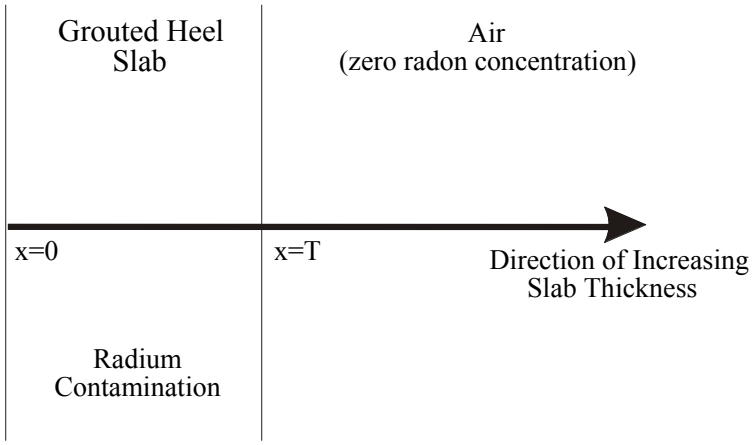

Figure 3-21. A diagram of the one-dimensional slab model.

$$\left.\frac{dC_{Rn}(x)}{dx}\right|_{x=0} = 0 \qquad (3\text{-}17)$$

$$C_{Rn}(x=T) = 0 \qquad (3\text{-}18)$$

Equation (3-17) is the condition that no flow is allowed out of the back surface of the slab, which allows for greater diffusive transport out of the front face of the slab. Equation (3-18) provides for continuity of concentration across the cement/air interface. This situation is analogous to the grouted heel setting on the ground surface in open air. Using these boundary conditions, the solution for the radon concentration is

$$C_{Rn}(x) = \frac{S_{Rn}}{\lambda_{Rn}}\left[1 - \frac{exp\left(\sqrt{\lambda_{Rn}/D_G}\cdot x\right) + exp\left(-\sqrt{\lambda_{Rn}/D_G}\cdot x\right)}{exp\left(\sqrt{\lambda_{Rn}/D_G}\cdot T\right) + exp\left(-\sqrt{\lambda_{Rn}/D_G}\cdot T\right)}\right] \qquad (3\text{-}19)$$

and the solution for the radon flux at the surface of the slab is[d]

$$J_{Rn}(x=T) = pS_{Rn}D_G\sqrt{\lambda_{Rn}/D_G}\left[\frac{\exp\left(\sqrt{\lambda_{Rn}/D_G}\cdot T\right) - \exp\left(-\sqrt{\lambda_{Rn}/D_G}\cdot T\right)}{\exp\left(\sqrt{\lambda_{Rn}/D_G}\cdot T\right) + \exp\left(-\sqrt{\lambda_{Rn}/D_G}\cdot T\right)}\right] \qquad (3\text{-}20)$$

By substituting appropriate values for the parameters in Equation (3-19), a value for the flux of radon from this slab can be evaluated.

d. The derivation of this expression is performed in Appendix H.

3.3.3.2 Appropriate Values for Radon Gas Transport Parameters. Table 3-9 lists the parameter values and the source of the information that was used for this analysis.

Substituting the transport parameter values listed in Table 3-9 along with the ^{226}Rn concentration (1.92E–04 Ci/tank; 1.73E+06 pCi/m^3) into Equation (3-20), the flux of ^{222}Rn out of the surface of the slab is 0.39 pCi/m^2/s after converting to pCi from Bq (1pCi=0.037 Bq). This value is more than an order of magnitude below the standard of 20 pCi/m^2/s given in DOE Manual 435.1-1 (DOE 2001a). The reason that such a conservative model was still able to meet the standard is that there is simply not much ^{226}Ra in the slab. Also, cement materials do not emanate or transport radon very well.

The situation for the short-lived isotopes ^{220}Rn and ^{219}Rn is not as simple as was seen previously for ^{222}Rn. This is due to the fact that these short-lived isotopes are flowing in the presence of the more long-lived, dominant isotope and are being swept along at higher diffusive velocities than would be the case if they were present alone (see Bird, Stewart, and Lightfoot 1960). Where the treatment of multiple isotopic flow is discussed herein, we assume that mass differences in the isotopes are negligible for such small distances of travel.

Table 3-9. Values of the gas transport parameters for the grouted heel along with the source of the information.

Parameter	Value	Source	Notes
Bulk diffusion coefficient for radon in grout (D_G)	4.6E–07 m^2/s	Renken and Rosenberg (1995)	Conservative upper limit for concrete
Emanation coefficient (ε)	0.3	Gadd and Borak (1995)	Conservative upper limit for concrete
Slab thickness (T)	2 ft (0.6 m)	Tank Farm Closure Study (INEEL 1999a)	Design minimum thickness of grouted heel
Decay constant for ^{226}Ra (λ_{Ra})	1.37E–11/s	Parrington et al. (1996)	
Decay constant for ^{222}Rn (λ_{Rn})	2.09E–06/s	Parrington et al. (1996)	
Porosity (p)	0.1	Gadd and Borak (1995)	

Assuming that ^{222}Rn dominates the diffusion process in the slab,[e] the steady state radon transport equation for the shorter-lived isotopes is

$$0 = D_G \frac{C_*(x)}{C_2(x)} \nabla^2 C_2(x) - \lambda_* C_*(x) + S_* \quad (3\text{-}21)$$

where the subscript 2 indicates a value for ^{222}Rn and the subscript * indicates a value for the shorter-lived isotope in question (i.e., either ^{220}Rn or ^{219}Rn). The solution for the flux of these isotopes at the surface of the slab is then given by[f]:

$$J_*(x=T) = \frac{\lambda_* S_*}{\lambda_2 S_2} J_2(x=T) \quad (3\text{-}22)$$

By substituting appropriate parameter values (i.e., half-lives [Parrington et al. 1996] and appropriate inventories for radium [Staiger and Millet 2000]) into Equation (3-22), the radon flux out of the surface of the slab can be calculated. When this substitution is made, however, the bare slab in open-air conservative calculation no longer meets the standard (by about two orders of magnitude) because the diffusive flux from ^{222}Rn is able to drive these nuclides out of the system more rapidly than would otherwise be the case. The following sections show, however, that even a modest overburden will prevent the migration of these two nuclides out of the system before they radioactively decay.

The analytical model used to demonstrate the inability of the short-lived isotopes to migrate from the system adds a diffusion barrier atop of the slab model shown previously. This model is shown pictorially in Figure 3-22.

Here, T_s is the system thickness and is the compliance point for the calculation. For simplicity and to make use of the relations derived for a bare slab, the interface condition in this model is that the flux at the interface between the slab and the overburden is identical to that determined by Equation (3-19). This is a conservative assumption because radon flows more easily out of a bare slab than out of one covered by an overburden. Also, for simplicity, the slab and overburden are assumed to have equal porosities. Again, the shorter-lived isotopes are flowing mainly in the presence of the dominant isotope, ^{222}Rn.

The steady-state transport equation for ^{222}Rn across the overburden is given as

$$0 = D_S \nabla^2 C_{2-S}(x) - \lambda_2 C_{2-S}(x) \quad (3\text{-}23)$$

e. This was shown to be a reasonable assumption in the previous section.

f. The derivation of this expression is given in Appendix H.

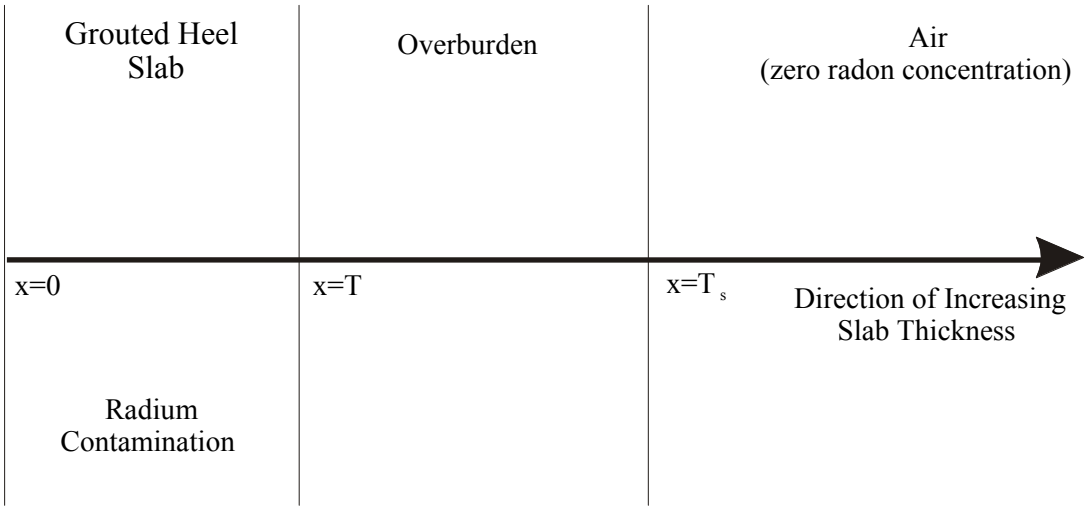

Figure 3-22. A diagram of the 1-dimensional slab model with overburden.

where

D_S = bulk diffusion coefficient for radon in the overburden (m^2/s)

$C_{2\text{-}S}$ = ^{222}Rn concentration as a function of position in overburden ($atoms/m^3$)

λ_2 = radioactive decay constant for ^{222}Rn (s^{-1}).

Here the subscript S denotes properties of the overburden (i.e., soil) and the subscript 2 denotes properties of ^{222}Rn. With the boundary conditions that the concentration of radon goes to zero at the outer boundary and the flux of radon into the overburden is given by Equation (3-20), the following equation gives the flux of ^{222}Rn out of the overburden:

$$\begin{aligned} J_{2-S}(x=T) &= J_{2-G}(x=T_s)\cdot\frac{\left[exp\left(-2\sqrt{\lambda_2/D_s}\cdot T_s\right)exp\left(\sqrt{\lambda_2/D_s}\cdot T_s\right)+exp\left(-\sqrt{\lambda_2/D_s}\cdot T_s\right)\right]}{\left[exp\left(-2\sqrt{\lambda_2/D_s}\cdot T_s\right)exp\left(\sqrt{\lambda_2/D_s}\cdot T\right)+exp\left(-\sqrt{\lambda_2/D_s}\cdot T\right)\right]} \\ &= J_{2-G}(x=T_s)\cdot\frac{2}{\left[exp\left(\sqrt{\lambda_2/D_s}\cdot(T_s-T)\right)+exp\left(-\sqrt{\lambda_2/D_s}\cdot(T_s-T)\right)\right]} \\ &= J_{2-G}(x=T_s)\cdot RF_{222} \end{aligned} \quad (3\text{-}24)$$

where

RF_{222} = reduction factor for radon due to decay while traversing the overburden.

Defining the mean migration time (t_m) as the average time it takes a radon atom to traverse the overburden, it follows that

$$RF_{222} = exp(-\lambda_2 t_m) \Rightarrow t_m = \frac{-ln(RF_{222})}{\lambda_{222}} \quad (3\text{-}25)$$

and

$$RF_* = exp\left(\frac{\lambda_*}{\lambda_{222}} ln\left(RF_{222}\right)\right) \quad (3\text{-}26)$$

Since the radioactive decay constants for ^{220}Rn and ^{219}Rn are well over three orders of magnitude larger than that of ^{222}Rn, and the natural log term is always less than zero, the reduction factor for the short-lived nuclides is vanishingly small for all but the thinnest of overburdens (i.e., where RF_{222} approaches unity). For reference, a 0.5-m-thick overburden of soil with a diffusion coefficient of 7E–06 m^2/s (the diffusion coefficient for radon in air, a conservative upper limit for radon diffusion in any medium [Rogers and Nielson 1992]) would have a reduction factor of about 10^{96}, with the reduction factor for ^{219}Rn being even smaller.

3.3.4 Volatile Radionuclide Model

The release of gaseous species of ^{3}H and ^{14}C to the air above the TFF was assumed to be controlled by gaseous diffusion in the air-filled pore space. Assuming that the concentration

gradient is constant over time, a conservative release rate, Q_i (in Ci/yr), can be estimated from a modified one-dimensional flux equation of the form

$$Q_i = D_{e,i} \times \left(\frac{C_{0,i}}{z} \right) \times A \qquad (3\text{-}27)$$

where

$D_{e,i}$ = effective diffusion coefficient of radionuclide i, in pore spaces (m^2/yr)

$C_{0,i}$ = initial air concentration of radionuclide i in the pores of the waste zone (Ci/m^3)

z = average length of diffusion path to surface (m)

A = total area of waste facility (m^2).

The expression above represents a maximum release rate because it assumes that the initial inventory is immediately available for release and that it is not significantly depleted over a year of release. Realistically, depletion from volatilization may greatly alter the concentration in the waste during a period of 1 yr.

To estimate $C_{0,i}$ for ^{3}H and ^{14}C, the chemical form of these radionuclides in the waste form must be taken into account. Tritium released to the pores of the waste form is assumed to be water vapor (i.e., tritiated water [HTO]). This assumption is conservative because the dose conversion factor for inhalation of HTO is many orders of magnitude greater than that for HT. ^{14}C is assumed to be solely associated with gaseous CO_2 in the air-filled pores.

To estimate the air concentration of HTO at the source, $C_{0,H\text{-}3}$, the concentration of ^{3}H in the pore water is assumed to equal its concentration in water vapor. The amount of water vapor, and thus HTO vapor, in the pores is a function of temperature and relative humidity. At 100% relative humidity, which can be assumed for the pores because of the presence of residual water, the concentration of water vapor, C_{v,H_2O} in g/m^3, was estimated from

$$C_{v,H_2O} = 10^3 \frac{P_v}{RT} \times MW \qquad (3\text{-}28)$$

where

10^3 = unit conversion factor (L/m^3)

P_v = vapor pressure at given temperature (atm)

R = gas constant (0.082 L-atm/ mol-^{o}K)

T = temperature (^{o}K)

MW = molecular weight of water (18 g/mol).

Equation (3-27) does not account for radioactive decay or the porosity of the overburden. The fluxes were determined for each radionuclide at the time of closure, which is conservative.

Assuming a subsurface temperature of about 283^{o}K (10^{o}C), corresponding to a vapor pressure of water of 1.2E–02 atm (9.1 mm Hg), the concentration of water vapor in the voids is approximately 9.3 g/m^3.

The waste form was assumed to have a porosity and water content equal to the values associated with the alluvium (for conservatism) to estimate the volume of water in the waste. The inventory was assumed to be diluted within this volume. Therefore, assuming a porosity of 0.24 a waste volume of approximately 27.8 m^3 (982 ft^3), and a 50-ft tank with a 6-in. heel, there is estimated to be about 6.7 m^3 (240 ft^3) of water in the waste form.

Assuming all of the ^{3}H disposed of in the TFF is initially associated with this water, an activity concentration, $C_{p,H\text{-}3}$, of 0.10 Ci/m^3 is estimated for the pore water. This value is based on the estimated, combined ^{3}H inventory at closure of 5.6E–01 Ci in the tank (Table 2-17), 2.47E–23 Ci in the sand pad (Table 2-18), and the 2.0 m^3 (71 ft^3) of water estimated in the pores. If the

concentration of ^3H in pore water is equivalent to its concentration in water vapor in the pores, the air-filled pore concentration, $C_{0,H-3}$, can be calculated from

$$C_{0,H-3} = C_{p,H-3} \times \frac{C_{v,H2O}}{\rho_w} \quad (3\text{-}29)$$

where

ρ_w = density of water (i.e., 10^6 g/m^3).

The estimated ^3H concentration in the pore gas following this procedure is 7.8E–07 Ci/m^3. The effective diffusion coefficient, D_{e,H_2O}, for H_2O through the vadose zone to the ground surface was estimated as

$$D_{e,H_2O} = D_{a,H_2O} \times 0.66 \times (\varepsilon - \theta_v) \quad (3\text{-}30)$$

where

D_{a,H_2O} = diffusivity of H_2O in air

0.66 = tortuosity coefficient

ε = total porosity (0.49)

θ_v = volumetric water content (0.073).

Equation (3-29) is the empirically-derived Penman relation (Hillel 1980) describing the relationship of effective diffusivity in soils to the unhindered diffusivity in air. The diffusion coefficient of water vapor in air is approximately 754 m^2/yr (8,120 ft^2/yr) (CRC Press 1981). Thus, the effective diffusion coefficient for water vapor in soil is approximately 208 m^2/yr (2,240 ft^2/yr).

Using a pore gas ^3H concentration of 7.8E–07 Ci/m^3 in Equation (3-22), an average diffusion path length of 3.0 m (i.e., 10 ft of cover soil), a tank area of 182 m^2 (1,960 ft^2), and a diffusion coefficient for water vapor in soil of 208 m^2/yr (2,240 ft^2/yr), the maximum release rate of HTO to the atmosphere at closure is estimated to be 9.8E–03 Ci/yr. This is an extremely conservative value because of (a) the simplified computational approach that does not account for the first-order dependence of the release rate on the pore water concentration, and (b) the assumption that HTO diffuses through the vadose zone without further exchange of ^3H with bound water in the soil. A more complicated realistic model was not warranted because the relatively short half-life of ^3H alone depletes the source sufficiently to prevent excessive doses from ^3H at the end of the institutional control. Calculations of offsite doses before cessation of institutional control are based on this conservative release rate.

To estimate the pore-water concentration of $^{14}CO_2$ at the source ($C_{p,C-14}$), a sorption coefficient of 5 m^3/kg was used to partition the ^{14}C from the waste to the pore water. The initial concentration of ^{14}C in the pore water at closure is estimated to be 1.7E–06 Ci/m^3 based on a total activity at closure of 0.49 Ci (Tables 2-17 and 2-18), a porosity of 0.24, and a total tank waste volume of 27.8 m^3 (982 ft^3).

The effective diffusivity of CO_2 in soil was estimated to be 121 m^2/yr (130E+01 ft^2/yr) based on diffusivity in the air of 440 m^2/yr (4,700 ft^2/yr). From Equation (3-27), the maximum flux of ^{14}C is estimated to be 0.012 Ci/yr, assuming a diffusion path length of 3.0 m (10 ft) of cover soil and a waste area of 182 m^2 (1,960 ft^2).

These release rates were adjusted to account for the eleven 300,000-gal tanks (i.e., they were multiplied by 11). They were then input into the CAP-88 PC model (EPA 1992) to determine doses to the general public from the atmospheric pathway.

The receptor was located 100 m (300 ft) from the TFF. The analysis used 1992 wind data from the INEEL Grid-3 meteorological station (obtained from the NOAA Office at the INEEL). Standard default values for agricultural products, based on the rural definition in CAP88-PC, were used in the analysis. The outputs from the modeling runs are provided in Appendix I.

3.3.5 Dose Model

The methodology used to calculate the all-pathways dose is based on the methodology present in reports by NRC (1977), Peterson (1983), and Maheras et al. (1997). This all-

pathways scenario assumes that a receptor receives radiation doses by consuming

- Contaminated groundwater
- Contaminated animal products (i.e., milk and beef from cattle that consume contaminated water and pasture grass irrigated with contaminated groundwater)
- Contaminated leafy vegetables and produce (i.e., all vegetation other than leafy vegetables).

Radionuclide concentrations as a function of time at the receptor well (calculated using the hydrological transport model, described previously) were used as input to these dose models. The receptor is located at the INEEL boundary during the operational and institutional control periods. During this time, the INEEL Site boundary is maintained and access by the public is not allowed. During the post-institutional control period, the member of the public is assumed to have a well located in the groundwater at the point of maximum concentration, which for analyses presented in this PA is located 600 m (2,000 ft) from the facility. Table 3-10 lists the parameters used in the all-pathways dose analysis, their distribution types and ranges, and the sources of information used to establish these ranges. These parameter distributions are used in this analysis, which is done stochastically for two reasons:

- To facilitate sensitivity analyses
- To examine the uncertainty on the final dose estimates.

The 95% confidence level will be used as the metric for comparison to the standards to "provide reasonable expectation" that the performance objective is met (DOE 2000).

For reference, Table 3-11 shows the parameter values used by Maheras et al. (1997) for a similar dose assessment at the INEEL. The values in Table 3-11 generally fall within the ranges found in Table 3-10. However, since many of the parameter distributions in Table 3-10 were from work performed for the Yucca Mountain Project (a site very similar in climate and geography to the INEEL) (LaPlante and Poor 1997), and since values from Maheras et al. (1997) were mostly national averages, some deviation is expected. The new values will be more representative of an arid environment and lifestyle.

3.3.6 The All-Pathways Dose Assessment Model

Figure 3-23 presents a block diagram of the all-pathways dose assessment model used herein, along with a listing of the input parameters to this dose model and where they reside in the calculation. The following paragraphs and equations describe the mathematical details of this model. The model is very similar to the model used by Maheras et al. (1997).

The dose from direct consumption of groundwater as drinking water was calculated as follows:

$$D_{DW} = \sum_i C_{GW-i} \times U_W \times DCF_i \times \frac{10^6\ pCi}{\mu Ci} \qquad (3\text{-}31)$$

where

D_{DW} = committed effective dose equivalent from one year's consumption of contaminated groundwater (mrem/yr)

$C_{GW\text{-}i}$ = concentration of radionuclide i in groundwater (μCi/L)

U_W = human consumption rate of water (L/yr)

DCF_i = ingestion dose conversion factor for radionuclide i (mrem/pCi).

The dose through water ingestion by beef and milk cattle assumes that cattle drink contaminated water. The receptor is then assumed to drink milk and eat meat from the cattle that drank the contaminated water. The dose from this pathway was calculated with the following equations:

Table 3-10. The input parameters and their distributions used in these analyses.

Parameter	Distribution[a]	Justification
Human Consumption Rate of Water (U_W)	Uniform on [184, 511]L/yr	Lower end is national average estimated daily intake of water-based foods and beverages (including drinking water) from Yang and Nelson (1986); upper end is national average intake of all liquid food stuffs from Yang and Nelson (1986)
Beef Cattle Consumption Rate of Water ($Q_{W\text{-}BC}$)	Uniform on [50, 60] L/d	Lower end is GENII-S default (Leigh et al. 1993); upper end is based on International Atomic Energy Agency (1994)
Milk Cattle Consumption Rate of Water ($Q_{W\text{-}MC}$)	Uniform on [60, 100] L/d	Lower end is GENII-S default (Leigh et al. 1993); upper end is based on International Atomic Energy Agency (1994)
Beef Cattle Consumption Rate of Fodder ($Q_{F\text{-}BC}$)	Uniform on [6.0, 12.0] kg/d	Lower end is based on International Atomic Energy Agency (1994); upper end is GENII-S default (Leigh et al. 1993) (Note: dry weights)
Milk Cattle Consumption Rate of Fodder ($Q_{F\text{-}MC}$)	Uniform on [11.0, 14.6] kg/d	Lower end is GENII-S default (Leigh et al. 1993); upper end is based on International Atomic Energy Agency (1994) (Note: dry weights)
Human Consumption Rate of Beef (U_B)	Normal μ=32 kg/yr σ= 0.4 kg/yr	National average from Yang and Nelson (1986)
Human Consumption Rate of Milk (U_M)	Uniform on [20, 180] L/yr	Range based on lower bound in LaPlante and Poor (1997); centroid value based on Hoffman, Gardner, and Eckerman (1982) and matches that in Yang and Nelson (1986)
Human Consumption Rate of Produce (U_P)	Normal μ=166 kg/yr σ= 40 kg/yr	Mean is from LaPlante and Poor (1997); standard deviation based on LaPlante and Poor (1997)
Human Consumption Rate of Leafy Vegetables (U_{LV})	Uniform on [4.3, 28.3] kg/yr	Based on Maheras et al. (1997) and LaPlante and Poor (1997)
Irrigation Rate (I)	Uniform on [3.5, 8.5] L/m^2/d	Lower bound is from LaPlante and Poor (1997); upper bound is from Maheras et al. (1997)
Wash-off Constant (k)	Uniform on [0.018, 0.032] L/mm	±25% from value in Maheras et al. (1997)
Leafy Vegetable Interception Fraction per Unit Yield (r/Y_{LV})	Uniform on [0.056, 0.096] m^2/kg	±25% from value in Maheras et al. (1997)
Produce Interception Fraction per Unit Yield (r/Y_P)	Uniform on [0.028, 0.048] m^2/kg	±25% from value in Maheras et al. (1997)
Fodder Interception Fraction per Unit Yield (r/Y_F)	Uniform on [1.5, 2.5] m^2/kg	±25% from value in Maheras et al. (1997)
Soil Areal Density (P)	Uniform on [180, 270] kg/m^2	From LaPlante and Poor (1997) for areal density in top 15 cm of soil; centroid value matches that used in Maheras et al. (1997)

Table 3-10. (continued).

Parameter	Distribution[a]	Justification
Irrigation Time (t_I)	Uniform on [60, 240] d	Based on LaPlante and Poor (1997) for all vegetation types; Maheras et al. (1997) used 90 days, which is in range
Buildup Time for Radionuclides in Soil (t_b)	Constant at 365 d	Conservative estimate from Maheras et al. (1997)
Irrigation Fraction of Year (f_I)	Irrigation Time/ 365 d	First principles
Leafy Vegetable Translocation Factor (T_{LV})	Constant at 1.0	Conservative estimate from default values in GENII-S (Leigh et al. 1993)
Produce Translocation Factor (T_P)	Uniform on [0.075, 0.125]	±25% from GENII-S default value (Leigh et al. 1993)
Leafy Vegetable Fraction of Activity after Processing (DF_{LV})	[0.375, 0.625]	±25% from value in Maheras et al. (1997)
Produce Fraction of Activity after Processing (DF_P)	Constant at 1.0	Conservative estimate assuming little of produce activity is on surface of vegetation (i.e., not washable)
Site Grown Factor for Vegetables and Produce (F_V)	Uniform on [0.25, 0.7]	Lower bound is estimate from intruder analysis (Section 5); upper bound is from Maheras et al. (1997)
Site Grown Factor for Beef (F_B)	Uniform on [0.25, 0.442]	Lower bound is estimate from intruder analysis (Section 5); upper bound is from Maheras et al. (1997)
Site Grown Factor for Milk (F_M)	Uniform on [0.25, 0.399]	Lower bound is estimate from intruder analysis (Section 5); upper bound is from Maheras et al. (1997)

a. μ=mean and σ=standard deviation.

Table 3-11. Parameter values used in the all pathway dose calculation in Maheras (1997).

Parameter	Value	Reference
Human Consumption Rate of Water (U_W)	258 L/yr	Yang and Nelson (1984)
Beef Cattle Consumption Rate of Water (Q_{W-BC})	50 L/d	NRC (1977)
Milk Cattle Consumption Rate of Water (Q_{W-MC})	60 L/d	NRC (1977)
Beef Cattle Consumption Rate of Fodder (Q_{F-BC})	12 kg/d	National Council on Radiation Protection and Measurement (1984)
Milk Cattle Consumption Rate of Fodder (Q_{F-MC})	16 kg/d	National Council on Radiation Protection and Measurement (1984)
Human Consumption Rate of Beef (U_B)	85 kg/yr	Rupp (1980)
Human Consumption Rate of Milk (U_M)	112 L/yr	Rupp (1980)
Human Consumption Rate of Produce (U_P)	176 kg/yr	Rupp (1980)
Human Consumption Rate of Leafy Vegetables (U_{LV})	18 kg/yr	Rupp (1980)
Irrigation Rate (I)	8.47 L/m^2/d	Maheras et al. (1997)
Wash-off Constant (k)	0.025/mm	Peterson (1983)
Leafy Vegetable Interception Fraction per Unit Yield (r/Y_{LV})	0.076 m^2/kg	Baes and Orton (1979) and Baes et al. (1984)
Produce Interception Fraction per Unit Yield (r/Y_P)	0.032 m^2/kg	Baes and Orton (1979) and Baes et al. (1984)
Fodder Interception Fraction per Unit Yield (r/Y_F)	2.0 m^2/kg	Baes and Orton (1979) and Baes et al. (1984)
Soil Areal Density (P)	225 kg/m^2	DOE (1987)
Irrigation Time (t_I)	90 d	Maheras et al. (1997)
Buildup Time for Radionuclides in Soil (t_b)	365 d	Maheras et al. (1997)
Irrigation Fraction of Year (f_I)	0.25	Maheras et al. (1997)
Leafy Vegetable Translocation Factor (T_{LV})	1.0	Ng et al. (1978)
Produce Translocation Factor (T_P)	0.1	Ng et al. (1978)
Leafy Vegetable Fraction of Activity after Processing (DF_{LV})	0.5	Ng et al. (1978)
Produce Fraction of Activity after Processing (DF_P)	1.0	Ng et al. (1978)
Site Grown Factor for Vegetables and Produce (F_V)	0.7	EPA (1989)
Site Grown Factor for Beef (F_B)	0.442	EPA (1989)
Site Grown Factor for Milk (F_M)	0.399	EPA (1989)

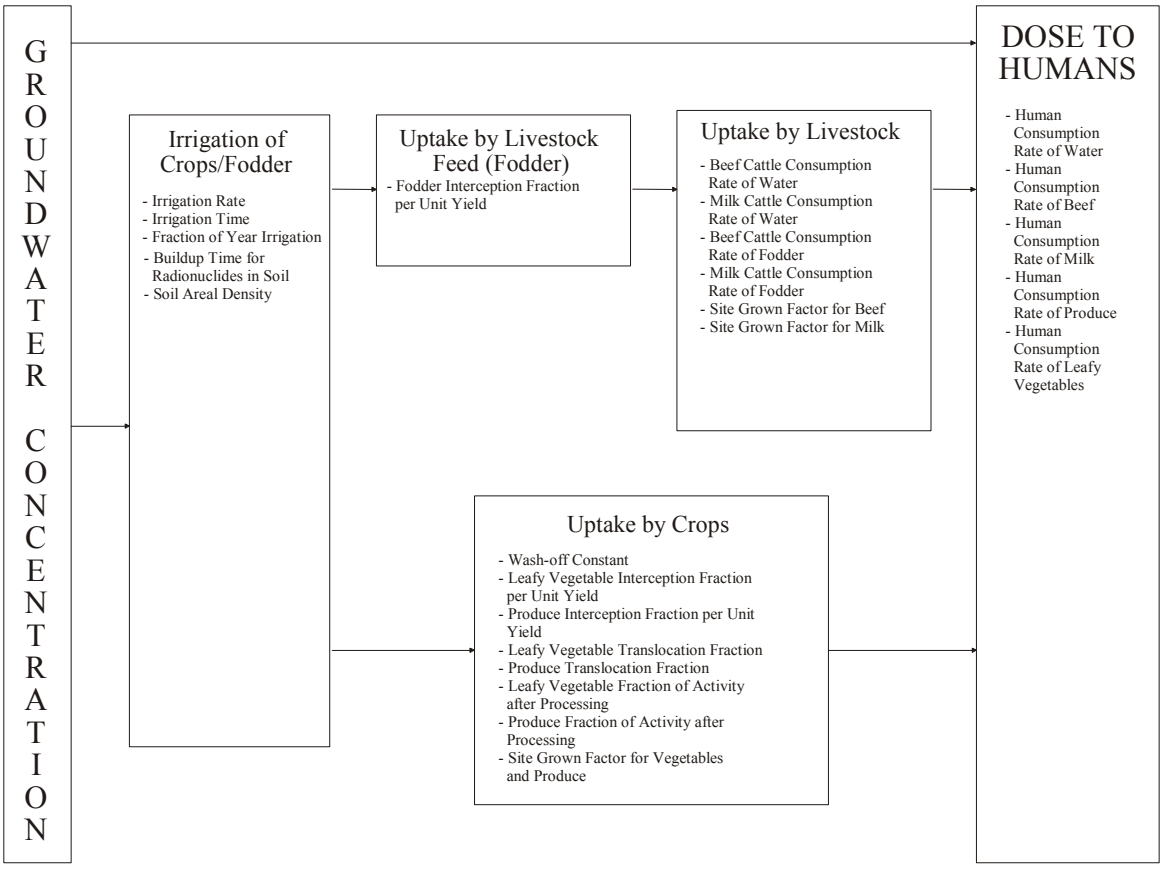

Figure 3-23. A block diagram of the all-pathways dose assessment and a description of where the parameter values enter the calculation.

Direct ingestion of beef contaminated by drinking water:

$$D_{B-DW} = \sum_i C_{GW-i} \times Q_{W-BC} \times F_b \times U_B \times DCF_i \times F_B \times \frac{10^6\ pCi}{\mu Ci} \quad (3\text{-}32)$$

where

$D_{B\text{-}DW}$ = committed effective dose equivalent from one year's consumption of beef contaminated by drinking water (mrem/yr)

$Q_{W\text{-}BC}$ = water consumption rate by beef cattle (L/yr)

F_b = beef transfer coefficient (d/kg)

U_B = human consumption rate of beef (kg/yr)

F_B = fraction of beef produced locally (unitless).

Direct ingestion of milk contaminated by drinking water:

$$D_{M-DW} = \sum_i C_{GW-i} \times Q_{W-MC} \times F_m \times U_M \times DCF_i \times F_M \times \frac{10^6\ pCi}{\mu Ci} \quad (3\text{-}33)$$

where

$D_{M\text{-}DW}$ = committed effective dose equivalent from one year's consumption of milk contaminated by drinking water (mrem/yr)

$Q_{W\text{-}MC}$ = water consumption rate by milk cattle (L/yr)

F_m = milk transfer coefficient (d/L)

U_M = human consumption rate of milk (L/yr)

F_M = fraction of milk produced locally (unitless).

The dose to humans from ingestion of contaminated leafy vegetables and produce was calculated assuming two contamination routes: direct deposition of contaminated irrigation water on plants and deposition of contaminated irrigation water on soil followed by root uptake by plants. Leafy vegetables and produce were treated separately. The dose through direct deposition was calculated as follows:

Leafy vegetables—direct deposition:

$$D_{LV-D} = \sum_i \left(\frac{C_{GW-i} \times I \times r}{Y_{LV}} \times \frac{1 - e^{-(\lambda_i + kI)t_I}}{\lambda_i + kI} \times U_{LV} \times DCF_i \times DF_{LV} \times T_{LV} \times F_V \times \frac{10^6\ pCi}{\mu Ci} \right) \quad (3\text{-}34)$$

where

$D_{LV\text{-}D}$ = committed effective dose equivalent from one year's consumption of leafy vegetables contaminated by direct deposition (mrem/yr)

I = irrigation rate (L/m^2/d)

r = interception fraction (unitless)

Y_{LV} = agricultural yield for leafy vegetables (kg/m^2, wet weight)

λ_i = radioactive decay constant for radionuclide i (d^{-1})

k = wash-off constant (mm^{-1})

t_I = irrigation time (d)

U_{LV} = human consumption rate of leafy vegetables (kg/yr)

DF_{LV} = fraction of activity remaining after preparation and processing of leafy vegetables (unitless)

T_{LV} = translocation factor for leafy vegetables (unitless)

F_V = fraction of leafy vegetables and produce produced locally (unitless).

Produce—direct deposition:

$$D_{P-D} = \sum_i \left(\frac{C_{GW-i} \times I \times r}{Y_P} \times \frac{1 - e^{-(\lambda_i + kI)t_I}}{\lambda_i + kI} \times U_P \times DCF_i \times DF_P \times T_P \times F_V \times \frac{10^6\ pCi}{\mu Ci} \right) \quad (3\text{-}35)$$

where

$D_{P\text{-}D}$ = committed effective dose equivalent from one year's consumption of produce contaminated by direct deposition (mrem/yr)

Y_P = agricultural yield for produce (kg/m^2, wet weight)

U_P = human consumption rate of produce (kg/yr)

DF_P = fraction of activity remaining after preparation and processing of produce (unitless)

T_P = translocation factor for produce (unitless).

The product kI is also known as the weathering-rate constant because of wash-off (Peterson 1983). This quantity describes the rate at which material is removed from plant surfaces by water and is analogous to λ_e, the weathering rate constant used in non-irrigation situations. The value of kI was calculated as follows:

$$kI = 0.025/mm \times \frac{8.47\ L}{m^2\ day} \times \frac{1\ m^3}{1{,}000\ L} \times \frac{1{,}000\ mm}{1\ m} = 0.212/d \quad \text{(3-36)}$$

The dose from deposition of contaminated irrigation water on soil followed by root uptake by plants and human consumption of plants was calculated using the following equations. Credit was not taken for leaching of radionuclides from the root zone of the plants. Also, buildup from successive years of farming was not taken into account.

Leafy vegetables—root uptake:

$$D_{LV-R} = \sum_i \left(\frac{C_{GW-i} \times I \times f_I}{P} \times \frac{1 - e^{-(\lambda_i \times t_b)}}{\lambda_i} \times CR_i \times U_{LV} \times DCF_i \times F_V \times \frac{10^6\ pCi}{\mu Ci} \right) \quad \text{(3-37)}$$

Produce—root uptake:

$$D_{P-R} = \sum_i \left(\frac{C_{GW-i} \times I \times f_I}{P} \times \frac{1 - e^{-(\lambda_i \times t_b)}}{\lambda_i} \times CR_i \times U_P \times DCF_i \times F_V \times \frac{10^6\ pCi}{\mu Ci} \right) \quad \text{(3-38)}$$

where

$D_{LV\text{-}R}$ = committed effective dose equivalent from one year's consumption of leafy vegetables contaminated by root uptake (mrem/yr)

$D_{P\text{-}R}$ = committed effective dose equivalent from one year's consumption of produce contaminated by root uptake (mrem/yr)

f_I = fraction of the year that crops are irrigated (unitless)

P = areal density (kg [dry weight soil]/m^2)

t_b = buildup time for radionuclides in soil (d)

CR_I = concentration ratio for radionuclide i (pCi/kg [wet weight plant] per pCi/kg [dry weight soil]).

The dose to humans from ingestion of animal products contaminated by contaminated feed was calculated assuming two contamination routes: direct deposition and root uptake. Meat and milk were treated separately. The dose through direct deposition was calculated as follows:

Beef—direct deposition:

$$D_{B-D} = \sum_i \left(\frac{C_{GW-i} \times I \times r}{Y_F} \times \frac{1 - e^{-(\lambda_i + kI)t_I}}{\lambda_i + kI} \times Q_{F-BC} \times TF_B \times U_B \times DCF_i \times F_B \times \frac{10^6\ pCi}{\mu Ci} \right) \quad \text{(3-39)}$$

$D_{B\text{-}D}$ = committed effective dose equivalent from one year's consumption of beef contaminated by direct deposition onto fodder (mrem/yr)

Y_F = agricultural yield for fodder (kg/m^2, dry weight)

$Q_{F\text{-}BC}$ = beef cow consumption rate of fodder (kg [dry]/d)

TF_B = transfer factor (fodder to beef)

U_B = human consumption rate of beef (kg/yr)

F_B = fraction of beef produced locally (unitless).

Milk—direct deposition:

$$D_{M-D} = \sum_i \left(\frac{C_{GW-i} \times I \times r}{Y_F} \times \frac{1 - e^{-(\lambda_i + kI)t_I}}{\lambda_i + kI} \times Q_{F-MC} \times TF_M \times U_M \times DCF_i \times F_M \times \frac{10^6\ pCi}{\mu Ci} \right) \quad \text{(3-40)}$$

where

$D_{M\text{-}D}$ = committed effective dose equivalent from one year's consumption of milk contaminated by direct deposition onto fodder (mrem/yr)

$Q_{F\text{-}MC}$ = milk cow consumption rate of fodder (kg [dry]/d)

TF_M = transfer factor (fodder to milk)

U_M = human consumption rate of milk (L/yr)

F_M = fraction of milk produced locally (unitless).

The dose through deposition on soil followed by root uptake was calculated using the following equations. As with produce and leafy vegetables, credit was not taken for leaching of radionuclides from the root zone of plants. Here again, buildup from successive years of farming also was not taken into account.

Beef—root uptake:

$$D_{B-R}=\sum_i \left(\frac{C_{GW-i} \times I \times f_I}{P} \times \frac{1-e^{-(\lambda_i \times t_b)}}{\lambda_i} \times CR_i \times Q_F \times TF_B \times U_B \times DCF_i \times F_B \times \frac{10^6\ pCi}{\mu Ci} \right) \quad (3\text{-}41)$$

Milk—root uptake:

$$D_{M-R}=\sum_i \left(\frac{C_{GW-i} \times I \times f_I}{P} \times \frac{1-e^{-(\lambda_i \times t_b)}}{\lambda_i} \times CR_i \times Q_F \times TF_M \times U_M \times DCF_i \times F_M \times \frac{10^6\ pCi}{\mu Ci} \right) \quad (3\text{-}42)$$

where

$D_{B\text{-}R}$ = committed effective dose equivalent from one year's consumption of beef contaminated by root uptake (mrem/yr)

$D_{M\text{-}R}$ = committed effective dose equivalent from one year's consumption of milk contaminated by root uptake (mrem/yr)

f_I = fraction of the year that crops are irrigated (unitless)

P = areal density (kg [dry weight soil]/m^2)

t_b = buildup time for radionuclides in soil (d)

CR_i = concentration ratio for radionuclide i (pCi/kg [wet weight plant] per pCi/kg [dry weight soil])

Q_F = animal consumption rate of fodder (kg [dry]/d).

Secondary and indirect pathways, such as inhalation of contaminated irrigation water, inhalation of contaminated dust, or external exposure from radionuclides deposited on the soil, were omitted from this scenario. These pathways were assumed to contribute relatively minor amounts when compared to direct pathways such as direct ingestion of contaminated water. This has been found to be the case for similar dose assessments for contamination introduced via the groundwater pathway (LaPlante and Poor 1997).

Note that the total human dose to be compared to the standards is the total received from all of the aforementioned pathways.

The equations described above are solved using a Formula Translation (FORTRAN) computer code developed for the TFF PA and presented in Appendix J. The code conducts 1,000 dose realizations based on data sampled from the distributions provided in Table 3-10. The results are then ordered from lowest to highest, based on dose. After this, the 950th realization on the list is chosen for the 95% confidence level (95% of the realizations are less than this value).

4. RESULTS OF ANALYSIS

This section describes the results of the analysis of performance for the TFF, conducted in accordance with the conceptual models and methodologies described in Section 3. Predicted releases to the environment, resulting groundwater concentrations, radon flux analysis, volatile radionuclide atmospheric transport, and the results of the dose analysis are presented.

Prior modeling of the TFF PA was conducted and a bounding analysis was completed. The results of these prior bounding analyses are provided in Appendix F. These analyses were re-evaluated based upon comments received from NRC and DOE. The focus of the new groundwater modeling analyses presented in this section are based on the four radionuclides (i.e., $^{90}Sr/^{90}Y$, ^{99}Tc, ^{129}I, and ^{14}C) determined from previous modeling (see Appendix F) to provide the majority of the groundwater pathway doses.

The source terms for the groundwater transport pathway are described first in Section 4.1. The results of the groundwater transport calculations are presented in Section 4.2. The radon flux results are presented in Section 4.3, and the volatile radionuclide atmospheric transport results are provided in Section 4.4. The groundwater protection doses and all-pathways results are presented in Section 4.5.

4.1 Groundwater Transport Source Term

As discussed in previous sections, DUST-MS was used to predict the release rates from the various waste forms at the INTEC facility. This approach was implemented to minimize computational time required by PORFLOW to predict release rates. The large hydraulic conductivity contrasts of the waste forms compared with the surrounding geological material required small time steps and subsequently time-consuming simulations using PORFLOW. However, comparative simulations were conducted to predict release rates using both DUST-MS and PORFLOW. The results showed that both models predicted similar contaminant transport rates using PORFLOW with the DUST-MS source term or the source term calculated by PORFLOW. These results showed that either source model yielded similar predictions on the rate and concentration of radionuclides released to the environment. In addition, the DUST-MS releases were compared to simple leaching models. These comparisons are provided in Section 7.

The results of the source term models for the groundwater pathway are described in this section. The contaminant releases for radon and the volatile radionuclides were described in Section 3. The results of the radon and volatile radionuclide analyses are provided in Sections 4.3 and 4.4, respectively.

4.1.1 Radionuclide Releases from the Piping, Sand Pad, and Tanks

Previous sections have

- Described the capabilities and features of the DUST-MS computer code
- Summarized the conceptual model used to model release rates out of the tank, sand pad, and concrete vault floor
- Provided DUST-MS input parameters used in all simulations and nuclide-specific input parameters.

The releases from piping at the TFF are based on the model presented in Section 3 for the degradation of the piping and the release of contaminants. In the previous analysis of the piping (see Appendix F), the piping was assumed to be released by diffusion to breaks in the piping. In this analysis, the piping is assumed to degrade in a manner similar to the tanks. Therefore, releases of contaminants from the piping begin to occur at 500 yr post-closure, the same time as releases from the tanks. The piping releases were assumed to follow the same release function as that for the tanks according to the DUST-MS results.

These releases were input into the groundwater model to determine groundwater concentrations, as discussed in Section 4.2.

Figure 4-1 displays the results from the DUST-MS simulations. The results are reasonable, considering the relative magnitudes of the partition coefficients and the types of releases. That is, releases from the sand pad occur earlier than releases from the tanks/piping. This is reasonable because radionuclides in the sand pad have a shorter transport path than radionuclides in the tank waste.

The output from DUST-MS simulations includes the total mass flux. These values were checked and they indicate a mass balance between releases from the source (initial inventory) and mass transported through the mass flux location. Additionally, maximum release rates compare favorably with hand-calculated values. Thus, the DUST-MS results also are quantitatively consistent with the expected values.

As is shown in Figure 4-1, two release peaks are present, the earlier peak being the sand pad releases beginning at 100 yr and the later peaks due to releases from the tanks/piping beginning at 500 yr. ^{14}C also is not released in significant quantities due to the large distribution coefficient (K_d) values present in the grouted waste and concrete.

The time of peak releases for each radionuclide and the peak release rates are provided in Table 4-1.

The releases determined using the DUST-MS computer model were input into the PORFLOW groundwater model as time history fluxes (Runchal 1997). The groundwater modeling results are presented in Section 4.2.

4.2 Groundwater Transport Results

Contaminant transport simulations were conducted for four radionuclides (i.e., ^{90}Sr, ^{99}Tc, ^{129}I, and ^{14}C) that were determined to provide the majority of the groundwater pathway doses for the 1,000-yr compliance period. Prior modeling analyses for the TFF, presented in Appendix F, assessed the other radionuclides for a period of one million years. These results indicate that the remaining radionuclides are not of concern for the TFF.

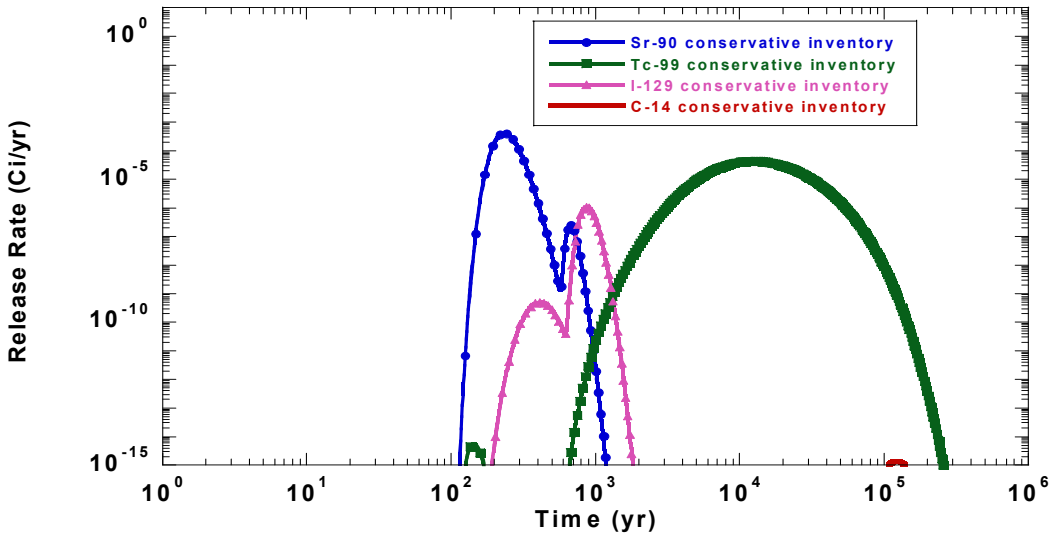

Figure 4-1. Releases of ^{90}Sr, ^{99}Tc, ^{129}I, and ^{14}C from the sand pad and tanks and piping.

Table 4-1. Peak releases rates, groundwater concentration, and doses for the groundwater pathway analyses.

	Peak Release Rate		Peak Groundwater Concentration		Peak Drinking Water Dose		Peak All-Pathway Dose	
Nuclide	Time (yr)	Ci/yr	Time (yr)	pCi/L	Time (yr)	mrem/yr	Time (yr)	mrem/yr
$^{90}Sr/^{90}Y$	232	0.005	551	0.01	551	0.001	551	0.006
^{99}Tc	12,206	5.0E!04	1.459E+04	116	1.459E+04	0.12	1.459E+04	0.87
^{129}I	867	1.3E!05	890	3.8	890	0.77	890	1.35
^{14}C	1.1998E+05	1.6E!14	1.216E+05	4.1E!09	1.216E+05	6.3E!12	1.216E+05	2.9E!11

Radionuclide releases were placed in the PORFLOW model domain where the sand pad and tanks were located. Degradation of the piping, vaults, and tanks were incorporated into the releases determined using the DUST-MS model. Radionuclide concentrations were observed in the regional aquifer at a point of maximum concentration.

Figure 4-2 shows a cross section of the unsaturated/saturated zone contaminant distribution of ^{99}Tc resulting from contaminant releases. ^{99}Tc was used in the figure because it has a long half-life and a source release that results in the center line of the plume being visible throughout the model domain. Therefore, ^{99}Tc was the best radionuclide for visual presentation. Other radionuclides were checked to make sure this was the point of entry of the plume center line.

Based on this contaminant distribution, the maximum observed contaminant concentrations occurs approximately 600 m (2,000 ft) downgradient from the tanks.[a] At this location, the nodes for the upper 10 m (30 ft) of the aquifer were averaged to obtain a contaminant concentration representative of a well water screen. Results of individual contaminant concentrations at this location for a one million year simulation are presented in Figure 4-3.

The model simulations were conducted using separated sources for the piping, sand pad, and tanks. These sources were simulated separately to assess the impact of the individual sources. The individual sources were then summed to obtain the total concentration in groundwater for the subsequent dose calculations.

4.2.1 General Transport Characteristics

The hydrostratigraphy, location of perched water zones, and transport characteristics of the individual radionuclides all impacted the results of the transport simulations. The perched water zones, or the absence thereof, have an important impact on the migration of contaminants through the vadose zone. Perched zones from seepage of the Big Lost River act as sources of water to the surrounding unsaturated material. As contaminants approach the perched zones, the total hydraulic head (defined as both capillary and gravitational forces) redirects the migration path around the perched water. While some contaminants enter the perched zones, the bulk of the flow is diverted around the perched zones (see Figure 4-2). Breaks in the perched zones where the impeding interbeds are absent play a major role in the downward migration of contamination. Consequently, the hydrostratigraphy defined by Anderson's USGS report plays a major role in the migration patterns of the subsurface contaminants (Anderson 1991).

This influence of the hydrostratigraphy is illustrated in Figure 4-2. As noted in Section 3, the low permeability of the D-DE2 interbed is a major factor in the formation of perched water bodies in the upper vadose zone. The hydrologic cross section for the site (shown in Section 3) shows that this interbed is discontinuous across the site. Hydraulic forces divert the downward migration of the contaminant plume to areas where this interbed

a. Model results were output in metric units. Therefore, in Section 4, measurements are given in metric units first, followed by U.S. customary units.

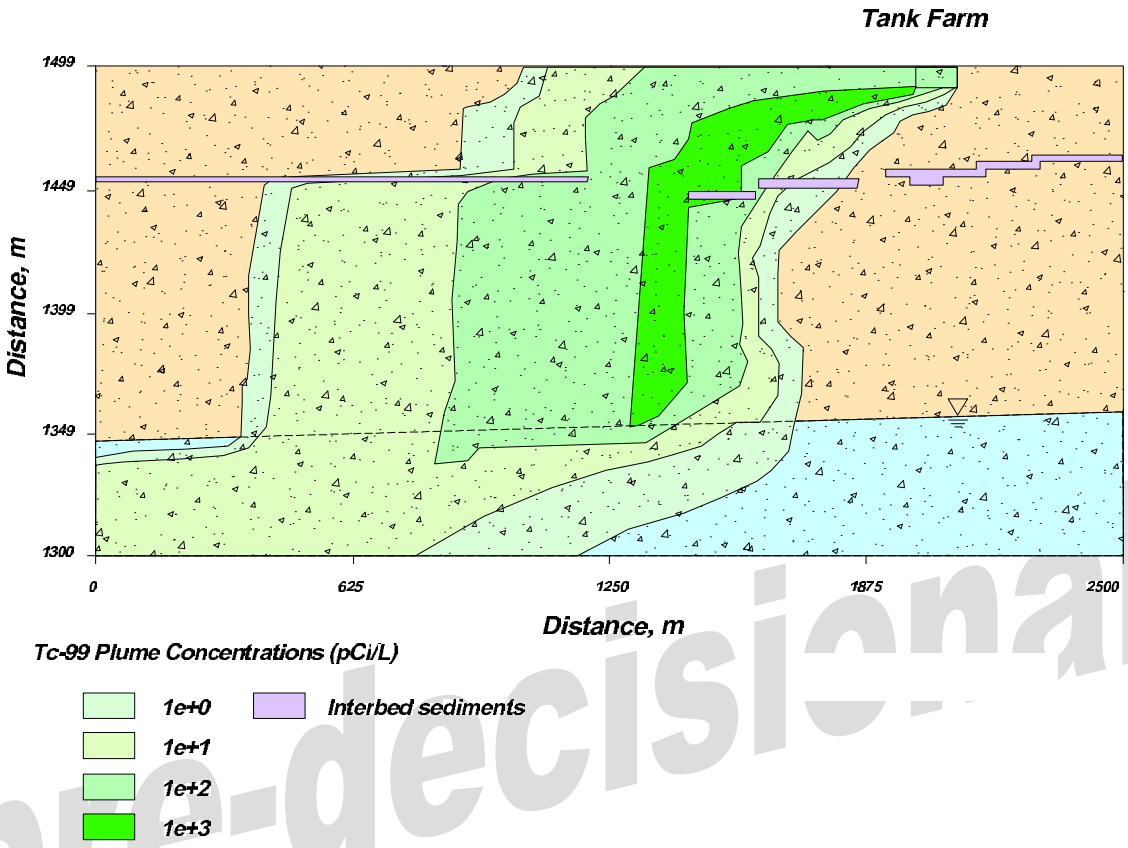

Figure 4-2. Groundwater modeling domain showing ^{99}Tc concentrations and location of maximum concentrations (all concentrations based on a unit source inventory).

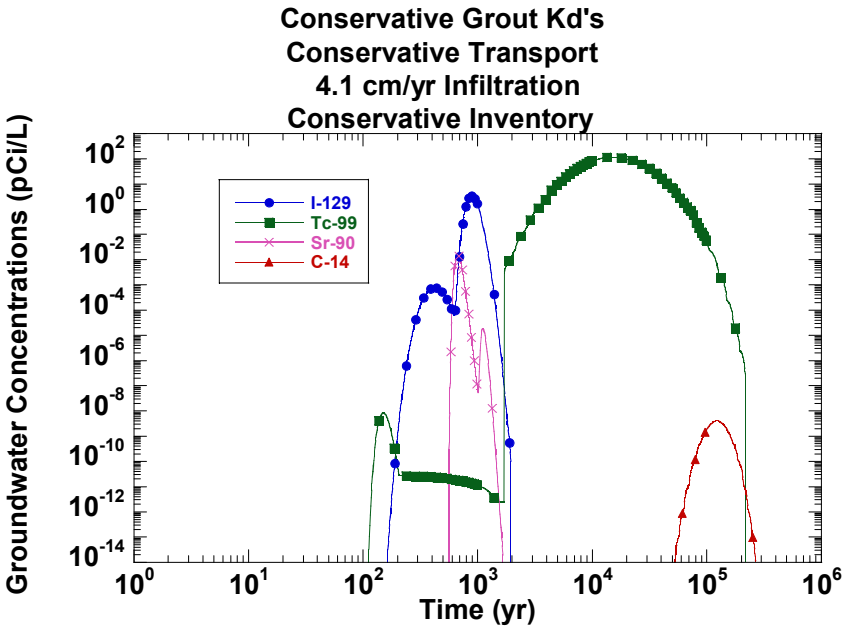

Figure 4-3. Groundwater concentrations for the conservative analysis.

is absent. The net result is that the center of the contaminant plume (where the highest concentrations enter the regional aquifer) is approximately 600 m (2,000 ft) downgradient of the release point. To a lesser degree, the discontinuity of the lower perched zones also impacts the migration patterns of the contaminants.

By the time the contaminants reach the water table, the difference in concentrations and arrival times below the two tanks in the groundwater modeling is diminished. The effects of the hydrostratigraphy and the lower perched water zones appear to cause a more uniform transport rate to the water table. Simulations were conducted using separate sources for the tanks (i.e., north and south tanks in the cross section); however, the resulting contaminant concentrations and arrival times were similar. Therefore, all contaminant runs were evaluated by placing the releases from two tanks at the location of the southern tank in the groundwater model domain.

The timing of contaminant releases from the sand pad and tanks/piping is evident from the observation point located 600 m (2,000 ft) downgradient in the groundwater. As expected, the arrival time and the time for peak concentrations to occur directly relate to the time of release.

Several factors affect the transport characteristics of the various radionuclides. Factors such as the K_d values and radionuclide half-lives are interrelated, and all of the factors impact the transport characteristics.

4.2.2 Results for Individual Radionuclides

The following sections discuss the transport characteristics of the individual radionuclides that resulted in significant aquifer concentrations and doses in the transport model. These radionuclides include ^{90}Sr, ^{99}Tc, ^{129}I, and ^{14}C. The remaining radionuclides were previously evaluated and were determined to provide no significant contribution to the groundwater pathway doses (see Appendix F).

The peak groundwater concentrations and the time of the peak are listed in Table 4-1.

4.2.2.1 Strontium-90. Peak concentrations for the groundwater occur for the sand pad source after approximately 550 yr at a concentration of 0.01 pCi/L. The peak groundwater concentration resulting from release from the tanks occurs approximately 1,110 yr after closure at a concentration of 1.8E!05 pCi/L. The peak groundwater concentration from the piping releases occurs at 1,110 yr after closure at a concentration of 4.4E!08 pCi/L.

4.2.2.2 Technetium-99. Peak concentrations for the groundwater occur for the sand pad source after approximately 150 yr at a concentration of 9.3E!09 pCi/L. The peak groundwater concentration resulting from release from the tanks occurs approximately 1.46E+04 yr after closure at a concentration of 116 pCi/L. The peak groundwater concentration from the piping releases occurs at 1.46E+04 yr after closure at a concentration of 0.27 pCi/L.

4.2.2.3 Iodine-129. Peak concentrations for the groundwater occur for the sand pad source after approximately 421 yr at a concentration of 8.9E!04 pCi/L. The peak groundwater concentration resulting from release from the tanks occurs approximately 888 yr after closure, at a concentration of 3.82 pCi/L. The peak groundwater concentration from the piping releases occurs at 888 yr after closure at a concentration of 0.02 pCi/L.

4.2.2.4 Carbon-14. Peak concentrations for the groundwater occur for the sand pad source after approximately E+05 yr at a concentration of 3.7E!14 pCi/L. The peak groundwater concentration resulting from release from the tanks occurs approximately 1.2E+05 yr after closure at a concentration of 4.1E!09 pCi/L. The peak groundwater concentration from the piping releases occurs at 1.2E+05 yr after closure at a concentration of 2.4E!16 pCi/L.

4.3 Radon Analysis Results

As discussed in Section 3, calculations were performed for a one-dimensional bare slab resting

on the ground surface to determine the radon flux at the surface of this slab. These calculations are highly conservative with respect to the actual performance of a grouted heel at the TFF. Because the slab is modeled in open air, no credit is taken for the vault or tank. Also, the radium inventory at the end of the 1,000-yr performance period is used for the source in the calculations, which is conservative for all times before the end of the performance period because of ingrowth from parent radionuclides. Modeling the slab in open air means radon can more easily diffuse out of the slab than would otherwise be expected. The model did not include pressure-driven transport of radon out of the slab for two reasons. First, cementitious materials are generally too impermeable for pressure-driven transport to be significant (Renken and Rosenberg 1995; Tanner 1990; Rogers and Nielson 1992). Second, it is difficult to envision a situation where a significant pressure gradient is maintained across the slab when it is buried at depth. In all cases for the radon analysis, the point of compliance is the surface of the TFF soils.

The conservative inventory ^{226}Ra concentration (1.92E–04 Ci/tank; 1.73E+06 pCi/m^3) resulted in a flux of ^{222}Rn out of the surface of the slab of 0.39 pCi/m^2/s after converting to pCi from Bq (1 pCi is equal to 0.037 Bq). This value is more than an order of magnitude below the standard of 20 pCi/m^2/s, given in DOE Manual 435.1-1 (DOE 2001a). The reason that such a conservative model was still able to meet the standard is that there is simply not much ^{226}Ra in the slab. Also, cement materials do not emanate or transport radon very well.

Since the radioactive decay constants for ^{220}Rn and ^{219}Rn are well over three orders of magnitude larger than that of ^{222}Rn and the natural log term is always less than zero, the reduction factor for the short-lived nuclides is vanishingly small for all but the thinnest of overburdens (i.e., where the reduction factor for ^{222}Rn approaches unity). For reference, a 0.5-m-thick (2-ft) overburden of soil with a diffusion coefficient of 7E–06 m^2/s (the diffusion coefficient for radon in air, a conservative upper limit for radon diffusion in any medium [Rogers and Nielson 1992]) would have a reduction factor of about 10^{96}, with the reduction factor for ^{219}Rn being even smaller.

4.4 Volatile Radionuclide Analysis Results

Based on the conservative inventory, volatile radionuclide release rates determined in Section 3 were input into the CAP88-PC computer model (EPA 1992) to determine the potential doses from the atmospheric pathway. The receptor was located 100 m (300 ft) from the TFF. The analysis used 1992 wind data from the INEEL Grid-3 meteorological station. Standard default values for agricultural products, based on the rural definition in CAP88-PC, were used in the analysis. The outputs from the modeling runs are provided in Appendix I.

The results of the CAP88-PC atmospheric transport runs for ^{3}H releases were determined to be 0.027 mrem/yr and ^{14}C doses were 1.28 mrem/yr, with a total dose of 1.3 mrem/yr. The point of compliance was at 100 m (300 ft) in a south-southwest direction from the TFF, which was the point of maximum dose. The performance objective for the air pathway is 10 mrem/yr. Therefore, the air transport pathway was found to be approximately 1/10th of the allowable dose limit.

4.5 Dose Analysis Results

4.5.1 Groundwater Protection

The groundwater pathway analysis was evaluated using conservative parameters. The analysis consisted of the conservative grout distribution coefficients, conservative transport parameters, 4.1 cm/yr (1.6 in./yr) infiltration, and the conservative inventory discussed previously in Sections 2 and 3.

The drinking water doses were calculated using Equation (3-31) in Section 3. The drinking water rate of 730 L/yr was used in the analysis. The point of compliance was at the point of maximum groundwater concentrations in the aquifer, 600 m (2,000 ft) south of the TFF.

The drinking water doses are shown in Figure 4-4. The peak drinking water doses and their time of peak for each radionuclide are listed in Table 4-1.

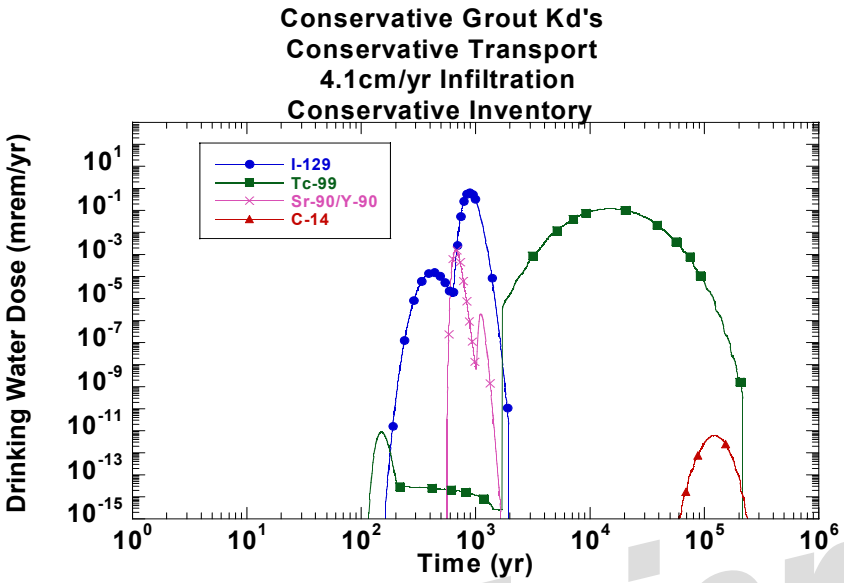

Figure 4-4. Drinking water doses for the conservative analysis.

4.5.1.1 Strontium-90. Peak drinking water doses occur for the sand pad source after approximately 550 yr at a dose of 0.001 mrem/yr. The peak drinking water doses resulting from release from the tanks occur approximately 1,110 yr after closure at a dose of 2.0E!06 mrem/yr. The peak drinking water dose from the piping releases occurs at 1,110 yr after closure at a dose of 4.9E!09 mrem/yr.

4.5.1.2 Technetium-99. Peak drinking water doses occur for the sand pad source after approximately 150 yr at a dose of 9.9E!12 mrem/yr. The peak drinking water dose resulting from release from the tanks occurs approximately 1.46E+04 yr after closure at a dose of 0.12 mrem/yr. The peak drinking water dose from the piping releases occurs at 1.46E+04 yr after closure at a dose of 2.9E!04 mrem/yr.

4.5.1.3 Iodine-129. Peak drinking water doses occur for the sand pad source after approximately 421 yr at a dose of 1.8E!04 mrem/yr. The peak drinking water dose resulting from release from the tanks occurs approximately 888 yr after closure at a dose of 0.77 mrem/yr. The peak drinking water dose from the piping releases occurs at 888 yr after closure at a dose of 0.004 mrem/yr.

4.5.1.4 Carbon-14. Peak drinking water doses occur for the sand pad source after approximately 1E+05 yr at a dose of 5.7E!17 mrem/yr. The peak drinking water dose resulting from release from the tanks occurs approximately 1.2E+05yr after closure at a dose of 6.3E!12 mrem/yr. The peak drinking water dose from the piping releases occur at 1.2E+05 yr after closure at a dose of 3.6E!19 mrem/yr.

The doses reported above are for the entire simulation time of one million years after closure of the TFF. The compliance period of 1,000 yr exhibited a peak dose of 0.77 mrem/yr from ^{129}I.

To ensure that the drinking water pathway doses are bounding, a sensitivity/uncertainty analysis was conducted. A discussion of the sensitivity/uncertainty results is provided in Section 7.

4.5.2 All-Pathways Dose

The groundwater all-pathway dose analysis was evaluated using conservative parameters. The analysis consisted of the conservative grout distribution coefficients, conservative transport parameters, 4.1 cm/yr (1.6 in./yr) infiltration, and the conservative inventory discussed previously in Sections 2 and 3.

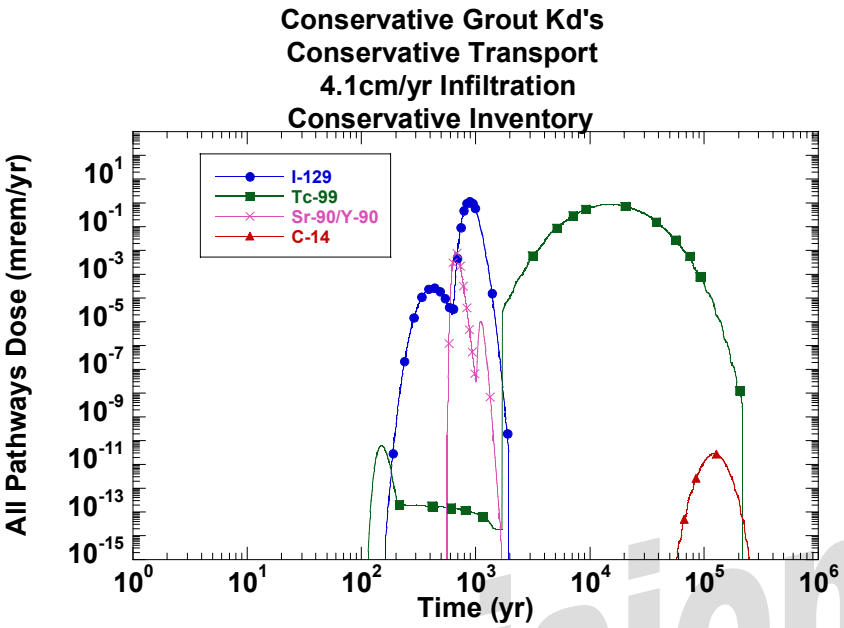

Figure 4-5. All-pathway doses for the conservative analysis.

The all-pathways doses are shown in Figure 4-5. The peak all-pathways doses and the tie of the peak for each radionuclide are summarized in Table 4-1.

4.5.2.1 Strontium-90. Peak all-pathways doses occur for the sand pad source after approximately 550 yr at a dose of 0.005 mrem/yr. The peak all-pathways doses resulting from release from the tanks occur approximately 1,110 yr after closure at a dose of 1.0E!05 mrem/yr. The peak all-pathways dose from the piping releases occurs at 1,110 yr after closure at a dose of 2.5E!08 mrem/yr.

4.5.2.2 Technetium-99. Peak all-pathways doses occur for the sand pad source after approximately 150 yr at a dose of 7.0E!11 mrem/yr. The peak all-pathways dose resulting from release from the tanks occurs approximately 1.46E+04 yr after closure at a dose of 0.87 mrem/yr. The peak all-pathways dose from the piping releases occurs at 1.46E+04 yr after closure at a dose of 2.0E!03 mrem/yr.

4.5.2.3 Iodine-129. Peak all-pathways doses occur for the sand pad source after approximately 421 yr at a dose of 3.1E!04 mrem/yr. The peak all-pathways dose resulting from release from the tanks occurs approximately 888 yr after closure at a dose of 1.4 mrem/yr. The peak all-pathways dose from the piping releases occurs at 888 yr after closure at a dose of 0.006 mrem/yr.

4.5.2.4 Carbon-14. Peak all-pathways doses occur for the sand pad source after approximately 1E+05yr at a dose of 2.6E!16 mrem/yr. The peak all-pathways dose resulting from release from the tanks occur approximately 1.2E+05 yr after closure at a dose of 2.9E!11 mrem/yr. The peak all-pathways dose from the piping releases occurs at 1.2E+05 yr after closure at a dose of 1.7E!18 mrem/yr.

The doses reported above are for the entire simulation time of 1 million years after closure of the TFF. The compliance period of 1,000 yr exhibited a peak dose of 1.4 mrem/yr from ^{129}I.

To ensure that the all-pathway doses are conservative, a sensitivity/uncertainty analysis was conducted. A discussion of the sensitivity/uncertainty results is provided in Section 7.

5. INADVERTENT INTRUDER ANALYSES

This section describes the potential intruder scenarios for the TFF. The intruder scenarios are screened based on the physical aspects of the facility (i.e., depth to the waste).

Intruder scenarios considered for use in this PA were limited to those previously described for low-level radioactive waste performance assessments (NRC 1982; Kennedy and Peloquin 1988). These intruder scenarios include both acute and chronic exposure scenarios. Acute exposure scenarios involve exposures of short duration, and include an intruder-construction scenario, a discovery scenario, and a drilling scenario.

Chronic, longer-duration, intruder scenarios include the intruder-agriculture, intruder-resident, and post-drilling scenario. The *Addendum to Radioactive Waste Management Complex Low-Level Waste Radiological Performance Assessment* (Maheras et al. 1997) considered two additional intruder scenarios at the INEEL: chronic intruder-radon and chronic biointrusion. All eight of these scenarios were screened for use in this PA and are discussed in this section.

The intruder scenarios used to support the waste classification limits in 10 CFR 61 (2003) were the intruder-construction, intruder-discovery, and intruder-agriculture scenarios. The more restrictive of the scenarios, intruder-construction and intruder-agriculture, were used for setting the Class A and Class C waste classification limits. The intruder-discovery scenario was used for setting the Class B waste limits for short-lived radionuclides (Oztunali and Roles 1986; NRC 1982).

When waste is disposed at depths greater than 5 m (20 ft), the intruder scenarios defined by NRC for surface excavation may not directly apply.[a] Disposal with special waste forms or at a depth greater than 5 m (20 ft) (which applies to the waste in the tanks and sand pads addressed by this PA), resembles the conditions anticipated for "Greater Confinement Disposal" operations for low-level waste at many of the operating DOE burial grounds (Oztunali and Roles 1986). These conditions require the definition of additional intruder scenarios. Kennedy and Peloquin (1988) and Oztunali and Roles (1986) present intruder-drilling and post-drilling scenarios to deal with waste disposed at depths greater than 5 m (20 ft).

The remainder of this section explores the intruder scenario definitions, presents the basis for the selection of appropriate intruder scenarios for the TFF, and explains the development of the mathematical representations and parameters of the intruder scenarios for both the acute and chronic exposures.

It should be noted that all of the intruder scenarios presented in this section were based on the conservative inventories presented in Section 2.3.

5.1 Intruder Scenario Screening

5.1.1 Intruder Inventory

The intruder analysis considers that active institutional control will be maintained over the disposal site for at least 100 yr after facility closure. This consideration eliminates from concern any radionuclide with a half-life less than about 5 yr, because the inventory in the waste at 100 yr after facility closure will be reduced to innocuous levels by radioactive decay (unless it appears in the initial inventory in extremely high concentrations). However, radionuclides with half-lives less than 5 yr cannot be neglected if the radionuclide appears in a decay chain, since its activity may increase with time because of the decay of a parent radionuclide, unless the parent is short-lived.

Using the 5-yr half-life screening criteria results in the elimination of the following radionuclides from further consideration: ^{102}Rh,

a. Model inputs and outputs are given in metric units. Therefore, in Section 5, measurements are given in metric units first, followed by U.S. customary units.

^{119m}Sn, ^{134}Cs, ^{150}Eu, ^{153}Gd, ^{155}Eu, and ^{171}Tm. In addition, the following radionuclides in short decay chains were eliminated from further analysis since the parent and progeny each have half-lives less than 5 yr: ^{106}Ru/^{106}Rh, ^{109}Cd/^{109m}Ag, ^{110m}Ag/^{110}Ag, ^{125}Sb/^{125m}Te, and ^{144}Ce/^{144m}Pr/^{144}Pr. Additional radionuclides were screened from further consideration because their half-lives indicate that they are either stable or have such long half-lives that their specific activity and thus, contribution to dose, would be insignificant. These radionuclides include ^{142}Ce (5E+16 yr), ^{149}Sm (1E+15 yr), ^{144}Nd (2.4E+15 yr), and ^{148}Sm (2E+14 yr).

5.1.2 Acute Intruder Scenarios

As suggested in the PA guidance (DOE 1999b), three potential acute intruder exposure scenarios were considered: the intruder-construction, intruder-discovery, and intruder-drilling scenarios. These scenarios are described below. Scenarios not considered applicable to the TFF were screened out from further consideration.

5.1.2.1 Intruder-Construction Scenario.

The intruder-construction scenario involves an inadvertent intruder who chooses to excavate or construct a building on the disposal site. In this scenario, the intruder is assumed to dig a basement excavation to a depth of approximately 3 m (10 ft) (Oztunali and Roles 1986). It is assumed that the intruder does not recognize the hazardous nature of the material excavated. He or she is exposed to radioactive constituents in the waste during the excavation of the basement. The intruder also is exposed to the exhumed waste by inhalation of resuspended contaminated soil and external irradiation from contaminated soil. Potato cellar excavation also was considered since these cellars are common in the agricultural region surrounding the INEEL. However, potato cellars are relatively shallow, with a typical depth of 1 m (3 ft) (Maheras et al. 1994, 1997).

The depth to the residual waste at the bottom of the tanks and/or sand pads (i.e., 3 m [10 ft] of soil plus 9 m [30 ft] of concrete) would preclude direct contact with the waste from the 3-m (10-ft) excavation. However, approximately 30% of the contaminated piping associated with the tanks is located within 3 m (10 ft) of the surface.

Due to the disposal depth of the waste in the tanks at the TFF (i.e., greater than 10 m [30 ft]) and the depth of the sand pad contamination, the intruder-construction scenario was not considered applicable to these waste. However, the intruder-construction scenario was considered for the radionuclide inventory located in the associated piping less than 3 m (10 ft) from the surface.

5.1.2.2 Intruder-Discovery Scenario.

The intruder-discovery scenario is conceptualized as a modification of the intruder-construction scenario. The basis for the intruder-discovery scenario is the same as the intruder-construction scenario except that the exposure time is reduced (Oztunali and Roles 1986). The scenario involves the intruder excavating a basement to a 3-m (10-ft) depth. The intruder is assumed to recognize that he or she is digging into very unusual soil immediately upon encountering the vault/tank/piping system and leaves the site. Consequently, the exposure time is reduced. The time typically applied to this scenario is 6 hr.

The depth to the residual waste at the bottom of the tanks and/or sand pads (i.e., 3 m [10 ft] of soil plus 9 m [30 ft] of concrete) would preclude direct contact with the waste from the 3-m (10-ft) excavation. However, approximately 30% of the contaminated piping associated with the tanks is located within 3 m (10 ft) of the surface.

The intruder-discovery scenario was not considered for further analysis since the exposure time of 6 hr would result in limited doses in comparison to the intruder-construction scenario with an exposure time of 160 hr which was retained for analysis of the piping radionuclide inventory.

5.1.2.3 Intruder-Drilling Scenario.

The intruder-drilling scenario assumes the short-term exposure of a hypothetical intruder to drill cuttings from a borehole penetrating the waste disposal site. This scenario involves wastes buried below the depth of typical construction excavations.

Oztunali and Roles (1986) indicate that for waste below 10 m (30 ft), the only applicable intrusion scenario is the intruder-drilling scenario. They also note that for grouted waste or waste disposed of in reinforced concrete structures, a time period of 500 yr after site closure is assumed as the effectiveness limit for this waste form. Therefore, this scenario is not considered applicable for drilling through reinforced concrete until 500 yr post-closure. However, they also note that the scenario is assumed to be fully applicable for grouted waste at any time. Because the waste could be contacted and moved to the surface, thereby exposing the intruder, the intruder-drilling scenario was retained for analysis in the TFF PA.

5.1.3 Chronic Exposure Scenarios

As suggested in the PA guidance (DOE 1999b), five potential chronic intruder exposure scenarios were considered: the intruder-agriculture, intruder-resident, intruder-radon, biointrusion, and post-drilling scenarios. These scenarios are described below. Those scenarios not considered applicable to the TFF were screened out from further consideration.

5.1.3.1 Intruder Post-Construction Scenario. The chronic intruder post-construction (i.e., agriculture) scenario is an extension of the acute intruder-construction scenario. It is assumed in this scenario that an intruder lives in the building constructed as part of the intruder-construction scenario and engages in agricultural activities on the contaminated site. The intruder is exposed to contamination by inhalation of resuspended contaminated soil, inhalation of gaseous radionuclides released from the waste, external irradiation, ingestion of contaminated soil, ingestion of contaminated beef and milk, and ingestion of contaminated vegetables.

As stated earlier, the intruder-construction scenario was only considered applicable to the piping associated with the TFF that is less than 3 m (10 ft) from the surface. The depth of the residual waste in the tanks and the sand pads prevents its excavation to the surface. Therefore, the intruder-agriculture scenario was retained for the piping inventory.

5.1.3.2 Intruder-Resident Scenario. The intruder-resident scenario assumes that the intruder constructs a residence on the waste form (i.e., concrete vault) after an excavation or some natural process exposes it. This scenario was not considered applicable to the TFF because of the depth of the waste and the shielding provided by the overlying grout and concrete. This shielding, along with the shielding provided by the house foundation, would reduce the external dose rates to very low levels. Therefore, the intruder-resident scenario was not considered for further analysis.

5.1.3.3 Intruder-Radon Scenario. The RWMC PA (Maheras et al. 1997) evaluated the intruder-radon scenario. The intruder-radon scenario assumes that the intruder excavates a $20 \times 10 \times 3$-m ($70 \times 30 \times 10$-ft) basement over the waste while constructing a home. The intruder is exposed to ^{222}Rn and its short-lived progeny while residing in the home. The exposure from radon emanating from the waste and migrating into the home is evaluated.

DOE Manual 435.1-1 (DOE 2001a) states that the intruder dose analyses are to exclude the total effective dose equivalent (TEDE) contribution from radon in air. Therefore, the RWMC chronic intruder-radon scenario was not considered for further analysis.

5.1.3.4 Biointrusion Scenario. The biointrusion scenario, assessed in the RWMC PA (Maheras et al. 1997), assumes that an intruder moves onto the site but does not excavate into the waste. Rather, radioactivity is brought to the surface by plants through root uptake and by burrowing animals. The RWMC discussion is given below.

Groves and Keller (1983) identified 10 species of small mammals nesting on or near the RWMC. Four species were the most numerous: deer mice (*Peromyscus maniculatus*), montane voles (*Microtus montanus*), Ord's kangaroo rats (*Dipodomys ordii*), and Townsend's ground squirrels (*Spermophilus townsendii*). Reynolds and Wakkinen (1987) studied the burrow depths of these four species in undisturbed soils. None of the deer mice burrows extended past 60 cm (20 in.), none of the montane vole burrows extended past

70 cm (30 in.), and none of the Ord's kangaroo rat burrows extended past 100 cm (40 in.). The maximum reported burrow depths for undisturbed soils was 138 cm (54.3 in.) for the Townsend's ground squirrel.

Harvester ants (*Pogonomyrmex salinus*) also were considered. Harvester ants burrow deeper than the small mammals. Blom, Clark, and Johnson (1991) state that harvester ants have been found as deep as 2.7 m (8.9 ft) in Wyoming and at the Hanford Site.

Reynolds and Fraley (1989) studied plant root profiles near the RWMC and determined the maximum rooting depth for big sagebrush (*Artemisia tridentata*) was 225 cm (88.6 in.), green rabbitbrush (*Chrysothamnus viscidiflorus*) was 190 cm (75 in.), and Great Basin wildrye (*Leymus cinereus*) was 200 cm (80 in.).

These studies give evidence that the biointrusion scenario is not applicable to the tanks and sand pads at the TFF because of the depth of the waste. The animal burrows and plant roots would not reach the residual waste in the tanks or sand pads. The animal burrows could contact waste in the piping located within the burrow depths. However, the amount of contamination excavated from the animal burrows would be far less than that involved in the intruder-construction/agricultural scenarios and this scenario would be bounded by the intruder-construction scenario for piping. Therefore, the biointrusion scenario was not considered further in this PA.

5.1.3.5 Post-Drilling Scenario. The chronic post-drilling scenario is an extension of the acute drilling scenario. It assumes that the intruder occupies the site after drilling a water well and grows crops on a mixture of clean soil and contaminated drill cuttings. After exhumation of the waste, the exposure pathways are the same as for the intruder-agriculture scenario. This intruder scenario was retained for further analysis.

5.2 Acute Intruder-Drilling Scenario Definition

The acute drilling scenario assumes that an inadvertent intruder drills a well into the contents of the tank and vault system. The intruder is exposed to contaminated drill cuttings spread over the ground and contaminated airborne dust. In the standard drilling scenario used in many PAs, the intruder is assumed to be exposed to contaminated drill cuttings in a mud pit. However, site-specific information developed through interviews with local well drilling contractors in the Idaho Falls area indicates that drillers spread the cuttings over the ground and do not use mud pits (Seitz 1991). The authors of the RWMC PA (Maheras et al. 1997) used this site-specific deviation of the standard drilling scenario and it also was incorporated into the TFF intruder-drilling scenario. The assumption that the drill cuttings are spread over the ground will result in higher dose estimates than if the cuttings were assumed to be in a mud pit because of the decrease in the shielding factor.

The drill cuttings are assumed to be spread over a 2,200 m^2 (24,000 ft^2) lot, which corresponds to about one-half acre. Typical lot sizes located outside of the Idaho Falls city limits are typically 1 to 3 acres. Therefore, a 2,200-m^2 lot size was considered conservative for use in the RWMC Radiological PA (Maheras et al. 1997), and also was incorporated into the TFF intruder-drilling scenario.

Well drilling contractors in the Idaho Falls area have reported that two types of wells are typically drilled: small-diameter residential wells and large irrigation wells. The small residential wells are typically 6 to 8 in. in diameter, serve a single residence, and also may provide enough water for a family garden and small quantities of livestock. The large-diameter irrigation wells are drilled to serve systems that irrigate hundreds of acres; the wells are located in the middle of farm fields, not near the farmer's residence. Therefore, a farmer would not drill an irrigation well to acquire water for his residence. Large-diameter irrigation wells are currently drilled in 18-in. diameters but drilling contractors indicated that

22-in.-diameter irrigation wells would be drilled in the future (Seitz 1991). An acute drilling exposure could result from drilling either a 6-in.-diameter residential well or 22-in.-diameter irrigation well. The larger 22-in.-diameter irrigation well was assessed for the acute intruder-drilling scenario.

The intruder is assumed to reside by the contaminated cuttings for 160 hr, the time local Idaho Falls well drilling contractors say it would take to drill and develop a 22-in.-diameter irrigation well (Seitz 1991). The exposure pathways for this acute drilling scenario include inhalation of resuspended drill cuttings, external exposure to the ground source, and inadvertent soil ingestion. Figure 5-1 illustrates the acute intruder-drilling scenario.

The TFF concrete vaults are reinforced concrete but the grout between the tank and vault and also inside of the tank is not reinforced concrete. However, considering that the depth to the waste in the tank is 10 m (30 ft), that the waste is contained within a stainless-steel tank, and that the overlying concrete vault roof is reinforced, credit beyond 100 yr could be taken for a barrier to intrusion. However, the intruder-drilling scenario was assumed to begin 100 yr after closure.

The activity concentration of radionuclides in the drill cuttings was determined as follows:

$$C_{s,i} = 1 \times 10^{12} \times C_{w,i} \times \frac{\pi r_{well}^2 t_w}{\pi r_{well}^2 D_b \rho} \qquad (5\text{-}1)$$

where

$C_{s,i}$ = soil activity concentration of radionuclide i (pCi/g)

1×10^{12} = factor for converting Ci to pCi

$C_{w,i}$ = waste activity concentration of radionuclide i at the time of intrusion (Ci/m^3)

r_{well} = radius of the well borehole (m)

t_w = thickness of the waste zone (m)

D_b = total depth of the borehole (m)

ρ = bulk density of the cuttings (g/m^3)

since

$$C_{w,i} = \frac{Ci_{Tank}}{\pi r_{Tank}^2 \ t_w} \qquad (5\text{-}2)$$

where

Ci_{Tank} = activity in the tank (Ci)

r_{Tank} = radius of the tank (m).

Then by substitution

$$C_{s,i} = 1 \times 10^{12} \times \frac{Ci_{Tank}}{\pi r_{Tank}^2 t_w} \times \frac{\pi r_{well}^2 t_w}{\pi r_{well}^2 D_b \rho} \qquad (5\text{-}3)$$

Simplifying results in

$$C_{s,i} = 1 \times 10^{12} \times \frac{Ci_{Tank}}{\pi r_{Tank}^2 D_b \rho} \qquad (5\text{-}4)$$

This equation is independent of the waste thickness or grout mixing thickness. Also, the radius of the well is not present in the equation. However, it must be noted that the concentration in the soil will be the same for any given well radius but the total amount of contaminated soil will vary with the well radius. This equation assumes that the radionuclide activity is completely mixed with the drill cuttings. The radionuclide activity would not likely be completely mixed with the drill cuttings. However, when considering the different possibilities, such as the cuttings from the tank being covered with cuttings from below the tank, it seems appropriate to make this gross assumption of complete mixing.

Contaminated sand pads are located beneath Tanks WM-185 and WM-187. Equation (5-4) can be expanded to include this contamination as follows:

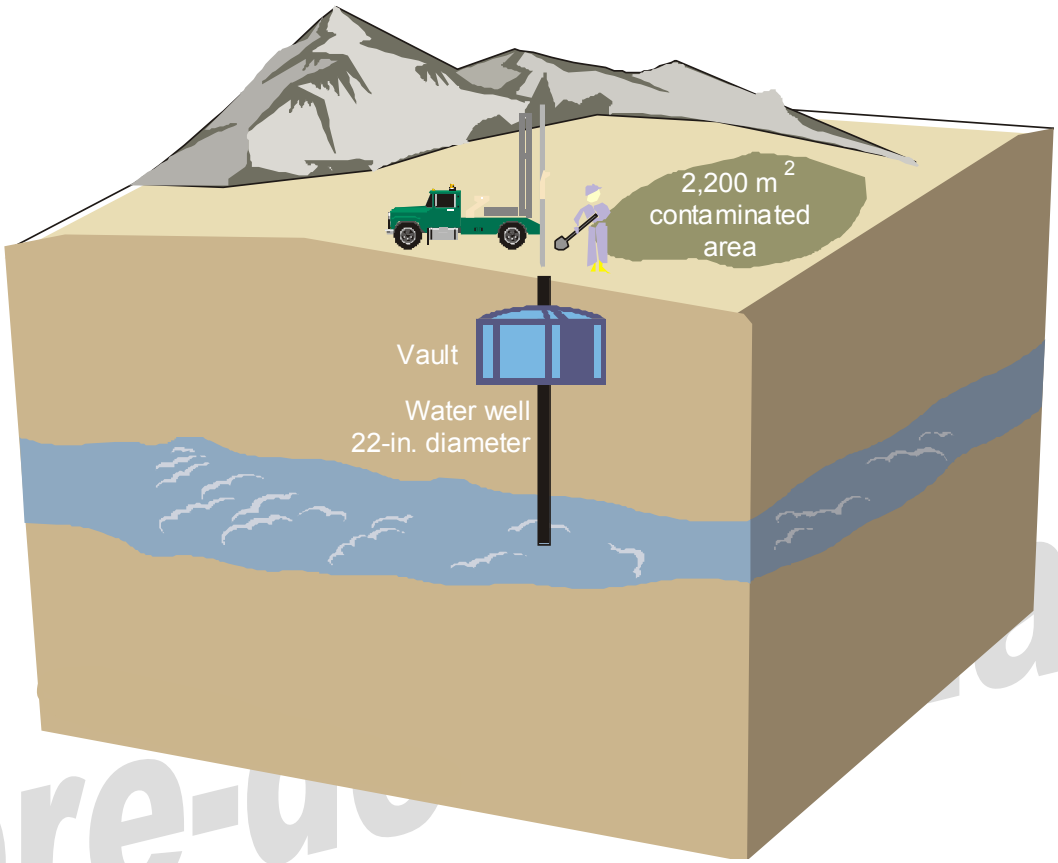

Figure 5-1. Graphical representation of the acute intruder-drilling scenario.

$$C_{s,i} = \frac{1\times10^{12}}{\pi D_b \rho} \times \left(\frac{Ci_{Tank}}{r^2_{Tank}} + \frac{Ci_{sand\ pad}}{r^2_{sand\ pad}} \right) \qquad (5\text{-}5)$$

where

$Ci_{sand\ pad}$ = activity in the sand pad (Ci)

$r_{sand\ pad}$ = radius of the sand pad (m).

In all cases, the depletion of the tank and sand pad radioactivities by leaching from water infiltration was not considered. The only mechanism for loss of activity in the tank and sand pad was by radioactive decay.

The depth of the borehole (D_b) was assumed to be 122 m (400 ft) to the aquifer (Rodriguez et al. 1997). The bulk density (ρ) was assumed to be 1.6E+06 g/m^3 (INEEL 1999b). When the volume of soil and waste excavated by the 22-in.-diameter well ($\pi r^2_{well} \times D_b$=30 m^3) is spread over 2,200 m^2, the final contaminated zone is approximately 0.014 m (0.54 in.) thick.

The unit concentration dose factor ($DF_{inh,i}$) for the inhalation of suspended cuttings was calculated as follows:

$$DF_{inh,i} = DCF_{inh,i} \times ASR \times f_{inh} \times I_{inh} \qquad (5\text{-}6)$$

where

$DF_{inh,i}$ = committed effective dose equivalent for inhalation of radionuclide i per unit soil concentration (mrem/yr per pCi/g)

$DCF_{inh,i}$ = inhalation dose conversion factor for radionuclide i (mrem/pCi)

ASR = soil mass loading in air (g/m^3)

f_{inh} = occupancy factor for inhalation pathway (dimensionless)

I_{inh} = annual intake of air (m^3/yr).

The committed effective dose equivalent (CEDE) from inhalation of suspended cuttings can be calculated for the radionuclide soil concentrations by multiplying them by the respective unit concentration dose factor ($DF_{inh,i}$).

The dose conversion factors used were taken from Federal Guidance Reports 11 and 12 (EPA 1988, 1993). The most conservative values were used in the intruder analysis. This approach is considered reasonable since no information is available on the chemical and physical form of the waste constituents. The soil mass loading was assumed to be 1 mg/m^3 (EG&G Idaho 1984), representative of construction activities. The inhalation occupancy factor is the fraction of time of a year spent onsite (0.018 or 160 hr/yr) (Seitz 1991). The annual intake of air was assumed to be 8,400 m^3/yr.

The unit concentration dose factor ($DF_{ext,i}$) for external radiation dose was calculated as follows:

$$DF_{ext,i} = DCF_{ext,i} \times f_{ext} \times \rho \quad (5\text{-}7)$$

where

$DF_{ext,i}$ = unit concentration dose factor for external exposure to radionuclide i per unit soil concentration (mrem/yr per pCi/g)

$DCF_{ext,i}$ = external dose conversion factor for radionuclide i (mrem/yr per pCi/m^3)

f_{ext} = occupancy factor for external radiation (dimensionless)

ρ = soil bulk density (g/m^3).

The EDE from external radiation exposure can be calculated for the radionuclide soil concentrations by multiplying them by the respective unit concentration dose factor ($DF_{ext,i}$). The occupancy factor for external radiation is the fraction of a year spent at the site (0.018 or 160 hr/yr) (Seitz 1991). The soil density was assumed to be 1.6E+06 g/m^3 (Rodriguez et al. 1997). External dose conversion factors for contaminated soil 1 cm (0.4 in.) thick with infinite lateral extent were used in the calculations from Federal Guidance Report 12 (EPA 1993).

The unit concentration dose factor ($DF_{ing,i}$) for inadvertent soil ingestion was calculated as follows:

$$DF_{ing,i} = DCF_{ing,i} \times f_{soil} \times I_{soil} \quad (5\text{-}8)$$

where

$DF_{ing,i}$ = unit concentration dose factor for inadvertent soil ingestion of radionuclide i per unit soil concentration (mrem/yr per pCi/g)

$DCF_{ing,i}$ = ingestion dose conversion factor for radionuclide i (mrem/pCi)

f_{soil} = occupancy factor for inadvertent soil ingestion (dimensionless)

I_{soil} = annual consumption rate of soil (g/yr).

The CEDE from inadvertent soil ingestion can be calculated for the radionuclide soil concentrations by multiplying them by the respective unit concentration dose factor ($DF_{ing,i}$).

The occupancy factor for inadvertent soil ingestion is the fraction of a year spent at the site (0.018 or 160 hr/yr) (Seitz 1991). The annual soil ingestion rate was assumed to be 40 g/yr (1.4 oz/yr) (Calabrese et al. 1990).

The dose from inhalation of ^{3}H was calculated assuming HTO was the only form present. The CEDE from inhalation and dermal absorption of HTO was calculated from

$$D_{inh,H-3} = 1.5 \times DCF_{inh} \times I_{inh} \times f_{inh} \times C_{a,H-3} \quad (5\text{-}9)$$

where

$D_{inh,H-3}$ = CEDE from inhalation and absorption of HTO (mrem/yr)

1.5 = factor to adjust the dose factor (DCF_{inh}) to account for absorption of ^{3}H through the skin

$C_{a,H-3}$ = activity concentration of HTO in air (pCi/m^3).

The concentration of HTO in air was calculated assuming that all of the HTO is in the soil pore water. The flux from the surface is the product of the soil pore water ^{3}H concentration and annual evapotranspiration. This flux is assumed to be mixed into a 2-m (7-ft) mixing zone. The concentration of HTO in air is given by

$$C_{a,H-3} = \frac{3.17 \times 10^{-8} \times 0.5 \times \frac{\rho C_s}{\theta_v} \times E_t \times \sqrt{A}}{H_{mix} \times U} \quad (5\text{-}10)$$

where

3.17×10^{-8} = conversion factor (yr/s)

0.5 = fraction of time wind is blowing toward receptor (dimensionless)

C_s = concentration in the soil (pCi/g)

θ_v = volumetric water content (dimensionless)

E_t = evapotranspiration rate (m/yr)

A = area of the contaminated zone (m^2)

H_{mix} = height of atmospheric mixing zone (m)

U = mean wind speed (m/s).

The volumetric water content of the well borehole cuttings was assumed to be the same as the near-surface alluvium, 0.28 (taken from the groundwater modeling results presented in Section 3). The evapotranspiration rate is the annual quantity of water evaporated from the surface, which was assigned a value of 0.15 m/yr (Maheras et al. 1994). The height of the atmospheric mixing zone and mean wind speed were conservatively assumed to be 2 m and 2 m/s, respectively.

The dose from inhalation of ^{14}C was calculated in a similar fashion. All airborne ^{14}C was assumed to be $^{14}CO_2$. The CEDE from inhalation of $^{14}CO_2$ was calculated as follows:

$$D_{inh,C-14} = DCF_{inh} \times I_{inh} \times f_{inh} \times C_{a,C-14} \quad (5\text{-}11)$$

where

$D_{inh,C-14}$ = CEDE from inhalation of $^{14}CO_2$ (mrem/yr)

$C_{a,C-14}$ = activity concentration of $^{14}CO_2$ in air (pCi/m^3).

The concentration of $^{14}CO_2$ in air was estimated from

$$C_{a,C-14} = \frac{3.17 \times 10^{-8} \times 0.5 \times EVSN \times \sqrt{A}}{H_{mix} \times U} \quad (5\text{-}12)$$

where

$EVSN$ = the $^{14}CO_2$ evasion rate (pCi/m^2/yr).

The carbon evasion rate was estimated from

$$EVSN = 1 \times 10^6 \times C_{s,C-14} \times E \times \rho \times d_{ref} \quad (5\text{-}13)$$

where

$C_{s,C-14}$ = concentration of ^{14}C in contaminated soil (pCi/g)

E = carbon evasion rate constant (per yr)

d_{ref} = reference soil depth (m).

The carbon evasion rate constant was assumed to be 22/yr, which is the default value used in the RESRAD computer model (Yu et al. 1993). The soil layer releasing $^{14}CO_2$ was assumed to be equal to the depth of the contaminated zone [i.e., 0.014 m (0.54 in.)]. The same values for the area, mixing height, and wind speed used for ^{3}H also were used for ^{14}C.

The dose conversion factors from Federal Guidance Reports 11 and 12 (EPA 1988 and 1993) are listed in Table 5-1. The parameter values used in the acute intruder-drilling scenario are summarized in Table 5-2. The resulting unit concentration dose factors for inhalation, external exposure, and inadvertent soil ingestion for the acute drilling scenario are provided in Table 5-3.

The results of the analyses are given in Section 5.6.

5.3 Acute Intruder-Construction Scenario

The acute intruder-construction scenario assumes that an inadvertent intruder moves onto the TFF and excavates a 20 × 10 × 3-m (70 × 30 × 10-ft) excavation for a basement (Oztunali and Roles 1986).

The intruder is assumed to spend 160 hr working on the excavation of the basement. The exposure pathways for this acute scenario include inhalation of resuspended soil, external exposure to the ground surface, and inadvertent soil ingestion.

The determination of the unit concentration dose factors for each exposure pathway were determined using the equations in Section 5.2 for the acute intruder-drilling scenario with the exception that the external dose factors for contaminated soil were based on infinite thickness and infinite lateral extent from Federal Guidance Report 12 (EPA 1993).

The activity concentration of radionuclides in the excavation were determined by assuming that the radionuclide inventory in the 30% of the piping located within 3 m (10 ft) of the surface was located over the 5-acre (20,234-m^2) area of the TFF. The soil activity concentration in the 20 × 10 × 3-m (70 × 30 × 10-ft) excavation was then determined as follows:

$$C_{s,i} = \frac{C_p \; x \; M_p \; x \; P_L \; x \; E_A}{P_{TL} \; x \; T_A \; x \; E_v \; x \; \rho_s} \qquad (5\text{-}14)$$

where

$C_{s,i}$ = soil activity concentration of radionuclide i (pCi/g)

C_p = piping activity concentration of radionuclide i at the time of intrusion (pCi/kg)

M_p = mass of residual contamination in the piping (kg)

P_L = length of piping within 3 m of the surface (m)

E_A = area of the excavation (m)

P_{TL} = total piping length at TFF (m)

T_A = area of the TFF

E_v = volume of excavation (m^3)

ρ_s = bulk density of the soil (g/m^3).

The piping activity concentrations (C_p) were based on the solid tank inventory provided in Section 2. The mass of residual contamination in the piping (M_p) was 15.5 kg (34.2 lb) based on the piping inventory analysis provided in Appendix A. The total length of process piping at the TFF located within 3 m (10 ft)of the surface (P_L) is 975.4 m (3,200. ft). The area of the excavation (E_A) is 200 m^2 (20 × 10 m[70 × 30-ft]). The total length of the process piping at the TFF (P_{TL}) is 3230.9 m (10,600. ft). The area of the TFF (T_A) is 5 acres (20,234 m^2). The volume of the excavation (E_V) is 600 m^3 (20 × 10 × 3 m [70 × 30 × 10-ft]). The bulk density of the soil (ρ_s) was assumed to be 1E+06 g/m^3.

Table 5-1. Dose conversion factors used in the acute intruder-drilling scenario.

Nuclide	Inhalation DCF (mrem/pCi)	External DCF 1 cm (mrem/yr per pCi/g)	External DCF 15 cm (mrem/yr per pCi/g)	Ingestion DCF (mrem/pCi)
^{10}Be	3.54E–04	3.62E–04	1.06E–03	4.66E–06
^{14}C	2.09E–06	8.03E–06	1.34E–05	2.09E–06
^{113m}Cd	1.53E–03	2.24E–04	6.39E–04	1.61E–04
^{60}Co	2.19E–04	2.84E+00	1.35E+01	2.69E–05
^{135}Cs	4.55E–06	1.96E–05	3.83E–05	7.07E–06
^{154}Eu	2.86E–04	1.42E+00	6.58E+00	9.55E–06
^{3}H	6.40E–08	0.00E+00	0.00E+00	6.40E–08
^{166m}Ho	7.73E–04	2.04E+00	9.15E+00	8.07E–06
^{129}I	1.74E–04	1.11E–02	1.29E–02	2.76E–04
^{115}In	3.74E–03	1.47E–04	3.96E–04	1.58E–04
^{138}La	1.37E–03	1.39E+00	6.63E+00	5.88E–06
^{94}Nb	4.44E–04	1.84E+00	8.46E+00	7.14E–06
^{63}Ni	3.10E–06	0.00E+00	0.00E+00	5.77E–07
^{107}Pd	1.28E–05	0.00E+00	0.00E+00	1.49E–07
^{146}Pm	1.47E–04	8.80E–01	3.94E+00	3.67E–06
^{87}Rb	3.23E–06	6.16E–05	1.40E–04	4.92E–06
^{79}Se	9.84E–06	1.08E–05	1.86E–05	8.70E–06
^{146}Sm	8.25E–02	0.00E+00	0.00E+00	2.04E–04
^{151}Sm	3.00E–05	9.75E–07	9.84E–07	3.89E–07
^{121m}Sn	1.15E–05	1.75E–03	1.96E–03	1.55E–06
^{98}Tc	2.29E–05	1.66E+00	7.58E+00	4.88E–06
^{99}Tc	8.33E–06	5.45E–05	1.25E–04	1.46E–06
^{123}Te	1.05E–05	6.26E–03	6.56E–03	4.18E–06
Short Decay Chains				
^{108}Ag	0.00E+00	2.34E–02	1.03E–01	0.00E+00
^{108m}Ag	2.83E–04	1.91E+00	8.61E+00	7.62E–06
^{137m}Ba	0.00E+00	7.02E–01	3.19E+00	0.00E+00
^{137}Cs	3.19E–05	2.50E–04	7.36E–04	5.00E–05
^{152}Eu	2.21E–04	1.31E+00	6.01E+00	6.48E–06
^{152}Gd	2.43E–01	0.00E+00	0.00E+00	1.61E–04

Table 5-1. (continued).

Nuclide	Inhalation DCF (mrem/pCi)	External DCF 1 cm (mrem/yr per pCi/g)	External DCF 15 cm (mrem/yr per pCi/g)	Ingestion DCF (mrem/pCi)
^{93m}Nb	2.92E–05	1.04E–04	1.04E–04	5.22E–07
^{147}Pm	3.92E–05	2.22E–05	4.99E–05	1.05E–06
^{126}Sb	1.17E–05	3.34E+00	1.52E+01	1.07E–05
^{126m}Sb	3.39E–08	1.83E+00	8.29E+00	9.36E–08
^{147}Sm	7.47E–02	0.00E+00	0.00E+00	1.85E–04
^{126}Sn	9.95E–05	5.32E–02	1.48E–01	1.95E–05
^{90}Sr	1.30E–03	2.45E–04	6.95E–04	1.42E–04
^{90}Y	8.44E–06	5.79E–03	2.24E–02	1.08E–05
^{93}Zr	3.21E–04	0.00E+00	0.00E+00	1.66E–06
Decay Chain 1				
^{228}Ac	3.08E–04	1.12E+00	5.16E+00	2.16E–06
^{212}Bi	2.16E–05	2.15E–01	1.00E+00	1.06E–06
^{252}Cf	1.57E–01	1.30E–04	1.76E–04	1.08E–03
^{244}Cm	2.48E–01	1.22E–04	1.26E–04	2.02E–03
^{248}Cm	1.65E+00	8.44E–05	8.78E–05	1.36E–02
^{240}Np	8.14E–08	1.51E+00	6.82E+00	2.37E–07
^{240m}Np	0.00E+00	3.89E–01	1.77E+00	0.00E+00
^{212}Pb	1.69E–04	1.70E–01	6.76E–01	4.55E–05
^{212}Po	0.00E+00	0.00E+00	0.00E+00	0.00E+00
^{216}Po	0.00E+00	1.98E–05	9.10E–05	0.00E+00
^{236}Pu	1.45E–01	1.56E–04	2.24E–04	1.17E–03
^{240}Pu	4.29E–01	1.16E–04	1.46E–04	3.54E–03
^{244}Pu	4.03E–01	7.19E–05	7.55E–05	3.32E–03
^{224}Ra	3.16E–03	1.16E–02	4.89E–02	3.66E–04
^{228}Ra	4.77E–03	0.00E+00	0.00E+00	1.44E–03
^{220}Rn	0.00E+00	4.58E–04	2.05E–03	0.00E+00
^{228}Th	3.42E–01	2.28E–03	7.79E–03	3.96E–04
^{232}Th	1.64E+00	2.17E–04	5.19E–04	2.73E–03
^{208}Tl	0.00E+00	3.66E+00	1.81E+01	0.00E+00
^{232}U	1.49E–02	3.51E–04	8.91E–04	1.31E–03

Table 5-1. (continued).

Nuclide	Inhalation DCF (mrem/pCi)	External DCF 1 cm (mrem/yr per pCi/g)	External DCF 15 cm (mrem/yr per pCi/g)	Ingestion DCF (mrem/pCi)
^{236}U	1.25E–01	1.22E–04	2.13E–04	2.69E–04
^{240}U	2.27E–06	1.05E–03	1.42E–03	4.44E–06
Decay Chain 2				
^{225}Ac	1.08E–02	1.79E–02	6.24E–02	1.11E–04
^{241}Am	4.44E–01	2.15E–02	4.37E–02	3.64E–03
^{217}At	0.00E+00	3.64E–04	1.61E–03	0.00E+00
^{213}Bi	1.71E–05	1.59E–01	7.01E–01	7.22E–07
^{249}Cf	5.77E–01	3.94E–01	1.72E+00	4.74E–03
^{245}Cm	4.55E–01	9.79E–02	3.36E–01	3.74E–03
^{221}Fr	0.00E+00	3.61E–02	1.48E–01	0.00E+00
^{237}Np	5.40E–01	2.58E–02	7.77E–02	4.44E–03
^{233}Pa	9.55E–06	2.32E–01	9.64E–01	3.63E–06
^{209}Pb	9.47E–08	2.62E–04	7.62E–04	2.13E–07
^{213}Po	0.00E+00	0.00E+00	0.00E+00	0.00E+00
^{241}Pu	8.25E–03	1.79E–06	5.88E–06	6.85E–05
^{225}Ra	7.77E–03	7.92E–03	1.10E–02	3.85E–04
^{229}Th	2.15E+00	9.51E–02	3.18E–01	3.53E–03
^{209}Tl	0.00E+00	2.30E+00	1.08E+01	0.00E+00
^{233}U	1.35E–01	4.03E–04	1.35E–03	2.89E–04
^{237}U	3.53E–06	1.49E–01	5.19E–01	3.17E–06
Decay Chain 3				
^{227}Ac	6.70E+00	1.44E–04	4.89E–04	1.41E–02
^{243}Am	4.40E–01	5.53E–02	1.42E–01	3.62E–03
^{211}Bi	0.00E+00	5.53E–02	2.39E–01	0.00E+00
^{251}Cf	5.88E–01	1.38E–01	5.16E–01	4.85E–03
^{243}Cm	3.07E–01	1.46E–01	5.64E–01	2.51E–03
^{247}Cm	4.14E–01	3.74E–01	1.64E+00	3.42E–03
^{223}Fr	7.84E–03	5.79E–02	1.89E–01	8.62E–06
^{239}Np	2.51E–06	1.91E–01	7.29E–01	3.26E–06
^{231}Pa	1.28E+00	4.30E–02	1.80E–01	1.06E–02

Table 5-1. (continued).

Nuclide	Inhalation DCF (mrem/pCi)	External DCF 1 cm (mrem/yr per pCi/g)	External DCF 15 cm (mrem/yr per pCi/g)	Ingestion DCF (mrem/pCi)
^{211}Pb	7.53E–06	6.07E–02	2.73E–01	5.25E–07
^{211}Po	0.00E+00	9.13E–03	4.18E–02	0.00E+00
^{215}Po	0.00E+00	2.11E–04	9.30E–04	0.00E+00
^{239}Pu	4.29E–01	1.05E–04	2.84E–04	3.54E–03
^{243}Pu	1.64E–07	2.58E–02	7.85E–02	3.34E–07
^{223}Ra	7.84E–03	1.51E–01	5.79E–01	6.59E–04
^{219}Rn	0.00E+00	6.65E–02	2.88E–01	0.00E+00
^{227}Th	1.62E–02	1.21E–01	4.95E–01	3.81E–05
^{231}Th	8.77E–07	1.32E–02	3.62E–02	1.35E–06
^{207}Tl	0.00E+00	4.22E–03	1.77E–02	0.00E+00
^{235}U	1.23E–01	1.77E–01	7.06E–01	2.66E–04
Decay Chain 4				
^{242}Am	5.85E–05	1.53E–02	4.99E–02	1.41E–06
^{242m}Am	4.26E–01	8.01E–04	1.68E–03	3.52E–03
^{210}Bi	1.96E–04	1.03E–03	3.47E–03	6.40E–06
^{214}Bi	6.59E–06	1.71E+00	8.14E+00	2.83E–07
^{250}Cf	2.62E–01	1.16E–04	1.18E–04	2.13E–03
^{242}Cm	1.73E–02	1.42E–04	1.69E–04	1.15E–04
^{246}Cm	4.51E–01	1.11E–04	1.16E–04	3.70E–03
^{238}Np	3.70E–05	6.31E–01	2.95E+00	4.00E–06
^{234}Pa	8.14E–07	2.20E+00	1.00E+01	2.16E–06
^{234m}Pa	0.00E+00	1.78E–02	7.85E–02	0.00E+00
^{210}Pb	1.36E–02	1.54E–03	2.45E–03	5.37E–03
^{214}Pb	7.81E–06	2.93E–01	1.25E+00	6.25E–07
^{210}Po	9.40E–03	9.94E–06	4.58E–05	1.90E–03
^{214}Po	0.00E+00	9.75E–05	4.48E–04	0.00E+00
^{218}Po	0.00E+00	1.06E–05	4.91E–05	0.00E+00
^{238}Pu	3.92E–01	1.18E–04	1.51E–04	3.20E–03
^{242}Pu	4.11E–01	9.77E–05	1.28E–04	3.36E–03
^{226}Ra	8.58E–03	7.75E–03	3.08E–02	1.32E–03

Table 5-1. (continued).

Nuclide	Inhalation DCF (mrem/pCi)	External DCF 1 cm (mrem/yr per pCi/g)	External DCF 15 cm (mrem/yr per pCi/g)	Ingestion DCF (mrem/pCi)
^{222}Rn	0.00E+00	4.74E–04	2.13E–03	0.00E+00
^{230}Th	3.26E–01	4.35E–04	1.19E–03	5.48E–04
^{234}Th	3.50E–05	8.52E–03	2.41E–02	1.37E–05
^{234}U	1.32E–01	1.89E–04	4.00E–04	2.83E–04
^{238}U	1.18E–01	8.26E–05	1.03E–04	2.55E–04

Table 5-2. Parameter values used in the acute intruder-drilling scenario.

Parameter	Description	Value
A	Area of contaminated zone (m^2)	2,200
ASR	Soil mass loading in air (g/m^3)	1E–03
D_b	Total depth of well borehole (m)	122
d_{ref}	Reference soil depth (m)	0.014
E	Carbon evasion rate constant (per yr)	22
E_t	Evapotranspiration rate (m/yr)	0.15
f_{ext}	Occupancy factor for external exposure (unitless)	0.018
f_{inh}	Occupancy factor for inhalation (unitless)	0.018
f_{soil}	Occupancy factor for soil ingestion (unitless)	0.018
H_{mix}	Height of mixing zone (m)	2
I_{inh}	Annual intake of air (m^3/yr)	8,400
I_{soil}	Annual consumption rate of soil (g/yr)	40
$r_{sand\ pad}$	Radius of the sand pad (m)	7.8
r_{Tank}	Radius of the tank (m)	7.6
r_{well}	Radius of the well (m)	0.28
ρ	Bulk density of the well cuttings (g/m^3)	1.6E+06
θ_v	Volumetric water content (unitless)	0.28
t_w	Thickness of waste zone (m)	0.15
U	Mean wind speed (m/s)	2

Table 5-3. Unit concentration dose factors for acute intruder-drilling scenario.

Nuclide	Unit DF Inhalation	Unit DF External	Unit DF Ingestion	Unit DF Total
	(mrem/yr per pCi/g)			
^{10}Be	5.44E–05	6.62E–06	3.41E–06	6.44E–05
^{14}C	3.21E–04	1.47E–07	1.53E–06	3.22E–04
^{113m}Cd	2.34E–04	4.09E–06	1.18E–04	3.56E–04
^{60}Co	3.35E–05	5.19E–02	1.97E–05	5.19E–02
^{135}Cs	6.98E–07	3.58E–07	5.16E–06	6.22E–06
^{154}Eu	4.39E–05	2.60E–02	6.97E–06	2.60E–02
^{3}H	1.47E–05	0.00E+00	4.68E–08	1.48E–05
^{166m}Ho	1.19E–04	3.72E–02	5.89E–06	3.73E–02
^{129}I	2.66E–05	2.03E–04	2.02E–04	4.31E–04
^{115}In	5.73E–04	2.69E–06	1.15E–04	6.91E–04
^{138}La	2.10E–04	2.55E–02	4.30E–06	2.57E–02
^{94}Nb	6.81E–05	3.36E–02	5.22E–06	3.37E–02
^{63}Ni	4.76E–07	0.00E+00	4.22E–07	8.98E–07
^{107}Pd	1.96E–06	0.00E+00	1.09E–07	2.07E–06
^{146}Pm	2.25E–05	1.61E–02	2.68E–06	1.61E–02
^{87}Rb	4.96E–07	1.13E–06	3.60E–06	5.22E–06
^{79}Se	1.51E–06	1.97E–07	6.35E–06	8.06E–06
^{146}Sm	1.27E–02	0.00E+00	1.49E–04	1.28E–02
^{151}Sm	4.60E–06	1.78E–08	2.84E–07	4.90E–06
^{121m}Sn	1.77E–06	3.20E–05	1.13E–06	3.49E–05
^{98}Tc	3.51E–06	3.04E–02	3.57E–06	3.04E–02
^{99}Tc	1.28E–06	9.96E–07	1.07E–06	3.34E–06
^{123}Te	1.62E–06	1.14E–04	3.05E–06	1.19E–04
Short Decay Chains				
^{108}Ag	0.00E+00	4.26E–04	0.00E+00	4.26E–04
^{108m}Ag	4.35E–05	3.48E–02	5.57E–06	3.49E–02
^{137m}Ba	0.00E+00	1.28E–02	0.00E+00	1.28E–02
^{137}Cs	4.90E–06	4.57E–06	3.65E–05	4.60E–05
^{152}Eu	3.39E–05	2.40E–02	4.73E–06	2.40E–02
^{152}Gd	3.74E–02	0.00E+00	1.17E–04	3.75E–02
^{93m}Nb	4.48E–06	1.91E–06	3.81E–07	6.77E–06
^{147}Pm	6.02E–06	4.06E–07	7.65E–07	7.19E–06

Table 5-3. (continued).

Nuclide	Unit DF Inhalation	Unit DF External	Unit DF Ingestion	Unit DF Total
	(mrem/yr per pCi/g)			
^{126}Sb	1.80E–06	6.11E–02	7.81E–06	6.11E–02
^{126m}Sb	5.21E–09	3.34E–02	6.84E–08	3.34E–02
^{147}Sm	1.15E–02	0.00E+00	1.35E–04	1.16E–02
^{126}Sn	1.53E–05	9.72E–04	1.42E–05	1.00E–03
^{90}Sr	1.99E–04	4.47E–06	1.04E–04	3.08E–04
^{90}Y	1.29E–06	1.06E–04	7.87E–06	1.15E–04
^{93}Zr	4.92E–05	0.00E+00	1.21E–06	5.04E–05
Decay Chain 1				
^{228}Ac	4.73E–05	2.04E–02	1.58E–06	2.04E–02
^{212}Bi	3.31E–06	3.92E–03	7.76E–07	3.93E–03
^{252}Cf	2.41E–02	2.37E–06	7.92E–04	2.49E–02
^{244}Cm	3.80E–02	2.23E–06	1.47E–03	3.95E–02
^{248}Cm	2.54E–01	1.54E–06	9.95E–03	2.64E–01
^{240}Np	1.25E–08	2.76E–02	1.73E–07	2.76E–02
^{240m}Np	0.00E+00	7.10E–03	0.00E+00	7.10E–03
^{212}Pb	2.59E–05	3.11E–03	3.32E–05	3.17E–03
^{212}Po	0.00E+00	0.00E+00	0.00E+00	0.00E+00
^{216}Po	0.00E+00	3.62E–07	0.00E+00	3.62E–07
^{236}Pu	2.22E–02	2.85E–06	8.52E–04	2.31E–02
^{240}Pu	6.59E–02	2.12E–06	2.58E–03	6.84E–02
^{244}Pu	6.19E–02	1.31E–06	2.42E–03	6.43E–02
^{224}Ra	4.84E–04	2.12E–04	2.67E–04	9.64E–04
^{228}Ra	7.32E–04	0.00E+00	1.05E–03	1.78E–03
^{220}Rn	0.00E+00	8.36E–06	0.00E+00	8.36E–06
^{228}Th	5.24E–02	4.16E–05	2.89E–04	5.27E–02
^{232}Th	2.51E–01	3.96E–06	1.99E–03	2.53E–01
^{208}Tl	0.00E+00	6.69E–02	0.00E+00	6.69E–02
^{232}U	2.28E–03	6.41E–06	9.57E–04	3.25E–03
^{236}U	1.92E–02	2.23E–06	1.96E–04	1.94E–02
^{240}U	3.48E–07	1.92E–05	3.24E–06	2.28E–05
Decay Chain 2				
^{225}Ac	1.66E–03	3.26E–04	8.11E–05	2.06E–03
^{241}Am	6.81E–02	3.92E–04	2.66E–03	7.12E–02

Table 5-3. (continued).

Nuclide	Unit DF Inhalation	Unit DF External	Unit DF Ingestion	Unit DF Total
	(mrem/yr per pCi/g)			
^{217}At	0.00E+00	6.65E–06	0.00E+00	6.65E–06
^{213}Bi	2.63E–06	2.91E–03	5.27E–07	2.91E–03
^{249}Cf	8.86E–02	7.20E–03	3.46E–03	9.92E–02
^{245}Cm	6.98E–02	1.79E–03	2.73E–03	7.43E–02
^{221}Fr	0.00E+00	6.58E–04	0.00E+00	6.58E–04
^{237}Np	8.29E–02	4.71E–04	3.24E–03	8.66E–02
^{233}Pa	1.46E–06	4.23E–03	2.65E–06	4.23E–03
^{209}Pb	1.45E–08	4.78E–06	1.55E–07	4.95E–06
^{213}Po	0.00E+00	0.00E+00	0.00E+00	0.00E+00
^{241}Pu	1.27E–03	3.28E–08	5.00E–05	1.32E–03
^{225}Ra	1.19E–03	1.45E–04	2.81E–04	1.62E–03
^{229}Th	3.29E–01	1.74E–03	2.58E–03	3.34E–01
^{209}Tl	0.00E+00	4.20E–02	0.00E+00	4.20E–02
^{233}U	2.08E–02	7.37E–06	2.11E–04	2.10E–02
^{237}U	5.42E–07	2.72E–03	2.32E–06	2.72E–03
Decay Chain 3				
^{227}Ac	1.03E+00	2.63E–06	1.03E–02	1.04E+00
^{243}Am	6.76E–02	1.01E–03	2.65E–03	7.12E–02
^{211}Bi	0.00E+00	1.01E–03	0.00E+00	1.01E–03
^{251}Cf	9.03E–02	2.52E–03	3.54E–03	9.63E–02
^{243}Cm	4.71E–02	2.66E–03	1.84E–03	5.16E–02
^{247}Cm	6.36E–02	6.82E–03	2.50E–03	7.29E–02
^{223}Fr	1.20E–03	1.06E–03	6.30E–06	2.27E–03
^{239}Np	3.85E–07	3.48E–03	2.38E–06	3.48E–03
^{231}Pa	1.97E–01	7.85E–04	7.73E–03	2.05E–01
^{211}Pb	1.16E–06	1.11E–03	3.84E–07	1.11E–03
^{211}Po	0.00E+00	1.67E–04	0.00E+00	1.67E–04
^{215}Po	0.00E+00	3.86E–06	0.00E+00	3.86E–06
^{239}Pu	6.59E–02	1.91E–06	2.58E–03	6.84E–02
^{243}Pu	2.52E–08	4.71E–04	2.44E–07	4.71E–04
^{223}Ra	1.20E–03	2.76E–03	4.81E–04	4.45E–03
^{219}Rn	0.00E+00	1.21E–03	0.00E+00	1.21E–03
^{227}Th	2.48E–03	2.21E–03	2.78E–05	4.72E–03

Table 5-3. (continued).

Nuclide	Unit DF Inhalation	Unit DF External	Unit DF Ingestion	Unit DF Total
	(mrem/yr per pCi/g)			
^{231}Th	1.35E–07	2.40E–04	9.87E–07	2.41E–04
^{207}Tl	0.00E+00	7.71E–05	0.00E+00	7.71E–05
^{235}U	1.88E–02	3.24E–03	1.94E–04	2.23E–02
Decay Chain 4				
^{242}Am	8.97E–06	2.79E–04	1.03E–06	2.89E–04
^{242m}Am	6.53E–02	1.46E–05	2.57E–03	6.79E–02
^{210}Bi	3.00E–05	1.89E–05	4.68E–06	5.36E–05
^{214}Bi	1.01E–06	3.12E–02	2.07E–07	3.12E–02
^{250}Cf	4.02E–02	2.12E–06	1.56E–03	4.18E–02
^{242}Cm	2.65E–03	2.59E–06	8.38E–05	2.74E–03
^{246}Cm	6.93E–02	2.03E–06	2.70E–03	7.20E–02
^{238}Np	5.68E–06	1.15E–02	2.92E–06	1.15E–02
^{234}Pa	1.25E–07	4.03E–02	1.58E–06	4.03E–02
^{234m}Pa	0.00E+00	3.25E–04	0.00E+00	3.25E–04
^{210}Pb	2.08E–03	2.82E–05	3.92E–03	6.03E–03
^{214}Pb	1.20E–06	5.36E–03	4.57E–07	5.36E–03
^{210}Po	1.44E–03	1.82E–07	1.39E–03	2.83E–03
^{214}Po	0.00E+00	1.78E–06	0.00E+00	1.78E–06
^{218}Po	0.00E+00	1.94E–07	0.00E+00	1.94E–07
^{238}Pu	6.02E–02	2.16E–06	2.34E–03	6.25E–02
^{242}Pu	6.30E–02	1.78E–06	2.45E–03	6.55E–02
^{226}Ra	1.32E–03	1.42E–04	9.68E–04	2.43E–03
^{222}Rn	0.00E+00	8.67E–06	0.00E+00	8.67E–06
^{230}Th	5.00E–02	7.95E–06	4.00E–04	5.04E–02
^{234Th}	5.38E–06	1.56E–04	9.97E–06	1.71E–04
^{234}U	2.03E–02	3.45E–06	2.07E–04	2.05E–02
^{238}U	1.82E–02	1.51E–06	1.86E–04	1.84E–02

The results of the intruder-construction analyses are given in Section 5.6.

5.4 Chronic Intruder Post-Drilling Scenario Definition

The chronic post-drilling scenario assumes that an inadvertent intruder moves onto the TFF and drills a residential well into the waste. The drilling portion of the scenario evaluates a 6-in. residential well. This type of well serves a single residence and provides sufficient water for a family garden and small quantities of livestock. As described in the acute drilling scenario, large-diameter wells are drilled to serve irrigation systems (i.e., hundreds of acres) that are located in the middle of farm fields, not near a farmer's residence. Therefore, in the chronic post-drilling scenario, the residence/home garden is evaluated using the traditional drinking water well diameter of 6 in.

The drill cuttings that are brought to the surface are assumed to be spread over 2,200 m^2 (24,000 ft or approximately one-half acre) of land surface. The waste is assumed to be mixed to a depth of 0.61 m (24 in.). The mixing depth of 0.61 m is based on using a deep tilling plow to increase the depth of the root zone and to break up soil compaction. To minimize erosion these plows are used in areas of southeast Idaho with highly erodible soils. Deep tilling plows have shanks that till to a depth of 24 in. and are sold at Idaho Falls implement dealers (Maheras et al. 1997).

The chronic post-drilling scenario assumes that the intruder is exposed to the drill cuttings during plowing and cultivation (i.e., dust inhalation). In addition, the intruder is assumed to ingest contaminated food products from the garden and from beef and milk cattle consuming contaminated forage. The intake of contaminated forage by cattle was adjusted according to the fraction of feed grown on contaminated cuttings and the necessary remaining feed obtained from uncontaminated ground. Figure 5-2 illustrates the chronic intruder post-drilling scenario.

The activity concentration of radionuclides in the contaminated zone is calculated as follows:

$$C_{s,i} = 1 \times 10^{12} \times C_{w,i} \times \frac{\pi r_{well}^2 t_w}{A_c D_c \rho} \qquad (5\text{-}15)$$

Figure 5-2. Chronic intruder post-drilling scenario.

where

$C_{s,i}$ = soil activity concentration of radionuclide i (pCi/g)

1×10^{12} = factor for converting Ci to pCi

$C_{w,i}$ = waste activity concentration of radionuclide i at the time of intrusion (Ci/m^3)

r_{well} = radius of the well borehole (m)

t_w = thickness of the waste zone (m)

A_c = area over which contamination is spread (m^2)

D_c = final depth of the contaminated zone after tilling (m)

ρ = bulk density of the soil (g/m^3)

since

$$C_{w,i} = \frac{Ci_{Tank}}{\pi r_{Tank}^2 t_w} \quad \text{and} \quad A_c = \pi r_{cont}^2 \qquad (5\text{-}16)$$

where

Ci_{Tank} = activity in the tank (Ci)

r_{Tank} = radius of the tank (m)

r_{cont} = radius of the contaminated zone (m).

Then by substitution

$$C_{s,i} = 1 \times 10^{12} \times \frac{Ci_{\text{Tank}}}{\pi r_{\text{Tank}}^2 t_w} \times \frac{\pi r_{well}^2 t_w}{\pi r_{cont}^2 D_c \rho} \qquad (5\text{-}17)$$

Simplifying results in

$$C_{s,i} = 1 \times 10^{12} \times \frac{Ci_{\text{Tank}} r_{well}^2}{\pi r_{\text{Tank}}^2 r_{cont}^2 D_c \rho} \qquad (5\text{-}18)$$

The equation can be expanded to include the contribution from sand pad contamination as follows:

$$C_{s,i} = 1 \times 10^{12} \times \left(\frac{Ci_{Tank} r_{well}^2}{\pi r_{Tank}^2 r_{cont}^2 D_c \rho} + \frac{Ci_{sand\ pad} r_{sand\ pad}^2}{\pi r_{sand\ pad}^2 r_{cont}^2 D_c \rho} \right) \qquad (5\text{-}19)$$

where

$Ci_{sand\ pad}$ = activity in the sand pad (Ci)

$r_{sand\ pad}$ = radius of the sand pad (m).

The unit concentration dose factor ($DF_{ing,soil,i}$) for inadvertent soil ingestion was calculated using Equation (5-8). The annual soil ingestion rate from outdoor air was assumed to be 10 mg/d or 3.65 g/yr (Konz et al. 1989).

The intruder was assumed to be indoors 50% of the time, outdoors 25% of the time, and offsite for 25% of the time, resulting in a soil ingestion occupancy factor of 0.75.

The unit concentration dose factor ($DF_{inh,i}$) for the inhalation of suspended cuttings was calculated as follows:

$$DF_{inh,i} = DCF_{inh,i} \times ASR \times \left[f_{inh,outdoor} + \left(f_{inh,indoor} \times S_{inh} \right) \right] \times I_{inh} \qquad (5\text{-}20)$$

where

$DF_{inh,i}$ = unit concentration dose factor for inhalation of radionuclide i per unit soil concentration (mrem/yr per pCi/g)

$DCF_{inh,i}$ = inhalation dose conversion factor for radionuclide i (mrem/pCi)

ASR = soil mass loading in air (g/m^3)

$f_{inh,outdoor}$ = occupancy factor for inhalation pathway outside the home (dimensionless)

$f_{inh,indoor}$ = occupancy factor for inhalation pathway inside the home (dimensionless)

S_{inh} = shielding factor for dust inside the home (dimensionless)

I_{inh} = annual intake of air (m^3/yr).

The CEDE from inhalation of suspended cuttings can be calculated for the actual radionuclide soil concentrations by multiplying the actual radionuclide soil concentrations by the respective unit concentration dose factor ($DF_{inh,i}$).

The inhalation occupancy factor assumes that indoor dust loading is 40% of outdoor levels. This results in an effective inhalation occupancy factor of 0.45 [i.e., indoor time fraction (0.5) × (0.4) + outdoor time fraction (0.25)].

The unit concentration dose factor ($DF_{ext,i}$) for external radiation dose was calculated as follows:

$$DF_{ext,i} = DCF_{ext,i} \times \left[\left(f_{ext,indoor} \times S_{ext,indoor}\right) + f_{ext,outdoor}\right] \times \rho \quad (5\text{-}21)$$

where

$DF_{ext,i}$ = unit concentration dose factor for external exposure to radionuclide i per unit soil concentration (mrem/yr per pCi/g)

$DCF_{ext,i}$ = external dose conversion factor for radionuclide i (mrem/yr per pCi/m^3)

$f_{ext,indoor}$ = occupancy factor for external radiation while inside the home (dimensionless)

$S_{ext,indoor}$ = shielding factor for indoor exposures (dimensionless)

$f_{ext,outdoor}$ = occupancy factor for external radiation while outside the home (dimensionless)

ρ = soil bulk density (g/m^3).

The EDE from external radiation exposure can be calculated for the radionuclide soil concentrations by multiplying them by the respective unit concentration dose factor ($DF_{ext,i}$).

The external exposure occupancy factor in this case includes a shielding factor for the residence of 0.7 for all radionuclides except $^{137}Cs/^{137m}Ba$, which was assigned an external exposure occupancy factor of 0.35. This was based on a separate analysis of the gamma exposure and attenuation by the foundation of the house. The analysis supporting this factor is provided in Appendix K.

Ingestion doses were calculated for ingestion of contaminated vegetables, beef, and dairy products. Since the area of contamination is small (i.e., 2,200 m^2 [24,000 ft^2]) and cannot fully support beef cattle or milk cows, the consumption rate of the contaminated pasture was adjusted to reflect the maximum amount of feed that could be produced on the lot. The adjustment factors provided in the *RWMC PA* (Maheras et al. 1997) were used in this analysis. The *RWMC PA* determined that 9% of the total pasture eaten by the cows would be contaminated. The consumption rate for contaminated pasture was calculated by Maheras et al. (1997) to be 5.4 kg/d for beef cattle and 7.2 kg/d for milk cows. In addition, 25% of the intruder's diet from vegetables was assumed to be contaminated.

The human consumption diet developed by Yang and Nelson (1984, 1986), based on a 1977–1978 United States Department of Agriculture survey (USDA 1983), was used in the assessment. The diet consists of 94 kg/yr of produce, 17 kg/yr of leafy vegetable, 89 L/yr of milk, and 55 kg/yr of beef products.

The radionuclide intake from vegetables and resulting unit concentration dose factors ($DF_{veg,i,k}$) assumes plant uptake by roots and foliar deposition.

$$DF_{veg,i,k} = DCF_{ing,i} \Big/ \Sigma_k f_{veg,k} \times I_{veg,k} \times \left[B_{iv,i} + (FA \times ASR_{foliar} \times FAR_k)\right] \quad (5\text{-}22)$$

where

$DF_{veg,i,k}$ = unit concentration dose factor for radionuclide i from plant ingestion of vegetation type k for a unit soil concentration (mrem/yr per pCi/g)

$DCF_{ing,i}$ = ingestion CEDE conversion factor for radionuclide i (mrem/pCi)

$f_{veg,k}$ = fraction of diet for vegetation type k derived from contaminated zone (dimensionless)

$I_{veg,k}$ = annual plant intake of vegetation type k (g/yr)

$B_{iv,i}$ = plant-soil concentration ratio for radionuclide i (pCi/g plant per pCi/g soil)

FA = area factor (dimensionless)

ASR_{foliar} = mass loading factor (g/m^3)

FAR_k = foliar deposition factor for vegetation type k (m^3/g).

Two vegetation types (k) were assumed: leafy vegetables and nonleafy vegetables such as fruits and grains. The fraction of the intruder's diet derived from the contaminated zone was assumed to be 0.25 for each of these vegetation types. The plant-soil concentration ratios used for the assessment are provided in Table 5-4. The area factor was 0.94. The foliar deposition factor was 0.054 m^3/g for fruits and nonleafy vegetables, 0.26 m^3/g for leafy vegetables, and 0.28 m^3/g for fodder (Maheras et al. 1997).

The unit concentration dose factor ($DF_{milk,i}$) received through consumption of milk was calculated as follows:

$$DF_{milk,i} = DCF_{ing,i} \times f_{milk} \times F_{milk} \times I_{milk} \times \left\{ I_{milk,fodder} \left[B_{iv,i} + (FA \times ASR \times FAR_k) + I_{cow,soil} \right] \right\} \quad (5\text{-}23)$$

where

$DF_{milk,i}$ = unit concentration dose factor for radionuclide i from ingestion of milk for a unit soil concentration (mrem/yr per pCi/g)

f_{milk} = fraction of milk derived from the contaminated site (dimensionless)

F_{milk} = milk transfer coefficient (d/L)

I_{milk} = annual intake of milk (L/yr)

$I_{milk,fodder}$ = intake of fodder by livestock (kg/d)

$I_{cow,soil}$ = intake of soil by livestock (kg/d).

The fodder-to-milk transfer coefficients used for this assessment are provided in Table 5-4. The intake of fodder by livestock was 7.2 kg/d, assuming 9% of the pasture would be contaminated (Maheras et al. 1997).

The unit concentration dose factor ($DF_{beef,i}$) received through consumption of beef products was determined as follows:

$$DF_{beef,i} = DCF_{ing,i} \times f_{beef} \times F_{beef} \times I_{beef} \times \left\{ I_{beef,fodder} \left[B_{iv,i} + (FA \times ASR \times FAR_k) + I_{cow,soil} \right] \right\} \quad (5\text{-}24)$$

where

$DF_{beef,i}$ = unit concentration dose factor for radionuclide i from ingestion of beef for a unit soil concentration (mrem/yr per pCi/g)

f_{beef} = fraction of beef derived from contaminated site (dimensionless)

F_{beef} = beef transfer coefficient (d/kg)

I_{beef} = annual intake of beef (g/yr)

$I_{beef,fodder}$ = intake of fodder by livestock (kg/d)

$I_{cow,soil}$ = intake of soil by livestock (kg/d).

The beef transfer coefficients used for this assessment are provided in Table 5-4. The intake of fodder by beef cows was 5.4 kg/d, assuming 9%

Table 5-4. Plant, beef, and milk uptake factors used in the chronic post-drilling scenario.

Nuclide	Vegetable/soil (pCi/g plant per pCi/g soil)	Beef (d/kg)	Milk (d/L)
^{10}Be	4.00E−03	1.00E−03	2.00E−06
^{14}C	5.5	3.10E−02	1.20E−02
^{113m}Cd	3.00E−01	4.00E−04	1.00E−03
^{60}Co	8.00E−02	2.00E−02	2.00E−03
^{135}Cs	4.00E−02	3.00E−02	8.00E−03
^{154}Eu	2.50E−03	2.00E−03	2.00E−05
^{3}H	4.8	1.20E−02	1.00E−02
^{166m}Ho	2.60E−03	2.00E−03	2.00E−05
^{129}I	2.00E−02	7.00E−03	1.00E−02
^{115}In	3.00E−03	4.00E−03	2.00E−04
^{138}La	2.50E−03	2.00E−03	2.00E−05
^{94}Nb	1.00E−02	3.00E−07	2.00E−06
^{63}Ni	5.00E−02	5.00E−03	2.00E−02
^{107}Pd	1.00E−01	1.00E−03	5.00E−03
^{146}Pm	2.50E−03	2.00E−03	2.00E−05
^{87}Rb	1.30E−01	1.50E−02	1.00E−02
^{79}Se	1.00E−01	1.00E−01	1.00E−02
^{146}Sm	2.50E−03	2.00E−03	2.00E−05
^{151}Sm	2.50E−03	2.00E−03	2.00E−05
^{121m}Sn	2.50E−03	1.00E−02	1.00E−03
^{98}Tc	5.00E+00	1.00E−04	1.00E−03
^{99}Tc	5.00E+00	1.00E−04	1.00E−03
^{123}Te	6.00E−01	7.00E−03	5.00E−04
Short Decay Chains			
^{108}Ag	1.50E−01	3.00E−03	2.50E−02
^{108m}Ag	1.50E−01	3.00E−03	2.50E−02
^{137m}Ba	4.00E−02	3.00E−02	8.00E−03
^{137}Cs	4.00E−02	3.00E−02	8.00E−03
^{152}Eu	2.50E−03	2.00E−03	2.00E−05
^{152}Gd	2.50E−03	2.00E−03	2.00E−05
^{93m}Nb	1.00E−02	3.00E−07	2.00E−06
^{147}Pm	2.50E−03	2.00E−03	2.00E−05

Table 5-4. (continued).

Nuclide	Vegetable/soil (pCi/g plant per pCi/g soil)	Beef (d/kg)	Milk (d/L)
^{126}Sb	1.00E−02	1.00E−03	1.00E−04
^{126m}Sb	1.00E−02	1.00E−03	1.00E−04
^{147}Sm	2.50E−03	2.00E−03	2.00E−05
^{126}Sn	2.50E−03	1.00E−02	1.00E−03
^{90}Sr	3.00E−01	8.00E−03	2.00E−03
^{90}Y	3.00E−01	8.00E−03	2.00E−03
^{93}Zr	1.00E−03	1.00E−06	6.00E−07
Decay Chain 1			
^{228}Ac	2.50E−03	2.00E−05	2.00E−05
^{212}Bi	1.00E−01	2.00E−03	5.00E−04
^{252}Cf	1.00E−03	6.00E−05	7.50E−07
^{244}Cm	1.00E−03	2.00E−05	2.00E−06
^{248}Cm	1.00E−03	2.00E−05	2.00E−06
^{240}Np	2.00E−02	1.00E−03	5.00E−06
^{240m}Np	2.00E−02	1.00E−03	5.00E−06
^{212}Pb	1.00E−02	8.00E−04	3.00E−04
^{212}Po	1.00E−03	5.00E−03	3.40E−04
^{216}Po	1.00E−03	5.00E−03	3.40E−04
^{236}Pu	1.00E−03	1.00E−04	1.00E−06
^{240}Pu	1.00E−03	1.00E−04	1.00E−06
^{244}Pu	1.00E−03	1.00E−04	1.00E−06
^{224}Ra	4.00E−02	1.00E−03	1.00E−03
^{228}Ra	4.00E−02	1.00E−03	1.00E−03
^{220}Rn	0.00E+00	0.00E+00	0.00E+00
^{228}Th	1.00E−03	1.00E−04	5.00E−06
^{232}Th	1.00E−03	1.00E−04	5.00E−06
^{208}Tl	2.00E−01	2.00E−03	3.00E−03
^{232}U	2.50E−03	3.40E−04	6.00E−04
^{236}U	2.50E−03	3.40E−04	6.00E−04
^{240}U	2.50E−03	3.40E−04	6.00E−04
Decay Chain 2			
^{225}Ac	2.50E−03	2.00E−05	2.00E−05

Table 5-4. (continued).

Nuclide	Vegetable/soil (pCi/g plant per pCi/g soil)	Beef (d/kg)	Milk (d/L)
^{241}Am	1.00E−03	5.00E−05	2.00E−06
^{217}At	2.00E−01	1.00E−02	1.00E−02
^{213}Bi	1.00E−01	2.00E−03	5.00E−04
^{249}Cf	1.00E−03	6.00E−05	7.50E−07
^{245}Cm	1.00E−03	2.00E−05	2.00E−06
^{221}Fr	3.00E−02	3.00E−02	8.00E−03
^{237}Np	2.00E−02	1.00E−03	5.00E−06
^{233}Pa	1.00E−02	5.00E−03	5.00E−06
^{209}Pb	1.00E−02	8.00E−04	3.00E−04
^{213}Po	1.00E−03	5.00E−03	3.40E−04
^{241}Pu	1.00E−03	1.00E−04	1.00E−06
^{225}Ra	4.00E−02	1.00E−03	1.00E−03
^{229}Th	1.00E−03	1.00E−04	5.00E−06
^{209}Tl	2.00E−01	2.00E−03	3.00E−03
^{233}U	2.50E−03	3.40E−04	6.00E−04
^{237}U	2.50E−03	3.40E−04	6.00E−04
Decay Chain 3			
^{227}Ac	2.50E−03	2.00E−05	2.00E−05
^{243}Am	1.00E−03	5.00E−05	2.00E−06
^{211}Bi	1.00E−01	2.00E−03	5.00E−04
^{251}Cf	1.00E−03	6.00E−05	7.50E−07
^{243}Cm	1.00E−03	2.00E−05	2.00E−06
^{247}Cm	1.00E−03	2.00E−05	2.00E−06
^{223}Fr	3.00E−02	3.00E−02	8.00E−03
^{239}Np	2.00E−02	1.00E−03	5.00E−06
^{231}Pa	1.00E−02	5.00E−03	5.00E−06
^{211}Pb	1.00E−02	8.00E−04	3.00E−04
^{211}Po	1.00E−03	5.00E−03	3.40E−04
^{215}Po	1.00E−03	5.00E−03	3.40E−04
^{239}Pu	1.00E−03	1.00E−04	1.00E−06
^{243}Pu	1.00E−03	1.00E−04	1.00E−06
^{223}Ra	4.00E−02	1.00E−03	1.00E−03

Table 5-4. (continued).

Nuclide	Vegetable/soil (pCi/g plant per pCi/g soil)	Beef (d/kg)	Milk (d/L)
^{219}Rn	0.00E+00	0.00E+00	0.00E+00
^{227}Th	1.00E−03	1.00E−04	5.00E−06
^{231}Th	1.00E−03	1.00E−04	5.00E−06
^{207}Tl	2.00E−01	2.00E−03	3.00E−03
^{235}U	2.50E−03	3.40E−04	6.00E−04
Decay Chain 4			
^{242}Am	1.00E−03	5.00E−05	2.00E−06
^{242m}Am	1.00E−03	5.00E−05	2.00E−06
^{210}Bi	1.00E−01	2.00E−03	5.00E−04
^{214}Bi	1.00E−01	2.00E−03	5.00E−04
^{250}Cf	1.00E−03	6.00E−05	7.50E−07
^{242}Cm	1.00E−03	2.00E−05	2.00E−06
^{246}Cm	1.00E−03	2.00E−05	2.00E−06
^{238}Np	2.00E−02	1.00E−03	5.00E−06
^{234}Pa	1.00E−02	5.00E−03	5.00E−06
^{234m}Pa	1.00E−02	5.00E−03	5.00E−06
^{210}Pb	1.00E−02	8.00E−04	3.00E−04
^{214}Pb	1.00E−02	8.00E−04	3.00E−04
^{210}Po	1.00E−03	5.00E−03	3.40E−04
^{214}Po	1.00E−03	5.00E−03	3.40E−04
^{218}Po	1.00E−03	5.00E−03	3.40E−04
^{238}Pu	1.00E−03	1.00E−04	1.00E−06
^{242}Pu	1.00E−03	1.00E−04	1.00E−06
^{226}Ra	4.00E−02	1.00E−03	1.00E−03
^{222}Rn	0.00E+00	0.00E+00	0.00E+00
^{230}Th	1.00E−03	1.00E−04	5.00E−06
^{234}Th	1.00E−03	1.00E−04	5.00E−06
^{234}U	2.50E−03	3.40E−04	6.00E−04
^{238}U	2.50E−03	3.40E−04	6.00E−04

of the pasture would be contaminated (Maheras et al. 1997). The intake of soil by beef cows was 0.5 kg/d.

A summary of the parameter values used in the intruder post-drilling scenario is listed in Table 5-5. Table 5-6 lists the unit concentration dose factors for the intruder post-drilling scenario. The unit concentration dose factors for ^{3}H and ^{14}C were determined using the RESRAD computer code (Yu et al. 1993) and default parameters.

The results of the intruder post-drilling scenario are provided in Section 5.6.

5.5 Chronic Intruder Post-Construction Scenario Definition

The chronic post-construction scenario assumes that an inadvertent intruder moves onto the TFF, excavates a basement, spreads the excavated material over the land, and subsequently farms the area.

The excavation soil is assumed to be spread over 2,200 m^2 (24,000 ft^2 or approximately one-half acre) of land surface. The waste is assumed to be mixed to a depth of 0.61 m (24 in.). The mixing depth of 0.61 m is based on using a deep tilling plow to increase the depth of the root zone and to break up soil compaction. These plows are used in areas of southeast Idaho with highly erodible soils to minimize erosion. Deep tilling plows have shanks that till to a depth of 24 in. and are sold at Idaho Falls implement dealers (Maheras et al. 1997).

The chronic post-construction scenario assumes that the intruder is exposed to the excavated soil during plowing and cultivation (i.e., dust inhalation). In addition, the intruder is assumed to ingest contaminated food products from the garden and from beef and milk cattle that consume contaminated forage. The intake of contaminated forage by cattle was adjusted according to the fraction of feed grown on contaminated cuttings and the necessary remaining feed obtained from uncontaminated ground.

The soil activity concentration in the soils was then determined using the equation presented in Section 5.3. However, since the excavated soil is spread over a 2,200 m^2 area, this results in the 600 m^3 of excavated soil being 0.27 m deep. The excavated waste soil is assumed to be mixed to a depth of 0.61 m. Therefore, the soil activity concentrations determined in Section 5.3 were reduced by a factor of 2.26 to account for the tilling and mixing of the soils to a depth of 0.61 m.

The determination of the unit concentration dose factors for each exposure pathway was determined using the equations in Section 5.4 for the intruder post-drilling scenario.

The results of the intruder post-construction scenario are provided in Section 5.6.

5.6 Intruder Analysis Results

5.6.1 Acute Intruder-Drilling Scenario

The soil concentrations and intruder doses resulting from the acute drilling scenario for each radionuclide for time periods of 100, 200, 300, 400, 500, 600, 700, 800, 900, and 1,000 yr post-closure are provided in Appendix L. Please see this appendix for intermediate results. Figure 5-3 shows the total intruder dose, dose from sand pad contamination, and dose from tank contamination. Figure 5-4 shows the doses from the major radionuclide contributors and the total from all nuclides. Figure 5-5 presents the intruder dose as a function of exposure pathway.

The maximum dose after institutional control (i.e., 100 yr) for the acute intruder was 232 mrem. The major radionuclide contributors to the total acute intruder dose were $^{137}Cs/^{137m}Ba$ with 188 mrem, ^{238}Pu with 15 mrem, $^{90}Sr/^{90}Y$ with 8.64 mrem, ^{239}Pu with 5.3 mrem, ^{241}Am with 5.1 mrem, and ^{240}Pu with 2.8 mrem. The acute drilling scenario dose results are less than the performance objective of 500 mrem for all times post-institutional control.

Table 5-5. Parameter values for the chronic post-drilling scenario.

Parameter	Description	Value
A_c	Area where contamination is spread (m^2)	2,200
ASR	Mass loading factor (g/m^3)	1.0E−03
ASR_{foliar}	Mass loading factor for garden (g/m^3)	1.0E−04
D_c	Final depth of contaminated zone after tilling (m)	0.61
f_{in}	Occupancy factor indoors (unitless)	0.5
$f_{veg,leafy}$	Fraction of leafy vegetation from site (unitless)	0.25
f_{beef}	Fraction of beef from site (unitless)	1
f_{milk}	Fraction of milk from site (unitless)	1
$f_{veg,nonleafy}$	Fraction of nonleafy vegetation from site (unitless)	0.25
$f_{offsite}$	Occupancy factor offsite (unitless)	0.25
f_{out}	Occupancy factor outdoors (unitless)	0.25
FA_{cow}	Area factor for resuspension on cow pathway (unitless)	0.94
FA_{milk}	Area factor for resuspension on milk pathway (unitless)	0.94
FA_{veg}	Area factor for resuspension in garden (unitless)	0.94
FAR_{fodder}	Foliar deposition factor for fodder (m^3/g)	0.28
FAR_{leafy}	Foliar deposition factor for leafy vegetation (m^3/g)	0.26
$FAR_{nonleafy}$	Foliar deposition factor for nonleafy vegetation (m^3/g)	0.54
$I_{beef,fodder}$	Beef animal intake of fodder (kg/d)	5.4
$I_{cow,soil}$	Soil ingestion rate for cows (kg/d)	0.5
$I_{inh,in}$	Breathing rate—indoors (m^3/yr)	8,400
I_{beef}	Intake of beef (g/yr)	55×10^4
I_{milk}	Intake of milk (L/yr)	89
$I_{milk,fodder}$	Milk animal intake of fodder (kg/d)	7.2
$I_{inh,out}$	Breathing rate—outdoors (m^3/yr)	8,400
I_{soil}	Soil ingestion rate (g/yr)	3.65
$I_{veg,leafy}$	Human consumption of leafy vegetation (g/yr)	1.8×10^4
$I_{veg,nonleafy}$	Human consumption of nonleafy vegetation (g/yr)	9.4E+04
r_{cont}	Radius of the contaminated zone (m)	26.5
$r_{sand\ pad}$	Radius of the sand pad (m)	7.8
r_{Tank}	Radius of the tank (m)	7.6
r_{well}	Radius of the well (m)	0.1
ρ	Bulk density of the contamination (g/m^3)	1.6E+06
S_{air}	Ratio of outdoor to indoor air (unitless)	0.4
$S_{ext,indoor}$	Shielding factor for indoor exposures (unitless)	0.7[b]
t_w	Thickness of waste zone (m)	0.15

a. Foliar deposition factors increased by a factor of ten for iodine.

b. $^{137}Cs/^{137m}Ba$ shielding factor is equal to 0.35 (see Appendix K).

Table 5-6. Unit concentration dose factors for the chronic post-drilling scenario.

Nuclide	Unit DCF Inhalation	Unit DCF External	Unit DCF Ingestion Vegetables	Unit DCF Ingestion Beef	Unit DCF Ingestion Milk	Unit DCF Ingestion Soil	Unit DCF Total
	(mrem/yr per pCi/g)						
^{10}Be	1.34E–03	6.35E–04	5.23E–04	1.34E–04	4.39E–07	1.28E–05	2.65E–03
^{14}C	1.77E–09	1.00E–09	7.60E–06	6.75E–07	5.59E–07	7.60E–10	8.84E–06
^{113m}Cd	5.78E–03	3.83E–04	1.35E+00	7.51E–03	3.81E–02	4.41E–04	1.40E+00
^{60}Co	8.27E–04	8.13E+00	6.03E–02	2.76E–02	5.16E–03	7.37E–05	8.22E+00
^{135}Cs	1.72E–05	2.30E–05	7.92E–03	8.35E–03	3.97E–03	1.93E–05	2.03E–02
^{154}Eu	1.08E–03	3.95E+00	6.70E–04	5.39E–04	8.81E–06	2.61E–05	3.95E+00
^{3}H	1.13E–09	0.00E+00	1.44E–07	1.17E–08	2.78E–08	1.53E–12	1.85E–07
^{166m}Ho	2.92E–03	5.49E+00	5.89E–04	4.56E–04	7.45E–06	2.21E–05	5.50E+00
^{129}I	6.56E–04	7.77E–03	1.55E–01	6.46E–02	1.59E–01	7.56E–04	3.88E–01
^{115}In	1.41E–02	2.38E–04	1.33E–02	1.79E–02	1.46E–03	4.31E–04	4.74E–02
^{138}La	5.17E–03	3.98E+00	4.13E–04	3.32E–04	5.43E–06	1.61E–05	3.98E+00
^{94}Nb	1.68E–03	5.08E+00	2.00E–03	6.53E–08	7.27E–07	1.95E–05	5.08E+00
^{63}Ni	1.17E–05	0.00E+00	8.08E–04	1.22E–04	8.84E–04	1.58E–06	1.83E–03
^{107}Pd	4.83E–05	0.00E+00	4.19E–04	8.55E–06	8.12E–05	4.09E–07	5.57E–04
^{146}Pm	5.54E–04	2.36E+00	2.58E–04	2.07E–04	3.38E–06	1.00E–05	2.37E+00
^{87}Rb	1.22E–05	8.43E–05	1.79E–02	4.88E–03	6.29E–03	1.35E–05	2.92E–02
^{79}Se	3.72E–05	1.12E–05	2.43E–02	4.97E–02	9.44E–03	2.38E–05	8.36E–02
^{146}Sm	3.12E–01	0.00E+00	1.43E–02	1.15E–02	1.88E–04	5.58E–04	3.38E–01
^{151}Sm	1.13E–04	5.91E–07	2.73E–05	2.20E–05	3.58E–07	1.06E–06	1.65E–04
^{121m}Sn	4.35E–05	1.18E–03	1.09E–04	4.38E–04	7.15E–05	4.24E–06	1.84E–03
^{98}Tc	8.64E–05	4.55E+00	6.84E–01	7.39E–04	1.59E–02	1.34E–05	5.25E+00
^{99}Tc	3.15E–05	7.51E–05	2.05E–01	2.21E–04	4.75E–03	4.00E–06	2.10E–01
^{123}Te	3.99E–05	3.93E–03	7.02E–02	6.02E–03	8.97E–04	1.14E–05	8.11E–02
Short Decay Chains							
^{108}Ag	0.00E+00	6.18E–02	0.00E+00	0.00E+00	0.00E+00	0.00E+00	6.18E–02
^{108m}Ag	1.07E–03	5.17E+00	3.20E–02	1.65E–03	2.68E–02	2.09E–05	5.23E+00
^{137m}Ba	0.00E+00	1.36E+00	0.00E+00	0.00E+00	0.00E+00	0.00E+00	1.36E+00
^{137}Cs	1.21E–04	3.13E–04	5.60E–02	5.90E–02	2.80E–02	1.37E–04	1.44E–01
^{152}Eu	8.35E–04	3.61E+00	4.55E–04	3.66E–04	5.97E–06	1.77E–05	3.61E+00

Table 5-6. (continued).

Nuclide	Unit DCF Inhalation	Unit DCF External	Unit DCF Ingestion Vegetables	Unit DCF Ingestion Beef	Unit DCF Ingestion Milk	Unit DCF Ingestion Soil	Unit DCF Total
	(mrem/yr per pCi/g)						
^{152}Gd	9.20E–01	0.00E+00	1.13E–02	9.07E–03	1.48E–04	4.40E–04	9.41E–01
^{93m}Nb	1.10E–04	6.24E–05	1.46E–04	4.77E–09	5.31E–08	1.43E–06	3.21E–04
^{147}Pm	1.48E–04	2.99E–05	7.35E–05	5.92E–05	9.66E–07	2.87E–06	3.15E–04
^{126}Sb	4.43E–05	9.11E+00	3.00E–03	3.26E–04	5.45E–05	2.93E–05	9.12E+00
^{126m}Sb	1.28E–07	4.98E+00	2.62E–05	2.85E–06	4.77E–07	2.56E–07	4.98E+00
^{147}Sm	2.83E–01	0.00E+00	1.30E–02	1.05E–02	1.71E–04	5.07E–04	3.07E–01
^{126}Sn	3.76E–04	8.85E–02	1.37E–03	5.51E–03	8.99E–04	5.34E–05	9.68E–02
^{90}Sr	4.91E–03	4.17E–04	1.20E+00	1.33E–01	6.75E–02	3.90E–04	1.40E+00
^{90}Y	3.19E–05	1.34E–02	9.04E–02	1.00E–02	5.10E–03	2.95E–05	1.19E–01
^{93}Zr	1.21E–03	0.00E+00	4.68E–05	4.61E–08	4.49E–08	4.54E–06	1.26E–03
Decay Chain 1							
^{228}Ac	1.17E–03	3.09E+00	1.52E–04	1.22E–06	2.00E–06	5.93E–06	3.09E+00
^{212}Bi	8.15E–05	6.01E–01	2.97E–03	1.21E–04	5.77E–05	2.91E–06	6.04E–01
^{252}Cf	5.93E–01	1.05E–04	3.06E–02	1.81E–03	3.67E–05	2.97E–03	6.29E–01
^{244}Cm	9.37E–01	7.55E–05	5.69E–02	1.12E–03	1.82E–04	5.52E–03	1.00E+00
^{248}Cm	6.25E+00	5.27E–05	3.84E–01	7.57E–03	1.23E–03	3.73E–02	6.68E+00
^{240}Np	3.08E–07	4.09E+00	1.33E–04	7.93E–06	6.79E–08	6.49E–07	4.09E+00
^{240m}Np	0.00E+00	1.06E+00	0.00E+00	0.00E+00	0.00E+00	0.00E+00	1.06E+00
^{212}Pb	6.38E–04	4.06E–01	1.28E–02	1.11E–03	6.95E–04	1.25E–04	4.21E–01
^{212}Po	0.00E+00	0.00E+00	0.00E+00	0.00E+00	0.00E+00	0.00E+00	0.00E+00
^{216}Po	0.00E+00	5.46E–05	0.00E+00	0.00E+00	0.00E+00	0.00E+00	5.46E–05
^{236}Pu	5.47E–01	1.34E–04	3.29E–02	3.24E–03	5.26E–05	3.19E–03	5.86E–01
^{240}Pu	1.62E+00	8.79E–05	9.99E–02	9.84E–03	1.60E–04	9.68E–03	1.74E+00
^{244}Pu	1.52E+00	4.53E–05	9.37E–02	9.23E–03	1.50E–04	9.09E–03	1.64E+00
^{224}Ra	1.19E–02	2.94E–02	4.10E–01	1.44E–02	2.57E–02	1.00E–03	4.92E–01
^{228}Ra	1.80E–02	0.00E+00	1.61E+00	5.65E–02	1.01E–01	3.93E–03	1.79E+00
^{220}Rn	0.00E+00	1.23E–03	0.00E+00	0.00E+00	0.00E+00	0.00E+00	1.23E–03
^{228}Th	1.29E+00	4.67E–03	1.12E–02	1.10E–03	8.94E–05	1.08E–03	1.31E+00
^{232}Th	6.20E+00	3.12E–04	7.71E–02	7.59E–03	6.17E–04	7.48E–03	6.29E+00

Table 5-6. (continued).

Nuclide	Unit DCF Inhalation	Unit DCF External	Unit DCF Ingestion Vegetables	Unit DCF Ingestion Beef	Unit DCF Ingestion Milk	Unit DCF Ingestion Soil	Unit DCF Total
	(mrem/yr per pCi/g)						
^{208}Tl	0.00E+00	1.08E+01	0.00E+00	0.00E+00	0.00E+00	0.00E+00	1.08E+01
^{232}U	5.62E–02	5.35E–04	9.20E–02	1.26E–02	3.62E–02	3.59E–03	2.01E–01
^{236}U	4.74E–01	1.28E–04	1.89E–02	2.58E–03	7.43E–03	7.35E–04	5.04E–01
^{240}U	8.57E–06	8.54E–04	3.12E–04	4.26E–05	1.23E–04	1.22E–05	1.35E–03
Decay Chain 2							
^{225}Ac	4.08E–02	3.74E–02	7.80E–03	6.27E–05	1.02E–04	3.04E–04	8.65E–02
^{241}Am	1.68E+00	2.62E–02	1.03E–01	5.06E–03	3.29E–04	9.97E–03	1.82E+00
^{217}At	0.00E+00	9.65E–04	0.00E+00	0.00E+00	0.00E+00	0.00E+00	9.65E–04
^{213}Bi	6.48E–05	4.20E–01	2.02E–03	8.26E–05	3.92E–05	1.98E–06	4.23E–01
^{249}Cf	2.18E+00	1.03E+00	1.34E–01	7.90E–03	1.60E–04	1.30E–02	3.37E+00
^{245}Cm	1.72E+00	2.02E–01	1.06E–01	2.08E–03	3.38E–04	1.02E–02	2.04E+00
^{221}Fr	0.00E+00	8.85E–02	0.00E+00	0.00E+00	0.00E+00	0.00E+00	8.85E–02
^{237}Np	2.04E+00	4.66E–02	2.49E+00	1.49E–01	1.27E–03	1.22E–02	4.74E+00
^{233}Pa	3.61E–05	5.78E–01	1.02E–03	5.53E–04	9.24E–07	9.94E–06	5.80E–01
^{209}Pb	3.58E–07	4.57E–04	5.96E–05	5.19E–06	3.25E–06	5.82E–07	5.26E–04
^{213}Po	0.00E+00	0.00E+00	0.00E+00	0.00E+00	0.00E+00	0.00E+00	0.00E+00
^{241}Pu	3.12E–02	3.53E–06	1.93E–03	1.90E–04	3.09E–06	1.87E–04	3.35E–02
^{225}Ra	2.94E–02	6.61E–03	4.31E–01	1.52E–02	2.70E–02	1.05E–03	5.10E–01
^{229}Th	8.11E+00	1.91E–01	9.97E–02	9.81E–03	7.97E–04	9.66E–03	8.42E+00
^{209}Tl	0.00E+00	6.49E+00	0.00E+00	0.00E+00	0.00E+00	0.00E+00	6.49E+00
^{233}U	5.12E–01	8.11E–04	2.03E–02	2.78E–03	8.00E–03	7.91E–04	5.45E–01
^{237}U	1.33E–05	3.12E–01	2.23E–04	3.05E–05	8.77E–05	8.68E–06	3.12E–01
Decay Chain 3							
^{227}Ac	2.53E+01	2.94E–04	9.87E–01	7.94E–03	1.30E–02	3.85E–02	2.64E+01
^{243}Am	1.66E+00	8.52E–02	1.02E–01	5.04E–03	3.27E–04	9.92E–03	1.87E+00
^{211}Bi	0.00E+00	1.43E–01	0.00E+00	0.00E+00	0.00E+00	0.00E+00	1.43E–01
^{251}Cf	2.22E+00	3.09E–01	1.37E–01	8.09E–03	1.64E–04	1.33E–02	2.69E+00
^{243}Cm	1.16E+00	3.38E–01	7.09E–02	1.40E–03	2.27E–04	6.88E–03	1.58E+00
^{247}Cm	1.57E+00	9.86E–01	9.65E–02	1.90E–03	3.09E–04	9.36E–03	2.66E+00
^{223}Fr	2.97E–02	1.13E–01	7.24E–03	9.42E–03	4.40E–03	2.36E–05	1.64E–01

Table 5-6. (continued).

Nuclide	Unit DCF Inhalation	Unit DCF External	Unit DCF Ingestion Vegetables	Unit DCF Ingestion Beef	Unit DCF Ingestion Milk	Unit DCF Ingestion Soil	Unit DCF Total
	(mrem/yr per pCi/g)						
^{239}Np	9.48E–06	4.37E–01	1.83E–03	1.09E–04	9.36E–07	8.93E–06	4.39E–01
^{231}Pa	4.85E+00	1.08E–01	2.97E+00	1.61E+00	2.69E–03	2.90E–02	9.57E+00
^{211}Pb	2.85E–05	1.64E–01	1.47E–04	1.28E–05	8.03E–06	1.44E–06	1.64E–01
^{211}Po	0.00E+00	2.51E–02	0.00E+00	0.00E+00	0.00E+00	0.00E+00	2.51E–02
^{215}Po	0.00E+00	5.58E–04	0.00E+00	0.00E+00	0.00E+00	0.00E+00	5.58E–04
^{239}Pu	1.62E+00	1.70E–04	9.99E–02	9.84E–03	1.60E–04	9.68E–03	1.74E+00
^{243}Pu	6.21E–07	4.71E–02	9.42E–06	9.28E–07	1.51E–08	9.14E–07	4.71E–02
^{223}Ra	2.97E–02	3.47E–01	7.38E–01	2.59E–02	4.62E–02	1.80E–03	1.19E+00
^{219}Rn	0.00E+00	1.73E–01	0.00E+00	0.00E+00	0.00E+00	0.00E+00	1.73E–01
^{227}Th	6.11E–02	2.97E–01	1.08E–03	1.06E–04	8.60E–06	1.04E–04	3.59E–01
^{231}Th	3.31E–06	2.17E–02	3.81E–05	3.76E–06	3.05E–07	3.70E–06	2.18E–02
^{207}Tl	0.00E+00	1.06E–02	0.00E+00	0.00E+00	0.00E+00	0.00E+00	1.06E–02
^{235}U	4.64E–01	4.24E–01	1.87E–02	2.56E–03	7.36E–03	7.28E–04	9.17E–01
Decay Chain 4							
^{242}Am	2.21E–04	2.99E–02	3.98E–05	1.96E–06	1.27E–07	3.86E–06	3.02E–02
^{242m}Am	1.61E+00	1.01E–03	9.92E–02	4.89E–03	3.17E–04	9.62E–03	1.72E+00
^{210}Bi	7.40E–04	2.08E–03	1.79E–02	7.32E–04	3.48E–04	1.75E–05	2.18E–02
^{214}Bi	2.49E–05	4.89E+00	7.92E–04	3.23E–05	1.53E–05	7.74E–07	4.89E+00
^{250}Cf	9.90E–01	7.11E–05	6.02E–02	3.56E–03	7.22E–05	5.83E–03	1.06E+00
^{242}Cm	6.53E–02	1.02E–04	3.24E–03	6.38E–05	1.04E–05	3.14E–04	6.90E–02
^{246}Cm	1.71E+00	6.97E–05	1.04E–01	2.06E–03	3.34E–04	1.01E–02	1.82E+00
^{238}Np	1.40E–04	1.77E+00	2.24E–03	1.34E–04	1.15E–06	1.09E–05	1.77E+00
^{234}Pa	3.08E–06	6.03E+00	6.06E–04	3.29E–04	5.50E–07	5.92E–06	6.03E+00
^{234m}Pa	0.00E+00	4.71E–02	0.00E+00	0.00E+00	0.00E+00	0.00E+00	4.71E–02
^{210}Pb	5.13E–02	1.47E–03	1.50E+00	1.31E–01	8.20E–02	1.47E–02	1.78E+00
^{214}Pb	2.95E–05	7.51E–01	1.75E–04	1.52E–05	9.55E–06	1.71E–06	7.51E–01
^{210}Po	3.55E–02	2.75E–05	5.37E–02	2.64E–01	2.92E–02	5.21E–03	3.88E–01
^{214}Po	0.00E+00	2.69E–04	0.00E+00	0.00E+00	0.00E+00	0.00E+00	2.69E–04
^{218}Po	0.00E+00	2.95E–05	0.00E+00	0.00E+00	0.00E+00	0.00E+00	2.95E–05

Table 5-6. (continued).

Nuclide	Unit DCF Inhalation	Unit DCF External	Unit DCF Ingestion Vegetables	Unit DCF Ingestion Beef	Unit DCF Ingestion Milk	Unit DCF Ingestion Soil	Unit DCF Total
	(mrem/yr per pCi/g)						
^{238}Pu	1.48E+00	9.04E–05	9.04E–02	8.90E–03	1.45E–04	8.76E–03	1.59E+00
^{242}Pu	1.55E+00	7.68E–05	9.48E–02	9.34E–03	1.52E–04	9.20E–03	1.67E+00
^{226}Ra	3.24E–02	1.85E–02	1.48E+00	5.22E–02	9.29E–02	3.63E–03	1.68E+00
^{222}Rn	0.00E+00	1.28E–03	0.00E+00	0.00E+00	0.00E+00	0.00E+00	1.28E–03
^{230}Th	1.23E+00	7.16E–04	1.55E–02	1.52E–03	1.24E–04	1.50E–03	1.25E+00
^{234}Th	1.32E–04	1.45E–02	3.85E–04	3.80E–05	3.08E–06	3.74E–05	1.51E–02
^{234}U	5.01E–01	2.40E–04	1.99E–02	2.72E–03	7.84E–03	7.76E–04	5.32E–01
^{238}U	4.48E–01	6.19E–05	1.79E–02	2.45E–03	7.04E–03	6.97E–04	4.76E–01

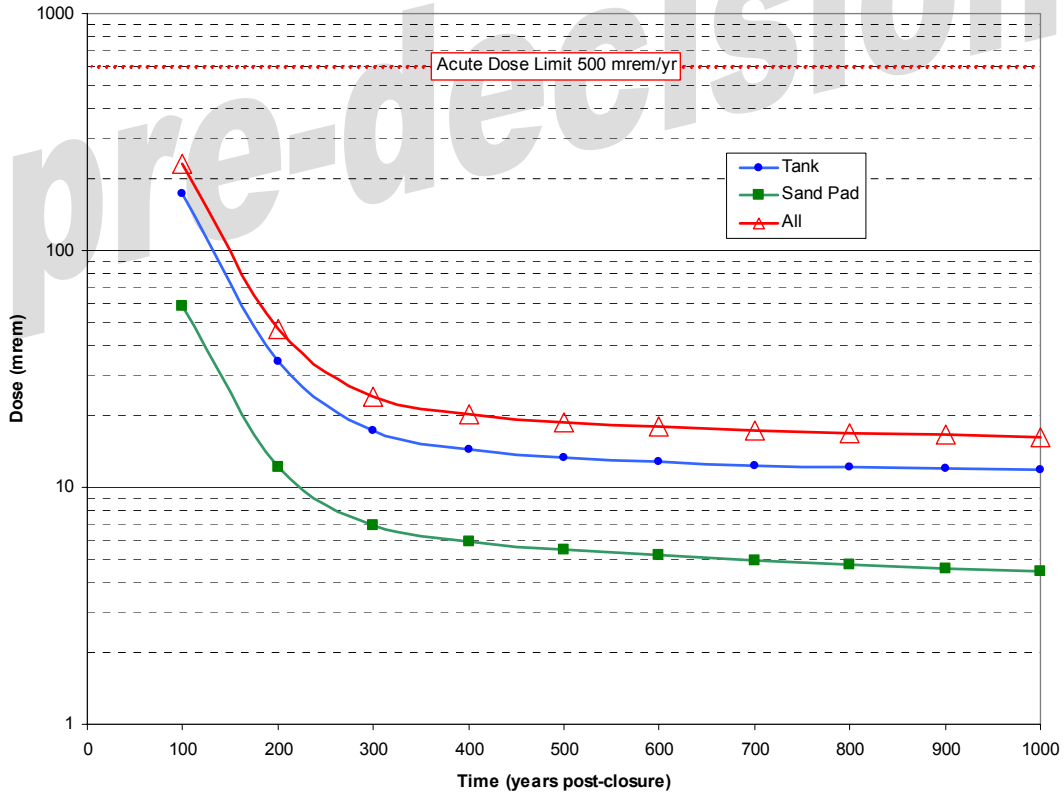

Figure 5-3. Results of the acute intruder-drilling scenario.

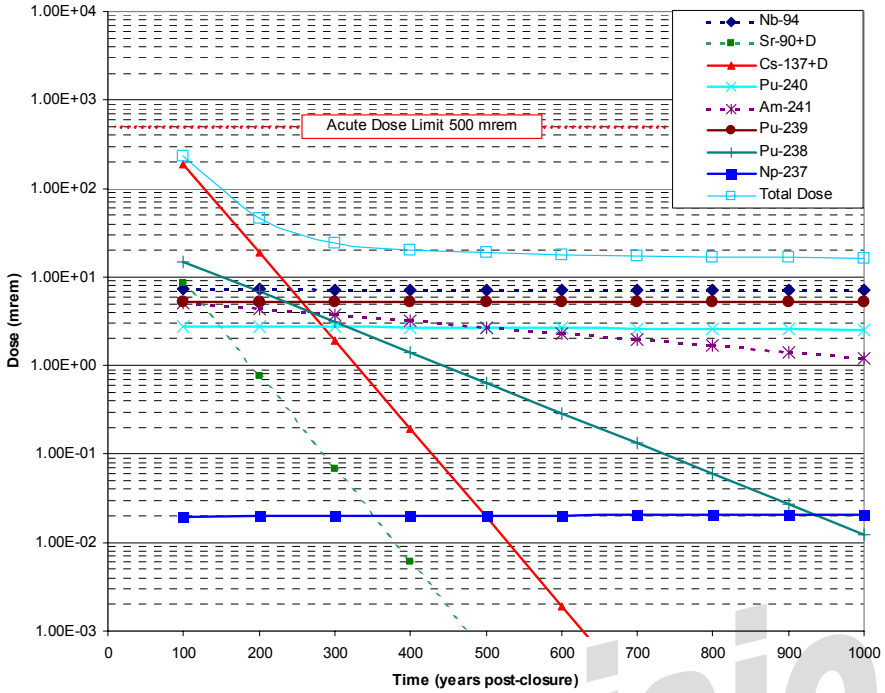

Figure 5-4. Results of the acute intruder-drilling scenario for individual radionuclides.

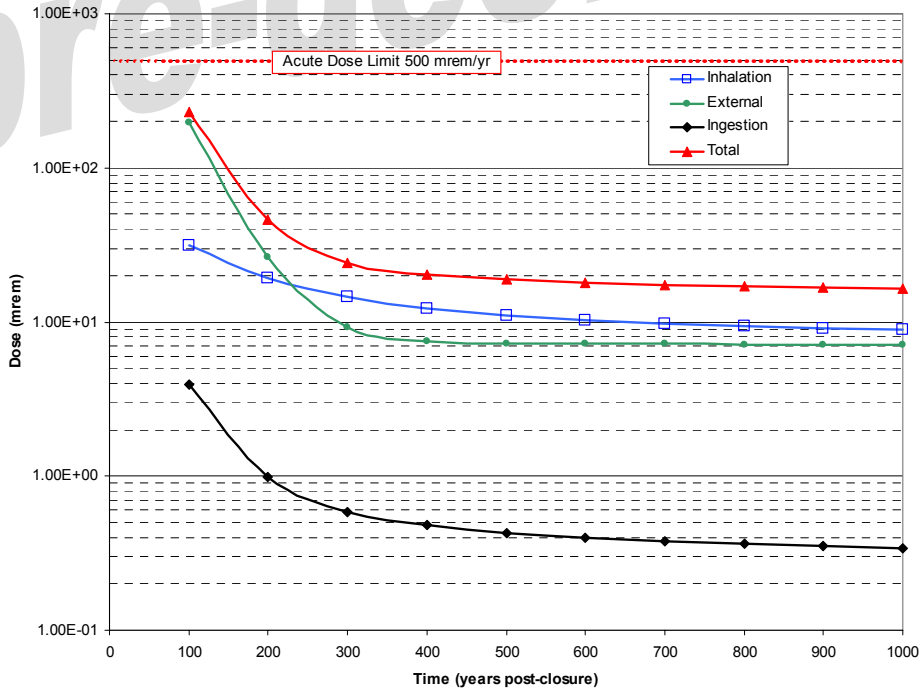

Figure 5-5. Results of the acute intruder-drilling scenario by exposure pathway.

5.6.2 Acute Intruder-Construction Scenario

The soil concentrations and intruder doses resulting from the acute drilling scenario for each radionuclide for time periods of 100, 200, 300, 400, 500, 600, 700, 800, 900, and 1,000 yr post-closure are provided in Appendix L. Please see this appendix for intermediate results. Figure 5-6 shows the doses from the major radionuclide contributors and the total from all nuclides. Figure 5-7 presents the intruder dose as a function of exposure pathway.

The maximum dose after institutional control (i.e., 100 yr) for the acute intruder-construction scenario was 0.93 mrem. The major radionuclide contributors to the total acute intruder dose were $^{137}Cs/^{137m}Ba$ with 0.72 mrem, ^{94}Nb with 0.045 mrem, $^{90}Sr/^{90}Y$ with 0.017 mrem, and ^{238}Pu with 0.013 mrem. The acute intruder-construction scenario dose results are less than the performance objective of 500 mrem for all times post-closure.

5.6.3 Chronic Intruder Post-Drilling Scenario

The soil concentrations and intruder doses resulting from the chronic post-drilling scenario for each radionuclide for time periods of 100, 200, 300, 400, 500, 600, 700, 800, 900, and 1,000 yr post-closure are provided in Appendix L. Please see this appendix for intermediate results. Figure 5-8 shows the total intruder dose, dose from sand pad contamination, and dose from tank contamination. Figure 5-9 shows the doses from the major radionuclide contributors and the total from all nuclides. Figure 5-10 presents the intruder dose as a function of exposure pathway.

The maximum dose after institutional control was 91.1 mrem/yr for the chronic intruder post-drilling scenario at 100 yr. The major radionuclide contributors to the total chronic intruder dose were $^{90}Sr/^{90}Y$ with 51.5 mrem/yr and $^{137}Cs/^{137m}Ba$ with 36.5 mrem/yr. The chronic intruder post-drilling scenario dose results do not exceed the performance objective of 100 mrem/yr during the compliance period.

5.6.4 Chronic Intruder Post-Construction Scenario

The soil concentrations and intruder doses resulting from the chronic post-construction scenario for each radionuclide for time periods of 100, 200, 300, 400, 500, 600, 700, 800, 900, and 1,000 yr post-closure are provided in Appendix L. Please see this appendix for intermediate results. Figure 5-11 shows the doses from the major radionuclide contributors and the total from all nuclides. Figure 5-12 presents the intruder dose as a function of exposure pathway.

The maximum dose was 26.1 mrem/yr for the chronic intruder post-construction scenario at 100 yr post-closure. The major radionuclide contributors to the total chronic intruder dose were $^{90}Sr/^{90}Y$ with 15.2 mrem/yr, $^{137}Cs/^{137m}Ba$ with 10.1 mrem/yr, ^{94}Nb with 0.58 mrem/yr, and ^{238}Pu with 0.15 mrem/yr. The chronic intruder post-construction scenario dose results do not exceed the performance objective of 100 mrem/yr for the 1,000-yr compliance period.

5.7 Intruder Sensitivity/ Uncertainty Analysis

DOE guidance for PAs (DOE 1999b) states that the sensitivity/uncertainty analysis for hypothetical inadvertent intruder analyses should be limited to qualitative arguments (e.g., explanation of the rationale for selected scenarios and parameters). Therefore, the discussion in this section is limited to qualitative rationale.

The preceding sections describe the TFF as a unique environment for the evaluation of intruder scenarios. Many of the standard scenarios were not considered applicable to the TFF because the depth of the waste in the tanks is 10 m (30 ft). Therefore, only the acute intruder-drilling and chronic post-drilling scenarios were considered applicable.

It is difficult to predict the future actions of humans, especially over a period of 1,000 yr. The fact that the intruder is assumed to drill a well directly through a tank is considered a very conservative assumption. It can be argued that the

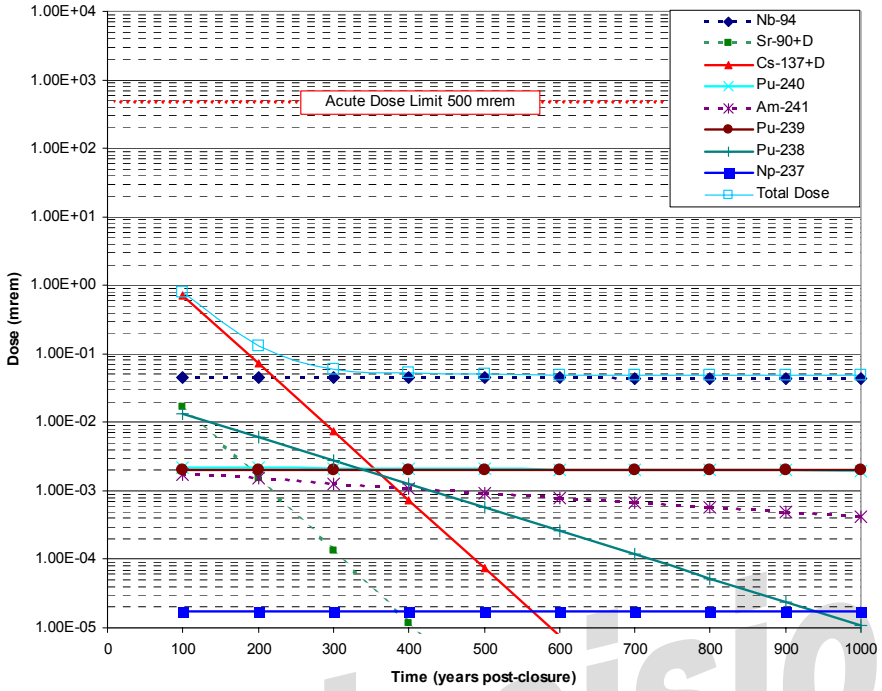

Figure 5-6. Results of the acute intruder-construction scenario for individual radionuclides.

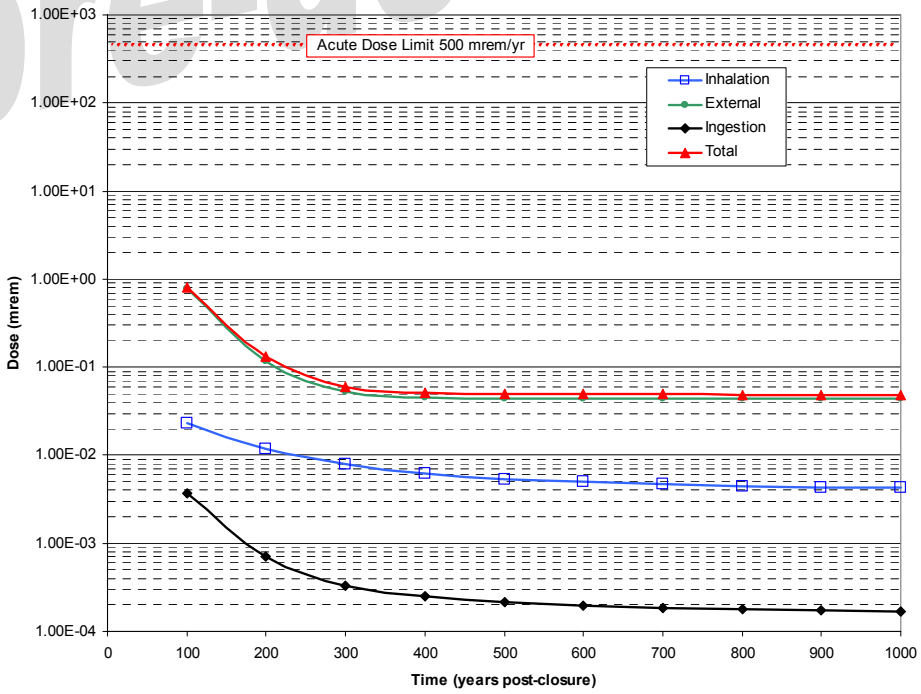

Figure 5-7. Results of the acute intruder-construction scenario by exposure pathway.

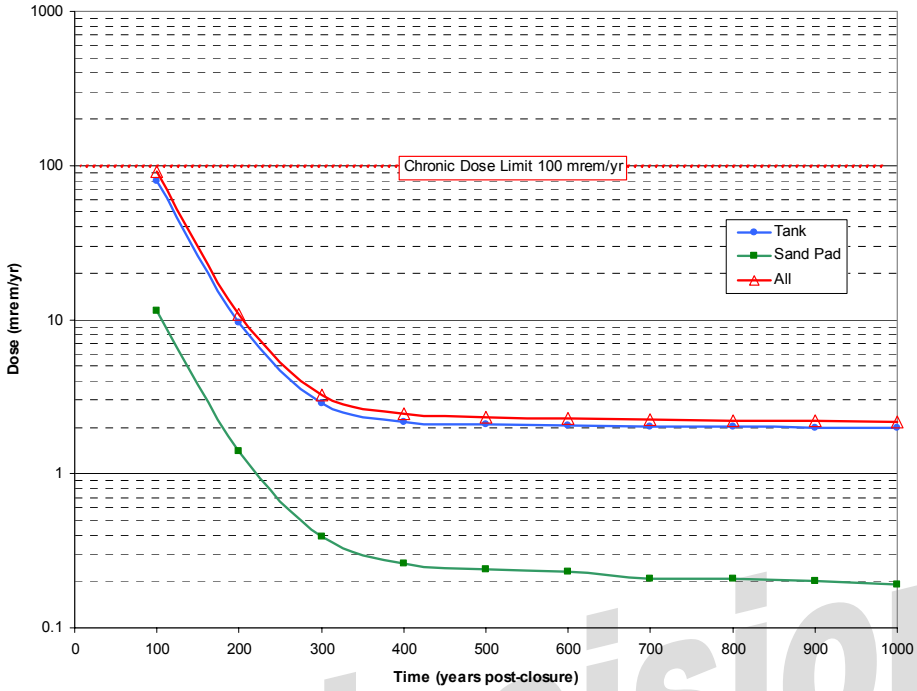

Figure 5-8. Results of the chronic intruder post-drilling scenario.

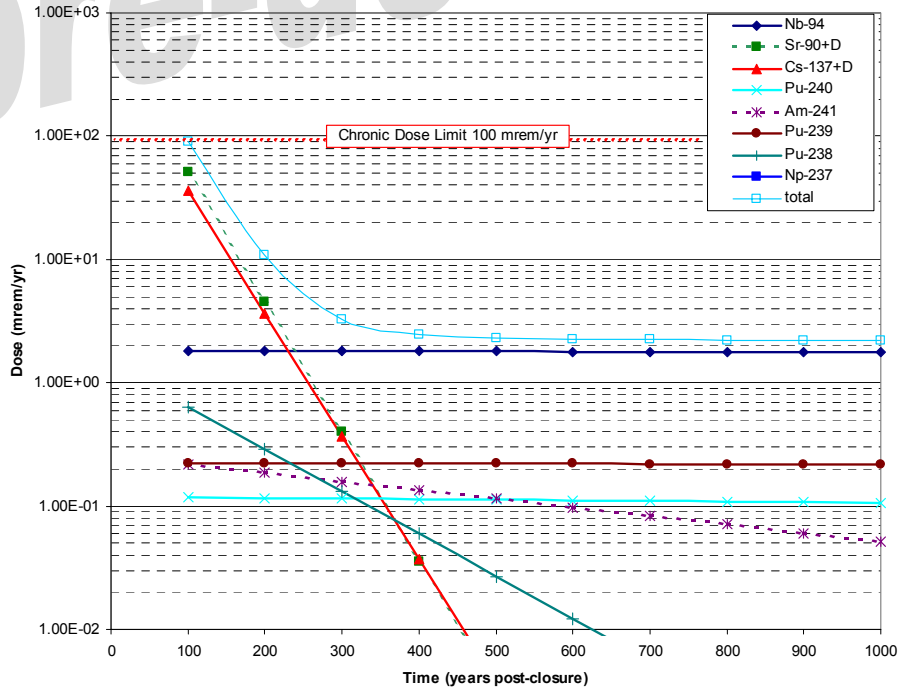

Figure 5-9. Results of the chronic intruder post-drilling scenario for individual radionuclides.

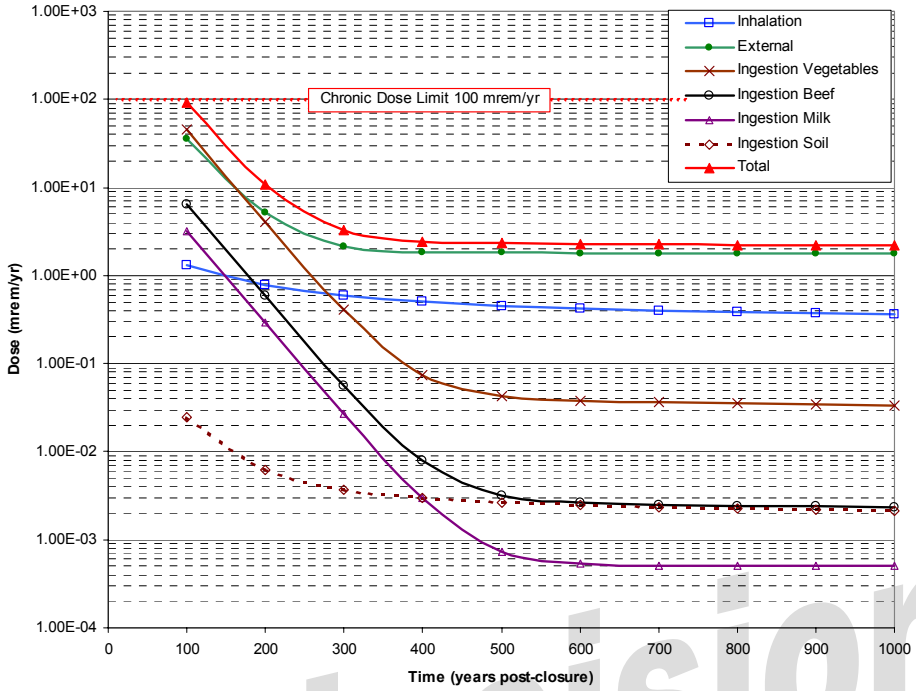

Figure 5-10. Results of the chronic intruder post-drilling scenario by exposure pathway.

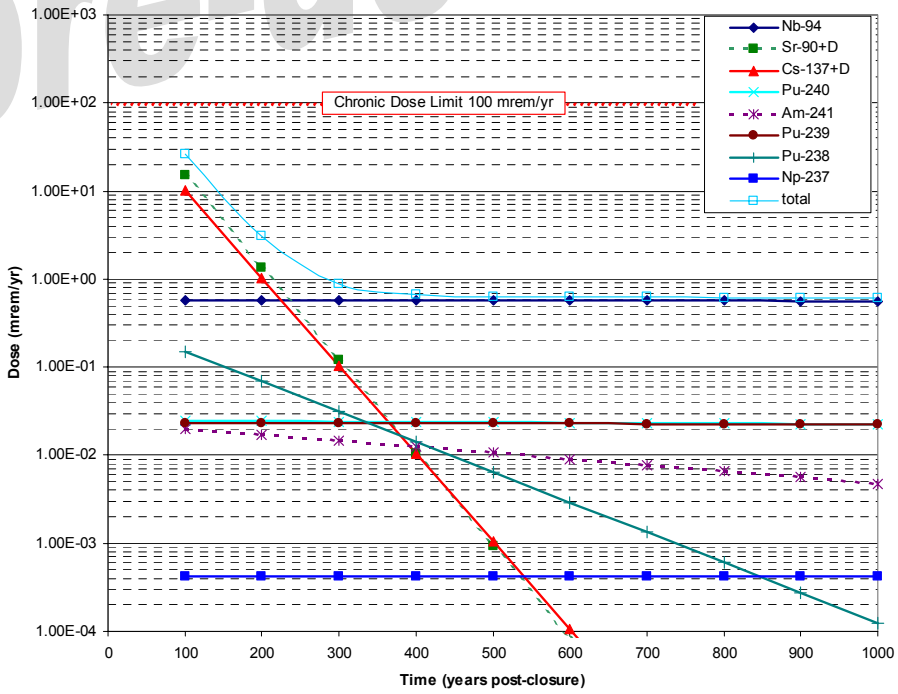

Figure 5-11. Results of the chronic intruder post-construction scenario for individual radionuclides.

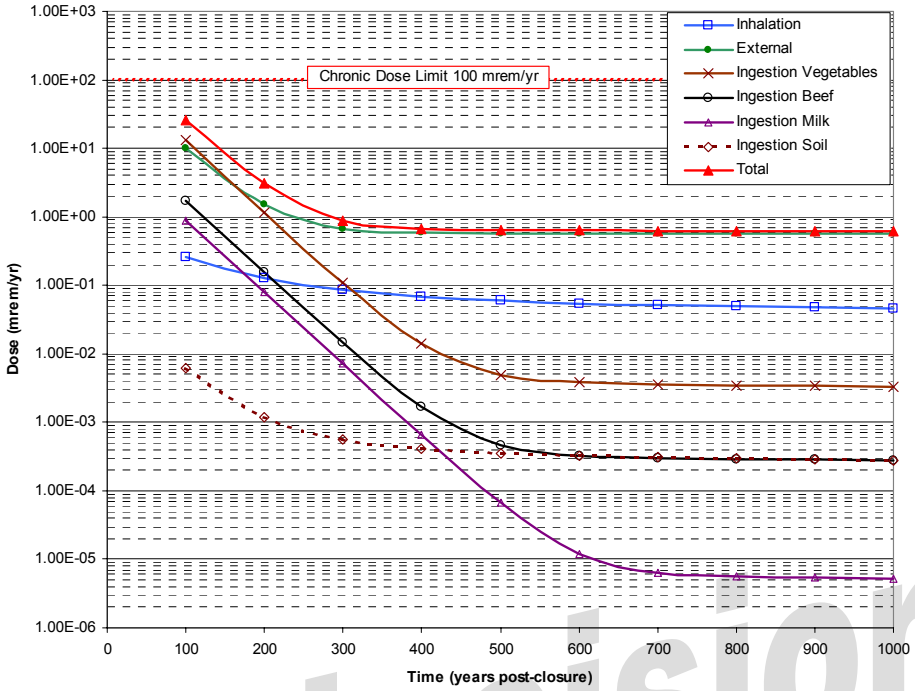

Figure 5-12. Results of the chronic intruder post-construction scenario by exposure pathway.

person drilling the well would not continue to drill through the concrete and stainless-steel tanks and grout unless it was completely degraded. However, to be conservative, it was assumed the intruder would drill the well through the waste at 100 yr post-closure.

Uncertainty exists in the state of the concrete systems over time. In this analysis, credit was taken for the concrete vault providing a barrier to intrusion. Oztunali and Roles (1986) state that "if resistance is encountered during drilling (as would be the case if the drill bit hit solid rocks or intact metal), the crew would simply move a few yards horizontally and drill a new hole. Drilling equipment and bits that can drill through solid rock and intact metal are available; however, they are more expensive than the equipment and bits that are normally required and used for water well installation. Similarly, it is anticipated that standard drill bits would have difficulty penetrating reinforced concrete structures, although little difficulty is expected for waste stabilized using grout backfill." Therefore, credit could be taken for the reinforced concrete vaults and the stainless-steel tanks, further reducing the doses for the intruder.

Intruder dose assessments include parameter uncertainty in radionuclide dose conversion factors and human intrusion and terrestrial transport models. The uncertainty in the radionuclide dose conversion factors is the subject of considerable research and is beyond the scope of these analyses. The dose conversion factors used were taken from Federal Guidance Reports 11 and 12 (EPA 1988 and 1993). The most conservative values were chosen for use in the intruder analysis. This approach is considered reasonable since there is no information available on the chemical and physical form of the waste constituents.

In Equation (5-4) for the acute intruder-drilling scenario, the radius of the well is not present in the equation. Note, however, that the concentration in the soil will be the same for any given well radius but the total amount of contaminated soil will vary with the well radius. This equation assumes that the radionuclide activity is completely mixed with the drill cuttings.

The radionuclide activity would not likely be completely mixed with the well cuttings. However, when considering the different possibilities such as the cuttings from the tank being covered with cuttings from below the tank and the varying radiation fields that would be encountered as the drilling commenced with time, it seems appropriate to make this assumption of complete mixing.

A 22-in.-diameter well provides 30 m^3 (1,000 ft^3) of contaminated zone (i.e., over the depth of the well borehole of 122 m [400 ft]). When the soil and waste are spread out over the assumed contaminated zone of 2,200 m^2 (24,000 ft^2), it results in a contaminated zone 0.014 m (0.54 in.) thick. As the well diameter is increased, the thickness of the contaminated zone also increases, thus affecting the external dose rate. However, in this intruder analysis, a very large diameter well was used for purposes of conservatism. Additionally, the assumption that the drill cuttings are spread out over the ground and are not located in a mud pit adds more conservatism and site-specific application that increases the external dose for this scenario.

Other conservative parameters were used in the acute intruder-drilling scenario as well. These include the assumptions that the intruder spends 160 hr drilling the well, respires at a rate of 8,400 m^3/yr, and is exposed to a dust loading of 1E+03 g/m^3. Standard drilling scenarios typically use an exposure time of 6 hr (Oztunali and Roles 1986).

In Equation (5-15) for the chronic post-drilling scenario, two parameters of importance are present in the form of the radius of the well (r_{well}) and the final depth of the contaminated zone after tilling (D_c). Variations in the values used for these parameters will result in proportional changes in the predicted radionuclide concentrations in the contaminated zone. Therefore, if the depth of the contaminated zone after tilling (D_c) is reduced by a factor of 2, the contaminated zone concentrations increase by a factor of 2. If the radius of the well (r_{well}) is increased by a factor of 2, the contaminated zone concentrations increase by a factor of 4. The selection of parameter values for D_c and r_{well} are considered to be appropriate and based on site-specific information.

The uncertainty in the intruder analyses is large and includes both the assumptions made during the development of the scenarios and the parameter values selected in the formulation of the mathematical representations. However, in this PA, every attempt was made to consider the site-specific environment and habits of the people currently in the region. Therefore, the analyses are considered to be representative of the INEEL region. The predicted doses are considered to be conservative, and there is a reasonable assurance that the performance objectives will not be exceeded for 1,000 yr post-closure.

Section 7 presents additional analysis of the uncertainty in the intruder dose results.

6. INTERPRETATION OF RESULTS

This section gives an interpretation of the results given in Sections 4 and 5. Section 7 provides additional discussion on the sensitivity and uncertainty in the analyses.

6.1 All-Pathways Dose

The all-pathways dose calculations were dominated by the groundwater pathway with a dose of 1.4 mrem/yr. The atmospheric dose contributes and additional 0.51 mrem/yr to the member of the public.

According to the results presented in Section 4, the doses to an individual of 1.4 mrem/yr at 890 yr for the all-pathways groundwater scenario did not exceed the performance objective of 25 mrem/yr for 1,000 yr after project completion. The long-term analysis in Section 4 also indicates that peak doses do not exceed the performance objective during the period of closure to 1 million years post-closure.

The atmospheric all-pathways dose of 0.51 mrem/yr, when added to the groundwater pathway dose of 1.4 mrem/yr, is still below the performace objective of 25 mrem/yr.

Uncertainty in the results is discussed in Section 7.

6.2 Radon Flux Results

Calculations were performed for a one-dimensional bare slab resting on the ground surface to determine the radon flux at the surface of the slab (Section 3). These calculations are highly conservative with respect to the actual performance of a grouted heel at the TFF because the slab is modeled in open air. This means that no credit is taken for the vault or tank. Also, the radium inventory at the end of the 1,000-yr analysis period is used for the source in the calculations, which is conservative for all times before the end of the performance period. This fact means that more radon can diffuse out of the slab than would otherwise be expected.

For ^{222}Rn (the dominant isotope in terms of atomic fraction), the flux of radon at the surface of the slab was 0.39 pCi/m^2/s, which is more than one order of magnitude below the performance objective of 20 pCi/m^2/s. Given the conservative nature of the calculation, there are two reasons that this value is so low: cementitious materials do not transport radon very well, and the radium content of the grouted heel is relatively low. Although the bare slab model could not be shown to meet the standard for the shorter-lived isotopes of radon (^{220}Rn, half-life of 55.6 s, and ^{219}Rn, half-life of 3.96 s), Section 3.3.3 shows that 0.5 m (2 ft) of overburden is capable of reducing these radon fluxes significantly. Therefore, the shorter-lived isotopes are quite incapable of penetrating even a modest overburden. Because of their shorter half-lives, the isotopes do not survive long enough to traverse the barrier.

6.3 Volatile Radionuclide Releases

The annual dose from volatile releases predicted by CAP88-PC atmospheric transport runs resulted in a dose for ^{3}H releases of 0.008 mrem/yr and ^{14}C doses of 0.5 mrem/yr, with a total dose of 0.5 mrem/yr. These doses are well below the atmospheric pathway performance objective of 10 mrem/yr. This was a very conservative analysis because flux rates were based on simplified models and the receptor was located at 100 m (300 ft) from the facility at all times (see Section 3.3.4). Also, the receptor would not be located near the TFF for the first 100 yr after closure because the site is assumed to be maintained and patrolled.

6.4 Groundwater Protection

The fundamental approach used in the numerical simulation of the unsaturated zone was to rely on the USGS definition of the site hydrostratigraphy, estimates of precipitation, and Big Lost River and percolation ponds seepage values, which were confirmed by several sources from the available literature (Anderson, Kuntz, and Davis 1999; Anderson 1991; Rodriguez et al.

1997). The hydraulic conductivity of the low-permeable interbed was varied within reasonable ranges, based on lithologic descriptions, to predict the location and extent of the numerous perched water bodies underlying the INTEC facility.

A two-dimensional groundwater flow and transport model was used to simulate contaminant releases from the tanks. The model domain dissected the center of two tanks, one sand pad, and included the releases from a break in the piping, providing the maximum release of contaminants to the underlying soil and groundwater. Since the dose limit calculation was applied to the two-dimensional slice through the center of the tanks, this approach ensures that all of the tanks will meet the groundwater performance objectives. In addition, the two-dimensional discretization of the problem domain allowed a high degree of resolution of the hydrostratigraphy, including the discontinuous interbeds that form the perched zones underlying the facility. By assuming that the USGS cross sections were accurate, the resulting numerical model predicted contaminant transport around the perched zones and through breaks in the interbeds. Dilution by perched water was minimized and the point where the maximum contaminant concentrations entered the regional aquifer was identified and selected as the compliance point.

According to the results presented in Section 4, the doses to an individual of 0.77 mrem/yr at 890 yr for the all-pathways scenario did not exceed the performance objective of 4 mrem/yr for 1,000 yr after project completion. The long-term analysis in Section 4 also indicates that peak doses do not exceed the performance objective during the period of closure to 1 million years post-closure.

Uncertainty in the results is discussed in Section 7.

6.5 Intruder Analysis Results

The maximum dose after institutional control (i.e., 100 yr) for the acute intruder-drilling scenario was 232 mrem. The major radionuclide contributors to the total acute intruder dose were $^{137}Cs/^{137m}Ba$ with 188 mrem, ^{238}Pu with 15 mrem, $^{90}Sr/^{90}Y$ with 8.64 mrem, ^{239}Pu with 5.3 mrem, ^{241}Am with 5.1 mrem, and ^{240}Pu with 2.8 mrem. The acute drilling scenario dose results are less than the performance objective of 500 mrem for all times post-institutional control.

The maximum dose post-institutional control (i.e., 100 yr) for the acute intruder-construction scenario was 0.93 mrem. The major radionuclide contributors to the total acute intruder dose were $^{137}Cs/^{137m}Ba$ with 0.72 mrem, ^{94}Nb with 0.045 mrem, $^{90}Sr/^{90}Y$ with 0.017 mrem, and ^{238}Pu with 0.013 mrem. The acute intruder-construction scenario dose results are less than the performance objective of 500 mrem for all times post-closure.

The maximum dose after loss of the concrete vault integrity was 91.1 mrem/yr for the chronic intruder post-drilling scenario at 100 yr post-closure. The major radionuclide contributors to the total chronic intruder dose were $^{90}Sr/^{90}Y$ with 51.5 mrem/yr and $^{137}Cs/^{137m}Ba$ with 36.5 mrem/yr. The chronic intruder post-drilling scenario dose results do not exceed the performance objective of 100 mrem/yr during the compliance period.

The maximum dose was 26.1 mrem/yr for the chronic intruder post-construction scenario at 100 years post-closure. The major radionuclide contributors to the total chronic intruder dose were $^{90}Sr/^{90}Y$ with 15.2 mrem/yr, $^{137}Cs/^{137m}Ba$ with 10.1 mrem/yr, ^{94}Nb with 0.58 mrem/yr, and ^{238}Pu with 0.15 mrem/yr. The chronic intruder post-construction scenario dose results do not exceed the performance objective of 100 mrem/yr for the 1,000-yr compliance period.

It is difficult to predict the future actions of humans, especially over a 1,000-yr period. The fact that the intruder is assumed to drill a well directly through a tank is considered a very conservative assumption. It can be argued that the person drilling the well would not continue to drill through the concrete and stainless-steel tanks and grout unless it was completely degraded. The analysis is very sensitive to the time of intrusion because the short-lived fission products are the main contributor to the intruder doses at 100 yr post-closure.

Uncertainty exists in the state of the concrete systems over time. In this analysis, credit was not taken for the concrete vault providing a barrier to intrusion. Oztunali and Roles (1986) state that "if resistance is encountered during drilling (as would be the case if the drill bit hit solid rocks or intact metal), the crew would simply move a few yards horizontally and drill a new hole. Drilling equipment and bits that can drill through solid rock and intact metal are available; however, they are more expensive than the equipment and bits that are normally required and used for water well installation. Similarly, it is anticipated that standard drill bits would have difficulty penetrating reinforced concrete structures, although little difficulty is expected for waste stabilized using grout backfill." Therefore, credit could be taken for the reinforced concrete vaults and the stainless-steel tanks, further reducing the doses for the intruder.

7. PERFORMANCE EVALUATION

A PA is the systematic analysis of the risks posed by a waste management system to the general public and the environment, and a comparison of those risks to the performance objectives. Section 7.1 provides an evaluation of the PA results with respect to the performance objectives listed in Section 1.4. A sensitivity/ uncertainty analysis is presented in Section 7.3. The results of the groundwater pathway analyses are discussed in comparison to the results presented in Section 7.1 to provide confidence that the projected performance and resulting doses are bounding. Selection criteria are discussed for the radionuclide inventory, radionuclide screening analysis, TFF degradation analysis, DUST-MS releases, and groundwater analysis.

The criteria for the selection and quantification of four radionuclide inventory and transport scenarios are presented. Section 7.3 contains a sensitivity/uncertainty analysis based on several scenarios involving the sensitive parameter for the transport of radionuclides. Different inventories, sorption coefficients, (K_d values) hydraulic diffusivity values, and infiltration rates are varied in numerical simulations for four different scenarios and the results are discussed in Section 7.4. The four scenarios include a best case, realistic case, conservative case, and worst case.

The final portions of this section present the uncertainties in the radon, volatile radionuclides, and intruder analyses. A discussion of future work completes this section.

7.1 Comparison of Results to Performance Objectives

This PA assesses the risk to two populations: the general public and hypothetical intruders. The risk to the general public has been assessed through the analysis of several conservative scenarios that reflect site-specific conditions at the TFF. The risk to hypothetical intruders was assessed through the analysis of four conservative scenarios. Tables 7-1 and 7-2 provide a summary of the PA results. The PA results indicate that all of the performance objectives are met for the TFF closure for all times post-closure.

7.1.1 Analysis of Airborne Emissions

The conservative case inventory, presented in Section 2.3, was used for the evaluation of the airborne emissions.

Table 7-1. Comparison of conservative results to the all-pathways, air emissions, and radon performance objectives.

Performance Objective	PA Result
Airborne emissions excluding radon 10 mrem/yr	0.51 mrem/yr
Average annual radon flux 20 pCi/m^2/s	0.39 pCi/m^2/s
Protection of groundwater[a] 4 mrem/yr	0.77 mrem/yr
All-pathways[a] 25 mrem/yr	1.86 mrem/yr

a. The all-pathways and protection of groundwater doses were never exceeded for the 1 million-yr analysis.

Table 7-2. Comparison of intruder results to the performance measures.

Performance Objective	PA Results			
	100 yr	200 yr	500 yr	1,000 yr
Acute drilling scenario 500 mrem	232 mrem	46.5 mrem	18.8 mrem	16.3 mrem
Acute construction scenario 500 mrem	0.80 mrem	0.13 mrem	0.05 mrem	0.05 mrem
Chronic post-drilling scenario 100 mrem/yr	91.1 mrem/yr	10.9 mrem/yr	2.3 mrem/yr	2.2 mrem/yr
Chronic post-construction scenario 100 mrem/yr	26.1 mrem/yr	3.1 mrem/yr	0.64 mrem/yr	0.61 mrem/yr

The annual dose from volatile releases predicted by CAP88-PC atmospheric transport runs resulted in a dose for ^{3}H releases of 0.008 mrem/yr and ^{14}C doses of 0.50 mrem/yr, with a total dose of 0.51 mrem/yr. These doses are well below the atmospheric pathway performance objective of 10 mrem/yr and also indicate that the atmospheric pathway will not contribute significantly to the all-pathways dose. This was a very conservative analysis because flux rates were based on simplified models and the receptor was located 100 m (300 ft) from the facility at all times (see Section 3.3.4). Also, the receptor would not be located near the TFF for the first 100 yr after closure because the site is assumed to be maintained and patrolled.

7.1.2 Analysis of Radon Flux

The conservative case inventory, presented in Section 2.3, was used for the evaluation of the radon flux rates.

Calculations were performed for a one-dimensional bare slab resting on the ground surface to determine the radon flux at the surface of the slab (Section 3). These calculations are highly conservative with respect to the actual performance of a grouted heel at the TFF because the slab is modeled in open air. This means that no credit is taken for the vault or tank. Also, the radium inventory at the end of the 1,000-yr analysis period is used for the source in the calculations, which is conservative for all times before the end of the performance period; therefore, more radon can diffuse out of the slab than would otherwise be expected.

For ^{222}Rn (the dominant isotope in terms of atomic fraction), the flux of radon at the surface of the slab was 0.39 pCi/m^2/s, which is more than one order of magnitude below the performance objective of 20 pCi/m^2/s. Given the conservative nature of the calculation, there are two reasons that this value is so low: cementitious materials do not transport radon very well and the radium content of the grouted heel is relatively low. Although the bare slab model could not be shown government to meet the standard for the shorter-lived isotopes of radon (^{220}Rn, half-life of 55.6 s and ^{219}Rn, half-life of 3.96 s), Section 3.3.3 shows that 0.5 m (2 ft) of overburden is capable of reducing these radon fluxes by at least a factor of 10^{96}. Therefore, the shorter-lived isotopes are quite incapable of penetrating even a modest overburden. Because of their shorter half-lives, the isotopes do not survive long enough to traverse the barrier.

7.1.3 Analysis of Groundwater Pathway Doses

The groundwater protection and all-pathways dose analyses were based on the conservative case inventory presented in Section 2.3. The results of the analyses presented in Sections 4 and 6 show that the performance objectives were not exceeded.

According to the results presented in Section 4, the realized doses to a receptor individual of 0.77 mrem/yr at 890 yr for the groundwater protection scenario (i.e., drinking water) did not exceed the performance objective of 4 mrem/yr for 1,000 yr after project completion. The long-term analysis in Section 4 also indicates that peak doses do not exceed the performance objective during the period of closure to one million years post-closure.

According to the results presented in Section 4, the realized doses to a receptor individual of 1.4 mrem/yr at 890 yr for the all-pathways scenario did not exceed the performance objective of 25 mrem/yr for 1,000 yr after project completion. The long-term analysis in Section 4 also indicates that peak doses do not exceed the performance objective during the period of closure to one million years post-closure.

A sensitivity/uncertainty analysis is presented in Section 7.3 for the groundwater pathway. The results of the conservative dose analysis are compared to the results of the uncertainty analysis to ensure that the projected doses are bounding.

7.1.4 Analysis of Chronic Intruder Post-Drilling Scenario

The conservative case inventory, presented in Section 2.3, was used for the evaluation of the intruder doses.

The maximum dose after institutional control (i.e., 100 yr) for the acute intruder-drilling scenario was 232 mrem. The major radionuclide contributors to the total acute intruder dose were $^{137}Cs/^{137m}Ba$ with 188 mrem, ^{238}Pu with 15.0 mrem, $^{90}Sr/^{90}Y$ with 8.64 mrem, ^{239}Pu with 15.3 mrem, ^{241}Am with 5.1 mrem, and ^{240}Pu with 2.8 mrem. The acute drilling scenario dose results are less than the performance objective of 500 mrem for all times post-institutional control.

The maximum dose post-institutional control (i.e., 100 yr) for the acute intruder-construction scenario was 0.80 mrem. The major radionuclide contributors to the total acute intruder dose were $^{137}Cs/^{137m}Ba$ with 0.72 mrem, ^{94}Nb with 0.04 mrem, $^{90}Sr/^{90}Y$ with 0.02 mrem, and ^{238}Pu with 0.01 mrem. The acute intruder-construction scenario dose results are less than the performance objective of 500 mrem for all times post-closure.

The maximum dose for the chronic intruder post-drilling scenario was 91.1 mrem/yr at 100 yr post-closure. The major radionuclide contributors to the total chronic intruder post-drilling scenario dose were $^{90}Sr/^{90}Y$ with 51.5 mrem/yr, and $^{137}Cs/^{137m}Ba$ with 36.5 mrem/yr. The chronic intruder post-drilling scenario dose results do not exceed the performance objective of 100 mrem/yr during the compliance period.

The maximum dose was 26.1 mrem/yr for the chronic intruder post-construction scenario at 100 yr post-closure. The major radionuclide contributors to the total chronic intruder dose were $^{90}Sr/^{90}Y$ with 15.2 mrem/yr, $^{137}Cs/^{137m}Ba$ with 10.1 mrem/yr, ^{94}Nb with 0.58 mrem/yr, and ^{238}Pu with 0.15 mrem/yr. The chronic intruder post-construction scenario dose results do not exceed the performance objective of 100 mrem/yr for the 1,000-yr compliance period

Uncertainty exists in the state of the concrete systems over time. In this analysis, credit was not taken for the concrete vault providing a barrier to intrusion. Oztunali and Roles (1986) state that "if resistance is encountered during drilling (as would be the case if the drill bit hit solid rocks or intact metal), the crew would simply move a few yards horizontally and drill a new hole. Drilling equipment and bits that can drill through solid rock and intact metal are available; however, they are more expensive than the equipment and bits that are normally required and used for water well installation. Similarly, it is anticipated that standard drill bits would have difficulty penetrating reinforced concrete structures, although little difficulty is expected for waste stabilized using grout backfill." Taking credit for both the reinforced concrete vault and the stainless-steel tank for additional years beyond 100 yr would reduce the intruder doses further because the dose is due to shorter-lived radionuclides.

The uncertainty in the results of the PA intruder analyses and potential effects on the projected doses is discussed in Section 7.10.

7.2 Use of Performance Assessment Results

The analyses presented in this PA were based on conservative assumptions and a conservative inventory. Based on the conservative analyses, all of the PA performance objectives were met.

The performance objective budget was allocated to the entire TFF closure. This is considered appropriate because all tanks to be closed are located within close proximity to one another. In other words, closure of facilities located in separate hydraulic flow regimes does not apply to the TFF closure. As demonstrated in the Savannah River Site Tank Closure study,[a] several facilities were considered during closure that were not within the same groundwater transport segments. The TFF is located within a flow regime in which all contaminants are considered within the specified groundwater transport segment modeled in this PA. Therefore, different performance objective budget allocations for each tank are not necessary.

The two-dimensional groundwater transport model considered a 1-m (3-ft) slice through the major axis of two tanks in a north-south cross section. This ensures that the maximum unit area of waste is input in the model and the downgradient groundwater concentrations are representative of the centroid of the contaminant plume that would be realized in a three-dimensional model.

The sensitivity/uncertainty analysis presented in Sections 7.3 through 7.11 provide additional discussion of the PA results in light of the uncertainties in the analyses.

a. Savannah River Site, 2000, *Industrial Wastewater Closure Plan for F- and H-Area High-Level Waste Tank Systems*, Preliminary Draft Revision 2, March 1.

7.3 Groundwater Pathway Sensitivity/Uncertainty Analysis

Several models and assumptions were used to assess the performance of the TFF, which results in several areas of the PA contributing to the uncertainty in the final results. Important areas of the PA analyses are discussed below and the sensitivity and uncertainty in the assumptions and parameter values are presented. A quantitative sensitivity/uncertainty analysis is provided for the groundwater pathway.

Four scenarios were developed for the groundwater pathway: 1) worst case, 2) conservative case, 3) realistic case, and 4) best case. The development of these four scenarios, with varying parameter values, was suggested by NRC. The four scenarios provide a means of evaluating the sensitivity and uncertainty of the analysis presented in Section 4. The bounding analysis presented in Section 4 was based upon the conservative scenario and associated parameter values. The parameter values chosen for each scenario are presented in Table 7-3. The following sections provide discussions on the selection of these parameter values.

7.3.1 Radionuclide Inventories

As recommended by NRC in the Request for Additional Information dated June 5, 2002,[b] the proposed changes for evaluating the TFF radionuclide inventory includes best, realistic, conservative, and worst-case scenarios. NRC suggested that four scenarios be developed to include radionuclide inventory and transport parameters. NRC recommended "best case, expected behavior, a reasonably conservative case, and a worst case."

b. Letter from Thomas H. Essig, Chief—Environmental and Performance Assessment Branch, Division of Waste Management, Office of Nuclear Safety and Safeguards, NRC, Joel T. Case, Director—INTEC Waste Programs, DOE-ID, 2002, "Request for Additional Information on the Idaho National Engineering and Environmental Laboratory Draft Waste Incidental to Reprocessing Determination for the Tank Farm Facility Residuals (DOE/ID-10777)," June 5.

Table 7-3. Overview of the parameter values for the sensitivity/uncertainty analysis.

		Nuclide Best Scenario	Realistic Scenario	Conservative Scenario	Worst-Case Scenario
Solid Radionuclide Inventory		50% reduction from worst case	25% reduction from worst case	10% reduction ^{129}I and ^{99}Tc inventories reduced	Depicts sodium-bearing waste (undiluted tank-heel residual)
Liquid Radionuclide Inventory		95% reduction from worst case	80% reduction from worst case	50% reduction ^{129}I and ^{99}Tc inventories reduced	Depicts sodium-bearing waste (undiluted tank-heel residual)
Infiltration		1.1 cm/yr	1.1 cm/yr	4.1 cm/yr	12.4 cm/yr
Grout Sorption Coefficients (m^3/kg)	Sr	0.006	0.006	0.003	0.001
	Tc	5	5	2.5	1
	I	0.03	0.03	0.008	0.002
	C	10	10	5.0	1.0
Unsaturated Zone Longitudinal Dispersivities (m)		0.52 (sediment) 3.36 (basalt)	0.52 (sediment) 3.36 (basalt)	0.29 (sediment) 1.85 (basalt)	0.052 (sediment) 0.34 (basalt)
Unsaturated Zone Transverse Dispersivities (m)		0.26 (sediment) 1.7 (basalt)	0.26 (sediment) 1.7 (basalt)	0.14 (sediment) 0.94 (basalt)	0.026 (sediment) 0.17 (basalt)
Interbed Sediment Sorption Coefficients (mL/g)	Sr	24	24	18	12
	Tc	0.1	0.1	0.01	0
	I	5	5	0.1	0.01
	C	20	20	10	2
Basalt Sorption Coefficients (mL/g)	Sr	13	13	6	1
	Tc	0.24	0.24	0.01	0
	I	1	1	0.1	0
	C	7.1	7.1	5.0	1.7

For conservatism, a conservative waste inventory was used to bound the worst condition that 100% sodium-bearing waste remained in the tank after emptying it to expected levels. The worst condition implies higher waste concentrations in the tanks than shown in recent sampling and historical data and shows the impacts if no tank cleaning was done.

The following discussions provide an overview of the development of the four inventory scenarios. A complete discussion on the development of the inventories is provided in Appendix A.

The sand pad inventory was held constant throughout the sensitivity/uncertainty analysis because the sand pad is not proposed to be washed like the tanks and piping.

7.3.1.1 Worst-Case Inventory. The worst-case radionuclide inventory initially was prepared to predict the greatest waste concentrations and masses that could remain at closure; it represents an upper estimate based on analytical data, numerical modeling, and knowledge of INTEC

operations (See Appendix F). This case considers that tank internal surfaces have been cleaned and the residual waste has been pumped out until there is about a 1.25-in. waste heel remaining in the tank.

The piping inventory for the worst-case scenario was based upon 15.5 kg of solid waste in the piping. The total piping inventory was assumed to be placed where the 11 tanks are located, resulting in 1/6 of the piping inventory being placed in the modeling domain for the two-dimensional groundwater model domain.

7.3.1.2 Conservative Inventory. The conservative case inventory differs from the worst case because it is assumed that limited tank cleaning has occurred. The basic difference is the liquid radionuclide concentration is assumed to be reduced by 50% and solids mass is assumed to be reduced by 10%. Like the worst case, this case considers that tank internal surfaces have been cleaned and the residual waste has been pumped out until there is about a 1.25-in waste heel remaining in the tank. The conservative case was prepared to predict the greatest waste concentrations and volumes that could remain at closure with only limited cleaning and represents a very conservative estimate based on analytical data, numerical modeling, and knowledge of INTEC operations.

The piping inventory for the conservative case was based upon 15.5 kg of solid waste in the piping, reduced by 10%.

7.3.1.3 Realistic Inventory. The realistic case inventory assumes that significant tank cleaning has occurred. The liquid radionuclide concentration is assumed to be reduced by 80% and solids mass is assumed to be reduced by 25% from the worst case. The realistic case was prepared to predict waste volumes that would remain at closure with significant cleaning and represents a conservatively realistic estimate based on analytical data, numerical modeling, and knowledge of INTEC operations. This scenario does not include the cleaning efficiencies shown in the mock-up of the tank cleaning but conservatively estimates the observed cleaning efficiencies of Tank WM-182. This case considers that tank internal surfaces have been cleaned and the residual waste has been pumped out until there is about a 1-in. waste heel remaining in the tank.

The piping inventory for the realistic case was based upon 15.5 kg of solid waste in the piping, reduced by 80%.

7.3.1.4 Best-Case Inventory. The best-case inventory of radionuclides differs significantly from the worst-case scenario. This scenario assumes a 95% reduction in liquid waste radionuclide concentrations and a 50% reduction in solid residual from the worst case. This case considers that tank internal surfaces have been cleaned and the residual waste has been pumped out until there is slightly over a 1-in. waste heel remaining in the tank. The best case was prepared to predict waste volumes that would remain at closure with thorough cleaning and represents a realistic but optimistic estimate based on analytical data, numerical modeling, and knowledge of INTEC operations. This scenario assumes that solid residual removal is about the same as that achieved in tank mock-up testing (INEEL 2001c). This conservatism allows for variability in the tank-to-tank solid inventory and structural and component differences; it also accounts for any reduced efficiency from cold mock-up conditions to field conditions.

The piping inventory for the best case was based upon 15.5 kg of solid waste in the piping, reduced by 95%.

7.3.2 Sorption Coefficients

A key area of uncertainty in the groundwater transport analyses is the sorption coefficients (K_d values). K_d values have been found to range over several orders of magnitude for selected radionuclides.

The following sections discuss the selection of distribution coefficients for the four sensitivity/ uncertainty scenarios.

7.3.2.1 Sediment and Basalt K_d Values. Knowledge of the sorptive properties of contaminants is key to understanding contaminant movement at the TFF. The subsurface comprises

surficial sediments, sedimentary interbeds, and basalt. There is limited site-specific adsorption information for contaminants in the subsurface environment at the INEEL (Del Debbio and Thomas 1989; Schmalz 1972). Distribution coefficients are available for cobalt, chromium, strontium, cesium, cadmium, mercury, and selenium for alluvium. For interbed sediments and basalt, distribution coefficients are available for cadmium, mercury, selenium, and strontium. Limited availability of site-specific adsorption information for other radionuclides for sediments and basalts at the INEEL has resulted in the use of adsorption parameters measured for sediments and basalts from other sites. Table 7-4 summarizes the measured K_d values for the INEEL.

Several investigators have published compendia of soil and sediment distribution coefficient data (Baes and Sharp 1983; Coughtrey, Jackson, and Thorne 1985; Sheppard and Thibault 1990). The most thorough of these compendia is Sheppard and Thibault (1990), which contains a breakout of the distribution coefficients by major soil types (i.e., sand, loam, clay, and organic). Past compendia grouped all soil types together.

Distribution coefficient data for basalts are not as readily available as data for soils and sediments. The main source of K_d values is basalts from the Nuclear Energy Agencies sorption database (Ticknor and Ruegger 1989). These basalt sorption values are provided in Table 7-5.

In addition, a survey of the literature for the WAG 3 modeling study (Rodriquez et al. 1997) is provided in Table 7-6.

K_d values are considered sensitive parameters in predictive modeling of radionuclide transport in the subsurface. There are a limited number of actual measurements available for the radionuclides that are specific to the INEEL soils and basalt as indicated by Table 7-4. Consequently, it was necessary to survey the literature for similar sites where actual radionuclide sorption studies have been conducted. Table 7-3 provides a list of K_d values for key radionuclides used in the predictive transport modeling. The rationale for the selection criteria is presented in Table 7-7. The sensitivity/uncertainty analysis consisted of the use of three separate combinations of the sorption coefficients: (1) worst-case transport, (2) conservative transport, and (3) realistic/best transport. The realistic/best scenarios used the same K_d values. This method provided a means of comparing the conservative case analysis, presented in Sections 3 and 4, with the range of values presented in the literature.

The appropriateness of using these K_d values at the INEEL is difficult to assess. The mineralogical differences have not been addressed, and the secondary minerals (e.g., clays and iron oxides) have not been quantified. The secondary minerals form in the fractures and may have a major impact on the adsorption of many radionuclides. Also, it is unclear if equilibrium is maintained during flow through the unsaturated zone. If local equilibrium is not valid, then the K_d value will overestimate the retardation of contaminants.

Column studies conducted on basalts at various moisture contents from saturation to 20% consistently resulted in essentially the same K_d values (Porro, Newman, and Dunnivant 2000). This evidence indicates that K_d values for the saturated zone are applicable to the unsaturated zone. While the reliability of K_d values obtained from batch tests is still being debated, using saturated K_d values for unsaturated transport simulation is not a specific concern.

The modeling study conducted for the *Remedial Investigation/Baseline Risk Assessment* (RI/BRA) for INTEC (Rodriguez et al. 1997) used the sediment distribution coefficient for the alluvium and the interbed sediments, a zero distribution coefficient for the vadose zone basalts, and 1/25 of the sediment distribution coefficient for the aquifer basalts. The vadose zone basalts were assumed to have a zero distribution coefficient in the RI/BRA based on the assumption that the water moves more quickly through vertical fractures in the vadose zone. This allows very little time for the contaminant to sorb to the basalt. In the aquifer, the RI/BRA modeling assumed that the water moves more slowly through the basalt fractures and matrix and there is sufficient time for the contaminants to sorb in the basalts.

Table 7-4. Summary of sorption coefficients measured at the INEEL.

	K_d Values (mL/g)[a]			
Element	Alluvium	Interbed Sediment	Basalt	Reference
Cd	4891-2864	10,115-8622	2319-785	Del Debbio and Thomas (1989)
Co	56	Not measured	Not measured	Schmalz (1972)
Cr	1.2	Not measured	Not measured	Schmalz (1972)
Cs	950	Not measured	Not measured	Schmalz (1972)
Hg	1921-236	673-72	87-9.2	Del Debbio and Thomas (1989)
Se	63-5.8	17-4.9	3.4-0.29	Del Debbio and Thomas (1989)
Sr	35-52	110-186	1.1-2.7	Del Debbio and Thomas (1989)
	24	Not measured	Not measured	Schmalz (1972)

a. K_d values reported by Del Debbio and Thomas (1989) were measured using batch equilibrium sorption methods on crushed materials that were passed through a 2-mm sieve.

Table 7-5. Basalt K_d values from the NEA database.

Element	NEA Basalt K_d Ranges (mL/g)
I	5.0E–02
Sr	2.0 to 1000
Tc	1.5E–01 to 5.5

Table 7-6. Sorption coefficient ranges identified in WAG 3.

Element	Sediment K_d (Range) mL/g	Basalt K_d (Range) mL/g
C	5 (2-20)[b]	—
I	0.1 (0.02-5)	—
Sr	60 (35-186)[c,d]	6 (1-13)[c,d]
Tc	0[d]	0[d]

a. Source: Rodriquez et al. 1997.

b. Range from NEA (Ticknor and Ruegger 1989) and Sheppard and Thibault (1990).

c. Source: Newman et al., in preparation, *Evaluation of the Mobility of Am, Cs, Co, Pu, Sr, and U through INEEL Basalt and Interbed Materials: Summary Report of the INEL/Clemson University Laboratory Studies*, ER-WAG7-82, INEEL internal report.

d. Source: Del Debbio and Thomas 1989.

Table 7-7. Selection rationale for the range of K_d values (mL/g) used in the sensitivity analysis.

Radionuclide	Range for K_d values (mL/g) used in transport model	Selection Rationale[a]
C (sediment)	2–20	Default: Ref. #1 loam soil K_d = 20 Site Values: WAG 3 Ref. #2 and #3 K_d = 2–20 Literature Confirmation: Sand Ref. #1 K_d = 5
C (basalt)	1.7–7.1	Site Values: WAG 3 K_d = not reported Literature Confirmation: The lowest reported Ref. #4 K_d = 1.7
I (sediment)	0.01–5	Default: Ref .#1 loam soil K_d = 5 Site Values: WAG 3 Ref. #2 K_d = 5 Literature Confirmation: No referenced value as low as K_d = 0.01
I (basalt)	0–1	Site Values: WAG 3 Ref. #2 K_d = 0 Literature Confirmation: Ref. #3 K_d = 0.05, Ref. #1 for sand K_d = 1
Sr (sediment)	12–24	Ref. #1 loam soil K_d = 20 Site Values: WAG 3 Ref.#2 K_d = 12–24 Literature Confirmation: Ref. #5 reports a range of 35–52 alluvium and 110–186 for interbed sediments
Sr (basalt)	1–13	Site Values: WAG 3 Ref. #2 K_d = 1–13 Literature Confirmation: Ref. #5 reports a range of 1.1–2.7 for crushed basalt column tests, Ref. #4 K_d = 2–1000
Tc (sediment)	0–0.1	Default: Ref. #1 loam soil K_d = 0.1 Site Values: WAG 3 Ref. #2 K_d = 0 Literature Confirmation: Ref. #3 lowest measured sand K_d = 0.02
Tc (basalt)	0–0.24	Site Values: WAG 3 Ref. #2 K_d = 0 Literature Confirmation: Ref. #5 measured K_d = 0.016 for crushed basalt column tests; Ref. #3 K_d = 0.15–5.5

a. References:

1. Sheppard and Thibault 1990.
2. Rodriquez et al. 1997.
3. NEA database (Ticknor and Ruegger 1989).
4. Thibault, Sheppard, and Smith 1990.
5. Del Debbio and Thomas 1989.

The RI/BRA modeling also based the aquifer basalt distribution coefficients on an evaluation of the ratio of the distribution coefficient for sediments to that for basalts from the Del Debbio and Thomas (1989) report. Here they found the ratio to the 1/25. The Del Debbio and Thomas (1989) report, however, provides conflicting information on the differences in sediment and basalt distribution coefficients. This report provides for higher distribution coefficients in the basalts (based on breakthrough curve studies) in comparison to the batch distribution coefficient study. Because of this, the appropriateness of the assignment of vadose and aquifer basalt distribution coefficient values is difficult to assess. Therefore, the distribution coefficients for basalts were treated as uncertain as well as the sediment distribution coefficients.

7.3.2.1.1 Strontium—The basalt values were based on the range presented in Table 7-7 with the worst-case scenario being assigned the lowest reported values in the range and the best/realistic case being assigned the highest value in the reported range. The conservative values were assigned the mid-point of the reported basalt K_d range.

The sediment (i.e., interbed sediments in the unsaturated zone) were assigned K_d values based upon the modeling conducted for WAG 3 CERCLA groundwater modeling at INTEC (Rodriquez et al., 1997). This modeling showed that a K_d value of 12 for the sediment resulted in ^{90}Sr groundwater concentrations higher then measured. A sediment value of 24 also was investigated and showed a closer match of the modeled concentrations with the measured concentrations. Therefore, the best/realistic scenario was assigned a K_d value of 24 for the interbed sediments, while the worst case was assigned a value of 12. The conservative case was assigned the mid-point value of the range.

7.3.2.1.2 Carbon—The basalt values were based on the range presented in Table 7-7. The worst-case scenario was assigned the lowest reported value, while the best/realistic scenario was assigned the high value for the range.

The sediment K_d values were taken from the range reported in Table 7-7 with the worst-case scenario being assigned the low value of the range and the best/realistic scenario being assigned the high value of the range. The conservative case was assigned a value of 5 mL/g, which was closer to the low end of the reported range.

As noted above, sand K_d values were selected for ^{14}C for transport simulations in the basalts where site-specific basalt K_d values were not available (Table 7-4). The published sand K_d values were obtained from Sheppard and Thibault (1990). It was assumed that the lower sand K_d values are more representative of the sorptive behavior of ^{14}C in basalt. This assumption is based on the coating of weathered mineral or chemical precipitates on sand grains and the irregular fracture surfaces that can react with the radionucludes. While the surface area to the void-space ratio for fractured media is less than a porous media (thereby reducing the sorptive capability for a fractured media), the presence of abundant iron oxides in basalt fractures capable of sorbing radionuclides offset the surface area effects. The degree of this offset is uncertain and difficult to apply to natural systems.

This approach allows a degree of retardation of ^{14}C in the basalts. The lower sand K_d values, compared to the higher K_d values for finer-grain sediment, are conservative on a relative basis. However, there is an acknowledged degree of uncertainty because of the lack of direct K_d measurements available for ^{14}C in basalt.

7.3.2.1.3 Technetium—The basalt value for the worst-case scenario was based on the value of zero in Table 7-7. The best/realistic case was assigned a value of 0.24, which is in the low end of the range. This was done to consider the fact that Tc has been found to be mobile at the INEEL Site. The conservative value was set to a very low value of 0.01, again due to reports that Tc is mobile at the INEEL.

The sediment K_d value for the worst case was taken as zero, while the realistic case was assigned a value of 0.1 based on values in Table 7-7 for loam soil. The conservative value

was assigned a value one order of magnitude less than the loam soil value.

7.3.2.1.4 Iodine—The basalt value for the worst case was assigned a value of zero, while the best/realistic case was assigned a value of 1.0 based on a reasonable upper end for the values reported in Table 7-7. The sediment K_d value for the worst case was assigned a value of 0.01, while the best/realistic case was assigned a value of 5.0. The conservative case was assigned a value of 0.1.

7.3.2.2 Grout K_d Values. The grout K_d values were evaluated for the four groundwater pathway scenarios. A review of the Bradbury and Sarott (1995) study on *Sorption Databases for the Cementitious Near-Field of a LLW Repository for Performance Assessment* indicates that the K_d values presented in their study were based on the conservative end of the possible choices (i.e., lower K_d values). Therefore, a combination of grout K_d values were chosen based on Bradbury and Sarott (1995), Allard (1985), and other studies specific to the elements of interest.

Concrete K_d values for reducing conditions have been chosen. The concrete is expected to exhibit strongly reducing conditions (Eh from –300 to –500 mV) as do most concrete systems. In addition, the closure system will also consist of a mix of concrete and fly ash, slag, or other substances to ensure reducing conditions in the grout.

The concrete K_d values were chosen from Region II of the Bradbury and Sarott study (1995). In Region II, the pore water composition is dominated by portlandite $Ca(OH)_2$, which fixes the pH at 12.5. The portlandite will be slowly removed by groundwater flow but the quantities contained in the cement are so large that this phase buffers the system over very long periods of time.

Bradbury and Sarott (1995) also discuss a Region III (Figure 1) for concrete systems, where the removal of $Ca(OH)_2$ has become significant and the pH falls continuously. The calcium-silicate-hydrate gel is no longer stable and begins to dissolve incongruently. However, investigation into the original paper on these concrete regions by Atkinson, Everitt, and Guppy (1989) reveals that concrete is not expected to reach this state until 100,000 yr. Since the PA compliance period is only 1,000 yr, the concrete K_d values are not expected to change over this period of time and therefore are held constant. This assumption is supported by the concrete degradation analysis presented in Appendix E. Graphs of the hydraulic conductivity for the tank/grout show no increase over the 1,000-yr time period. The concrete degradation sensitivity analysis also shows that the tank/grout hydraulic conductivity does not increase until 800 yr for the least conservative case with only a one order of magnitude change in the hydraulic conductivity. Thus, the amount of water available for loss of $Ca(OH)_2$ is still minimal. For conservatism, the PA assumes that the tank fails at 500 yr; however, the degradation analysis indicates the tank/grout life is much longer. In addition, graphs of carbonation degradation and $Ca(OH)_2$ leaching do not show any significant changes during the 1,000-yr compliance period for loss of $Ca(OH)_2$.

The selection of concrete K_d values for the three groundwater pathway scenarios are presented in Table 7-3. The following discussion provides justification for each set of sorption K_d values for each element shown in Table 7-3.

7.3.2.2.1 Strontium—Ewart, Terry, and Williams (1985) report Sr distribution ratios for hardened cement paste and concrete between 0.001 and 0.004 m^3/kg, with very little dependency on concentration. Atkinson and Nickerson (1988) summarized the results from different types of tests and give a best-estimate range for Sr of 0.003 to 0.006 m^3/kg. Due to the small difference in K_d values reported for Sr, the worst-case scenario was assigned the low value of 0.001 m^3/kg, and the value was scaled for the other scenarios to a high value of 0.006 m^3/kg for the best/realistic scenario.

7.3.2.2.2 Technetium—Sorption data for Tc on cementitious materials are sparse. Under reducing conditions, Tc is present as hydrolyzed Tc^{+4} species. In some recent work, using Tc^{+4} at trace levels, distribution ratios of 5 m^3/kg have been reported (Bayliss et al. 1991). Tc may be expected to sorb strongly under

reducing conditions at a high pH. Bradbury & Sarott (1995) chose a conservative value (i.e., low value) of 1 m^3/kg for reducing conditions. Therefore, for the TFF PA, the conservative value of 1 m^3/kg was chosen for the worst-case scenario, with the K_d values being scaled up to the measured value of 5 m^3/kg for the best/realistic K_d value.

7.3.2.2.3 Iodine—Iodine is assumed to be present as I^- under oxidizing and reducing conditions (Bradbury and Sarott 1995). Many studies on the sorption of I^- on cement paste at a high pH indicate that its sorption is low but finite. Bradbury and Sarott (1995) selected a conservative value (i.e., lower value) of 0.002 m^3/kg for iodine in reducing trichloroethylene (TCE) concrete systems. Allard, Persson, and Terstenfelt (1985) recommended a K_d value of 0.03 m^3/kg for I^- in concrete systems. Therefore, for the TFF PA, the conservative value of 0.002 m^3/kg was chosen for the worst-case scenario, with the K_d value being scaled up to the recommend value of 0.03 m^3/kg by Allard, Persson, and Terstenfelt (1985) for the best/realistic case.

7.3.2.2.4 Carbon—Allard, Persson, and Terstenfelt (1985) recommend a K_d value for C of 5 m^3/kg. Studies by Allard, Torstenfelt, and Andersson (1981) and Bayliss et al. (1988) have investigated the sorption of ^{14}C as $^{14}CO_3^{2-}$ in cement/concrete systems. Generally, very high sorption values (approximately 10 m^3/kg) have been reported. Therefore, for the TFF PA, the value of 10 m^3/kg has been chosen for the best/realistic case and the scaled-down value of 1 m^3/kg for the worst-case scenario.

7.3.3 Hydraulic Dispersivity Variations

Dispersivity is a scale-dependent term used in the advective-dispersion equation to compensate for the variation in transport of solute particles. Ideally, the transport of solute particles could be described by the processes of advection and diffusion if it were possible to define the velocities throughout the porous media. Because this is impractical, averaging the groundwater velocities over some representative scale results in a scale-dependency of the dispersion term. A rule of thumb for estimating longitudinal dispersivity is 1/10 of the transport distance and a transverse dispersivity of one-half of the longitudinal value (Mills et al. 1985). Mills et al. (1985) also state that the unsaturated zone dispersivities are normally observed to be lower than the 1/10 rule. Inverse modeling of the INEEL Test Area North's TCE and tritium plume suggests the fracture basalt has a smaller value than rule-of-thumb dispersivity values.

Pickens and Grisak (1981) provide a comparison of scale-dependent dispersion based on field and laboratory studies. The longitudinal dispersivity ranges from 12 to 61 m based on computer modeling studies in granular geologic material associated with larger contaminated zones. Results of field tracer tests yield a range in longitudinal dispersivities of 0.012 to 15.2 m. Small-scale laboratory tests using repacked granular material yield a range in longitudinal dispersivities on the order of 0.01 to 1 cm. Work conducted by Sudicky and Cherry (1979) and Lee, Cherry, and Pickens (1980) showed that point sampling compared to samples from large screen intervals was a large factor in dispersivities reported in the literature. These researchers showed a range of longitudinal dispersivities based on point sampling methods of 0.01 to 0.22 m.

In evaluating the best estimate of dispersivity values for the unsaturated zone modeling, several factors were incorporated into the analysis. The transport scale is on the order of 130 m for transport through the unsaturated zone to the underlying water table. There are 20 separate zones that are assigned a specific hydraulic conductivity value that differs from the adjacent zones. The variations in hydraulic conductivity inherently impart dispersion on the transport of solutes. The scale of transport in the individual geologic units or zones is on the order of a few to tens of meters. As shown in Figure 7-1, the scale of transport distances for the individual stratigraphic units results in a range of longitudinal dispersivity of 0.01 to 1.0 m. The INEEL WAG 3 modeling for the INTEC facility, where the TFF is located, used a dispersivity value of 5 m for their unsaturated zone modeling (Rodriquez et al. 1997).

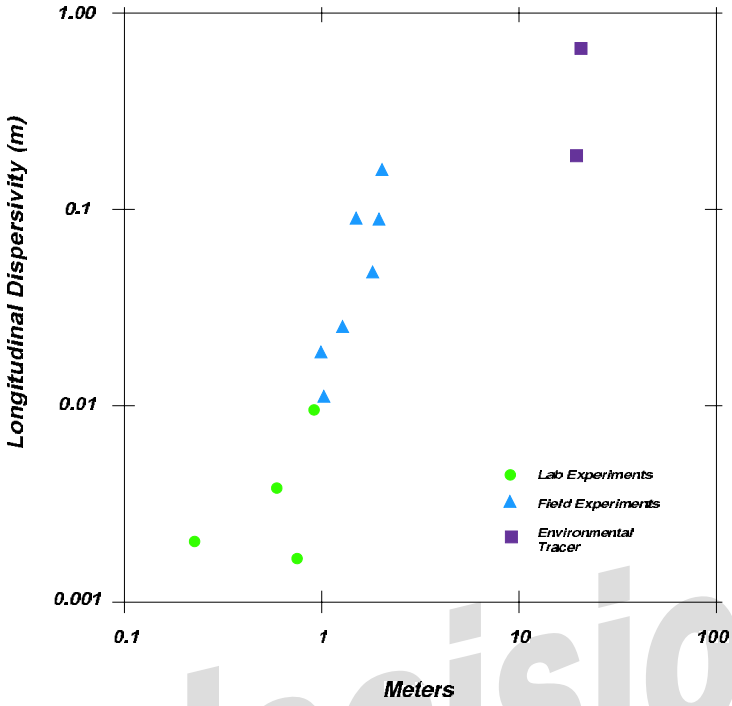

Figure 7-1. Longitudinal dispersivity graph (Mills et al. 1985).

The results of an extensive review of the literature for measured dispersivity values in porous and fractured material are presented in Table 7-8. The range in measured dispersivity values is significantly less than the calculated site values for the Snake River Plain Aquifer. In addition, the measurement scale for literature values reported in Table 7-8 are closer to the scale of transport for the individual geologic units in the unsaturated zone underlying the site. Consequently, the best/realistic, conservative, and worst-case scenarios were chosen from the values listed below.

For the realistic scenario, the highest values presented in Table 7-8 were selected. These values represented the highest measured or estimated values available in the literature. For the best/realistic scenarios, the interbed sediments will be assigned a value of 0.52 m for the longitudinal dispersivity and one-half that value, or 0.26 m for the transverse dispersivity. For basalt portions of the unsaturated zone, the selected values were 3.36 m for the longitudinal dispersivity and 1.7 m for the transverse dispersivity for the best/ realistic scenarios. The worst-case scenario was assigned 1/10 of the dispersivity values used for the best/realistic case. The conservative case was assigned values that are in the mid-point of the ranges of dispersivities used for the best/realistic and worst-case scenarios.

7.3.4 Infiltration Variations

A wide range in the infiltration rates at the site is reported in the literature and site-specific studies. These values range from a low of 0.16 in./yr (0.4 cm/yr) to a high of 4.9 in./yr (12.4 cm/yr). Most of the reported values in the literature are estimates based on the amount of precipitation and best-guess estimates of the evapotranspiration rates for the area.

One of the few actual field measurements conducted at the site is reported by Cecil et al. (1992). By measuring tritium and ^{36}Cl profiles in the soil, test results yielded a range of 0.4 to 1.1 cm/yr (0.2 to 0.43 in./yr) infiltration.

A detailed investigation of water infiltration rates was conducted at the CFA Landfill by

Table 7-8. Dispersivity values measured or calculated and reported in the literature (in meters).

	Boateng and Cawlfield (1999)	Bresler and Dagan (1983)	Broermann et al. (1997)	Hinsby et al. (1996)	Mallants et al. (2000)	Pickens and Grisak (1981)	Pistre et al. (2002)	Pohll et al. (1999)	Russo and Bresler (1981)	Sudicky, Cherry, and Frind (1983)
Unsaturated soil	α_L=0.005 α_T=0.001	α_L=0.03							α_L=0.08–0.52	
Saturated soil			α_L=0.67–6.51		α_L=0.09 α_T=0.0085	α_L=0.7				α_L=0.01–0.08 α_T=0.005–0.03
Unsaturated Fractures										
Saturated Fractures				α_L=0			α_L=0.01–3.36	α_L=1 α_T=1		

Miller et al. (1990). The CFA Landfill is covered by an earthen-based material from the surrounding area. Based on soil analysis, precipitation, and evapotranspiration estimates, a range of infiltration rates from 1.0 in. (2.5 cm) to 1.6 in./yr (4.1 cm/yr) was reported. This measured value is the same infiltration rate used in the WAG 3 modeling analysis (Rodriquez et al. 1997) for the Tank Farm area.

The measured value of 1.6 in./yr (4.1 cm/yr) for the CFA Landfill is considered an appropriate value for the conservative case since the TFF area will be covered with an engineered barrier under the CERCLA program. Therefore, this infiltration rate was considered for the realistic and base-case modeling estimates.

Three infiltration rates were considered in the uncertainty analysis, 12.4 cm/yr (4.88 in./yr) as the highest rate for the worst-case scenario, 4.1 cm/yr (1.6 in./yr) as the base-case infiltration for the conservative scenario, and 1.1 cm/yr (0.43 in./yr)as the realistic/best case infiltration. The low infiltration rate of 1.1 cm/yr (0.43 in./yr) is considered applicable to a well-engineered landfill cover that is required for the TFF.

7.3.5 Time of Degradation

Degradation analyses were conducted for the TFF closure system, which includes the vaults, tanks, grout, and piping. The degradation analyses were conducted to provide support for the PA analyses that assumed degradation step changes of 100 yr for the vault and grout between the vault and tanks, 500 yr for the tanks and grout inside of the tanks, and 500 yr for the piping.

Table 7-9 gives a summary of the degradation analyses using the assumption that a 50% loss of grout is the point of degradation failure of the system hydraulically. Table 7-9 shows the degradation times assumed in the PA, those for the base-case degradation analysis, and also the minimum and maximum degradation times from the sensitivity analysis (see Appendix E).

As indicated by the data in Table 7-9, the assumptions for degradation step changes in the PA are well within the ranges predicted by the degradation analysis. The uncertainty in the degradation of the TFF system components is large, as indicated in Table 7-9. However, the degradation steps assumed for the PA are equal to or less than the minimum failure times predicted by the degradation analysis. The data indicate that additional credit for a system component failure times could be taken.

Table 7-9. Summary of the degradation analysis, showing the time of failure for each component.

TFF System Component	PA Failure Time Assumption (yr)	Base Case Degradation Failure Time (yr)	Minimum Degradation Failure Time (yr)	Maximum Degradation Failure Time (yr)
Vault	100	175	100	> 10,000
Grout (between vault and tank)	100	3,500	500	> 10,000
Piping[a]	500	8,000	1,750	> 10,000
Tank and grout inside tank	500	8,000	1,750	> 10,000

a. Based on the degradation analysis, taking credit for the stainless-steel piping, and thus being equal to the tank degradation time.

However, to ensure that the analysis was bounding, conservative failure times were used for the analyses.

Corrosion rates from Palmer et al. (1999) are used to estimate the vault failure time from the expansion-corrosion reaction of the reinforcing steel and the times of the tank and the piping failure from corrosion. The corrosion rates are based on the maximum uniform corrosion rate observed in Tanks WM-180 through WM-189 as reported in Palmer et al. (1999) for stainless-steel coupons placed in these tanks for times ranging from 10 to 30 yr. From these studies, the maximum uniform corrosion rates ranged from 2.0E−05 to 5.3 E−02 mpy, where mpy is mils per year and mils are 0.001 in. The degradation calculations used a conservative value of 10^{-5} m/yr (3.9 E−01 mpy), which is greater than the maximum observed corrosion rate and is considered reasonable and conservative given the available data are not consistent with the expected grouted vault and tank conditions and do not account for corrosion over the time period of interest (i.e., 1,000 yr).

In the vault, tank, and piping degradation calculations, the thickness of the reinforcing steel, tank wall, and piping were assumed to be 0.5 in. (1 cm), 3/16 in. (0.5 cm), and 0.1 in. (0.3 cm), respectively. These values were selected based on design information and represent a conservative (i.e., minimum thickness) value. For example, the tank wall thickness was assumed to be 3/16 in. (0.5 cm), while the tank wall thickness varied from 3/16 in. (0.5 cm) on the dome, to 1/4 in. (0.6 cm) on the upper walls, to 5/16 in. (0.8 cm) on the lower walls.

For the tank and piping, corrosion was modeled as occurring inside and outside of the walls (i.e., from the grout inside and outside the walls). Since corrosion was modeled from the inside and outside of the walls, complete corrosion of the tank and piping was assumed to occur when one-half of the wall thickness corroded. Corrosion of reinforcing steel was assumed to occur from the outside of the cylindrical reinforcing steel/concrete vault interface and complete corrosion was assumed once 50% of the reinforcing steel corroded.

Using the extreme values from the range of maximum uniform corrosion rates in Palmer et al. (1999) and the assumptions of vault, tank, and piping stainless steel thickness and direction of corrosion attack, the failure times of the stainless steel in the vault, tank, and piping range from 10 million to 5,000 yr, 5 million to 2,000 yr, and 3 million to 1,000 yr for the minimum and maximum corrosion rates, respectively. In the DUST-MS calculations, the times for the vault and tank/piping failure of 100 and 500 yr were used. Additionally, the possible corrosion

mechanisms for the stainless-steel coupons in the tanks (Palmer et al. 1999) are for conditions that are more aggressive than those expected in the grouted vault, tank, and piping.

Thus, the failure times used to determine the onset of radionuclide release rates in DUST-MS for the vault, tank, and piping are conservative when compared to the available corrosion data. The corrosion model is considered to have provided bounding times for corrosion failure of the vault, tank, and piping. Furthermore, the release rate analysis used initial times for releases that were earlier than the times predicted by the most conservative of the corrosion rates.

The assumed degradation times were not altered in the groundwater pathway sensitivity/ uncertainty analysis.

7.3.6 Groundwater Pathway-Sensitivity and Uncertainty Analysis Results

This section discusses the results of the sensitivity and uncertainty analysis. The results are divided into two categories: (1) sensitivity and uncertainty analysis based upon the four groundwater pathway scenarios in a matrix of combinations, and (2) sensitivity/uncertainty analysis based upon individual changes in a specified parameter.

7.3.6.1 Groundwater Scenario Sensitivity/Uncertainty Results. The four groundwater scenarios: (1) worst-case, (2) conservative, (3) realistic, and (4) best, were analyzed for the groundwater protection scenario (i.e., drinking water) and the all-pathways scenario doses. These four scenarios were run for the matrix of possibilities: (1) inventory, (2) infiltration, and (3) transport parameters (i.e., distribution coefficients). This matrix resulted in 36 groundwater run combinations.

The sensitivity/uncertainty analysis was conducted for radionuclides ^{129}I, ^{99}Tc, $^{90}Sr/^{90}Y$, and ^{14}C, which were determined to be the major dose drivers for the groundwater pathway in Section 4.

The dose results of the sensitivity/uncertainty matrix for the four scenarios are provided in Tables 7-10 and 7-11. The conservative case (i.e., conservative grout and transport K_d values, 4.1 cm/yr infiltration, and the conservative inventory) used in the dose compliance analysis in Section 4 is highlighted in yellow.

The use of the matrix allows for an interpretation of the sensitivity and uncertainty in the parameters of interest in the groundwater analysis.

All graphs of the radionuclide releases and groundwater doses for each matrix combination shown in Tables 7-10 and 7-11 are provided in Appendix M.

The drinking water doses for the four main scenarios are shown in Figures 7-2 through 7-5 for the radionuclides of interest. The four main groundwater scenarios consisted of (refer to Table 7-3 for parameter values):

- Worst-case scenario—consisting of the worst-case grout K_d values, worst-case transport K_d values, 12.4 cm/yr (4.88 in./yr) infiltration, and worst-case inventory
- Conservative scenario—consisting of the conservative grout K_d values, conservative transport K_d values, 4.1 cm/yr (1.6 in./yr) infiltration, and conservative inventory
- Realistic scenario—consisting of the realistic grout K_d values, realistic transport K_d values, 1.1 cm/yr (0.43 in./yr) infiltration, and realistic inventory
- Best scenario—consisting of the same transport parameters as the realistic scenario with the best inventory.

The locations of the time of peak drinking water dose and magnitude of the peak drinking water doses for all other cases would be located between the two extremes of the worst-case scenario and the best scenario for each radionuclide of interest shown in Figures 7-2 through 7-5.

Table 7-10. Drinking water doses for sensitivity/uncertainty groundwater analyses.[a]

Parameterization				Drinking Water Dose (yr post-closure) (mrem/yr)				
Grout K_d	Transport K_d	Infiltration	Inventory	^{129}I	^{99}Tc	$^{90}Sr/^{90}Y$	^{14}C	Total (yr post-closure)
Worst-Case	Worst-Case	12.4	Worst-Case	23.1 (538)	1.07 (2370)	17.3 (294)	0.008 (1.4E–04)	23.1 (538)
			Conservative	8.7	0.99	17.3	0.004	17.3 (294)
			Realistic	6.7	0.09	17.3	0.002	17.3
			Best	4.4	0.05	17.3	0.0004	17.3
Worst-Case	Worst-Case	4.1	Worst-Case	9.09 (607)	0.38 (5060)	3.02 (342)	1E–4 (3.78E+04)	9.09 (607)
			Conservative	3.42	0.35	3.02	5E–05	3.42
			Realistic	2.64	0.03	3.02	2E–05	3.02 (342)
			Best	1.75	0.02	3.02	5E–06	3.02
Worst-Case	Worst-Case	1.1	Worst-Case	2.66 (844)	0.09 (1.75E+04)	0.04 (461)	9E–10 (1.0E+05)	2.66(884)
			Conservative	1.0	0.09	0.04	4E–10	1.0
			Realistic	0.77	0.008	0.04	2E–10	0.77
			Best	0.51	0.005	0.04	5E–11	0.51
Conservative	Conservative	12.4	Worst-Case	5.72 (635)	0.47 (4270)	0.02 (453)	4E–06 (5.53E+04)	5.72 (635)
			Conservative	2.15	0.43	0.02	2E–06	2.15
			Realistic	1.66	0.04	0.02	9E–07	1.66
			Best	1.10	0.02	0.02	2E–07	1.10
Conservative	Conservative	4.1	Worst-Case	2.05 (890)	0.13 (1.46E+04)	0.001 (551)	1E–11 (1.22E+05)	2.05 (890)
			Conservative	0.77	0.12	0.001	6E–12	0.77
			Realistic	0.60	0.011	0.001	2E–12	0.60
			Best	0.39	0.007	0.001	6E–13	0.39
Conservative	Conservative	1.1	Worst-Case	0.49 (1890)	0.04 (4.13E+04)	3.4E–07 (891)	0	0.49 (1890)
			Conservative	0.18	0.03	3.4E–07	0	0.18
			Realistic	0.14	0.003	3.4E–07	0	0.14
			Best	0.09	0.002	3.4E–07	0	0.09
Realistic/Best	Realistic/Best	12.4	Worst-Case	1.49 (1060)	0.23 (8100)	4.77E–05 (856)	5E–09 (9.14E+04)	1.49 (1060)
			Conservative	0.56	0.21	4.77E–05	2E–09	0.56
			Realistic	0.43	0.02	4.77E–05	9E–10	0.43
			Best	0.29	0.01	4.77E–05	2E–10	0.29
Realistic/Best	Realistic/Best	4.1	Worst-Case	0.50 (1960)	0.07 (2.33E+04)	3.53E–07 (988)	2E–17 (1.83E+05)	0.50 (1960)
			Conservative	0.19	0.07	3.53E–07	9E–18	0.19
			Realistic	0.14	0.006	3.53E–07	4E–18	0.14
			Best	0.09	0.004	3.53E–07	9E–19	0.09
Realistic/Best	Realistic/Best	1.1	Worst-Case	0.14 (5670)	0.02 (8.05E+04)	1.14E–12 (1310)	0	0.14 (5670)
			Conservative	0.05	0.01	1.14E–12	0	0.05
			Realistic	0.04	0.001	1.14E–12	0	0.04
			Best	0.03	0.0008	1.14E–12	0	0.03

a. Conservative-case used in dose analysis is highlighted in yellow; green shows the worst-case scenario with the conservative inventory.

Table 7-11. All-pathway doses for sensitivity/uncertainty groundwater analyses.[a]

Parameterization				All-Pathways Dose (yr post-closure) (mrem/yr)				
Grout K_d	Transport K_d	Infiltration	Inventory	^{129}I	^{99}Tc	$^{90}Sr/^{90}Y$	^{14}C	Total (yr post-closure)
Worst-Case	Worst-Case	12.4	Worst-Case	40.4 (538)	7.52 (2370)	85.8 (294)	0.04 (1.41E+04)	85.8 (294)
			Conservative	15.2	6.98	85.8	0.02	85.8
			Realistic	11.7	0.630	85.8	0.008	85.8
			Best	7.76	0.38	85.8	0.002	85.8
Worst-Case	Worst-Case	4.1	Worst-Case	15.9 (607)	2.65 (5060)	15.0 (342)	4.95E–04 (3.78E+04)	15.9 (607)
			Conservative	5.97	2.46	15.0	2.48E–04	15.0 (342)
			Realistic	4.61	0.22	15.0	9.94E–05	15.0
			Best	3.05	0.13	15.0	2.48E–05	15.0
Worst-Case	Worst-Case	1.1	Worst-Case	4.65 (884)	0.685 (1.75E+04)	0.18 (461)	4.31E–09 (1.0E+05)	4.65 (884)
			Conservative	1.75	0.64	0.18	2.16E–09	1.75
			Realistic	1.35	0.06	0.18	8.66E–10	1.35
			Best	0.89	0.03	0.18	2.16E–10	0.89
Conservative	Conservative	12.4	Worst-Case	9.98 (635)	3.29 (4270)	0.12 (453)	2.01E–05 (5.53E+04)	9.98 (635)
			Conservative	3.75	3.05	0.12	1.01E–05	3.75
			Realistic	2.89	0.28	0.12	4.03E–06	2.89
			Best	1.92	0.16	0.12	1.01E–06	1.92
Conservative	Conservative	4.1	Worst-Case	3.59 (890)	0.94 (1.46E+04)	0.006 (551)	5.75E–11 (1.22E+05)	3.59 (890)
			Conservative	1.35	0.87	0.006	2.88E–11	1.35
			Realistic	1.04	0.08	0.006	1.15E–11	1.04
			Best	0.69	0.05	0.006	2.88E–12	0.69
Conservative	Conservative	1.1	Worst-Case	0.86 (1890)	0.25 (4.13E+04)	1.68E–06 (891)	0	0.86 (1890)
			Conservative	0.32	0.23	1.68E–06	0	0.32
			Realistic	0.25	0.21	1.68E–06	0	0.25
			Best	0.17	0.01	1.68E–06	0	0.17
Realistic/Best	Realistic/Best	12.4	Worst-Case	2.61 (1060)	1.62 (8100)	2.36E–04 (856)	2.23E–8 (9.14E+04)	2.61 (1060)
			Conservative	0.98	1.50	2.36E–04	1.11E–08	1.5
			Realistic	0.76	0.14	2.36E–04	4.47E–09	0.76
			Best	0.50	0.08	2.36E–04	1.11E–09	0.50
Realistic/Best	Realistic/Best	4.1	Worst-Case	0.87 (1960)	0.5 (2.33E+04)	1.75E–06 (988)	9.02E–17 (1.83E+05)	0.87(1960)
			Conservative	0.33	0.46	1.75E–06	4.51E–17	0.46
			Realistic	0.25	0.04	1.75E–06	1.81E–17	0.25
			Best	0.17	0.02	1.75E–06	4.52E–18	0.17
Realistic/Best	Realistic/Best	1.1	Worst-Case	0.24 (5670)	0.11 (8.05E+04)	5.65E–12 (1310)	0	0.24 (5670)
			Conservative	0.088	0.1	5.65E–12	0	0.10
			Realistic	0.068	0.009	5.65E–12	0	0.07
			Best	0.045	0.005	5.65E–12	0	0.04

a. Conservative-case used in dose analysis is highlighted in yellow; green shows the worst-case scenario with the conservative inventory.

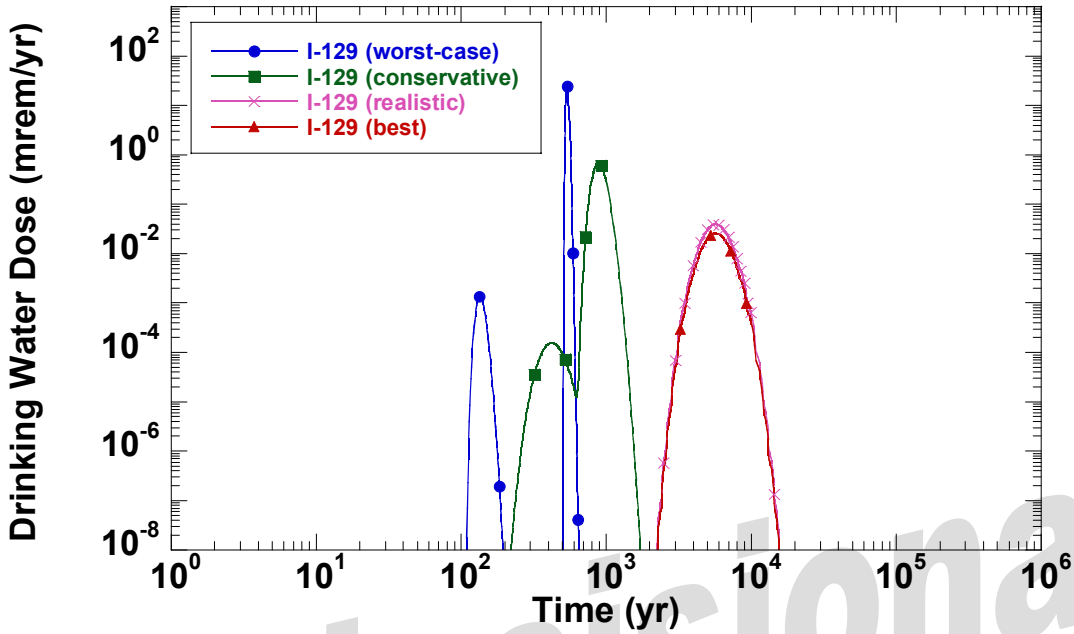

Figure 7-2. ^{129}I drinking water doses for the four groundwater scenarios.

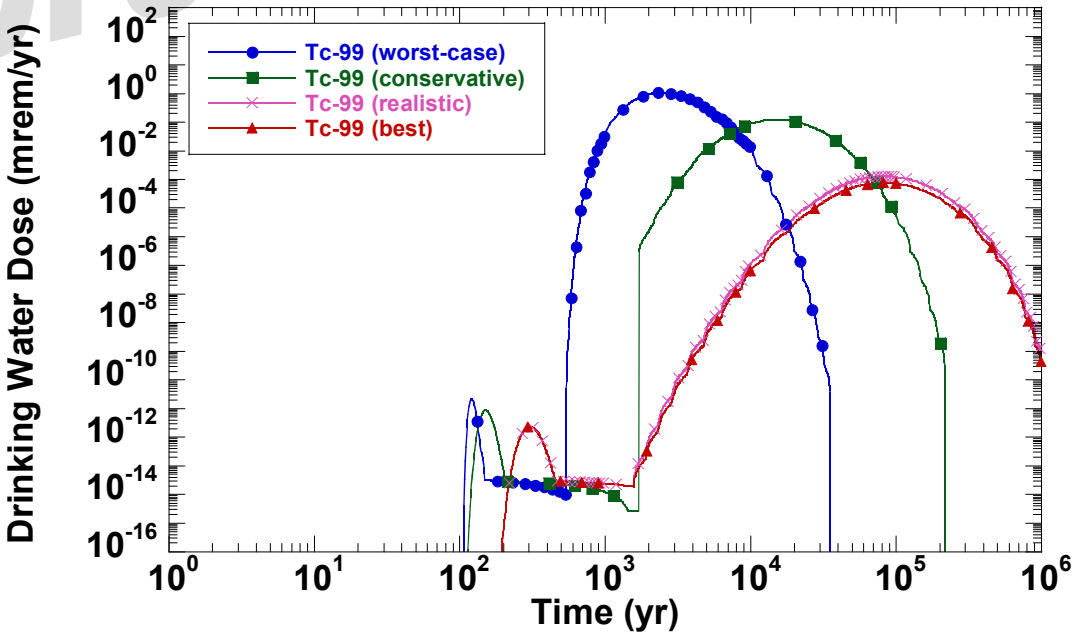

Figure 7-3. ^{99}Tc drinking water doses for the four groundwater scenarios.

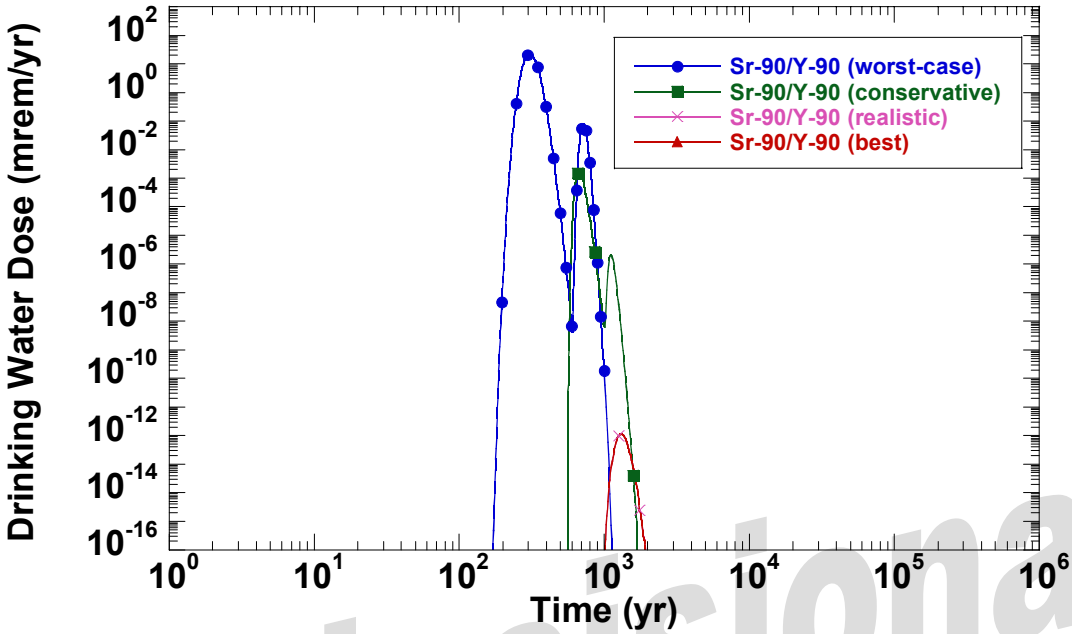

Figure 7-4. $^{90}Sr/^{90}Y$ drinking water doses for the four groundwater scenarios.

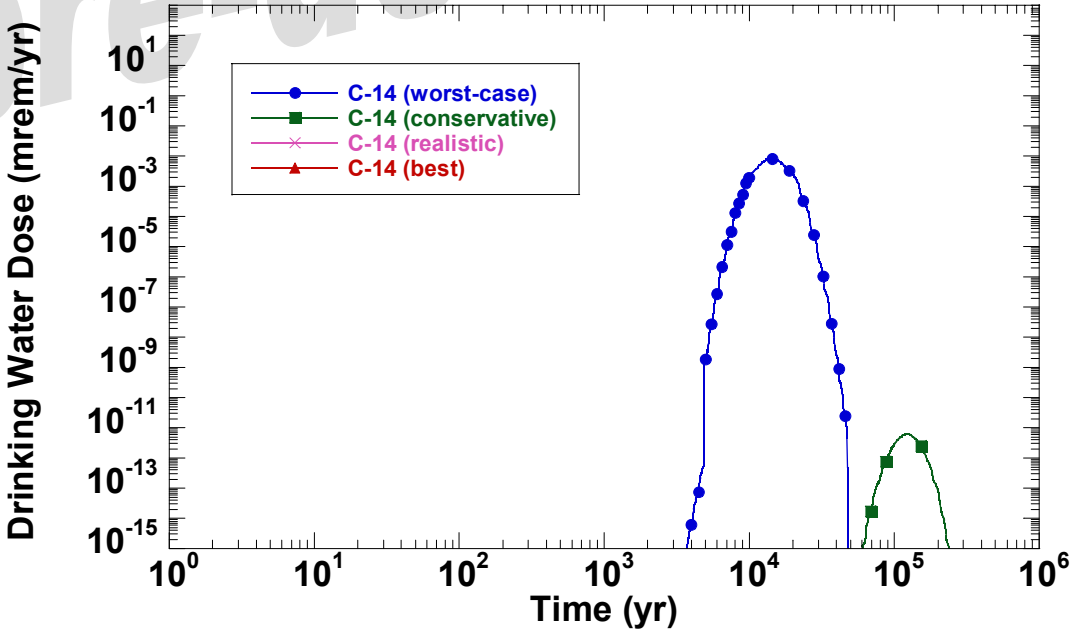

Figure 7-5. ^{14}C drinking water doses for the four groundwater scenarios.

The doses for the all-pathways scenarios are provided in Appendix M and are not shown here because they are similar in character to the drinking water dose graphs in terms of arrival time and location of the peak dose. The only difference is the magnitude of the doses, as can be seen from a comparison of Tables 7-10 and 7-11.

The drinking water doses presented in Table 7-10 for the matrix of scenarios shows a maximum drinking water dose of 23.1 mrem/yr at 538 yr post-closure for the worst-case scenario. This dose is the result of ^{129}I releases from the tanks. The next highest contributor to the drinking water dose for the worst-case scenario is from $^{90}Sr/^{90}Y$ with a drinking water dose of 17.3 mrem/yr at 294 yr post-closure. This dose is due to releases from the sand pad. The $^{90}Sr/^{90}Y$ doses are the same for all inventory combinations because the sand pad inventory was held constant throughout the analyses. The sand pad releases dominate the $^{90}Sr/^{90}Y$ doses because the releases occur at 100 yr and the decay time is less than the releases from the tank inventory.

^{99}Tc and ^{14}C doses are low for all scenarios and do not contribute significantly to the overall doses from the TFF. This is due to the grout K_d values, which limit the releases of these radionuclides from the tanks and vaults.

The conservative case was used in the Section 4 dose analysis (highlighted in yellow in Tables 7-10 and 7-11). This case is considered the applicable set of parameter values for comparison to the performance objectives. The infiltration rate of 4.1 cm/yr (1.6 in./yr) was considered applicable to an earthen cover. Currently the TFF is covered by 10 ft (3 m) of earthen material. In addition, future closure work at the TFF for CERCLA actions will provide an additional engineered cover over the TFF, reducing the infiltration further than that assumed in the conservative case. The conservative inventory also is considered appropriate for the conservative case, because current knowledge of the cleaning process, completed on Tank WM-182, shows that the process is effective. The conservative case was based on the conservative K_d values for the grout and unsaturated zone interbeds and sediments. There is a large uncertainty in the distribution coefficients; therefore, the conservative case used the average values of the reported ranges in the literature.

The large uncertainty in the grout and transport distribution coefficients is addressed in Tables 7-10 and 7-11. The uncertainty is shown by evaluation of the worst-case scenario grout and transport K_d values, in combination with an infiltration rate of 4.1 cm/yr (1.6 in./yr) and the conservative inventory (i.e., highlighted in green in Tables 7-10 and 7-11). In this case, it has been shown that the resulting doses are less than the performance objectives. In other words, even if the distribution coefficients for grout and transport are selected at the worst-case level, the doses do not exceed the performance objectives.

The doses in Tables 7-10 and 7-11 for the worst-case combinations located above the highlighted green area (worst-case K_d values, 4.1 cm/yr (1.6 in./yr) infiltration, and conservative inventory) are provided to show the worst possible combinations of parameters. However, these combinations of parameter values are not considered applicable to the TFF.

Tables 7-10 and 7-11 can be used to evaluate the sensitivity and uncertainty of the parameter values. Based on the results of the sensitivity/ uncertainty analysis, the following observations were made:

- Model runs are not sensitive to inventory changes due to the small changes in inventory in comparison to the ranges of possibilities for the other parameters in the analysis.

- Grout K_d values have a broader range reported in the literature than the K_d values for the stratigraphic units. Therefore, the groundwater scenario doses are affected more by the selection of the grout K_d values than the transport K_d values.

- Sand pad releases dominate the resultant dose calculations for $^{90}Sr/^{90}Y$ transport simulations due to the release time of 100 yr, compared to the tanks at 500 yr and the subsequent decay.

- Dose peaks shift in time (i.e., later arrival time for increasing K_d values) for variations in sorption coefficients in the unsaturated zone and cause a subsequent decrease in the doses.

- Decreases in infiltration shift the dose peak to later arrival times and also cause a decrease in the radionuclide doses.

- Changes in predicted radionuclide doses and peak arrival times are less sensitive to variations in hydraulic dispersivity values.

7.3.6.2 Sensitivity and Uncertainty of Individual Parameters. The sensitivity and uncertainty in each parameter selection also was investigated. The sensitivity and uncertainty of the drinking water doses based on variations in dispersion, unsaturated zone K_d values, infiltration rates, grout K_d values, and inventory were investigated separately.

Figure 7-6 provides a comparison of the effect of changing the dispersion coefficient from the worst-case values to the best-case values (refer to Table 7-3 for parameter values). The doses are based on the worst-case parameter values for all remaining parameters; therefore, only the dispersion coefficients were changed.

The use of the best-case dispersion coefficients (i.e., higher values of dispersion) results in lower doses than the worst-case dispersion coefficients (i.e., lower values of dispersion) due to additional dispersion of the contaminant plume during transport. The peak dose arrival time also decreases as expected. However, in comparison to the other parameter changes, the dispersion coefficient is a less sensitive parameter.

Figure 7-7 provides a comparison of the effect of changing the unsaturated zone K_d values for basalts and interbed sediments. The evaluation of the K_d values was done using four cases: (1) zero K_d values for basalts and interbed sediments, (2) basalt and sediment K_d values assigned to each appropriate unit, (3) only the sediment K_d value assigned and the basalt assigned zero K_d values, and (4) basalt K_d value assigned and the sediment K_d assigned zero K_d values.

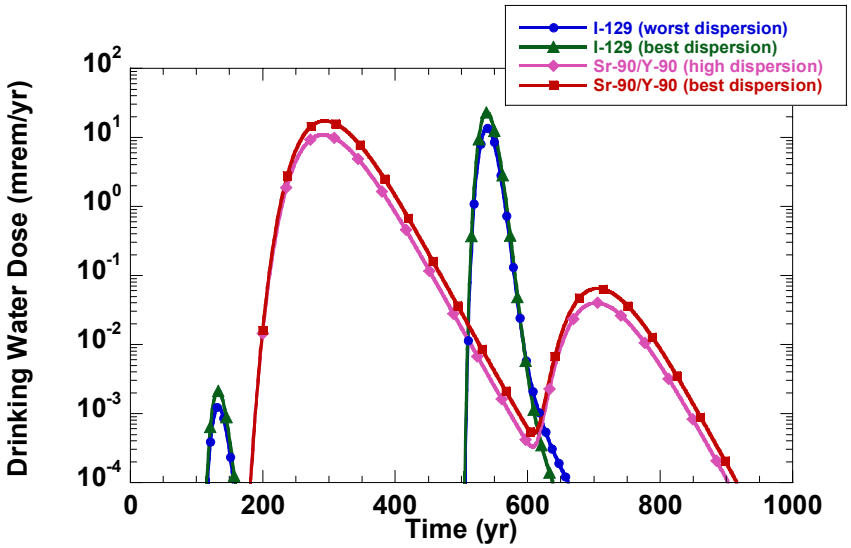

Radionuclide	Best-Case Dispersion	Worst-Case Dispersion
I-129	13.7 mrem/yr (535 yr)	23.1 mrem/yr (538 yr)
Sr-90/Y-90	10.8 mrem/yr (291 yr)	17.3 mrem/yr (294 yr)

Figure 7-6. Sensitivity/uncertainty of dispersion coefficients on drinking water doses.

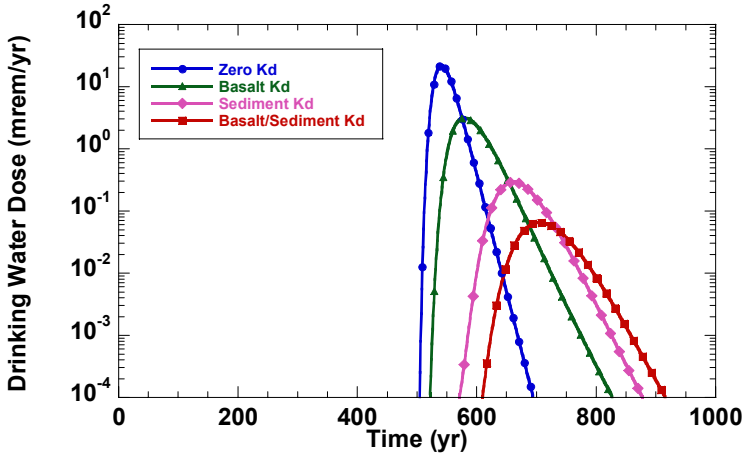

Radionuclide	Zero Kd	Basalt/Sediment Kd	Sediment Kd	Basalt Kd
I-129	23.1 mrem/yr (538 yr)	23.1 mrem/yr (538 yr)	23.1 mrem/yr (538 yr)	22.9 mrem/yr (539 yr)
Sr-90/Y-90	21.7 mrem/yr (541 yr)	0.065 mrem/yr (706 yr)	0.29 mrem/yr (661 yr)	3.2 mrem/yr (579 yr)

Figure 7-7. Sensitivity/uncertainty of unsaturated zone Kd values on 129I and 90Sr/90Y drinking water doses.

First, the importance of the interbed sediment K_d values and the basalt K_d values were investigated using ^{129}I. The basalt and interbed sediments were independently assigned the same values in the sensitivity analysis, (i.e., 0.01 mL/g). This analysis shows that the basalts and interbeds are of equal importance in the transport analysis when assigned the same K_d value independently.

The sensitivity and uncertainty in the ^{90}Sr groundwater transport analysis was investigated by assigning different K_d values to the interbed sediments (12 mL/g) and the basalts (6 mL/g). The analysis shows that the interbed sediments with the higher K_d value were the most important parameter in the analysis as expected. This is important because the interbed sediments tend to have higher K_d values but are less uncertain in the analysis than the assignment of K_d values for the basalt units.

The sensitivity and uncertainty in the infiltration rate also was investigated. Figures 7-8 and 7-9 present the results of the infiltration sensitivity/uncertainty analysis. The infiltration rate is an important factor in the analysis as can be seen by these results. The infiltration rate affects not only the transport rate through the unsaturated zone but also the release rate from the waste form.

The infiltration analysis for ^{129}I, shown in Figure 7-8, shows the change in arrival time of the peak dose being increased in time for the lower infiltration rate, as expected. In addition, the resulting doses also decrease with the decreasing infiltration rate due to the reduction in the release of contaminants from the waste forms.

The infiltration analysis for $^{90}Sr/^{90}Y$, shown in Figure 7-9, again shows that the arrival time of the peak doses are shifted to an increased time for the lower infiltration rates. In addition, the doses are reduced for lower infiltration rates due to the lower infiltration releasing less contaminant from the waste forms. The $^{90}Sr/^{90}Y$ dose results are more sensitive to changes in infiltration than ^{129}I because to the increased arrival times and subsequent decay.

The sensitivity and uncertainty in the grout distribution coefficients (K_d values) also was investigated. Figures 7-10 and 7-11 show the

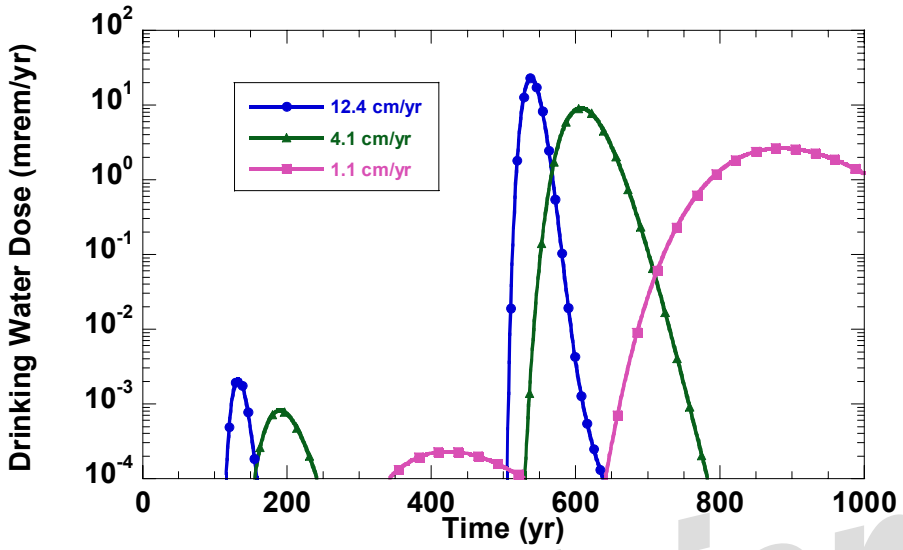

	12.4 cm/yr	4.1 cm/yr	1.1 cm/yr
I-129	23.1 mrem/yr (538 yr)	9.1 mrem/yr (607 yr)	2.7 mrem/yr (883 yr)

Figure 7-8. Sensitivity/uncertainty of infiltration on ^{129}I drinking water doses.

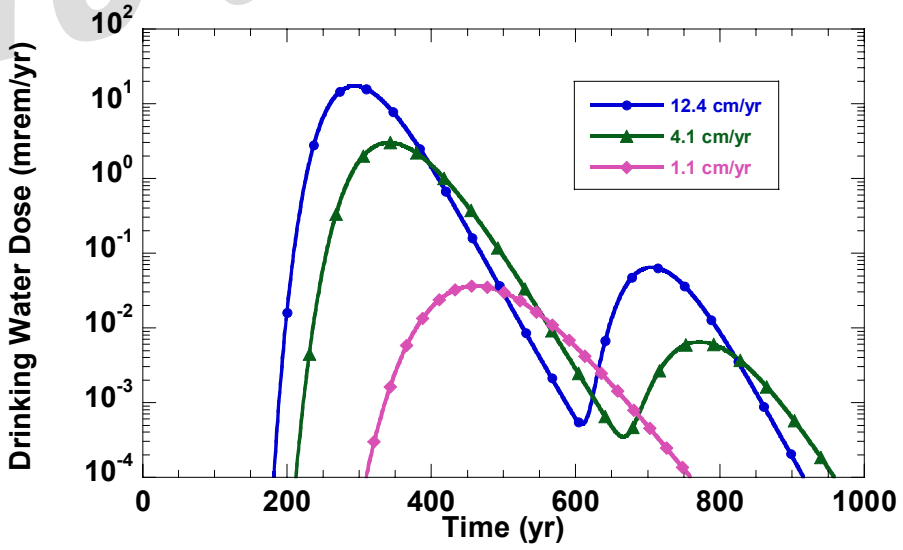

	12.4 cm/yr	4.1 cm/yr	1.1 cm/yr
Sr-90/Y-90	17.3 mrem/yr (294 yr)	3.0 mrem/yr (341 yr)	0.036 mrem/yr (457 yr)

Figure 7-9. Sensitivity/uncertainty of infiltration on $^{90}Sr/^{90}Y$ drinking water doses.

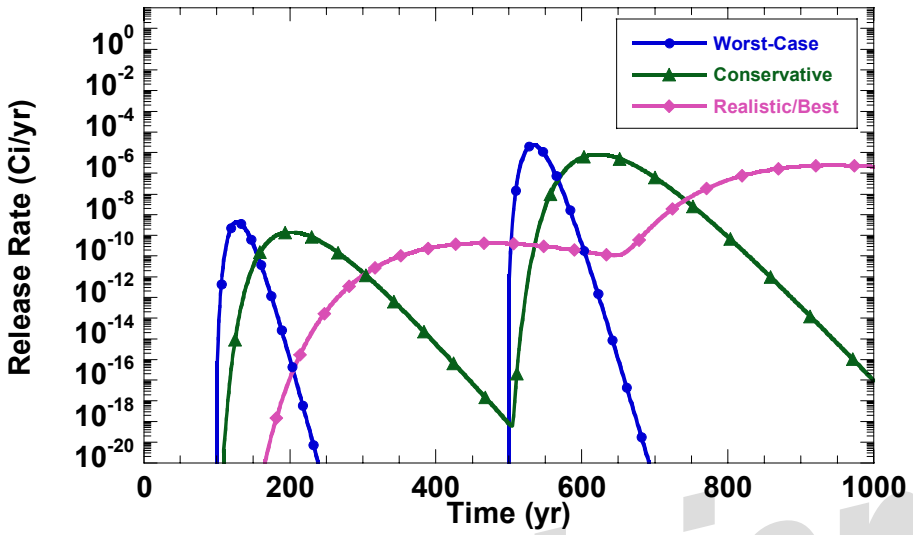

	Worst-Case	Conservative	Realistic/Best
I-129	2.38E–05 Ci/yr (534 yr)	8.18E–06 (620 yr)	2.42E–06 (940 yr)

Figure 7-10. Sensitivity/uncertainty of grout K_d values on ^{129}I releases.

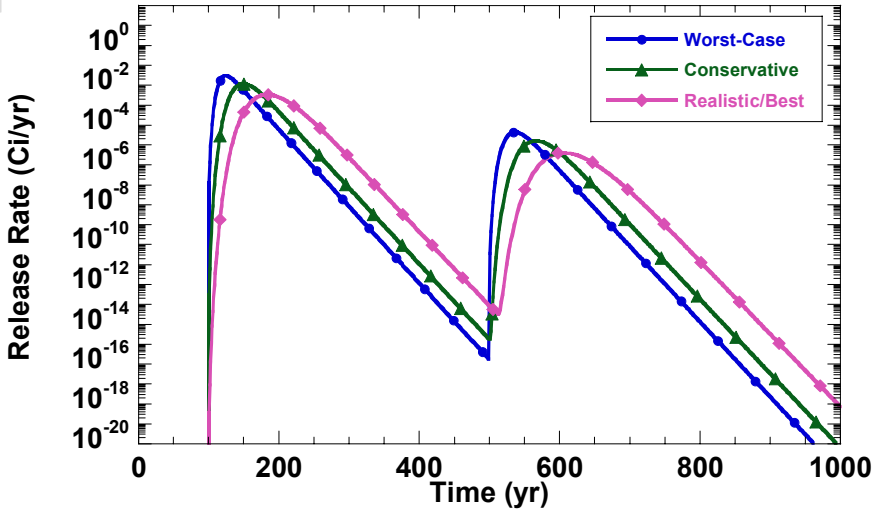

	Worst-Case	Conservative	Realistic/Best
Sr-90	0.031Ci/yr (124 yr)	0.012 Ci/yr (147 yr)	0.0034 Ci/yr (182 yr)

Figure 7-11. Sensitivity/uncertainty of grout K_d values on $^{90}Sr/^{90}Y$ releases.

sensitivity and uncertainty in the release rates for ^{129}I and ^{90}Sr. Again, the result of increasing the K_d value from the worst-case parameter value (i.e., lower grout K_d value) to the best case (i.e., higher grout K_d value) is a delay in the time of peak release and a decrease in the release rate. The groundwater pathway dose analyses are sensitive to the grout K_d value because the reported ranges in the grout K_d values are large.

The sensitivity and uncertainty in the inventories also was investigated. Figures 7-12 and 7-13 provide the change in the drinking water doses based on the four tank inventories. The peak dose arrival times are the same for each case because the transport parameters were held constant. The sensitivity and uncertainty in the inventories shows a reduction in the doses in direct proportion to the decreases in the radionuclide inventories. The groundwater pathway dose analyses are not very sensitive to the inventory changes because the range of inventories is not as great as the range of other parameter values.

7.4 Sensitivity/Uncertainty in Hydraulic Parameters

The modeling approach discussed in detail in Section 3 attempts to minimize subsurface water transport uncertainties due to lack of data. By adopting a detailed stratigraphic model representation, using site data that was confirmed by two or more sources and using basalt permeabilities based on detailed lithologic analysis presented in Anderson, Kuntz, and Davis (1999), the magnitude of model uncertainty was significantly lowered. Model calibration with the existing perched zone data yielded a reasonable approximation of the system—further reducing model uncertainty. The following discussion provides an analysis of the sensitivity of the vertical conductivity parameter value on the formation of perched water in the model.

7.4.1 Vertical Conductivity Sensitivity Analysis

Figure 7-14 compares the distribution of perched zones as a function of vertical permeability variations in the D-DE2 interbed (Zone 9). This interbed is associated with the upper-most perched zone at several locations across the site and has been identified by borehole data as containing low permeable sediments capable of restricting infiltrating water. The simulations were conducted using recharge solely from the Big Lost River versus the model calibration that was conducted using the additional source of recharge from the percolation ponds. Before the 1000-yr simulations, the percolation ponds will be removed from service. Consequently, the sensitivity analysis is conducted on representative moisture conditions during future model simulation.

For the simulation, a calibrated vertical permeability value of 0.0025 m/d was incorporated into the model for D-DE2 interbed. As shown in the Figure 7-14, this permeability value was varied by plus and minus one order of magnitude to evaluate the impact on perched zone distribution. The upper-perched zones vary from nearly nonexistent to relatively extensive in the Tank Farm area. These results show that the model is sensitive to permeability changes in the important stratigraphic units. The calibrated permeability is within the measured range for the type of interbed lithology. Therefore, the permeability values used in the model are reasonable and the model is dynamic in responding to input variations.

7.4.2 Transport Resulting From Dam Failure Flood

The worst-case flooding scenario reported in the site literature is a dam failure analysis conducted by Van Haaften et al. (1984). A PMF event above Mackay Dam results in a 1.1 m (3.7 ft) overtopping of the dam, with a 0.5-hr dam failure, 42.6-m (140-ft) breach in the dam, and no flow losses downstream. The result of this worst-case scenario is flooding of the INTEC facility with 1 to 2 m (3 to 7 ft) of water covering the site and a peak flow of 3292.5 m^3/s (116,272 ft^3/s). The flood hydrograph for the base-case discharge shows a peak flow that lasts only 7.5 hr (Figure 2-17, Section 2). Since the INTEC facility is located at the margins of the flood, the area would be inundated for a lesser a period of time.

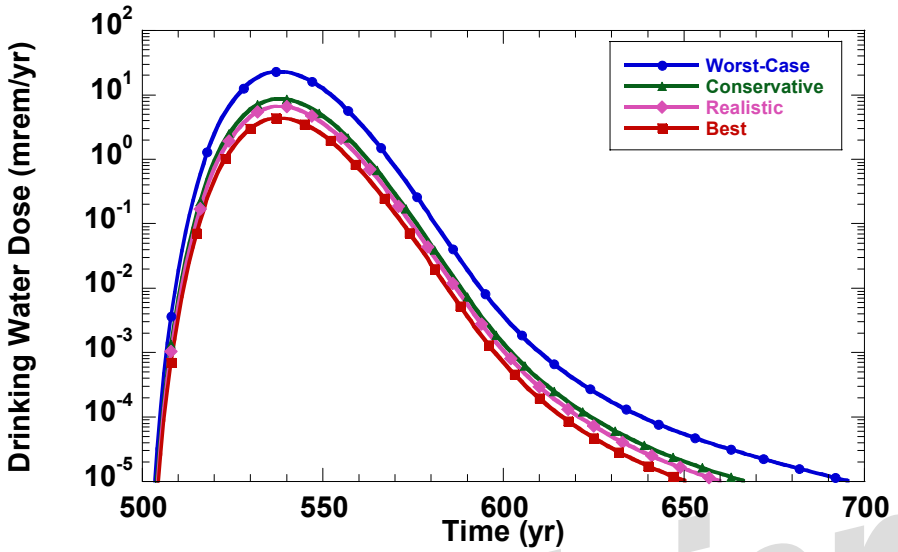

	Worst-Case	Conservative	Realistic	Best
I-129	23.1 mrem/y	8.7 mrem/yr	6.7 mrem/yr	4.4 mrem/yr

Figure 7-12. Sensitivity/uncertainty of inventory on ^{129}I drinking water doses.

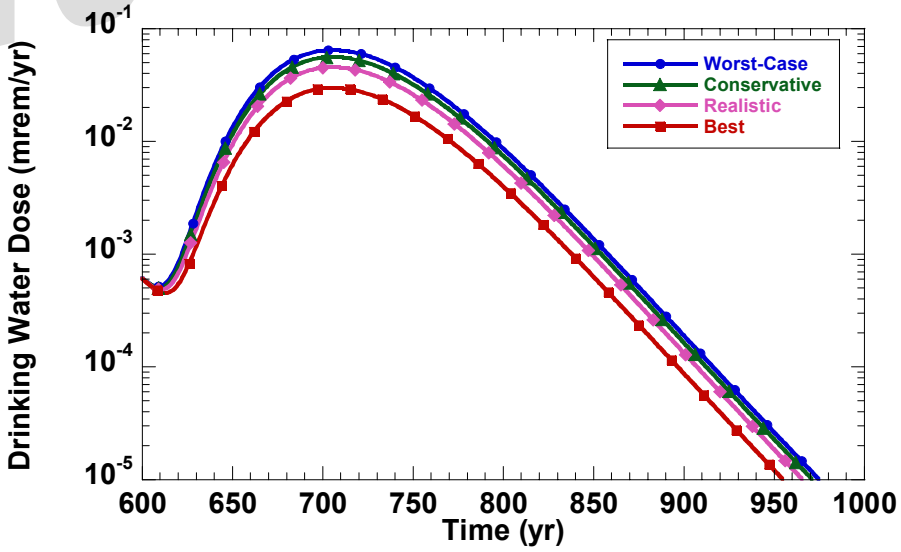

	Worst-Case	Conservative	Realistic	Best
Sr-90/Y-90	0.065 mrem/yr	0.056 mrem/yr	0.046 mrem/yr	0.030 mrem/yr

Figure 7-13. Sensitivity/uncertainty of inventory on ^{90}Sr/^{90}Y drinking water doses.

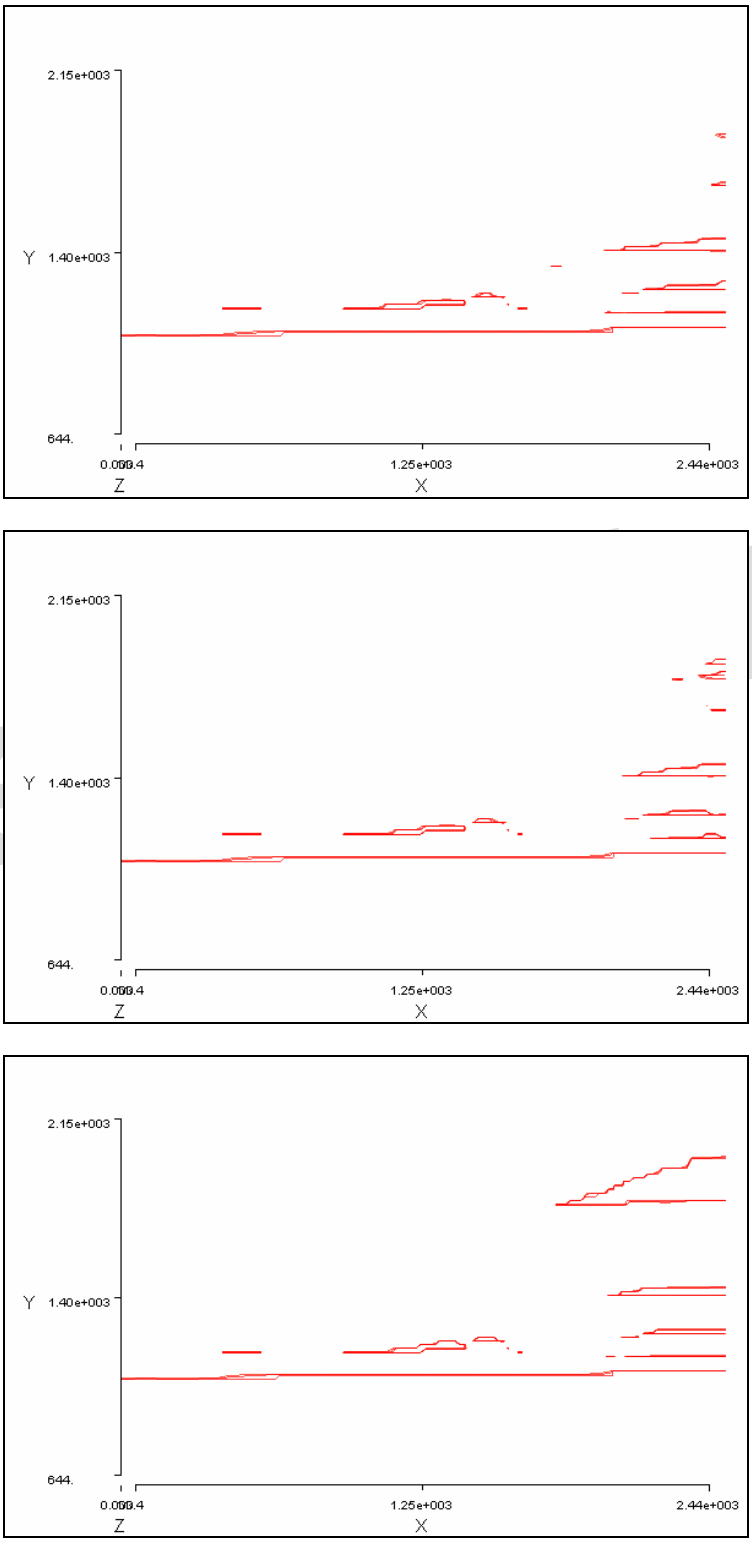

Figure 7-14. Sensitivity of the moisture content distribution in the unsaturated zones with variations in vertical hydraulic conductivity values in the D-DE–2 interbed (Zone 9) of 0.025, 0.0025, and 0.00025 m/d.

The impact on radionuclide transport resulting from such a flooding event was evaluated by simulating increased infiltration in the region of the flood. It was assumed that flood occurred at 500 yr—the same time as when the tanks failed. Based on double-ring infiltrometer tests conducted on desert alluvial soils by Kearl (1981), the infiltration rate was measured at 2.5 cm/hr (0.98 in./hr). Assuming the flood at the facility and subsequent ponding water continues to infiltrate for a full day, a total of 61 cm (24 in.) of water was input in the simulation. Transport simulations indicate this large amount of infiltration forced radionuclide migrations laterally in the model domain due to the dominant influence of the Big Lost River boundary condition under higher saturation conditions. Consequently, in order to evaluate the impact of flooding and subsequent increases in perching water on present transport pathways, the infiltration due to flooding was lowered to a rate of 100 times the 12.4 cm/yr (4.88 in./yr) infiltration rate. The extent of the flooding as illustrated in Figure 2-18 shows that the entire modeling domain is covered with water.

A transport comparison for a unit concentration of ^{129}I under non-flooding and flooding conditions is presented in Figure 7-15. For non-flooding conditions, a peak concentration is reached during the early portion of the simulation with a continual decrease in concentration values. For the flooding conditions, a peak concentration is reached slightly earlier than non-flooding conditions. However, the peak concentration resulting for flooding conditions is less than for non-flooding conditions. The perching layers below the Tank Farm increase in thickness and extent during the flooding scenario and retard the movement of contaminants downward (Figure 7-16). As contaminants spread across the surface of the perched zones, dilution occurs from mixing with the perched water and infiltration from precipitation. The rate of decline in ^{129}I concentrations in the flooding simulation is due to the amount of additional water that must move through the system. Once the water from the flooding event has passed, concentrations continue to decline to minimal levels.

7.4.3 Transmissivity in the Regional Aquifer

There is a large range of transmissivity values for the basalt aquifer reported in site literature. There are numerous investigations of magnitude and distribution of hydraulic conductivity in the regional aquifer. This includes work by Thomas (1988), Ackerman (1991), and Anderson, Kuntz, and Davis (1999). Based on the available data, the highest range of hydraulic conductivity resulting in the highest transport rates were used in the model simulations resulting in a conservative approach to the modeling.

7.4.4 Big Lost River Seepage

Seepage from the Big Lost River is a major driving force for water movement in the unsaturated zone underlying the INTEC facility. Detailed stream loss measurements were conducted by Bennett (1990) for the Big Lost River. These measurements showed seepage losses in the vicinity of the INTEC facility. The losses were used to estimate recharge to the unsaturated zone at the site.

The modeling assumed that the bulk of the perched water zones underlying the site were the result of seepage from the Big Lost River. Resulting calibration simulations using existing perched zone data compared favorably with measured seepage rates, increasing confidence in the seepage values and reducing uncertainty.

7.4.5 Basalt Porosity

The value chosen for the basalt porosity controls the rate of water and contaminant transport, particularly in the aquifer. Transport rates are moderately affected by the selection of this parameter. Available porosity measurements show a range of 5 to 15% with a historical acceptable value of 10%. A value of 10% porosity was used in the modeling.

7.4.6 Unsaturated Hydraulic Characteristic

Unsaturated hydraulic characteristic curves are based on measurements for porous media and

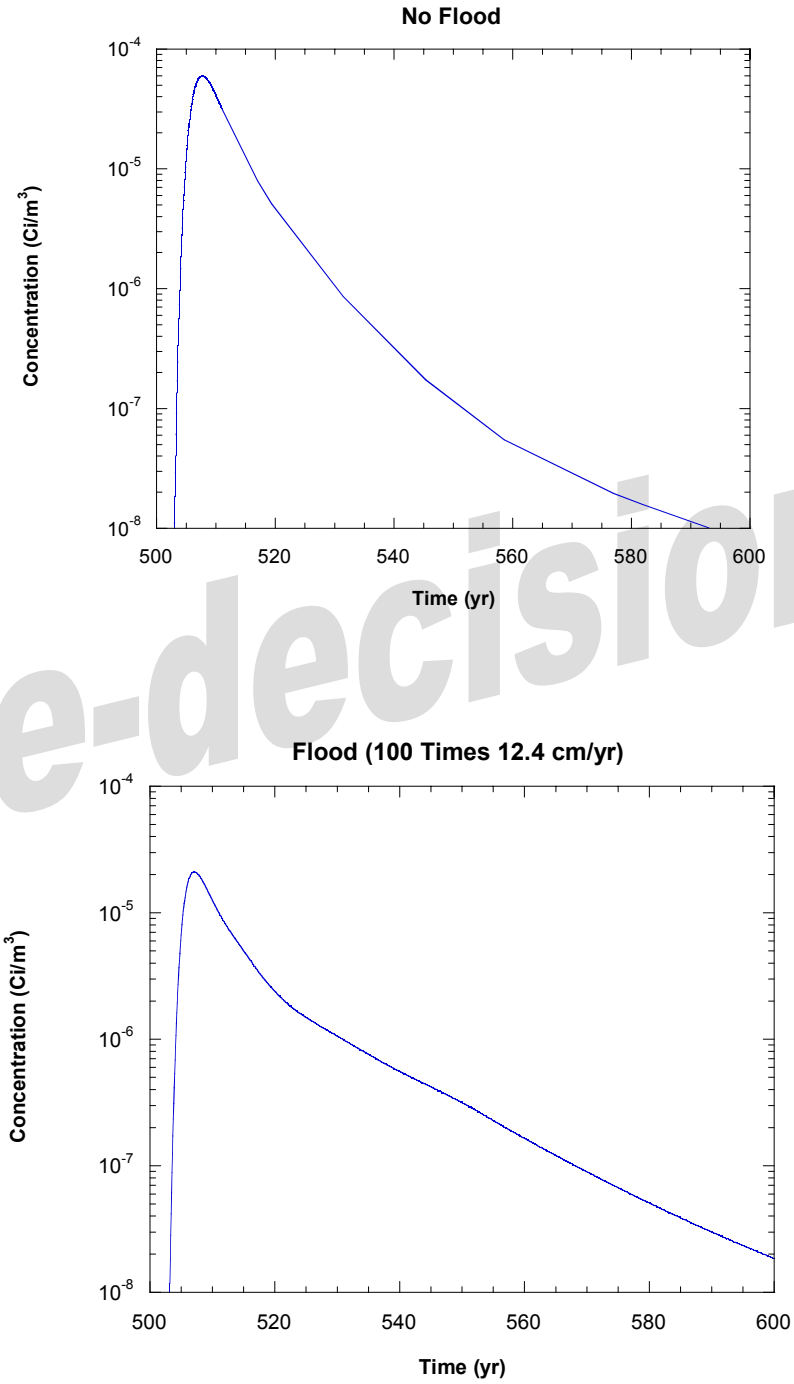

Figure 7-15. Comparison of radionuclide concentrations at the water table for non-flooding and flooding conditions.

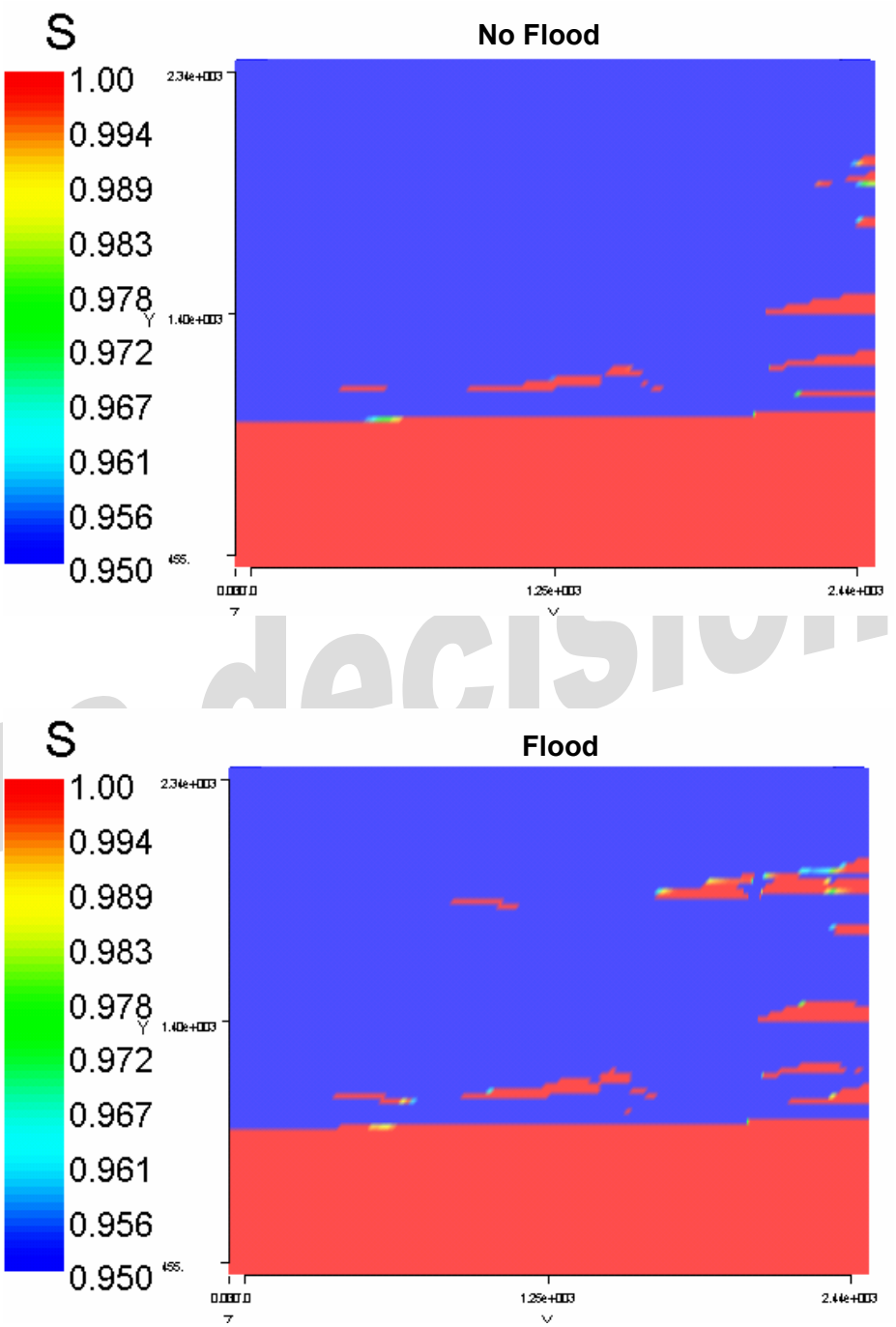

Figure 7-16. Extent of perched water due to non-flooding conditions and flooding conditions.

are poorly defined for water movement in unsaturated basalt fractures. Based on work conducted by Magnuson (1995), characteristic curves for basalt units were adapted for use in the model. These curves assume the instantaneous movement of water in the basalts with only a minor decrease in capillary pressures.

This parameter impacts transport rates in the unsaturated basalts. The rapid movement of water in response to small capillary pressure decreases actually predicts, conservatively, the movement of water and contaminants, which mitigates model uncertainty.

7.5 Piping Inventory Uncertainty

The inventory in the piping is presented in Section 2.3 and Appendix A. The piping was assumed to be released at the same time as the tank inventory at 500 yr. Previous TFF PA analyses, presented in Appendix F, were based on the inventory releases being controlled by diffusion to initial breaks in the pipes beginning at the time of closure. The analysis presented in this report is based on the fact that the piping is stainless steel and the insides of the pipes will be grouted along with the concrete trenches that provide secondary containment. Therefore, the piping degradation would be similar to the tank degradation.

The uncertainty in the piping inventory can be evaluated by simple evaluation of the original mass assumed to be located in the piping (see Section 2.3 and Appendix A). The original mass assumed to be located in the piping was 15.5 kg. The piping drinking water doses are directly proportional to the initial mass of contaminants assumed to be in the piping. The drinking water doses from piping releases for the conservative case were $^{90}Sr/^{90}Y$ at 4.0E–09 mrem/yr, ^{99}Tc at 2.9E–04 mrem/yr, ^{14}C at 3.6 E–19 mrem/yr, and ^{129}I at 3.7E–03 mrem/yr. As can be seen, the doses from the piping releases are low. An order of magnitude increase in the assumption of the original contaminant mass in the piping would not result in a significant increase in the drinking water or all-pathways doses due to piping contamination.

7.6 Sand Pad Uncertainty

The sand pad analysis presented in Section 2.3 was based on the assumption that the sand pad was saturated during the vault contamination event. Therefore, the contaminants in the vault liquid were assumed to reach the sand pad only by diffusion from the vault liquid to the sand pad pore space. The diffusion assumption was assessed against the assumption that the sand pad was at residual saturation during the contamination event. Therefore, the contaminants from the vault liquid would directly fill the sand pad pore volume.

Two assumptions were made in the analysis: (1) sand pad residual saturation is 0.3 and (2) total sand pad porosity is 0.34. The contaminated vault liquid was assumed to fill the pore voids in the sand pad. The sand pad was then washed and decayed as discussed in Section 2.3 and Appendix A. Table 7-12 compares the two conceptual model results for the sand pad.

Table 7-12 presents the increase of activity in the sand pad based on the pore-filling assumption in comparison to the original diffusion assumption. As can be seen, the change in the activity estimates are less than one order of magnitude.

The results of this analysis show that the change in conceptualization of the sand pad contamination events does not change the results significantly. The differences in the drinking water doses due to the sand pad conceptual models are compared in Table 7-13 for the conservative case.

Table 7-13 shows that the difference in the conceptualization of the original contamination event does not result in a significant increase in the drinking water doses due to the sand pad. The same can be said for the all-pathways doses. Therefore, the uncertainty in the sand pad inventories due to conceptual model differences does not result in a change in compliance with the performance objectives.

Table 7-12. Comparison of the sand pad conceptual models.

Radionuclide	Diffusional Model Sand Pad Activity at 2016 (Ci)	Pore-Filled Model Sand Pad Activity at 2016 (Ci)	Activity Factor Increase
^{90}Sr	226	295	1.3
^{99}Tc	2.0E−12	1.9E−11	9.5
^{14}C	3.9E−07	8.7E−07	2.2
^{129}I	1.1E−06	5.0E−06	4.5

Table 7-13. Comparison of the sand pad drinking water doses for each conceptual model.

Radionuclide	Diffusional Model Dose Results (mrem/yr)	Pore-Filled Model Dose Results (mrem/yr)
$^{90}Sr/^{90}Y$	1.2E−03	1.6E−03
^{99}Tc	9.93E−12	9.4E−11
^{14}C	5.7E−17	1.2E−16
^{129}I	1.8E−04	8.1E−04

7.7 DUST-MS Release Model Uncertainty

7.7.1 Heterogeneity in Tank Grout

This section presents a qualitative discussion showing considerations in the release rate modeling approach and selection of input parameters followed by a quantitative analysis relating the implications to modeling heterogeneities in the source term conceptual model.

The effects of heterogeneities in the tank grout (i.e., shrinkage cracks) on degradation and release rates are not directly modeled in the DUST-MS source term release rate calculations. However, because of the lack of available site-specific information and uncertainty and variability in the available information, reasonable and conservative assumptions were made in the source term release rate calculations. When site-specific data were not available, upper-limit assumptions were made (e.g., diffusion coefficient). These assumptions are described throughout this document.

For example, the DUST-MS estimations of release rates from the tank and sand pad are based on a number of conservative assumptions. Piping, vault, and tank failure times used in the release rate determinations are 0, 100, and 500 yr. These values are earlier than the times predicted from the degradation analysis. Moreover, the degradation analyses used parameters that were considered reasonable and conservative based on the available data.

A quantitative analysis was conducted to explore and compare the release rates using DUST-MS and also using a first-order release rate model. Releases were computed assuming matrix diffusion into the shrinkage cracks between the grout and tank wall. In both models, the bottom 1 ft (0.3 m) of the grout tank was assumed to contain the radionuclides present in the tank.

In the first-order model release rate, a mass balance equation based on a control volume approach was employed. This same approach was used in the hand calculation performed for the sensitivity analyses to verify DUST-MS release rates. Following this description, the approach to

compute release rates based on diffusion from the source into concrete cracks when fracture flow occurs is presented. This approach is consistent with the analysis used to determine the mass of radionuclides in the sand pad. The radionuclide ^{129}I is modeled in these analyses using worst-case scenario values.

7.7.1.1 Release Rates from Analytical Model. The rate of change of mass inside the control volume (i.e., the tank source) decreases from water infiltrating and mobilizing radionuclides in the tank source. This relationship is expressed in Equation (7-1).

$$\frac{dM_T}{dt} = C_P \times Q_{\text{inf }il} \times SA \qquad (7\text{-}1)$$

where

M_T = total mass in the tank source (Ci, assumed initially to be a unit source)

t = time (yr)

C_p = pore water concentration in the tank source (Ci/cm^3)

Q_{infil} = flow rate of infiltrating water in the tank source (12.6 cm/yr)

SA = source surface area normal to flow (cm^2, circle with a radius of 760 cm).

The tank source is assumed to be cylindrical with a radius of 7.6 m (25 ft) and a height of 1 ft (0.3 m). In this vault/tank conceptualization, the radionuclides in the tank are completely mixed in the tank source volume.

To determine the mass remaining in the tank source, M_T, it was assumed that the radionuclides partitioned between the water in the pore space and the solid (i.e., degraded grout) and the radionuclide concentrations are at equilibrium according to the partition coefficient. The relationship between the pore water concentration and the total mass contained in the tank source is described by Equation (7-2).

$$C_p = \frac{M_T}{K_d \times M_{soil} + V_W} \qquad (7\text{-}2)$$

where

M_{soil} = mass of the source (5.56E+07 cm^3 at a bulk density of 2.12 g/cm^3)

V_w = volume of source water (cm^3, assuming a moisture content of 0.242).

Substituting Equation (7-2) into Equation (7-1) and solving for the total mass in the tank as a function of time, M_T, yields Equation (7-3).

$$M_T = M_0 \exp[-\alpha\ (t-500)] \qquad (7\text{-}3)$$

where

M_0 = initial mass in tank (Ci, unit initial source)

$$\alpha = \frac{Q_{\text{inf }il}\, SA}{K_d \times M_{soil} + V_W}$$

$t\text{-}500$ = time since the beginning of the release at 500 yr.

The mass release rate from the tank is obtained by differentiating Equation (7-3) with respect to time, t and is expressed in Equation (7-4).

$$\frac{dM_T}{dt} = -M_0\ \alpha \exp[-\alpha\ (t-500)] \qquad (7\text{-}4)$$

Equation (7-4) was evaluated for the same times used in the DUST-MS release rate calculations shown in Figure 7-17. The DUST-MS release rates from the tank source, together with the release rates computed using the analytical solution in Equation (7-4) are provided in Figure 7-17.

7.7.1.2 Release Rates into Concrete Cracks. To determine the release rate into shrinkage cracks between the grout and tank, it

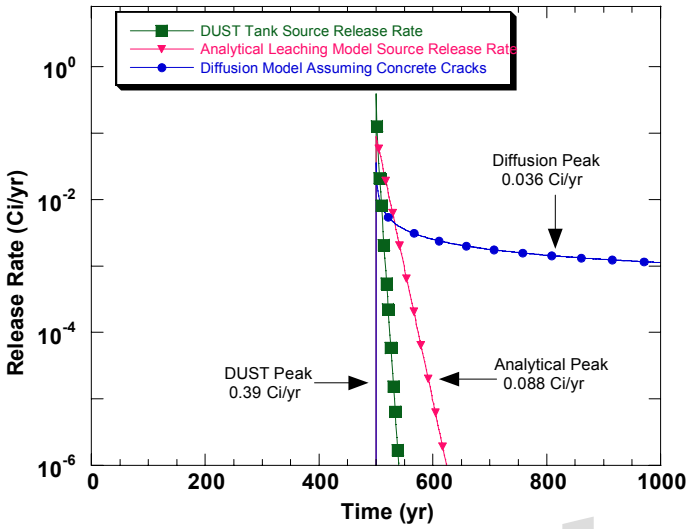

Figure 7-17. Comparison of DUST-MS tank release rates and analytical calculations for the ^{129}I Tank source using worst-case scenario parameters with release rates estimated assuming diffusion into concrete cracks with fracture flow.

was conservatively assumed that the entire circumference of the grout/tank interface served as a preferential water flow pathway and radionuclides diffused from the grout to the grout/tank interface crack. At this interface, the radionuclide concentration was assumed to be maintained at zero. That is, the radionuclides were swept away by the water flowing at the grout/tank interface crack. The approach and parameters used to model diffusion from the grout to the shrinkage crack is consistent with the approach used to model diffusion into the sand pad. This approach is provided in Section 2.3.2 and is summarized below.

To model diffusion, numerous published reference materials provided solutions to diffusion equations (e.g., Crank 1975; Choy and Reible 2000). The following equation describes one-dimensional diffusion from a semi-infinite media

$$\frac{\partial C_A}{\partial t} = \left(\frac{D_{A(eff)}}{R_{fA}} \right) \frac{\partial^2 C_A}{\partial x^2} \qquad z \in [0, \infty) \qquad (7\text{-}5)$$

where

C_A = concentration of radionuclide A (M/L^3)

$D_{A(eff)}$ = diffusion coefficient of radionuclide A, assumed to be 10^{-5} cm^2/s, which is conservative for sand/degraded grout (L^2/T)

R_{fA} = retardation factor of radionuclide A in grout (unitless)

z = distance (L).

where

C_{A0} = initial concentration of radionuclide A (M/L^3).

with uniform initial concentration and zero concentration at the surface. Equation (7-5) is presented in Choy and Reible (2000).

The boundary conditions associated with Equation (7-5) and its solution include the following:

$$C_A(z,t)\big|_{z=0} = 0 \qquad t > 0 \qquad (7\text{-}6)$$

$$C_A(z,t)\big|_{z\to\infty} = C_{A0} \qquad t > 0 \qquad (7\text{-}7)$$

$$C_A(z,t)\big|_{t=0} = C_{A0} \qquad z \in [0,\infty) \qquad (7\text{-}8)$$

The boundary and initial conditions Equations (7-6) through (7-8) for Equation (7-5) describe a semi-infinite system with a constant initial concentration of radionuclide A (C_{A0}) and represent transport (diffusion) toward the surface where the concentration is maintained at zero. The zero concentration boundary condition implies that as soon as the contaminant diffuses to the surface it is immediately removed. For mass transport in the grout to the grout/tank interface shrinkage crack, this assumption is conservative (i.e., does not underestimate mass transfer at the grout/tank interface shrinkage crack).

The analytical solution to Equation (7-5), using boundary and initial conditions in Equations (7-6) through (7-8) for the surface flux, $j_A(t)$, in units of M/L^2T is offered in Choy and Reible (2000).

$$j_A(t)\big|_{z=0} = C_{A0}\sqrt{\frac{D_{A\,(eff)}\,R_{fA}}{\pi\, t}} \qquad t > 0 \qquad (7\text{-}9)$$

Equation (7-9) determines the amount of a contaminant that diffuses from the grout to the grout/tank interface shrinkage crack. The flux computed using Equation (7-9) is multiplied by the area normal to flow in the grout/tank interface shrinkage crack. This area is the product of the tank circumference (i.e., $2\pi r$, where r is the tank radius, 7.6 m [25. ft]) and the height of grout at the bottom of the tank that contains radionuclides (i.e., 1 ft [0.3 m]). The release rates from the grout/tank interface shrinkage cracks computed using this approach and Equation (7-9) result in the values shown in Figure 7-17.

From Figure 7-17, the peak release rates computed using DUST-MS and the first-order release rate model are 0.39 and 0.88 Ci/yr, respectively, while the peak release rate, determined assuming diffusion from the grout/tank interface shrinkage crack is 0.036 Ci/yr. Thus, conservatively assuming that the entire grout/tank wall interface is a preferential water pathway and that radionuclides diffuse from the bottom 1 ft (0.3 m) of the grout, the peak DUST-MS release rate is an order of magnitude greater than the peak release rate computed assuming diffusion. Even if two or three cracks similar to the shrinkage crack at the grout/tank interface are assumed, the peak diffusion release rates would be less than the DUST-MS and first-order model release rates. Moreover, if the shrinkage cracks are assumed to occur earlier (e.g., at $t = 0$), the peak diffusion release rates are still less than the DUST-MS and first-order model release rates.

Consequently, since the peak dose serves as the performance measure, the conservative assumptions described at the beginning of this section and the results shown in Figure (7-17) indicate that the DUST-MS peak release rates are reasonable when compared to analytical results. Additionally, assuming a large enough tank infiltration exists in the grout tank to cause fracture flow, peak release rates arising from heterogeneities in tank grout cracks are expected to be an order of magnitude smaller than the DUST-MS peak release rate. This analysis confirms that (1) modeling release rates using DUST-MS and assuming surface rinsing are reasonable and conservative and (2) even if conservative assumptions are made, the effects of heterogeneities on the peak release when compared to the DUST-MS peak release rate is small.

7.7.2 Comparison to Analytical Calculations

Release rates of radionuclides from the TFF vaults were estimated using the DUST-MS computer code (Sullivan 1993, 1996). One-dimensional DUST-MS transport simulations were conducted for radionuclide sources in the grouted tank and in the sand pad beneath the tank to estimate the radionuclide release rates. To evaluate the sensitivity of these release rates to the selected DUST-MS release rate model (i.e.,

surface rinsing), the following comparative analysis was conducted between release rates computed using DUST-MS and release rates from an analytical solution to a first-order mass balance equation.

DUST-MS simulations were conducted for ^{129}I release rates from the tank assuming worst-case scenario parameters. Release rates were calculated from the source in the tank and from the concrete vault at the vault floor/basalt interface (i.e., following transport through the tank, sand pad, and vault floor). These results are provided in Figure 7-18. The release rates begin at 500 yr when the tank is assumed to have totally corroded and grout inside the tank is completely degraded. The results in Figure 7-18 show the effects of transport through the tank, sand pad, and vault floor on the release rates from the source in the tank.

For comparison with DUST-MS results, an analytical solution to a first-order mass balance equation based on a control volume approach was employed. The rate of change of mass inside the control volume (i.e., the tank source) decreases from water infiltrating and mobilizing radionuclides in the tank source. This relationship is expressed in Equation (7-10).

$$\frac{dM_T}{dt} = C_P \times Q_{\text{inf}\,il} \times SA \qquad (7\text{-}10)$$

where

M_T = total mass in the tank source (Ci, assumed initially to be a unit source)

t = time (yr)

C_p = pore water concentration in the tank source (Ci/cm^3) Q_{infil}= flow rate of infiltrating water in the tank source (12.6 cm/yr)

SA = source surface area normal to flow (cm^2, circular with a radius of 760 cm).

The tank source is assumed to be cylindrical with a radius of 7.6 m (25. ft) and the height of 1 ft (0.3 m). In this vault/tank conceptualization, the radionuclides in the tank are completely mixed in the tank source volume.

To determine the mass remaining in the tank source, M_T, it was assumed that the radionuclides partitioned between the water in the pore space

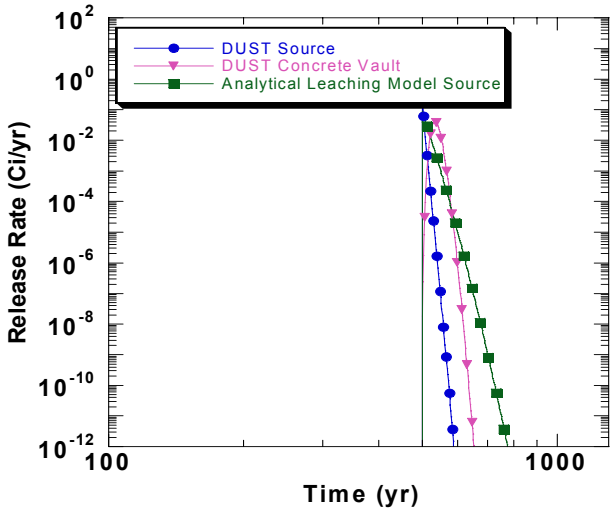

Figure 7-18. Comparison of DUST-MS release rates with analytical calculations for the ^{129}I tank source using worst-case scenario parameters.

and the solid (i.e., degraded grout) is at equilibrium according to the partition coefficient, K_d. The relationship between the pore water concentration and the total mass contained in the tank source is described by Equation (7-11).

$$C_p = \frac{M_T}{K_d \times M_{soil} + V_W} \qquad (7\text{-}11)$$

where

M_{soil} = mass of the source (5.56E+07 cm^3 at a bulk density of 2.12 g/cm^3)

V_w = volume of source water (cm^3, assuming a moisture content of 0.242).

Substituting Equation (7-11) into Equation (7-10) and solving for the total mass in the tank as a function of time, M_T, yields Equation (7-12).

$$M_T = M_0 \exp[-\alpha\ (t-500)] \qquad (7\text{-}12)$$

where

M_0 = initial mass in tank (Ci, unit initial source)

$$\alpha = \frac{Q_{\inf il}\, SA}{K_d \times M_{soil} + V_W}$$

t-500 = time since the beginning of the release at 500 yr.

The mass release rate from the tank is obtained by differentiating Equation (7-12) with respect to time, *t*, and is expressed in Equation (7-13).

$$\frac{dM_T}{dt} = -M_0\ \alpha \exp[-\alpha\ (t-500)] \qquad (7\text{-}13)$$

Equation (7-13) was evaluated for the same times used in the DUST-MS release rate calculations shown in Figure 7-18. The DUST-MS release rates from the tank source and from the vault floor together with the release rates computed using the analytical solution in Equation (7-13) are provided in Figure 7-18.

In Figure 7-18, the DUST-MS release rate peak is larger (about 0.4 versus 0.09) than the analytically-based release rate peak. The DUST-MS releases occur sooner than the analytically-based releases as evidenced in the slopes of these release rates following the peak releases. Thus, it is concluded from the results in Figure 7-18 that the DUST-MS release rates computed with the surface rinsing model are consistent and conservative relative to release rates determined with a mass balance, equilibrium-partitioning-based analytical model.

7.8 Radon Analysis

The radon transport analysis was based on a very conservative diffusion model. Due to the very low flux results for radon, it is difficult to pose a situation in which a significant change in the result could occur. The most important parameter would be the radium concentrations in the waste. However, there is no conceivable way for the inventory to change enough to increase the radon fluxes and make them near the performance objective. Table 7-14 summarizes the radon flux results for the four inventories (i.e., worst-case, conservative, realistic, and best).

7.9 Volatile Radionuclide Analysis

The analysis of atmospheric doses for volatile radionuclides was conducted in a very conservative manner for ^3H and ^{14}C. The inventory for the releases was based upon the conservative inventory. The total dose for the atmospheric pathway was 0.51 mrem/yr, which is very low in comparison to the performance objective of 10 mrem/yr.

It is difficult to pose a situation in which a parameter could change significantly enough to cause the atmospheric doses to be near the performance objective. Table 7-14 summarizes the atmospheric dose results for the four inventories (i.e., worst-case, conservative, realistic, and best).

Table 7-14. Doses for each inventory option for radon flux, atmospheric releases, and intruder scenarios.

	Worst-Case Inventory	Conservative Inventory	Realistic Inventory	Best Inventory
Acute Drilling Intruder (mrem)	276	232	193	144
Chronic Drilling Intruder (mrem/yr)	106	91.1	75.1	52.8
Acute Construction Intruder (mrem)	0.89	0.80	0.67	0.45
Chronic Construction Intruder (mrem/yr)	29.1	26.1	21.8	14.5
Radon Flux ($pCi/m^2/s$)	0.48	0.39	0.29	0.19
Atmospheric (mrem/yr)	1.1	0.51	0.22	0.05

7.10 Intruder Analyses

DOE guidance for PAs (DOE 1999b) states that the sensitivity/uncertainty analysis for hypothetical inadvertent intruder analyses should be limited to qualitative arguments (e.g., explanation of the rationale for selected scenarios and parameters).

The discussions in Section 5 show that the TFF is a unique environment for the evaluation of intruder scenarios. Many of the standard scenarios were not considered applicable to the TFF because the depth of the waste in the tanks is 10 m (30 ft). Therefore, only the intruder-drilling and post-drilling scenarios were considered applicable for the tank and sand pad contamination. Additional scenarios were evaluated for the piping inventory located less than 3 m (10 ft) below the surface. These scenarios included the intruder-construction scenario and the post intruder-construction scenario.

It is difficult to predict the future actions of humans, especially over a period of 1,000 yr. The fact that the intruder is assumed to drill a well directly through a tank is considered a very conservative assumption. It can be argued that the person drilling the well would not continue to drill through the concrete and stainless-steel tanks and grout unless it was completely degraded. However, to be conservative, the well was assumed to be drilled through the waste at 100 yr post-closure. The analysis is very sensitive to the time of intrusion since the short-lived fission products are the main contributor to the intruder doses at 100 yr post-closure.

Uncertainty exists in the state of the concrete systems over time. In this analysis, credit was taken for the concrete vault providing a barrier to intrusion. Oztunali and Roles (1986) state that "if resistance is encountered during drilling (as would be the case if the drill bit hit solid rocks or intact metal), the crew would simply move a few yards horizontally and drill a new hole. Drilling equipment and bits that can drill through solid rock and intact metal are available; however, they are more expensive than the equipment and bits that are normally required and used for water well installation. Similarly, it is anticipated that standard drill bits would have difficulty penetrating reinforced concrete structures, although little difficulty is expected for waste stabilized using grout backfill." Therefore, credit could be taken for the reinforced concrete vaults and the stainless-steel tanks, further reducing the doses for the intruder.

In Equation (5-4) for the acute intruder-drilling scenario, the radius of the well is not present in the equation. Note, however, that the concentration in the soil will be the same for any given well radius, but the total amount of contaminated soil will vary with the well radius. This equation assumes that the radionuclide activity is completely mixed with the drill cuttings. The radionuclide activity would not

likely be completely mixed with the well cuttings. However, when considering the different possibilities such as the cuttings from the tank being covered with cuttings from below the tank and the varying radiation fields that would be encountered as the drilling commenced with time, it seems appropriate to make this assumption of complete mixing.

A 22-in.-diameter well provides 30 m^3 (1,000 ft^3) of contaminated zone (i.e., over the depth of the well borehole of 122 m [400. ft]). When the soil and waste are spread out over the assumed contaminated zone of 2,200 m^2 (24,000 ft^2), it results in a contaminated zone 0.014 m (0.54 in.) thick. As the well diameter is increased, the thickness of the contaminated zone also increases, thus affecting the external dose rate. However, in this intruder analysis, a very large-diameter well was used for purposes of conservatism. Additionally, the assumption that the drill cuttings are spread out over the ground and are not located in a mud pit adds more conservatism and site-specific application, which increases the external dose for this scenario.

Other conservative parameters were used in the acute intruder-drilling scenario as well. These include the assumption that the intruder spends 160 hr drilling the well. Standard drilling scenarios typically use an exposure time of 6 hr (Oztunali and Roles 1986).

In Equation (5-14) for the chronic post-drilling scenario, two parameters of importance are present in the form of the radius of the well (r_{well}) and the final depth of the contaminated zone after tilling (D_c). Variations in the values used for these parameters will result in proportional changes in the predicted radionuclide concentrations in the contaminated zone. Therefore, if the depth of the contaminated zone after tilling (D_c) is reduced by a factor of 2, the contaminated zone concentrations increase by a factor of 2. If the radius of the well (r_{well}) is increased by a factor of 2, the contaminated zone concentrations increase by a factor of 4. The selection of parameter values for r_{well} and D_c are considered to be appropriate and based on site-specific information.

For both the acute and chronic intruder scenarios, the conservative inventory was used. Table 7-14 summarizes the intruder dose results for the four inventories (i.e., worst-case, conservative, realistic, and best).

The uncertainty in the intruder analyses is large and includes both the assumptions made during the development of the scenarios and the parameter values selected in the formulation of the mathematical representations. However, in this PA, every attempt was made to consider the site-specific environment and habits of the people currently in the region. Therefore, the analyses are considered to be representative of the INEEL region. The predicted doses are considered to be conservative, and there is a reasonable assurance that the performance objectives will not be exceeded for 1,000 yr post-closure.

7.11 Dose Analyses

The dose analyses for the groundwater pathway contain many parameters dealing with human exposure. For the groundwater protection pathway, standard drinking water intake rates (i.e., 730 L/yr) were used to bound the doses.

The all-pathways doses were calculated stochastically to account for the variations in human exposure parameters. Each parameter in the dose calculations was represented by a distribution of values. These distributions were then sampled, and the dose results were ranked from lowest to highest for 1,000 realizations. The 950^{th} dose value in the ranking was then used as the 95% confidence level.

In certain circumstances, national average data have been used for formulating some of the biosphere dose parameter distributions; however, site-specific information has been used for others as referenced from Maheras et al. (1997), where appropriate. Other site-related information (i.e., from Yucca Mountain dose analysis, a similar semi-arid environment) also has been used where appropriate (LaPlante and Poor 1997).

To the best knowledge of the authors, no reliable site-specific information is known to exist for the human consumption rate of locally-

generated water. For reference, Maheras et al. (1997) used a constant value of 258 L/yr from Yang and Nelson (1984) that was based on national data. This parameter was shown to be the most important for sensitivity/uncertainty analyses. In this case, national average data were used to generate the parameter distribution. Since national average data would include more data from warmer climates than data from cooler climates (compared to the INEEL), and because the drinking water rate is greater in warmer climates, the distribution used for this parameter tends toward greater consumption rates than those expected for locally-generated data. Hence, the rate is conservative. (The values used in the Maheras et al. (1997) report are provided in Section 3 along with the parameter distributions used in the TFF PA analyses for comparison.)

7.12 Future Work

Because this PA is considered a living document for closure projects such as the TFF, it will be reviewed as additional information and studies are conducted to determine if it still bounds the TFF environment. As additional data become available and the PA needs to be revised, additional analysis will be required. The following areas of future work are presented to facilitate discussion for improving the PA in future revisions.

Further work should be conducted to refine and confirm the existing radionuclide inventories that will be present at the INTEC facility at site closure. This work includes additional sampling and analysis of existing waste and refinement of potential waste estimates for unsampled areas, such as the piping and sand pads. Sampling of the tanks before closure will be necessary to evaluate the ^{129}I inventory to ensure that the groundwater protection performance objectives are met.

Future research and development studies should be reviewed and incorporated into the PA as they become available to reduce the uncertainty and address data gaps identified in this PA. Specifically, work conducted in the areas of unsaturated hydraulic parameters, distribution coefficients, and the behavior of fracture flow in the basalt units would be useful for future iterations of the PA analyses. Unsaturated hydraulic properties needing refinement include the moisture characteristic curves, unsaturated hydraulic conductivities, and moisture retention values used for the interbed. In addition, unsaturated data that are representative of the behavior of fracture flow under unsaturated conditions would improve the analysis of the groundwater pathway in the PA. This is particularly important in the model simulations because the fracture flow is represented as a porous flow in the model.

Future research or literature studies that refine the distribution coefficients used in the model simulations would be useful for the transport calculations in the PA. For example, similar investigations conducted at the Hanford facility could be evaluated to locate specific tests conducted to measure K_d values for basalt and interbed units. New information obtained from similar site studies should be examined to adequately address the sensitivity of this important parameter on transport rates of specific radionuclides in the subsurface at INTEC.

8. PREPARERS

Mark S. Jarzemba, Ph.D.
Ph.D., Nuclear Engineering, The Ohio State University, 1993
M.S., Nuclear Engineering, The Ohio State University, 1991
B.S., Engineering Physics, The Ohio State University, 1988

Dr. Jarzemba is a Nuclear Engineer/Health Physicist with 8 years of experience in radiation transport, dosimetry, and environmental radioactivity (man-made and naturally occurring). He is the author of 12 peer-reviewed journal articles, 10 conference proceedings, and numerous contractor reports on these subjects. Much of his professional experience is in both high- and low-level waste repository performance assessment.

Dr. Jarzemba provided technical support for the evaluation of intruder doses, the all-pathways dose assessment, and the radon release assessment for the TFF PA.

Peter M. Kearl, CGWP
M.S., Hydrology/Hydrogeology, University of Nevada-Reno, 1982
B.S., Geology, Mesa State College, 1979

Mr. Kearl is a Certified Ground Water Professional with over 20 years of experience in environmental transport modeling and hydrologic assessments. He has been involved in technical aspects of performance assessments for the Savannah River Site.

Mr. Kearl conducted the hydrologic assessment and groundwater modeling involving the contaminant transport simulations for this PA. Mr. Kearl has performed hydrologic studies in 40 states and five foreign countries.

Robert W. Rice
M.S., Chemical Engineering, Arizona State University, 1987
B.S., Chemical Engineering, University of Colorado, 1983
B.S., Business, University of Colorado, 1983

Mr. Rice has 16 years of experience in the fields of chemical and process engineering and modeling. He participated in the development of the Nuclear Regulatory Commission's Total System Performance Assessment computer code that is used to conduct probabilistic performance assessments for the proposed high-level waste repository at Yucca Mountain. This code checks the results and assumptions in DOE's Total System Performance Assessment for Yucca Mountain. His work experience includes unsaturated and saturated zone flow and transport modeling, code development and testing, behavior of the near-field environment surrounding the waste packages, waste package degradation, infiltration from the ground surface, and determination of dose at the receptor location.

For this PA report, Mr. Rice was involved in the degradation analysis of the tank, vault, grout, and piping systems used to estimate the changes in permeability over time.

Edward Kirk Roemer
B.S., Environmental Management, Columbia Southern University, 2001
A.S., Geology, Mesa State College, 1995

Mr. Roemer has 17 years of experience in environmental field characterization, transport modeling, and GPS/GIS graphics. He has been involved in technical aspects of performance assessments for the Savannah River Site, Nevada Test Site, and Yucca Mountain.

Mr. Roemer provided overall report preparation, graphics, and databases for the TFF PA. He was involved in the evaluation of the intruder doses, all-pathways dose assessment, and general development of the PA report.

David J. Thorne, CHP
M.S., Health Physics, Colorado State University, 1988
B.S., Geology, Mesa State College, 1985

Mr. Thorne is a Certified Health Physicist with 17 years of experience in environmental transport modeling and dose assessment. He has

been involved in technical aspects of performance assessments for the Savannah River Site, Nevada Test Site, and Yucca Mountain.

Mr. Thorne provided project coordination and technical oversight for the TFF PA. He was involved in the evaluation of the intruder doses, all-pathways dose assessment, and overall development of the PA report.

John C. Walton, Ph. D.
Ph.D., Chemical Engineering, University of Idaho, 1991
M.S., Chemical Engineering, University of Washington, 1988
M.S., Environmental Science, University of Virginia, 1981
B.S., Biology and Geology, Western Illinois University, 1979

Dr. Walton has over 20 years of experience in the environmental field. His work has involved the development of predictive models for concrete degradation and the analysis of fluid flow and mass transport through concrete vaults and waste forms used to isolate nuclear waste. Dr. Walton also developed a model for leakage from flaws in geomembrane liners used in landfills and surface impoundments, and a mechanistic corrosion model for waste package degradation. Other work has included the development of a generalized reactive transport code used for release rate and corrosion models. This code has supported the Nuclear Regulatory Commission's analysis of the engineered barriers performance for the proposed high-level waste repository at Yucca Mountain. Dr. Walton is currently an associate professor at the University of Texas at El Paso.

For this PA report, Dr. Walton was involved in the application of concrete degradation and corrosion models to the tank, vault, grout, and piping systems that were used in the degradation analysis to estimate the changes in permeability over time.

9. REFERENCES

10 CFR 20, 2003, "Standards for Protection against Radiation," *Code of Federal Regulations*, Office of the Federal Register, January 1.

10 CFR 61, 2003, "Licensing Requirements for Land Disposal of Radioactive Waste," *Code of Federal Regulations,* Office of the Federal Register, January 1.

40 CFR 61, Subpart H, 2002, "National Emission Standards for Emissions of Radionuclides Other than Radon from Department of Energy Facilities," *Code of Federal Regulations*, Office of the Federal Register, July 1.

40 CFR 141, 2002, "National Primary Drinking Water Regulations," *Code of Federal Regulations*, Office of the Federal Register, July 1.

40 CFR 264, 2002, "Standards for Owners and Operators of Hazardous Waste Treatment, Storage, and Disposal Facilities," *Code of Federal Regulations*, Office of the Federal Register, July 1.

40 CFR 265, 2002, "Interim Status Standards for Owners and Operators of Hazardous Waste Treatment, Storage, and Disposal Facilities," *Code of Federal Regulations*, Office of the Federal Register, July 1.

40 CFR 265.193, 2002, "Containment and Detection of Releases," *Code of Federal Regulations*, Office of the Federal Register, July 1.

40 CFR 265.197, 2002, "Closure and Post-Closure Care," *Code of Federal Regulations*, Office of the Federal Register, July 1.

41 FR 298, 1975, "National Interim Primary Drinking Water Regulations," *Federal Register*, Environmental Protection Agency, pp. 59566–59574, December 24.

58 FR 138, 1991, "Sole Source Designation of the Eastern Snake River Plain Aquifer, Southern Idaho," *Federal Register*, Environmental Protection Agency, pp. 50634–50638, October 7.

65 FR 236, 2000, "National Primary Drinking Water Regulations; Radionuclides; Final Rule," *Federal Register*, Environmental Protection Agency, pp. 76707–76753, December 7.

42 USC 6901 et. seq., 1976, "Resource Conservation and Recovery Act of 1976," October 21.

42 USC 9601–9675, 1980, "Comprehensive Environmental Response, Compensation, and Liability Act of 1980," December 11.

Ackerman, D. J., 1991, *Transmissivity of the Snake River Plain Aquifer at the Idaho National Engineering Laboratory Site, Idaho,* U.S. Geological Survey Water-Resources Investigations Report 91-4058, DOE/ID-22097.

ACRi, 2000, *PORFLOW Users Manual*, Version 4.0, Rev. 4, Bel Air, California.

Allard, B., 1985, *Radionuclide Sorption on Concrete*, NAGRA Technical Report NTB 85-21, NAGRA, Wettingen, Switzerland.

Allard, B., G. Persson, and B. Torstenfelt, 1985, *Technical Reports 85-18 Actinide Solubilities and Speciation in a Repository Environment; 85-19 Organic Complexing Agents in Low- and Medium-Level Radioactive Waste; 85-20 Radionuclide Sorption on Carbonate-Clayish Rock; and 85-21 Radionuclide Sorption on Concrete,* NAGRA, Radiochemistry Consultant Group for Kematka Consultants Co., Stockholm, Sweden.

Allard, B., B. Torstenfelt, and K. Andersson, 1981, *Sorption Studies of $H^{14}CO_3^-$ on Some Geologic Media and Concrete*, Scientific Basis for Nuclear Waste Management, Volume 3, J. Moore (ed.), New York: Plenum Press, p. 465.

American Ornithologist's Union, 1983, *Checklist of North American Birds,* Lawrence, Kansas: Allen Press.

Anderson, S. R., 1991, *Stratigraphy of the Unsaturated Zone and Uppermost Part of the Snake River Plain Aquifer at the Idaho Chemical Processing Plant and Test Reactor Area, Idaho National Engineering Laboratory, Idaho,* U.S. Geological Survey Water-Resources Investigations Report 91-4010, DOE/ID-22095.

Anderson, S. R., and R. C. Bartholomay, 1995, "Use of Natural Gamma Logs and Cores for Determining the Stratigraphic Relationship at the Radioactive Waste Management Complex, Idaho National Engineering Laboratory, Idaho," *Journal of the Idaho Academy of Science,* Vol. 31, No. 1, pp. 1–10.

Anderson, S. R., D. J. Ackerman, and M. J. Liszewski, 1996, *Stratigraphic Data for Wells at and near the Idaho National Engineering Laboratory, Idaho,* U.S. Geological Survey Open-File Report 96-248, DOE/ID-22127.

Anderson, S. R., M. A. Kuntz, and L. C. Davis, 1999, *Geologic Controls of Hydraulic Conductivity in the Snake River Plain Aquifer at and near the Idaho National Engineering and Environmental Laboratory, Idaho,* U.S. Geological Survey Water-Resources Investigations Report 99-4033, DOE/ID-22155.

Anderson, S. R., M. J. Liszewski, and L. D. Cecil, 1997, *Geologic Ages and Accumulation Rates of Basalt-Flow Groups and Sedimentary Interbeds in Selected Wells at the Idaho National Engineering Laboratory, Idaho,* U.S. Geological Survey Water-Resources Investigations Report 97-4010.

ANSI, 1970, " Welded and Seamless Wrought Steel Pip," ANSI B36.10.

Army Corps of Engineers, 1995, "Engineering and Design for Periodic Inspection and Continuing Evaluation of Completed Civil Works Structures," ER-1110-2-100, February 15.

Arthur, W. J., 1982, "Radionuclide Concentrations in Vegetation at a Solid Radioactive Waste Disposal Area in Southeastern Idaho," *Journal of Environmental Quality,* Vol. 11, No. 3, pp. 394–399.

Arthur, W. J., J. C. Grant, and O. D. Markham, 1983, "Importance of Biota in Radionuclide Transport at the SL-1 Radioactive Waste Disposal Area," *Idaho National Engineering Laboratory Radioecology and Ecology Programs, 1983 Progress Report,* DOE/ID-12098.

Atkinson, A., and A. K. Nickerson, 1988, "Diffusion and Sorption of Cesium, Strontium, and Iodine in Water-Saturated Cement," *Nuclear Technology,* Vol. 81, No. 1, pp. 100–113.

Atkinson, A., N. M. Everitt, and R. Guppy, 1989, *Evolution of pH in a Radwaste Repository: Experimental Simulation of Cement Leaching*, AERE-R12594, DOE/RW/89/025, Part 1, Harwell Laboratory, UKAEA.

Baes, C. F., et al., 1984, *A Review and Analysis of Parameters for Assessing Transport of Environmentally Released Radionuclides through Agriculture,* ORNL-5786.

Baes, C. F., III, and T. H. Orton, 1979, *Productivity of Agricultural Crops and Forage, Yv,* in *A Statistical Analysis of Selected Parameters for Predicting Food Chain Transport and Internal Dose of Radionuclides*, F. O. Hoffman and C. F. Baes (eds.), NUREG/CR-1004, ORNL/NUREG/TM-282, October.

Baes, C. F., III, and R. D. Sharp, 1983, "A Proposal for Estimation of Soil Leaching and Leaching Constants for Use in Assessment Models," *Journal of Environmental Quality,* Vol. 12, pp. 17–28.

Barraclough, J. T., et al., 1967, *Hydrology of the National Reactor Testing Station, Idaho, 1966,* U.S. Geological Survey Water-Resources Open File Report, IDO-22049.

Barraclough, J. T., B. D. Lewis, and R. G. Jensen, 1982, *Hydrologic Conditions at the Idaho National Engineering Laboratory, Idaho Emphasis: 1974-1978*, U.S. Geological Survey, Water-Supply Paper 2191, Washington.

Bates, R. L., and J. A. Jackson, 1980, *Glossary of Geology, 2nd Edition*, Falls Church, Virginia: American Geological Institute.

Bayliss, S., F. Ewart, R. Howse, J. Smith-Briggs, H. Thomason, and H. Willmott, 1988, "The Solubility and Sorption of Lead-210 and Carbon-14 in a Near-Field Environment," *Scientific Basis for Nuclear Waste Management*, M. Apted and R. Westerman (eds.), Volume 112, p. 33, Material Research Society, Pittsburgh, Pennsylvania.

Bayliss, S., A. Haworth, R. McCrohon, A. Moreton, P. Oliver, N. Pilkington, A. Smith, and J. Smith-Briggs, 1991, "Radioelement Behaviour in a Cementitious Environment," *E-MRS Symposium on the Scientific Basis for Nuclear Waste Management, Strasbourg, France.*

Bennett, C. M., 1990, *Streamflow Losses and Groundwater Level Changes along the Big Lost River at the INEL, Idaho,* U.S. Geological Survey Water-Resources Investigations Report 86-4204, DOE/ID-22091.

Berenbrock, C., and L. C. Kjelstrom, 1998, *Preliminary Water-Surface Elevations and Boundary of the 100-Year Peak Flow in the Big Lost River at the Idaho National Engineering and Environmental Laboratory, Idaho,* U.S. Geological Survey Water Resources Investigations Report 98-4065, DOE/ID-22148.

Bird, R. B., W. E. Stewart, and E. N. Lightfoot, 1960, *Transport Phenomena,* New York: John Wiley and Sons, pp. 495–518.

Blom, P. E., W. H. Clark, and J. B. Johnson, 1991, "Colony Densities of the Seed Harvesting Ant *Pogonomyrmex* salinus in Seven Plant Communities on the Idaho National Engineering Laboratory," *Journal of the Idaho Academy of Science*, Vol. 27, No. 1, pp. 28–36.

Blumb, A. C., C. L. Murphy, and L. G. Everett, 1992, "A Comparison of Three Functional Forms for Representing Soil Moisture Characteristics," *Ground Water*, Vol. 30, No. 2, pp. 175–185.

Boateng, S., and J. D. Cawlfield, 1999, "Two-Dimensional Sensitivity Analysis of Contaminant Transport in the Unsaturated Zone," *Ground Water*, Vol. 37, No. 2, pp. 185–193.

Bradbury, M. H., and F. A. Sarott, 1995, *Sorption Databases for the Cementitious Near-Field of a LLW Repository for Performance Assessment,* Paul Scherrer Institute, 95-12, March.

Bresler, E., and G. Dagan, 1983, "Unsaturated Flow in Spacially Variable Fields, 3. Solute Transport Models and Their Application to Two Fields," *Water Resources Research,* Vol. 19, No. 2, pp. 429–435.

Breysse, D., and B. Gerard, 1997, "Modeling of Permeability in Cement-based Materials: Part 1—Uncracked Medium," *Cement and Concrete Research,* Vol. 27, No. 5, pp. 761–775.

Broermann, J., R. L. Bassettt, E. P. Weeks, and M. Borgstrom, 1997, "Estimation of α_L, Velocity, K_d and Confidence Limits from Tracer Injection Test Data," *Ground Water,* Vol. 35, No. 6, pp. 1066–1076.

Calabrese, E. J., E. J. Stanek, C. E. Gilbert, R. M. Barnes, 1990, "Preliminary Adult Soil Ingestion Estimates: Results of a Pilot Study," *Regulatory Toxicology Pharmacology*, Vol. 12, pp. 88–95.

Carrigan, P. H., Jr., 1972, *Probability of Exceeding Capacity of Flood-Control System at the National Reactor Testing Station, Idaho,* USGS Open-File Report, IDO-22052.

Case, M. J., and M. D. Otis, 1988, *Guidelines for Radiological Performance Assessment of DOE Low-Level Radioactive Waste Disposal Sites,* DOE/LLW-62T, July.

Cecil, L. D., et al., 1992, "Water Infiltration Rates in the Unsaturated Zone at the Idaho National Engineering Laboratory Estimated by Chlorine-36 and Tritium Profiles, and Neutron Logging," *Proceedings of the 7th International Symposium on Water-Rock Interactions, Park City, Utah, July 13–18*, WRI-7, Y. K. Kharaka and A. S. Meest (eds.).

Cecil, L. D., et al., 1991, *Formation of Perched Ground-water Zones and Concentrations of Selected Chemical Constituents in Water, Idaho National Engineering Laboratory, Idaho 1986–1988,* U.S. Geological Survey Water-Resources Investigations Report 91-4166, DOE/ID-22100.

Cholewa, A. F., and D. M. Henderson, 1984, "A Survey and Assessment of the Rare Vascular Plants of the Idaho National Engineering Laboratory," *Great Basin Naturalist,* Vol. 44, pp. 140–144.

Choy, B., and D. D. Reible, 2000, *Diffusion Models of Environmental Transport*, Boca Raton: Lewis Publishers.

Clawson, K. L., G. E. Start, and N. R. Ricks, 1989, *Climatography of the Idaho National Engineering Laboratory*, U.S. Department of Commerce, National Oceanic and Atmospheric Administration, Environmental Research Laboratories, Air Resources Laboratory, Field Research Division, Idaho Falls, Idaho, DOE/ID-12118, December.

Crank, J., 1975, *The Mathematics of Diffusion*, 2nd Edition, Oxford: Oxford University Press.

Croff, A. G., 1980, *A User's Manual for the ORIGEN2 Computer Code*, ORNL/TM-7175, July.

Coats, D. W., and R. C. Murray, 1985, *Natural Phenomena Hazards Modeling Project: Extreme Wind/Tornado Hazard Models for Department of Energy Site,* UCRL-53526, Rev. 1, Lawrence Livermore National Laboratory, Livermore, California.

Coughtrey, P. J., D. Jackson, and M. C. Thorne, 1985, *Radionuclides Distribution and Transport in Terrestrial and Aquatic Ecosystem: A Compendium of Data,* A. A. Balkema (ed.).

CRC Press, Inc., 1981, *CRC Handbook of Chemistry and Physics,* Robert C. Weast and Melvin J. Astle (eds.), Boca Raton, Florida.

Del Debbio, J. A., and T. R. Thomas, 1989, *Transport Properties of Radionuclides and Hazardous Chemical Species in Soils at the Idaho Chemical Processing Plant,* WINCO-1068.

Department of Commerce, 2001, *Profiles of General Demographic Characteristics, 2000 Census of Population and Housing, Idaho,* Economics and Statistics Administration, U.S. Census Bureau, May.

Department of Commerce, 2000, *County Population Estimates and Demographic Components of Population Change: Annual Time Series, July 1, 1990 to July 1, 1999 (Includes Revised April 1, 1990 Population Estimates Base)*, CO-99-8, Statistical Information Staff, Population Division, March 9, available at http://eire.census.gov/popest/archives/county/co-99-8/99C8_16.txt.

Department of Commerce, 1997, *Current Population Reports, Population Projections: States, 1995–2025,* P25-1131, Economics and Statistics Administration, May, available at http://www.census.gov/prod/2/pop/p25/p25-1131.pdf, web page visited November 25, 2002.

Department of Commerce, 1995, Population of Counties by Decennial Census: 1900 to 1990, Population Division, March 27, available at http://www.census.gov/population/cencounts/id190090.txt.

Department of Commerce, 1990, *1990 Census of Population: General Population Characteristics, Idaho*, 1990 CP-1-14, Economics and Statistics Administration, Bureau of the Census.

Department of Commerce, 1963, *Maximum Permissible Body Burdens and Maximum Permissible Concentration of Radionuclides in Air or Water for Occupational Exposure,* National Bureau of Standards Handbook 69 as amended, August.

DOE, 2002, *Idaho High-Level Waste & Facilities Disposition Final Environmental Impact Statement,* DOE/EIS-0287, September.

DOE, 2001a, "Radioactive Waste Management Manual," DOE M 435.1-1, Change 1, Department of Energy, June 19.

DOE, 2001b, "Radioactive Waste Management," DOE O 435.1, Change 1, Department of Energy, August 28.

DOE, 2000, *Department of Energy Deactivated High-Level Waste Facility Closure (HLWFC) Manual,* Office of Environmental Management, Office of Integration and Disposition (EM-22), Revision 0, August.

DOE, 1999a, "Implementation Guide for Use with DOE M-435.1-1," DOE G 435.1-1, Department of Energy, July 9.

DOE, 1999b, *Format and Content Guide for U.S. Department of Energy Low-Level Waste Disposal Facility Performance Assessments and Composite Analyses*, December 7.

DOE 1999c, "Remarks by Secretary of Energy Bill Richardson, Land Transfer Event, Idaho National Engineering and Environmental Laboratory, July 17, 1999," *United States Department of Energy Secretarial Notices*, available at http://www.energy.gov/HQDocs/speeches/1999/julss/landtrans.htm, Web page updated July 27, 1999, Web page visited December 4, 2001.

DOE, 1998, "Radioactive Waste Management," DOE O 5820.2A, Department of Energy, September 26.

DOE, 1995, *Department of Energy Programmatic Spent Nuclear Fuel Management and Idaho National Engineering Laboratory Environmental Restoration and Waste Management Programs Final Environmental Impact Statement,* DOE/EIS-0203-F, April.

DOE, 1993, "Radiation Protection of the Public and the Environment," DOE O 5400.5, Department of Energy, January 7.

DOE, 1987, *Environmental Assessment: Fuel Reprocessing and Restoration at the Idaho National Engineering Laboratory,* DOE/EA-0306.

DOE-ID, 2003a, *Tier 1 Closure Plan for the Idaho Nuclear Technology and Engineering Center Tank Farm Facility at the INEEL,* DOE/ID-10975, March.

DOE-ID, 2003b, *Composite Analysis for Tank Farm Closure*, DOE/ID-10974, February.

DOE-ID, 2002, *Idaho Nuclear Technology and Engineering Center Tank Farm Facility Residuals—Waste-Incidental-to-Reprocessing Report*, Draft B, DOE/ID-10777, December.

DOE-ID, 2001a, *Idaho Hazardous Waste Management Act/Resource Conservation and Recovery Act Closure Plan for Idaho Nuclear Technology and Engineering Center Tanks WM-182 and WM-183*, DOE/ID-10802, Revision 2, November.

DOE-ID, 2002b, *Contingent Landfill Closure and Post-Closure Plan for Idaho Nuclear Technology and Engineering Center Tanks WM-182 and WM-183*, DOE/ID-10841, Revision 2, November.

DOE-ID, 2000, *Operable Unit 3-14 Tank Farm Soil and Groundwater Phase I Remedial Investigation/Feasibility Study Work Plan,* DOE/ID-10676, Revision 0, December.

DOE-ID, 1999, *Final Record of Decision, Idaho Nuclear Technology and Engineering Center, Operable Unit 3-13, Idaho National Engineering and Environmental Laboratory, Idaho Falls, Idaho*, DOE/ID-10660, Revision 0, Idaho DEQ; DOE-ID; EPA, Region 10; October.

DOE-ID, 1998, *Idaho National Engineering and Environmental Laboratory Storm Water Pollution Prevention Plan for Industrial Activities,* DOE/ID-10431, Revision 30, October.

DOE-ID, 1997a, *Idaho National Engineering and Environmental Laboratory Comprehensive Facility and Land Use Plan*, DOE/ID-10514, December.

DOE-ID 1997b, *Idaho National Engineering and Environmental Laboratory Site Environmental Report for Calendar Year 1996*, DOE/ID-12082(96), August.

DOE-ID, 1997c, *INEEL National Emissions Standard for Hazardous Air Pollutants—Radionuclides,* DOE/ID-10342(96), June.

DOE-ID, 1996, *1995 INEL National Emissions Standards for Hazardous Air Pollutants—Radionuclides,* DOE/ID-10342(95), June.

DOE-ID, 1995a, *Long-Term Land Use Future Scenarios for the Idaho National Engineering Laboratory,* DOE/ID-10440, August.

DOE-ID, 1995b, *Department of Energy Programmatic Spent Nuclear Fuel Management and Idaho National Engineering Laboratory Environmental Restoration and Waste Management Programs Final Environmental Impact Statement,* Vol. 2, Pt. A, DOE/EIS-0203-F, April.

DOE-ID, 1994, *Comprehensive Well Survey for the Idaho National Engineering Laboratory*, Volume II, DOE/ID-10402, Revision 3, May.

Dunne, T., and L. B. Leopold, 1978, *Water in Environmental Planning*, New York: W. H. Freeman and Co., pg. 102.

Dunnivant, F. M., et al., 1998, "Water and Radioactive Tracer Flow in a Heterogeneous Field-Scale System," *Ground Water*, Vol. 36, No. 6, pp. 949–958.

Dykes, J. W., (ed.) 1963, *MTR Progress Report, Cycle No. 198, September 30, 1962–October 21, 1963*, IDO-16952, Phillips Petroleum Company, INEEL.

Edvardsen, C., 1999, "Water Permeability and Autogenous Healing of Cracks in Concrete," *American Concrete Institute Materials Journal,* Vol. 96, No. 4, pp. 448–454.

EG&G Idaho, 1984, *Environmental and Other Evaluations of Low-Level Waste at the Radioactive Waste Management Complex,* EGG-WM-6523.

EPA, 2001, *Who is Responsible for Drinking Water Quality?,* available at http://www.epa.gov/safewater/dwh/who.html, Web page updated September 23, 2002, Web page visited November 25, 2002.

EPA, 1993, *External Exposure to Radionuclides in Air, Water, and Soil,* Federal Guidance Report No. 12, EPA-402-R-93-081, Office of Radiation and Indoor Air, Washington, D.C.

EPA, 1992, *User's Guide for CAP88-PC: Version 1.0*, 402-B-92-001, Office of Radiation Programs, Las Vegas, Nevada, March.

EPA, 1990, *EPA Support Document for the EPA Designation of the Eastern Snake River Plain Aquifer as a Sole Source Aquifer*, 910/9-90-020, August.

EPA, 1989, *Risk Assessments Methodology, Environmental Impact Statement, NESHAPs for Radionuclides, Background Information Document – Volume I,* EPA/520/1-89-005.

EPA, 1988, *Limiting Values of Radionuclide Intake and Air Concentration and Dose Conversion Factors for Inhalation, Submersion, and Ingestion,* Federal Guidance Report No. 11, EPA-520/1-88-020, Office of Radiation Programs, Washington, D.C.

Ewart, F., S. Terry, and S. Williams, 1985, *Near-Field Sorption Data for Caesium and Strontium*, UKAEA Report AERE M3452, Harwell, United Kingdom.

Freeze, R. A., and J. C. Cherry, 1979, *Groundwater*, Englewood, New Jersey: Prentice-Hall.

Gad, M. S., and T. B. Borak, 1995, "In-Situ Determination of the Diffusion Coefficient of Rn-222 in Concrete," *Health Physics*, Vol. 68, No. 6, pp. 817–822.

Garabedian, S. P., 1986, *Application of a Parameter-Estimation Technique to Modeling the Regional Aquifer Underlying the Eastern Snake River Plain, Idaho,* U.S. Geological Survey Water-Supply Paper 2278, Washington, D.C.

Gorman, V. W., and R. C. Guenzler, 1983, *The 1983 Borah Peak Earthquake and INEL Structural Performance*, EGG-EA-6501, pg. 76.

Grove Engineering, Inc., 1990, "RadDecay," *Microshield User's Manual,* Rockville, Maryland: Grove Engineering, Inc.

Groves, C. R., and B. L. Keller, 1983, "Ecological Characteristics of Small Mammals on a Radioactive Waste Disposal Area in Southeastern Idaho," *The American Midland Naturalist,* Vol. 109, No. 2, pp. 253–265.

Hackett, W. R., and R. P. Smith, 1992, "Quaternary Volcanism, Tectonics, and Sedimentation in the Idaho National Engineering Laboratory Area," *Field Guide to Geologic Excursions in Utah and Adjacent Areas of Nevada, Idaho, and Wyoming,* J. K. Wilson (ed.), Utah Geological Survey, Miscellaneous Publication 92-3, pp. 1–17.

Harniss, R. O., and N. E. West, 1973, "Vegetation Patterns of the National Reactor Testing Station, Southeastern Idaho," *Northwest Science*, Vol. 47, pp. 30–43.

Hearn, N., 1999, "Effect of Shrinkage and Load-Induced Cracking on Water Permeability of Concrete," *American Concrete Institute Materials Journal*, Vol. 96, No. 2.

Hearn, N., R. J. Detwiler, and C. Sframeli, 1994, "Water Permeabililty of Three Old Concretes," *Cement and Concrete Research,* Vol. 24, No. 4, pp. 633–640.

Hillel, D., 1980, *Fundamentals of Soil Physics,* New York: Academic Press.

Hinsby, K., L. D. McKay, P. Jorgensen, M. Lenczewski, and C. P. Gerba, 1996, "Fracture Aperture Measurements and Migration of Solites, Viruses, and Immiscible Creosote in a Column of Clay-Rich Till," *Ground Water,* Vol. 34, No. 6, pp. 1065–1079.

Hitchcock, C. L., and A. Cronquist, 1974, *Flora of the Pacific Northwest,* Seattle: University of Washington Press.

Hoff, D. L., R. G. Mitchell, G. C. Bowman, R. Moore, 1991, *The Idaho National Engineering Laboratory Site Environmental Report for Calendar Year 1990*, DOE/ID-12082(90).

Hoff, D. L., R. G. Mitchell, G. C. Bowman, R. Moore, 1990, *The Idaho National Engineering Laboratory Site Environmental Report for Calendar Year 1989*, DOE/ID-12082(89).

Hoffman, F. O., R. H. Gardner, and K. F. Eckerman, 1982, *Variability in Dose Estimates Associated with the Food Chain Transport and Ingestion of Selected Radionuclides,* NUREG/CR-2612.

Hull, L. C., 1989, *Conceptual Model and Description of the Affected Environment for the TRA Warm Waste Pond (Waste Management Unit TRA-03),* EGG-ER-8644.

IDAPA 58.01.05.009, 2002, "Interim Status Standards for Owners and Operators of Hazardous Waste Treatment, Storage, and Disposal Facilities," Idaho Administrative Procedures Act, Department of Environmental Quality, March 15.

IDAPA 58.01.11, 2002, "Ground Water Quality Rules," Idaho Administrative Procedures Act, Department of Environmental Quality, March 15.

IDAPA 58.01.11.200, 1997, "Ground Water Quality Standards," Idaho Administrative Procedures Act, Department of Environmental Quality, March 20.

IDHW, 1998, "Second Modification to Consent Order," Idaho Code § 39-4413, July 31.

IDHW, 1992, "Consent Order to the Notice of Noncompliance," Idaho Code § 39-4413, April 3.

IDHW, EPA, and DOE-ID, 1991, *Federal Facility Agreement and Consent Order for the Idaho National Engineering Laboratory,* State of Idaho Department of Health and Welfare, Division of Environmental Quality; U.S. Environmental Protection Agency, Region 10; U.S. Department of Energy, Idaho Field Office, December 4.

INEEL, 2001a, *Idaho Nuclear Technology and Engineering Center Safety Analysis Report, Tank Farm Facilities*, SAR-107, Revision 0, July.

INEEL, 2001b, *Idaho National Engineering and Environmental Laboratory Impacts 2001, An Analysis of the INEEL's Impact on Idaho's Economy*, 01-GA50944.

INEEL, 2001, *FY-2000 Tank Farm Closure Mock-up Test Report*, INEEL/EXT-2001-00299, EDF-15722-048, Revision 0, April 26.

INEEL, 2000a, *Conceptual Design Report, INTEC Tank Farm Facility Closure*, Project File 015722, Revision 0, September 29.

INEEL, 2000b, *FY 2001-2005 Institutional Plan, Idaho National Engineering and Environmental Laboratory*, INEEL/EXT-2000-00462, August.

INEEL, 1999a, *Idaho Nuclear Technology and Engineering Center Tank Farm Facility Conceptual DOE and HWMA/RCRA Closure Approach,* INEEL/EXT-99-01066.

INEEL, 1999b, *TMI-2 Safety Analysis Report,* Rev. 1, SARII-8.4, March 16.

INEEL, 1998, *Idaho Chemical Processing Plant Safety Document*, Section 4.2 "Aqueous Liquid Waste Management," PSD-4.2, Rev. 10, February 19.

INEL, 1994, *Interim Data Results From the FY 93/94 Perched Ground Water Investigation,* February.

INEL, 1983, *Hydrogeologic and Geochemical Assessment of Contaminated Groundwater at the Idaho Chemical Processing Plant*.

International Atomic Energy Agency, 1994, *Handbook of Parameter Values for the Prediction of Radionuclide Doses to the Public in the Event of a Nuclear Accident or Radiological Emergency,* Safety Series No. 81, International Atomic Energy Agency, Vienna, Austria.

Iriya, K., Y. Itoh, M. Hosoda, A. Fujiwara, and Y. Tsuji, 1992, "Experimental Study on the Water Permeability of a Reinforced Concrete Silo for Radioactive Waste Repository," *Nuclear Engineering and Design*, Vol. 138, pp. 165–170.

Irving, J. S., 1993, *Environmental Resource Document for the Idaho National Engineering Laboratory,* EGG-WMO-10279, July.

Jackson, S. M., 1985, *Acceleration Data from the 1983 Borah Peak, Idaho, Earthquake Recorded at the Idaho National Engineering Laboratory, in Workshop XXVIII on the Borah Peak, Idaho, Earthquake*, U.S. Geological Survey Open-File Report, 85-290, pp. 385–400.

Jackson, S. M., I. G. Wong, G. S. Carpenter, D. M. Anderson, and S. M. Martin, 1993, "Contemporary Seismicity in the Eastern Snake River Plain, Idaho, Based on Microearthquake Monitoring," *Bulletin of the Seismological Society of America,* Vol. 83, pp. 680–695.

Jeppson, R. J., and K. E. Holte, 1978, "Flora of the Idaho National Engineering Laboratory Site," *Ecological Studies on the Idaho National Engineering Laboratory Site, 1978 Progress Report,* IDO-12087.

Jones, J. K., Jr., B. C. Carter, and H. H. Genoways, 1979, *Revised Checklist of North American Mammals North of Mexico, 1979,* Occasional Papers Museum Texas Tech University, No. 62, Lubbock, Texas.

Kearl, P. M., 1981, *Water Transport in Desert Alluvial Soil*, University of Nevada, Reno, Desert Research Institute Water Resources Center, Publication No. 45024.

Kennedy, W. E., Jr., and R. A. Peloquin, 1988, *Intruder Scenarios for Site-Specific Low-Level Radioactive Waste Classification,* DOE/LLW-71T, Department of Energy, Idaho Operations Office.

Knutson, C. F., et al., 1992, *3D RWMC Vadose Zone Modeling (including FY-89 to FY-90 Basalt Characterization Results),* EGG-ERD-10246, May.

Konz, J. J., et al., 1989, *Exposure Factors Handbook*, EPA/600/8-89/043.

Koslow, K. N., and D. H. Van Haaften, 1986, *Flood Routing Analysis for a Failure of Mackay Dam,* EGG-EP-7184, June.

Kuntz, M. A., H. R. Covington, and L. J. Schorr, 1992, "An Overview of Basaltic Volcanism of the Eastern Snake River Plain, Idaho," *Regional Geology of Eastern Idaho and Western Wyoming,* P. K. Link, M. A. Kuntz, and L. B Platt (eds.), Memoir 179, Geological Society of America, Denver, Colorado, pp. 227–267.

Kuntz, M. A., B. Skipp, M. A. Lanphere, W. E. Scott, K. L. Pierce, G. B. Dalrymple, D. E. Champion, G. F. Embree, W. R. Page, L. A. Morgan, R. P. Smith, W. R. Hackett, and D. W. Rodgers, 1994, *Geologic Map of the Idaho National Engineering Laboratory and Adjoining Areas, Eastern Idaho,* U.S. Geological Survey Miscellaneous Investigations Map I-2330, 1:100,000 scale.

Lamke, R. D., 1969, *Stage Discharge Relations on Big Lost River Within National Reactor Testing Station, Idaho,* U.S. Geological Survey Open File Report, ID0-22050.

LaPlante, P. A., and K. Poor, 1997, *Information and Analyses to Support Selection of Critical Groups and Reference Biospheres for Yucca Mountain Exposure Scenarios,* CNWRA 97-009, Center for Nuclear Waste Regulatory Analyses, Southwest Research Institute, San Antonio, Texas.

Latchum, J. W., A. L. Biladeau, E. S. Brown, D. D. Deming, B. L. Schmalz, F. M. Warzel, and L. J. Weber, 1962, *Report of the Investigating Committee, CPP Waste Tank WM-187 Leakage of March 17, 1962*, La-53-62A, INEEL, Phillips Petroleum Company.

Leigh, C. D., B. M. Thompson, J. E. Campbell, D. E. Longsine, R. A. Kennedy, B. A. Napier, et al., 1993, *User's Guide for GENII-S: A Code for Statistical and Deterministic Simulation of Radiation Doses to Humans from Radionuclides in the Environment,* SAND 91-0561, Sandia National Laboratories, Albuquerque, New Mexico.

LITCO, 1994, *ICPP Safety Analysis Report,* INEL-94/022.

LMITCO, 1998, *INTEC TFF Tanks WM-182 and WM-183 Closure Study (Draft),* August 31.

Magnuson, S. O., 1995, *Inverse Modeling for Field-Scale Hydrologic and Transport Parameters of Fractured Basalt,* INEL-95/0637.

Magnuson, S. O., and D. L. McElroy, 1993, *Estimation of Infiltration From In Situ Moisture Contents and Representative Moisture Characteristic Curves for the 30', 110', and 240' Interbeds,* EDF RWMC-93-001.1, EG&G Idaho, August.

Maheras, S. J., A. S. Rood, S. O. Magnuson, E. M. Sussman, and R. N. Bhatt, 1997, *Addendum to Radioactive Waste Management Complex Low-Level Waste Radiological Performance Assessment (EGG-WM-8773),* INEEL/EXT-97-00462, April.

Maheras, S. J., A. S. Rood, S. O. Magnuson, E. M. Sussman, and R. N. Bhatt, 1994, *Radioactive Waste Management Complex Low-Level Radiological Performance Assessment,* EGG-WM-8773, April.

Malde, H. E., 1991, "Quaternary Geology and Structural History of the Snake River Plain, Idaho and Oregon," *Quaternary Non-Glacial Geology, Coterminous United States*, R. B. Morrison, (ed.), Geological Society of America, Boulder Colorado, The Geology of North America, Vol. K-2, pp. 251–281.

Mallants, D., A. Espino, V. Van Hoorick, J. Feyen, N. Vandenberghe, and W. Loy, 2000, "Dispersivity Estimates from a Tracer Experiment in a Sandy Aquifer," *Ground Water*, Vol. 38, No. 2, pp. 304–310.

Markham, O. D., 1987, *Summaries of the Idaho National Engineering Laboratory Radioecology and Ecology Programs Research Projects,* DOE/ID-12111.

McBride, R., et al., 1978, *Vegetation Types and Surface Soils of the Idaho National Engineering Laboratory Site,* IDO-12084.

McElroy, D. L., 1993, *Soil Moisture Monitoring Results at the Radioactive Waste Management Complex of the Idaho National Engineering Laboratory, FY-1993,* EGG-WM-11066, November.

McKenzie, D. H., L. L. Cadwell, L. E. Eberhardt, W. E. Kennedy, Jr., R. A. Peloquin, and M. A. Simmons, 1983, *Relevance of Biotic Pathways to the Long-Term Regulation of Nuclear Waste Disposal,* Topical Report on Reference Eastern Humid Low-Level Sites, NUREG/CR-2675, PNL-4241, Vol. 3, Pacific Northwest Laboratory, Richland, Washington.

Miller, S. M., J. E. Hammel, and L. F. Hall, 1990, *Characterization of Soil Cover and Estimation of Water Infiltration at Central Facilities Area II, Idaho National Engineering Laboratory,* Research Technical Completion Report, Idaho Water Resources Institute, University of Idaho, June.

Mills, W. B., D. B. Porcello, M. J. Ungs, S. A. Gherini, K. V. Summers, Lingfung Muk, G. L. Rupp, G. L. Bowie, and D. A. Haith, 1985, *Water Quality Assessment: A Screening Procedure for Toxic and Conventional Pollutants, Part II*, EPA/600/6-85/002b, September 1985.

Mitchell, J. C., L. L. Johnson, and J. E. Anderson, 1980, *Geothermal Investigations in Idaho, Part 9: Potential for Direct Heal Application of Geothermal Resources,* Water Information Bulletin No. 30, Plate 1, Idaho Department of Water Resources, Boise.

Mosely, R., and C. Groves, 1990, "Rare, Threatened, and Endangered Plants and Animals of Idaho," *Natural Heritage Section, Nongame and Endangered Wildlife Program,* Idaho Department of Fish and Game.

Mundorff, M. J., E. G. Crosthwaite, and C. Kilburn, 1964, *Groundwater for Irrigation in the Snake River Basin in Idaho,* U.S. Geological Survey Water Supply Paper 1654.

Myers, D. R., and D. A. Duranceau (eds.), 1994, *Prototype Hanford Surface Barrier: Design Basis Document*, BHI-00007, Bechtel Hanford, Inc., Richland, Washington.

Nace, R. L., et al., 1959, *Geography, Geology, and Water Resources of the National Reactor Testing Station, Idaho, Part 3: Hydrology and Water Resources,* IDO-22034-USGS.

National Council on Radiation Protection and Measurement, 1984, *Radiological Assessment: Predicting the Transport, Bioaccumulation, and Uptake by Man of Radionuclides Released to the Environment,* NCRP Report No. 76, March.

National Weather Service, 1991, *DAMBRK*, Version 6120188-4, Revision 4, August.

Ng, Y. C., et al., 1978, *Methodology for Assessing Dose Commitment to Individuals and to the Population from Ingestion of Terrestrial Foods Contaminated by Emissions from a Nuclear Fuel Reprocessing Plant at the Savannah River Plant,* UCID-17743, Lawrence Livermore Laboratory, March.

NOAA, 1984, *Climatography of the Idaho National Engineering Laboratory, Site Specific Summary NPR Primary and Alternate Site (Draft),* G. E. Start (ed.), IDO-12048B, November.

NRC, 1982, *Final Environmental Impact Statement on 10 CFR 61, Licensing Requirements for Land Disposal of Radioactive Waste,* NUREG/0945, November.

NRC, 1977, *Calculation of Annual Doses to Man From Routine Releases of Reactor Effluents for the Purpose of Evaluating Compliance with 10 CFR Part 50*, Regulatory Guide 1.109, Appendix I, Revision 1.

Noss, R. F., E. T. LaRoe III, and J. M. Scott, 1995, "Endangered Ecosystems of the United States: A Preliminary Assessment of Loss and Degradation," *Biological Report 28*, National Biological Service, Department of the Interior.

Nussbaum, R. A., E. D. Brodie, Jr., and R. M. Storm, 1983, *Amphibians and Reptiles of the Pacific Northwest,* Moscow, Idaho: University Press of Idaho.

Odler, I., and I. Jawed, 1991, "Expansive Reactions in Concrete," *Material Science of Concrete II,* J. Skalny and S. Mindess (eds.), American Ceramic Society, Inc.

Olmsted, F. H., 1962, *Chemical and Physical Character of Groundwater in the National Reactor Testing Station, Idaho,* IDO-22043.

Orr, B. R., and L. D. Cecil, 1991, *Hydrologic Conditions and Distribution of Selected Chemical Constituents in Water, Snake River Plain Aquifer, INEL, Idaho, 1986 to 1988*, USGS Water-Resources Investigation Report 89-4008, DOE/ID-22078, pg. 73.

Ostenaa, D. A., D. R. Levish, R. E. Klinger, and D. R. H. O'Connell, 1999, *Phase 2 Paleohydrologic and Geomorphic Studies for the Assessment of Flood Risk for the Idaho National Engineering and Environmental Laboratory, Idaho,* Report 99-7, U.S. Bureau of Reclamation, Geophysics, Paleohydrology, and Seismotechonics Group, Technical Service Center, Denver, Colorado, July.

Overton, C. K., et al., 1976, "Big Lost River Fisheries," *Summaries of the Idaho National Engineering Laboratory Site Ecological Information Meeting, July 10–11, 1975,* U.S. Energy Research and Development Administration, Idaho Operations Office, pp. 42–43.

Oztunali, O. I., and G. W. Roles, 1986, *Update of Part 61: Impacts Analysis Methodology, Methodology Report,* NUREG/CR-4370, Vol. 1, U.S. Nuclear Regulatory Commission, Washington, D.C, January.

Palmer, W. B., P. A. Anderson, W. J. Dirk, M. D. Staiger, M. C. Swenson, and F. S. Ward, 1999, *Status and Estimated Life of the 300,000-gal INTEC Tanks*, INEEL/EXT-99-00743, Revision 1, November.

Parrington, J. R., H. D. Knox, S. L. Breneman, E. M. Baum, and F. Feiner, 1996, *Nuclides and Isotopes,* 15th Ed., GE Nuclear Energy, San Jose, California.

Patterson, M., 1999, *Light Duty Utility Arm Deployment in Tank WM-188*, INEEL/EXT-99-01302, December 1.

Pelton, J. R., R. J. Vincent, and N. J. Anderson, 1990, "Microearthquakes in the Middle Butte/East Butte Area, Eastern Snake River Plain, Idaho," *Bulletin of the Seismological Society of America,* Vol. 80, No. 1, pp. 209–212.

Peterson, H. T., Jr., 1983, "Terrestrial and Aquatic Food Chain Pathways," *Radiological Assessment – A Textbook on Environmental Dose Analysis*, J. E. Till and H. R. Meyer (eds.), NUREG/CR-3332.

Pickens, J. F., and G. E. Grisak, 1981, "Scale-Dependent Dispersion in a Stratified Granular Aquifer," *Water Resources Research*, Vol. 17, No. 4, pp. 1191–1211.

Pistre, S., S. Marliac, H. Jourde, and P. Bidaux, 2002, "New Combined Log and Tracer Test Interpretation Method for Identifying Transfers in Fissured Aquifers," *Ground Water*, Vol. 40, No. 2, pp. 232–241.

Pohll, G., A. E. Hassan, J. B. Chapman, C. Papelis, and R. Andricevic, 1999, "Modeling Ground Water Flow and Radioactive Transport in a Fractured Aquifer," *Ground Water,* Vol. 37, No. 5, pp. 770–780.

Poloski, A. P., 2000, "Sandpad Contamination Analysis," EDF-15722-046, July 21, in *Conceptual Design Report, Book 6: EDFs, Volume 3 of 3, INTEC Tank Farm Facility Closure, Draft*, INEEL Project File Number 015722, Revision 0.

Porro, I., M. E. Newman, and F. M. Dunnivant, 2000, "Comparison of Batch and Column Methods for Determining Strontium Distribution Coefficients for Unsaturated Transport in Basalt," *Environmental Science & Technology*, Vol. 34, No. 9, pp. 1679–1686.

Portage Environmental, 2002, *Sampling and Analysis Plan for the Post-Decontamination Characterization of the WM-182 and WM-183 Tank Residuals,* INEEL/EXT-01-00666, Revision 2, prepared for the INEEL, August.

Portage Environmental, 2001, *Sampling and Analysis Plan for the Post-Decontamination Characterization of the Process Waste Lines from INTEC Tank Farm Facility Tanks WM-182 and WM-183*, INEEL/EXT-01-01543, Revision 1, prepared for the INEEL, November.

Radiation Safety Information Computational Center, 2002, *RSICC Computer Code CC-371*, http://www-rsicc.ornl.gov/codes/ccc/ccc3/ccc%2D371.html, updated June 2002, Web page visited April 7, 2003.

Renken, K. J., and T. Rosenberg, 1995, "Laboratory Measurements of the Transport of Radon Gas through Concrete Samples," *Health Physics,* Vol. 68, No. 6, pp. 800–808.

Reynolds, T. D., et al., 1986, "Vertebrate Fauna of the Idaho National Environmental Research Park," *Great-Basin Naturalist,* Vol. 46, pp. 513–527.

Reynolds, T. D., and L. Fraley, Jr., 1989, "Root Profiles of Some Native and Exotic Plant Species in Southeastern Idaho," *Environmental and Experimental Botany,* Vol. 29, pp. 241–248.

Reynolds, T. D., and J. W. Laundre, 1988, "Vertical Distribution of Soil Removed by Four Species of Burrowing Rodents in Disturbed and Undisturbed Soils," *Health Physics,* Vol. 54, No. 4, pp. 445–450.

Reynolds, T. D., and W. L. Wakkinen, 1987, "Characteristics of the Burrows of Four Species of Rodents in Undisturbed Soils in Southeastern Idaho," *The American Midland Naturalist,* Vol. 188, No. 2, pp. 245–250.

Rightmire, C. T., and B. D. Lewis, 1987, *Hydrogeology and Geochemistry of the Unsaturated Zone, Radioactive Waste Management Complex, Idaho National Engineering Laboratory, Idaho,* U.S. Geological Survey Water Resources Investigation Report 87-4198, DOE/ID-22073.

Robertson, J. B., R. Schoen, and J. T. Barraclough, 1974, *The Influence of Liquid Waste Disposal on the Geochemistry of Water at the National Reactor Testing Station, 1952–1970,* U.S. Geological Survey Open-File Report, IDP-22053, TID-4500, February.

Rodriguez, R. R., A. L. Shafer, J. McCarthy, P. Martian, D. E. Burns, D. E. Raunig, N. A. Burch, and R. L. VanHorn, 1997, *Comprehensive RI/FS for the Idaho Chemical Processing Plant OU 3-13 at the INEEL – Part A, RI/BRA Report (Final),* DOE/ID-10534, Binders 1–3, November.

Rogers, V. C., and K. K. Nielson, 1992, "Data and Models for Radon Transport through Concrete," *The 1992 International Symposium on Radon and Radon Reduction Technology*, Vol. 2:VI-3, Environmental Protection Agency.

Rood, A. S., 1998, *GWSCREEN: A Semi-Analytical Model for Assessment of the Groundwater Pathway from Surface or Buried Contamination,* Version 2.5, INEEL/EXT-98-00750, August.

Runchal, A., 1997, *PORFLOW Software and User Manual,* Version 4.0, Analytic and Computational Research Inc., Bel Air, California.

Russo, D., and E. Bresler, 1981, "Effect of Field Variability in Soil Hydraulic Properties on Solutions of Unsaturated Water and Salt Flows," *Soil Science Society of America Journal,* Vol. 45, No. 4, pp. 675–681.

Rupp, E. M., 1980, "Age-Dependent Values of Dietary Intake for Assessing Human Exposures to Environmental Pollutants," *Health Physics,* Vol. 39, pp. 151–163.

Savannah River Site, 2000, *Industrial Wastewater Closure Plan for F- and H-Area High-Level Waste Tank Systems*, Preliminary Draft Revision 2, March 1.

Schmalz, B. L., 1972, *Radionuclide Distribution in Soil Mantle of the Lithosphere as a Consequence of Waste Disposal at the National Reactor Testing Station,* IDO-10049.

Sehlke, G., F. E. Bickford, 1993, *Idaho National Engineering Laboratory Groundwater Monitoring Plan,* DOE/ID-10441, Volumes 1 and 2, June.

Seitz, R. R., 1991, *Well Parameters for Intruder Drilling Scenario at RWMC,* SEM-RWMC-91-002, EG&G Idaho, August.

Seitz, R. R., and J. C. Walton, 1993, *Modeling Approaches for Concrete Barriers Used in Low-Level Waste Disposal*, NUREG/CR-6070, EGG-2701, November.

Sheppard, M. I., and D. H. Thibault, 1990, "Default Soil Solid/Liquid Partition Coefficients, K_ds, for Four Major Soil Types: A Compendium," *Health Physics,* Vol. 59, pp. 471–482.

Simpson, J. C., and R. L. Wallace, 1978, *Fishes of Idaho,* Moscow, Idaho: University Press of Idaho.

Staiger, M. D., and C. B. Millet, 2000, *Inventory Estimates for the Tank Farm and CCSF,* MDS-01-00/Mil-01-00, March 21.

State of Idaho, 1983, "Hazardous Waste Management," Idaho Statute, Title 39, "Health and Safety," Chapter 44, "Hazardous Waste Management" (also known as the Hazardous Waste Management Act of 1983).

Sudicky, E. A., and J. A. Cherry, 1979, "Field Observations of Tracer Dispersion Under Natural Flow Conditions in an Unconfined Sandy Aquifer," *Water Pollution Resources Canada*, Vol. 14, pp. 1–17.

Sudicky, E. A., J. A. Cherry, and E. O. Frind, 1983, "Migration of Contaminants in Groundwater at a Landfill: A Case Study," *Journal of Hydrology,* Vol. 63, pp. 81–108.

Sullivan, T. M., 1998, *DUST-MS—Disposal Unit Source Term—Multiple Species*, Informal Report, BNL-EWMG.

Sullivan, T. M., 1996, *DUST-MS—Model Equations for Waste Form Leaching and Transport with Ingrowth Due to Radioactive Progeny,* Brookhaven National Laboratory, Environmental and Waste Technology Center.

Sullivan, T. M., 1993, *DUST: Disposal Unit Source: Term Data Input Guide,* NUREG/CR-6041, BNL-NUREG-52375.

Tanner, A. B., 1990, "The Role of Diffusion in Radon Entry into Houses," *The 1990 International Symposium on Radon and Radon Reduction Technology*, Vol. 2:V-2, Environmental Protection Agency.

Thomas, T. R., 1988, *Modeling Hypothetical Groundwater Transport of Nitrates, Chromium, and Cadmium at the Idaho Chemical Processing Plant,* WINCO-1060.

Thorne, D. J., et al., 2000, *Performance Assessment for the Tank Farm Facility Idaho Nuclear Technology and Engineering Center, Draft*, Portage Environmental, July.

Ticknor, K. V., and B. Ruegger, 1989, *A Guide to the NEA's Sorption Data Base,* Version 2.0, September.

Tullis, J. A., and K. N. Koslow, 1983, *Characterization of Big Lost River Floods with Recurrence Intervals Greater than 25 Years,* RE-PB-83-044, EG&G Idaho.

Tyson, D. R., 2002, "Validation of the Radionuclide Mass Balance Used in the INTEC SBW WIR Determination Report," EDF-1920, Revision 4, August 29.

USDA, 1983, *Food Intakes: Individuals in 48 States, Year 1977-1978*, NFCS 1977-1978, Report No. I-2, Human Nutrition Information Service, Washington, D.C.

Van Genuchten, R., 1978, *Calculating the Unsaturated Hydraulic Conductivity with a New Closed-Form Analytical Model,* Princeton University, Rpt. 78-WR-08, Department of Civil Engineering, Princeton, New Jersey.

Van Haaften, D. H., K. N. Koslow, and C. J. Naretto, 1984, *Hydrologic Analysis of a Mackay Dam Failure During a Probable Maximum Flood on Big Lost River, Idaho*, SE-A-84-018, INEEL internal report.

Volcanism Working Group, 1990, *Assessment of Potential Volcanic Hazards for the New Production Reactor Site at the Idaho National Engineering Laboratory,* EGG-NPR 10624, October.

Walker, E. H., 1960, *Analysis of Aquifer Tests, January 1958–June 1959, at the National Reactor Testing Station, Idaho,* Atomic Energy Commission.

Walton, J. C., and R. R. Seitz, 1991, *Performance of Intact and Partially Degraded Concrete Barriers in Limiting Fluid Flow*, NUREG/CR-5614, July.

Walton, J. C., M. Rahman, D. Casey, M. Picornell, and F. Johnson, 1997, "Leakage through Flaws in Geomembrane Liners," *Journal of Geotechnical and Geoenvironmental Engineering,* June.

Wang, K., D. C. Jansen, and S. P. Shah, 1997, "Permeability Study of Cracked Concrete," *Cement and Concrete Research*, Vol. 27, No. 3, pp. 381–393.

Ward, A. L., and G. W. Gee, 2000, "Hanford Site Barrier Technology," *Vadose Zone Science and Technology Solutions*, B. B. Looney and R. W. Falta (eds.), Columbus, Ohio: Battelle Press, pp. 1415–1423.

Wenzel, D. R., 1997, "Evaluation of Contaminated Soil Site CPP-31 Activity," EDF-CPP-058, functional file number 1000-50, INEEL.

Westinghouse Savannah River Company, 1992, *Radiological Performance Assessment for the Z-Area Saltstone Disposal Facility*, WSRC-RP-92-1360, Wilhite, E. L., J. Cook, J. Fowler, R. Hiergesell (Westinghouse Savannah River Company), L. M. McDowell-Boyer, P. Kearl, and D. J. Thorne (Oak Ridge National Laboratory); and J. Walton, C. Smith, R. Smith, and R. Seitz (INEEL).

Whitehead, R. L., 1992, *Geohydrologic Framework of the Snake River Plain Regional Aquifer System, Idaho and Eastern Oregon,* U.S. Geological Survey Paper 1408-B, 32 pp., 6 pls. in pocket.

Wilcox, M. R., 2000, "INTEC Tank Farm Facility Ancillary Process Waste Line Mass Estimate," EDF-015722-39, July 17, in *Conceptual Design Report, Book 6: EDFs, Volume 2 of 3, INTEC Tank Farm Facility Closure, Draft*, INEEL Project File Number 015722, Revision 0.

Wilson, L. G., L. G. Everett, and S. J. Cullen, 1995, *Handbook of Vadose Zone Characterization and Monitoring*, ISBN 0-87371-610-8, Boca Raton: Lewis Publishers.

Woodward-Clyde Consultants, 1990, *Assessment of Potential Volcanic Hazards for the New Production Reactor Site at the Idaho National Engineering Laboratory,* EGG-NPR–10624, October.

Woodward-Clyde Federal Services, 1996, *Site-Specific Probabilistic Seismic Hazard Analyses for the Idaho National Engineering Laboratory, Volume 1, Final Report, and Volume 2, Appendix,* INEL-95/0536, Lockheed Idaho Technologies Company, Idaho Falls, Idaho, May.

Yang, Y. Y., and C. B. Nelson, 1986, "An Estimation of Daily Food Usage Factors for Assessing Radionuclide Intakes in the U.S. Population," *Health Physics,* Vol. 50, No. 2, pp. 245–257.

Yang, Y. Y., and C. B. Nelson, 1984, *An Estimation of the Daily Average Food Intake by Age and Sex for Use in Assessing the Radionuclide Intake of Individuals in the General Population,* EPA 520/1-84-021.

Yu, C., A. J. Zielen, J. J. Cheng, Y. C. Yuan, L. G. Jones, D. J. LePoire, Y. Y. Wang, C. O. Loureiro, E. Gnanapragasam, E. Faillace, A. Wallo III, W. A. Williams, and H. Peterson, 1993, *Manual For Implementing Residual Radioactive Material Guidelines Using RESRAD,* Version 5.0,

ANL/EAD/LD-2, Environmental Assessment Division, Argonne National Laboratory, Argonne, Illinois.